



REFERENCE ONLY

UNIVERSITY OF LONDON THESIS

Degree PhD

Year 2006

Name of Author LEBELO, C-M

COPYRIGHT

This is a thesis accepted for a Higher Degree of the University of London. It is an unpublished typescript and the copyright is held by the author. All persons consulting the thesis must read and abide by the Copyright Declaration below.

COPYRIGHT DECLARATION

I recognise that the copyright of the above-described thesis rests with the author and that no quotation from it or information derived from it may be published without the prior written consent of the author.

LOANS

Theses may not be lent to individuals, but the Senate House Library may lend a copy to approved libraries within the United Kingdom, for consultation solely on the premises of those libraries. Application should be made to: Inter-Library Loans, Senate House Library, Senate House, Malet Street, London WC1E 7HU.

REPRODUCTION

University of London theses may not be reproduced without explicit written permission from the Senate House Library. Enquiries should be addressed to the Theses Section of the Library. Regulations concerning reproduction vary according to the date of acceptance of the thesis and are listed below as guidelines.

- A. Before 1962. Permission granted only upon the prior written consent of the author. (The Senate House Library will provide addresses where possible).
- B. 1962 - 1974. In many cases the author has agreed to permit copying upon completion of a Copyright Declaration.
- C. 1975 - 1988. Most theses may be copied upon completion of a Copyright Declaration.
- D. 1989 onwards. Most theses may be copied.

This thesis comes within category D.



This copy has been deposited in the Library of UCL



This copy has been deposited in the Senate House Library, Senate House, Malet Street, London WC1E 7HU.

TEMPORAL-BNDF MODEL BASED APPROACH TO
CHANGE DETECTION,
The development of a ~~generic change detection~~
~~scheme~~. An application to the identification and
delineation of fire affected areas

Lisa-Maria Rebelo

Remote Sensing Unit
Department of Geography
University College London

Thesis Submitted for the Fulfilment
of the Degree of Doctorate of Philosophy

UMI Number: U592335

All rights reserved

INFORMATION TO ALL USERS

The quality of this reproduction is dependent upon the quality of the copy submitted.

In the unlikely event that the author did not send a complete manuscript and there are missing pages, these will be noted. Also, if material had to be removed, a note will indicate the deletion.



UMI U592335

Published by ProQuest LLC 2013. Copyright in the Dissertation held by the Author.
Microform Edition © ProQuest LLC.

All rights reserved. This work is protected against
unauthorized copying under Title 17, United States Code.



ProQuest LLC
789 East Eisenhower Parkway
P.O. Box 1346
Ann Arbor, MI 48106-1346

Abstract

Although large quantities of southern Africa burn every year, minimal information is available relating to the fire regimes of this area. This study develops a new, generic approach to change detection, applicable to the identification of land cover change from high temporal and moderate spatial resolution satellite data. Traditional change detection techniques have several key limitations which are identified and addressed in this work. In particular these approaches fail to account for directional effects in the remote sensing signal introduced by variations in the solar and sensing geometry, and are sensitive to underlying phenological changes in the surface as well as noise in the data due to cloud or atmospheric contamination.

This research develops a bi-directional, model-based change detection algorithm. An empirical temporal component is incorporated into a semi-empirical linear BRDF model. This may be fitted to a long time series of reflectance with less sensitivity to the presence of underlying phenological change. Outliers are identified based on an estimation of noise in the data and the calculation of uncertainty in the model parameters and are removed from the sequence. A “step function kernel” is incorporated into the formulation in order to detect explicitly sudden step-like changes in the surface reflectance induced by burning.

The change detection model is applied to the problem of locating and mapping fire affected areas from daily moderate spatial resolution satellite data, and an indicator of burn severity is introduced. Monthly burned area datasets for a 2400km by 1200km area of southern Africa detailing the day and severity of burning are created for a five year period (2000-2004). These data are analysed and the fire regimes of southern African ecosystems during this time are characterised. The results highlight the extent of the burning which is taking place within southern Africa, with between 27-32% of the study area burning during each of the five years of observation. Higher fire frequencies are exhibited by savanna and grassland ecosystems, while more dense vegetation types such as shrublands and deciduous broadleaf forests burn less frequently. In addition the areas which burn more frequently do so with a greater severity, with a positive relationship identified between the frequency and the severity of burning.

Acknowledgements

First, I would like to thank Dr Philip Lewis who, in addition to being my supervisor, has been a mentor since I started at UCL all those years ago. I wouldn't have got this far without your constant help, advice and support. Thanks also to my colleagues in the Geography Department at University College London for all the discussions, help and encouragement over the years. In particular I would like to thank Tristan for his endless patience, guidance and friendship. Thanks must go to Addie and Ian - for so much love and help along the way, and for always believing I would get there in the end. And finally, to my parents for their constant love and support, without which this thesis would not have been possible.

This work was carried out under a Teaching Studentship in the Department of Geography, University College London. The field data was provided by Drs Alistair Smith and Martin Wooster, King's College London. Field work was funded by Drs Martin Wooster and Nick Drake. All are gratefully acknowledged.

Contents

1	Introduction	21
1.1	Global vegetation burning	22
1.1.1	The need for monitoring	24
1.1.2	Principal research programmes	26
1.1.3	The role of remote sensing	28
1.2	Research objectives	29
1.3	Thesis plan	31
2	Remote Sensing Change Detection	33
2.1	Multi-temporal change detection	34
2.1.1	Image enhancement techniques	35
2.1.2	Post-classification techniques	44
2.1.3	Overview	46
2.1.4	Spectral mixture analysis	47
2.1.5	Mapping fire affected areas at a global scale	49
2.2	Limitations of traditional change detection techniques	50
2.2.1	Issues implicit in multi-temporal studies	56
2.3	The detection of active fires	58
2.3.1	Fixed threshold algorithms	59
2.3.2	Contextual algorithms	61
2.4	Global fire products	62
2.4.1	The MODIS active fire product	64
2.4.2	Global burned area products	67

2.5	Summary	72
3	Fire characteristics of southern Africa	75
3.1	Introduction	76
3.2	The role of fire in southern African ecosystems	76
3.3	The area of interest	80
3.4	Fire characteristics of southern Africa	86
3.4.1	Thermal Anomalies	86
3.4.2	The temporal distribution of fire activity	87
3.4.3	The spatial distribution of fire activity	97
3.5	The spectral characteristics of burned and unburned surfaces	99
3.5.1	Field-based spectral measurements	100
3.5.2	Fire induced spectral change	103
3.5.3	Perturbing factors	106
3.6	The MODIS burn signal	107
3.6.1	The proportional change in MODIS reflectances	111
3.6.2	The duration of the MODIS burn signal	113
3.7	Summary	119
4	A new approach to change detection	122
4.1	Anisotropic surface reflectance	123
4.2	Models of the BRDF	125
4.2.1	Physically based models	126
4.2.2	Empirical models	128
4.2.3	Semi-empirical models	129
4.2.4	Analytical inversion	137
4.2.5	Overview	138
4.3	A new approach to change detection	139
4.4	Rationale	143
4.5	Temporal angular models of the surface	144
4.5.1	A cubic function of time	147

- 4.5.2 Model assumptions 152
- 4.6 Filtering for outliers 163
- 4.7 Detecting step changes 172
- 4.8 Summary 179
- 5 Model implementation 181**
 - 5.1 Introduction 182
 - 5.2 The MODerate resolution Imaging Spectroradiometer 182
 - 5.2.1 Sensor Characteristics 183
 - 5.2.2 Data Products from MODIS 184
 - 5.2.3 Surface Reflectance 187
 - 5.2.4 Surface State 190
 - 5.2.5 Geolocation Angles 190
 - 5.3 Data preprocessing 194
 - 5.4 Identifying fire induced surface change 195
 - 5.4.1 Determining the day of the change 196
 - 5.4.2 A spectral filter 199
 - 5.5 The creation of monthly burned area datasets 203
 - 5.5.1 The selection of burn candidates 204
 - 5.5.2 The proportional change in reflectance 208
 - 5.5.3 Excluding confusing spectral change 218
 - 5.6 Summary 229
- 6 Analysis of results 230**
 - 6.1 MODIS 500m fire affected areas 231
 - 6.2 MODIS 1km Thermal Anomalies 233
 - 6.2.1 Scaling between active fire counts and the area burned 240
 - 6.3 SAFARI 2000 MODIS 500m burned areas 245
 - 6.3.1 Errors of omission 246
 - 6.3.2 Errors of commission 251
 - 6.4 GBA2000 1km burned areas 263

6.4.1	Errors of omission	263
6.4.2	Errors of commission	270
6.5	Summary	278
7	Characterisation of the fire regime	280
7.1	The fire regime	281
7.2	The fire frequency	283
7.2.1	Fire frequencies in southern Africa, 2000-2004	285
7.2.2	Fire return intervals	296
7.3	The seasonality of burning	299
7.3.1	The temporal distribution of burning within the study area	300
7.4	The spatial extent of burning	307
7.5	Annual burned area totals	308
7.5.1	Burned area totals in each vegetation type	311
7.6	The severity of burning	315
7.6.1	An indicator of burn severity	318
7.7	Summary	337
8	Conclusions	340
8.1	Summary of work	341
8.2	Aims of the study	342
8.2.1	Objective 1: A change detection model	342
8.2.2	Objective 2: Mapping fire affected areas	344
8.2.3	Objective 3: Analysis of the fire regime of southern Africa	346
8.3	Principal contributions	347
8.4	Further Research	349
	References	352
	Appendices	386
A	Sitemap	388

<i>CONTENTS</i>	<i>7</i>
B Active fires and burned areas	391
C Monthly burned area totals	392
D Number of burn pixels	395
E Fire frequencies	396
F Burned area totals	398
G Burn severity classes	404

List of Figures

2.1	The effect of burning on MODIS band 5 reflectances and NDVI, Site 2A, Zimbabwe 2001: The vertical line indicates the day of the MODIS active fire detection	52
2.2	Mongu (Zambia) core validation site and MODIS Landcover Product	54
2.3	Directional effects in MODIS 500m reflectances, Mongu (Zambia), 4th April 2001	55
3.1	The study area, shown in the red box: Adapted from ESRI (1999)	81
3.2	Land cover classes	85
3.3	Fires detected by Terra MODIS, 2000 - 2004	88
3.4	Active fire detections from MODIS Aqua and Terra: Monthly totals	90
3.5	Typical diurnal burn cycle, Adapted from: Giglio and Pinzon (2003)	91
3.6	The difference in the number of fires detected by Aqua and Terra as a proportion of the total	92
3.7	The difference in the number of fires detected by Terra and Aqua as a proportion of the total detected in each cover type	93
3.8	Phenology of deciduous broadleaf forest and grasslands, 2000-2004	96
3.9	Mean EVI profile and MODIS Terra active fire detections, 2000-2004	97
3.10	Location of the field study site (Smith 2004)	100
3.11	The spectral characteristics of savanna surfaces	102
3.12	MODIS burned and unburned reflectances	109
3.13	Separability (mean values of M)	110
3.14	Standard deviations of burned (filled circles) and unburned (empty circles) reflectances	110
3.15	Proportional changes in reflectance ($\delta\rho(\lambda)$)	112
3.16	Duration of the MODIS burn signal	115

4.1	Angular effects caused by sensor characteristics and orbital patterns	124
4.2	Isotropic, volumetric and geometric forms of vegetation scattering	130
4.3	Rossthick and LiSparse kernels for a solar zenith angle of 45°	133
4.4	Observed and modelled reflectances, Zambia, Site 4A, January-May 2003	150
4.5	Observed and modelled reflectances, Democratic Republic of the Congo, Site 4B May-August 2003	151
4.6	Variations in surface brightness	155
4.7	Variations in brightness	155
4.8	Additive model: Parameter values at near-infrared wavelengths	158
4.9	Multiplicative model: Parameter values at near-infrared wavelengths	159
4.10	MODIS 500m band 2 reflectance as a function of view zenith angle	161
4.11	Temporal sequence of MODIS 500m band 2 reflectance	161
4.12	MODIS 500m band 2 reflectances: Sampling in the solar plane	162
4.13	Observed and modelled MODIS band 2 reflectance: Additive and multiplicative results	163
4.14	Isolated spikes in MODIS 500m band 2 reflectance	164
4.15	Filtering for outliers: Z-score values, additive model results	166
4.16	Observed and modelled MODIS 500m band 2 reflectances: Additive model results	166
4.17	The removal of noisy observations: Site 4G, Democratic Republic of the Congo .	168
4.18	The removal of noisy observations of MODIS band 2 reflectances: Site 4G, Democratic Republic of the Congo	169
4.19	Observed and modelled MODIS band 2 reflectances: 16 day moving window (Site 4G, Democratic Republic of the Congo)	170
4.20	Change in reflectance due to burning	173
4.21	The heaviside function	174
4.22	Detecting step changes: Observed and modelled MODIS band 2 reflectances, June-September 2003, Site 4H, Democratic Republic of the Congo	177
4.23	Identifying the day of change: Filtered Z-scores, 16 day moving window ap- proach (Site 4H, Democratic Republic of the Congo)	178
4.24	Identifying the day of change: RMSE, Additive temporal model (Site 4H, Demo- cratic Republic of the Congo)	178

5.1	MODIS Sinusoidal grid (<i>Source</i> : http://nsidc.org/data/modis/landgrid.html) . . .	186
5.2	MODIS atmospheric correction (<i>Source</i> : Adapted from Vermote and Vermeulen (1999a))	189
5.3	Uncertainty in predictions of reflectance	197
5.4	Locating the day of greatest change: Site 5A, central Angola	198
5.5	The prediction of a step change, Site 5A, central Angola	200
5.6	MODIS band 2 reflectances: Site 5B, southern Angola	201
5.7	Step changes in reflectance ($M(\lambda)$) Site 5B, southern Angola	202
5.8	Prediction of burn-type change (Site 5B, southern Angola)	203
5.9	Temporal range of model inputs and outputs	204
5.10	The proportional change ($\delta\rho$) in band 5 reflectances at active fire locations	209
5.11	Selection of change candidate values	210
5.12	$\delta\rho(band2)$ and $\delta\rho(band5)$ at active fire locations	211
5.13	Sites 5C, 5D and MODIS Landcover Product	216
5.14	Disagreement between 1km active fire locations and 500m potential burn candidates: red pixels indicate active fire detections which are not identified as burns; black areas indicate burn candidates	217
5.15	Canopy level reflectance modelled with different leaf equivalent water thickness using the Kuusk model (Kuusk 1996)	219
5.16	Site 5E and MODIS Landcover Product	222
5.17	Proportional change in reflectance ($\delta\rho(band2)$): Changes due to flooding, April 2003: Site 5E, Botswana	223
5.18	Magnitude of the change ($M(band2)$): Additive model results, site 5E, Botswana	224
5.19	Site 5F and MODIS Landcover Product	225
5.20	Proportional change in reflectance ($\delta\rho(\lambda)$) due to burning, July 2000: Multiplicative model results: Site 5F, southern Angola	226
5.21	Magnitude of the change ($M(band2)$): Additive model results, Site 6F (southern Angola)	226
5.22	Changes due to flooding (black pixels), Site 5E (northern Botswana) April 2003 .	227
5.23	Magnitude of the change ($M(band2)$): Site 5G, central Angola	229

6.1	Sites 6A, 6B and MODIS Landcover Product	232
6.2	Burned area information, August 2004: Multiplicative model results	234
6.3	An area of burning, August 2001	235
6.4	Sites 6C, 6D, 6E and MODIS Landcover Product	238
6.5	Discrepancies between 1km active fire detections and 500m burned areas (additive model results), April 2003: black pixels = no burn or fire, red pixels = fire only, green = burn only, dark blue = fire and burn (Sites 6C and 6D, Angola) . . .	239
6.6	Discrepancies between 1km active fire detections and 500m burned areas (additive model results), July 2003: black pixels = no burn or fire, red pixels = fire only, green = burn only, dark blue = fire and burn (Site 6E, Angola)	239
6.7	Discrepancies between SK2 500m burned areas and SABA (multiplicative model results): black pixels = burn in both, red pixels = burn in SK2 only, white pixels = no burn in SK2	248
6.8	Sites 6F, 6G and MODIS Landcover Product	250
6.9	Sites 6H, 6I and MODIS Landcover Product	254
6.10	Discrepancies between SK2 500m burned areas and SABA (multiplicative model results): black pixels = burn in both, red pixels = burn in SABA only, white = no burn in SABA	255
6.11	SABA errors of commission: 500m burn pixels not identified by the SK2 product	256
6.12	Site 6L and MODIS Landcover Product	258
6.13	Discrepancies between SABA (multiplicative model results) and SK2 500m burned areas	260
6.14	Errors of commission: distribution of SABA day of burn	261
6.15	Discrepancies between SABA (multiplicative model results) and SK2 500m burned areas, Site 6L (northern Angola)	262
6.16	Site 6M and MODIS Landcover Product	265
6.17	A semi-permanent water body identified as a burn in the GBA2000 product, Site 6M, Zambia, April 2000	266
6.18	Semi-permanent water features, 29th April 2000, Site 6M (Zambia)	266
6.19	Site 6N and MODIS Landcover Product	269

6.20 SABA errors of omission: GBA2000 burned areas, Site 6N, western Angola, May 2000	270
6.21 SABA errors of omission: Site 6P, western Angola, May 2000	270
6.22 Site 6Q and MODIS Landcover Product	274
6.23 Errors of commission: black pixels = burn in both SABA and GBA2000, red pixels = burn in SABA only (Site 6Q)	275
6.24 SABA burned areas, Site 6Q, northern Zambia	276
6.25 Distribution of SABA/GBA2000 errors of commission within each land cover class	277
7.1 The determinants and components of a fire regime. Adapted from Diaz-Delgado <i>et al.</i> (2004)	283
7.2 Fire frequency: Proportion of each cover type which burns more than once be- tween 2000-2004	288
7.3 Fire frequency (2000-2004): Multiplicative model results	292
7.4 (b) Site 7B (Angola): Fire frequency (2000-2004): Multiplicative model results .	293
7.5 (b) Site 7B (Angola): Land cover	294
7.6 Digital Elevation Model, (<i>Source</i> : USGS 2006)	295
7.7 Mean fire return intervals (2000-2004)	297
7.8 Mean fire return interval (2000-2004) as a function of land cover	298
7.9 Monthly area burned as a proportion of the annual total: multiplicative model results	301
7.10 Eastern half of study area (MODIS tile “h20v10”): Mean MODIS EVI, 6th April 2000-2004	302
7.11 Seasonality of burning 2004: Multiplicative model results	305
7.12 Mean fire return intervals of savanna fires as a function of the timing of initial burning	306
7.13 Total area burned per month between April 2000 and November 2004: Multi- plicative model results	309
7.14 Vegetation phenology (savannas), October to May: MODIS EVI	310
7.15 Proportion of each vegetation type burned per month between April 2000 and November 2004: Multiplicative model results	312

7.16 MODIS EVI profiles (January 2000 to November 2004). The vertical red and black lines indicate the start and end of the annual fire season respectively. 313

7.17 Sites 7C, 7D and MODIS Landcover Product 320

7.18 Spatial patterns of burn severity at two locations: Multiplicative model results . . 321

7.19 Distribution of MODIS band 7 proportional changes in reflectance: Sites 7C and 7D (northern and southern Angola) 322

7.20 Spatial patterns of burn severity at two locations 324

7.21 Burn severity 2004 325

7.22 Temporal distribution of mean burn severity and MODIS EVI, 2000-2004 327

7.23 Mean severity of burning for each of the main vegetation types present in the study area 329

7.24 The relationship between the mean burn severity and fire frequency in each vegetation type: Multiplicative model results 334

7.25 Changes in woody and grass biomass with levels of fire frequency. Solid lines indicate stable equilibria, dashed lines unstable equilibria, and arrows the direction of development. Source: Langevelde *et al.* (2003) 336

A.1 The locations of pixel examples used in the text 390

List of Tables

2.1	Fire related statistics: MODIS Thermal Anomalies product	66
2.2	GBA2000 Classification rules (<i>Source: Tansey et al. (2004b)</i>)	70
3.1	IGBP Land Cover units	82
3.2	Land cover characteristics of the study area	84
3.3	Predominant vegetation types	84
3.4	Percent and area of land surface on fire	97
3.5	Proportion of cover type detected as fire	98
3.6	Properties of the GER 3700 spectroradiometer (GER 2000)	101
3.7	Duration of the MODIS burn signal (M)	116
3.8	Duration of the MODIS burn signal ($\delta\rho(band2)$)	117
4.1	Effects of noisy data on model fitting: Additive model results	170
5.1	EOS measurements	183
5.2	MODIS land surface reflectance wavebands	184
5.3	MODIS Sinusoidal projection parameters (<i>Source: http://landweb.nascom.nasa.gov/</i>)	186
5.4	MODIS Surface State product: Quality Assurance (QA) bits	191
5.5	MODIS Surface State product: Quality Assurance (QA) bits	192
5.6	Percentage of MODIS active fire detections which exhibit a proportional decrease in MODIS band 2 <i>and</i> band 5 reflectances	212
5.7	Percentage of MODIS active fire detections which exhibit a proportional decrease in MODIS band 2 <i>and</i> band 5 reflectances below a particular threshold value	213

5.8	Proportional change ($\delta\rho$) in canopy level reflectance due to varying leaf equivalent water thickness	220
5.9	Proportional change in reflectance at a single pixel location due to flooding: 9th April 2003	223
5.10	Proportional change in reflectance at a single pixel location due to burning: 15th July 2000	227
6.1	Percentage of MODIS (Aqua and Terra) 1km active fire locations identified as burned	236
6.2	Percentage of MODIS (Terra and/or Aqua) 1km active fire locations identified as burned in each cover type	241
6.3	Percentage of 500m burned areas detected as active fires: Multiplicative model results	243
6.4	Percentage of 500m burned areas detected annually as active fires in each vegetation type: Multiplicative model results	244
6.5	Number of pixels and percentage of SK2 burned areas also identified as burned by SABA	246
6.6	Rejection criteria of pixels identified as burns in the SK2 but not the SABA dataset	247
6.7	Percentage of SABA burned areas <i>not</i> identified as burned in SK2 as a function of vegetation type	251
6.8	Number of pixels and percentage of SABA burned areas <i>not</i> identified as burned in SK2	251
6.9	Percentage of SABA burned areas <i>not</i> identified as burned in SK2 as a function of vegetation type	259
6.10	Number of 1km pixels and percentage of GBA2000 burned areas <i>not</i> identified as burned in the SABA dataset	264
6.11	Percentage of 1km GBA2000 burned areas identified water induced surface change	267
6.12	Number of pixels and the percentage of SABA burned areas <i>not</i> identified as burned by GBA2000	271
6.13	Percentage of each 1km pixel identified as burned in SABA but <i>not</i> in GBA2000 .	272

7.1	Percentage of total area burned which burn between one and three times during a single fire season	286
7.2	Percentage of each land cover type which burns more than once in a single fire season	287
7.3	Fire frequency across the study area: Percentage of land surface which burns between one and five times during the five year period	287
7.4	Fire frequency across the study area: Percentage of each land cover type which burns between one and five times during the five year period: Multiplicative model results	289
7.5	Percentage of total annual area burned within each cover type: Multiplicative model results	304
7.6	Total area burned (million hectares): Multiplicative model results	308
7.7	Percentage of the total land area which has burned: Multiplicative model results	309
7.8	Total area burned (million hectares): Multiplicative model results	312
7.9	Percentage of vegetation class which burns: Multiplicative model results	312
7.10	Classification of burn severity based on the propotional change in MODIS band 5 reflectances	323
7.11	Proportion of low, moderate and high severity burns in each cover class between 2000-2004: Multiplicative model results	331
A.1	Pixel locations referred to in the text: Sites which are of a greater spatial extent than a single pixel are indexed by the upper left row and column, while the latitude and longitude refer to the centre of the pixel. Each site is indexed by the chapter number in which it appears.	389
B.1	Percentage of 500m burned areas detected as active fires: Additive model results	391
C.1	Percentage of 500m burned areas detected as active fires: Additive model results	393
C.2	Percentage of 500m burned areas detected as active fires: Multiplicative model results	394
D.1	Number of pixels identified as burning between one and three times during a single fire season	395

E.1	Fire frequency across the study area: Percentage of each land cover type which burns between one and five times during the five year period: Additive model results	397
F.1	Total area burned (million hectares): Additive model results	398
F.2	Percentage of the total land area which has burned: Additive model results	399
F.3	Total area burned (100000 hectares): Additive model results	400
F.4	Total area burned (100000 hectares): Multiplicative model results	401
F.5	Percentage of vegetation class which has burned: Multiplicative model results . .	402
F.6	Percentage of vegetation class which has burned: Multiplicative model results . .	403
G.1	Proportion of low, moderate and high severity burns in each cover class between 2000-2004: Additive model results	405

List of acronyms

API	<i>Application Programming Interface</i>
ASTER	<i>Advanced Spaceborne Thermal Emission and Reflectance Radiometer</i>
ATSR	<i>Along Track Scanning Radiometer</i>
AVHRR	<i>Advanced Very High Resolution Radiometer</i>
BIBEX	<i>Biomass Burning Experiments</i>
BIP	<i>Band Interleaved by Pixel</i>
BRDF	<i>Bidirectional Reflectance Distribution Function</i>
BSQ	<i>Band sequentially</i>
BT	<i>Brightness Temperature</i>
CEOS	<i>Committee on Earth Observation Satellites</i>
CERES	<i>Cloud and Earth's Radiant Energy System</i>
CVA	<i>Change Vector Analysis</i>
DMSP	<i>Defense Mapping Satellite Program</i>
EOS	<i>Earth Observing System</i>
ESA	<i>European Space Agency</i>
EVI	<i>Enhanced Vegetation Index</i>
FASIR-NDVI	<i>Fourier-Adjusted, Solar-zenith angle corrected, Interpolated, Reconstructed -NDVI</i>
GBA2000	<i>Global Burned Area 2000</i>
GEMI	<i>Global Environment Monitoring Index</i>
GLOBSCAR	<i>GLObal Burn Scar dataset</i>
GOFC	<i>Global Observation of Forest Cover</i>
GTOS	<i>Global Terrestrial Observing System</i>
GVM	<i>Global Vegetation Monitoring unit of the Joint Research Centre</i>

HDF	<i>Hierarchical Data Format</i>
HDF	<i>Hierarchichal Data Format</i>
IGAC	<i>International Global Atmospheric Chemistry</i>
IGBP	<i>International Geosphere and Biosphere Program</i>
IGOS	<i>International Global Observing System partners</i>
IRS-1C	<i>Indian Remote Sensing satellite</i>
JRC	<i>Joint Research Centre</i>
LAI	<i>Leaf Area Index</i>
Landsat MSS	<i>Landsat Multi-Spectral Scanner</i>
Landsat TM	<i>Landsat Thematic Mapper</i>
Landsat ETM	<i>Landsat Enhanced Thematic Mapper</i>
MIR	<i>Middle Infra-Red</i>
MISR	<i>Multi-angle Imaging SpectroRadiometer</i>
MODIS	<i>MODerate resolution Imaging Spectroradiometer</i>
MVC	<i>Maximum Value Composite</i>
NBAR	<i>Nadir Adjusted BRDF Reflectance</i>
NBR	<i>Normalised Burn Ratio</i>
NDVI	<i>Normalised Difference Vegetation Index</i>
NDWI	<i>Normalised Difference Water Index</i>
NIR	<i>Near Infra-Red</i>
NOAA	<i>National Oceanic and Atmospheric Administration</i>
NPP	<i>net Primary Productivity</i>
NSCA	<i>National Center for Supercomputing Applications</i>
NTAM	<i>Nonlinear Temporal Angular Model</i>
PCA	<i>Principal Components Analysis</i>
POLDER	<i>Polarisation and Directionality of Earth Reflectances</i>
RMSE	<i>Root Mean Square Error</i>
SABA	<i>Southern Africa Burned Areas</i>
SAFARI	<i>Southern African Regional Science Initiative</i>
SAFNET	<i>Southern Africa Fire NETWORK</i>

SK2	<i>SAFARI 2000 burned areas</i>
SMA	<i>Spectral Mixture Analysis</i>
SPOT-VGT	<i>VEGETATION</i>
STARE	<i>Suthern Tropical Atlantic Regional Experiment</i>
SWVI	<i>Short Wave Vegetation Index</i>
TRACE-A	<i>TRansport and Atmospheric Chemistry near the Equator-Atlantic</i>
TRMM	<i>Tropical Rainfall Measuring Mission</i>

Chapter 1

Introduction

1.1 Global vegetation burning

The terrestrial surface is in a state of permanent flux with changes occurring due to both natural and anthropogenic causes and at a variety of spatial and temporal scales. The identification, analysis, and interpretation of the physical changes taking place to the Earth's surface is not only of significance in the management of these areas, but is also a fundamental input to models of global climate and biogeochemical cycles (Coppin *et al.* 2004). The importance of monitoring, mapping and managing these changes has long been a priority of the scientific community with emphasis on the effects of land cover change on ecological processes and cycles as well as on Earth-atmosphere systems. Vegetation fires (both naturally and anthropogenically ignited) occur recurrently in a large proportion of the world's major biomes and are a key driver in the dynamics of these. The complex feedbacks which exist between land cover modifications, biogeochemical cycling and climate change cannot be fully determined without a detailed understanding of the nature of these changes.

Vegetation fires emit a range of greenhouse gases and particulate matter which modify atmospheric composition and chemistry, and as such are increasingly recognised as a key contributor to global climate change (Scholes *et al.* 1996a, Lobert *et al.* 1999). It has been estimated that approximately 38% of the tropospheric ozone, 39% of particulate organic carbon, 32% of carbon monoxide, and over 20% of the global hydrogen, nonmethane hydrocarbons, methyl chloride and nitrous oxides are produced annually by vegetation fires (Levine 1991). It is therefore hardly surprising that a large proportion of the global interannual variability in atmospheric carbon dioxide, carbon monoxide, methane and hydrogen between 1992 and 1999 has been attributed to biomass burning (Langenfelds *et al.* 2002). Smoke aerosols emitted during the combustion process are also of importance and have the potential to cause direct or indirect radiative forcing. Aerosols may have a direct impact on climate by reflecting incoming solar radiation, while indirect modifications arise from their ability to act as cloud condensation nuclei thereby affecting cloud formation and the amount of solar radiation reaching the Earth's surface. Although aerosols emitted by biomass burning are generally considered to have a cooling effect in contrast to the warming caused by greenhouse gases, assessments of the combined climatic impacts have proved to be problematic and controversial due to the uneven spatial distribution of the two effects (IPCC 2001). In addition a major uncertainty in the modelling of the climatic im-

impact of aerosols currently arises from the lack of accurate information describing the emission of these (Tansey *et al.* 2004a). Vegetation fires are also thought to significantly alter the surface albedo thereby affecting the quantity of solar radiation received and reflected from the Earth's surface. A relative decrease in the surface albedo of up to 25% has been identified over burned surfaces in Northern Hemisphere Africa due to the darkening of the surface due to the presence of charcoal and ash, increasing the capacity of these to absorb solar radiation (Govaerts *et al.* 2002). Although the exact amplitude of fire-induced variations in the albedo cycle have yet to be quantified, it is suggested that these modifications may be sufficiently large to alter regional atmospheric circulations and associated rainfall patterns (*ibid*).

Changes in the global carbon cycle occur due to the release of fossil CO₂ into the atmosphere, and through land cover transformations. In addition to the gaseous emissions produced directly through the combustion process the role of vegetation fires in the global carbon budget is now recognised and emphasis is currently placed on improving our understanding of the relationships between the global climate, biomass burning and the carbon cycle. It is estimated that 3.9 gigatons of carbon, the equivalent of over 70% of anthropogenic emissions from fossil fuels are released annually by global vegetation fires (Andreae 1991). Carbon is stored in vegetation and when this burns the carbon is released into the atmosphere. As a result biomass burning alters the role of vegetation from a carbon sink to a source thereby changing the distribution of carbon sources and sinks across the terrestrial surface. In the past, fires have typically been viewed as part of a 'steady state' world where carbon loss due to combustion in one location is compensated for by accumulation of biomass in another (Crutzen and Andreae 1990). However the net strength of the terrestrial sink is highly variable from year to year as the carbon balance of terrestrial ecosystems responds strongly and rapidly to climate variability and interannual changes in fires (Bousquet *et al.* 2000, Van der Werf *et al.* 2004). In fire-dependent ecosystems such as the savannas of southern Africa the emissions of CO₂ from fires has little impact on the long-term trend of atmospheric CO₂ concentration as similar quantities are sequestered during the following years growth (Andreae 1991). In contrast to this short-term cycling of carbon, ecosystems with greater biomass such as forests and woodlands vegetation recovery is much slower after burning and as a result the quantities of CO₂ emitted may alter atmospheric concentrations for decades (Hicke *et al.* 2003). Increases in vegetation fires are thus frequently cited as one of the consequences of global warming, and under current predictions of climate change these are

likely to increase in frequency and severity in boreal forests resulting in the loss of up to a quarter of the carbon stored within these ecosystems (Kasischke *et al.* 1995).

Biomass burning is a key driver in global vegetation dynamics affecting ecosystem structure, function and composition. Burning has a direct impact on the vegetation with species adapted to fire more likely to survive than those which are less resistant. The timing, frequency and interval between recurrent fires will determine the plant species composition through selection in most ecosystems (Thonicke *et al.* 2001). While the distribution of the worlds major biomes are frequently considered to be climate dependent, the physiognomic characteristics of ecosystems which undergo frequent burning may not be determined by climate. Recent simulations using a Dynamic Vegetation Growth model indicate that in the absence of fire the grassland and savanna ecosystems of Africa and South America have the climatic potential to form forests (Bond *et al.* 2004). Frequent fires convert areas of forest to savanna and grasslands by suppressing the regrowth of trees and favouring the development of shrubs and grasses. Conversely under a regime of infrequent fires or total fire suppression grass biomass decreases as tree cover increases resulting in lower fuel loads and less intense fires which subsequently cause less damage to the trees. In the absence of fire and anthropogenic land cover modifications closed forests on the Earth's surface would more than double. This suggests that vegetation fires may be a primary determinant of global biome distributions by promoting the development and maintaining the presence of flammable fire prone ecosystems where the climate can in fact support forests. Although the feedbacks between biomass burning and climate are not well constrained, simulations of a General Circulation Model have identified a positive feedback loop between fire frequency and climate whereby a reduction of tree cover results in a warmer and drier climate, accelerated fire frequencies and thus further tree loss which in turn contribute to an increase in temperature and a decrease in precipitation (Hoffmann *et al.* 2002).

1.1.1 The need for monitoring

The requirement for information relating to the occurrence of vegetation fires at both a regional and global scale has various motivations. These are primarily associated with (i) the loss of human lives, livelihood and property, (ii) ecosystem health and sustainability, and (iii) climate change.

The effective management of vegetation fires as well as the sustainability of fire dependent ecosystems requires a sound understanding of the spatial and temporal distribution of burning. Detailed characterisations of global fire regimes are required to inform policy and are a prerequisite in the formulation of appropriate ecosystem dependent management plans. A lack of information relating to the fire regime of an area may result in poorly conceived fire management strategies and the implementation of unsuitable policies of suppression or inappropriate prescribed fire regimes. Changes in an established fire regime may result in previously adapted plants no longer able to survive, while complete exclusion may result in a decrease in higher frequency less intense fires but an increase in less frequent but extremely destructive high severity fires (Thonicke *et al.* 2001, Bond *et al.* 2004). The alteration of fire regimes will therefore have implications for the conservation of ecosystem biodiversity and the maintenance of ecosystem health, structure and functioning. The mechanisms which influence fire regimes and the extent to which these are being altered by human activity are not well understood.

A great deal of uncertainty is currently also associated with the amount of biomass combusted globally and therefore the quantities and constituents of gases and aerosols emitted at regional to global scales (Levine 1991, Andrews and Queen 2001, Tansey *et al.* 2004a). Information relating to the occurrence of vegetation fires is required to understand and model the impact of biomass burning emissions on atmospheric chemistry and the radiative budget of the Earth. Although the links between the increasing levels of atmospheric carbon dioxide and global climate change are well understood, anthropogenic perturbations to the global carbon budget as a result of biomass burning are not. An improved understanding of the contribution of vegetation fires to the dynamics of the global carbon cycle, and the extent to which this can be managed in order to stabilise atmospheric concentrations of greenhouse gases is required (Candell *et al.* 2004). The fire regime of a region will determine both the quantity and type of gases emitted by biomass burning. Two aspects of this - the area and type of vegetation which burns annually - currently provide the greatest uncertainty in the calculation of gaseous and aerosol emissions due to burning (Tansey *et al.* 2004b).

Accurate and systematic information detailing the quantity of biomass burned and associated emissions released is needed not only to characterise present interactions between the carbon-climate system and to understand the processes which contribute to higher fire frequencies, but also to model the effect of changing and future climates on fire occurrence and intensity. Cur-

rently the vulnerability of the carbon-climate system to increasing fire frequencies and the future dynamics of the carbon cycle remain unclear. Feedbacks between a changing climate and fire frequency and intensity are not represented in climate change models as the interactions between climate and fire are not well understood. There is therefore a pressing need to incorporate fire information into global change scenarios, and to represent fire processes in global scale modelling of the vegetation-climate system (Hoffmann *et al.* 2002). However despite this need for information the occurrence and interannual variability of burning at both the regional and global scale is largely undocumented. There is currently a lack of coherent and consistent information describing the spatial and temporal distribution of vegetation fires and their characteristics. As a result, fire is typically under-appreciated as a global control of vegetation structure and biome distribution (Thonicke *et al.* 2001). In addition, this lack of consistent information has resulted in large variations in emissions calculations, with estimates of global carbon losses due to fire ranging from 1.5 to 5.0 Pg C yr⁻¹ (Seiler and Crutzen 1980, Crutzen and Andreae 1990, Hao and Liu 1994). There is therefore an urgent need to quantify and characterise the interannual variability of biomass burning in order to improve understanding of the processes and feedbacks involved.

1.1.2 Principal research programmes

The Global Observation of Forest Cover (GOFC) was developed in 1997 by the Committee on Earth Observation Satellites (CEOS). In 2000 GOFC became the first of five projects of the Global Terrestrial Observing System (GTOS), which is sponsored by the International Global Observing System (IGOS). In 2001 the GOFC was transformed into the Global Observation of Forest Cover and Global Observation of Landcover Dynamics (GOFC-GOLD) in order to incorporate research into nonforested in addition to forested areas. The aim of GOFC-GOLD is to provide both space-based and *in situ* observations of forests as well as other vegetation types in order to achieve an accurate, reliable and quantitative understanding of the terrestrial carbon budget (GOFC-GOLD 2003). This is conducted through three primary themes of research; (i) forest cover change, (ii) forest biophysical processes, and (iii) forest fire monitoring. GOFC-GOLD-Fire is concerned with the third theme of this project and aims to demonstrate the operational utility of satellite observations of fire and to refine current capabilities in order to

meet the needs of the fire community. Goals of this project include the development of fire early warning systems and improvement in the availability of multi-source fire data over the internet, the establishment of an operational network of fire validation sites and protocols, and the creation of a suite of emissions products (GOFC 2005).

Several large international research projects have been undertaken over the past fifteen years with the aim of characterising the emissions of gases and aerosols from vegetation fires. The Biomass Burning Experiments (BIBEX) were initiated in 1990 and conducted under the International Global Atmospheric Chemistry (IGAC) programme, a core initiative of the International Geosphere and Biosphere Project (IGBP) launched with the aim of studying global change. The goal of BIBEX was to characterise and quantify global trace gas and aerosol emissions from vegetation fires (Andreae 1998). Observations from satellites and the space shuttle as well as measurements made during field campaigns in the Amazon basin had indicated high levels of tropospheric ozone and carbon monoxide annually over this region and the southern Atlantic Ocean between August and October. It was speculated that these observations might be explained by vegetation fires in Africa.

The Southern Tropical Atlantic Regional Experiment (STARE) was initiated as an air and ground based measurement programme in 1990 with the aim of investigating the source of trace gases over the Southern Atlantic and characterising their atmospheric transport. The project was formed as part of BIBEX and involved two components. The first, the TRansport and Atmospheric Chemistry near the Equator-Atlantic (TRACE-A) was designed to investigate the extent, characteristics and origin of the elevated levels of ozone over the South Atlantic through *in situ* measurements, and to assess the contribution of emissions from Africa and Brazil to the atmospheric composition above these regions. The second, the Southern African Fire/Atmosphere Research Initiative (SAFARI-92) was formed with the aim of investigating the emissions from African fires and their impact on atmospheric circulation as well as the ecological impact of burning on African savannas. The major achievements of this research was the identification of the main gases and aerosols produced as a result of biomass burning in these ecosystems and an increased understanding of the contribution of these to the high levels of tropospheric ozone over the South Atlantic. Prior to STARE investigations into the complex interactions between the ecology, chemistry and atmospheric emissions from southern African fires had not been performed. The results of these programmes are documented in Lindesay *et al.* (1996).

Following on from the 1992 campaign SAFARI 2000 (the Southern African Regional Science Initiative) was designed to be a more comprehensive study into emissions processes in southern Africa, in order to improve understanding and prediction capabilities of the regional sensitivity to and effect on global change (Swap 2000). In particular the goal of the 2000 programme was to identify the key linkages between selected aspects of the southern African earth-atmosphere-human system. The main themes of the research were stated as; (i) terrestrial ecology, (ii) land use and land cover change, (iii) aerosols and trace gas chemistry and transport, (iv) surface radiation and (v) cloud characterization and radiative effects. To date this is the largest coordinated research effort into the characterisation of emissions from African savanna fires. As a result of the extensive surveys conducted in the savannas, grasslands and woodlands of southern Zambia and South Africa during these programmes an inventory of emission factors for savanna ecosystems now exist.

1.1.3 The role of remote sensing

Systematic monitoring of fires at regional to global scales is problematic due to the rapidity with which they occur and their unpredictable nature. Measurements from satellites provide the only feasible means of observing large portions of the Earth's surface at a high temporal frequency and in a consistent manner. As such the detection of fires from space has received a great deal of attention over the past few decades. Global or near global datasets documenting the locations of "active fires" are available to the scientific community from mid-1996 to the present from the Along Track Scanning Radiometer (ATSR) (Arino *et al.* 1999), from 1998 to the present from the Tropical Rainfall Measuring Mission (TRMM) Visible and InfraRed Spectrometer (VIRS) (Giglio *et al.* 2003b), and from early 2000 to the present from the Moderate Resolution Imaging Spectroradiometer (MODIS) (Giglio *et al.* 2003a). Although the availability of active fire data is an extremely valuable source of information documenting the occurrence of fires at a global scale over the last decade, this data only provides a brief snapshot of fires which are burning and unobscured by cloud at the time of the satellite overpass. It does not therefore provide the information required to quantify the area and type of vegetation which has burned.

In contrast to the near real time active fire information required by fire managers, the global change research community needs data detailing the location, spatial extent, intensity and fre-

quency of burning. While numerous studies have quantified the area burned from remote sensing data these have typically been performed over a limited temporal and spatial scale. This lack of information has resulted in the estimation of burned areas from ancillary information, indirectly from active fire data or extrapolated from these to larger spatial scales. Although recent efforts have been made to produce inventories of the total global area burned from satellite data, these have been performed over a limited temporal scale, for example of a single year (Simon *et al.* 2004, Tansey *et al.* 2004b). They therefore do not contain sufficient temporal information with which to quantify the interannual variability of fire regimes. While all of the above datasets provide useful information relating to the occurrence of vegetation fires at a variety of spatial and temporal scales and estimations of burned areas have improved significantly through the use of remote sensing data, the availability of multiple years of daily moderate spatial resolution satellite data has yet to be fully exploited in a consistent and systematic manner.

1.2 Research objectives

The previous section has documented the need for fire monitoring at the regional and global scale. The shift from a natural to an anthropogenically driven fire regime is evident no more so than in the savannas, grasslands and woodlands of southern Africa. These are the most frequently burned biomes in the world and are considered to be most at variance with their climate potential. Past or future changes in the diversity and extent of these ecosystems cannot be fully understood without an understanding of their fire regimes (Bond and Keeley 2005). A great deal is still unknown about the spatial extent of burning in Africa, the type of vegetation which burns and the interannual variabilities of these factors. While savanna fires are thought to be of little importance as a source of carbon dioxide, this is only the case if the ecosystem is in a stable state and the carbon released due to burning is replaced during the subsequent year via vegetation regrowth. All African savanna fires however produce a range of trace gases and aerosols with the quantity of carbon monoxide released annually due to burning estimated to be equivalent to 30% of the global industrial source (Hao *et al.* 1990). As discussed above, these fires are the primary cause of the pronounced annual peak in tropospheric ozone which extends across the Atlantic Ocean between Africa and South America during September and October (Fishman

et al. 1991). It has been suggested that anthropogenic modifications to African fire regimes have resulted in emissions from savanna fires up to three times greater than those predicted under natural scenarios (Hoffa *et al.* 1999). Emissions from these fires have significant consequences to atmospheric chemistry with emissions in a high fire year estimated to be double those in a low fire year (Barbosa *et al.* 1999). Despite this the interannual variability in the extent, season, and frequency of burning in southern Africa has yet to be quantified.

Locating and mapping areas of burning within southern African ecosystems provides a greater challenge than in more densely vegetated biomes such as the boreal forests of North America or Siberia, or the tropical forests of South East Asia and South America, due to the characteristics of the fires which occur in these ecosystems. The majority of the biomass burning which occurs in southern hemisphere Africa is due to surface fires which burn through the herbaceous and understorey layer with trees greater than 2-4m in height typically unaffected (Frost and Robertson 1985). The change in the signal which is measured at the satellite sensor as a result of burning may therefore be subtle. As many of the species within these ecosystems are adapted to and in some cases stimulated by fire, post fire regrowth occurs rapidly. While crown fires in boreal or tropical forests typically leave a fire scar which may be detectable for several years after the fire, the fast recovery of southern African ecosystems means a detectable signal may only be present for as little as one to two weeks after burning (Trigg and Flasse 2000, Roy *et al.* 2005a). Coupled with the possibility of missing satellite observations due to cloud or smoke this necessitates the use of high temporal resolution satellite data. Current burned area detection methodologies do not fully exploit the availability or the information content of daily global data from satellite sensors such as MODIS. In addition they tend to be ecosystem dependent and unsuitable for application at large spatial scales. Although recent advances have been made in the characterisations of trace gas and aerosol emissions released by biomass burning and the effects of these on atmospheric composition, large uncertainties still exist. These are predominantly related to the spatial extent, the seasonality and the quantity of biomass which burns annually. Despite the frequency and extent of biomass burning and the focus of the various international experimental campaigns described above, adequate burned area data for southern Africa do not exist. There is therefore an urgent need for systematic and consistent information describing the occurrence and interannual variability of biomass burning within this region.

The principal aims of this research are defined in the context of the needs detailed above.

These are stated as three objectives;

1. **The development of an algorithm suitable for the detection of sudden surface change from daily moderate spatial resolution optical remote sensing data**
2. **The application of this methodology to the identification and delineation of burned areas in southern Africa on a daily basis for a five year period (2000-2004)**
3. **The characterisation and analysis of the fire regimes of southern African ecosystems from the data produced via Objectives 1 and 2 over the five annual fire seasons**

These objectives are addressed as outlined in the following paragraphs.

1.3 Thesis plan

Objective 1 is defined within the context of a change detection problem. Chapter 2 is therefore concerned with a review of the methods typically used in the remote sensing of land cover change and the limitations of these traditional approaches. This is followed by a description of the approaches applied to the detection of active fires and the identification of burned areas from satellite data, and the operational fire-related remote sensing products currently available to the scientific community.

Chapter 3 provides a discussion of the causes and ecological impacts of fire within southern African ecosystems. This is followed by a characterisation of the diurnal, seasonal and interannual distribution of burning within this region through an analysis of MODIS daily active fire locations for the five year period 2000 to 2004. The spectral features of burned surfaces at active fire locations identified in the previous analysis are investigated and the change in the optical remote sensing signal which occurs due to burning as well as the duration of this is defined. Objective 1 is met in Chapter 4 following the needs identified in the previous two chapters. Based on the requirements identified in Chapter 3 and the shortcomings of the traditional approaches to change detection described in Chapter 2, Chapter 4 develops a new, generic approach to the detection of surface change from high temporal resolution satellite data.

Chapter 5 is concerned with a description of the data sources used in the subsequent Chapters and the preprocessing of these. This is followed by the application of the generic change detec-

tion model developed in Chapter 4 to the detection and delineation of fire affected areas across southern Africa over five annual fire seasons (2000-2004). The separation of burned areas from areas which exhibit spectrally similar changes is discussed, and the post-processing methods applied to the datasets described. Objective 2 is thus met over the course of Chapter 5. In Chapter 6 the burned area data is compared to two alternative burned area products as well as an active fire dataset currently available to the scientific community.

Chapter 7 fulfills Objective 3 through an analysis of the daily burned area results presented in Chapter 6. These data are used to characterise the fire regimes of savanna, grassland and forest ecosystems in southern Africa over five consecutive annual fire seasons during the period 2000 to 2004. Chapter 8 provides conclusions of the research and the potential for further work.

Chapter 2

Remote Sensing Change Detection

The preceeding chapter has discussed the need for information relating to the occurrence, timing and spatial extent of vegetation fires at regional to global scales, as well as the suitability of remote sensing data for this purpose. Due to the role of fire as an agent of land cover change, the detection of fire affected areas has typically been achieved through the analysis of multi-temporal remote sensing datasets using a change detection scheme. Over the past two decades numerous automated change detection procedures have been developed. The aim of this chapter is to provide a review of the methods which have been used in the detection of land surface change and their relative advantages and disadvantages, and the application of these to the detection of fire affected areas. This is followed by a discussion of the detection of active fires from Earth Observation (EO) data sources and an overview of the global and operational fire and burned area products currently available to the scientific community.

2.1 Multi-temporal change detection

Remote sensing change detection studies are based on the principle that areas of change within a multi-temporal co-registered dataset will be statistically different to those where the land surface has remained invariant over the time period of interest. Although a great variety of change detection methods and comparative studies of these exist in the literature, there is no general consensus as to the most suitable method for detecting a particular type of change. Techniques based on the analysis of multi-temporal and multi-spectral satellite data at a range of spatial resolutions have demonstrated potential as a means to detect, identify and monitor ecosystem changes irrespective of their cause (Coppin *et al.* 2004). The technique chosen for a particular study tends to depend on the analyst's knowledge of and skill in handling remote sensing data, the type of data available, and the characteristics of the study area (Yuanbo *et al.* 2004). While all remote sensing data sources offer potentially useful information relating to the properties of the Earth's surface, a handful have proved more popular than others in the detection of land cover change. While historically the Landsat series (MSS, TM and ETM+)¹, SPOT Vegetation, and AVHRR sensors as well as aerial photographs have been the most common optical data sources, MODIS and ASTER are becoming increasingly important (Lu *et al.* 2004). The most appropriate

¹A list of acronyms used in the text can be found on page 18

data source for a particular study will be determined by both the temporal and spatial scales of the change of interest, as well as the spectral nature of this change.

2.1.1 Image enhancement techniques

The simplest approach to digital change detection involves the comparison of the same area at two points in time, and encompasses the techniques of image differencing, regression, ratioing, transformation and change vector analysis. Common features of this category are (i) the enhancement of the change signal through the mathematical combination of multi-temporal images, and (ii) the requirement for a threshold (or set of thresholds) to identify areas of change. Apart from the more complex approach of change vector analysis these techniques are all simple to implement and the results are easy to interpret, but they only provide information relating to the magnitude of the change rather than complete matrices of change information (Lu *et al.* 2004).

Image differencing and ratioing

The simple technique of image differencing involves the subtraction of pixel values for one image date from the corresponding pixel values at a subsequent image date. The resulting histogram will have values ranging from negative to positive with those clustered around zero representing areas of no change, and those in the tails of the distribution representing areas which have changed between the two image dates (Jensen 1996). This technique has been popular due to its computational simplicity and ease of interpretation, and has been used frequently to identify areas of land cover and land use change (Pilon *et al.* 1988, Muchoney and Haack 1994, Sohl 1999). A major drawback of the approach however is the difficulty in the determination of a suitable threshold value with which to separate changes of interest from background changes and noise. Fung and LeDrew (1988) have investigated the use of various accuracy indices in the determination of optimal threshold levels and recommend the Kappa coefficient of agreement based on an error matrix of image and reference data. In addition as the result of image differencing is solely an indication of the magnitude of change, it is not possible to interpret the changes as a function of their original spectral value (Yuan *et al.* 1999). Coppin and Bauer (1994) have thus suggested standardizing the difference algorithm in order to address this issue, thereby

minimising the occurrence of different change events which exhibit similar change values.

Numerous data transformation techniques have been used to reduce the dimensionality of the data and to enhance the remote sensing change signal prior to the difference operation. The most frequently used of these techniques in change detection studies are band ratioing, vegetation indices, principal components analysis and the tasseled-cap transformation (Lunetta 1999).

Image transformation

The Principal Components Analysis (PCA) and Kauth Thomas or tasseled-cap transformation have been popular in remote sensing change detection studies as they reduce the redundancy within a multi-band dataset and emphasize different information in the derived components (Lu *et al.* 2004). The PCA exploits the variance within a dataset by rotating the axis to new orientations which are orthogonal to each other, and may be performed in one of two ways for the purpose of change detection: (i) on each image separately with image differencing subsequently applied to the corresponding components for each date, or (ii) to the entire dataset simultaneously. When applied to a multi-temporal dataset the first two components tend to correspond to areas of no change and lower order components to changes in the land surface (Macleod and Congalton 1998, Pereira *et al.* 1997). However the interpretation of the various components and the changes which are represented often require prior knowledge of the dataset used and may need further analysis using techniques such as image differencing or ratioing and the definition of a suitable threshold level to extract change information (Yuan *et al.* 1999). The approach has been used to identify changes in forest cover (Jha and Unni 1994), forest defoliation (Muchoney and Haack 1994) and forest mortality (Collins and Woodcock 1995).

The tasseled-cap transformation was developed by Kauth and Thomas (1976) to monitor agricultural crops from Landsat imagery. The objective of the technique is the transformation of the original spectral channels into several discrete bands of information, each of which can be associated with a specific physical characteristic of the land surface. The output from the transformation is three vectors representing brightness, wetness and greenness. The brightness vector primarily identifies variation in soil reflectance, the greenness vector is an indication of the amount of green vegetation present within the scene, and the wetness vector is related to both the canopy and soil moisture. This transformation technique has been used successfully to monitor

forest mortality (Collins and Woodcock 1995), identify changes in forest biomass (Coppin *et al.* 2001), and to locate areas of land-use change (Fung 1990, Seto *et al.* 2002). Studies which have performed comparisons between the PCA and tasseled-cap transformations have generally found the tasseled-cap to be a more suitable change detection technique than the PCA (Fung and LeDrew 1987, Collins and Woodcock 1995, Rogan and Yool 2001). Fung and LeDrew (1987) note the importance of a thorough understanding of the study area prior to performing a PCA for the purpose of detecting land cover changes in order to avoid drawing false conclusions from the results. In contrast the occurrence of land cover and land use change is more easily interpreted from the tasseled-cap coefficients as these are independent of the image scenes (Collins and Woodcock 1994, Coppin *et al.* 2004, Lu *et al.* 2004). Disadvantages of this group of techniques in general include the lack of detailed change matrices, the need for thresholds to identify areas of change, and the difficulty in identifying and interpreting the change information from the transformed images (Lu *et al.* 2004).

Linear transformation techniques have almost exclusively been applied to high resolution remote sensing data for the detection and delineation of fire affected areas. While some authors have performed a PCA on multi-temporal datasets at their full spectral resolution (Richards 1984) others have selected suitable bands prior to performing the transformation (Siljestrom and Moreno 1995). The order of the principal components which contain the majority of the information varies between studies, and is affected by the relative proportions of stable and changed areas in the datasets (Pereira *et al.* 1997). Thus in a study of bushfire damage in Australia Richards (1984) found that localised change was enhanced in the third and fourth principal components of a multi-temporal Landsat MSS timeseries, Garcia-Haro *et al.* (2001) have found that the third principal component of a multi-temporal Landsat TM dataset was best related to fire induced vegetation change in the Mediterranean. In contrast Salvador *et al.* (2000) discovered that the PCA did not group all burn pixels in a long time series of Landsat MSS data over the Mediterranean within a few components, and instead areas affected by fire appeared in almost all of the principal components.

Band ratioing and vegetation indices

Selection of appropriate spectral bands prior to image differencing may highlight specific changes and provide insights into the nature of these changes. The normalization of the difference between visible and near-infrared reflectances (the 'NDVI') is commonly used as an indicator of vegetation health and amount (Tucker 1979). The NDVI provides a measure of the 'greenness' of vegetation, and is therefore commonly used as an indicator of change for vegetated surfaces. The approach typically involves the calculation of the NDVI for each image and changes in vegetation cover which have taken place between the image dates can then be identified by subtracting the corresponding NDVI images. Various studies have demonstrated that land cover changes are easier to identify if vegetation indices are used to enhance the data prior to image differencing (Rogan *et al.* 2002). Although numerous other multi-band combinations have been used to investigate land cover change, a comparison of seven vegetation indices has indicated that the NDVI difference images were the most successful at separating changes (Lyon 1998).

The calculation of the ratio of two image dates for each waveband on a pixel-by-pixel basis ('image ratioing') has also been employed in identifying land use and land cover change (Prakash and Gupta 1998, Coppin *et al.* 2004). Areas which have not changed between the image acquisition dates will have ratio values of one, while areas of change will exhibit higher or lower values. A study by Nelson (1983) has found the difference of a Landsat MSS band 5 and 7 ratio more successful in monitoring defoliation than single band differencing or ratioing, while a comparison of image differencing, ratioing and NDVI differencing in the detection of land-use changes from a multi-temporal Landsat TM dataset indicated no significant differences between the results of the three approaches (Prakash and Gupta 1998).

Vegetation indices involving combinations of wavebands which are sensitive to fire induced surface change have been popular in the detection of burned areas as they enhance the vegetation signal while minimising atmospheric effects in the remote sensing signal as well as the contribution of the soil background (Huete and Jackson 1988). Traditionally the most commonly used in the identification of fire affected areas has been the NDVI. Until recently the AVHRR instrument on board the NOAA polar orbiting satellite has been the main source of moderate spatial resolution remote sensing data of the land surface. Its low cost long-term archive (since 1978), high temporal resolution and global coverage have made it a more suitable data source

for the detection of fire affected areas at a regional scale than other optical sensors. As a result numerous burned area studies have been conducted using AVHRR data, the majority of which have involved the analysis of multi-temporal NDVI images. These have typically involved the subtraction of pre and post-fire NDVI composites with the subsequent identification of a suitable threshold to locate areas of change. Burned areas have been identified successfully using this method in, for example, Alaskan boreal forest (Kasischke *et al.* 1993, Kasischke and French 1995), Canadian boreal forest (Li *et al.* 1997, Fraser *et al.* 2000a, Li *et al.* 2000a) and Indonesian tropical forests (Malingreau *et al.* 1985, Fuller and Fulk 2001). While the majority of studies have used AVHRR data from a single fire season, Kasischke and French (1995) have demonstrated a 20-30% increase in accuracy with the use of multi-year NDVI images.

Despite the widespread use of temporal NDVI composites or single date images for the identification of burned areas there are certain limitations associated with this approach. A major problem with the use of vegetation index differencing approach at large spatial scales is that the thresholds required to identify burned pixels may be spatially and temporally variable (Kasischke and French 1995, Li *et al.* 2000b). An additional drawback in the use of NDVI differencing to locate burned pixels is that decreases will occur in the NDVI unrelated to fire, for example due to seasonal vegetation senescence, deforestation or harvesting, drought, cloud contamination or misregistration of multi-date images, all of which will contribute to large errors of commission (Li *et al.* 2000b, Fuller and Fulk 2001). The use of the NDVI has been shown to be particularly problematic in the detection of burning within African savannas as fires typically occur after the senescence of vegetation and therefore the ndvi falls before a fire event (Eva and Lambin 1998a). Various studies have therefore investigated the feasibility of using alternate spectral indices to locate fire affected areas. Pereira (1999) has performed a comparative evaluation of the utility of several vegetation indices for mapping burned areas from AVHRR data. The results suggest that the NDVI is not a suitable indicator of burned vegetation in Mediterranean landscapes, and instead a new index ('GEMI3') is proposed. This is a modified version of the Global Environment Monitoring Index which is less sensitive to soil and atmospheric variations than the NDVI (Pinty and Verstraete 1992), with the shortwave infrared waveband replacing the red band thus making the index a more sensitive and improved discriminator of burned areas than either the NDVI or GEMI (Pereira 1999). The GEMI3 has also been used successfully to map burned areas at a continental scale from AVHRR data (Barbosa *et al.* 1999). However an assessment of various

spectral indices by Chuvieco *et al.* (2002) concludes that for the Mediterranean environment the Burned Area Index (BAI) based on red and near infrared spectral space and computed as the distance between each pixel and a reference spectral point, provides the highest burned area discrimination with AVHRR data.

The Vegetation (VGT) instrument onboard SPOT-4 has broadly similar characteristics to NOAA-AVHRR. With a spatial resolution of approximately 1.1km, a large swath width (2000km) resulting in a high temporal resolution with daily global coverage, and wavebands selected specifically for large scale vegetation monitoring, VGT data has been used frequently to map burned areas. In addition the inclusion of a middle infrared waveband (1.55-1.75um) not present on the earlier of the AVHRR sensors (pre NOAA-14) increases the utility of VGT data in burned area mapping studies. A study by Eastwood *et al.* (1998) has demonstrated that the differentiation between burned and unburned vegetation may be achieved more accurately using the middle infrared waveband than either other individual wavebands or the NDVI, while research conducted by Fraser *et al.* (2000b) and Fraser and Li (2002) has exploited the sensitivity of this waveband to burning by formulating a 'Short-Wave Vegetation Index' (SWVI) which follows the form of the NDVI but replaces the red channel with the middle (shortwave) infrared VGT waveband. Results demonstrate that the magnitude of the change between pre burn and post burn surfaces in an area of Canadian boreal forest is greater using the SWVI than the NDVI. In addition the authors highlight the lower sensitivity of the middle infrared channel to smoke contamination as an additional advantage over the use of the conventional NDVI. Zhan *et al.* (2003) have followed a similar approach using the red and shortwave infrared channels along with the NDVI and SWVI and a set of temporally varying thresholds to create monthly burned area maps for the boreal forests of the Russian Federation, while from an analysis of burned area spectral signatures for a region of Australian savanna Stroppiana *et al.* (2003) have found the Global Environmental Monitoring Index (GEMI) based on the red, near and middle infrared wavebands (Pinty and Verstraete 1992) to be the most appropriate index for the detection of burned areas. Silva *et al.* (2004) however have assessed the separability between burned vegetation and the unburned background using the individual VGT wavebands (excluding the blue band) and three indices - an 'Albedo Index' calculated as the mean of the red, NIR and shortwave infrared reflectances, the NDVI and the SWVI - with the conclusion that only the NIR band allows for accurate discrimination of burned areas in all of the study sites, with the most suitable index varying between vegetation type and

regions.

The Along Track Scanning Radiometer (ATSR) and ATSR-2 onboard the ERS-1 and ERS-2 satellites have a similar spatial resolution (1km) to both the AVHRR and SPOT-VGT sensors as well as a spectral configuration suitable for burned area mapping (a shortwave infrared channel and two thermal infrared channels), although with a much narrower swath width (500km) they are less suitable for high temporal large scale mapping than either the AVHRR or SPOT-VGT. Eva and Lambin (1998a) and Eva *et al.* (1998) have successfully used ATSR imagery to map fire affected areas in Central Africa using a methodology which exploits the sharp fall in shortwave infrared reflectance and simultaneous rise in surface brightness temperature exhibited by recently burned surfaces. An advantage of this approach is that relative spectral changes are used to detect burned surfaces as opposed to absolute spectral values, thereby taking into account spatial and temporal variability and resulting in less confusion between burned areas and other cover types (Eva and Lambin 1998a).

Single or multi-band thresholding techniques have also been applied to moderate and higher spatial resolution optical data in the identification and delineation of fire affected areas. Vaquez *et al.* (2001) have investigated the feasibility of using images from the medium spatial resolution (180m) Wide Field Sensor (WiFS) onboard the Indian Remote Sensing Satellite (IRS-1C) to map burned areas. Their methodology involved the analysis of pre burn and post burn NDVI images with results indicating the potential of the data for estimating burned areas at both regional and national scales. The Landsat series of sensors provide high resolution data, and several studies have investigated the use of vegetation indices with both Landsat MSS and TM data for mapping burned areas. Jakubauskas *et al.* (1990) have used NDVI values in order to map burned areas and to investigate burn severity in a Michigan mixed forest, while Salvador *et al.* (2000) have produced burned area maps of Spain using a long (1975-1993) NDVI time series created from Landsat MSS data and Lopez and Caselles (1991) have performed an analysis of bispectral space using Landsat TM wavebands in an attempt to develop a vegetation index suitable for the detection of burned areas, on the basis of which they suggest an index following the form of the NDVI but substituting the red band for the shortwave infrared band.

Image regression

The regression approach to change detection involves the establishment of a linear relationship between two images acquired on different dates. Pixel values may then be estimated for the later date image through the regression function, and changes are subsequently identified by subtracting these estimates from the earlier date image with areas of change exhibiting higher residuals than those which have remained stable between the two dates (Pereira *et al.* 1997). Although image regression has been used to detect land cover changes results have been only marginally better than those produced by image differencing techniques (Singh 1989, Ridd and Liu 1998). An advantage of the approach is the reduction of the impact of atmospheric, radiometric and environmental differences between the two images on the results (Lu *et al.* 2004). However as with the techniques described above the requirement of a change threshold is a major limitation of the method (Coppin *et al.* 2004).

Despite this drawback several studies have successfully applied the technique to the detection of burned areas. Fernandez *et al.* (1996) have performed a linear regression analysis of NDVI values calculated from AVHRR images acquired immediately before and after a forest fire event in Spain. The results have been compared to those produced by NDVI differencing, with the linear regression proving to be more successful of the two approaches. Koutsias and Karteris (1998) and Koutsias and Karteris (2000) have introduced a logistic regression approach to map burned areas in the Mediterranean from multi-temporal and single date Landsat TM data. In this case the logistic expression defines the probability of a pixel belonging to a burn (as opposed to unburned) class. A model consisting of near infrared, middle infrared and visible wavebands was found to provide the best spectral separability for the detection of burned areas, and proved to be capable of mapping burns with an accuracy of 97.62%. This method was subsequently extended to include spatial information, with the probability of a pixel belonging to a burn class dependent on whether the neighbouring pixels also belong to the same class (Koutsias 2003). Logistic regression models have also been applied to moderate resolution data, with work by Fraser *et al.* (2002) locating burned areas at a continental scale and Silva *et al.* (2004) across several vegetation types from SPOT VGT data. Both of these studies have applied a multiple logistic regression model to the individual wavebands as well as to the NDVI and SWVI (Fraser *et al.* 2000b). Fraser *et al.* (2002) have also introduced a series of change metrics in order to

account for seasonal phenological variations in the time series of reflectance, as well as three spatial tests which are applied to potential burn pixels in order to reduce errors of commission and increase the sensitivity of detection. A major drawback of this approach is the necessity of developing accurate regression functions for the specific wavebands prior to implementing the model (Lu *et al.* 2004), and different functions may be required to accurately identify changes over different ecosystem types and times of year. In addition the assumption of the approach is that a pixel location at time A is linearly related to the same location at time B, which implies that the majority of the pixels within the image have not changed significantly during the time interval between acquisitions (Vogelmann 1988, Coppin *et al.* 2004). Any variations in the reflectance signal between these two dates which are not related to the surface change of interest will thus decrease the accuracy of the method.

Change vector analysis

Change Vector Analysis (CVA) is a conceptual extension of image differencing, and has frequently been employed in change detection studies (Lu *et al.* 2004). The procedure is capable of processing the full dimensionality of a multi-spectral and multi-temporal dataset, and involves the calculation of the vector difference between subsequent time trajectories with the length of the vector representing the magnitude of the change and its direction the nature of the change (Lambin and Strahler 1994a). There are therefore two outputs from the algorithm - the direction of the change vector and the multi-spectral change magnitude, both of which may be used to describe the characteristics of a particular change event. The direction of the change vector has been shown to be useful in the identification of different types of physical change, while the magnitude has proved to be useful for relative comparisons within and among different change categories (Johnson and Kasischke 1998). It is therefore particularly suited to situations where the land cover change and the associated spectral characteristics are not known in advance, the changes may have a high spectral variability, or information relating to both changes in land cover type and condition are required (Johnson and Kasischke 1998). In addition the ability to analyse all of the spectral information within a multi-temporal dataset concurrently as opposed to a single band at a time is a major advantage (Coppin *et al.* 2004). Johnson and Kasischke (1998) have demonstrated the usefulness of CVA in processing the full dimensionality of multi-

spectral remote sensing datasets and in extracting and exploiting the components of change from the data. However the method suffers from similar problems to the image differencing and ratioing approach due to the use of thresholds to locate areas of change, sensitivity to misregistration of the data, and radiometric differences between the images (Yuan *et al.* 1999). Despite these drawbacks it has been used successfully to examine forest change (Cohen and Fiorella 1998) and to detect and identify seasonal and annual variations in landscape variables (Lambin and Strahler 1994b, Lambin 1996). In addition a comparison of various change detection techniques including CVA, image differencing, vegetation index differencing and post-classification differencing has highlighted the success of CVA in particular for providing details relating to the nature of the change (Sohl 1999). Due to the capability of CVA in providing information relating to the type (in addition to the magnitude) of change as well as the maturity of this approach in comparison to other available change detection techniques, it is the primary method used in the creation of the MODIS land cover change product, designed to quantify progressive transformations as well as more instantaneous land cover conversions at a global scale (Strahler *et al.* 1999b).

The drawbacks of this method are similar to those for the image differencing approach described above. As with these methods CVA is sensitive to changes which are not related to land cover, such as changes in seasonality and ecosystem dynamics, changes in atmospheric conditions, and changes which are due to the solar and sensing geometry of the acquisitions. In addition problems arise due to the difficulty in identifying the type of land cover change from the results, and in achieving consistent and accurate interpretation of the magnitude and direction of the change vector (Lambin and Ehrlich 1996).

2.1.2 Post-classification techniques

The post-classification approach to change detection involves the comparative analysis of independently produced spectral classification results spanning the time period of interest (Singh 1989). Although the need for radiometric calibration between the two dates is avoided as each image has been classified separately, the accuracy of the final change map is dependent on the quality of the individual classifications and is essentially a product of the accuracies of these (Lambin and Strahler 1994a). As errors in the original data due to misregistration as well as misclassification are compounded, a study by Townshend *et al.* (1992) has identified a need for 0.2%

pixel positional accuracy in order to avoid change detection errors of up to 10%, while Serra *et al.* (2003) have found more than 30% of change information to be unreliable in the presence of a RMSE of 1 pixel in the original classifications. An additional disadvantage of the approach is the large amount of time and expertise required to create the classification products (Lu *et al.* 2004). However an advantage of the post-classification approach is the capability of providing a matrix of the change information, as well as the reduction of the impact of atmospheric, sensor and environmental differences between multi-temporal images, and thus it still remains one of the more popular change detection methodologies (Coppin and Bauer 1994, Lu *et al.* 2004). Hall *et al.* (1991) have performed a post-classification comparison of two Landsat TM images for the identification of five forest successional classes, while a comparison of six conventional change detection techniques by (Mas 1999) has found the post-classification comparison approach to be the most accurate for the detection of changes from multi-temporal Landsat MSS data, with the added advantage of providing an indication of the nature of the changes. Neural network classifiers have also proved to be successful and have been used to detect forest mortality from multi-date Landsat TM data with improved results over more conventional methods of change detection (Gopal and Woodcock 1996), while a comparison between conventional classification algorithms and a back-propagation neural network classifier by (Kushardono *et al.* 1995) has indicated higher accuracies with the latter.

As the detection and mapping of burned areas has typically been approached as a single feature extraction problem conventional image classification methodologies have not been applied as widely as in other areas of change detection, and studies which exist in the literature have mainly focused on the use of these techniques with high resolution data (Pereira *et al.* 1997). Although the supervised approach has been more popular, unsupervised classification techniques have successfully been used to map burned areas from multi-temporal Landsat TM data using a minimum distance to means classifier (Jakubauskas *et al.* 1990) as well as with multi-temporal NDVI images and a maximum likelihood algorithm (Garcia-Haro *et al.* 2001). A supervised classification approach has been adopted by Patterson and Yool (1998) to map burned areas in Arizona from a single post-fire Landsat TM image using a minimum distance algorithm, and by Hudak and Brockett (2004) to identify areas of burned savanna in southern Africa from multi-date Landsat TM images using a parallelepiped classifier. Research conducted by Hudak and Brockett (2004) indicates higher accuracies when a principal components transformation is

performed prior to the classification process, while Patterson and Yool (1998) have found that burned areas are mapped more accurately when the data is preprocessed using a Kauth Thomas transformation (Kauth and Thomas 1976) rather than a principal components transformation.

In recent years more complex automated classification procedures have been developed and applied to moderate resolution data in an attempt to separate burned areas from the surrounding vegetation over a larger spatial or more frequent temporal scale. A study by Gitas *et al.* (2004) has introduced a method to map a large fire in Spain incorporating contextual information into the classification procedure. The authors developed an object-based model using the spectral and spatial characteristics of the dataset which was successful at mapping the area burned, although it is suggested that further research is needed before the method can be considered robust *ibid.* Al-Rawi *et al.* (2001) have employed a supervised ART-II artificial neural network to detect areas of burning in Spain from a multi-temporal AVHRR dataset, while Brivio *et al.* (2003) have used a supervised classification strategy based on the hierarchical use of a Multi-Layer Perceptron neural network to create daily burned area maps of north Africa for a period of three months from SPOT VGT data. Stroppiana *et al.* (2003) have also used daily SPOT VGT images as well as ten day composites to successfully map burned areas of a woodland savanna ecosystem in Australia. The methodology involved a supervised classification scheme based on a homogenous univariate classification tree which successfully identified burned three area classes of varying severity, although the accuracy of the results was found to vary with vegetation type. A disadvantage of these methods however is the length of training time required and the sensitivity of the results to the amount and quality of the training data used (Lu *et al.* 2004).

2.1.3 Overview

While the respective advantages and disadvantages of each of the individual techniques have been discussed above, there are several major unifying limitations. Although these methods provide useful information detailing land cover change, their accuracy is limited by a range of complicating factors relating the surface state to the remote sensing signal (Roy *et al.* 2002). In particular image enhancement techniques are extremely sensitive to changes in seasonality and ecosystem dynamics which may have occurred between the dates of image acquisitions, to the extent that they have been shown to be unable to differentiate accurately between variations due

to soil moisture, atmospheric conditions and vegetation phenology from those due to land cover change (Mas 1999). A second disadvantage is the need for a spatially and temporally specific change/no change threshold in order to identify areas of significant change. Although this latter point is not applicable to classification techniques and these are still sensitive to background changes and atmospheric conditions, the accuracy of the final change map will be a product of the individual classifications. In addition a great amount of time and expertise is required in the creation of accurate (supervised) classification products (Lu *et al.* 2004). While a number of the above techniques have nevertheless been successfully applied to the detection of land cover changes at a local scale and from high spatial resolution data, few have been applied successfully to moderate spatial resolution data at a global scale (Strahler *et al.* 1999b). The main reason for this is the problems of interpretation which arise from the application of these techniques over larger scales (Lambin and Ehrlich 1997).

2.1.4 Spectral mixture analysis

Subtle land cover changes as well as the physical nature of these changes may be identified from a multi-temporal dataset using spectral mixture analysis (SMA). The development of this technique has been encouraged by the increased dimensionality of high spectral resolution data, and is based on the assumption that the remote sensing signal measured by a sensor for a particular location will be a linear mixture of the separate spectra of each of the individual components or ‘endmembers’ within the scene (Coppin *et al.* 2004). Spectral mixture analysis is the process of calculating the fraction of each of these endmembers. The first step involves determining the spectral response of the endmembers. The spectral characteristics may be extracted from training areas within the images or from spectral libraries collated from either field or laboratory measurements (Lu *et al.* 2004). The second step involves the formulation of the ‘mixture model’ which describes the contribution of each of the endmembers to the observed reflectance. In the case of a linear mixture model the reflectance from each pixel is considered to be a linear combination of the reflectances of the endmembers, weighted by their areal proportions. The pixel reflectances may then be inverted to determine the areal proportions of each of the endmembers within the scene.

The technique is particularly useful and more robust when applied to datasets where the

number of useful wavebands is significantly higher than the number of endmembers of interest (Okin *et al.* 2001). Advantages of the approach include the capability of providing information at a subpixel level and thus relating to subtle changes in the surface, as well as the physical and quantitative nature of the individual fraction images which makes them well suited to studies of surface change. Tompkins *et al.* (1997) emphasize however that all of the strengths of SMA are dependent on the accuracy of the definition of the endmembers, and inaccuracies in these will lead to incorrect and potentially meaningless fractional images. The selection of endmembers has been investigated and is described in detail by Adams *et al.* (1995), Bateson and Curtiss (1996), and Tompkins *et al.* (1997). SMA has been used successfully in a variety of change detection studies including the identification of land cover change (Adams *et al.* 1995), in monitoring forest defoliation (Radeloff *et al.* 1999), and in mapping changes in vegetation cover (Rogan *et al.* 2002). Adams *et al.* (1995) have used four endmembers (green vegetation, non-photosynthetic vegetation, soil and shade) to investigate land cover changes in the Brazilian Amazon which proved to be a more successful approach than traditional classification methods, while Rogan *et al.* (2002) have used the same four endmembers to map land cover change in California with a higher degree of accuracy than that achieved with the tasseled-cap approach.

Despite the fact that SMA is the most commonly used technique in the analysis of remote sensing data at sub-pixel resolution, minimal studies have applied the approach to the detection of sub-pixel burned areas (Sa *et al.* 2003). Spectral unmixing techniques have, however, been applied to the identification of burned areas from an IRS LISS scene by Roan-Cuesta *et al.* (2003). Four endmembers were defined (charred vegetation, bare soil, green vegetation and shadow) in order to classify a forest fire in north-east Spain, with the method proving to be more successful than the use of NDVI images.

Although the major advantage of this approach lies in its capability to recover change signals at much finer scales (Coppin *et al.* 2004) disadvantages include the need for the accurate identification (either manually or from a spectral library) of the endmembers, as well as the requirement for a much greater number of wavebands than endmembers. This latter point makes the technique more suitable for application to hyperspectral remote sensing data.

2.1.5 Mapping fire affected areas at a global scale

Despite the large number of studies which have been carried out into the detection of burned areas at a regional or national scale, minimal attempts have been made to produce a method applicable to the global identification of burned areas. Various studies have successfully mapped fire-affected areas at a regional or ecosystem level including southern (Scholes *et al.* 1996b), western (Kennedy *et al.* 1994), and central African ecosystems (Eva and Lambin 1998a), Alaskan boreal forest (Kasischke and French 1995), Mediterranean forest (Pereira 1999), and South American tropical forest (Kaufman *et al.* 1990), while at a continental scale Barbosa *et al.* (1999) have mapped annual burned areas for the whole of Africa. Although the individual approaches used in these studies have proved successful at locating burned surfaces at these scales, it is apparent that the methods required to detect burned areas differ from one vegetation type to another (Gregoire *et al.* 2003). This is primarily due to the spatial and temporal variability of the spectral characteristics of fire affected areas and the complex and diverse nature exhibited by these surfaces (Pereira *et al.* 1997). The threshold approach for example which has been applied by many authors to AVHRR NDVI composites (Kasischke and French 1995, Fraser *et al.* 2000a, Li *et al.* 1997, Li *et al.* 2000b, Fuller and Fulk 2001) is problematic when used with multi-temporal datasets or to areas spanning different vegetation types due to the difficulty in determining of a suitable threshold. Not only may a different threshold be required for each vegetation type, but an appropriate threshold level may vary from image to image (Al-Rawi *et al.* 2001). Although methodologies have been investigated which avoid this problem - Fernandez *et al.* (1996) for example have developed a method whereby the threshold value is determined contextually - few of these have been tested on a global dataset. Due to issues such as these Pereira *et al.* (1997) have concluded that the development of a generic, optimal, context-independent methodology for detecting and mapping burned areas may prove problematic, and suggest that region-specific ecological knowledge may be required to complement a spectral dataset. Despite this a handful of studies do exist in the literature which have attempted to design a single algorithm capable of delineating burned areas on a global scale. Roy *et al.* (1999) have investigated a multi-temporal burn scar detection algorithm designed for global application which is presented as the basis for operational burn scar monitoring using AVHRR and MODIS imagery. The VI3 vegetation index which follows of the form of the NDVI with the reflective component of the middle infrared sub-

stituted for the red band, is applied to a temporal sequence of AVHRR data to produce a burn scar index change map, which is then classified into burned and unburned pixels. A generic change detection algorithm designed for global application has also been presented by Roy *et al.* (2002), and is described in detail in Section 4.3. The methodology involves fitting a model of surface reflectance against a set of recent observations, in order to produce an expectation of subsequent measurements of reflectance. Large discrepancies between the observed and the modelled reflectance are then attributed to surface change or “bad data” (i.e. noise, residual cloud, cloud shadow). Originally prototyped with AVHRR data (Roy and Lewis 2000), the model has subsequently been applied to daily MODIS imagery for an area of Southern Africa with promising results (Roy *et al.* 2002). The few global burned area datasets which do exist are described in detail in Section 2.4.2.

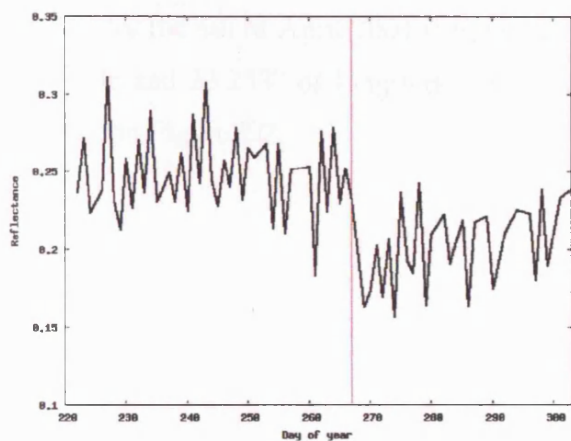
2.2 Limitations of traditional change detection techniques

The ability of the methods described above to separate areas which have been affected by fire from those which have not is highly dependent on the magnitude of the change in the signal which has occurred due to the change of interest (i.e. burning) in addition to the threshold level used (if required) to identify the change. The determination of a suitable threshold level is critical to the accurate identification of change, but as this may vary spatially and temporally the identification of an appropriate level is not a simple matter. Areas of change selected via an interactively or statistically defined threshold will include external influences caused by varying atmospheric conditions, sun angles, soil moisture and phenological states in addition to the actual changes of interest (Lu *et al.* 2004). Although more advanced techniques such as spectral mixture analysis or artificial neural networks do not require the definition of a threshold and produce higher quality change information, the results are still highly dependent on the magnitude of the change in comparison to background “noise” in the data. A study by Stroppiana *et al.* (2002) has shown that between 60-70% of the variability in SPOT-VGT surface reflectance data is caused by geometrical effects, with only 30-40% of the variability actually due to changes in the vegetation. Attempts have typically been made to reduce such effects prior to the detection of changes through the use of temporal composites. While the most popular approach has been

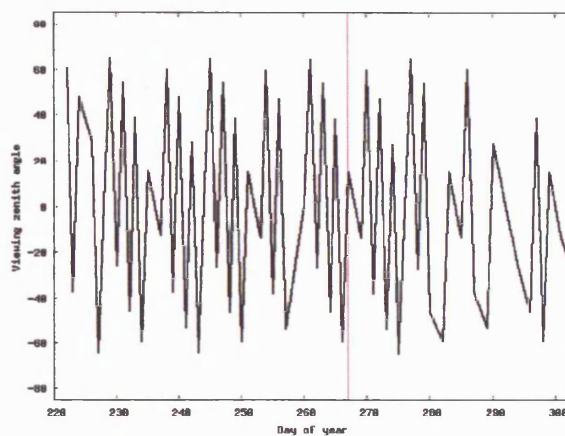
based on maximum NDVI values with the assumption that lower values of the NDVI will occur due to atmospheric effects, contamination from clouds and the soil background and variations due to sun and sensor positions. However problems with this approach occur as high NDVI values may be observed due to directional effects resulting in the preferential selection of off-nadir pixels (Lu *et al.* 2004). Other compositing procedures have been introduced such as the maximum surface temperature as clouds and cloud shadow will decrease the thermal infrared response (Cihlar *et al.* 1994, Roy 1997), or the use of maximum NDVI values followed by a minimum scan angle criteria (Cihlar 1994). Alternately the methods used have been dictated by the specific type of change which is being identified. Barbosa *et al.* (1998) have thus used a minimum albedo criteria in the detection of burned areas in order to preserve any information relating to the burned surfaces which will exhibit a low albedo.

Although compositing procedures may reduce the impact of external effects which are not directly related to the changes of interest, they do not remove them completely. The approach is therefore not ideal as the presence of these effects may mask the occurrence of low magnitude changes in the signal. This is demonstrated by Figure 2.1a which contains a temporal sequence of MODIS band 5 ($1.23\mu m - 1.25\mu m$) reflectances. The data corresponds to a single 500m pixel location from an area of northern Zimbabwe which has been flagged as containing an active fire on day 267 in the MODIS Thermal Anomalies product (see Section 2.3). The exact location of this pixel is documented as Site 2A in Table A.1 and Figure A.1 in Appendix A. This waveband (along with band 5) has been shown to exhibit higher sensitivity to fire induced surface change than the remaining five MODIS land surface reflectance wavebands (Roy *et al.* 2002, Trigg and Flasse 2000). The view zenith angle under which each observation is acquired is displayed in 2.1b and the NDVI for the same sequence in Figure 2.1c.

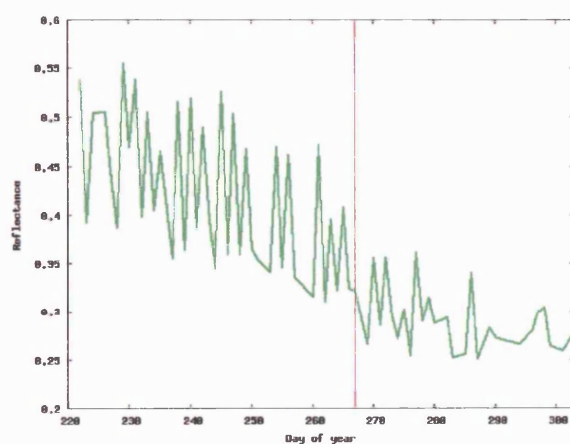
Despite the decrease in reflectance which is evident in the temporal sequence on the day of the fire, the magnitude of this change is within the variance of the data prior to the burn due to directional effects. It is clear from the NDVI (Figure 2.1c) values for this pixel location that the identification of the fire induced land cover change would be extremely difficult due to the variations which are present in the data due to “background” effects. The presence of these effects in surface reflectance data will decrease the separability between land cover classes if they are not accounted for. This is demonstrated by Figures 2.3a and 2.3b which contains atmospherically corrected reflectance data extracted for an area of 5km by 20km at the two



(a) MODIS band 5 reflectances



(b) View zenith sampling



(c) NDVI

Figure 2.1: The effect of burning on MODIS band 5 reflectances and NDVI, Site 2A, Zimbabwe 2001: The vertical line indicates the day of the MODIS active fire detection

sites indicated in Figure 2.3c. Figure 2.3a displays MODIS band 1 ($0.62\text{-}0.67\mu\text{m}$) and band 2 ($0.841\text{-}0.876\mu\text{m}$) 500m reflectances for the two sites, while Figure 2.3b contains the same data corrected for angular effects. These data have been extracted from the MODIS Core Validation (Mongu site, Zambia) 500m Surface Reflectance and Nadir Adjusted BRDF Reflectance products (NBAR) for the 4th of April 2001 (Strahler *et al.* 1999a). The Mongu site is located at -15.438° of latitude and 23.253° of longitude. The location of the image within the area of interest is displayed in Figure 2.2.

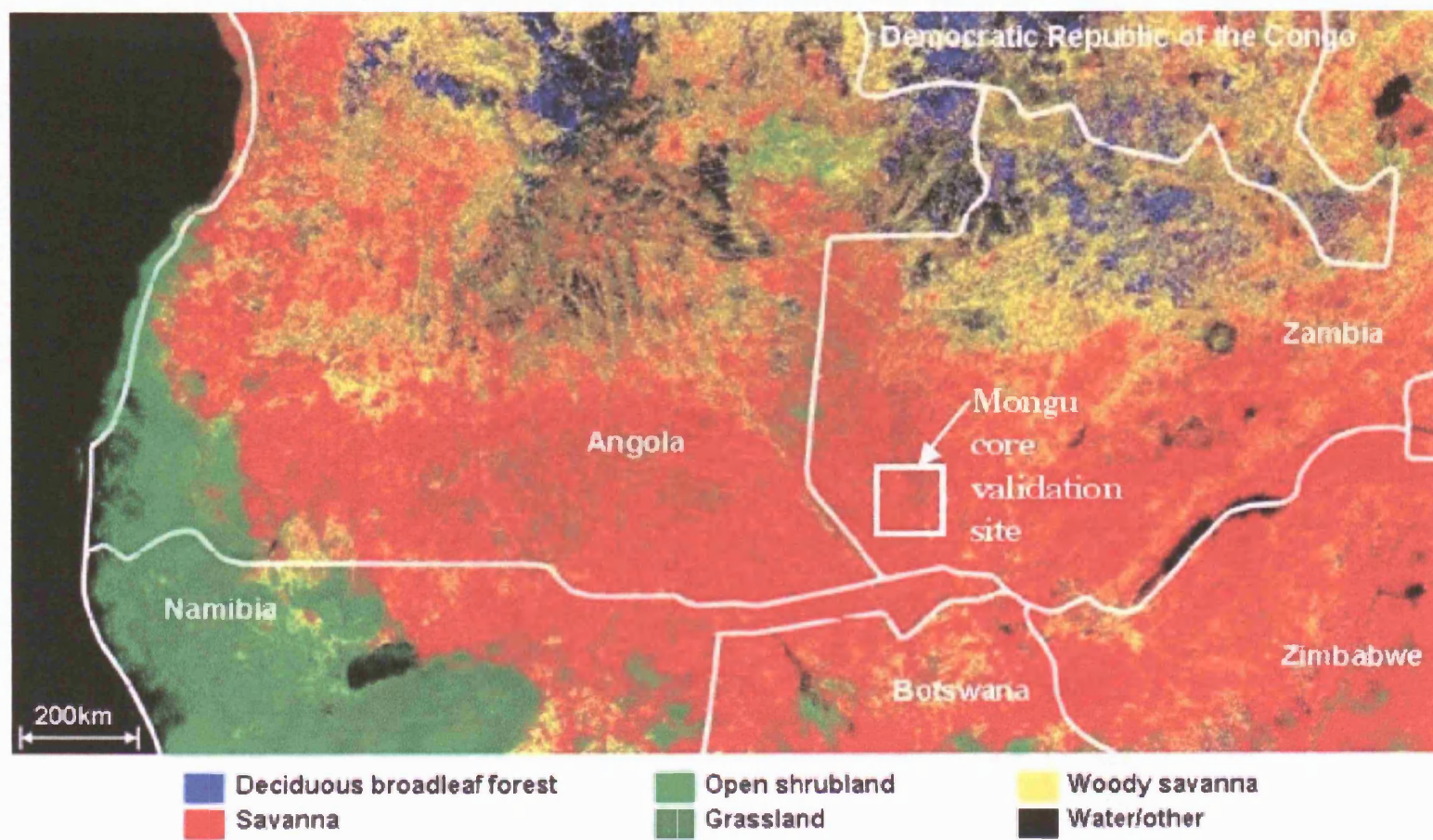
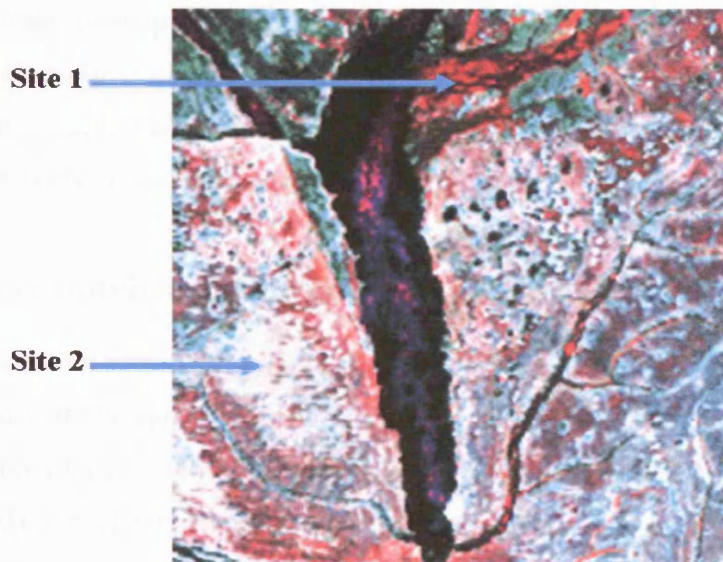
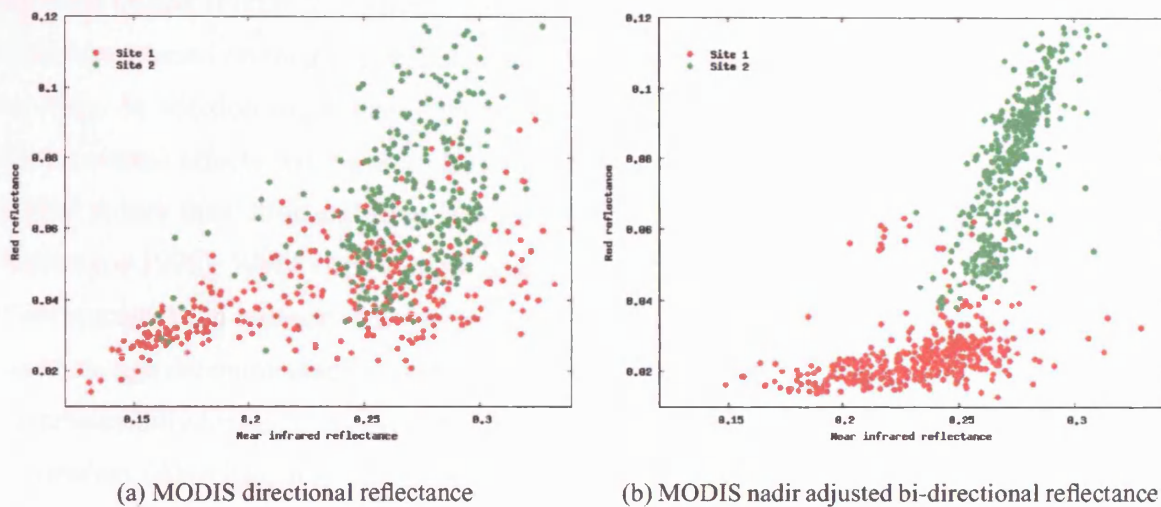


Figure 2.2: Mongu (Zambia) core validation site and MODIS Landcover Product



(c) MODIS nadir adjusted bi-directional reflectance: False colour composite of bands 2, 1, 4

Figure 2.3: Directional effects in MODIS 500m reflectances, Mongu (Zambia), 4th April 2001

Although from a visual examination of the NBAR image in the Figure 2.3c the two sites appear to be physically distinct, when directional effects are present in the data the distributions of the two classes in visible/near-infrared space overlap (Figure 2.3a) making it impossible to separate them based solely on this information. However once the data have been corrected

for these effects (Figure 2.3a) the overlap is reduced enabling a classification of the two land-cover types based on their spectral characteristics to be achieved with a much higher degree of accuracy. In addition single band reflectances or vegetation indices which have been corrected for directional effects will have a clearer physical meaning than uncorrected temporally composited values thus allowing for a better quantitative description of the biosphere (Leroy and Hautecoeur 1999). While such variations have traditionally been viewed as a source of error and have typically been reduced through the use of composited data as described above, a handful of recent change detection studies have exploited the information contained in this domain indicating substantially higher land cover classification accuracies with the incorporation of directional information (Abuelgasim *et al.* 1996, Barnsley *et al.* 1997). The incorporation of this information into the analysis adds an additional domain of information which has typically not been exploited in traditional approaches to change detection. As the spatial and temporal variability of the spectral response of burned areas is often extremely diverse and complex (Pereira *et al.* 1997), failure to exploit all of the information available in the remote sensing signal will result in decreased change detection capabilities.

2.2.1 Issues implicit in multi-temporal studies

All change detection methodologies will be sensitive to variations present in the data which are not associated with the surfaces changes of interest (Roy *et al.* 2002). The precise registration of a multi-temporal dataset to a common spatial framework is a prerequisite for the accurate detection of land cover change on a pixel by pixel basis. Dai and Khorram (1998) demonstrate that a registration accuracy of at least one-fifth of a pixel is necessary in order to achieve a change detection error of less than 10%. With an increasing emphasis on the need for more reliable quantitative estimates of the Earth's biophysical properties, considerable efforts have been made with the latest generation of sensors to address the need for accurate image registration (Townshend *et al.* 1992, Wolfe *et al.* 1998). The operational geolocation goal of the MODIS Science Team is thus an accuracy of 0.1 pixels for the 1km wavebands which corresponds to 10% of a 500m pixels (Nishihama *et al.* 1997). The utility of multi-temporal datasets in studies of change detection may also be reduced by atmospheric, environmental and radiometric differences, variations in pixel size across the image swath, and the variations in the sensor and solar geometries at

the time of data acquisition as discussed above (Roy 2000). While the impact of environmental effects have tended to be addressed through the use of anniversary date images, accurate atmospheric and radiometric correction and calibration of the images is required (Coppin *et al.* 2004). Problems such as the inaccurate detection of clouds and poor spectral calibration of the data are less prevalent however in data acquired by newer sensors such as MODIS than in comparable sensors such as the AVHRR (Roy *et al.* 2002). The position of the first seven MODIS reflective wavebands and their bandwidths have been chosen based on experience with the AVHRR and Landsat TM sensors in order to maximise radiometric precision and to avoid atmospheric absorption, and as a result all of these seven wavebands are of potential use in the discrimination of land cover units and in the identification of land cover change (Townshend *et al.* 1991, Strahler *et al.* 1999b).

In any land cover change detection study utilising remote sensing data, a choice needs to be made between the use of high spatial but low temporal resolution data, or moderate/low spatial but high temporal resolution data. The most appropriate data source will be dictated by the nature of the change which is to be identified, the spatial and temporal scale of the study, and the availability of data. While changes may be detected more accurately from higher spatial resolution systems such as Landsat TM due to the lower heterogeneity of the surface at the single pixel scale (30m for Landsat TM), this is achieved at the expense of low revisit periods. Sixteen days will therefore elapse before the same location on the Earth's surface is imaged again by the Landsat sensor. Combined with the possibility of cloud cover (or smoke/haze from fires) this low revisit period means that only a few good quality observations of the surface may be available over a period of several months. In contrast high temporal resolution sensors such as MODIS, AVHRR and SPOT VGT acquire near daily data at a global scale, but at a considerably lower spatial resolution. The first seven MODIS land surface reflectance bands are thus acquired at a resolution of 500m, while the spatial resolution of the AVHRR and SPOT VGT sensors are approximately 1km. The accurate identification of fire affected areas over large scales necessitates the use of high temporal resolution data due to the sudden and evolutionary nature of vegetation fires and the subsequent burned surface. While the "burn scar" produced by a fire may be identifiable within highly vegetated areas such as the boreal forests of Siberia for more than a year after the occurrence of a fire (Fraser and Li 2002), burned surfaces in southern Africa may exhibit a rapid post-fire recovery with an identifiable signal no longer present in as little as

a month after burning (Trigg and Flasse 2000). This aspect of the fire regime is discussed further in Section 3.6.2. The most appropriate remote sensing data source for a particular problem thus requires a careful consideration of both the spatial and the temporal characteristics of the changes of interest.

2.3 The detection of active fires

Over the past decade a large number of studies have been conducted into the detection of active fires from satellite data, and this is therefore a very well developed research field. Although the majority of work has been conducted at a regional or ecosystem scale the methodologies developed tend to be more widely applicable. All active fire detection algorithms are designed with the aim of separating those pixels in a dataset which contain active fires, from those that do not. The majority of methodologies have been designed for use with data from the Advanced Very High Resolution Radiometer (AVHRR). Until the launch of MODIS (Terra) in December 1999 the AVHRR sensor was the most suitable for large scale fire detection due to its high temporal resolution providing near daily global coverage and long term archive (25 years) of data at a moderate spatial resolution of approximately 1km. In addition the spectral configuration of the sensor makes it suitable for monitoring various characteristics of fires. A key aspect of the instrument is the location of the thermal infrared band (channel 3) between $3.55\mu m$ and $3.93\mu m$ near the spectral maximum of radiative emissions for objects radiating at temperatures around 800K, the temperature of burning grass. In comparison channels 4 ($10.3\mu m - 11.3\mu m$) and 5 ($11.5\mu m - 12.5\mu m$) are located near the spectral maximum for average environmental temperatures (approximately 300K). The underlying basis of the majority of fire detection algorithms is thus the assumption that a pixel containing an active fire will receive much more radiant energy at channel 3 wavelengths than at either channels 4 or 5. Existing fire detection algorithms fall into two broad categories; fixed threshold and contextual techniques. The fixed threshold approach involves the definition of an absolute threshold to which the value of each pixel is compared individually. In contrast a contextual algorithm defines a relative threshold through an examination of the statistics of neighbouring pixels. Contextual algorithms are the more recent technique and have been designed in an attempt to improve the accuracy of fire detection from remote sensing

data in a global context as although fixed threshold algorithms produce acceptable localized results, in general they have not been as successful in the analysis of large multi-regional datasets.

2.3.1 Fixed threshold algorithms

Traditional methods of fire detection are typically referred to as ‘fixed threshold’ algorithms as they employ an empirically defined threshold of, for example, AVHRR channel 3, to locate pixels which contain hotspots. The simplest approach is to assume that all saturated pixels in the thermal infrared channel contain fires. Saturation of the AVHRR sensor occurs at brightness temperatures of approximately 320 degrees Kelvin (K), and as this value is much higher than the temperatures of typical ground features the saturation of pixels is assumed to be an indication of the presence of fires (Cahoon *et al.* 1991, Kennedy *et al.* 1994). Thresholding AVHRR channel 3 at this level however leads to a large number of false identifications due to sunglint effects and the presence of other highly reflective surfaces. Research has indicated that while a single channel 3 threshold is sufficient to detect all fires within an AVHRR dataset, an additional threshold may be required to eliminate hot surfaces (Brustet *et al.* 1991). Various methodologies have thus been suggested to address the problem of saturation of non-fire pixels in an attempt to reduce the number of false fire detections.

Kaufman *et al.* (1990) implement three tests to identify forest fires in Brazil from AVHRR data. The first test ($\text{Channel 3} \geq 316\text{K}$) ensures that the pixel is hot. The second compares the difference between channel 3 and 4 to a pre-defined threshold, and the third ($\text{Channel 4} \geq 250\text{K}$) screens out clouds, as they may be highly reflective in channel 3 but will have a cooler temperature at channel 4 wavelengths. Li *et al.* (2000a) have also introduced three tests to eliminate false fires. The first examines the difference in brightness between AVHRR channels 3 and 4 in order to identify any false fire pixels caused by a warm background such as bare soil which may emit enough heat to saturate channel 3. The second test involves an examination of channel 4 values in order to eliminate false fire identifications caused by highly reflective clouds. Finally the reflectance values of channel 2 are examined, as true fire pixels will have a low reflectance in channel 2 due to decreased biomass and the presence of ash (Kennedy *et al.* 1994). Randriambelo *et al.* (1998) have used a similar approach. A multi-channel (AVHRR channels 3 and 4) algorithm is used to detect fires in south-eastern Africa and Madagascar. The method

assigns thresholds to the channel 3 and channel 4 data through an analysis of the histograms for each channel. A fixed threshold of 320K was used in the analysis of savanna regions, while a lower threshold of 316K was used for areas with denser vegetation cover. The channel 4 threshold is used to eliminate pixels which are contaminated by clouds or which contain warm surfaces (such as bare soil) as these will exhibit high reflectances. The values for the channel 4 threshold are determined by an examination of the Normalised Difference Vegetation Index (NDVI). Low or negative values of the NDVI are likely to correspond to clouds or bare surfaces, and these are thus eliminated.

In contrast to methodologies which are based purely on thresholding the individual or some multi-band combination of the thermal wavebands, various alternative approaches have been suggested. Chuvieco and Martin (1994) for example, have performed an initial classification of the dataset with thresholds subsequently applied only to vegetated areas in an attempt to avoid confusion between fire pixels and bare soils, while Setzer and Pereira (1992) only identify saturated pixels as active fires if a smoke plume is also identified in AVHRR channel 1.

Another approach to deal with the problem of sensor saturation due to the presence of highly reflective surfaces has been the use of night time images. Langaas (1993) has successfully used night time AVHRR channel 3 data over an area of West Africa to locate and analyse the characteristics of fires. A modification of the Dozier model (Matson and Dozier 1981) which provides algorithms for calculating the size and temperature of sub-resolution hotspots is utilised in order to identify high temperature sources within the images. Cahoon *et al.* (1992)) have used Defense Mapping Satellite Program (DMSP) night time data to detect fires over the African continent. This data proved to be particularly useful for the detection of fires in areas where there are few city lights such as the African savanna. However, despite the advantages which it may provide, night time datasets have not been widely used in fire detection studies. This is because the night time satellite overpass does not coincide with the occurrence of maximum fire activity, as the majority of vegetation fires generally begin during the afternoon when the ground is drier and the wind stronger, and tend to be short-lived lasting only for a few hours (Kennedy *et al.* 1994). In addition fires which persist for several days typically exhibit a diurnal cycle whereby they burn strongly during the afternoon and die down at night (Belward *et al.* 1994).

2.3.2 Contextual algorithms

In comparison to the fixed-threshold approach, contextual algorithms work by establishing a temperature difference threshold. This typically involves an examination of local background information in order to set the levels dynamically. Thresholds are thus derived on a pixel-by-pixel basis from the values of pixels in a surrounding window. The method relies on the fact that high temperature sources produce a high middle-infrared signal but have little effect on longer infrared wavelengths. Studies by Flasse and Ceccato (1996) and Wooster *et al.* (1998) thus identify potential fire pixels where the middle-infrared and longwave-infrared signals appear widely divergent. This fire detection process consists of two stages. First, pixels which may contain a fire are identified using a simple threshold which is low enough to ensure that all potential fire pixels are retained, but high enough to reject the majority of pixels which are definitely not fires. A pixel will be flagged as a potential fire if $T_3 > 311\text{k}$ and $(T_3 - T_4) > 8\text{k}$, where T_3 and T_4 are AVHRR channel three and four values. In addition a threshold may be applied to the channel 4 values, in order to ensure that the pixel is free of clouds and water bodies, as these may result in high reflectance values and lead to the incorrect identification of a pixel as a potential fire (Stroppiana *et al.* 2000). The second stage is the confirmation of a hotspot as a fire. This is achieved by comparing the pixel with its neighbours through the use of statistical measures such as the mean and the standard deviation of the background temperature difference. An expanding window technique (a maximum window size is defined to ensure that the statistics collected are representative of the pixel's background) is used to produce an acceptable set of background pixels, and potential fire pixels or pixels which contain clouds are not included within this. If the potential fire pixel is sufficiently different from its background, then it is classified as a fire. The criteria defined by Justice *et al.* (1996) require the value of a potential fire pixel to be at least two standard deviations greater than the mean background value in order to be classified as a definite fire pixel.

Following a contextual approach a fire pixel is thus identified by comparing the values of a potential hotspot with its neighbours and consequently confirming the presence of fire if the contrast between the pixel and the background is large enough. This method has several advantages over traditional fixed threshold algorithms. The main difference is that the decision to define a pixel as a fire is made on a relative, rather than an absolute basis. As a result the algorithm can

be applied to different areas or using data from a different season without requiring modification. For example forest fires in a cooler environment may not necessarily saturate AVHRR channel 3 as they have a lower temperature than savanna fires. However they will still be detected on the basis of the contrast between the fire and the background. If a fixed threshold algorithm which would apply the same thresholds to the two environments were to be used, either the forest fires would not be detected, or if they were then a large number of 'warm' pixels in the savanna environment which did not contain fires would also be classified as fire pixels. The main advantages of contextual algorithms are thus their self-adaptive nature and applicability to a wide range of seasons and environments (Flasse and Ceccato 1996).

2.4 Global fire products

At the time of writing the only global operational active fire information available is the MODIS Thermal Anomalies product. This is described in detail in Section (2.4.1). However several international programmes have been initiated with the aim of providing information on fire activity at a global scale using satellite data. In particular global active fire datasets include the International Geosphere and Biosphere Program's Global Fire Product, the Joint Research Centre's World Fire Web, and the European Space Agency's World Fire Atlas, and the Tropical Rainfall Measuring Mission's Fire Product which has near-global coverage. However as the Global Fire Product is only available for the period April 1992 to December 1993 it will not be discussed further.

The World Fire Web

Produced by the Global Vegetation Monitoring unit (GVM) of the Joint Research Centre (JRC) the World Fire Web is a global active fire dataset for the period October 1996 to December 2001. The dataset is available daily at a spatial resolution of 0.5 by 0.5 of a degree. The locations of active fires have been determined from 1km by 1km spatial resolution AVHRR data using a contextual algorithm (Flasse and Ceccato 1996). However errors of both commission (caused by warm highly reflective surfaces) and omission (due to the presence of smoke and clouds) exist in the dataset with large fires often remaining undetected due to the contextual threshold levels

used.

The World Fire Atlas

The World Fire Atlas produced by the European Space Agency (ESA) documents the global locations of active fire detections between 1995 and June 2004 at the time of writing with processing ongoing, synthesized into monthly fire maps over this period. The dataset has been created using a fixed threshold algorithm applied to night-time data from the Along Track Scanning Radiometer (ATSR) and ATSR-2. Although the detection of hotspots from night-time results in lower errors of commission due to sun-glint or the presence of warm surfaces, the timing of the satellite overpass may not coincide with the peak of fire activity in certain ecosystems. In addition to the use of night-time data the orbital characteristics of the ERS satellites result in a night-time revisit period of between three and six days at the equator. Both of these factors can contribute to the underestimation of fires. In comparison an alternative problem with the use of ATSR and ATSR-2 data is the overlap of the ATSR and ATSR-2 frames which may result in multiple detections of the same fire. However the main limitation of the dataset is the underestimation of the number of fire pixels, and it is suggested that the algorithms employed in its creation should be used with caution in the detection of agricultural, savanna and small fires (Arino and Plummer 2000).

The TRMM VIRS Fire Product

This fire product has been compiled using data from the Visible and Infrared Scanner (VIRS) onboard the Tropical Rainfall Measuring Mission (TRMM) satellite. Active fire detections are documented at a spatial resolution of 0.5 by 0.5 of a degree for the period January 1998 to August 2004 at the time of writing, with processing ongoing. The sensor has a near-global geographical coverage spanning the latitudes 38 degrees South and 28 degrees North, with the same location observed once every two days. The product has been created using a contextual fire detection algorithm (Giglio *et al.* 1999). An evaluation of the results has indicated at least a moderate probability of detection for all of the test sites, with a higher probability of detection for fires occurring in non-forest land cover classes (Giglio *et al.* 2003b). Study sites which exhibited a high level of fire activity such as areas of woodland or forest within central Africa (the Central African Republic, Angola and Zambia) where the fire activity also occurred primarily within

forest or woodland pixels demonstrated the lowest probabilities of detection by the algorithm (*ibid*).

2.4.1 The MODIS active fire product

The algorithms used to produce the MODIS active fire product are based on heritage algorithms developed to detect fires from AVHRR data. One of the major problems involved in the use of AVHRR imagery for fire detection is the saturation of channel 3, resulting in the false identification of fire pixels. In contrast, MODIS has two $4\mu m$ channels (bands 21 and 22) which saturate at temperatures of 500K and 335K respectively as well as an $11\mu m$ channel which saturates at approximately 400K, thereby offering unique fire detection capabilities (Justice *et al.* 2002). Four daily MODIS observations, two from Terra (10.30am and pm local equator crossing time) and two from Aqua (1.30pm and am local equator crossing time) are used to produce a suite of active fire products. The algorithm employed to detect fires is a hybrid approach combining both absolute and relative criteria, and as is the case with most satellite based fire detection methodologies it exploits the different responses of the middle-infrared and the longwave-infrared wavebands to the presence of fire (Kaufman *et al.* 2003). The data used in the current research is the “version 4” MODIS product. This has been created using an updated post-launch algorithm which was introduced due to two particular problems in the initial results. The problems with the earlier version of the algorithm involved the detection of a large number of false fires over deserts and sparsely vegetated surfaces, while relatively small fires were frequently not identified (Giglio *et al.* 2003a).

The MODIS fire detection algorithm follows the same approach as the first and the majority of subsequent hotspot detection algorithms, exploiting the difference in the responses of the middle and long wave infrared wavebands to the presence of a hot subpixel target (Dozier 1981). The basis of the version 4 algorithm is the absolute increase in radiance at $4\mu m$ as well as the increase at this wavelength relative to the radiance measured at $11\mu m$. In the following discussion T_4 will refer to the $4\mu m$ channel, and T_{11} the $11\mu m$ channel (MODIS bands 22 and 31 respectively) and K to degrees Kelvin. The version 4 algorithm involves four main processes. The first locates any potential fire pixels while the second involves a fixed threshold approach to identify larger or more intense fires. A background characterisation is then performed, and

finally a contextual approach is used to locate any smaller fires.

The first step in the fire detection algorithm involves the identification of any potential fire pixels. For daytime data this is achieved through three tests. If the three conditions

$$T_4 > 310k$$

and

$$\Delta T > 10K$$

where

$$\Delta T = T_4 - T_{11}$$

and

$$\rho_{(band2)} < 0.3$$

are not met then the pixel is automatically rejected as a non-fire pixel. For nighttime data no reflective test is performed and the threshold of the first test is reduced to 305 degrees Kelvin. Any pixels which pass these conditions are assumed to be potential fire pixels and are subjected to two further tests. An absolute threshold is used to identify pixels which are definite fires and therefore have a very low chance of being false alarms (Kaufman *et al.* 1998). The threshold level is therefore set high enough to ensure only unambiguous fire pixels are identified:

$$T_4 > 360k \text{ (day)}$$

$$T_4 > 320k \text{ (night)}$$

The third test is also performed on all the pixels which have passed the first test, irrespective of whether they have passed the absolute threshold test or not, and involves the characterisation of radiometric background signal of each potential fire pixel. This is achieved using all “usable” pixels within a window surrounding the potential fire observation as input. Usable pixels are defined as those which are land pixels, are cloudfree, and are not background fire pixels (Giglio *et al.* 2003a). Background fire pixels are identified as those where:

$$T_4 > 325k$$

and

$$\Delta T > 20K$$

for daytime observations, and where:

$$T_4 > 310k$$

and

$$\Delta T > 10K$$

for nighttime observations. If the potential fire pixel has a sufficient number of usable observations (as least 25 percent of the window), various statistical measures are then computed as detailed in Table 2.1. The mean absolute deviation is used in preference to the standard deviation

Statistic	Definition
\overline{T}_4	respective mean of T_4
δ_4	mean absolute deviation of T_4
\overline{T}_{11}	respective mean of T_{11}
δ_{11}	mean absolute deviation of T_{11}
$\overline{\Delta T}$	respective mean of ΔT
$\delta_{\Delta T}$	mean absolute deviation of ΔT

Table 2.1: Fire related statistics: MODIS Thermal Anomalies product

as a measure of dispersion as it is more resistant to outliers, which may be present in the data due to undetected clouds, water or fires (Giglio *et al.* 1999, Giglio *et al.* 2003a). Pixels which pass the background characterisations are then subjected to a series of contextual tests. The aim of this process is to locate pixels which display T_4 and ΔT values which are sufficiently different from the values of the non-fire background, and thresholds are therefore determined from the variability of the background values. This is achieved through three tests;

1. $\Delta T > \overline{\Delta T} + 3.5\delta_{\Delta T}$
2. $\Delta T > \overline{\Delta T} + 6K$
3. $T_4 > \overline{T}_4 + 3\delta_4$

In the case of nighttime observations unambiguous fire detection is performed based on the information collected so far. Nighttime fire pixels are identified as observations which pass the absolute threshold test or where the above three contextual tests are true. For daytime observations the pixel is identified as a tentative fire if it passes the absolute threshold test or all of the three contextual conditions are met. For the pixel to be identified unambiguously as a fire it is subjected to a further three steps which are designed to eliminate false detections due to sun glint, hot desert surfaces or coastlines. For a description of the rejection criteria the reader is referred to Giglio *et al.* (2003a).

Performance of the algorithm

Results from the global (i.e. over all biomes) validation of the version 4 MODIS fire detection algorithm indicate that under ideal daytime and nighttime conditions a flaming fire needs to be approximately 100 m^2 in order to have at least a 50 percent chance of detection, while smoldering fires typically need to be between 10 and 20 times larger to achieve the same probability of detection (Giglio *et al.* 2003a). The greatest source of error in the Version 4 product is the persistent false detection of fires along the banks of (as well as on islands within) some rivers, and improvements are thus necessary in the ancillary water mask used in the algorithm (*ibid*).

2.4.2 Global burned area products

At the time of writing no global burned area information is produced operationally. However several global burned area datasets have been created from remote sensing data sources.

The GLOBSCAR dataset

The GLOBal Burn SCAR (GLOBSCAR) project was initiated in 2001 under the European Space Agency's Data User Programme, with the aim of producing monthly global burned area maps from daytime ATSR-2 imagery for the year 2000. This sensor was chosen in particular due to its high spectral resolution thermal and near infrared channels, both of which have been shown to be the most appropriate wavebands for the global detection of burned surfaces (Trigg and Flasse 2000, Stroppiana *et al.* 2002). In addition the repeat cycle of the ERS-2 satellite which results in coverage at the equator at least once every three days, its equatorial crossing time of 10.30am, and moderate spatial resolution (1 by 1km) make it an appropriate data source for the detection of burned areas globally (Simon *et al.* 2004).

The methodology employed in the creation of the GLOBSCAR dataset consists of two algorithms which exploit the two main changes which occur to the remotely sensed signal as a result of burning. The first involves the decrease in near infrared reflectance which occurs due to the removal of vegetation as a result of burning independent of the vegetation type, while the second is dependent on the increase in temperature of a recently burned surface as a result of increased absorption of solar radiation, decreased evapotranspiration due to the loss of the vegetative cover,

and the blanketing presence of ash and carbon constituents (Simon *et al.* 2004). The first algorithm (“K1”) is based on the geometrical characteristics of the burn pixels in bi-spectral (near and thermal infrared) space (Piccolini and Arino 2000). Burn pixels are expected to move away from the distribution irrespective of the vegetation type or atmospheric conditions due to the higher brightness temperature and lower near infrared reflectance exhibited by burned surfaces. The K1 algorithm is applied to the data in fixed size windows as defined in Equation 2.1:

$$K1(i, j) = mean(NIR) - NIR + 2 \times TIR - 2 \times mean(TIR) - variance(TIR) \quad (2.1)$$

where TIR (thermal infrared), mean(TIR) and variance(TIR) are expressed in Kelvin, NIR (near infrared) and mean(NIR) are integer expressions of the actual percentages, and only ‘burnable’ pixels are used in the calculation of the mean and variance quantities. A 50km by 30km window size has been chosen as these dimensions present a compromise between the need for a sufficiently homogenous land surface in terms of the cover type, and a sufficient number of observations to derive the mean quantities required by the algorithm (Simon *et al.* 2004). A problem with this approach is the requirement of a high degree of separability in the NIR-TIR spectral space, which is not always the case in particular in the presence of smaller burns and mixed pixels.

The second algorithm (“E1”) consists of a series of fixed threshold tests which were initially designed for the detection of burned areas within tropical savannas, involving information from four ATSR-2 wavebands (Eva and Lambin 1998a). A pixel is identified as a burn if:

1. $RED_{0.67} < 10\%$
2. $NDVI < 0.4$
3. $SWIR_{1.6} < 20\%$
4. $NIR_{0.8} < SWIR_{1.6}$
5. $BT_{11} > 300K$

Where RED, SWIR and NIR denote the reflectance in red, short wave and near infrared wavebands respectively, and BT is the brightness temperature. In order to achieve acceptable global

results and to minimise errors of commission the K1 and E1 algorithms cannot be used individually, and therefore both have been used in the creation of the GLOBSCAR datasets with pixels only labelled as burns in the final output if they have been identified as potential burns by both algorithms. Although errors of commission occur with the K1 algorithm due to the presence of dark bare soil or mixed pixels, these are reduced considerably by the E1 thresholds. The main limitation of the E1 algorithm is confusion between water pixels and burn pixels in particular in the Okavango delta, but it is possible to avoid such errors through the use of a water mask (Fierens 2002). Thus when both algorithms are used although under-detection of burned pixels occurs frequently and is significant in some areas, for example croplands in Zimbabwe, errors of commission rarely occur and tend to be limited to isolated pixels (Simon *et al.* 2004).

Validation of the results has indicated that inaccuracies in the geolocation of the data in conjunction with the coarse spatial resolution (1km by 1km) of the ATSR-2 data results in poor quantitative results at a local scale (in particular for smaller fires) which are not necessarily representative of the performance of the product at a global scale (Simon *et al.* 2004). The main limitation of the algorithms is the application of single threshold levels applied at global scale. The reason given for this is the lack of reliable land cover information at the time of creation of the product, and it is suggested that the problem of under-detection of burn pixels in certain ecosystems may be avoided through the application of modulated thresholds which would require the use of a detailed land cover map (*ibid*).

The GBA2000 dataset

The main aim of the Global Burnt Area 2000 (GBA2000) project was to provide reliable and quantitative information relating to the magnitude and spatial distribution of biomass burning at a global scale. Co-ordinated by the Global Vegetation Monitoring unit (GVM) of the Joint Research Centre (JRC) a network approach involving national institutions from six countries and two international institutions has been used to develop and test a series of regional algorithms which may be applied to the problem of locating burned areas in moderate spatial resolution satellite data. The algorithms are applied to daily global data for the year 2000 acquired by the Vegetation (VGT) instrument onboard the SPOT4 satellite.

Under the assumption that a different methodology is required to identify burned areas in

different climatic zones or ecosystem types, seven regional algorithms are used to create the final global product, with the algorithm used for a particular region dependent on the landcover characteristics of that region. This approach was followed in order to overcome problems which arise in the detection of burned surfaces due to phenology, varying snow cover and flooding (Gregoire *et al.* 2003). The burned area algorithm applied to the southern Africa region is based on a supervised classification trees approach. The classification trees are applied to monthly composites of VGT data, and a pixel is classified as a burn if it satisfies all of the conditions of any of the classification rules listed in Table 2.2. The variables used in the classification process

Rule	Conditions
A	$NIR_2 \leq 256.5; \Delta_{12}NIR > 51.5; \Delta_{12}NIR \leq 70.5; NDVI_2 \leq 0.309$
B	$NIR_2 \leq 256.5; \Delta_{12}NIR > 51.5; \Delta_{12}NIR \leq 70.5$
C	$NIR_2 \leq 256.5; NDVI_2 \leq 0.198; \Delta_{12}NDWI > 0.06; NDWI_2 \leq -0.19$
D	$NIR_2 > 256.5; NDVI_2 > 0.198; NIR_2 \leq 272.5; \Delta_{12}NIR > 80.5; NDVI_2 \leq 0.290$
E	$NIR_2 > 256.5; NDVI_2 > 0.198; NIR_2 > 272.5; NDVI_2 \leq 0.231; \Delta_{12}NDWI \leq 0.076; \Delta_{12}NIR > 69.5; RED_2 \leq 213.5$
F	$NIR_2 > 256.5; NDVI_2 >^0 .198; NIR_2 > 272.5; NDVI_2 \leq 0.231; \Delta_{12}NDWI \leq 0.076; NDWI_2 \leq -0.212$

Table 2.2: GBA2000 Classification rules (*Source: Tansey et al. (2004b)*)

are the red, near infrared (NIR) and middle infrared (MIR) SPOT VGT bands. The NDVI and the Normalised Difference Water Index (NDWI, defined as $(NIR-MIR)/(NIR+MIR)$) are also computed. The Δ_{ij} variable in Table 2.2 refers to $variable_{timei} - variable_{timej}$ where times i and j refer to the monthly composite images at time 1 and 2 respectively.

An initial accuracy assessment has been performed on the preliminary burned area maps over a limited area for four sites in south-eastern Africa (Gregoire *et al.* 2003). Linear regression analysis using high resolution (Landsat TM) data to identify burned areas has been performed, with r^2 coefficients of at least 0.88 for three of the sites. The r^2 coefficient for the fourth test site located in Mozambique is however only 0.4. Overall errors for sub-saharan Africa include false detections due to flooding of non-permanent water features and hot dark rocks. However it is suggested that compared to the magnitude of burning which is taking place in this region such false detections are not significant (Tansey *et al.* 2004b). More detailed statistics relating to the accuracy of the product are not available at the time of writing, although a validation protocol is

in place to produce a statistically sound assessment of the results at a continental scale (Boschetti *et al.* 2004).

2.5 Summary

This chapter has reviewed a range of change detection methods which are typically applied to the problem of identifying and monitoring ecosystem changes from remote sensing data. Particular reference has been made to the application of these to the detection and mapping of fire affected areas at a variety of spatial and temporal scales and within different ecosystem types. In addition the approaches used to detect active fires have been defined and the current production of global operational active fire datasets discussed. The detection of active fires from remote sensing data is a relatively mature field with sophisticated algorithms applied to a range of data sources for the production of global datasets as well as a general consensus as to the most appropriate algorithms for this purpose. In contrast a wide range of burned area mapping methodologies exist in the literature with no general agreement on the most appropriate method for a particular data source or study area, and no operational burned area product currently available to the scientific community. The majority of approaches have only been applied to a single study area or season with the methods used to separate areas of burning from areas of no-change dependent on the characteristics of the particular ecosystem and the time of year. In addition with the exception of the two global burned area products described in Section 2.4.2 which document the occurrence of burning on a monthly scale for a single year, and the algorithm of Roy *et al.* (2002) which is applied to daily data for a single month, none of the methodologies discussed above have been applied to the detection of fire affected areas at a high temporal resolution or over multiple fire seasons. Although the change detection studies reviewed above provide useful information, various limitations are associated with the approaches used. These are summarised as follows;

1. Thresholding The majority of the methods described above require the definition of a threshold with which to differentiate between the changes of interest and background variations. The determination of a suitable threshold level is critical to the accurate identification of significant land cover change. Over large areas however the identification of an appropriate threshold may be difficult due to variations in the surface which are unrelated to the changes of interest, and variations imposed by the sensing system (Roy *et al.* 2002). In addition to the changes of interest, areas of change which have been identified via thresholding (whether interactively or statistically defined) will include external influences caused by variations in factors such as the

phenological state of the vegetation, the atmospheric conditions, and the sensor and solar geometry under which the data was acquired. The presence of these factors may have a considerable impact on the accuracy of the change detection results.

2. Low frequency surface variations The change detection techniques described above generally assume overall phenological conditions to be comparable, whether they are performed at a bi-temporal or a continuous time scale (Coppin *et al.* 2004). These methods tend to be very sensitive to changes in seasonality or ecosystem dynamics. Variations in the surface which occur over the time periods of the study but are unrelated to the changes of interest may complicate the identification of these. While the impact of such variations have traditionally been reduced through the use of anniversary date images, this approach is not possible in the detection of high temporal resolution changes which necessitate the need for data sensed frequently over long periods. Although the impact of low frequency phenological variations on the detectability of the remote sensing change signal will be dependent on the magnitude of these in comparison to the magnitude of the changes which are to be identified, they constitute a perturbing factor in the identification of significant surface change. The accurate identification of land cover changes from high temporal resolution remote sensing data will therefore be facilitated by the incorporation of these phenological variations into the change detection approach.

3. Atmospheric and directional effects The majority of the change detection techniques discussed in Section 2.1 are extremely sensitive to noise in the data due to the presence of cloud or cloud shadows, atmospheric effects, and variations in solar angles and the geometry of the sensor (Coppin *et al.* 2004). While such effects have typically been addressed through temporal compositing procedures involving, for example, the use of maximum NDVI values, this approach is not ideal. A major drawback is the subsequent data reduction associated with the compositing process, with the temporal frequency of observations essentially reduced to the length of the temporal compositing period. In addition the use of maximum value NDVI composites frequently fails to identify all cloud contaminated pixels (Lambin and Strahler 1994a), and have been shown to preferentially select off-nadir pixels (Cihlar 1994). The impact of directional effects on the remote sensing signal and the effects which these have on the identification of land cover change has been illustrated in Section 2.2. The presence of these effects or noise in the temporal se-

quence will significantly reduce the capability of the change detection algorithm to accurately identify the changes of interest.

In light of these three major limitations the current work aims to develop a generic change detection technique applicable to the detection of high temporal resolution surface change from moderate spatial resolution remote sensing data. The model addresses the drawbacks of traditional approaches by;

1. Accounting for low frequency phenological surface change
2. Accounting for directional effects in the remote sensing signal
3. Identifying and removing noisy observations of reflectance

The following chapter investigates the occurrence of vegetation fires within southern African ecosystems and characterises their effects on the remote sensing signal. Based on these findings a further set of recommendations are defined for the application of the change detection algorithm to the specific problem of identifying and mapping fire affected areas in southern Africa. Following on from the limitations of traditional approaches defined above and the recommendations made in Chapter 3 a new, generic approach to change detection which is applicable to the identification and delineation of fire affected areas is developed in Chapter 4.

Chapter 3

Fire characteristics of southern Africa

3.1 Introduction

The previous chapter has introduced the field of remote sensing change detection with particular reference to the detection of burned areas and active fires. For any change detection study to be effective a thorough understanding of the nature of the change is required. The aim of this chapter is therefore to provide an overview of biomass burning in southern Africa. As the wider impact of fire and its effect on atmospheric constituents has been dealt with in Chapter 1, the aim of the discussion below is to provide a description of the effect of fire on the terrestrial components of southern African ecosystems. This is followed by a description of the study site and a characterisation of the fire regime of the area using a five year data set of daily active fire detections. The temporal and spatial distribution of fires over the five year period is described, and the spectral characteristics of burned surfaces within the study area investigated. Finally, based on this information a set of recommendations for an effective southern Africa burned area mapping algorithm are defined.

3.2 The role of fire in southern African ecosystems

Although a primary agent of disturbance, fire is integral to many African ecosystems with Africa frequently referred to as the “fire continent” due to the regular and widespread occurrence of vegetation fires (Goldammer and Mutch 2001). Vegetation fires have occurred in Africa for millenia and their presence thus maintains habitats for species which are adapted to and have evolved with frequent burning, and as such the continued occurrence of fire is essential in maintaining the structure, composition, diversity and productivity of these ecosystems. Although in the absence of burning these fire-dependent ecosystems have the climate potential to form forests, this transformation would result in a loss of species and decreased biodiversity (Bond *et al.* 2004). Past and future changes in the extent and species composition of these ecosystems cannot be fully understood without an understanding of the ecology of fire (Bond and Keeley 2005).

The ignition sources of southern African vegetation fires are varied and range from lightning strikes to prescribed burning for agricultural or ecosystem management. A study at a site in South Africa over the period 1980 to 1992 suggests that lightning fires occurred most frequently between October and January when thunderstorms were most frequent, while anthropogenic fires

mainly occurred between the months of June and September (Trollope 2000). Most of the rainfall in southern Africa occurs during convective lightning storms which may cause fires in the early part of the wet season when fuels are still dry enough to ignite and sustain a fire (Goldammer and Mutch 2001). Although lightning strikes may still be the primary cause of fire in areas where human ignition sources are not present this is generally no longer the case with lightning accounting for less than 10% of observed ignitions and humans now recognised as the main cause of southern African fires (Dwyer *et al.* 1998, Goldammer and Mutch 2001).

As a land management tool fire is embedded in the culture of many African societies as it is the cheapest and easiest method with which to clear land and is therefore commonly used in agricultural areas to remove unwanted biomass, to prepare land for cultivation, to remove agricultural residues and to control bush encroachment (Frost 1999). It is also used to increase the fertility of nutrient deficient soils by releasing the nutrients sequestered in plant biomass, and in addition forms the main source of domestic energy for cooking and heating (Goldammer and Mutch 2001). Fire is frequently used as a wildlife management tool in southern Africa as burning stimulates the sprouting of plants thereby improving the forage quality and attracting ungulates, and is used for the same reasons by pastoralists in particular towards the end of the dry season when above ground plant biomass is at a minimum (Trollope 1982, Zavala and Holdo 2005). The human driven shift in the fire regime of southern African ecosystems has resulted in an increase in the frequency as well as in the return rate of fires (Saarnak 2001). Both of these aspects of the fire regime are characterised in Chapter 7. This shift in the periodicity of fires has resulted in a change in the vegetation composition of these ecosystems, to the extent that some authors suggest that African savannas are in fact fire-maintained sub-climax formations derived from repeated burning (Frost 1999, Goldammer and Mutch 2001, Bond *et al.* 2004). Southern Africa has an ideal fire climate comprising a wet season during which plant biomass increases and accumulates, and a dry season when the vegetation senesces and forms extremely flammable plant fuels (Trollope 2000). The majority of fires within this region are surface fires which are spread by fuels close to the ground such as dead leaf matter, grass and stem material. Surface fires feed selectively consuming plants in the herbaceous layer (where grass species dominate) with little effect on trees taller than 2-4m (Frost and Robertson 1985, Bond and Keeley 2005). The characteristics of vegetation fires (the intensity, frequency and spatial extent) are dependent on the following six factors and their interactions (Sousa 1984, Goldammer and Mutch 2001,

Trollope and Trollope 2002);

1. Frequency and seasonality of ignition sources As discussed above fires are ignited both naturally and anthropogenically. The intensity and spatial extent of the fire will be dependent on the timing of the ignition in relation to the five factors described below.

2. Moisture content of the vegetation This factor is critical as it will determine the probability of ignition, the ability of the fuel to carry a fire, the quantity of fuel consumed and the rate of combustion. It will be dependent on the characteristics of the soil and the amount of precipitation received during the wet season.

3. The rate of fuel accumulation Soil type and water availability are major factors in determining the rate of accumulation in southern African ecosystems. The amount of energy available for release during a fire is related to the quantity of fuel, with a positive feedback thus observed between fuel loads and fire intensity as fuel accumulation determines the quantity of biomass available for burning at any given time. The accumulation rate is controlled by the difference in the rate of production and the rate of decomposition of plant matter and the more fuel that has accumulated since the last burn, the more intense the fire will be.

4. Structural and chemical characteristics of the fuel These factors will also influence the intensity of the fire. High intensity crown fires are common in ecosystems where the surface to volume ratio of vegetation is large such as coniferous forests. In contrast savanna ecosystems where the fuel is distributed in widely-separated strata tend to burn with a lower intensity.

5. Heterogeneity of the landscape The spatial extent of vegetation fires is strongly influenced by the topography and spatial characteristics of the vegetation, as well as the presence of natural or artificial fire breaks.

6. Weather conditions at the time of the fire The climate will have an indirect influence on frequency and intensity of fires through its influence on the rate of accumulation of fuel loads. Factors such as precipitation, air temperature, humidity, wind speed and wind direction will

affect the intensity of the fire, its size and the rate at which it spreads, with rapidly moving fires tending to consume less fuel and exhibiting lower intensities.

As all of these factors will vary both spatially and temporally, fire regimes may be extremely variable, as will be the effects of fire on the vegetation and the nature of the fire residues. A reciprocal relationship typically exists between the vegetation and fire where the condition of the vegetation affects the fire, and the interval between fires determines the composition, structure and quantity of living and dead fuels (Sousa 1984). Recurrent fires have the potential to influence the structure and the composition of vegetation, and the extent to which this happens will be dependent on factors such as the species composition of the vegetation, their sensitivity to fire and their capacity to recover afterwards, as well as the factors discussed above (Frost and Robertson 1985). In addition while the initial impact of a fire may be an increase in soil nutrients via ash deposits, the post fire surface will be more sensitive to nutrient leaching and soil erosion (Menaut *et al.* 1993). Although the extent of the destruction of a vegetation community will vary according to the timing of the fire in relation to the plant phenology and the six factors described above, the overall effect of fire is a reduction in the living and dead plant material. Fires which occur early in the dry season have a lower combustion efficiency due to the higher moisture content of the vegetation as the water vapour released from the burning fuel has a smothering effect on the fire (Hoffa *et al.* 1999). The negative effect of fuel moisture on fire intensity in an ecosystem in South Africa has been demonstrated by Trollope and Trollope (2002). In contrast fires which occur late in the dry season thus tend to be more intense and destructive than early dry season fires due to the lower fuel moisture content, higher air temperatures and wind speed (Desanker *et al.* 1995). In addition, the late dry season is a period of rapid growth and nutrient cycling by woody plants and fires will affect woody plants more than grasses which are usually dormant at this time (Frost 1999). The effect of frequent late dry season fires is thus an eventual transformation of woodland areas to savanna and grassland with only isolated stands of fire tolerant trees remaining (Desanker *et al.* 1995). The increase in grasses results in higher dry season fuel loads which results in more frequent and intense fires and the further suppression of woody plants (*ibid*). In contrast the complete absence of burning and to a lesser extent the occurrence of early dry season fires has been shown to encourage the growth of woody plants (Trapnell 1959, Trollope 2000).

The fire regime of southern Africa is clearly highly complex and dependent on the interactions of a large number of factors. Although numerous studies exist which have investigated the occurrence of fire in this region, the majority of these have been performed over a short temporal period or limited spatial scale. As stated above the construction of an effective remote sensing change detection algorithm requires a detailed understanding of the temporal, spatial and spectral nature of the change which is to be identified. The remainder of this chapter is therefore dedicated to the characterisation of the occurrence of fire within the study area over the past five years in terms of these three variables.

3.3 The area of interest

The study area encompasses the region of southern Africa spanning -10.0 to -20.0 degrees of latitude and 10.15 to 31.92 degrees of longitude as detailed in Figure 3.1. This is an area of approximately 1200 by 2400km containing portions of Angola, Namibia, Botswana, Zambia, Zimbabwe, Zaire and Mozambique, which corresponds to the spatial extent of two neighbouring MODIS tiles. The locations of these within the global grid are horizontal 19 and 20 and vertical 10 (“h19v10” and “h20v10”). The MODIS sensor and the data products available from it are discussed in Chapter 5. The MODIS Land Cover Product has been used to identify the vegetation classes present within the study area. This product consists of a land cover classification of the globe at a spatial resolution of 1km. A full description of the product and the methodology used to create it can be found in Strahler *et al.* (1999b). The results of four different classification schemes are included in the Land Cover product along with an assessment of the quality of the classification. The schemes used are:

1. The International Geosphere-Biosphere Program classification - IGBP (Belward *et al.* 1999)
2. The University of Maryland land cover classes - UMD (Hansen *et al.* 2000)
3. The Biogeochemical biome model classification - BGC (Running *et al.* 1994b)
4. The Leaf Area Index/fraction of Photosynthetically Active Radiation biome - LAI/fPAR (Myneni *et al.* 1997)

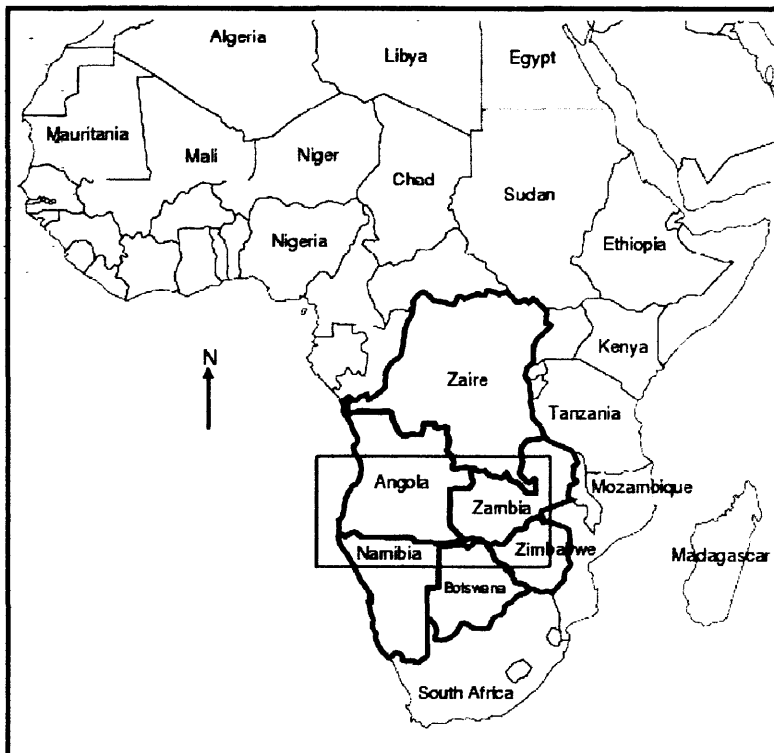


Figure 3.1: The study area, shown in the red box: Adapted from ESRI (1999)

The main difference between each of these is the number of categories into which the land surface is divided. The UMD scheme only contains one class of shrub and one class of savanna and only a single category combining grasses and cereal crops with no individual grassland class. The LAI/fPAR scheme does not include a savanna category and only a combined grasses/cereal class. As the vegetation type for the areas used in this study is expected to mainly consist of grassland, savannas and shrublands the IGBP classification was used in preference to the alternative schemes. The IGBP approach encompasses seventeen land cover categories which include eleven categories of natural vegetation separated by life form (woody and herbaceous cover), three of developed and mosaic lands, and three classes of non-vegetated land (Strahler *et al.* 1999b). These are detailed in Table 3.1. At the time of writing this product was only available

Natural Vegetation
Evergreen Needleleaf Forests
Evergreen Broadleaf Forests
Deciduous Needleleaf Forests
Deciduous Broadleaf Forests
Mixed Forests
Closed Shrublands
Open Shrublands
Woody Savannas
Savannas
Grasslands
Permanent Wetlands
Developed and Mosaic Lands
Croplands
Urban and Built-up Lands
Cropland/Natural Vegetation Mosaics
Non-Vegetated Lands
Snow and Ice
Barren or Sparsely Vegetated
Water Bodies

Table 3.1: IGBP Land Cover units

for 2000 and 2001. This was created from one year's worth of data (10/15/00-10/15/01), excluding June 2001 which is missing due to problems with the sensor during this period. The

only other operational land cover products available for the region are the GLC2000 produced by the Global Vegetation Monitoring unit of the Joint Research Centre (Bartholome and Belward 2005), and the International Geosphere Biosphere Programme's global land cover classification (Townshend *et al.* 1994). The global GLC2000 maps have been produced using 14 months of daily 1km resolution SPOT VEGETATION data and cover the period from November 1999 to December 2000. The IGBP global land cover classification was produced from 12 months of 1km resolution AVHRR data and covers the period April 1992 to March 1993. The MODIS land cover classification thus provides the most recent global, satellite derived land cover information.

The MODIS land cover product for each of the two years has been produced using 365 days of MODIS surface reflectance data. The 2000 map covers the time period beginning on the 15th October 2000 and ending on the 15th October 2001, while the 2001 product covers the period between the 1st of January to the 31st December 2001. The difference in the temporal coverage of the input data used to create the two products is therefore only 77 days. Although the 2001 product is available at version 004 and has thus been validated and is ready for use in scientific publications, the 2000 map is only a version 003 product and therefore the quality may not be optimal (NASA 2001). Due to the lower version of the 2000 product and the overlap in the time period of the input data for the 2000 and 2001 land cover maps, only the 2001 product will be used in the current research.

The vegetation classes present in the study area and the percentage of each are displayed in Table 3.2. Savannas, water, woody savannas and grasslands account for over 80 percent of the land surface within the area of interest. The five main vegetation classes across the entire study area will be used as individual case studies for the purpose of the current research. These are deciduous broadleaf forests, open shrublands, grasslands, woody savannas and savannas which (along with water) contribute to 92.9 percent of the total area. A detailed definition of each of these classes is provided in Table 3.3, and their spatial distribution is displayed in Figure 3.2. There is a distinct north to south change in vegetation type over the area of interest. The majority of woody savannas and deciduous broadleaf forests are located in the north of the study site, giving way to savannas towards the southern half. Open shrublands and grasslands are predominantly located in the southwest along the coast, stretching further inland towards the south. A band of savanna vegetation interspersed with patches of woody savanna stretches across the southern half of the study area (Figure 3.2).

IGBP Class	Percent cover
Water	11.4
Evergreen Needleleaf Forests	0.1
Evergreen Broadleaf Forests	3.6
Deciduous Broadleaf Forests	5.1
Mixed Forests	0.3
Closed Shrublands	0.8
Open Shrublands	6.1
Woody Savannas	22.7
Savannas	41.1
Grasslands	6.5
Permanent Wetlands	0.1
Croplands	0.3
Urban and Built-up Lands	0.2
Cropland/Natural Vegetation Mosaics	0.6
Barren or Sparsely Vegetated	1.6

Table 3.2: Land cover characteristics of the study area

Vegetation type	IGBP description
Deciduous broadleaf forest	Lands dominated by woody vegetation with a percent cover greater than 60 percent. Height exceeds 2m. An annual cycle of leaf-on and leaf-off periods
Open shrublands	Lands with woody vegetation less than 2m tall with shrub canopy cover between 30 and 60 percent. The forest cover height exceeds 2m
Grasslands	Lands with herbaceous types of cover. Tree and shrub cover is less than 10 percent.
Woody savannas	Lands with herbaceous and other understory systems with forest canopy cover between 30 and 60 percent. The forest cover height exceeds 2m
Savannas	Lands with herbaceous and other understory systems with forest canopy cover between 10 and 30 percent. The forest cover height exceeds 2m

Table 3.3: Predominant vegetation types

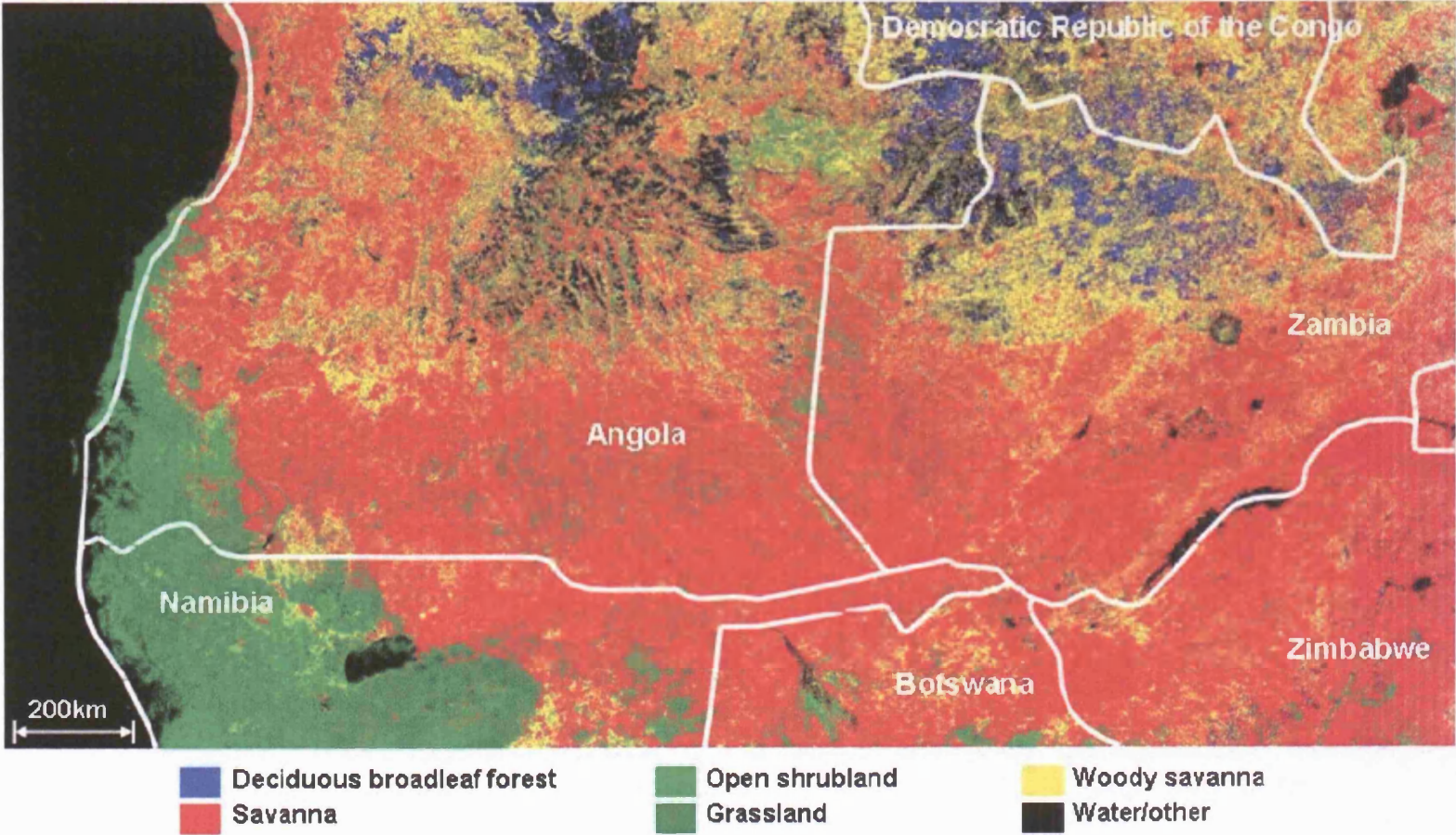


Figure 3.2: MODIS Landcover Product

3.4 Fire characteristics of southern Africa

MODIS active fire detections for the period March 2000 to December 2004 have been used to perform an initial characterisation of the occurrence of fire within the study area. At the time of writing no global or southern African burned area data set exists for the past five years. The only burned area products available for the region are the GBA2000 (Gregoire *et al.* 2003) and the GLOBSCAR (Simon *et al.* 2004) data sets, both of which only document global burned areas for the year 2000. The spatial and temporal locations of active fires as detected by MODIS provide the only account of fire activity in the study area over the past five years, and as such form an important companion and test data set in the examination of burned areas in this region over this period.

3.4.1 Thermal Anomalies

The MODIS fire products were designed with the aim of providing a global time series of fire data to the global change research community as well as for assisting in the formulation of land management schemes (Justice *et al.* 2002). In particular the products are aimed at supporting the modelling of trace gas and particulate emissions from biomass burning, and are a response to the growing demand for spatially detailed fire information needed to parameterize and validate various regional and global models (Kaufman and Justice 1998). The algorithm uses MODIS channel 21 ($3.929\mu m$ - $3.989\mu m$) which saturates at nearly 500K, and channel 22 ($3.929\mu m$ - $3.989\mu m$) which saturates at 331K. The identification of fires is based on their absolute detection if the fire produces enough heat, or their detection relative to the thermal emission of the surrounding pixels for smaller and/or cooler fires (Justice *et al.* 2002). A detailed description of the methodology has been provided in Section 2.4.1. The product is freely available to the public at various levels:

- Level 2
- Level 2G
- Level 3 8-Day Composite
- Level 3 8-Day Summary

The Level 2 product is the most basic and is used to create all of the higher order fire data sets. It is produced from data acquired during approximately five minutes of MODIS sensing and is stored in the MODIS orbit geometry (see Section 5.2.2). The Level 2G product details the daily location of potential fire pixels, while the Level 3 8-day product has eight days of daily 1km gridded data packaged into a single file for convenience. The Level 3 summary product provides a composite of all 1km gridded fire pixels detected within each 8 day period. All of the data sets are produced using daytime and nighttime data sensed by both the MODIS Terra and MODIS Aqua instruments. As the aim of the current research is to characterise the fire regime of the study area in as much detail as possible the Level 3 8-day composite product is used as it details daily (day and night) detections. In addition using a gridded product greatly facilitates comparisons between different MODIS data products at the same location.

3.4.2 The temporal distribution of fire activity

The southern Africa burn season coincides with the annual dry season which occurs between May and October, although this may vary from year to year. The timing of fire activity is important for a variety of reasons. In southern African savannas, for example, fires which occur earlier in the year when the vegetation moisture is high will have a lower combustion efficiency than burning which occurs later in the dry season, thereby emitting fewer emission products of complete combustion and more products of incomplete combustion. Results from a study in Zambia suggest that in comparison to late dry season fires, those which occur earlier in the dry season will emit at least three times more CH_4 and NMHC even though lower quantities of biomass are consumed (Hoffa *et al.* 1999). The implications of these results is that the vegetation moisture content at the time of the fire has the potential to alter the type and quantity of carbon emissions, and therefore Hoffa *et al.* (1999) have made the recommendation that the seasonal dynamics of fire regimes are included in global estimates of carbon flux. In addition the timing and intensity of the burning will determine the effect which it has on the vegetation and soil as well as on the rate of succession and regeneration of the vegetation, and is thus of importance in the management of these areas (Perez and Moreno 1998, Tansey *et al.* 2004b). The factors which determine the timing of the burn season are discussed in Section 3.2 and include meteorological conditions which affect the fuel loads available as well as the moisture content of these (Sousa 1984).

The total number of pixels detected as containing an active fire and documented in the MODIS (Terra) daily 1km Thermal Anomalies product is shown in Figure 3.3a, with the number of fires detected per month displayed as a percentage of the total number detected over each year in Figure 3.3b. Although the active fire data do not provide a comprehensive description of fire activity as only fires which are burning at the time of the satellite overpass have the potential to be identified, it does provide an indication of the annual distribution of fire occurrence in the study area over the five year period. During each of the five years of observations the annual

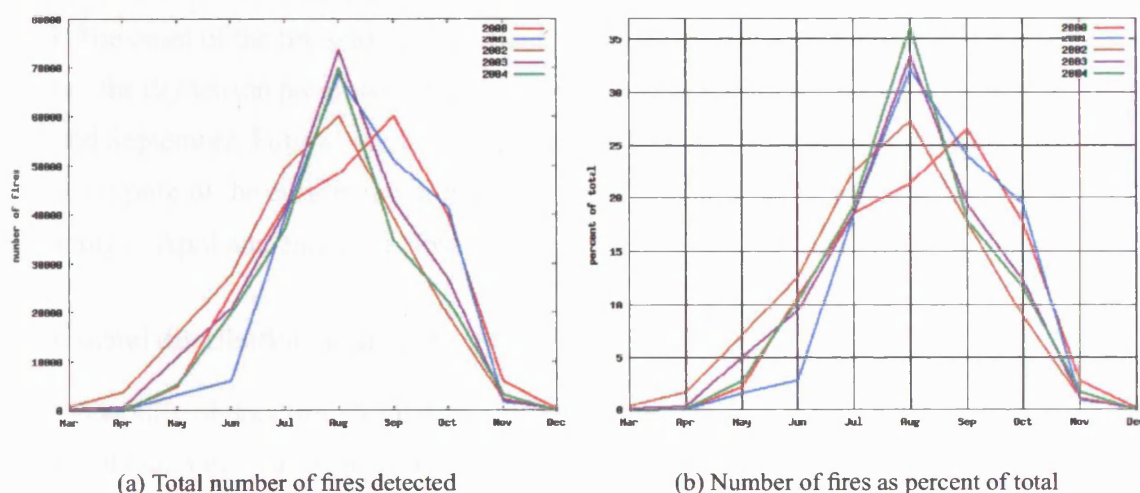


Figure 3.3: Fires detected by Terra MODIS, 2000 - 2004

peak of fire activity occurs between the beginning of August and the end of September, with over 25% of the total number of fires detected occurring during a single month at the peak of the burn season. During each of these five years over 95% of the active fires detected during each year occur between the beginning of April and the end of November. There appears to be more consistency in the end point of the burn season with the total number of fires falling to below 5% of the total after the end of October each year, than in the starting point, with a rise in fire detections to over 5% of the total occurring at some point between the beginning of May and the end of July.

Although many studies have characterised the temporal and spatial distribution of fires in Africa, the majority of these have tended to be at a continent scale and over a maximum of two

fire seasons. Cahoon *et al.* (1992) have used nighttime images from the Defense Meteorological Satellite Program (DMSP) for 1986 and 1987 for this purpose. The study shows very low fire activity in southern hemisphere Africa in April, with a rapid increase between March and June as drier conditions move south and eastwards. Fire is widespread in Angola, Zambia, southern Zaire and Zimbabwe by May. Between September and October fire frequency increases in eastern Africa and wanes in the western and interior nations, following the return of moist conditions to most of these areas during October. The same general trends were identified in a study by Dwyer *et al.* (2000) which used daily daytime 1km AVHRR data for the period April 1992 to December 1993. The onset of the fire season in southern hemisphere Africa was found to coincide with the onset of the dry season progressing from west to east with the peak of burning occurring between July and September. Following on from this information and the results contained in Figure 3.3, for the purpose of the current research the temporal extent of the burn season will be defined as beginning in April and ending in November.

The diurnal distribution of fire activity

The availability of data from MODIS Terra provides an insight into the temporal distribution of fire activity on a daily as well as an annual scale. The addition of MODIS Aqua fire detections (available from July 2002 onwards) to those from MODIS Terra allows an investigation to be performed into the diurnal nature of the fire activity during the annual fire season. This is possible due to the differences in the overpass time of the two satellites, with Terra crossing the equator twice daily at 10.30am and 10.30pm local time, and Aqua at 1.30pm and 1.30am local time. The number of fire pixels detected in the data acquired during the Terra and Aqua overpass over the two years that Aqua MODIS data have been available for the entire burn season at the time of writing are shown in Figure 3.4.

From the data contained in Figure 3.4 it is clear that for most months of the 2003 and 2004 fire seasons the number of fire detections is much higher in the data collected by MODIS Aqua than in that collected by MODIS Terra during the earlier overpass. This suggests that there is a strong diurnal pattern to the fire activity within the study area, with a much higher number of fires occurring later in the day at the time of the Aqua overpass. Although the study of Cahoon *et al.* (1992) found that contrary to their expectations there was no strong diurnal cycle in the frequency

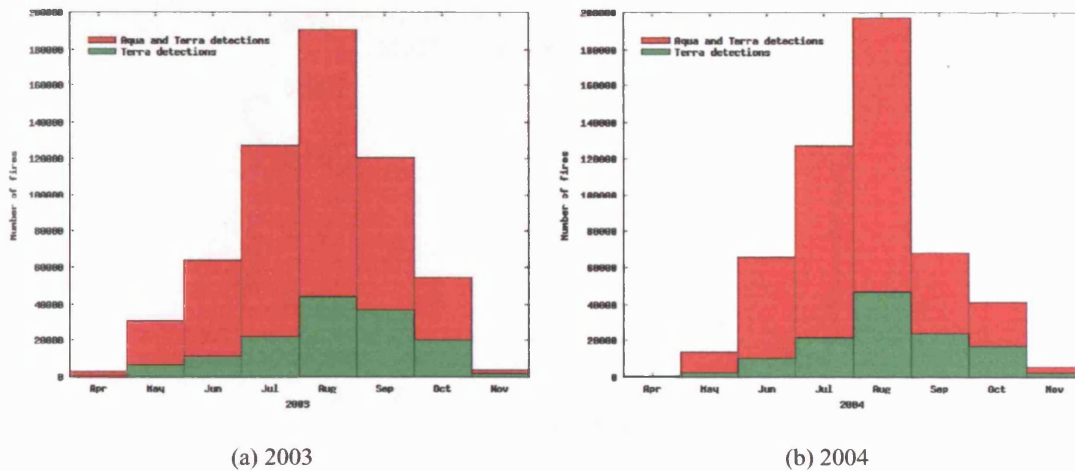


Figure 3.4: Active fire detections from MODIS Aqua and Terra: Monthly totals

of African fires which they attributed to the fact that most fires were left to burn uncontrolled, the diurnal nature of vegetation fires has been observed in several studies (Langaas 1993, Arino and Melinotte 1997, Justice *et al.* 2002). The typical form of the daily fire cycle is displayed in Figure 3.5 with a peak in activity observed in the afternoon. The data in Figure 3.5 express the diurnal fire cycle as a probability density function (PDF) for data derived for the 1999-2001 fire season in Borneo using TRMM VIRS observations, fitted with a Gaussian + cubic polynomial (Giglio and Pinzon 2003). Although the data are for Southeast Asia, they are representative of the diurnal burning cycle in most regions (*ibid*). The Equatorial overpass times of MODIS Terra and Aqua have been added for illustrative purposes. It has been suggested that this pattern of burning occurs due to several reasons which include the timing of human daily activity, the drying out of the ground and the decrease in vegetation moisture as the day progresses both of which encourage flaming, and the presence of stronger winds in the afternoon which result in the faster movement of the fires (Kennedy *et al.* 1994, Arino and Melinotte 1997).

An examination of the daily MODIS observations for the five years suggests however that this diurnal pattern in fire activity is not uniform across the annual burn season. This is evident from Figure 3.6 which displays the difference in the number of fires detected by MODIS Terra and MODIS Aqua each month as a percentage of the total detected each month. A greater proportion

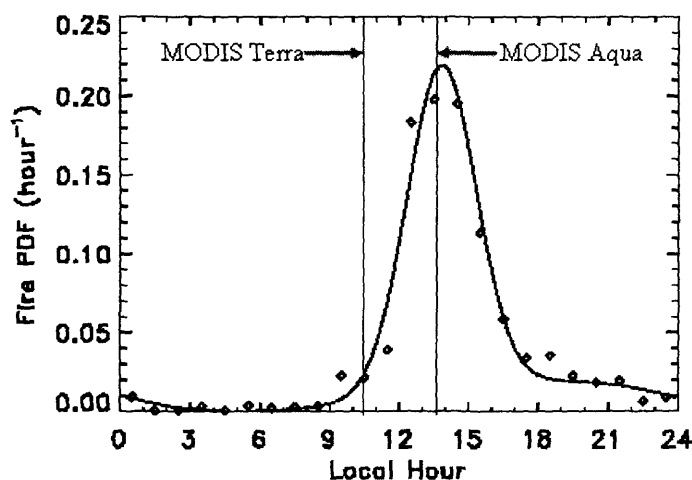
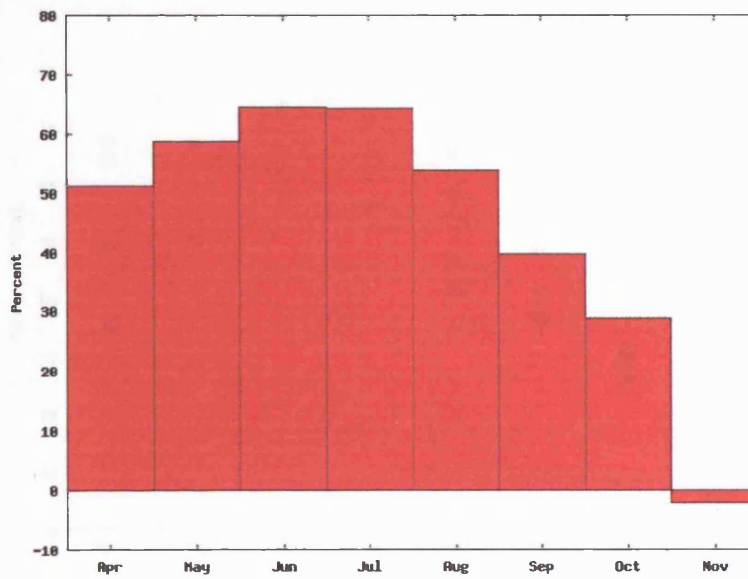


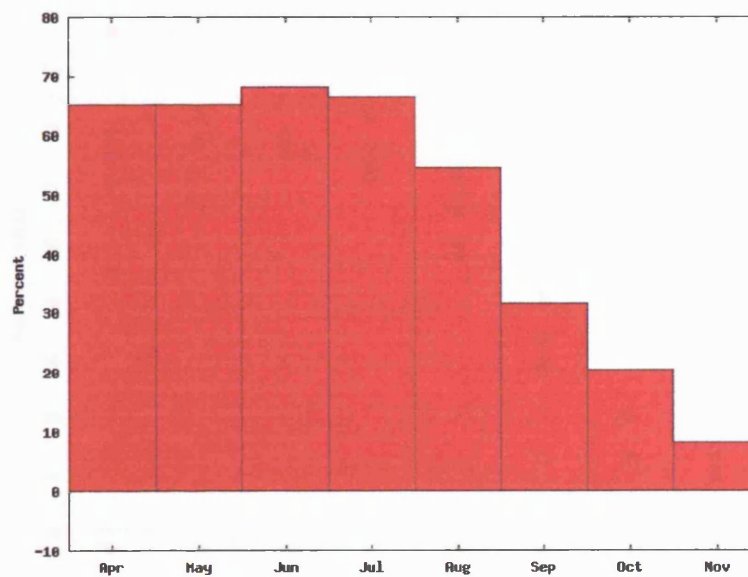
Figure 3.5: Typical diurnal burn cycle, Adapted from: Giglio and Pinzon (2003)

of the total number of fires detected start later in the day at the peak of the fire season, with 64.4 and 68 percent more fires detected in the afternoon during July 2003 and 2004. Later in the year towards the end of the fire season the proportion of fires detected in the afternoon decreases but is still substantially larger than the number of fires occurring earlier in the day, with over 30 percent more fires detected by the Aqua overpass during October in both 2003 and 2004. The increase in the proportion of fires detected in the afternoon at the peak of the burn season may be due to the fact that fires which persist for several days have been shown to exhibit a diurnal cycle as they tend to burn strongly during the afternoons and then die down at night (Belward *et al.* 1994), as well as due to the drier and more favourable meteorological conditions (Kennedy *et al.* 1994).

The difference between the number of fires detected by MODIS Aqua and Terra for each of the five main cover types in the study area (see Tables 3.2 and 3.3) is displayed in Figure 3.7 as a proportion of the total number of fires detected in each cover type each month. The pattern is very similar for both years between May and October, with a higher percentage of the total fires detected in deciduous broadleaf forest detected during the afternoon overpass, and the lowest proportions of afternoon burning occurring in grasslands or savannas for most months of the burn season. The two months at the tails of the fire season (April and November) exhibit much more variability in the proportional difference of fire occurrence within each vegetation class. In November 2003 a higher proportion of fires occurring in savanna, woody savanna and open shrubland are detected in the morning overpass, while in 2004 this is the case for detections

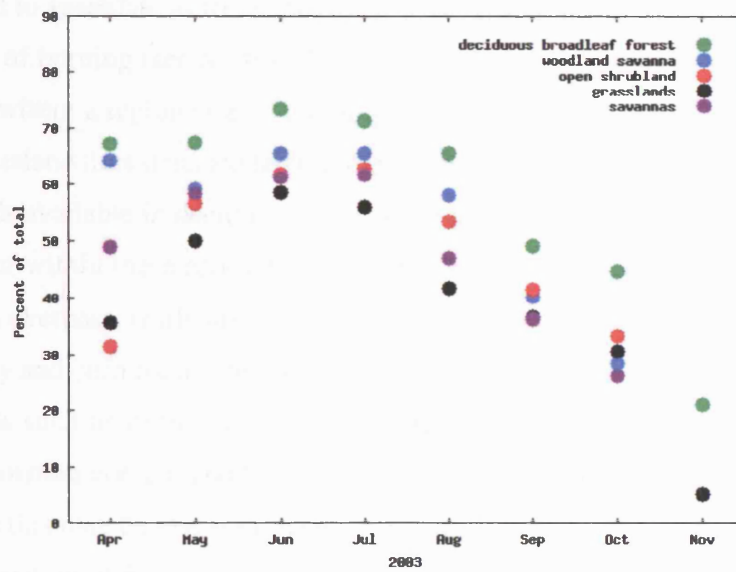


(a) 2003

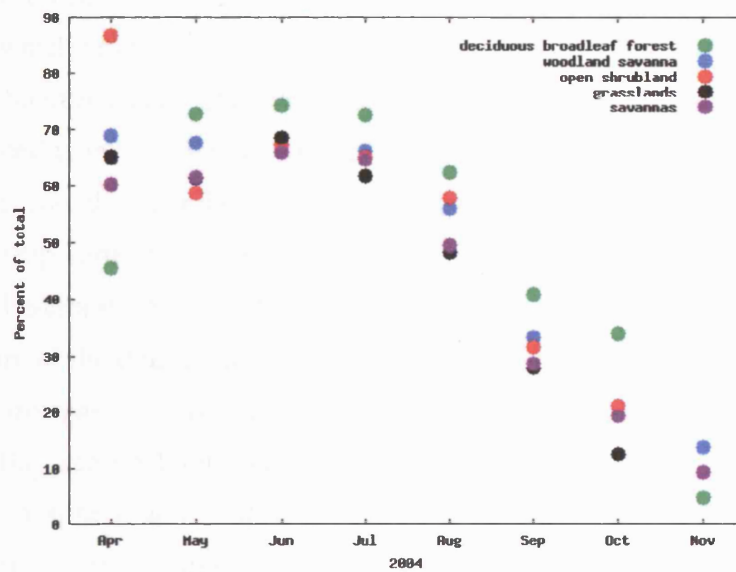


(b) 2004

Figure 3.6: The difference in the number of fires detected by Aqua and Terra as a proportion of the total



(a) 2003



(b) 2004

Figure 3.7: The difference in the number of fires detected by Terra and Aqua as a proportion of the total detected in each cover type

within open shrubland and grassland classes. The reasons for these observations are unknown and it is difficult to speculate as to the possible causes due to the number of factors which influence the timing of burning (see Section 3.2) and the subsequent complexity of the fire characteristics exhibited within a region or ecosystem type. A possible factor for the lower proportion of savanna and grassland fires detected later in the day however is the fire rate of spread. Due to the greater fuel loads available in deciduous broadleaf and woody savanna ecosystems for example, fires which occur within these ecosystems burn for longer increasing their chances of detection by the afternoon overpass, while fires which occur within grassland and savanna ecosystems tend to spread quickly and burn for a short period (Van der Werf *et al.* 2003). In addition classes with higher fuel loads such as deciduous broadleaf forests and woody savannas the vegetation will have a higher moisture content and therefore may be more likely to burn later in the day as this decreases, while this may be less significant for vegetation types such as savanna and grasslands.

The diurnal pattern of fire activity described above and displayed in Figures 3.4, 3.5 and 3.6 has implications for studies which have used satellite observed fire counts to scale between active fires and the area burned (Eva and Lambin 1998a, Pereira and Setzer 1996, Scholes *et al.* 1996a), as well as those which have used active fire detections to derive information such as aerosol distribution (Ji and Stocker 2002). The relationship between MODIS (Terra and Aqua) fire counts and the area burned is investigated in Chapter 6. Studies which have attempted to achieve the former have either found weak relationships between fire counts and burned areas, or alternately that this relationship varies temporally and spatially as a function of individual fire events or ecosystem type (Pereira and Setzer 1996, Scholes *et al.* 1996a). In addition to the recognition of the variable nature of the diurnal fire activity over the annual fire season it is necessary to take into account the overpass time of the sensor. The study of Ji and Stocker (2002) for example has investigated the “seasonal, intraseasonal and interannual variability of global land fires and their effects on atmospheric aerosol distribution”, with the conclusion that vegetation fires in the tropics and sub-tropics exhibit significant intraseasonal oscillations. However as highlighted by Giglio and Pinzon (2003) the fire data used in this study has been acquired by the TRMM-VIRS satellite whose local overpass time drifts significantly each day, in order to allow for complete sampling of the diurnal rainfall cycle. The fire information used by Ji and Stocker (2002) has been constructed from five day composites of TRMM data, without taking into account the diurnal pattern of fire activity and the orbital shifts in the TRMM overpass time during the five days.

As a result Giglio and Pinzon (2003) have shown that the intraseasonal oscillations identified by Ji and Stocker (2002) are an artefact of the compositing strategy used in the study, and suggest that these sampling induced periodicities may be averaged-out through the use of an appropriate latitude-dependent average interval based on the TRMM orbital characteristics.

Phenology of the vegetation

The phenological state of the vegetation at the time of burning will determine not only the fuel loads available, the moisture content of these and thus the severity of the fire, but it will also determine the ability of the vegetation to recover after the fire. Fire severity has been shown to impact the regeneration of the vegetation as well as the species abundance and composition of the post fire ecosystem (Wang and Kevin 2005). In particular fires which occur early in the dry season will be less destructive to savanna vegetation than fires which occur later in the dry season (Stromgaard 1992, Eva and Lambin 1998a). As discussed above the southern Africa fire season follows the onset of the dry season and is brought to a halt by the return of the rains (Cahoon *et al.* 1992). The phenology of the vegetation within the study area is investigated using the MODIS Enhanced Vegetation Index (EVI) product (Huete *et al.* 1999). The EVI is a vegetation index which has been formulated using isolines in red/near-infrared space which have been designed to approximate vegetation biophysical isolines derived from radiative transfer theory as well as observed biophysical relationships. The EVI is described in Equation 3.1;

$$EVI = G \times \frac{\rho_{nir} - \rho_{red}}{\rho_{nir} + C_1 \times \rho_{red} - C_2 \times \rho_{blue} + L} \quad (3.1)$$

where ρ_{nir} , ρ_{red} and ρ_{blue} are the near infrared, red and blue reflectances, C_1 and C_2 are atmosphere resistant correction coefficients in the red and blue waveband, L is a canopy background brightness correction factor, and G is a gain factor. The MODIS EVI product is available every 16 days at a spatial resolution of 250m, 500m or 1km. The advantages of using this enhanced index over the conventional NDVI include (i) reduction in atmospheric influences due to the use of the more atmosphere-sensitive blue band to correct the red band (ii) insensitivity to most canopy backgrounds through the use of factor L and (iii) sensitivity to high biomass regions (*ibid*).

In order to characterise the temporal profile of the vegetation growth and senescence during the annual burn season mean EVI profiles have been calculated across the area of interest for

each of the five years of observation. The annual profiles for deciduous broadleaf forests and grasslands are displayed in Figure 3.8. These two cover types have been chosen to illustrate the phenological trends over the study area as they encompass the full range of variability. Of the five main vegetation classes (see Table 3.3) deciduous broadleaf forests exhibit the highest and greatest changes in EVI values each year, while grasslands vary the least and have the lowest mean EVI values. It is apparent from these data that the phenology of both types of vegetation

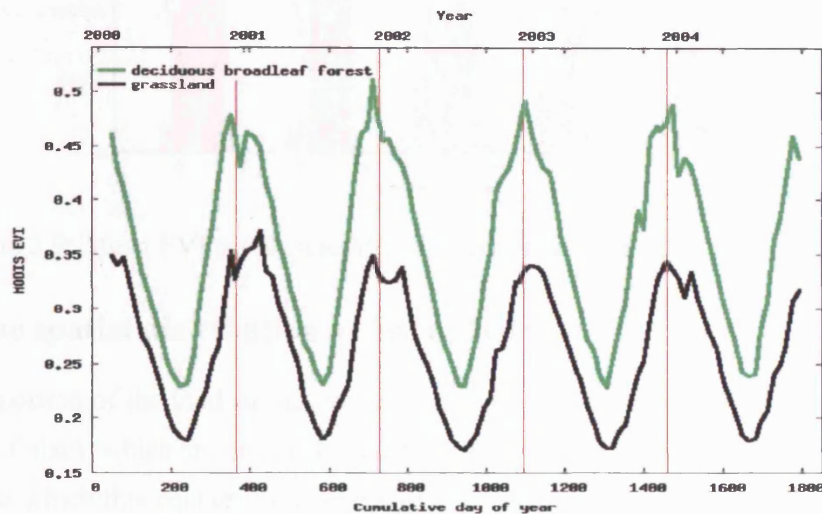


Figure 3.8: Phenology of deciduous broadleaf forest and grasslands, 2000-2004

follow similar trends from year to year, with little variation in the minimum and maximum EVI values or their seasonal distributions over the five year period. The growth cycle of the vegetation within the study area tends to reach a peak between December and January during each of the five years of observations. Over the following six to seven months the vegetation senesces and is at its driest between August and September each year. The relationship between vegetation senescence and the occurrence of fires is evident from Figure 3.9 which displays the total number of active fires detected each month over the five year period by the Terra satellite, as well as the mean EVI calculated over the study area. The temporal distribution of fires follows the vegetation growth cycle, with the peak of the fire season corresponding to the height of the dry season. This inverse relationship between the EVI and the number of fires detected is evident for each of the five years of observation.

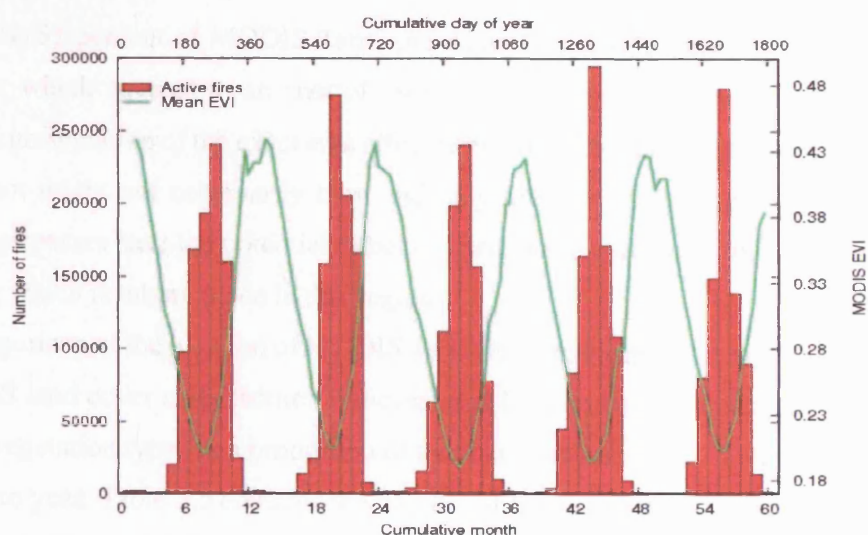


Figure 3.9: Mean EVI profile and MODIS Terra active fire detections, 2000-2004

3.4.3 The spatial distribution of fire activity

A large proportion of the land surface within the study area is affected by fire each year. The percentage of pixels which are detected as containing an active fire during the past five years and the land area which this equates to (assuming the entire 1km by 1km pixel burns) is shown in Table 3.4. As the Aqua satellite was not launched until May 2002 the first annual burn season for which an entire MODIS Aqua data set is available is 2003. The figures in Table 3.4 indicate the total number of pixels detected as containing a hotspot at some point during each year - if a pixel burns more than once during the year, or is recorded as a fire in both the Terra and Aqua products it is only counted as a single fire event.

Year	MODIS Terra		MODIS Aqua and Terra	
	Percentage of total area	Land area (million ha)	Percentage of total area	Land area (million ha)
2000	8.9	22.6	N/A	N/A
2001	8.4	21.3	N/A	N/A
2002	8.6	22.0	N/A	N/A
2003	8.6	22.0	31.1	79.4
2004	7.6	19.3	31.0	79.1

Table 3.4: Percent and area of land surface on fire

In 2004, 31 percent of MODIS Terra and Aqua 1km pixels were detected as containing an active fire, which equates to an area of 79 million hectares. Although this is not an entirely accurate representation of the exact area affected by fire as the entire 1km² area of a pixel detected as a hotspot might not necessarily burn and only fires which coincide with the timing of the satellite overpasses have the potential to be detected, it does provide some indication of the scale of burning which is taking place in this region.

A comparison of the location of MODIS Terra fire detections for each of the five years against the MODIS land cover classification indicates that the number of fires occurring in each of the five main vegetation types as a proportion of the total number of fires remains relatively constant from year to year. Table 3.5 contains the number of fire pixels detected in each of the five main vegetation classes present in the study area, as a percentage of the total number of pixels for each cover class. Fire activity is greatest in areas of savanna, with between 10.8 and 11.3 percent of savanna pixels detected as containing a fire each year, and lowest in areas of open shrubland.

Vegetation Type	2000	2001	2002	2003	2004
Savanna	11.2	10.8	11.3	11.3	11.2
Deciduous broadleaf forest	9.9	9.7	9.3	9.5	9.7
Woody savanna	8.6	8.2	8.1	8.4	8.2
Grassland	5.1	4.2	4.8	4.8	4.7
Open shrubland	4.2	3.5	3.4	3.6	3.5

Table 3.5: Proportion of cover type detected as fire

Similar patterns of burning have been found by Dwyer *et al.* (2000) who investigated the global spatial and temporal distribution of active fires using twenty months (April 1992 to December 1993) of 1km AVHRR data. Savanna fires were found to be predominant and accounted for the largest proportion of pixels containing fires. However when calculated as a percentage of the total vegetation cover, deciduous broadleaf forests exhibited the highest burning with 78% of the total fires identified occurring within this cover class in comparison to only 27% in savannas. The reasons for the greater proportion of active fires observed within deciduous forests during this study is unknown, but may be due to the lower quantities of this cover type within the current study area in comparison to the larger southern Africa region used in the Dwyer *et al.* (2000) study.

3.5 The spectral characteristics of burned and unburned surfaces

The aim of this section is to review the research relating to the spectral properties of fire affected surfaces in order to identify the nature of, to quantify, and to attempt to explain the spectral changes which occur as a result of the transition of the surface from pre-burn to post-burn conditions. This will be achieved through;

1. A review of the spectral response of burned surfaces as described in the literature
2. An examination of ground-based spectral data of pre-fire and post fire surfaces collected in the field
3. An examination of the effect of fire on the first seven MODIS land surface reflectance wavebands

The identification of an area within a remote sensing image which has been affected by fire relies on the assumption that the occurrence of the fire has altered the radiometric properties of the surface in some way, and that this change has some degree of temporal persistence. Burned area mapping methodologies to date have almost exclusively exploited changes in the spectral response of the land surface as a means of identify burning (see Chapter 2). The magnitude and the persistence of any fire induced changes in the remote sensing signal (which will be referred to as the “burn signal”) will be dependent on the extent to which the properties of the surface have been altered by the fire. This in turn is a function of the characteristics of the fire itself as well as the vegetation type, and the condition of the vegetation prior to burning, and will therefore vary temporally as well as spatially. The occurrence of fire typically results in the alteration of the vegetation structure through the partial or total destruction of the vegetated layer, the deposition of charcoal and ash, and the exposure of the underlying soil surface. The nature of any residues left by the fire and the length of time for which they are present (which will be dependent on the post fire climatic conditions) will also determine the temporal persistence and the magnitude of any changes in the remote sensing signal. Although the post fire presence of char, a carbon residue of partially combusted vegetation and the most abundant post fire residue provides a large contrast with brighter unburned vegetation, its presence may be shortlived as it may be removed

rapidly by the wind exposing the underlying soil surface (Trigg and Flasse 2000, Govaerts *et al.* 2002). An understanding of the spectral nature as well as the temporal persistence of the burn signal is necessary in order to select the most appropriate wavebands for the detection of fire affected areas from remotely sensed data.

3.5.1 Field-based spectral measurements

A ground-based spectral data set collected by Smith (2004) in an area of savanna within the current area of interest will be used as a companion example for the following discussion. The study site was located within the Chobe National Park in north-eastern Botswana, as indicated by the blue box in Figure 3.10.



Figure 3.10: Location of the field study site (Smith 2004)

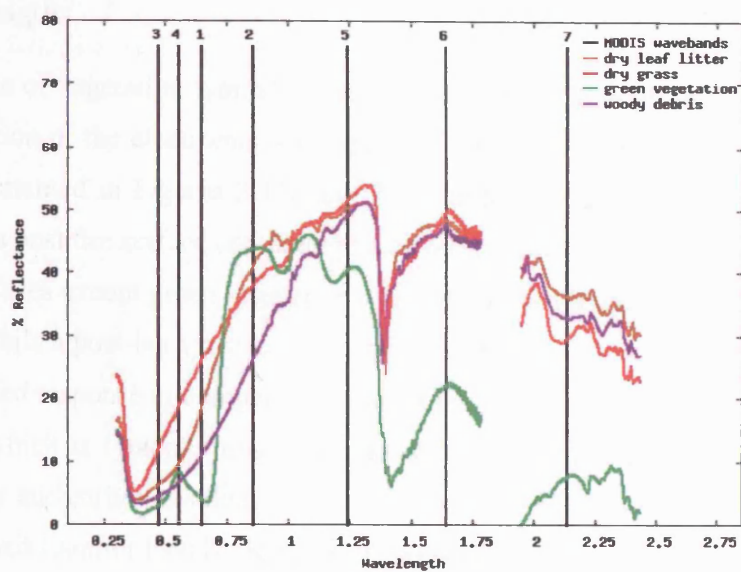
The data set was collected using a GER-3700 spectroradiometer to measure the reflectance from a series of burned and unburned savanna surfaces. The characteristics of the GER-3700 instrument are detailed in Table 3.6 (GER 2000). The data were acquired by mounting the spectroradiometer

on a tripod at a height of approximately 0.75m directly above the surface, with each individual spectra recorded consisting of a mean of eight measurements sampled over five seconds. The experimental plots were located specifically in areas where the individual surface components entirely filled the field of view of the instrument. Three such measurements were collected within each plot with a distance of a few centimetres between them in order to minimise the occurrence of small scale variations in the surface reflectance (*ibid*).

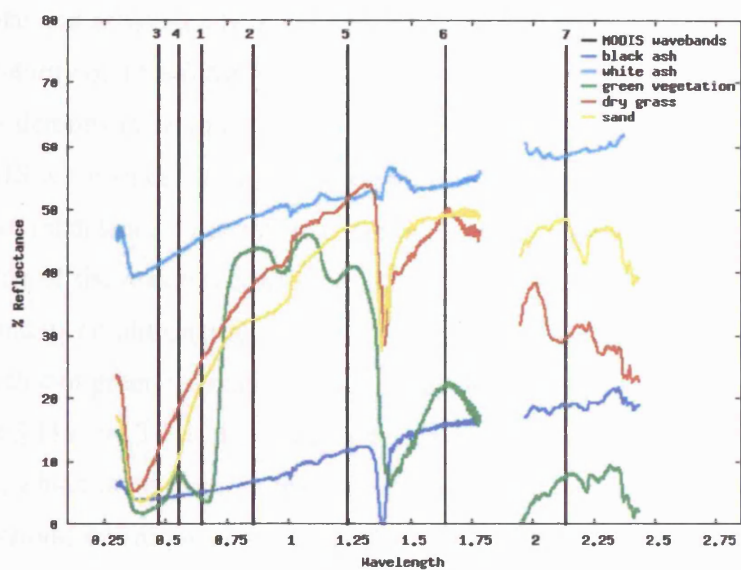
Spectral range	350nm to 2500nm
Channels	704
Bandwidth	1.5nm: 350nm to 1050nm 6.5nm: 1050nm to 1900nm 9.5nm: 1900nm to 2500nm
Field of view	3 degrees
Digitisation	16 bit
Radiometric calibration accuracy	400nm: 5% 700nm: 4% 1000nm: 5% 2200nm: 7%
Spectral resolution	0.3nm: 350nm to 1050nm 1.1nm: 1050nm to 1090nm 1.6nm: 1090nm to 2050

Table 3.6: Properties of the GER 3700 spectroradiometer (GER 2000)

Preprocessing of the measured radiance requires normalisation of the data using a spectralon reference panel which has a known reflectance at each waveband. The reflectance spectra were subsequently interpolated to 1nm intervals and a mean of all measurements from each experimental plot calculated. These data are displayed in Figures 3.11a (unburned classes) and 3.11b (burned and unburned classes). The central wavelength of each of the first seven MODIS land surface reflectance wavebands are also shown for reference. The unburned surfaces include Kalahari sands, green vegetation, senesced grasses, senesced leaf litter, and woody debris, while the burned surfaces contained either white or black ash. It should be noted that measurements below $0.35\mu m$ are not reliable as this region lies outside the prescribed spectral range of the GER-3700, and an increase in sensor noise occurs between $1.4 - 1.8\mu m$ as well as at wavelengths longer than $2.2\mu m$ (Smith 2004).



(a) Unburned surfaces



(b) Burned and unburned surfaces

Figure 3.11: The spectral characteristics of savanna surfaces

3.5.2 Fire induced spectral change

Visible wavelengths

The combustion of vegetation typically results in a decrease in reflectance at all wavebands in the visible portion of the electromagnetic spectrum (Stroppiana *et al.* 2002, Roy *et al.* 2002). The spectra contained in Figures 3.11a and 3.11b indicate that at visible wavelengths the reflectance from a post fire surface containing black ash is lower or of a similar magnitude to all of the pre-fire surfaces except green vegetation which exhibits a lower reflectance at red and green wavelengths, while a post-burn surface containing predominantly white ash demonstrates a substantially elevated response in comparison to all of the measured pre-fire surfaces. The decrease in reflectance which is typically observed immediately after a fire has been explained by the presence of char and carbon residues which result in a darkening of the surface and a reduction in albedo (Eva and Lambin 1998b). Research however has indicated that visible wavebands tend to be much less sensitive to fire induced changes than infrared wavebands (Razafimpanilo *et al.* 1995, Silva *et al.* 2004, Stroppiana *et al.* 2003), and in addition are much more sensitive to the presence of smoke and aerosols which are emitted by the fire (Miura *et al.* 1998). An examination of the separability of 15000 MODIS 500m pixels across an area of southern Africa by Roy *et al.* (2002) has demonstrated that although burning reduces the mean reflectance of all of the first seven MODIS wavebands, at visible wavelengths the difference between the mean pre-fire and mean post fire reflectance values were small in comparison to their standard deviations.

The magnitude of the spectral change at all visible wavelengths is dependent on both the vegetation type and its condition prior to the fire. The reflectance of senescent vegetation tends to be higher than that of green vegetation although this will vary with vegetation type, as demonstrated in Figures 3.11a and 3.11b. In southern Africa the peak of fire activity occurs at the height of the dry season, which is the point in the phenological cycle of herbaceous vegetation (such as grassland and savanna) where the above-ground plant sections are dead and dry (Govaerts *et al.* 2002). The change from bright dry grass to darker burned surface typically results in a decrease in reflectance at all wavelengths in the range $0.25\mu\text{m}$ to $4\mu\text{m}$ spectral range, which includes MODIS bands 1-7 (Govaerts *et al.* 2002, Stroppiana *et al.* 2003). In contrast the magnitude of the burn signal is smaller in forest and shrubland ecosystems where the above ground vegetation is live and green with a lower reflectance in the red spectral region than that of dry grass.

This is exhibited by the measured spectra displayed in Figure 3.11a, where the reflectance of dry grass is significantly lower than that of green vegetation in the red waveband (MODIS band 1). This results in a lower contrast between the pre-fire vegetative and the post fire charred surface (Govaerts *et al.* 2002, Stroppiana *et al.* 2003).

Near to mid-infrared wavelengths

The occurrence of fire typically results in a decrease in surface reflectance at near-infrared to mid-infrared wavelengths (Zhan *et al.* 2003, Roy *et al.* 2005b). Although the presence of white ash (Figure 3.11b) suggests an increase in reflectance immediately after burning within all of the measured cover types, this is likely to be short-lived as the ash will be removed rapidly by meteorological factors revealing charred remains of the vegetation and the underlying soil surface. The lower reflectance in this spectral region of the post-burn (black ash) surfaces measured in the field in comparison to all of the pre-burn surfaces is apparent in Figures 3.11a and 3.11b. In the presence of green vegetation this decrease occurs at near to mid-infrared wavelengths due to the removal of the photosynthetically active material as the vegetation burns, as this is brighter than the post fire surface which in contrast exhibits low reflectance values due to the absorption of the radiation by char and ash (Eva and Lambin 1998a). In addition at this spectral range the reflectance of senescent vegetation is typically higher than that of green vegetation, and the reflectance of burned areas is generally lower than that of senescent vegetation (Figures 3.11a and 3.11b), resulting in a large change between a pre-fire surface containing dry vegetation and the subsequent post fire charred surface (Brustet *et al.* 1991, Pereira and Setzer 1993, Eva and Lambin 1998a).

The magnitude of the change at near-infrared to mid-infrared wavelengths will therefore be a function of both the condition of the vegetation prior to the fire as well as the vegetation type (Govaerts *et al.* 2002). Research indicates that in general the reflective portion of the infrared region of the electromagnetic spectrum provides the best separability between burned and unburned vegetation (Koutsias and Karteris 1998, Trigg and Flasse 2000, Trigg and Flasse 2001), and in particular for southern African savanna ecosystems MODIS wavebands in this spectral region (bands 2, 5 and 6) provide the highest separation between burned and unburned pixels (Roy *et al.* 2002, Sa *et al.* 2003). An investigation into the spectral response of burned

surfaces in south-eastern Africa, the Iberian Peninsula, and Siberia by Silva *et al.* (2004) has indicated that only the near-infrared decreases after burning in all land cover types, while the response at middle infrared ($1.58\mu m$ - $1.74\mu m$) wavelengths is dependent on the land cover type. A decrease in the spectral response at middle infrared wavelengths was consistently observed over areas of grassland and cropland, while over forest and woodland areas the response was more variable and either decreased or increased immediately after the fire (*ibid*). Although a decrease in the signal might be expected immediately after the fire due to the strong absorption of middle infrared radiation by charcoal (Fraser and Li 2002), this response may be a function of the combustion completeness as well as the phenological state of the vegetation prior to the fire (Roy *et al.* 1999). If the vegetation is senescing at the time of the fire the combustion completeness will be high, resulting in large amounts of burn residue which will contribute to a significant decrease in reflectance at middle infrared wavelengths, whereas the burning of green vegetation will exhibit lower levels of combustion completeness and a rise in the middle infrared reflectance due to a decrease in the water content of the vegetation as a result of the fire (Silva *et al.* 2004).

Longwave-infrared wavelengths

Although MODIS band 7 ($2.105\mu m$ - $2.155\mu m$) reflectances have generally been found to decrease as a result of fire (Trigg and Flasse 2000, Roy *et al.* 2002), the magnitude of the change which occurs at this spectral region is small and provides less discrimination between pre-fire and post fire surfaces than at shorter infrared wavelengths (Sa *et al.* 2003, Roy *et al.* 2005b). An examination of the measured spectra displayed in Figures 3.11a and 3.11b suggests that for senesced vegetation this occurs due to higher reflectance from post fire surfaces (black ash) at longer infrared wavelengths than at shorter infrared wavelengths, while conversely the reflectance of dry vegetation is lower at longwave infrared than at near-infrared and mid-infrared wavelengths. These characteristics result in a spectral change of lower magnitude from pre-fire to post fire conditions at MODIS band 7 wavelengths in comparison to that which occurs within the spectral regions occupied by bands 2, 5 and 6. However the data displayed in Figures 3.11a and 3.11b indicate a different pattern for green vegetation, with a lower reflectance exhibited by this surface in contrast to that of the black ash. This would result in an increase in MODIS band 7

reflectances due to the occurrence of fire in areas with photosynthetically active material. This is supported by a study of burned surfaces using Landsat TM data which demonstrated an increase in post fire reflectances at this spectral range, which the authors suggest is due to a decrease in the vegetation moisture content as a result of the fire (Pereira 1999). In addition a characterisation of the spectral evolution of post fire savanna surfaces using field spectroradiometry has shown that the direction and magnitude of the post-burn change is not only small but also extremely variable between $2.05\mu m$ and $2.25\mu m$, as although the reflectance at this wavelength decreases initially immediately after the occurrence of a fire it rises quickly and remains higher than pre-fire levels for several weeks (Trigg and Flasse 2000). Stroppiana *et al.* (2000) have also observed an increase in post fire savanna reflectances at $2.2\mu m$ compared to the surrounding unburned vegetation, however it is suggested that this is due to the removal of senesced plant material which has a low spectral response, and the exposure of the underlying soil surface which exhibits a higher reflectance in this spectral region.

3.5.3 Perturbing factors

For any change detection scheme to be effective, it is necessary to use wavebands which exhibit sensitivity to the changes of interest. While the change from pre-fire to post fire surface conditions may exhibit a distinct spectral response, this response may not necessarily be specific to biomass burning and other changes may be characterised by similar spectral changes. An understanding of the nature of these ‘perturbing factors’ which may confuse the burn signal is important as if they are not taken into account high errors of commission may occur due to the false detection of fire affected areas (Trigg and Flasse 2001).

Burned surfaces are characterised by the removal of the vegetative layer and the exposure of the underlying soil surface, resulting in a decrease in near to mid-infrared wavelengths. Similar changes may however occur due to vegetation senescence, harvesting or pests (Roy *et al.* 2005b). Events not associated with the removal or decrease in vegetation such as snow melt and flooding may also result in a decrease in reflectance in the near and middle infrared (MODIS bands 2,5 and 6), thereby confusing the identification of fire induced change (*ibid*). Confusion may also arise between burned areas and water bodies or moist vegetation as all have low reflectance in the shortwave infrared (Pereira and Setzer 1993, Razafimpanilo *et al.* 1995, Eva and Lambin 1998a).

In addition variations in the pre-fire surface due to factors such as differing photosynthetic states or types of vegetation within an area of interest may cause significant perturbations (Trigg *et al.* 2005). The success of a change detection algorithm will be influenced by the magnitude of the spectral change which occurs due to the changes of interest, and the wavebands used to identify this change. The effect of burning on the seven MODIS land surface reflectance wavebands is therefore investigated in the following paragraphs.

3.6 The MODIS burn signal

In order to quantify the magnitude of the changes which occur due to burning in each of the spectral regions occupied by the first seven MODIS land surface reflectance wavebands, the fire induced spectral change and the separability of the MODIS pre-fire and post fire spectral signal has been examined. This is necessary in order to determine the ability of each of the wavebands to discriminate between surfaces which have been affected by fire and those which have not, as a means of characterising the burn signal and to aid the selection of the most appropriate wavebands with which to identify burned areas. It is noted that while the reflective component of the middle infrared may provide useful information in the separation of burned from unburned surfaces, this product is not used in the current study as it is still experimental (Peticolin and Vermote 2002).

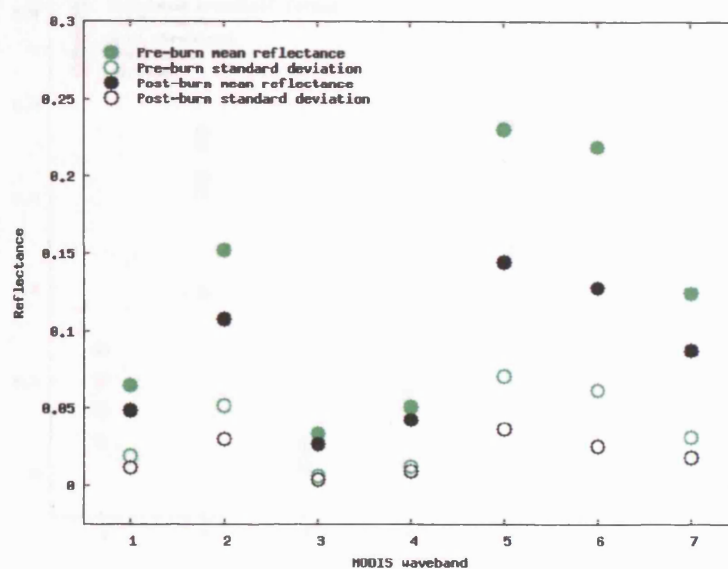
The MODIS data set used for this purpose contains pre-fire and post fire reflectances for each of the land surface channels (bands 1-7). Data have been examined for the four days preceding the fire and the four days preceding the day of the fire as documented in the MODIS Thermal Anomalies product, with the observation closest to the day of the fire which is cloudfree and acquired with a view zenith angle of $\pm 10^\circ$ selected. Although the exclusion of off nadir and cloudy pixels decreases the number of available samples by approximately 40%, this approach has been followed as the aim of this section is to identify the wavebands which will afford the highest separation between burned and unburned areas. The inclusion of directional effects will decrease the burned-unburned separability of the data making it harder to identify the most suitable wavebands with which to detect burn type changes. This is demonstrated by the data displayed in Figure 3.12. Figure 3.12a shows the mean reflectance for a single pixel calculated

from the daily reflectances for the seven days preceding (pre burn) and the seven days following (post burn) the occurrence of a fire as well as the standard deviations of these data, for each of the seven MODIS land surface reflectance wavebands. The difference between the mean burned and the mean unburned reflectances is of a comparable magnitude to the standard deviations of the observations at all wavelengths, and thus the magnitude of the change from pre burn to post burn conditions is within the variance of the data prior to the fire event. Figure 3.12b shows the individual band 5 reflectances for the seven days either side of the fire as a function of the viewing zenith angle at which they were acquired. The effects which variations in the viewing angle have on the magnitude of the mid-infrared reflectances is clearly evident, and are of the same order of magnitude as the burn signal.

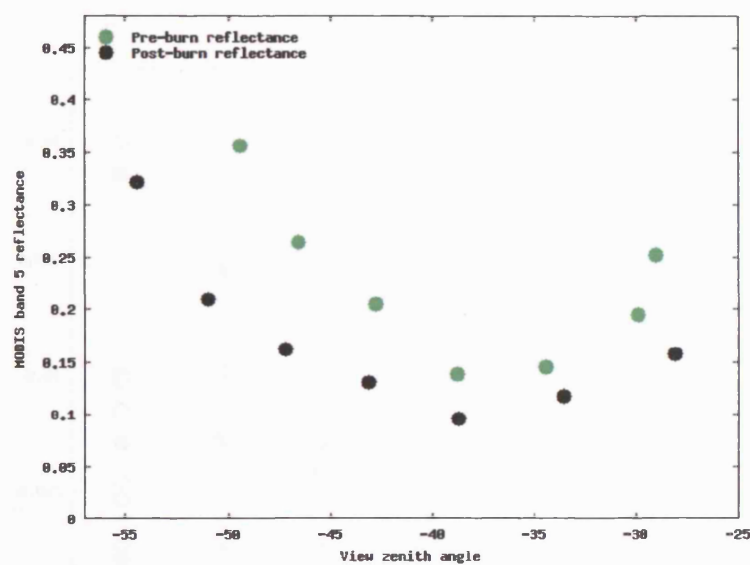
The data set used to investigate the burned-unburned separability consists of 5000 observations selected at random and according to the criteria described above for the five main cover types for the 2001 burn season. The separability of the data are examined using the measure defined in Equation 3.2;

$$M(\lambda) = \left(\frac{\rho_{post} - \rho_{pre}}{\sqrt{\sigma_{post}^2 + \sigma_{pre}^2}} \right) \quad (3.2)$$

where ρ_{post} and ρ_{pre} are the post burn and pre burn reflectances selected according to the criteria described above, and σ_{post} and σ_{pre} are the standard deviation of these data. This measure (M) thus provides an indication of the magnitude of the change in reflectance which occurs at each band normalised by the standard deviation of the data and is used to quantify the burned-unburned separability of the data as it is essentially the same as the quantity which is used to locate fire induced spectral change in the change detection model introduced in Section 4.5. The mean values of $M(\lambda)$ for each vegetation type are displayed in Figure 3.13, and the standard deviations of the data in Figure 3.14. As discussed in Section 3.5 the burned and unburned reflectances are expected to have a higher separability at near-infrared and mid-infrared wavelengths. This is exhibited by the data contained in Figure 3.13, with MODIS bands 2, 5 and 6 indicating higher burned-unburned separabilities for all five vegetation classes than the remaining four wavebands, although the separability values at bands 2, 5 and 6 are still low. The effect of burning is a decrease in reflectance for all classes and at all MODIS land surface reflectance wavebands.



(a) Summary statistics



(b) Directional effects

Figure 3.12: MODIS burned and unburned reflectances

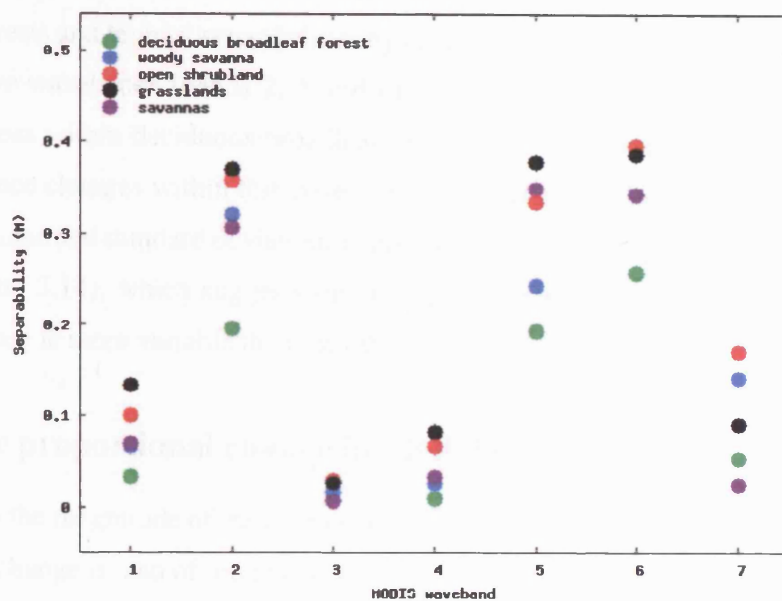
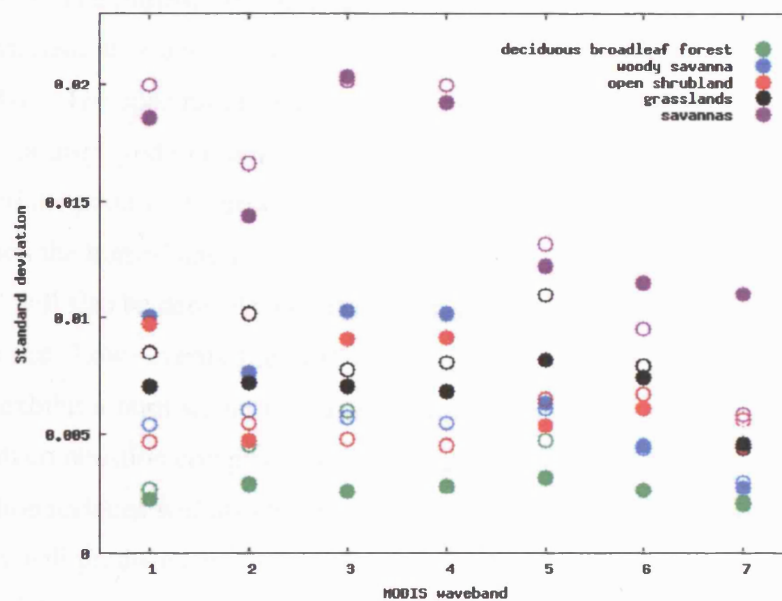
Figure 3.13: Separability (mean values of M)

Figure 3.14: Standard deviations of burned (filled circles) and unburned (empty circles) reflectances

The lowest separabilities (values of M closest to zero) are demonstrated by areas of deciduous broadleaf forests and highest separabilities by areas of grassland and open shrubland for all three burn-sensitive wavebands (bands 2, 5 and 6). These data have implications for the detection of burned areas within deciduous broadleaf forests, and indicate that the magnitude of the fire induced surface changes within this cover type are small. The savanna data set exhibits higher burned and unburned standard deviations at each waveband in comparison to the other vegetation classes (Figure 3.14), which suggests that the spectral response of the pre burn and post burn savanna surface is more variable than the other four cover types.

3.6.1 The proportional change in MODIS reflectances

In addition to the magnitude of the change in reflectance which has occurred due to burning, the proportional change is also of interest as this may be a more appropriate measure with which to separate areas which have been affected by fire from those which have not. The magnitude of the spectral change which occurs as a result of burning is expected to vary both spatially and temporally, as a function of the characteristics of the pre-fire surface as well as the nature of the fire (see Section 3.2). The intrinsic spectral variability of fire affected areas is primarily dependent on the photosynthetic state and type of the vegetation prior to burning (Pereira *et al.* 1999, Trigg and Flasse 2001). The spectral changes which occur as vegetation senesces are evident in the measured spectra displayed in Figure 3.11b (Section 3.5). It is clear from this data that the vegetation type and the point in its growth cycle at which the fire occurs will determine the spectral contrast between the burned and unburned surfaces (Trigg and Flasse 2001). The magnitude of the burn signal will also be dependent on the combustion completeness and the properties of any residues of the fire. Low severity fires will result in a more heterogeneous post fire surface and will therefore exhibit a burn signal of lower magnitude than areas of high severity fires which will have a high combustion completeness leaving a more uniform post fire surface. The nature of the combustion residues will also have an impact on the burn signal and fires of different levels of efficiency will produce combustion residues varying from dark coloured char and ash as a result of incomplete combustion, and white ash for more efficient combustion (Stronach and Mcnaughton 1989). These surfaces have variable reflectances which will determine the magnitude of the spectral change from pre-burn to post-burn conditions as demonstrated by the measured

spectra in Figure 3.11b. In contrast to the magnitude of the spectral change which has occurred due to a fire, a measure describing the proportional change in reflectance will allow for variability in the pre-fire and post fire reflectance levels. Such a measure is defined in Equation 3.3 which takes into account the intrinsic variability of the burn signal by weighting the magnitude of the change in the reflectance due to fire by the pre-change reflectance level:

$$\delta\rho(\lambda) = \left(\frac{\rho_{post} - \rho_{pre}}{\rho_{pre}} \right) \quad (3.3)$$

where ρ_{pre} and ρ_{post} are the pre burn and post burn reflectances on the day before and the day after the change respectively. Figure 3.15 shows mean values of $\delta\rho(\lambda)$ calculated from the same data set as used in Section 3.6. All cover types exhibit a proportional change in reflectance of at

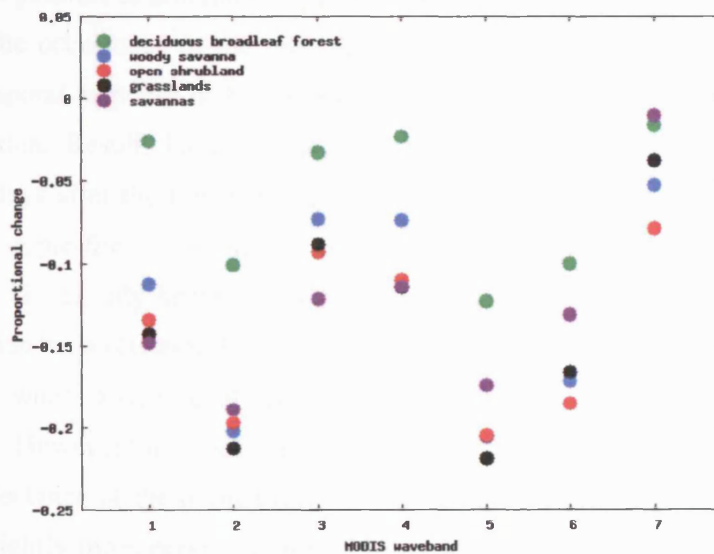


Figure 3.15: Proportional changes in reflectance ($\delta\rho(\lambda)$)

least -0.1 at MODIS bands 2, 5 and 6 which equates to a 10% decrease in reflectance as a result of burning. Similar to the separability data in Figure 3.13, deciduous broadleaf forests demonstrate the smallest proportional change in reflectance levels at these wavelengths in comparison to the other cover types. This is likely to be due to the fact that fires which occur within this vegetation type tend to burn only the understorey vegetation leaving the canopy components unaffected, thus having a relatively lower impact on the reflectance signal.

3.6.2 The duration of the MODIS burn signal

It is not only the relative change in and magnitude of fire induced spectral change which is of importance in the identification of the most appropriate wavebands for the separation of burned and unburned pixels, but the persistence of these changes in the remote sensing signal is also significant as not only will it influence the choice of wavebands, but it will determine the temporal sampling required in order to successfully identify the changes of interest. In particular high spatial resolution sensors such as the Landsat series which only revisit the same location once every sixteen days may not be suitable for the detection of sudden but short lived surface change.

Minimal work exists which characterises the temporal evolution and the duration of the burn signal in the spectral response of post fire surfaces, although several studies have investigated whether it is still possible to accurately separate burned from unburned pixels at various temporal intervals after the occurrence of the fire. A study by Trigg and Flasse (2000) has examined the spectral-temporal response of burned savanna using *in-situ* spectroradiometry for a site in north-east Namibia. Results indicate that a significant signal exists in MODIS bands 2 and 5 for at least 13 days after the fire, bands 1, 4 and 6 tend to be sensitive immediately after the burn and return to pre-fire levels within 7, 7 and 11 days respectively, while at longer infrared wavelengths the signal only becomes significant one day after the fire and rises thereafter. A similar pattern has been observed by Savage and Vermeulen (1983) for an area of grassland in southern Africa, where a significant decrease in reflectance occurred in the entire $0.3\mu m-3\mu m$ range after a fire. However four weeks after the date of the fire there was no significant difference between the reflectance of the burned surface and the surrounding unaffected vegetation. The burn signal is slightly more persistent in burned areas of woody savanna in central Africa. A study by Eva and Lambin (1998a) has shown that it is possible to separate fire affected areas from the surrounding woody savanna for up to 17 days after the fire at near and shortwave infrared wavelengths while after longer time periods confusion arises between senesced vegetation and the burned surfaces due to the removal of the ash deposits by the elements and the regrowth of the vegetation. In contrast an investigation of the temporal trend of reflectance for a post fire woody savanna surface in Northern Australia has demonstrated that while the near infrared reflectance remains lower than pre-fire levels for up to several weeks after the fire, reflectance in the middle infrared demonstrates a quick post fire recovery reducing the chances of detection

only two weeks after the fire (Stroppiana *et al.* 2003). It is suggested that this may be due to the dispersal of the charcoal and ash by meteorological processes, resulting in exposure of the underlying soil surface and a middle infrared signal which is increasingly influenced by the soil signal and the presence of dry vegetation (Trigg and Flasse 2000, Stroppiana *et al.* 2003). The reflectance at near infrared wavelengths is less sensitive to such changes and is more dependent on the state of the vegetation which remains comparatively consistent for the weeks immediately after the fire, resulting in a longer persistence of the burn signal at this wavelength (Stroppiana *et al.* 2003). The persistence of burn surfaces in the MODIS spectral response over the area of interest has been examined using the separability measure described in Equation 3.2 as well as the proportional change in reflectance (Equation 3.3) at four temporal periods; 1 day after the fire, 7 days after the fire, 14 days after the fire, and 21 days after the fire. As in the previous sections only cloudfree observations which have been acquired with a view zenith angle of $\pm 10^\circ$ have been considered from the same data set as used above, with the occurrence of fire determined from the MODIS Thermal Anomalies product. The results for savanna pixels are displayed graphically in Figure 3.16, and the results for all of the vegetation classes are contained in Table 3.7 and 3.8. Separability values of at least 0.2 have been highlighted in Table 3.7 for the purpose of the following discussion.

The values of M contained in Table 3.7 and Figure 3.16a indicate that the separability of the burned and unburned surfaces for all five vegetation types decreases markedly over time. While MODIS bands 2, 5 and 6 demonstrate the highest separabilities (>0.30) for most vegetation classes immediately after the occurrence of a fire, after a period of only seven days M values of at least 0.30 are only observed over areas of burned grassland and open shrubland for these wavebands. After a period of 14 days although lower band 2, 5 and 6 reflectances in comparison to the pre-fire levels (as indicated by a positive value of M) are still evident over all vegetation types except for deciduous broadleaf forests, the separabilities are extremely low with M values of less than 0.2 for all classes except grassland where $M(\text{band2})=0.21$ and $M(\text{band5})=0.22$. Thus in contrast to the studies discussed above where, for example, a significant signal was found to exist over burned savanna at MODIS bands 2 and 5 for at least 13 days after the fire (Trigg and Flasse 2000), for the areas examined while all vegetation classes except for deciduous broadleaf forests exhibit separabilities of at least 0.30 immediately after the fire at band 2, 5 and 6 wavelengths, within 14 days after the fire the surface reflectance has returned to pre-fire levels

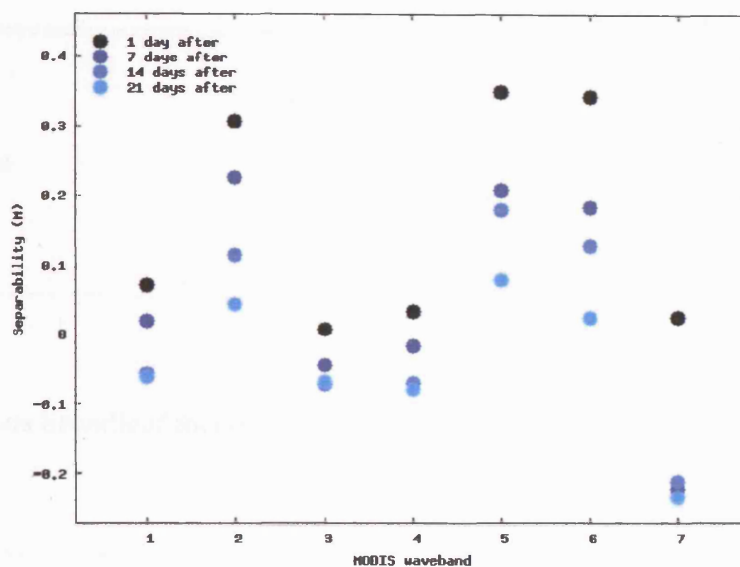
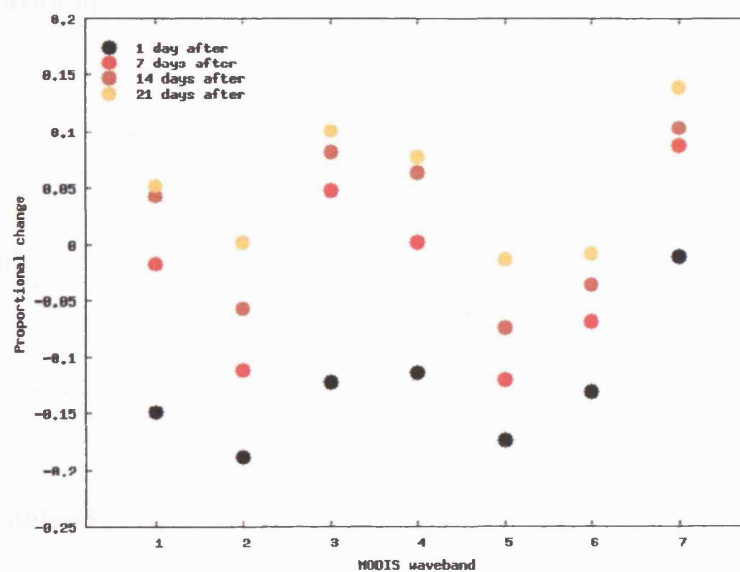
(a) Mean separability (M)(b) Proportional change in reflectance ($\delta\rho$)

Figure 3.16: Duration of the MODIS burn signal

Vegetation Type	Waveband	Time after fire:			
		1 day	7 days	14 days	21 days
Savanna	1	0.07	0.02	-0.06	-0.06
	2	0.31	0.23	0.11	0.04
	3	0.01	-0.04	-0.07	-0.07
	4	0.03	-0.02	-0.07	-0.08
	5	0.35	0.21	0.18	0.08
	6	0.34	0.18	0.13	0.02
	7	0.02	-0.22	-0.21	-0.23
Deciduous broadleaf forest	1	0.03	-0.06	-0.11	-0.09
	2	0.25	0.07	-0.01	-0.10
	3	0.01	-0.05	-0.06	-0.06
	4	0.01	-0.06	-0.10	-0.10
	5	0.22	0.05	0.01	-0.01
	6	0.26	0.01	-0.03	-0.05
	7	0.05	-0.19	-0.22	-0.18
Woody savanna	1	0.07	-0.03	-0.07	-0.07
	2	0.32	0.13	0.08	0.01
	3	0.02	-0.04	-0.06	-0.05
	4	0.03	-0.04	-0.07	-0.08
	5	0.24	0.11	0.11	0.10
	6	0.34	0.06	0.03	0.07
	7	0.14	-0.12	-0.23	-0.20
Grassland	1	0.13	0.13	0.06	-0.02
	2	0.37	0.30	0.21	0.11
	3	0.03	0.03	-0.01	-0.04
	4	0.08	0.07	0.02	-0.04
	5	0.38	0.30	0.22	0.21
	6	0.39	0.28	0.16	0.12
	7	0.09	-0.06	-0.13	-0.17
Open shrubland	1	0.10	0.19	0.02	0.01
	2	0.36	0.31	0.15	0.13
	3	0.02	0.04	-0.05	-0.03
	4	0.07	0.13	-0.01	-0.02
	5	0.33	0.30	0.18	0.18
	6	0.40	0.30	0.15	0.12
	7	0.17	0.05	-0.12	-0.16

Table 3.7: Duration of the MODIS burn signal (M)

Vegetation Type	Waveband	Time after fire:			
		1 day	7 days	14 days	21 days
Savanna	1	-0.15	-0.12	0.04	0.05
	2	-0.19	-0.11	-0.06	0.01
	3	-0.12	0.15	0.08	0.10
	4	-0.11	0.01	0.06	0.08
	5	-0.17	-0.12	-0.07	-0.01
	6	-0.13	-0.07	-0.04	-0.01
	7	-0.01	0.09	0.10	0.14
Deciduous broadleaf forest	1	-0.03	0.06	0.11	0.13
	2	-0.14	-0.05	0.00	0.09
	3	-0.03	0.07	0.10	0.13
	4	-0.02	0.06	0.11	0.14
	5	-0.15	-0.06	-0.02	0.04
	6	-0.14	-0.02	0.02	0.05
	7	-0.02	0.10	0.12	0.14
Woody savanna	1	-0.11	0.04	0.09	0.08
	2	-0.20	-0.07	-0.03	0.01
	3	-0.07	0.05	0.11	0.10
	4	-0.07	0.04	0.09	0.11
	5	-0.21	-0.09	-0.04	0.01
	6	-0.17	-0.04	-0.01	-0.00
	7	-0.05	0.07	0.12	0.08
Grassland	1	-0.14	-0.19	-0.10	-0.03
	2	-0.21	-0.23	-0.15	-0.08
	3	-0.09	-0.14	-0.07	-0.03
	4	-0.12	-0.18	-0.09	-0.02
	5	-0.22	-0.21	-0.12	-0.07
	6	-0.17	-0.14	-0.09	-0.03
	7	-0.04	0.02	0.05	0.11
Open shrubland	1	-0.13	-0.18	-0.01	-0.03
	2	-0.20	-0.22	-0.08	-0.07
	3	-0.10	-0.13	0.02	-0.04
	4	-0.11	-0.16	0.00	-0.03
	5	-0.21	-0.21	-0.08	-0.07
	6	-0.19	-0.17	-0.07	-0.05
	7	-0.08	-0.03	0.05	0.08

Table 3.8: Duration of the MODIS burn signal ($\delta\rho(band2)$)

with very low separabilities indicated at this point. Although the separabilities are low the most persistent burn signal is observed at bands 2 and 5 for grassland pixels (Table 3.7) with M values of at least 0.2 at 14 days. In contrast deciduous broadleaf forests and woody savannas show the highest recovery with the post fire signal hardly separable only 7 days after the fire. A similar pattern is observed in the proportional changes in reflectance which occur at MODIS bands 2, 5 and 6 wavelengths. A decrease in reflectance of at least 10 % (a $\delta\rho$ value of at least -0.1) occurs at these three wavelengths across all cover types immediately after the fire. These values have been highlighted in Table 3.8 for convenience. The fastest recovery of the signal to pre-fire levels is observed over deciduous broadleaf forests and woody savannas with only a 5, 6 and 2 % decrease in reflectance evident at band 2, 5 and 6 wavelengths over deciduous broadleaf forests 7 days after the fire, and a change of 7, 9 and 4 % ($\delta\rho$ values of -0.05, -0.06 and -0.02 respectively) over woody savannas. In contrast the most persistent signal is observed over grassland pixels, where an equivalent decrease in reflectance of 15, 12 and 9 % at bands 2, 5 and 6 is still evident 14 days after the occurrence of the fire. The persistence of the signal over grassland areas is likely to be related to the vegetation type. Grassland ecosystems have tree and shrub cover of less than 10% (see Table 3.3). In contrast to deciduous broadleaf forests which have a canopy cover of at least 60% and open shrublands which have a canopy cover between 30 and 60%, the burned areas of grassland will be less obscured by canopy components and thus more visible to the satellite sensor.

The burn signal at MODIS band 7 wavelengths exhibits a similar pattern to that identified by Trigg and Flasse (2000) at a burned savanna site in Namibia where the signal at longer infrared wavelengths was only found to be significant one day after the fire and rose thereafter. The data contained in Table 3.8 and Figure 3.16 indicate that for all vegetation classes the signal is hardly separable one day after the fire, but becomes more separable as time progresses with increasingly higher reflectance levels (a negative M value) observed within 7, 14 and 21 days after the occurrence of the fire. The proportional changes in reflectance which occur at band 7 wavelengths are extremely variable immediately after the fire, with a 1% ($\delta\rho=-0.01$) change occurring over savannas and an 8% change over open shrublands. Except for areas of open shrubland where a decrease in reflectance (a negative $\delta\rho$ value) is still observed a week after the fire, band 7 reflectances rise within seven days after the fire with an increase of between 8 and 14 % in the surface reflectance occurring up to 21 days after the fire.

3.7 Summary

This chapter has provided an overview of vegetation fires in southern Africa. The causes and ecological effects of biomass burning within this region have been discussed and the study site introduced. In addition the occurrence of fire within the study area has been characterised in terms of the temporal and spatial distribution of fire activity, and the spectral characteristics of burned surfaces have been investigated. The significant findings of this work are summarised below.

1. Temporal distribution of fire activity The southern Africa fire season coincides with the dry season which usually encompasses the months of May to October, with 95 percent of the total number of active fires detected by MODIS over the area of interest occurring between the beginning of April and the end of November during the past five years. A comparison of the data acquired by the morning (equatorial crossing of 10.30am local time) and afternoon (equatorial crossing of 1.30pm local time) MODIS overpass suggests that the fire activity within this area has a strong diurnal pattern, with almost three times as many fires detected later in the day at the peak of the 2003 and 2004 fire season.

2. Spatial distribution of fire activity A large proportion of southern Africa burns every year with the fire activity moving from west to east as the burn season progresses. Fire activity is greatest in areas of savanna with between 10.8 and 11.3 percent of savanna pixels detected as containing a fire during the five annual fire seasons examined, and lowest in areas of open shrubland.

3. Spectral characteristics of burned surfaces With a few exceptions (Trigg and Flasse 2000, Sa *et al.* 2003, Stroppiana *et al.* 2003) minimal field research has been performed describing the reflectance characteristics of fire affected surfaces, or the duration and temporal evolution of the burn signal. The vegetation classes in the area of interest tend to reach the peak of their growth cycle by the end June, and senesce during the following months until the onset of the rainy season, with the peak of fire activity occurring at the height of the dry season. An examination of the separability of pre-fire and post fire reflectances for each of the individual MODIS land

surface wavebands over the burn season suggests that although the classes are extremely similar at all wavelengths, separation of burned and unburned pixels may be achieved more effectively using near or middle infrared wavebands which exhibit a decrease in reflectance as a result of burning.

4. Duration of the burn signal The temporal persistence of the change in the remote sensing signal which occurs as a result of fire is of importance in the detection of fire affected areas as it will determine the temporal sampling required for a high detection probability. While burn scars in open shrubland and grassland ecosystems may be detectable up to 7 and 14 days respectively after the occurrence of a fire, for the remaining three classes within 7 days the surfaces exhibit very low burned-unburned separabilities, with deciduous broadleaf forests and woody savannas showing the fastest post fire recovery.

Detailed knowledge of the temporal and spatial variability of fires within the area of interest can greatly reduce the extent of satellite coverage required to determine and monitor the total area burned throughout the year (Cahoon *et al.* 1992). For the purpose of this Thesis, the temporal extent of the southern Africa fire season is defined as the eight months beginning with April and ending with November. In order for a change detection scheme to be effective it is necessary to use wavebands which are sensitive and as unique as possible to the changes of interest. The work presented above suggests that MODIS bands 2, 5 and 6 offer the greatest separability between burned and unburned surfaces within the study area. However the separability of these surfaces are not uniform across the study area, with areas of deciduous broadleaf forests indicating substantially smaller changes from pre-burn to post-burn conditions than the other cover types. This suggests that it will be significantly harder to detect areas of burning which have occurred within deciduous broadleaf forests due to the smaller magnitude of the fire induced change. The low magnitude of the fire induced spectral change which is observed immediately after the fire emphasises further the need to exploit all of the information available and thus the importance of utilising directional information within the remote sensing signal in the detection of burned areas within these ecosystems. The persistence of these changes is also of significance with the results presented indicating that recovery of the burned surfaces may occur within as little as seven days after the fire. In order to ensure the maximum probability of detection of these burned areas it is

therefore necessary to acquire images as near to the day of burning and with as high a revisit period as possible. Near-daily satellite acquisitions from high temporal resolution sensors provide the only feasible means of identifying these changes.

Following on from these requirements and the shortcomings of traditional change detection techniques discussed in Chapter 2, a change detection scheme is presented in the next chapter which accounts for the directional information contained in the remote sensing signal, and which may be applied to the daily detection of burned surfaces from high temporal resolution satellite data.

Chapter 4

A new approach to change detection

Chapters 2 and 3 have discussed the need for a burned area detection algorithm which accounts for directional effects in surface reflectance, and which is applicable to the high temporal resolution monitoring of burned surfaces. This chapter provides a description of the models and methods commonly used to describe the anisotropy of surface reflectance and its manifestation in remote sensing data. Following on from this a new generic approach to change detection which incorporates directional information is introduced and its application to burned area detection described.

4.1 Anisotropic surface reflectance

The Earth's surface is not a Lambertian reflector, and therefore does not reflect light equally in all directions. The degree of anisotropy displayed by a particular surface is determined by both the optical and the physical nature of that surface. Although the angular distribution of reflectance will have a spectral dependence as the interaction between the downwelling radiation and the objects on the surface varies as a function of wavelength, the primary source of anisotropy is the three-dimensional character of the surface (Liang *et al.* 2000). The shape, size and spacing of objects will directly influence the scattering of radiation from the surface producing a distinctive pattern of shadows which will vary with viewing position. Over a plant canopy for example the remote sensing signal will depend mainly on the relative proportions of sunlit leaf and soil visible from a particular viewing angle. This will be determined by the size and orientation of the scatterers (the leaves) in the direction of the sun and the satellite. As a result research has indicated that it is possible to separate vegetation cover types based solely on the structural (as opposed to spectral) characteristics of the surface from the directional information contained within the remote sensing signal (Asner 2000).

The spectral reflectance from a land surface is not only dependent on the spectral and spatial properties of the surface, but will vary as a function of the angle at which it is illuminated and the angle at which it is viewed from (Nicodemus *et al.* 1977, Roujean *et al.* 1992, Wanner *et al.* 1995). As measurements of reflectance from the earth's surface may be acquired under very different illumination and viewing angles, characterisation of this anisotropy is of importance in the understanding of earth surface properties. Directional effects may be apparent in remote sensing

measurements from a variety of sources. Wide field of view sensors (for example AVHRR and MODIS) acquire data under very different viewing angles across an individual swath, resulting in angular variations in the data sensed at different locations within the single swath, as illustrated in Figure 4.1a. The Instantaneous Field Of View (IFOV) of MODIS is 110° at the satellite

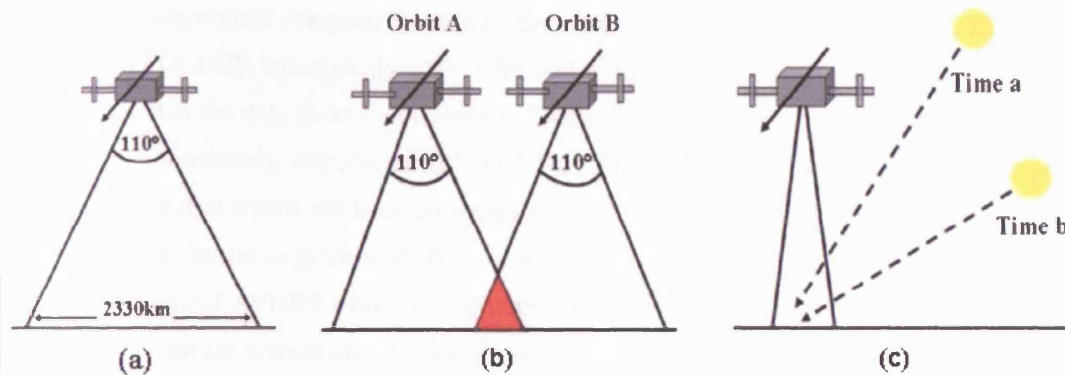


Figure 4.1: Angular effects caused by sensor characteristics and orbital patterns

which results in viewing angles which range between 0° at nadir to 70° at the edges of a single image. In addition angular variations will be present in data acquired for the same location on the earth's surface during different orbital passes as highlighted by the red area in Figure 4.1b. Similar effects will be present in data acquired by sensors such as POLDER (Polarisation and Directionality of Earth Reflectances) and MISR (Multiangle Imaging Spectra-Radiometer). An examination of daily vegetation indices calculated from POLDER data show variations in the range of 0.2-0.5 as a result of different viewing angles (Leroy and Hauteceur 1999). The source of such effects is not limited to variations in the viewing geometry under which the data is acquired as the surface reflectance is also dependent on the position of the sun. Images sensed over the same area at a constant viewing angle but at different times of the day (for example by a geostationary sensor such as METEOSAT), or at different times of the year will be affected by variations in the angle of illumination as illustrated in Figure 4.1c. These effects make the comparison of temporal series of remote sensing data, or the analysis of data within a single wide swath problematic.

Until relatively recently the analysis of remotely sensed images has typically regarded the

surface as a Lambertian reflector, ignoring directional affects. As discussed in Section 2.2 a common approach in change detection studies has been to use Maximum Value Composites (MVCs) in order to reduce the impact of these effects within a time series of images (Holben 1986). The importance of taking directional effects into account when comparing surface reflectance data acquired under varying illumination and viewing conditions is now generally accepted, and algorithms designed to evaluate data from sensors such as MODIS, VEGETATION, MISR and POLDER increasingly correct for and in some cases actually exploit the angular effects implicit in the data (Lucht and Roujean 2000a). The “Fourier-Adjusted, Solar-zenith angle corrected, Interpolated, Reconstructed” NDVI (FASIR-NDVI) dataset for example is a global vegetation dataset which has been corrected for effects within the data which are not related to actual changes in the vegetation (Sellers *et al.* 1994). The dataset has been constructed from 17 years of global AVHRR observations with variations in the reflectance observations due to atmospheric and calibration effects and differing view and illumination geometries corrected for. With the launch of MODIS Terra at the end of 1999 an operational product which corrects for angular effects has been available to the scientific community, alongside the standard surface reflectance products (Justice *et al.* 1998, Schaaf *et al.* 2002). The importance of accounting for such effects prior to the use of a multi-temporal dataset for the purpose of detecting changes in the land surface has been described in Chapter 2. Directional effects within remote sensing data may be normalised to a standard viewing and illumination geometry allowing for comparison between measurements acquired under different viewing and illumination conditions. The following section discusses the ways in which this is typically achieved.

4.2 Models of the BRDF

The anisotropy of the surface may be modelled by the Bidirectional Reflectance Distribution Function (BRDF), which describes the dependence of surface spectral reflectance on the geometry at which the surface is illuminated and viewed from (Nicodemus *et al.* 1977). This function may be fitted using empirical or physical models with numbers of parameters ranging from a few to dozens (Liang *et al.* 2000). A third group of models referred to as “semi-empirical” also exist, which provide a compromise between an empirical and a purely physical approach. These

three classes of model differ in (i) the detail with which the scattering of light within a scene is described (ii) the degree of *a priori* knowledge required about the landcover characteristics of the scene and (iii) the minimum number of observations needed to accurately derive the model parameters (Wanner *et al.* 1995).

4.2.1 Physically based models

Physical models of the BRDF are more complex than semi-empirical or empirical approaches as they attempt to realistically describe the reflectance from a vegetation canopy based on an abstraction of the canopy. The shape of the BRDF is described using a number of parameters related to the surface characteristics, such as the size, shape and distribution of elements within a vegetation canopy. An advantage of using a physically based model to describe the surface BRDF is thus that in comparison to a purely empirical approach, the model parameters will have some physical meaning. Models of the directional reflectance from vegetation typically trace the path of a photon as it interacts with the canopy and the individual canopy components, thereby explicitly describing the scattering of light within a scene. However as a description of all processes within a scene would be impossible, it is necessary to make certain assumptions and approximations relating to the physics of the scene. Despite these abstractions physical models are inherently more complex than empirical ones and contain a larger number of parameters and are thus more computationally expensive. They are however particularly useful for deriving surface variables such as the Leaf Area Index (LAI) from the remote sensing signal, which may subsequently be used to estimate parameters such as surface roughness or the fraction of photosynthetically absorbed radiation which are of importance in modelling biogeochemical cycles (Kalluri *et al.* 2001). Although a wide range of canopy reflectance models applicable to a diverse range of cover types have been developed, physical models of canopy reflectance typically fall into one of four broad categories; geometric optics, radiative transfer, hybrids of the two, and numerical simulations (Goel 1989). A comprehensive review of these may be found in Goel and Thompson (2000), Chen and Leblanc (2000), Qin and Liang (2000) and Disney *et al.* (2000).

The first class uses geometric optics to describe the reflectance from vegetation as a function of the structural and spatial characteristics of the canopy (Li and Strahler 1985). Vegetation canopies are modelled as discrete three dimensional objects which are viewed and illuminated

from different directions within the hemisphere. Geometrical models such as that of Li and Strahler (1985,1986,1992) represent the scene as a collection of geometric shapes (such as cones and cylinders) on a Lambertian surface. The geometry of a scene is then dependent on the size and density of these shapes, and the reflectance of the scene is modelled as a combination of four individual parameters, the sunlit and shadowed proportions of the objects in the scene and the ground when viewed and illuminated from a particular direction. This group of models has been applied successfully to sparse or moderately closed canopies (such as shrublands), row crops and bare soil surfaces.

The second category have typically been based on radiative transfer theory, and describe a vegetation canopy as a horizontally homogenous layer of absorbing and scattering particles with known optical properties. Radiative transfer models tend to be more appropriate for modelling dense and horizontally uniform canopies such as forests or crops (Nilson and Kuusk 1989, Kuusk 1995). The majority of work in this area has modelled vegetation at the canopy level, although leaf level models such as PROSPECT (Jacquemoud and Baret 1990) do exist. The physical basis for canopy radiative transfer models is the treatment of the canopy as a turbid medium consisting of randomly distributed scatterers (e.g. leaves) in horizontal layers with specific orientations (Goel 1989). The model parameters are then the optical and structural properties of these individual scattering elements. The directional reflectance from the canopy may be calculated using numerical or analytical methods. Analytical solutions are typically achieved by either approximating the canopy radiative transfer equation with a set of integro-differential equations which may then be solved for diffuse and specular fluxes travelling in the downward and upward directions, or by separating the canopy radiation into unscattered, single scattering and multiple scattering components (Qin and Liang 2000). In contrast to these numerical methods are more accurate but also more computationally expensive and many iterations may be required to reach an acceptable solution. The hybrid category combines aspects of both geometric optical and radiative transfer models, with geometric shapes representing the canopy in a turbid medium (Ni *et al.* 1999). Hybrid models are therefore more flexible than the other two approaches, but also more complex.

Computer simulation models are more complex than the approaches described above, and involve the specification of the position and dimensions of the canopy elements as well as their arrangement within the canopy. The interactions between the photons and the canopy are then

simulated using, for example, Monte Carlo methods (Lewis and Muller 1992) or radiosity techniques (Borel *et al.* 1991). However although such models are useful in quantifying and investigating the nature of the radiation regime within a canopy, they are computationally expensive and require *a priori* knowledge of the surface in order to set the model parameters to suitable limits prior to inversion.

4.2.2 Empirical models

In contrast to the physically based approaches described above, empirical models are formulated solely to describe mathematically the shape of the surface BRDF. Statistical coefficients are typically derived by fitting a polynomial function to the observed directional reflectances. An advantage of this approach is the lack of assumptions regarding the landcover type and therefore the model may be equally applicable to a homogenous or spatially discrete canopy. However this may also be a disadvantage as empirical models do not have any physical basis and the parameters which comprise the model are not measurable properties of the surface. Thus while models of this form are useful in accounting for angular effects, they do not provide us with any information relating to the biophysical nature of the scene (Cihlar *et al.* 1994).

An example of an empirical model is that of Walthall *et al.* (1985), which has subsequently been modified by Nilson and Kuusk (1989) to satisfy the reciprocity principle. Based on a set of polynomials the surface BRDF is described as;

$$\rho(\theta_i, \theta_v, \phi) = f_0(\theta_i^2 + \theta_v^2) + f_1\theta_i^2\theta_v^2 + f_2\theta_i\theta_v\cos\phi + f_3 \quad (4.1)$$

where θ_i, θ_v, ϕ refer to the illumination and viewing zenith angles, and the relative azimuth (the angle between the illumination and viewing azimuths) respectively. As the model is linear it may be inverted against a set of directional measurements of reflectance ($\rho(\theta_i, \theta_v, \phi)$) using linear algebra to provide an estimate of the four parameters (f_n). Due to its simple linear and robust nature, this model may be inverted rapidly and has therefore been used extensively in the angular normalisation of multiangular remote sensing datasets (Huete *et al.* 1999). Zhang *et al.* (1998) have applied the modified version of the Walthall model to a global 10-day composite AVHRR dataset, with results indicating consistent nadir reflectance values (f_3) across different vegetation

types. However a comparison between ten different BRDF models for the calculation of nadir reflectance as well as the spectral albedo by Privette *et al.* (1997) found the Walthall model to perform poorly in comparison to the semi-empirical alternatives. Due to the empirical nature of the model it is less suited to extrapolation to wider sampling conditions or to a reduced number of observations than those which follow a semi-empirical approach.

4.2.3 Semi-empirical models

The third class of models has developed out of the two described previously. In comparison to physical models the semi-empirical approach provides a simpler parameterisation of the BRDF, albeit still more complex than a purely empirical approach. As this class of models essentially provides an approximation to physical models of the BRDF they are mathematically simpler while at the same time their parameters retain some of their physical and more important characteristics (Wanner *et al.* 1995). Semi-empirical models thus offer a compromise as they require fewer observations than empirical models while in contrast to a purely physical approach they successfully model heterogeneity within a scene and do not require *a priori* knowledge of the surface characteristics. In addition they have fewer parameters than physical models and are therefore easier to implement.

Two types of semi-empirical models will be discussed, as both approaches are used in the current research. The first is the 'kernel-driven' approach introduced by Roujean *et al.* (1992) and further developed by Wanner *et al.* (1995), which has been developed from an explicit consideration of the remote sensing inversion problem (Lucht and Roujean 2000b). The scene is represented as a linear combination BRDF shapes which are functions of illumination and viewing angles only. The model takes the form of Equation 4.2,

$$\rho(\lambda, \theta_i, \theta_v, \phi) = \sum_n f_n(\lambda) K_n(\theta_i, \theta_v, \phi) \quad (4.2)$$

where ρ is the spectral reflectance and θ_i, θ_v and ϕ represent the illumination and viewing zeniths and the relative azimuth. K_n are the geometric expressions of BRDF shapes, and are typically referred to as 'kernels'. The model parameters (f_n) describe the relative contribution of each of the BRDF shapes to the overall reflectance of the scene. A great deal of flexibility is possible

in defining appropriate kernels for the model, and various formulations of the volumetric (K_{vol}) and geometric (K_{geo}) kernels have been developed (Roujean *et al.* 1992, Wanner *et al.* 1995). In the original implementation three kernels are used, each describing a different form of scattering to model the surface BRDF. These three types of scattering are described schematically in Figure 4.2 and are modelled using (i) an isotropic parameter (the nadir reflectance with nadir illumination - a constant typically set to unity) to describe isotropic scattering from the surface (Figure 4.2a) (ii) a volumetric kernel which provides a single scattering approximation to radiative transfer (Figure 4.2b) (iii) a geometric-optical term which accounts for shadowing effects (Figure 4.2c). It is assumed that the BRDF may be decomposed into the two types of scatter-

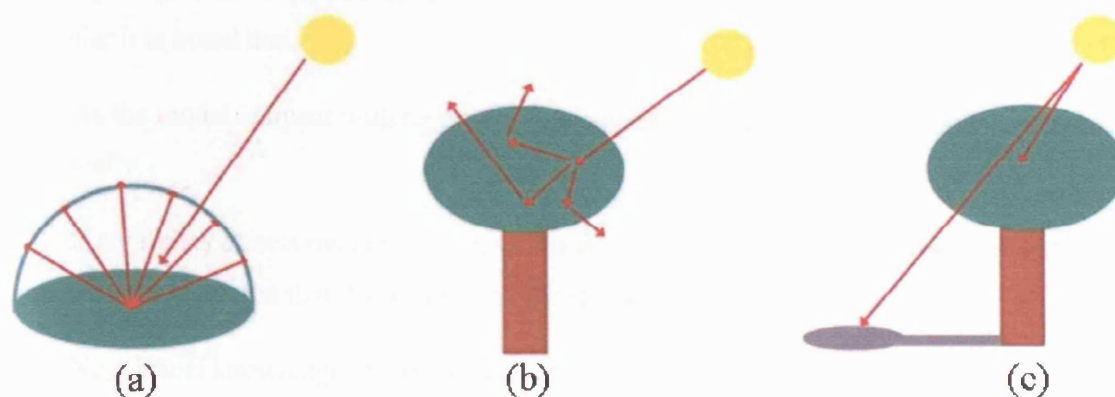


Figure 4.2: Isotropic, volumetric and geometric forms of vegetation scattering

ing described by the kernels, and that these are mutually exclusive and therefore do not overlap (Roujean *et al.* 1992). Thus over a forest canopy, for example, while the reflectance from the crowns will typically be characterised by geometric scattering, volumetric contributions will be made by scattering within the canopy (Roujean *et al.* 1992). The isotropic term is included in order to compensate for the single scattering assumption as reflectance from an anisotropic surface will tend to become increasingly isotropic with higher order scattering. The model thus assumes that multiple scattering from the surface will have no directional dependence. Although more than three kernels may be used (Hu *et al.* 1997), it is generally accepted that the three kernels described above provide a sufficient description of most BRDF shapes of naturally occurring surfaces (Lucht and Roujean 2000b). For the operational application of this model little difference

is observed between the kernels within the same family, and the combination of RossThick and LiSparse has been found to best represent observed reflectances over a wide variety of surfaces (Schaaf *et al.* 2002). In this case the model takes the form of Equation 4.3.

$$\rho(\lambda, \theta_i, \theta_v, \phi) = f_{iso}(\lambda) + f_{vol}(\lambda)K_{vol}(\theta_i, \theta_v, \phi) + f_{geo}(\lambda)K_{geo}(\theta_i, \theta_v, \phi) \quad (4.3)$$

The development of the semi-empirical approach described above has arisen out of the need for the operational normalisation of directional effects and generation of estimates of albedo from large datasets such as those acquired by the MODIS sensor (Lucht and Roujean 2000b). The properties of these models offer several advantages in the examination of large datasets. In particular it is noted that:

1. As the model is linear with respect to its parameters it may be inverted rapidly and analytically
2. If adjacency effects over heterogenous areas are ignored the model can be assumed to scale linearly with area thereby accounting for spatial heterogeneity
3. No *a priori* knowledge of the surface is therefore required
4. There is some physical basis to the model parameters and they may therefore provide information relating to the biophysical characteristics of the surface

AMBRALS

The Algorithm for MODIS Bi-directional Reflectance Anisotropy of the Land Surface (AMBRALS) is a model consisting of a collection of semi-empirical kernels which describe the angular reflectance for a variety of surface cover types, and are combined as described in Equation 4.2 to form a linear BRDF model. AMBRALS was designed specifically for use with MODIS data, and is used operationally to produce the MODIS BRDF/Albedo product (Wanner *et al.* 1997, Strahler *et al.* 1999a). The kernels used in the creation of this dataset are the RossThick and the LiSparse Reciprocal. These (along with an isotropic parameter) are inverted over 16 days of directional reflectances. A period of 16 days is used as this is the MODIS orbital repeat cycle.

The volumetric kernel was developed by Roujean *et al.* (1992) and Wanner *et al.* (1995) from the work of Ross (1981) for optically thick canopies (i.e. with a Leaf Area Index greater than 1) as a first order approximation to radiative transfer for infinitesimal scatterers. The kernel takes the form of Equation 4.4:

$$K_{vol} = \frac{(\pi/2 - \xi) \cos \xi + \sin \xi}{\cos \theta_i + \cos \theta_v} - \frac{\pi}{4} \quad (4.4)$$

where θ_i and θ_v refer to the illumination and viewing zenith angles respectively, and ξ is the scattering phase angle described as:

$$\cos \xi = \cos \theta_i \cos \theta_v + \sin \theta_i \sin \theta_v \cos \phi \quad (4.5)$$

The model assumes a single scattering approximation to radiative transfer. i.e. photons scattered more than once are ignored. In addition the scattering facets (leaves) are assumed to be randomly orientated, with equal leaf transmission and reflectance (Roujean *et al.* 1992).

The LiSparse is a geometric kernel developed by Wanner *et al.* (1995) from the geometric-optical BRDF model introduced by Li and Strahler (1992). It provides an approximation to protrusion and shadowing effects for an optically thin surface, and has subsequently been modified for conditions of reciprocity as the original parameterisation was formulated for a fixed solar zenith angle (Lucht 1998, Strahler *et al.* 1999a). The canopy is represented as a collection of spheroids (the canopy) on sticks (the trunks), and is parameterised by the geometry of the canopy (the base to height and tree-height to crown-height ratios) and the brightness and arrangement of the protrusions. The kernel takes the form of Equation 4.6;

$$K_{geo} = O(\theta_i, \theta_v, \phi) - \sec \theta'_i - \sec \theta'_v + \frac{1}{2}(1 + \cos \xi') \sec \theta'_i \sec \theta'_v \quad (4.6)$$

where θ_i and θ_v refer to the illumination and viewing zenith angles respectively, and O is the proportion of shadows which overlap. This is defined as;

$$O = \frac{1}{\pi}(t - \sin t \cos t)(\sec \theta'_i + \theta'_v) \quad (4.7)$$

The shape of the shadows is defined by the cosine of the parameter t ;

$$\cos t = \frac{h \sqrt{D^2 + (\tan \theta'_i \tan \theta'_i \sin \theta'_v)^2}}{b \sec \theta'_i + \sec \theta'_v} \quad (4.8)$$

which is a function of both h (the height of the spheroid) and the distance between the two centres of the shadows D , which in turn is a function of the illumination and viewing geometries.

The model is parameterised by the density of objects within the scene (the trees), the brightness of the crowns and the background, and the geometry of the objects (the relative crown height (h) and base to height ratio). The model assumes illuminated ground and illuminated crowns have the same brightness, and that areas of shadow are completely black. In addition in the Li Sparse formulation the mutual shadowing of objects is ignored. Both kernel formulations are displayed graphically in Figure 4.3. An asymmetric “bowl shape” is evident in both kernels,

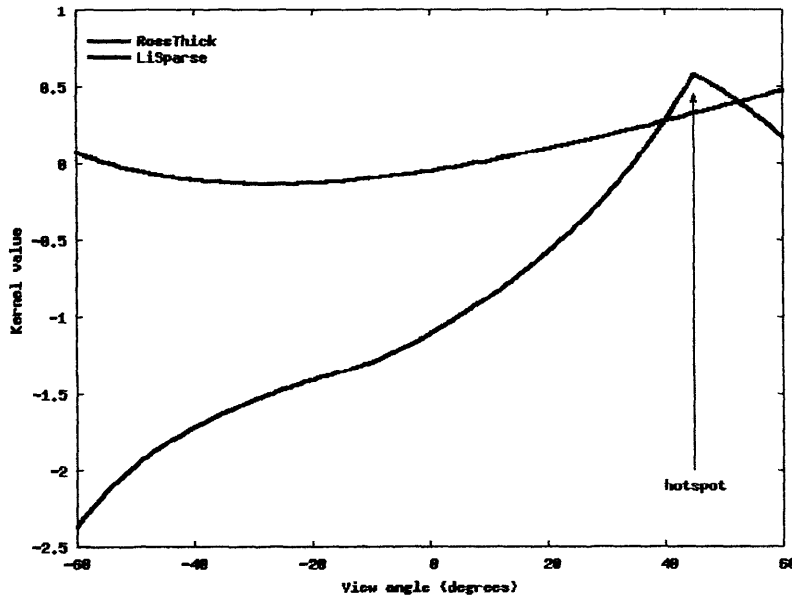


Figure 4.3: Rossthick and LiSparse kernels for a solar zenith angle of 45°

with the volumetric kernel exhibiting an upward bowl, and the geometric kernel a downward bowl. The hotspot (the peak in reflectance in the backscatter direction) is not present in the Ross kernel as it is formulated for infinitesimal scatterers and the hotspot is therefore not described by the radiative transfer approximation. The hotspot is evident in the Li kernel however as it accounts implicitly for shadowing effects.

The RossThick and LiSparse kernels are combined with an isotropic kernel which describes the reflectance from a surface under nadir viewing and illumination conditions and whose value is always unity. Under this angular geometry the BRDF kernels are expressed as;

$$K_{geo}(\theta_i = 0, \theta_v = 0) = K_{vol}(\theta_i = 0, \theta_v = 0) = 0 \quad (4.9)$$

and therefore $\rho(\theta_i = 0, \theta_v = 0) = f_{iso}$. Although various other formulations of volumetric and geometric kernels have been defined, the combination of the two described above has been shown to describe sufficiently the scattering characteristics of a wide variety of land cover types (Lucht and Roujean 2000a, Schaaf *et al.* 2002), and several studies have identified these kernels as most suited to the operational MODIS BRDF/Albedo product (Wanner *et al.* 1995, Privette *et al.* 1997, Lucht *et al.* 2000). As these two kernels are employed in the production of the MODIS BRDF/albedo product they have been tested extensively (Schaaf *et al.* 2002). In particular they have been shown to perform well under sparse angular sampling and when extrapolated to angular scenarios where sampling has not taken place, to perform consistently well over a wide range of surface covers, and to be relatively insensitive to the presence of noise in the data (Privette *et al.* 1997, Lucht 1998, Lucht and Lewis 2000). However, the set of kernels used in this research is not of great importance as the interest lies in the ability of the model to accurately predict the reflectance values under similar angular scenarios, rather than in the behaviour of the individual model parameters.

MRPV

An alternative set of semi-empirical models describe the reflectance as a product of a collection of terms t_n which determine the characteristics of the BRDF shape. These follow the form of Equation 4.10:

$$\rho(\lambda, \theta_i, \theta_v, \phi) = \prod_n K_n((\theta_i, \theta_v, \phi); f_n(\lambda)) \quad (4.10)$$

where f_n are the model parameters and the BRDF shape is described as a product of the t_n terms. The underlying concept of such models is that the reflectance from a surface may be described

by the determinants of the BRDF shape and their functioning in terms of the control they exert on particular aspects of the angular dependence of the reflectance and the multiplicative nature of these models results in a much wider representation of BRDF shapes than in additive models such as AMBRALS (Lucht and Roujean 2000a).

The original three parameter model of Rahman, Pinty and Verstraete (Rahman *et al.* 1993b, Rahman *et al.* 1993a) commonly referred to as RPV is a multiplicative model of the form described in Equation 4.10. The model is formulated from an explicit consideration of the shape of the BRDF which is defined as the product of three terms (i) the amplitude of the reflectance, (ii) the shape of the BRDF, and (iii) the relative amount of forward and backward scattering. However as the third term contains a Henyey-Greenstein function the model is not linear with respect to its parameters. A modified version has been defined by Marchonik *et al.* (1998) for operational use in the MISR (Multiangle Imaging SpectroRadiometer) BRDF product, which approximates the Henyey-Greenstein function with an exponential function resulting in a semi-linear model (Lucht and Roujean 2000a). The model takes the form of Equation 4.11:

$$\rho(\lambda, \theta_i, \theta_v, \phi) = \rho_0 K_1^{f_1} K_2^{f_2} K_3^{f_3} \quad (4.11)$$

where θ_i , θ_v and ϕ represent the illumination and viewing zenith and the relative azimuth angle, ρ_0 is a brightness term, and f_n are the model parameters. A logarithm of the model needs to be calculated in order to linearise it, after which it may be inverted analytically:

$$\ln(\rho(\lambda, \theta_i, \theta_v, \phi)) = \ln \rho_0 + f_1 \ln K_1 + f_2 \ln K_2 + f_3 \ln K_3 \quad (4.12)$$

The functions K_n are defined as follows:

$$K_1(\lambda, \theta_i, \theta_v, k) = \frac{\cos^{k-1} \theta_i \cos^{k-1} \theta_v}{(\cos \theta_i + \cos \theta_v)^{1-k}} \quad (4.13)$$

$$K_2(g, \xi) = (e^{-b_m \cos \xi}) \quad (4.14)$$

$$K_3(\rho_0, G) = 1 + \frac{1 - \rho_0}{1 + G} \quad (4.15)$$

where K_1 is the Minnaert model which describes the basic shape of the BRDF as a function of the viewing and illumination geometry (Minnaert 1941), K_2 is the Henyey Greenstein phase function which controls the relative amount of forward and backward scattering (Henyey and Greenstein (1941) in Rahman *et al.* (1993a)), and K_3 is an approximation to the hotspot effect. At all spatial scales objects in a three dimensional scene will cast shadows resulting in a “hotspot” effect of emergence and occlusion as a function of the viewing and illumination geometry, which will result in a peak in reflectance in the retrosolar direction and a decrease in reflectance away from the direction of illumination (Lucht and Roujean 2000a). In the definition of K_3 , when $\theta_i = \theta_v$ and $\phi_i = \phi_v$ (i.e. the hotspot), $G = 0$ and K_3 reaches it maximum value, and thus the value of the total reflectance increases (Rahman *et al.* 1993b). The geometric factor G is defined in Equation 4.16.

$$G = \sqrt{[\tan^2 \theta_i + \tan^2 \theta_v - 2(\tan \theta_i \times \tan \theta_v \times \cos \phi)]} \quad (4.16)$$

The difference between the MRPV model and the AMBRALS type approach is essentially limited to the treatment of the hotspot. MRPV has more flexibility in fitting around this region than AMBRALS which has a fixed hotspot width. However as sensors such as MODIS do not sample extensively within this region this feature is of little practical importance in the current research. The two approaches have been shown to perform similarly, with only marginal differences in output (Lucht 1998, Lucht *et al.* 2000). Research indicates that the extrapolative and interpolative abilities of the two models are comparable (Lucht 1998), with both approaches displaying fitting errors of a similar order of magnitude (Zhang *et al.* 1998).

4.2.4 Analytical inversion

Estimations of the BRDF may be produced by inverting semi-empirical models such as AMBRALS and MRPV provided a sufficiently large set of multiangular reflectances is available to derive the model parameters. An advantage of using the additive or multiplicative linear or semi-linear combination of kernels defined above (Equations 4.3,4.11) to model the BRDF is that they provide an analytical solution that reduces to the inversion of a small matrix (Lucht and Roujean 2000b). While such models have traditionally been inverted using angular measurements of reflectance derived from satellite observations of the surface, the use of *a priori* information has recently received attention. This information may take the form of field measurements (Li *et al.* 2001) or general knowledge relating to the surface characteristics derived from both ground and spaceborne measurements (Gao *et al.* 2003), and is applied when observations of the surface are noisy or acquired under poor angular sampling conditions which result in a limited number of good quality observations and low accuracies in model inversion. *A priori* knowledge has been used to (i) indicate when the retrieved kernel weights (or albedos) are outside expected bounds, (ii) to smooth noisy data, and (iii) to produce *a posteriori* estimates of unknown kernel weights under poor angular sampling scenarios (Li *et al.* 2001, Susaki *et al.* 2004). In the production of the MODIS BRDF/Albedo product if at least seven cloud-free observations of the surface are available during a 16 day period then a full inversion is attempted. However in the case of insufficient data, poor angular sampling or a poor model fit a ‘magnitude’ inversion is performed which exploits *a priori* knowledge (Schaaf *et al.* 2002). This process is described in more detail in Section 4.5.2.

Semi-empirical linear kernel driven BRDF models are typically inverted using standard linear algebraic techniques. This requires an error function to be defined in order to minimise the differences between the observations and the modelled reflectances. The method most commonly used is that of least squares, whereby the model parameters are determined by minimising the square of the errors between the modelled and the observed reflectances. The observed reflectances are assumed to have a Gaussian distribution with errors equally distributed between positive and negative values. If the observations are unbiased the assumption is that any deviation of the modelled from the observed data is due either to noise in the measurements or an inability of the model to describe the observed BRDF (Lucht and Lewis 2000). The error function to be

minimised has only a single minimum and is defined as:

$$e^2 = \sum_{i=1}^n (\rho_{i(\text{observed})} - \rho_{i(\text{modelled})})^2 \quad (4.17)$$

where $i = 1 \dots n$ is the index of observations and $\rho(\text{observed})$ and $\rho(\text{modelled})$ the observed and modelled reflectances. The partial derivatives of e^2 are then calculated with respect to each of the model parameters in order to find the values for which e^2 is a minimum. The model to be inverted may be written as:

$$\rho = \sum_{i=1}^n f_i K_i \quad (4.18)$$

where ρ are the modelled reflectances, n is the number of kernels (K_i), and f_i are the weights to be determined (i.e. the model parameters). The values of the f_i terms which minimise the error function (Equation 4.17) need to be found. Using matrix notation this can be stated as:

$$\mathbf{p} = \mathbf{k} \cdot \mathbf{M} \quad (4.19)$$

where \mathbf{p} represents a vector containing the summed observed reflectances, \mathbf{M} is the matrix containing the kernel product values and \mathbf{k} is a vector containing the model parameters which we wish to solve for. A generic linear system such as that defined in Equation 4.19 may be solved by multiplying \mathbf{M} by its transverse \mathbf{M}^T producing a variance-covariance matrix of the model kernels. This is then inverted to give $[\mathbf{M}\mathbf{M}^T]^{-1}$. The parameter vector \mathbf{k} can then be calculated by multiplying $[\mathbf{M}\mathbf{M}^T]^{-1}$ by the observations vector \mathbf{p} .

4.2.5 Overview

The anisotropy of surface reflectivity and the methods typically used to normalise remote sensing data for these effects has been discussed in the preceding sections. Semi-empirical linear kernel driven BRDF models have proved a popular means to this end, and are the chosen approach for the operational production of the MODIS BRDF/Albedo product (Schaaf *et al.* 2002). Although the importance of accounting for angular effects in the remote sensing signal is increasingly

acknowledged, change detection studies typically assign these effects to “noise” and attempt to reduce their impact rather than account for or exploit their information content. The remainder of this chapter is therefore concerned with the development of a new approach to change detection which explicitly accounts for directional effects in earth observation data using the linear and semi-linear kernel driven approaches discussed above.

4.3 A new approach to change detection

The primary aim of the work documented here is to derive a change detection algorithm which addresses the drawbacks of traditional approaches, and which may be applied to the identification of fire induced surface change from high temporal and moderate spatial resolution remote sensing data. Traditional remote sensing change detection techniques have been reviewed in Chapter 2. In light of the limitations identified with these, the change detection model developed in the following sections is formulated to;

1. Account for phenological changes in the surface
2. Account for directional effects in the remote sensing signal
3. Enable the identification and removal of noisy data within a time series

The research follows on from that of Roy and Lewis (2000) and Roy *et al.* (2002) who implemented a new, generic approach to change detection. This work was novel in its approach due to the incorporation of angular effects in the remote sensing signal into a change detection model of the surface. Coupled with the use of statistical measures (as opposed to the traditional approach of thresholding arbitrary signal levels) to identify change, the incorporation of a BRDF model was shown to provide an increased accuracy over previous methods in the detection of fire induced changes to the surface (Roy *et al.* 2002). Although the approach detailed in the subsequent sections follows on from the work of Roy *et al.* (2002) in particular through the incorporation of a BRDF model of the surface into the change detection model, the various modifications have resulted in a burn scar detection algorithm which is substantially different to the original version. The following section provides a description of the original model of Roy

and Lewis (2000) and Roy *et al.* (2002) and the drawbacks associated with it. Leading on from this the change detection model is developed, and its implementation described.

The change detection algorithm of Roy and Lewis (2000) involved the inversion of a BRDF model against a time series of reflectance data, with the resulting model parameters used to provide a prediction of reflectance under the viewing and illumination conditions of a subsequent observation or set of observations. This expectation of reflectance was then compared to the observed value with areas of potential surface change identified as large discrepancies between the observed and predicted values. The linear semi-empirical kernel driven approach of Roujean *et al.* (1992) was followed in order to model the angular variations in surface reflectance for reasons including the linearity of the model which allows for rapid analytical inversion, the implicit modelling of heterogeneity, and the ability to produce rapid predictions of uncertainty associated with the estimates of the model parameters. Using a volumetric and a geometric kernel the model takes the form of Equation 4.3. The kernels used to account for geometric and volumetric contributions of surface scattering are a reciprocal version of the LiSparse geometric-optical kernel, and the RossThick volumetric kernel (Schaaf *et al.* 2002). As the BRDF model takes a linear form it is inverted analytically against a set of m observations of reflectance following the approach defined in Section 4.2.4. Under the assumption of a normal distribution of residuals a Z-score is then defined as a normalized measure relating to the probability of a new observation belonging to the same set as that used in the model inversion (Roy *et al.* 2002):

$$Z(\lambda) = \frac{\rho_{modelled}(\lambda, \theta_i, \theta_v, \phi) - \rho_{observed}(\lambda, \theta_i, \theta_v, \phi)}{\varepsilon} \quad (4.20)$$

where $\rho_{modelled}(\lambda, \theta_i, \theta_v, \phi)$ is the modelled bidirectional reflectance, $\rho_{observed}(\lambda, \theta_i, \theta_v, \phi)$ is the measured reflectance and e is the error in model prediction as defined in Equation 4.17 and ε is the mean error in a prediction of the bidirectional reflectance at the angles θ_i , θ_v , and ϕ , defined in Equation 4.21. The sign of the Z-score provides an indication of the direction in which the modelled reflectance diverges from the measured value.

$$\varepsilon = e \sqrt{\frac{1}{w}} \quad (4.21)$$

The term $\frac{1}{w}$ is the ‘weight of determination’ of the model (Lucht and Lewis 2000) which is defined as:

$$\frac{1}{w} = \mathbf{u}^T \mathbf{M}^{-1} \mathbf{u} \quad (4.22)$$

The weight of determination of the model parameters is a function of the angular sampling of the observed reflectances. This term is thus useful in determining the contribution of the angular sampling to the error associated with the model parameters (Lucht and Lewis 2000).

The model defined above represents a generic approach to detecting changes which have taken place on a vegetated surface. A linear semi-empirical model of the BRDF is inverted against a set of multiangular reflectances, and the parameters of the model are then inverted to predict the surface reflectance under the angular geometry of the next observation in the time series. In addition a Z-score is calculated as the magnitude of this is related to the probability of the next observation of reflectance *not* belonging to the same set as the previous observations used to calculate the model parameters, with the sign of the Z-score indicating whether the modelled value is higher or lower than the subsequent observation. If the absolute value of the Z-score for a pixel is greater than a specified threshold ($|Z| \geq Z_{threshold}$) then the pixel is identified as a potential change. Once a pixel has been identified as a potential change candidate, the next step in the algorithm is to separate temporary surface changes from persistent ones. Temporary changes may be caused by short term increases or decreases in soil moisture, the presence of undetected clouds or cloud shadows, or by artifacts in the data (Roy *et al.* 2002). In the original implementation of the model this is achieved through the use of a temporal consistency threshold. The algorithm is applied in fixed temporal increments through a time series of reflectance data, with the Z-score defined in Equation 4.20 calculated at each point. The pixel is then identified as a change candidate if it has a minimum number of observations (N_{pass}) within an defined time period ($N_{duration}$) which are above the value of the $Z_{threshold}$, with the day of change selected as the one with the greatest $|Z|$ value. It is suggested that a suitable value of (i) N_{pass} observations might be estimated from an examination of the frequency of the satellite overpass in addition to the presence of cloud cover; (ii) $N_{duration}$ may be derived empirically for a given $Z_{threshold}$ or may be based on field observations or spectral measurements of the duration of the burn signal; (iii) $Z_{threshold}$ is chosen arbitrarily after an examination of the data (Roy *et al.* 2002).

After a persistent change has been identified, it is necessary to determine the nature of the change. This is achieved by an examination of the magnitude and the difference in the sign between the modelled nadir reflectance calculated for the mean solar zenith angle of the 16 days prior to the day of change and after the day of change, in an attempt to differentiate between changes due to burning and changes as a result of factors other than the occurrence of fire. This is based on the assumption that different types of land cover change will vary spectrally. The relative change in nadir modelled reflectance is described in Equation 4.23.

$$\delta\rho_{nadir} = \frac{\rho_{nadir(\lambda)}^+ - \rho_{nadir(\lambda)}^-}{\rho_{nadir(\lambda)}^-} \quad (4.23)$$

where $\rho_{nadir(\lambda)}^-$ is the nadir reflectance calculated from the 16 days prior to the day of change, and $\rho_{nadir(\lambda)}^+$ is the nadir reflectance for the day after the change. Areas which have changed as a result of burning are expected to exhibit a decrease in reflectance (see Chapter 3), which will result in a negative value of $\delta\rho_{nadir}$. Changes due to other factors (e.g. cloud contamination) will result in an increase in reflectance, and thus will have a positive value of $\delta\rho_{nadir}$.

The model described above was applied to a time series of approximately two months of band 5 ($1.24\mu m$) MODIS 500m surface reflectance data (Roy *et al.* 2002). Preliminary regional verification shows that the timing and location of larger areas of burning correspond to MODIS active fire detections, and a qualitative examination suggests that it is possible to track the spatial and temporal progression of burning from the model results.

Although the preliminary results indicate that the algorithm maps both the location and approximate day of burning successfully at a regional scale (Roy *et al.* 2002), various issues are identified with the approach described. The primary aim of the research presented here is to refine this original algorithm in particular by addressing these problems in addition to the limitations identified in Chapter 2, through the development of a new approach to change detection. This model is introduced in the following section.

4.4 Rationale

The change detection algorithm of Roy *et al.* (2002) was introduced in the previous section. This original implementation of the model uses a sliding window approach to invert the semi-empirical kernel driven BRDF model of Wanner *et al.* (1995) over a temporal sequence of surface reflectance, and to provide a prediction of reflectance for a subsequent day in the time series. The BRDF of the surface is modelled from day $T - n$ (where T is the day of the current observation and n is the size of the window) to day T , to provide a prediction of reflectance for the next observation (day $T + 1$). The window is moved in daily increments through the data, providing a prediction of reflectance for each pixel (excluding the first n observations in the time period), based on the previous n observations. Following the criteria used in the production of the MODIS BRDF/Albedo product Roy *et al.* (2002) have used a window size of 16 days, with a minimum of seven cloud free observations required during this period to perform the inversion. The size of the window is an important factor as it will affect the accuracy with which the model predictions fit the observed reflectances. The wider the window size used the larger the number of samples available for inversion and therefore the more accurate the model predictions will be, while too small a window may result in large uncertainties in the model predictions.

A major assumption of this approach is that the surface state remains invariant over the time period of the window (n days). The validity of this assumption is dependent on various factors. The magnitude of any variations in the state of the land surface will be determined by the dynamics of the vegetation which in turn will be a function of the vegetation type, as well as the meteorological conditions prior to as well as over the temporal sequence of the model inversion. If a short window size is used it may be reasonable to assume that the surface does remain static over this time period. However if there is persistent cloud in the data, it may be necessary to use a larger window size in order to have a sufficient number of cloud free observations (m) to perform the inversion. If the window size is too large the results may be smoothed and the probability of underlying change occurring increased, which will pose problems when trying to detect sudden changes in the data. Roy *et al.* (2002) have set the value of m to be seven. Thus following this approach a minimum of seven cloud free observations are required over the sixteen day period in order to invert the model. While this criteria might be easily met in datasets collected over southern Africa during the burn season, it may prove to be problematic in studies of northern

latitudes where the likelihood of persistent cloud in the data is greater. In a comparison of BRDF models for the angular normalisation of data collected over northern latitudes Latifovic *et al.* (2003) emphasize that even with the use of data acquired by multiple sensors and an enlarged temporal window, the routine acquisition of a sufficient number of cloud-free observations remains a serious challenge. In addition, the inherent presence of smoke, haze and aerosols over an area subjected to burning may reduce the number of cloud free or good quality observations, although the extent to which this occurs will be dependent on the intensity of the fire and the weather conditions at the time of burning. In this case a larger window size may be needed in order to provide a sufficient number of samples with which to accurately determine the model parameters and to reliably invert the model, and the validity of the assumption of a static surface may be questionable.

The following section describes the development of two temporal BRDF models which may be applied to a long time series of reflectance data, and which are used as a basis for a change detection scheme.

4.5 Temporal angular models of the surface

In order to model the angular variations in a temporal sequence of multi-angular remote sensing data, it is necessary to use a model which is applicable to the surface characteristics for the entire period of interest. As described above the approach typically used in the angular normalisation of remote sensing data or the retrieval of BRDF model parameters has been to apply the model over a short (e.g. 16 day) temporal window. Variations in the surface are considered unimportant over this period and are therefore not accounted for. The author is only aware of two studies in the literature which have described the development of a temporal angular model of the surface applicable to a long time series of data. Latifovic *et al.* (2003) have introduced a nonlinear temporal angular model (NTAM) which combines aspects of existing models and responds to seasonal changes in land cover properties. The NTAM consists of an angular component which follows the kernel driven approach of Roujean *et al.* (1992) to describe the geometric and volumetric scattering from the surface, a hotspot expression (Chen and Cihlar 1997), and a temporal component which uses vegetation indices as a surrogate temporal measure. The model is de-

scribed in Equation 4.24:

$$\begin{aligned} \rho_i(\theta_i, \theta_v, \phi, \Delta_i) = & 1 + (a_1 + a_2(1 - \Delta_i) + a_3(1 - \Delta_i)^2) \times f_1(\theta_i, \theta_v, \phi) \\ & + (a_4 + a_5\Delta_i + a_6\Delta_i^2) \times f_2(\theta_i, \theta_v, \phi) \times (1 + a_7e^{-\xi/\pi a_8}) \end{aligned} \quad (4.24)$$

where f_1 and f_2 refer to the geometric and volumetric components which are functions of the illumination and viewing geometries only (Roujean *et al.* 1992), the final term is the hotspot definition and

$$\Delta_1 = (\rho_2 - \rho_1)/(\rho_2 + \rho_1) \text{ (visible waveband)}$$

$$\Delta_2 = \rho_2 - \rho_1 \text{ (near-infrared waveband)}$$

where ρ_1 is the visible waveband, and ρ_2 the near infrared. The introduction of the Δ_i term allows for tracking of seasonal variations in the BRDF shapes, while the a_i coefficients remain time invariant. The temporal variations in the geometric and volumetric parameters are supposed to be related to the amount of vegetation. In the model this is described by a polynomial function in the form of two vegetation indices, consisting of the NDVI for the visible wavebands and the difference between the red and near-infrared for the near-infrared waveband. This model was tested along with the empirical modified Walthall (Walthall *et al.* 1985) model, the semi-empirical model of Roujean *et al.* (1992) and the Ross-Li geometric-optics model (Lucht and Roujean 2000b), on a multi-angular dataset spanning an entire growing season. The highest overall r^2 values were produced by the NTAM model, with less pronounced interannual variations in r^2 demonstrated by this temporal model, while the linear models did not perform as well due to the changing target characteristics during the period of inversion (Latifovic *et al.* 2003).

Despite the improvement exhibited by the NTAM model over the non-temporal approaches its formulation is not ideal. The temporal components of this model are approximated by polynomials which are related to vegetation indices, in an attempt to account for variations in green leaf area during the growing season and the land cover dependent patterns of geometric and volumetric scattering components (Latifovic *et al.* 2003). Various problems are associated with the NDVI. These have been discussed in Section 2.1.1 and include its sensitivity to external perturbations such as variations in the soil background and atmospheric conditions. In addition it is not a good indicator of plant growth as it saturates at high levels of biomass. The ability of the NDVI

to describe temporal variations in the surface is therefore likely to be spatially and temporally variable.

The second temporal BRDF model which has been introduced in the literature is that of Zhang *et al.* (1998) which is used to account for angular variations in a long time series of AVHRR data. The authors emphasize that although almost all models of the BRDF describe the reflectance from a surface purely as a function of the geometry at which the surface is illuminated at and viewed from thereby assuming that the target does not change significantly over the period of measurement, seasonal and annual variations in vegetation do occur and need to be taken into account when looking at long time series of data. In particular land cover types such as grasslands and deciduous forests (which together cover approximately 30 percent of the land surface of the current southern Africa study area) exhibit seasonality, and it is therefore necessary to account for these phenological variations (Kalluri *et al.* 1997). In order to achieve this Zhang *et al.* (1998) implement a temporal angular model using a Fourier series to approximate the temporal component of reflectance, and a modified version of the empirical Walthall model (Walthall *et al.* 1985) to account for the angular component of surface reflectance. This temporal model of the surface BRDF is described in Equation 4.25:

$$\begin{aligned} \rho(\lambda, \theta_i, \theta_v, \phi, t) = & a_0(\theta_v^2 + \theta_i^2) + a_1\theta_v^2\theta_i^2 + a_2\theta_v\theta_i\cos\phi + a_3 \\ & + a_4\cos\frac{2\pi t}{N} + a_5\sin\frac{2\pi t}{N} + a_6\cos\frac{4\pi t}{N} + a_7\sin\frac{4\pi t}{N} \end{aligned} \quad (4.25)$$

where N is the number of measurements in the time series, and t varies between 0 and $N - 1$. The model is tested on 4 years of AVHRR data in the form of 10-day NDVI Maximum Value Composites (MVC). In addition the time series was split into intervals of three months and the modified Walthall model (Walthall *et al.* 1985) and the modified RPV model (Rahman *et al.* 1993a) used to model the surface over this time period, as well as over the entire four years. The results from this study indicate that while for seasonally invariant land cover types such as the Sahara all three models perform equally well, in higher latitudes over areas of deciduous vegetation the temporal model performs better (Zhang *et al.* 1998). In addition for the full four year dataset the temporal model gives better results than both the modified Walthall or modified RPV models, as it accounts for phenological change over this period. Kalluri *et al.* (1997) have

found however that errors in the reflectances modelled by the temporal model were higher in temperate regions of Asia, Europe and North America, as well as across the Sahel. These are attributed to the greater inter annual variations in surface conditions which occur in these areas.

While the two temporal models described above remove the requirement to partition a time series of reflectance data due to variations in the surface phenology, the temporal components used to represent the surface variations are not ideal. The latter algorithm has been formulated for application to at least a year's worth of reflectance data in order to account for phenological variations over this period. In comparison the requirements of the current research are slightly different. Although one of the principal objectives is to account for low frequency changes in the surface over the time period of the observations, the motivation for doing this is the improved detection of land cover change. As these changes may occur at the same location more than once a year the temporal length of the observation period is unlikely to be greater than six months. The aim of the following section is therefore to develop a temporal angular model which is capable of accounting for phenological variations at this scale, and which therefore allows for the accurate detection of land cover changes which have occurred during this period.

4.5.1 A cubic function of time

The aim of this section is to introduce two temporal angular models of the surface which may be applied to long time periods (on the order of several months) of high temporal and moderate spatial resolution remote sensing data, for the purpose of detecting land cover change. The development of the temporal angular models has involved the incorporation of an empirical temporal model along with two different BRDF models of the surface. This is similar to the approach suggested by Zhang *et al.* (1998) and Latifovic *et al.* (2003) in so far as an empirical temporal model is coupled with an angular model of reflectance to produce a temporal BRDF model of the surface. However it is desirable to keep the number of nonlinear parameters in particular as well as the total number of model parameters to a minimum, thereby maintaining a simple and fast solution to inversion. This is of particular importance if the model is to be used with a spatially or temporally large dataset, or if it is intended for operational use. A four term temporal model has therefore been used to account for small scale phenological variations occurring on the surface over the period of the inversion, in the form of a cubic function of time. Two temporal BRDF

models are developed through the incorporation of this empirical model along with an angular model of the surface reflectance. The first uses the semi-empirical kernel driven approach of Wanner *et al.* (1995) to model the BRDF, with the temporal model attached to the brightness (the isotropic) component of the BRDF kernels. In this additive case the temporal component takes the form of a cubic function of time with the BRDF modelled as:

$$\rho(\lambda, \Omega, \Omega') = f_{iso}(\lambda) + f_{isot}(\lambda)t + f_{isot2}(\lambda)t^2 + f_{isot3}(\lambda)t^3 + f_{vol}(\lambda)K_{vol} + f_{geo}(\lambda)K_{geo} \quad (4.26)$$

where t represents the relative location of each observation within the time series, (Ω, Ω') represent the viewing and illumination vectors respectively, K_{vol} and K_{geo} are the kernels which describe the scattering of reflectance from the surface, and the f terms are the model parameters.

The second temporal approach utilises the modified RPV model of Rahman *et al.* (1993a) to describe the anisotropy of the surface. In this multiplicative case the temporal model takes the form of an exponentially transformed cubic, and the BRDF is modelled as:

$$\ln\rho(\lambda, \Omega, \Omega') = \ln\rho_0(\lambda) + \ln\rho_0(\lambda)t + \ln\rho_0(\lambda)t^2 + \ln\rho_0(\lambda)t^3 + f_1\ln K_1 + f_2\ln K_2 + f_3\ln K_3 \quad (4.27)$$

As above t represents the relative location of each observation within the time series, (Ω, Ω') refer to the viewing and illumination vectors respectively, and f_n are the model parameters. The angular components of both of these models are described in more detail in Section 4.2.3.

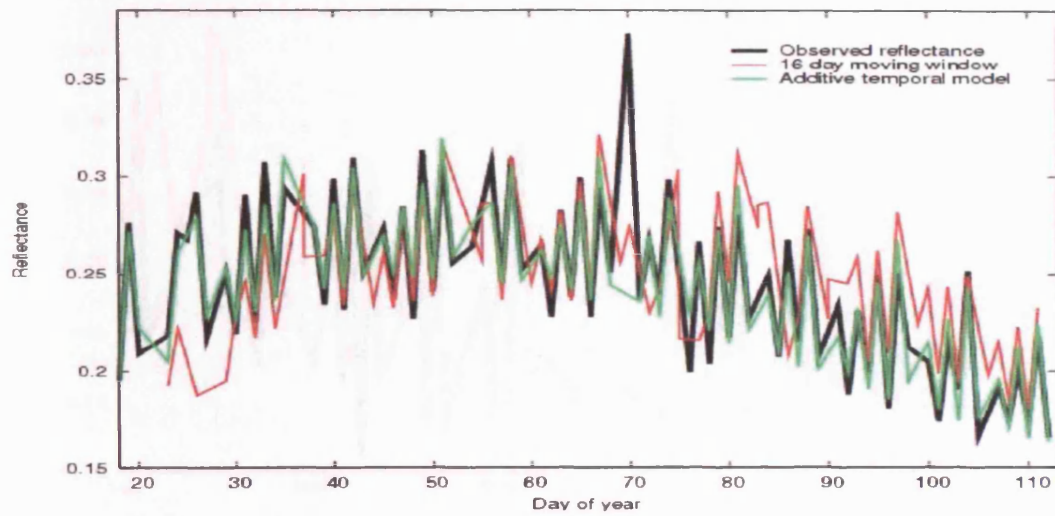
Each of the temporal BRDF models described in Equations 4.26 and 4.27 now consists of six parameters (per waveband), and explicitly account for temporal variations within the time period of the observations. As a result it is possible to invert the models over a much longer temporal sequence than traditional approaches. With the moving window approach typically used to invert BRDF models it is necessary to update the parameter values $f_{vol}(\lambda)$ and $f_{geo}(\lambda)$ for each new observation of reflectance. In contrast, for the temporal BRDF model described in Equation 4.26 only the three parameters $f_{isot}(\lambda)t$, $f_{isot2}(\lambda)t^2$ and $f_{isot3}(\lambda)t^3$ vary as a function of time while $f_{vol}(\lambda)$ and $f_{geo}(\lambda)$ remain constant. Similarly in the multiplicative case (Equation 4.27) only the three parameters $\rho_0(\lambda)t$, $\rho_0(\lambda)t^2$, and $\rho_0(\lambda)t^3$ are allowed to vary as a function of time, while the remaining parameters f_1 , f_2 and f_3 are constant over the time period of the inversion. In

comparison to the model of Roy *et al.* (2002) or the approach used in the creation of the MODIS BRDF/Albedo product (Strahler *et al.* 1999a) where three parameters per waveband are fitted to each sixteen day window, with either the additive temporal or multiplicative temporal BRDF model there are only six parameters for the entire temporal sequence.

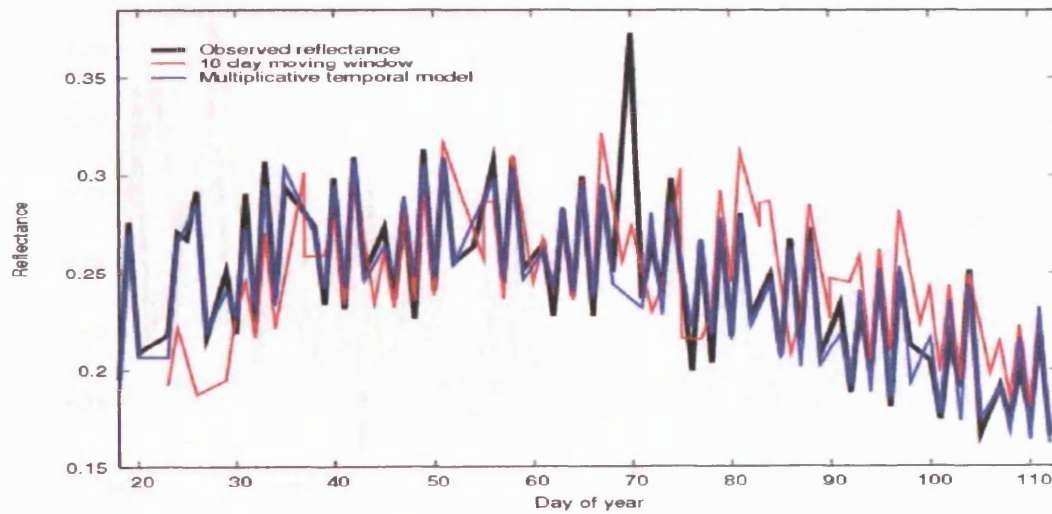
Two examples are employed to demonstrate the performance of the two temporal models. The first corresponds to the temporal sequence for an individual pixel, and illustrates the performance of the temporal models in the presence of low frequency surface change, while the second highlights the effect of cloudy samples on the model behaviour. Figure 4.4 displays a temporal sequence of 100 days of near infrared reflectances and the results from three different BRDF models. The first is the semi-empirical linear kernel driven approach described in Equation 4.3 which has been applied incrementally to the reflectance data using a 16 day window, with a minimum number of 7 cloud free samples required to perform the inversion. The second is the temporal version of this model defined in Equation 4.26 above and referred to as the “additive temporal” approach. The final model is the temporal angular version of the MRPV model introduced in Equation 4.27, and referred to as the “multiplicative temporal” approach.

Site 4A is located in western Zambia, as documented in Table A.1 and Figure A.1 in Appendix A. Figure 4.4a displays the observed (MODIS band 2) reflectances and the values predicted by the additive temporal model and the 16 day moving window approach, while Figure 4.4b displays the observed and the multiplicative temporal as well as the 16 day moving window modelled reflectances. A phenological trend is clearly evident in the temporal sequence as corresponding to the growth and senescence of the vegetation. While this change in the surface is modelled well by the two temporal BRDF models, it is apparent from the modelled reflectances in Figure 4.4 that problems arise with the 16 day moving window approach. Figure 4.4c displays a scatter plot of the observed and modelled reflectances for each of the three models. The r^2 values calculated between the observed and modelled reflectances are high for the additive temporal and multiplicative temporal results (0.91 and 0.93 respectively), but demonstrate a poor fit for the 16 day moving window approach ($r^2 = 0.54$).

The second temporal sequence is displayed in Figure 4.5. This corresponds to approximately three and a half months of daily MODIS 500m near infrared (band 2) reflectance data. The pixel is located in the Democratic Republic of the Congo (DCR) and is documented in Table A.1 and Figure A.1 in the Appendix A as Site 4B. Figure 4.5a displays the observed and modelled



(a) Additive temporal model and additive 16 day moving window approach



(b) Multiplicative temporal model and additive 16 day moving window approach

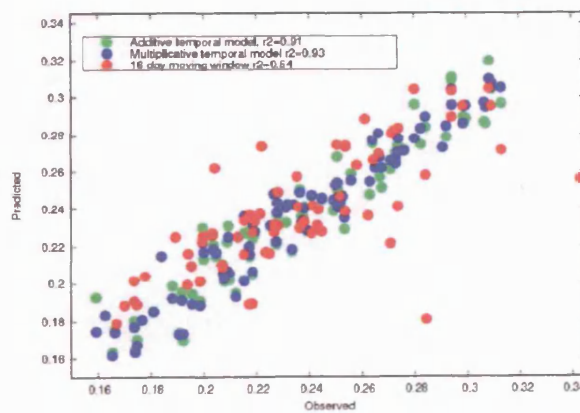
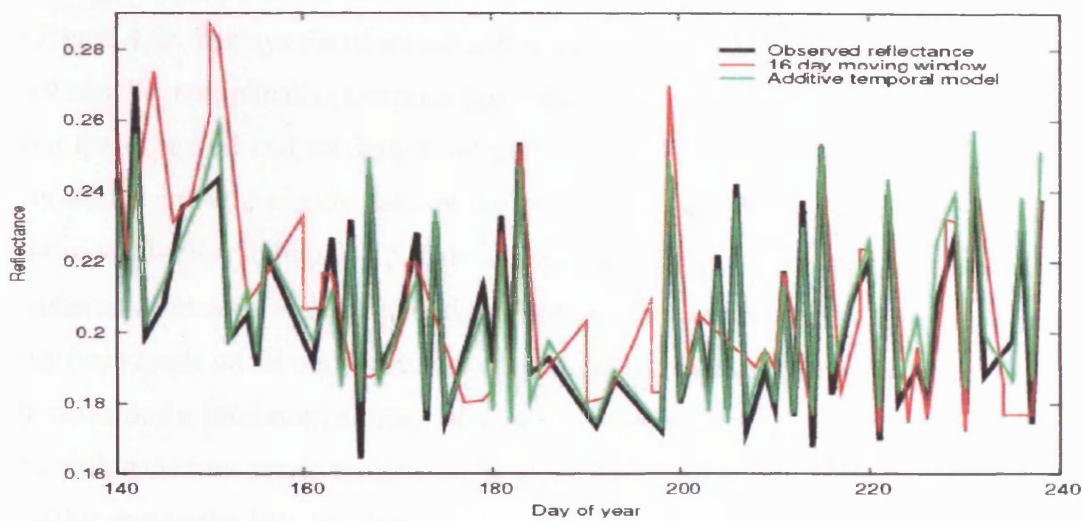
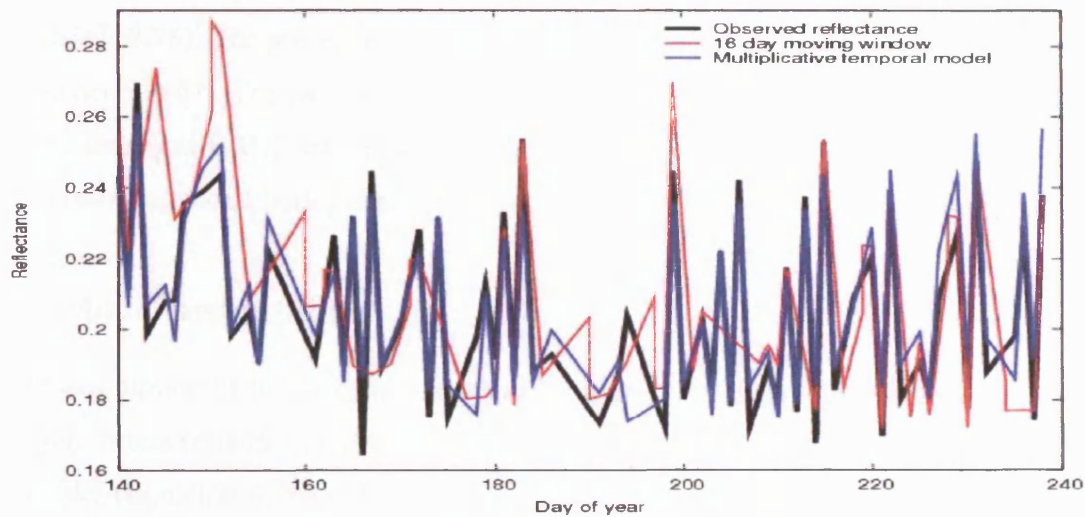


Figure 4.4: Observed and modelled reflectances, Zambia, Site 4A, January-May 2003



(a) Additive temporal model and additive 16 day moving window approach



(b) Multiplicative temporal model and additive 16 day moving window approach

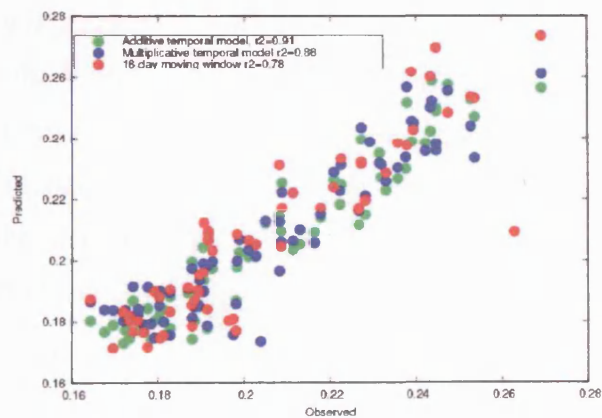


Figure 4.5: Observed and modelled reflectances, Democratic Republic of the Congo, Site 4B May-August 2003

reflectances using both the traditional 16 day window and the new additive temporal model, while Figure 4.5b displays the observed and modelled reflectances using both the 16 day moving window and the multiplicative temporal approach. All three datasets and the r^2 values calculated between the observed and modelled reflectances are displayed in Figure 4.5c. The effect of missing samples due to cloudy data on the predictions of reflectance from the 16 day moving window model is clear in Figure 4.5. Due to fewer than the minimum number of samples required to perform an inversion (at least 7 cloud free observations during the 16 day period) a prediction has only been made on 69 out of the 100 days in the time series (this does not include the initial 16). In contrast the minimum number of samples is set to be 25 for the temporal models, but as all days within the time series are used as input for each prediction a larger number of predictions are possible during the 100 day time period. While all three models fit the observed reflectances relatively well, the results of both temporal models are more accurate ($r^2=0.91$ and $r^2=0.86$ for the additive and multiplicative temporal models respectively) than the 16 day moving window approach ($r^2=0.78$). The presence and removal of noisy observations of reflectance are discussed further in Section 4.6. The two examples displayed in Figures 4.4 and 4.5 illustrate the advantage in using a temporal BRDF model to account for the angular component of the remote sensing signal in the presence of both phenological change and missing observations due to bad data.

4.5.2 Model assumptions

A major assumption of the temporal approach described in Equations 4.26 and 4.27 is that the BRDF parameters remain constant over the time period of the inversion. In the case of the additive model (Equation 4.26) only the isotropic coefficient is allowed to vary as a function of time, while the geometric and volumetric BRDF shape parameters remain constant over this period. It is thus assumed that while the magnitude of the brightness will vary, the shape of the BRDF (the volumetric and geometric contributions) will remain the same over the entire temporal period over which the inversion is performed. With the temporal version of the modified RPV model (Equation 4.26) the shape parameters are again assumed to be constant over this period. However as this model is multiplicative such an assumption has a different effect on the model behaviour. With the modified RPV model although the shape parameters will only have a single value over the period of the inversion the assumption is not that the overall BRDF shape

remains constant. Instead as the model parameters are combined in a multiplicative manner the BRDF shape will scale with changes in brightness. This is extremely similar to the assumptions made in the MODIS BRDF/Albedo back-up algorithm. The primary MODIS BRDF/Albedo algorithm uses a semi-empirical kernel-driven approach to describe the surface BRDF and Albedo as detailed in Section 4.2.3. An operational requirement in the creation of this product is for a minimum of seven cloud free observations within a sixteen day period in order to perform a full BRDF retrieval. The data within a sixteen day window are initially evaluated to discard any outliers, the weights of determination (Lucht and Lewis 2000) are calculated to ascertain the confidence of the product, and additional checks are performed to ensure that the kernel weights and model parameters are positive (Schaaf *et al.* 2002). If the data do not pass all of these evaluations then a backup algorithm is used as an alternative to a full inversion with a “magnitude inversion” approach followed instead. This involves the retrieval of the appropriate BRDF shape from a predetermined global BRDF database which has previously been derived for each MODIS pixel from the Olsen land cover map (Olson 1994). The 94 Olsen land cover types are converted into 24 BRDF appropriate land cover classes following the scheme of Strugnell and Lucht (2001) where an archetypal BRDF shape is associated *a priori* with a particular surface cover. A seasonal model is used in addition to the land cover information in order to account for seasonal anisotropic variability within the BRDF shapes. The assumption of this method is that the BRDFs associated with a particular surface cover will have broadly similar shapes with variations being merely a matter of degree (Schaaf *et al.* 2002). In order to determine the magnitude of these variations the archetypal shapes are adjusted by a scaling factor which provides the best fit for all of the directional observations at each pixel, thereby allowing for realistic variation within each class (Strugnell and Lucht 2001). This method can be expressed as:

$$\rho = s \times f \tag{4.28}$$

where the underlying BRDF shape (f) is a function of the three BRDF parameters (isotropic, volumetric and geomteric) which are a function of the illumination and viewing geometries of the surface only. The surface reflectance (ρ) is thus calculated by adjusting the BRDF shape with the actual observations through the determination of a scaling factor s , which can be calculated using a least squares approach (Gao *et al.* 2003). The current use of the land cover map and the seasonal

model is only an interim solution until a sufficient number of stable high quality retrievals have been performed globally from MODIS data, and these will eventually be used instead. The magnitude inversion approach is employed as the MODIS BRDF/Albedo backup algorithm due to its reliability which has been demonstrated through its application to and rigorous testing on a global AVHRR dataset (Strugnell *et al.* 2001, Schaaf *et al.* 2002).

The assumption made with the multiplicative temporal model introduced in Equation 4.27 relating to the temporal nature of the surface BRDF is similar to that associated with the magnitude inversion approach described above. For both the multiplicative temporal model and the MODIS back up algorithm it is assumed that the BRDF shape at a particular location will scale with changes in brightness. In contrast with the additive temporal model (Equation 4.26) the assumption is that while the overall brightness changes temporally, the shape of the BRDF does not. This is essentially the same so long as the magnitude of the change in brightness is not too great over the time period of interest. This is illustrated by Figure 4.6 which displays the variation in brightness for a series of individual pixels. This is the nadir modelled reflectance ($\Omega=0$, $\Omega'=0$) calculated as:

$$\rho(\lambda, \Omega, \Omega') = f_{iso} + f_{iso_t}t + f_{iso_{t^2}}t^2 + f_{iso_{t^3}}t^3 \quad (4.29)$$

where t is the day of the observation and f_{iso} , f_{vol} , and f_{geo} are the additive temporal BRDF model parameters. The inversions have been performed for a sequence of observations of MODIS band 2 reflectance acquired over a period of 120 days at five pixel locations. Figure 4.6a contains the results for the first four months of the burn season (April to July), while Figure 4.6b contains the results for the last four months of the burn season (August to November). As these data are the nadir modelled reflectance the temporal variability is essentially caused by variations in the characteristics of the surface.

The general trend in the near infrared reflectance for each of the five main vegetation classes is a decrease in brightness over the first half of the burn season between the beginning of April and the end of July, while over the second half of the season (August to November) the surface exhibits a general increase in brightness, although the exact nature of the change is dependent on the vegetation type. This pattern in the near infrared reflectance is observed over all vegetation types as the vegetation becomes increasingly dry as the burn season progresses until the onset

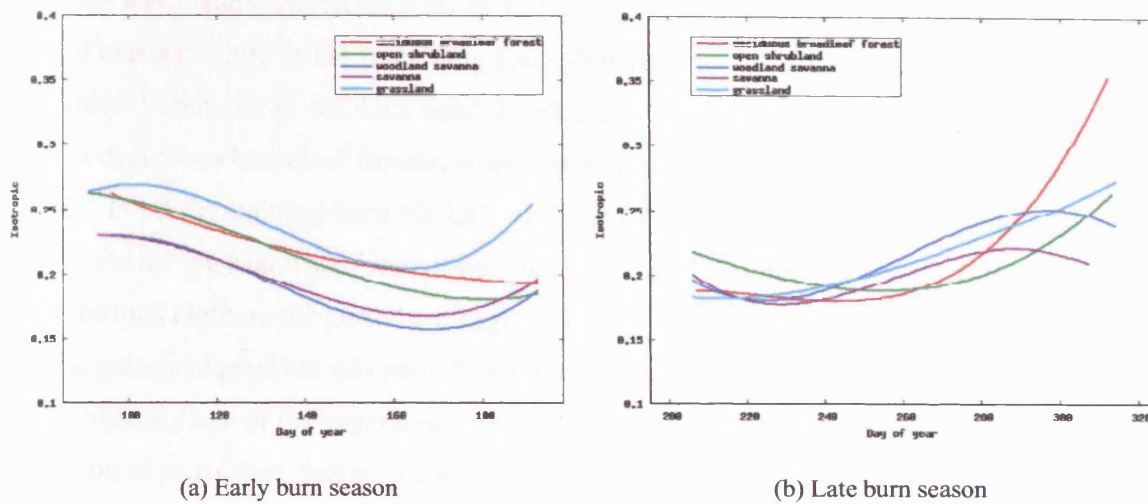


Figure 4.6: Variations in surface brightness

of the rains which occurs towards the end of the southern Africa fire season (Roy *et al.* 2002). The data contained in Figure 4.6 are representative of the general trends observed within the study area over the annual burn season. Figure 4.7 contains the magnitude of the changes in brightness for each of these pixels at each waveband over the entire 8 months of the burn season. The change in brightness over this period for all five vegetation types is less than 0.35 at all

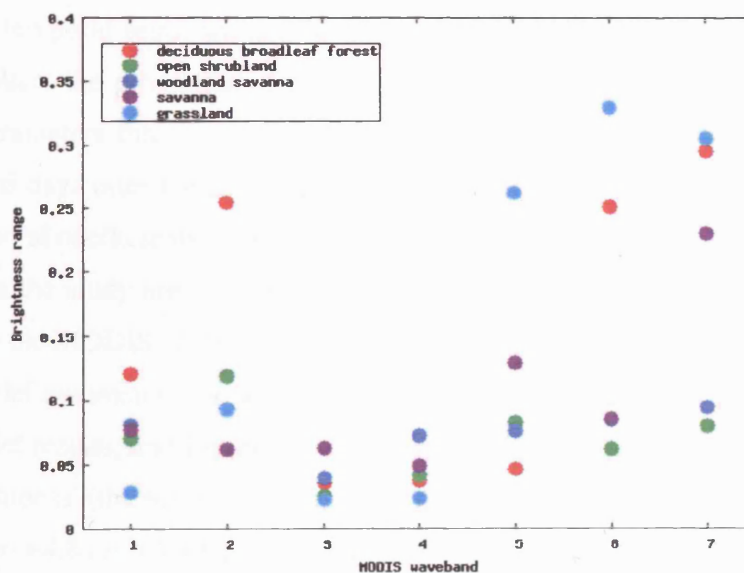


Figure 4.7: Variations in brightness

MODIS wavebands. At MODIS bands 1, 3 and 4 the magnitude of the change is small (<0.15) for all classes, while at the remaining four MODIS land surface wavebands changes are more variable. Variations in MODIS band 2 reflectance are less than 0.15 for all vegetation types except deciduous broadleaf forests, where the magnitude of the change during the eight months is 0.25. For the remaining three MODIS wavebands (5, 6 and 7) the greatest changes in brightness occurs for the grassland pixel with magnitudes of 0.26, 0.33 and 0.31 respectively. The variations over the total eight month period are large for certain cover types (e.g. 0.33 at band 6 wavelengths for the grassland pixel) as this period (April to November) encompasses a large proportion of the phenological cycle of the vegetation (see Section 3.4.2). As the aim of the current research is the detection of land cover change due to burning, the temporal models will not be implemented over periods longer than four months. This is due to the characteristics of the fires observed within the area of interest and described in Section 3.4. Due to the length of the southern Africa fire season (approximately 8 months long) and the possibility of multiple fire events occurring at the same location during this time, for accurate identification of these the change detection model should not be implemented over periods greater than four months.

In addition to the magnitude of phenological changes in the vegetation which occur over the time period of the inversion, the validity of the assumptions associated with the two temporal models described in Equations 4.26 and 4.27 are dependent on the stability of the shape of the BRDF over the temporal sequence and thus the extent to which the occurrence of fire within the study area alters the properties of the surface. This is investigated through a comparison of the model parameters fitted over a temporal sequence of 16 days before the occurrence of a fire, and the 16 days after the fire. The additive and multiplicative models have been fitted without the temporal coefficients to 10000 pre-fire and post-fire sequences of reflectance selected at random across the study area for the 2003 fire season. The occurrence of burning has been determined from the MODIS active fire product. Scatter plots of the pre-fire and post-fire values for the three model parameters for MODIS band 2 wavelengths are displayed in Figure 4.8 for the additive model results, and Figure 4.9 for the multiplicative model results. While a general decrease in 'brightness' (the first model parameter in both the additive and multiplicative models) is evident in Figures 4.8a and 4.9b, the values of the remaining parameters are extremely variable. The changes in the model parameters from pre-burn to post-burn conditions are likely to vary depending on the nature of the fire induced surface change as well as the characteristics of the

surface prior to the fire. The variability in the pre-burn and post-burn model parameters (Figures 4.8 and 4.9) are likely to be a function of this, as well as the noise in the data and the accuracy of the model fit over the 16 day sequence.

A study by Trigg *et al.* (2005) has investigated the effects of burning on the anisotropy of two savanna surfaces at a study site in Namibia using field spectroradiometry. These results indicate that at a grassland site the occurrence of fire reduces the anisotropy of the surface in comparison to its pre-fire state, while in contrast at a shrubland site the effect of burning is to either increase or decrease the surface anisotropy. In addition while the burned grassland site is only weakly anisotropic, the reflectance from the burned shrubland is found to be considerably more so, and while the effect of the grassland fire is to change the shape of the BRDF from an ‘upward bowl’ shape (i.e. higher reflectance at high negative and high positive solar angles) to a flatter shape with extremely similar reflectance across the solar plane, the effect of the shrubland fire is to decrease the magnitude of the reflectance more uniformly across all angles with the burned surface still exhibiting a slight upward bowl shape. This is thought to be due to the characteristics of the post-fire surface, as in contrast to the fire at the grassland site which burned most of the material present leaving a flat surface with low anisotropy, the fire at the shrubland site did not burn all of the vegetative material leaving a more structured surface due to the presence of charred stems (which cast shadows) resulting in greater surface anisotropy. The authors thus conclude that the anisotropy of burned vegetation may be expected to vary as a function of the fire intensity and combustion completeness as well as the timing of burning within the fire season (Trigg *et al.* 2005).

In addition to the distributions of parameter values displayed in Figures 4.8 and 4.9 an examination of the reflectance from a variety of pre-fire and post-fire surfaces suggests that the BRDF shape of the post-fire surface as well as the change in the BRDF shape as a result of the occurrence of a fire is extremely variable. This is illustrated through a temporal sequence of MODIS band 2 reflectances for two individual woody savanna pixels. The surface reflectance for the forty-five days before the detection of a fire as well as for the forty-five days after the fire is displayed as a function of the viewing zenith angle of each acquisition for the two pixel locations (Figures 4.10, 4.11 and 4.12). A fire has occurred on day 169 at the first location and on day 197 at the second. The band 2 reflectances are also displayed as a function of the day of the observation in Figures 4.11a and 4.11b. The occurrence of fire is clearly evident in both of these sequences

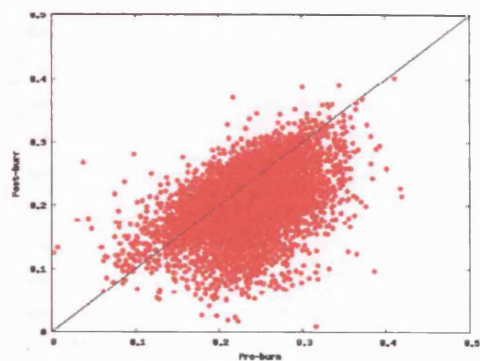
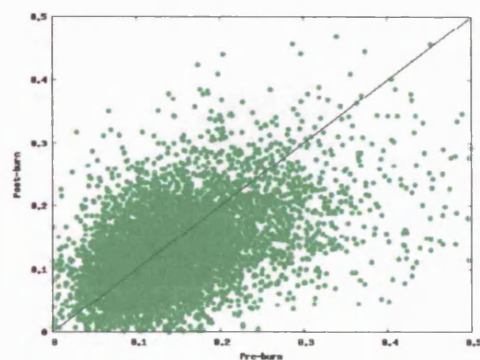
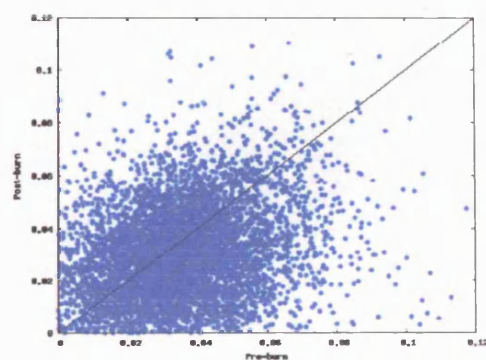
(a) Parameter 1 (f_{iso})(b) Parameter 2 (f_{vol})(c) Parameter 3 (f_{geo})

Figure 4.8: Additive model: Parameter values at near-infrared wavelengths

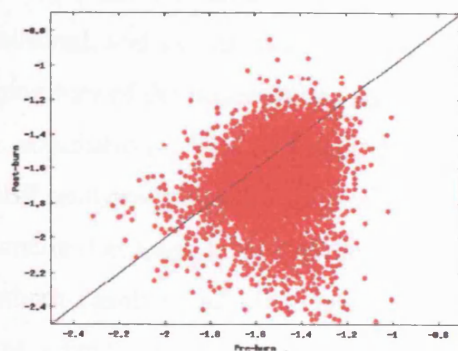
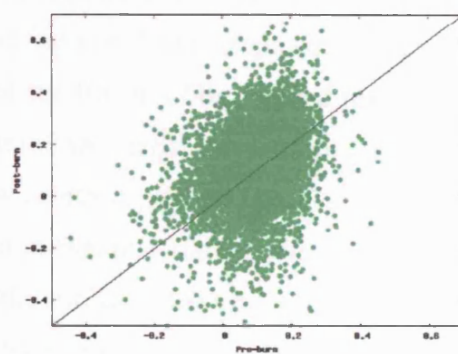
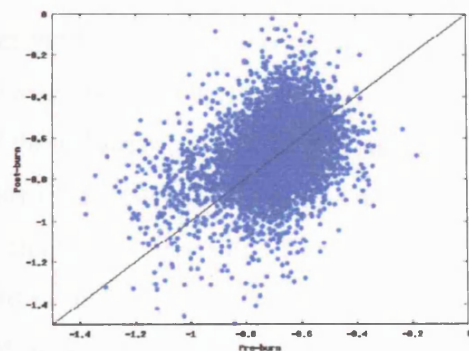
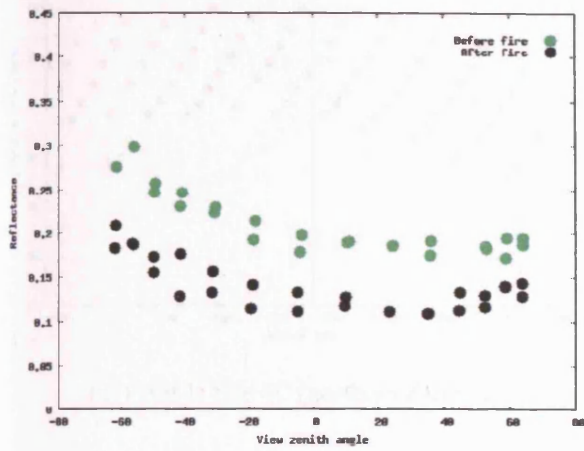
(a) Parameter 1 (ρ_0)(b) Parameter 2 (k)(c) Parameter 3 (b)

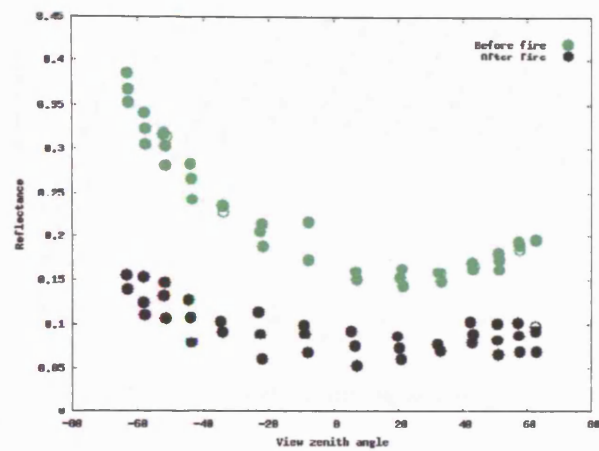
Figure 4.9: Multiplicative model: Parameter values at near-infrared wavelengths

of reflectance. The variations in the solar zenith angles over the period of the acquisitions is displayed in Figures 4.12a and 4.12b. The difference between the pre-burn and post-burn sampling in the solar plane is minimal, and variations in the reflectance are therefore predominantly a function of the viewing geometry of the observations and the changes taking place on the surface over the period of the acquisitions. The two pixel locations are documented as “woody savanna” in the MODIS IGBP land cover classification (see Section 3.3). Their locations within the area of interest are documented as Sites 4C and 4D in Table A.1 and Figure A.1 in Appendix A. Site 4C is located in northern Zambia, and 4D in north-eastern Angola. The woody savanna vegetation class is defined as a land surface which supports herbaceous and other understorey systems with forest canopy cover between 30 and 60%, and forest cover height exceeding 2m (IGBP 1988). Both of the pre-burn temporal sequences of reflectance (Figures 4.11a and 4.11b) exhibit a slightly asymmetric ‘upward bowl’ shape when plotted as a function of viewing zenith angle, although the shape of the BRDF of the second pixel is more pronounced than the first. This shape is typical of near infrared reflectances from a vegetation canopy as shadows tend to be less visible at larger view zenith angles resulting in a higher contribution of scattering from the vegetation. As is evident in Figure 4.10a the effect of fire at the first location is a reduction in the overall brightness of the surface. However the burning has not had a large impact on the surface anisotropy and the shape of the post-fire BRDF is extremely similar to that exhibited by the pre-fire surface. In contrast at the second location (Figure 4.10b) the occurrence of fire has a much larger impact on the anisotropy of the reflectance, with the post-fire surface exhibiting a much flatter shape than either the pre-fire BRDF or the post-fire BRDF at the first location. An examination of the temporal sequences plotted as a function of time (Figures 4.11a and 4.11b) indicate that the variance of the reflectance prior to the burn is much greater at the second location, and that the magnitude of the change from pre-fire to post-fire reflectance is also much greater at this location in comparison to the first. It is likely that this is due to factors such as the characteristics and condition of the vegetation prior to burning, as well as the combustion completeness and intensity of the fire (Trigg *et al.* 2005).

In the case of the first pixel as the occurrence of fire has a minimal effect on the shape of the BRDF and simply reduces the brightness of the surface by an order of magnitude, either of the temporal models described in Equations 4.26 and 4.27 are theoretically suited to modelling the changes in the surface. However in the second example, as the magnitude of the shape

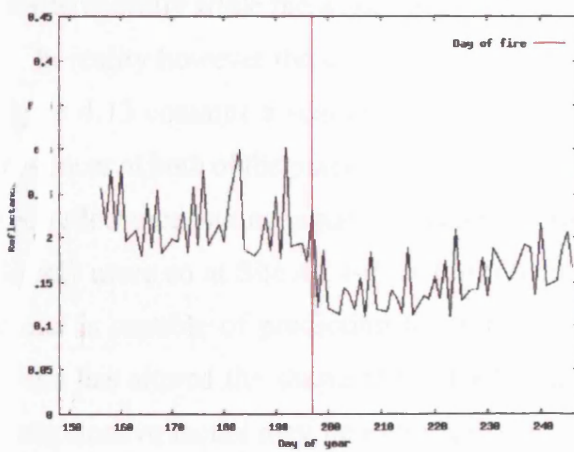


(a) Pixel 1: Site 4C (northern Zambia)

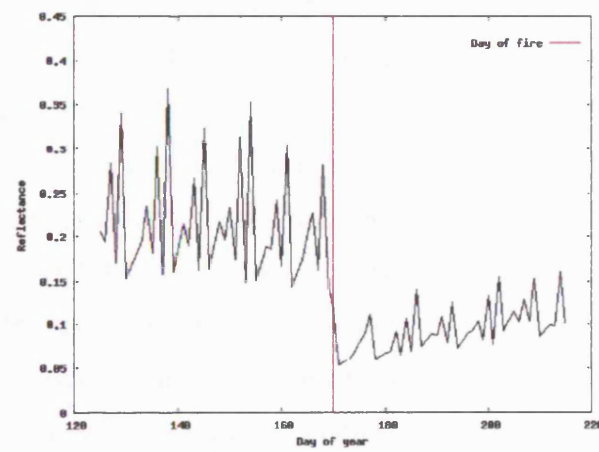


(b) Pixel 2: Site 4D (north-eastern Angola)

Figure 4.10: MODIS 500m band 2 reflectance as a function of view zenith angle



(a) Pixel 1: Site 4C (northern Zambia)



(b) Pixel 2: Site 4D (north-eastern Angola)

Figure 4.11: Temporal sequence of MODIS 500m band 2 reflectance

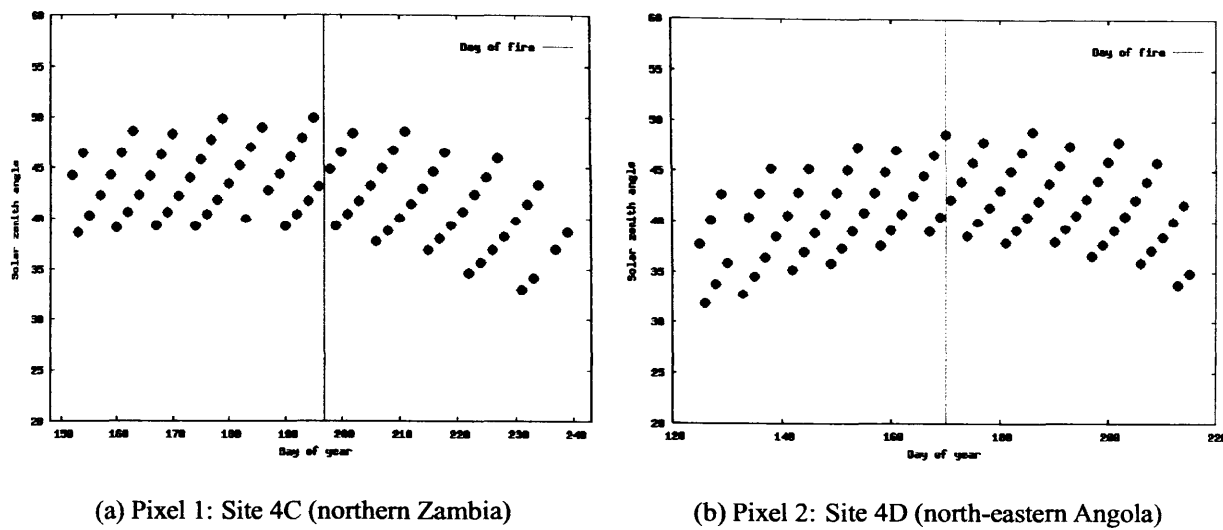


Figure 4.12: MODIS 500m band 2 reflectances: Sampling in the solar plane

of the BRDF decreases with decreasing reflectance (Figure 4.10b) the multiplicative empirical temporal BRDF model (Equation 4.26) may be more appropriate as the assumption with this approach is not that the actual shape of the BRDF remains constant over the time period of the inversion, but that it scales with changes in brightness. In contrast the assumption of the additive temporal model is that only the isotropic parameter and thus the overall level of reflectance will vary temporally while the actual shape of the BRDF will remain constant.

In reality however the choice of model makes little difference to the modelled reflectances. Figure 4.13 contains a scatterplot of model predicted values for the MODIS band 2 temporal sequences at both of the pixel locations using the multiplicative and the additive temporal models. The reflectance values modelled using the two different approaches are very similar although slightly more so at Site 4C ($r^2 = 0.97$) than at Site 4D ($r^2 = 0.93$). This suggests that either model is capable of predicting the surface reflectance accurately, although if the occurrence of fire has altered the shape of the BRDF as opposed to just the brightness of the surface the multiplicative model may be more appropriate. The difference in the predictions of reflectance from the two approaches is however extremely small. This is likely to be due to the fact that the overall magnitude of the brightness does not vary a great deal between pre-burn and post-burn conditions (approximately 0.1 in the above examples), and as a result both of the models are equally effective in characterising the angular variations in the surface reflectance. It should also

product, and their cloud state is documented as “clear”. The pixel locations are documented as Sites 4E and 4F in Table A.1 and Figure A.1 in Appendix A. Site 4E is located in southern Angola, and 4F in eastern Angola.

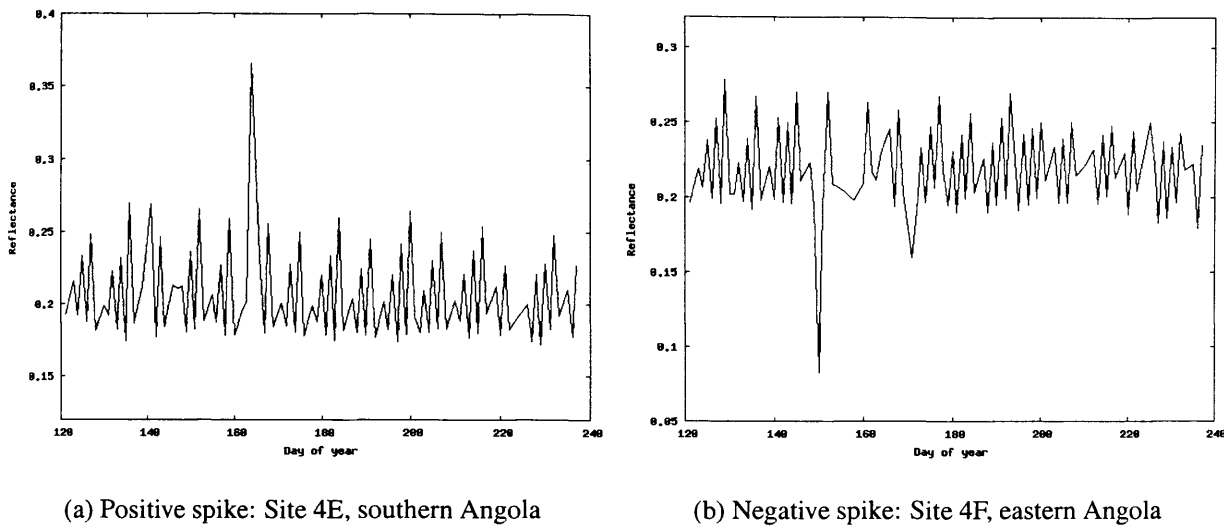


Figure 4.14: Isolated spikes in MODIS 500m band 2 reflectance

In the change detection model of Roy *et al.* (2002) isolated spikes such as these are not removed from the temporal sequence prior to inversion. An assumption implicit in this approach is the equal weighting of all observations, with all observations within the temporal window used to perform the inversion contributing equally to a subsequent prediction of reflectance, regardless of their quality. This assumption is only strictly valid if the expected variance for each observation is equal, which may not necessarily be the case. In particular the presence of isolated spikes in the data due to residual clouds, cloud shadow or ‘noise’ will invalidate this assumption. Although the change detection algorithm of Roy *et al.* (2002) does not identify such anomalies in the data as changes in the surface state due to the use of the temporal consistency threshold, they are not removed from the dataset and will therefore contribute to subsequent predictions of reflectance.

In order to identify and remove isolated bad data from the temporal sequence a Z-score has been defined. This is a probabilistic quantity related to the likelihood of a new observation belonging to the same set as that used in the model inversion, and is calculated after the first pass (and at every subsequent pass) of the model. Following the method of Roy *et al.* (2002)

described in Section 4.3 this measure takes the form of Equation 4.30:

$$Z = \frac{\rho_{observed}(\lambda, \Omega, \Omega') - \rho_{predicted}(\lambda, \Omega, \Omega')}{\varepsilon} \quad (4.30)$$

where $\rho_{observed}(\lambda, \Omega, \Omega')$ and $\rho_{predicted}(\lambda, \Omega, \Omega')$ are the observed and model predicted reflectance respectively, and ε is the error in the model prediction. This is defined as:

$$\varepsilon = e \sqrt{\frac{1}{w}} \quad (4.31)$$

where e is the expectation of error in the data assuming a normal distribution of residuals, and is approximated from the residuals according to Equation 4.32:

$$e^2 = \frac{1}{m-6} \sum_{i=1}^{i=m} (\rho_{observed}(\lambda, \Omega_i, \Omega'_i) - \rho_{predicted}(\lambda, \Omega_i, \Omega'_i))^2 \quad (4.32)$$

where m refers to the number of observations in the sequence and $m-6$ the degrees of freedom of the system. $\frac{1}{w}$ in Equation 4.31 is the “weight of determination” or the noise amplification factor (Lucht and Lewis 2000) defined as:

$$\frac{1}{w} = [\mathbf{u}]^T [\mathbf{M}]^{-1} [\mathbf{u}] \quad (4.33)$$

where $[\mathbf{u}]$ is a vector containing the model coefficients, T denotes the transpose operation and $[\mathbf{M}]^{-1}$ is the inverse matrix. The weights of determination of $[\mathbf{u}]$ are directly related to the standard deviation of the uncertainty or error associated with the model parameters themselves (Lucht 1998).

The corresponding Z-scores calculated for the two temporal sequences displayed in Figure 4.14 are shown in Figure 4.15. Figure 4.16 contains the observed and model predicted values for the two pixels. The Z-score defined in Equation 4.30 has been calculated for these sequences (Figure 4.30) and these values have been filtered using a threshold of 1.5 to identify isolated spikes. Any observations with a Z-score greater than 1.5 or less than -1.5 have been removed from the sequence and therefore do not contribute to the subsequent predictions of reflectance.

In some situations and in particular towards the end of the burn season as cloud cover in-

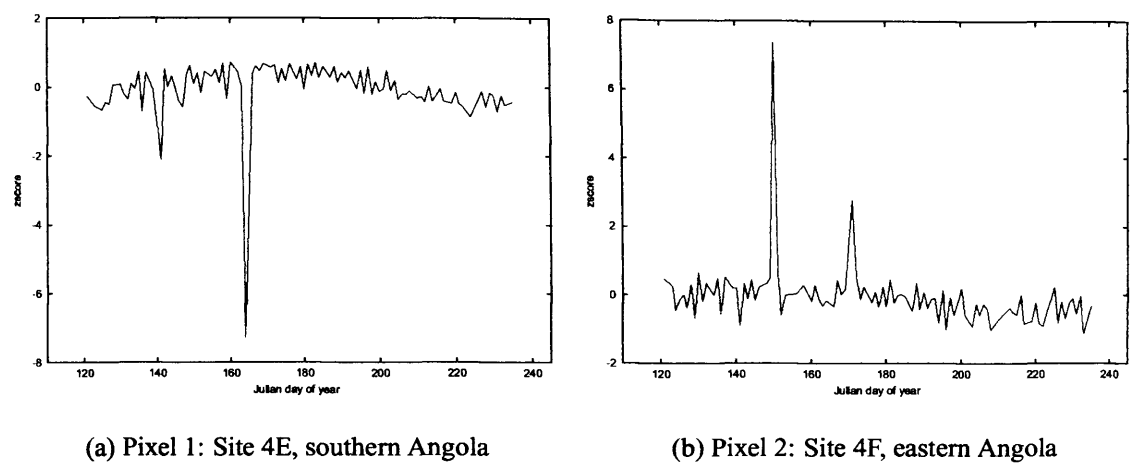


Figure 4.15: Filtering for outliers: Z-score values, additive model results

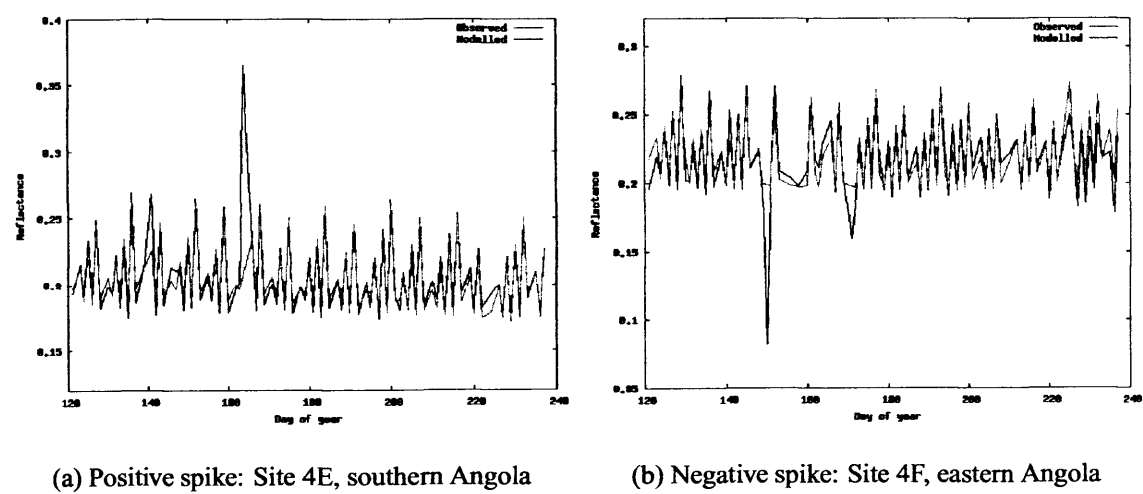
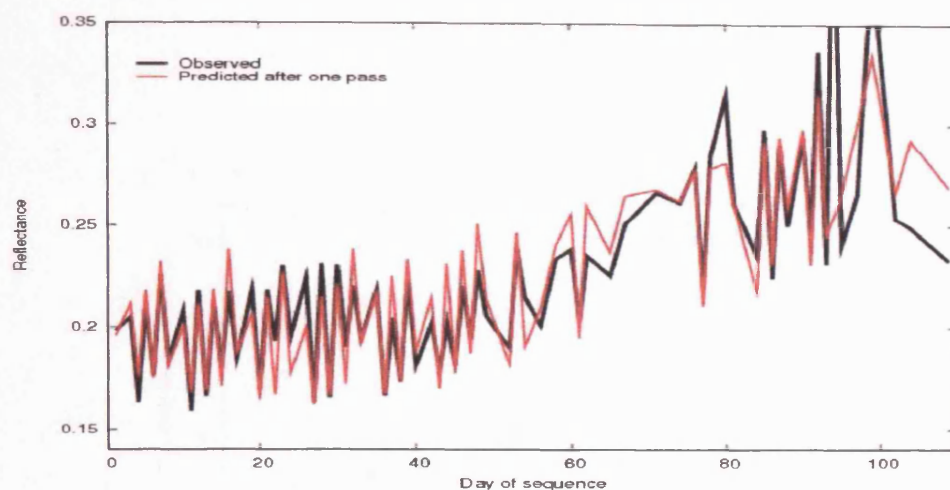
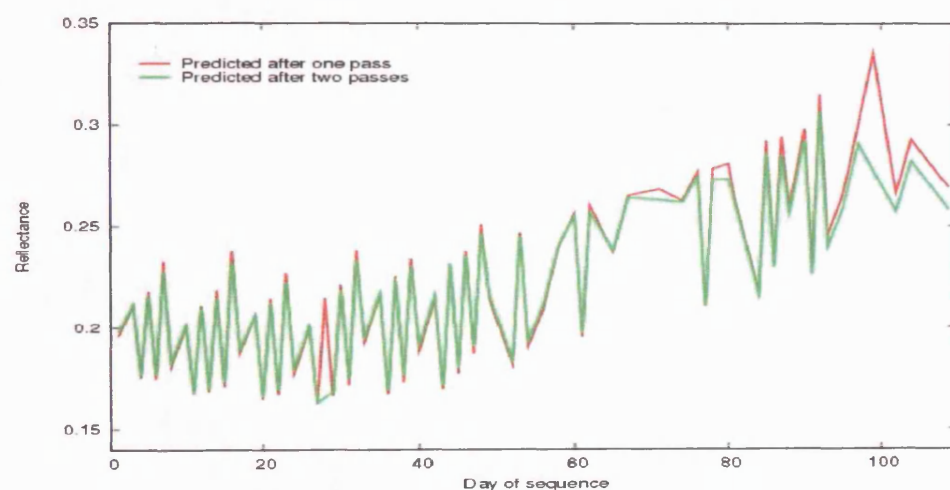


Figure 4.16: Observed and modelled MODIS 500m band 2 reflectances: Additive model results

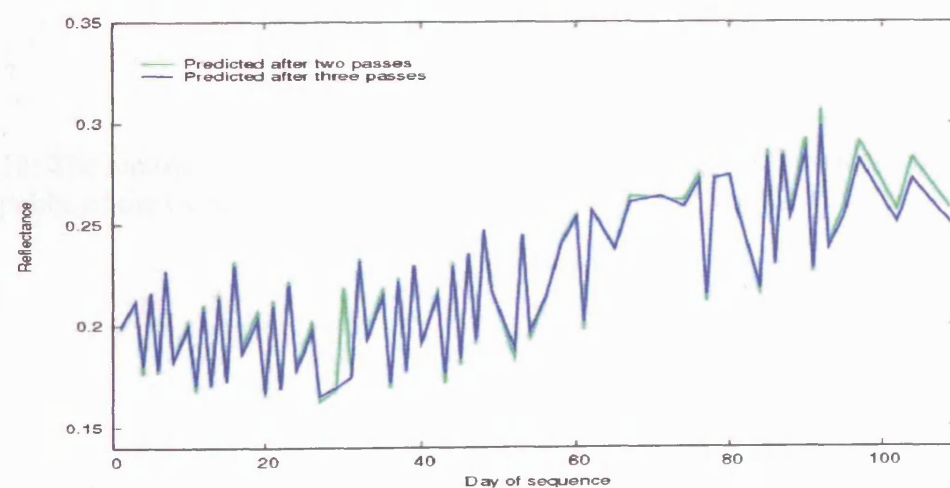
creases over the area of interest, a higher number of observations tend to contain undetected cloud in comparison to the examples in Figure 4.14, both of which contain only a single large isolated outlier over the period of approximately 120 days. A single iteration is not always sufficient to detect and remove multiple outliers especially if neighbouring observations in a sequence are also noisy. Multiple iterations of the model are therefore performed with isolated outliers removed at each pass using the best knowledge of noise in the data and parameter estimation at each iteration. This is demonstrated for a single pixel inverted over approximately three and a half months (110 days) of daily MODIS 500m band 2 reflectances. The pixel is located in southern DCR and is documented in Table A.1 and Figure A.1 in Appendix A as Site 4G. The temporal sequence (day 1 corresponds to the 1st of August 2002) of observed and predicted reflectances using the additive temporal model are displayed in Figure 4.17. All of the observations are documented as high quality and cloud-free in the MODIS Surface State product (see Section 5.2.4). Figure 4.17a displays the observed band 2 reflectances and the model predicted values after a single iteration. A $|Z|$ threshold of 1.5 has been used in all cases. Figure 4.17b displays the modelled values after a single and after two passes, while Figure 4.17c displays the modelled values after two and three iterations. The measured reflectances are also displayed in Figure 4.18 as a function of viewing zenith angle, and the ‘noisy’ observations which have been identified and removed during each subsequent model iteration are highlighted. A single large positive outlier (day 94) which is likely to be an undetected cloud is identified and removed on the first pass (Figures 4.17a and 4.18a). Two more noisy observations are identified on days 28 and 99 on the second pass, and one more (day 30) on the third pass (Figures 4.17b, 4.17c and 4.18b). No more observations with a $|Z|$ value greater than the threshold ($|Z| = 1.5$) are identified with additional iterations. The necessity of identifying and removing outliers from the time series of observations prior to calculation of the model parameters and forward modelling of the reflectance is highlighted by the RMSE values displayed in Table 4.1. These correspond to the temporal sequence displayed in Figures 4.17 and 4.18 above. The unfiltered values are the RMSEs calculated between the observed and modelled reflectances with none of the outliers removed. In contrast the filtered values have been calculated from the observed and modelled reflectances after three model iterations and using a $|Z|$ threshold of 1.5. The removal of outliers allows for more accurate predictions of reflectance and consequently more robust detection of changes within the data. Three passes are generally sufficient to remove potential cloud identifications



(a) Observed reflectances and predicted values (one pass)

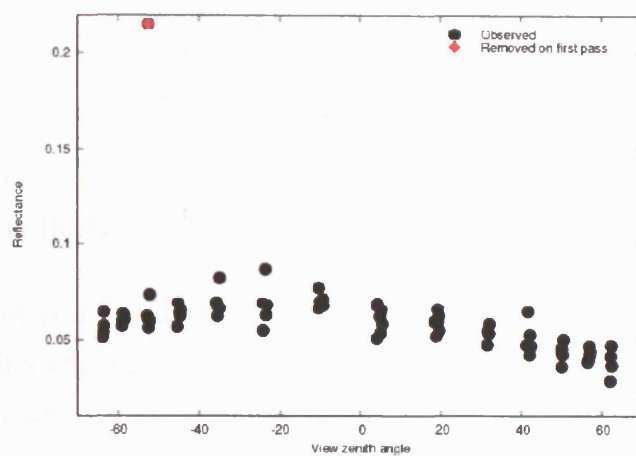


(b) Predicted reflectances after one and two passes

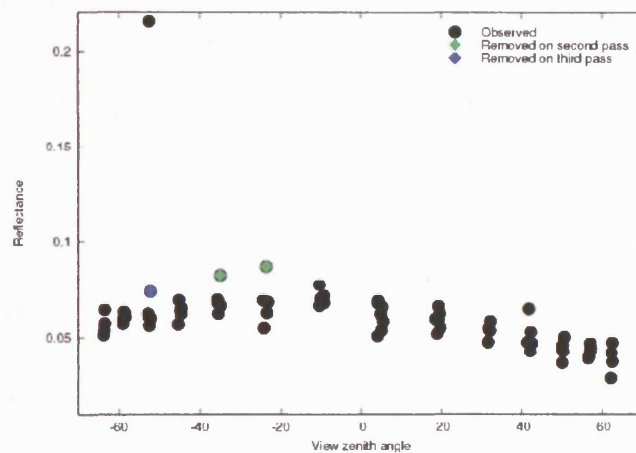


(c) Predicted reflectances after two and three passes

Figure 4.17: The removal of noisy observations: Site 4G, Democratic Republic of the Congo



(a) Observation removed after a single pass



(b) Observation removed after multiple passes

Figure 4.18: The removal of noisy observations of MODIS band 2 reflectances: Site 4G, Democratic Republic of the Congo

	Unfiltered RMSE	Filtered RMSE
Band 1	0.018	0.004
Band 2	0.020	0.013
Band 3	0.017	0.002
Band 4	0.018	0.003
Band 5	0.021	0.016
Band 6	0.013	0.009
Band 7	0.013	0.009

Table 4.1: Effects of noisy data on model fitting: Additive model results

and ‘bad’ observations acquired during the burn season data over the area of interest, and all model runs conducted for the purpose of the current research have thus used three iterations and a $|Z|$ value of 1.5 to remove outliers from the temporal sequences of MODIS surface reflectance data.

The improved identification of noisy data which is enabled by the greater number of samples through the use of the temporal model is displayed in Figure 4.19. This contains the observed

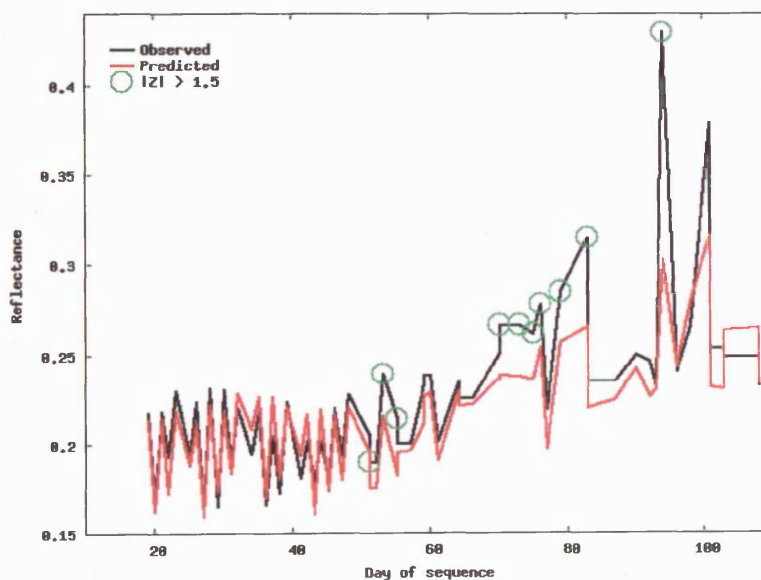


Figure 4.19: Observed and modelled MODIS band 2 reflectances: 16 day moving window (Site 4G, Democratic Republic of the Congo)

and model predicted reflectances for the same pixel location and temporal sequence as displayed

in Figures 4.17 and 4.18. Only the observations of reflectance for which a prediction have been made are included. As in approach of Roy *et al.* (2002) the reflectances in Figure 4.19 have been modelled using a sixteen day window, with a minimum of 7 observations required to perform an inversion over this time. During the 110 day temporal sequence 49 of the daily observations during this period have been labelled as containing cloud by the MODIS Surface State product. Only 62 predictions have been made over this time period due to missing samples, and the effect of cloudy data on the 16 day moving window predictions in Figure 4.19 are clear. The observations which correspond to predictions with a Z-score greater than 1.5 and would therefore be identified as outliers following the procedure described above have been highlighted in Figure 4.19. The large number of cloudy observations in the temporal sequence results in a higher RMSE in the predictions over a 16 day window due to a lower number of available samples during this time. This contributes to the higher Z-score values in comparison to those calculated using the temporal model, and subsequently the identification of a greater number of outliers in the sequence. In comparison to the traditional 16 day moving window approach the longer temporal sequence over which the inversions are performed using the two temporal models allows for better estimation of noise within the data and uncertainty in the model parameters. This results in more efficient identification of outliers which in turn allows for more accurate predictions of reflectance and consequently more reliable detection of changes within the sequence.

4.7 Detecting step changes

The model described in Section 4.5.1 fits a semi-empirical kernel driven BRDF model to a time series of multi-angular surface reflectance data, allowing for subtle variations in the surface state over the period of the temporal sequence. The next step in the development of a change detection algorithm needs to be the incorporation of a function to detect the changes of interest. In the change detection model of Roy *et al.* (2002) described in Section 4.3 this is performed through two main steps. The first involves the detection of potential change pixels and is achieved through the use of a statistical measure. The model predicted reflectance (inverted over a minimum of seven cloudfree observations from the previous sixteen days) is compared to the next observation of reflectance in the time series, and a Z-score is defined as a normalized measure related to the probability of this new observation belonging to the same set as that used in the model inversion. The derivation of this measure is described in detail in Section 4.3. The magnitude of the Z-score is related to the probability of the subsequent observation not belonging to the same set as the previous observations, and its sign is related to the increase or decrease of the new observation relative to the model predicted value. If the sign of the Z-score indicates a change in the expected direction this measure is then thresholded to identify significant changes. An additional operation is included in order to separate temporary changes which may be due to factors such as short term changes in soil moisture or the presence of cloud shadow, from persistent ones. This involves an examination of the temporal consistency of the Z-score values, with persistent changes defined as those where a subsequent number of observations over a specified time period each have a Z-score with the same sign and a value above the threshold. The authors suggest that a suitable time period may be derived empirically for a given Z-score threshold, or may be based on field observations or spectral measurements of burn persistence. Once a persistent change has been identified, the second step in the change detection process involves the determination of the nature of the change. This is achieved through an examination of both the magnitude and the sign difference between the modelled nadir reflectance calculated before and after the date of the persistent change in order to differentiate between different types of surface change, following the concept that different types of change will have different trajectories in spectral space (Roy *et al.* 2002). This procedure is defined in more detail in Section 4.3 and Equation 4.23.

In contrast to the change detection approach described above a function has been incorporated

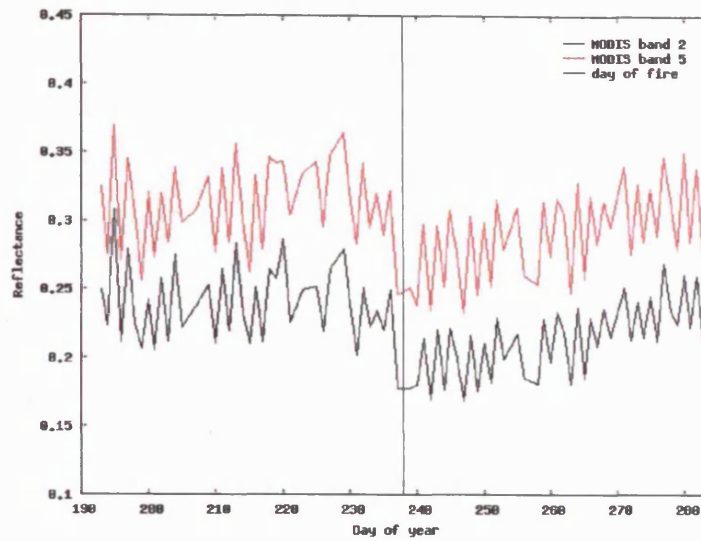


Figure 4.20: Change in reflectance due to burning

into the temporal BRDF models in order to explicitly model for changes in the land surface thus reducing the reliance of the methodology on the incorporation of heuristics to identify change. The occurrence of a fire results in a sudden decrease in near-infrared and short-wave infrared reflectances (MODIS bands 2 and 5), as shown in the temporal sequence for a single MODIS 500m surface reflectance pixel which was detected as containing an active fire on day 229 (Figure 4.20). In order to model for this type of change a 'step function kernel' has been incorporated directly into the model. This is achieved through the introduction of an additional non-linear model:

$$a(\lambda, t) = s(\lambda)H_c(t) \quad (4.34)$$

where $a(\lambda, t)$ represents the isotropic term (f_{iso}) in the case of the additive model, or the brightness term (ρ_0) in the case of the multiplicative model. The coefficient $s(\lambda)$ is the magnitude of the change, and $H_c(t)$ is a heaviside function, represented graphically in Figure 4.21 with Time (t) along the x-axis and the value of the function along the y-axis.

The heaviside is a discontinuous step function which is commonly used in signal processing to describe a signal that switches on at a specific time and stays on indefinitely. Defined

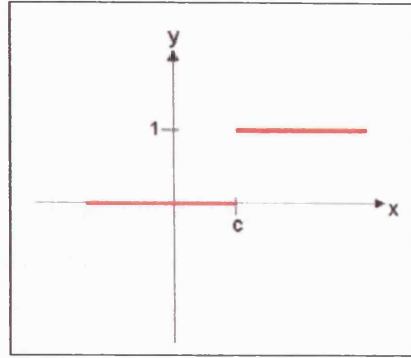


Figure 4.21: The heaviside function

mathematically in Equation 4.35:

$$H_c(t) = \begin{cases} 0 & : t < c \\ 0.5 & : t = c \\ 1 & : t > c \end{cases} \quad (4.35)$$

the heaviside function is a switch that has a value of zero (i.e. is off) until $t = c$ at which point it takes on a value of one (i.e. is switched on), with the non-linear parameter c representing the time of the step change.

The change detection model now has eight parameters, with $a(\lambda)$ and $s(\lambda)$ effectively representing the brightness or overall reflectance level before the change, and the magnitude (and thus direction) of the change respectively. The additive temporal model is defined in Equation 4.36 and the multiplicative temporal model in Equation 4.37.

$$\begin{aligned} \rho(\lambda, \Omega, \Omega') = & f_{iso}(\lambda) + f_{iso_t}(\lambda)t + f_{iso_{t^2}}(\lambda)t^2 + f_{iso_{t^3}}(\lambda)t^3 \\ & + f_{vol}(\lambda)K_{vol} + f_{geo}(\lambda)K_{geo} + a(\lambda, t) \end{aligned} \quad (4.36)$$

$$\begin{aligned}
\ln \rho(\lambda, \Omega, \Omega') = & \ln \rho_0(\lambda) + \ln \rho_0 t(\lambda) t + \ln \rho_0 t^2(\lambda) t^2 + \ln \rho_0 t^3(\lambda) t^3 \\
& + f_1 \ln K_1 + f_2 \ln K_2 + f_3 \ln K_3 + a(\lambda, t)
\end{aligned}
\tag{4.37}$$

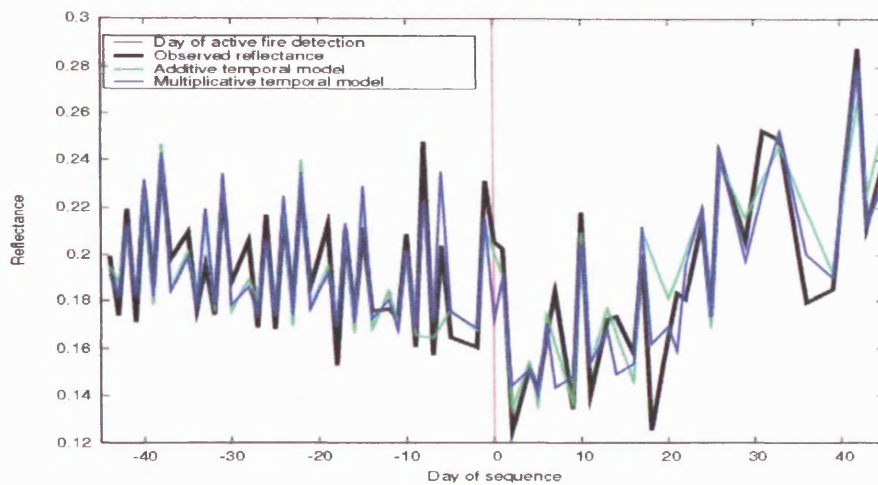
The non-linear parameter c (Equation 4.34) represents the day in the temporal sequence at which the change occurs. For a generic change detection model the most appropriate value for c may be found by stepping through each possible value (each day within the time series), and examining the error in model fit with the value of c which gives the lowest error selected as the day on which the greatest step change has occurred. As c is wavelength independent if the best value for c is chosen by minimising the error in model fit the change detected will be the largest which occurs over the period of the inversion across all wavebands. Therefore if the interest lies in detecting a particular type of change which is known to demonstrate a specific spectral response then there may be more appropriate ways of determining the best value of c . This is discussed in detail in Section 5.4.

As the additive temporal BRDF model is linear it may be inverted analytically. Although it is not inherently linear inversion of the multiplicative temporal BRDF model may also be achieved relatively simply requiring only a few iterations to reach a suitable initial estimate of the parameter ρ_0 . However, with the addition of the step function kernel (Equation 4.34) the temporal models now contain a non-linear parameter c which must therefore be inverted using non-linear methods. The method chosen to achieve this involves stepping through all possible values of parameter c (i.e. each day in the times series) while solving for the seven linear parameters using the method of least squares. In order to ensure sufficient samples for a robust determination of both $a(\lambda)$ and $s(\lambda)$ a buffer of at least 10 days is applied at the beginning and end of the time series over which the inversion is performed. This is discussed further in Section 5.5.

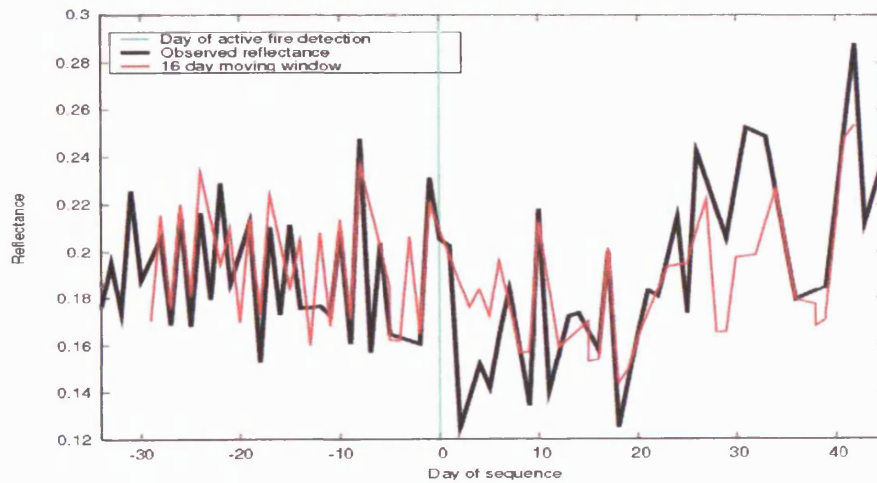
The operation of the two change detection models are displayed in Figure 4.22. The models have been applied to a sequence of MODIS band 2 reflectances for a 90 day period for a single pixel located in southern DCR and documented in Table A.1 and Figure A.1 (Appendix A) as Site 4H (Democratic Republic of the Congo). A fire has been identified by the MODIS active fire product in the middle of the sequence on day 0, which corresponds to the 23rd of July, 2003. Figure 4.22a displays the additive and multiplicative model results, with the horizontal

line indicating the day of the active fire detection. Parameter c , the day of the step change is 0 for the additive and 1 for the multiplicative temporal model. The reflectances modelled using the 16 day moving window (additive) approach are displayed in Figure 4.22b for comparison. This particular location has been chosen to illustrate the operation of the models as it contains potential outliers in the first half of the sequence, and exhibits a phenological change in the surface during the second half of the sequence. The Z-scores for the 16 day moving window approach are displayed in Figure 4.22c, as a means of identifying the occurrence of burning within the time series (Roy *et al.* 2002). The two temporal models fit the reflectance well, with both identifying the occurrence of a step change within a day of the active fire detection. In contrast problems arise with the 16 day moving window approach due to the presence of potentially noisy data in the first half of the sequence before the fire induced change, changes in the surface which occur towards the end of the time sequence but are unrelated to the change of interest as well as missing samples in the second half of the sequence due to cloud. As a result locating the day of burning is problematic. Z-scores above the threshold value occur on four days before the fire. Although these are all isolated occurrences and therefore following the approach of Roy *et al.* (2002) would not be identified as burn candidates, towards the end of the sequence (days 29-33) a series of high Z-score values are evident (Figure 4.22c) which would be identified as a burn event. Isolated outliers such as these are not removed prior to inversion in the change detection model of Roy *et al.* (2002) (see Section 4.3), although the presence of noisy data is addressed in a subsequent refinement (Roy *et al.* 2005b). Figure 4.23 displays the Z-scores for the 16 day moving window approach calculated for the same sequence, but with all the observations which have been identified as outliers by either of the temporal models removed prior to inversion. Despite the removal of noisy observations identifying the correct day of burn is still problematic with the change still identified on day 29 of the sequence. The RMSE for the additive temporal model which is minimised to locate the day of the step change (parameter c) is displayed in Figure 4.24 for comparison. This provides a much clearer signal with which to identify the changes of interest than the Z-scores displayed in Figure 4.23. Although a local minima occurs in the rmse on day 21, it is small compared to the minimum of the entire sequence which corresponds to the day of the actual change (day 0).

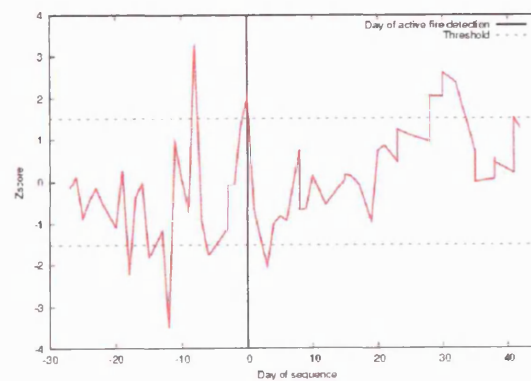
The detection of step changes is achieved more robustly through the use of the temporal change detection models due to the longer time sequence and the greater number of samples over



(a) Additive and multiplicative temporal model: Observed and modelled reflectance



(b) 16 day moving window approach: Observed and modelled reflectance



(c) Z-scores: 16 day moving window approach

Figure 4.22: Detecting step changes: Observed and modelled MODIS band 2 reflectances, June-September 2003, Site 4H, Democratic Republic of the Congo

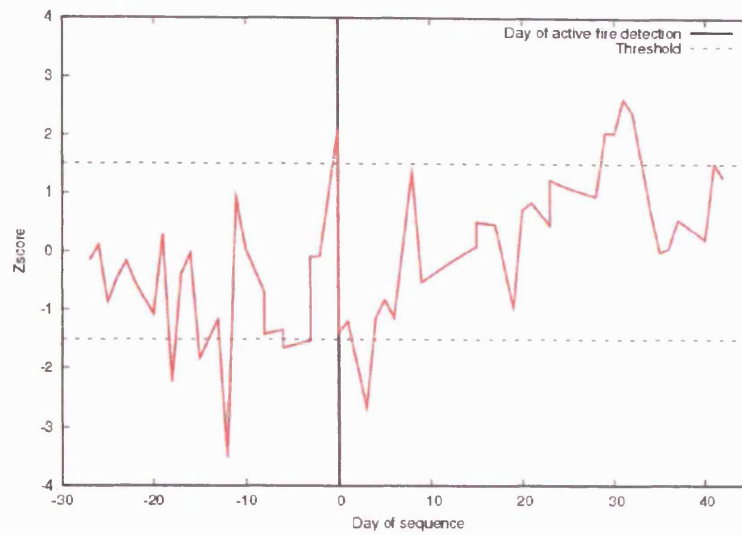


Figure 4.23: Identifying the day of change: Filtered Z-scores, 16 day moving window approach (Site 4H, Democratic Republic of the Congo)

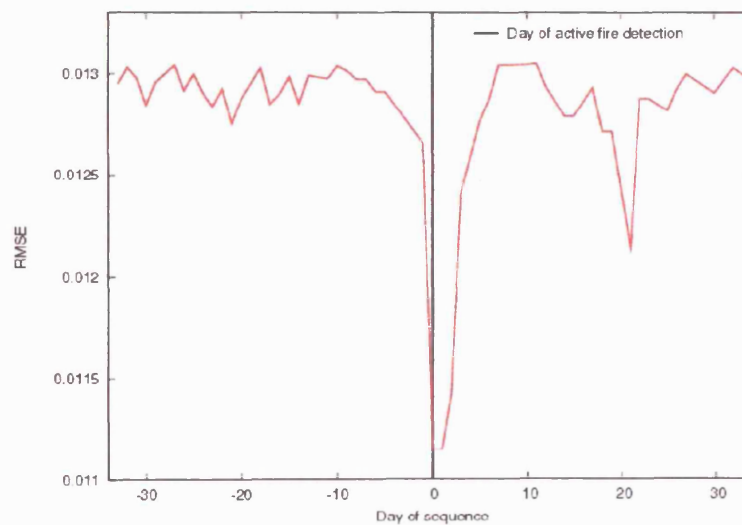


Figure 4.24: Identifying the day of change: RMSE, Additive temporal model (Site 4H, Democratic Republic of the Congo)

which the inversions are performed. This allows for improved estimation of the noise within the data which results in better identification of outliers, better estimation of the model parameters and subsequently more accurate predictions of reflectance. This is of particular importance in the presence of missing samples and phenological changes in the surface. As demonstrated in Figure 4.24 the use of a longer time sequence and the explicit detection of step changes provides a clearer change signal with which to identify the changes of interest.

4.8 Summary

This chapter has described the presence of directional effects in the remote sensing signal, and introduced the models which are commonly used to normalise the signal for these effects. Following on from this a new generic approach to change detection applicable to the identification of sudden changes in the surface has been introduced. The model has been designed to address the shortcomings of traditional change detection techniques identified in Chapter 2 and is developed from the approach introduced by Roy *et al.* (2002). The model has been formulated to address three main issues;

1. Directional effects The directional effects present in remote sensing data in particular from wide field of view sensors such as the AVHRR and MODIS are typically ignored in the detection of land cover change. The presence of these will significantly reduce the capability of any change detection algorithm to accurately identify the changes of interest. The change detection models introduced in Section 4.5 incorporate a BRDF model in order to account for directional effects in the remote sensing signal. This allows for the more accurate detection of subtle changes in the surface which may be of a similar magnitude to those induced by the solar and sensing geometry. In addition in comparison to compositing techniques which attempt to minimise directional effects in the remote sensing signal, the incorporation of an angular model into the change detection scheme allows for the use of all as opposed to just near-nadir observations.

2. Low frequency surface change The change detection techniques reviewed in Section 2.1 in general and the model of Roy *et al.* (2002) in particular ignore phenological variations and assume these to be comparable across the time period of the study. Any low frequency variations

in the characteristics of the surface which occur over the temporal sequence will complicate the identification of the changes of interest. This issue is addressed in Section 4.5.1 through the introduction of two temporal angular models of the surface. Both of these models account for temporal variations in the surface state and may be fitted to considerably longer time periods than, for example, the moving window approach typically used to invert angular models of reflectance (Strahler *et al.* 1999a, Roy *et al.* 2002). The use of a longer time series facilitates more stable inversions (in particular in the presence of missing samples due to cloud) which are necessary when attempting to identify sudden and potentially low magnitude change within the data.

3. Noisy observations All change detection techniques will be sensitive to the presence of noisy observations within the time series. Under the current approach if outliers are not removed from the temporal sequence they will contribute to subsequent predictions of reflectance and will reduce the capability of the model to accurately identify the changes of interest. A filter is therefore incorporated into the algorithm in order to detect isolated outliers based on an estimation of the noise within the data at each iteration of the model. The use of a temporal angular model of the surface allows for improved identification of outliers over a traditional 16 day moving window approach. The longer sequence of observations and thus the greater number of samples over which the inversion is performed enables better estimation of noise within the data. This subsequently allows for improved estimation of the model parameters and better predictions of reflectance which results in more accurate detection of land surface change.

The model presented in this chapter is a generic approach to change detection which is applied here to the problem of detecting sudden changes in the remote sensing signal through the incorporation of a step function kernel. This allows for the explicit detection of step changes within the data, and may be tailored to a particular type of change based on the spectral characteristics of the changes of interest. The implementation of this model and its application to the identification and delineation of fire-affected areas from daily moderate resolution satellite data is described in the next chapter.

Chapter 5

Model implementation

5.1 Introduction

The aim of this chapter is to introduce the data sources used and to describe the application of the change detection model introduced in the previous chapter to the detection of fire affected areas within the southern Africa region of interest over the five year study period. Fire is a dynamic process which can move rapidly across the land surface. The characterisation of the burn signal in Section 3.6 indicates that post fire surfaces within the study area recover quickly with chances of detection decreasing significantly after only seven days after the occurrence of a fire. In order to have the highest possible chance of detecting fire induced surface change it is therefore necessary to use daily or near daily data. The first section of this chapter introduces the high temporal resolution data available from the MODIS sensor, and the production of monthly change maps through the implementation of the change detection models developed in Chapter 4 with daily MODIS 500m surface reflectances. The second half of the chapter discusses the post-processing steps applied to the results for the specific purpose of detecting fire induced surface change.

5.2 The MODerate resolution Imaging Spectroradiometer

NASA's Earth Observing System (EOS) incorporates a series of polar orbiting and low inclination satellites. As part of this family the Terra and Aqua satellites were launched in December 1999 and May 2002 respectively and form the second phase of NASA's Earth Science Enterprise, with the first having focused on free-flying satellites and space shuttle missions as well as various airborne and ground-based studies. The launch of Terra saw the start of the second phase, with the aim of providing observations of the key physical variables needed to advance our understanding of the Earth as an integrated system. To this end twenty-four key measurements of the Earth's processes (documented in Table 5.1) are collected by the various sensors on board to provide long term global observations of the land surface, biosphere, solid earth, atmosphere and oceans. The Moderate Resolution Imaging Spectroradiometer (MODIS) was launched on both the Terra and Aqua satellites with the aim of facilitating understanding of global dynamics and processes, through the provision of improved monitoring for the purpose of land, ocean and atmospheric research. The data collected by MODIS is designed to complement the spectral,

spatial and temporal coverage of the other instruments on board. These include the Advanced Spaceborne Thermal Emission and Reflectance Radiometer (ASTER, Yamagushi *et al.* (1998)), the Multi-angle Imaging SpectroRadiometer (MISR, Diner *et al.* (1998)), and the Cloud and Earth's Radiant Energy System (CERES, Wielicki *et al.* (1998)).

EOS Measurements	
Atmosphere	Cloud properties Radiative Energy Fluxes Precipitation Tropospheric Chemistry Stratospheric Chemistry Aerosol Properties Atmospheric Temperature Atmospheric Humidity Lightning
Solar	Total Solar Irradiance Solar Spectral Irradiance
Land	Land Cover and Land Use Change Vegetation Dynamics Surface Temperature Fire occurrence Volcanic Effects Surface Wetness
Oceans	Surface Temperature Phytoplankton and Dissolved Organic Matter Surface Wind Fields Ocean Surface Topography
Cryosphere	Land Ice Sea Ice Snow Cover

Table 5.1: EOS measurements

5.2.1 Sensor Characteristics

Both Terra and Aqua are in sun-synchronous near-polar circular orbits which result in a repeat cycle of approximately 16 days. Terra passes from north to south ('descending') with an equatorial crossing of 10:30am local time, and Aqua is in 'ascending' node passing from south to

north with an equatorial crossing of 1:30pm local time. A ± 55 degree scanning pattern at a height of 705km results in a viewing swath width of 2330 km and global coverage every 1 to 2 days. In terms of angular sampling the variation is thus primarily in the sensor zenith angle. Both satellites have a 16 day revisit period at the equator and the surface is therefore viewed from a different direction by each consecutive MODIS overpass during this repeat cycle. Data are recorded in 36 spectral bands between $0.405\mu m$ and $14.385\mu m$. The first two spectral bands (red and near-infrared wavelengths) are acquired at a nominal spatial resolution of 250m at nadir, the next five at 500m (bands 3-7) and the remaining 28 (bands 8-36) at 1000m. The first seven 'land surface reflectance' wavebands which are recorded at a spatial resolution of 500m and used in this study are detailed in Table 5.2. The components of the sensor designed for the purpose

Primary Use	Band	Bandwidth(nm)	Resolution(m)
Land/Cloud/Aerosols Boundaries	1	620 - 670	250
	2	841 - 876	250
Land/Cloud/Aerosols Properties	3	459 - 479	500
	4	545 - 555	500
	5	1230 - 1250	500
	6	1628 - 1652	500
	7	2105 - 2155	500

Table 5.2: MODIS land surface reflectance wavebands

of land imaging combine features of the AVHRR instrument and the Landsat Thematic Mapper, with the addition of middle and long-wave infrared wavebands. In addition spectral channels which facilitate improved atmospheric and cloud correction have been incorporated in order to remove the effects of the atmosphere on observations of the surface (Justice *et al.* 1998)

5.2.2 Data Products from MODIS

There are 44 standard data products created from MODIS data, which have been designed with the aim of fulfilling the needs of the global change research community (Justice *et al.* 1998). Each of these have been produced using peer reviewed algorithms developed by the MODIS Science team (Running *et al.* 1994a). The standard data products incorporate a combination of surface state variables such as spectral reflectance, albedo and land temperature, as well a

collection of higher order variables such as leaf area index (LAI), active fire locations and snow and ice cover, produced to meet the goals of NASA's Earth Science Enterprise. The products are organised into five categories; (i) calibration, (ii) atmosphere, (iii) land, (iv) cryosphere, (v) ocean. As only the land products are of relevance to the current research the other four categories will not be discussed further. The MODIS land products are available at five different levels of processing. The raw instrument data are archived at their original resolution as level 0, with each of the subsequent levels containing increasingly refined data products. This methodology is followed in order to enable efficient processing and reprocessing of MODIS land products, to support subsequent applications of the data, and to provide users with the original data along with subpixel geolocation information (Wolfe *et al.* 1998).

Level 1: MODIS level-1a products contain reformatted and packaged raw instrument (level 0) data at their original resolution. Quality information is added at this point, indicating missing or bad pixels. Level 1b data are created by calibrating at aperture radiances generated from MODIS level-1a sensor counts which are then geolocated to subpixel accuracy. Multiple onboard calibration systems are used in conjunction with vicarious calibrations techniques (i.e. using radiances of known targets) in order to ensure a high calibration accuracy. The emphasis on calibration is a direct response to the problems experienced with optical data from the AVHRR sensor due to the lack of onboard calibration systems (Justice *et al.* 1998).

Level 2: Level 2 products are derived from the Level 1 calibrated radiances and ancillary data and are stored in the original sensor sampling space. The smallest amount of data stored as Level 1 and Level 2 products is referred to as a 'granule', and corresponds to approximately five minutes of MODIS sensing covering approximately 2340 km by 2000 km. In addition Level-2 gridded products (Level 2G) are available, generated from a single day of Level 2 data which are organised into an Earth-based grid. The Level 2 grids contain all observations which fall within each grid cell over a twenty-four hour period, thus storing multiple observations overlapping or intersecting each grid cell, which can then be used as input to higher level products in an accurate and robust manner (Wolfe *et al.* 1998).

Level 3: The gridded Level 3 products are stored as fixed, non-overlapping, earth located 'tiles'. There are 326 tiles which contain land (460 global tiles in total), each covering a geographic area of 1200km by 1200km (Wolfe *et al.* 1998). These products are spatially resampled, geometrically corrected Level 2 data which may have been temporally composited and/or aver-

aged in order to produce a single estimate of a geophysical variable for each grid location (Justice *et al.* 1998).

All of the data used for the purpose of the current research are Level 3 gridded products which are available in a Sinusoidal projection. The projection parameters are contained in Table 5.3. The tiles are 10 by 10 degrees at the equator, and the tile coordinate system starts at 0,0

Parameter	Value	Description
Sphere	6371007.181	Radius of reference sphere (m)
Central Meridian	0.0	Longitude of central meridian
False Easting	0.0	False Easting in the same units as the sphere radius
False Northing	0.0	False Northing in the same units as the sphere radius

Table 5.3: MODIS Sinusoidal projection parameters (*Source:* <http://landweb.nascom.nasa.gov/>)

(horizontal and vertical tile numbers) in the upper left corner as indicated in Figure 5.1. Two

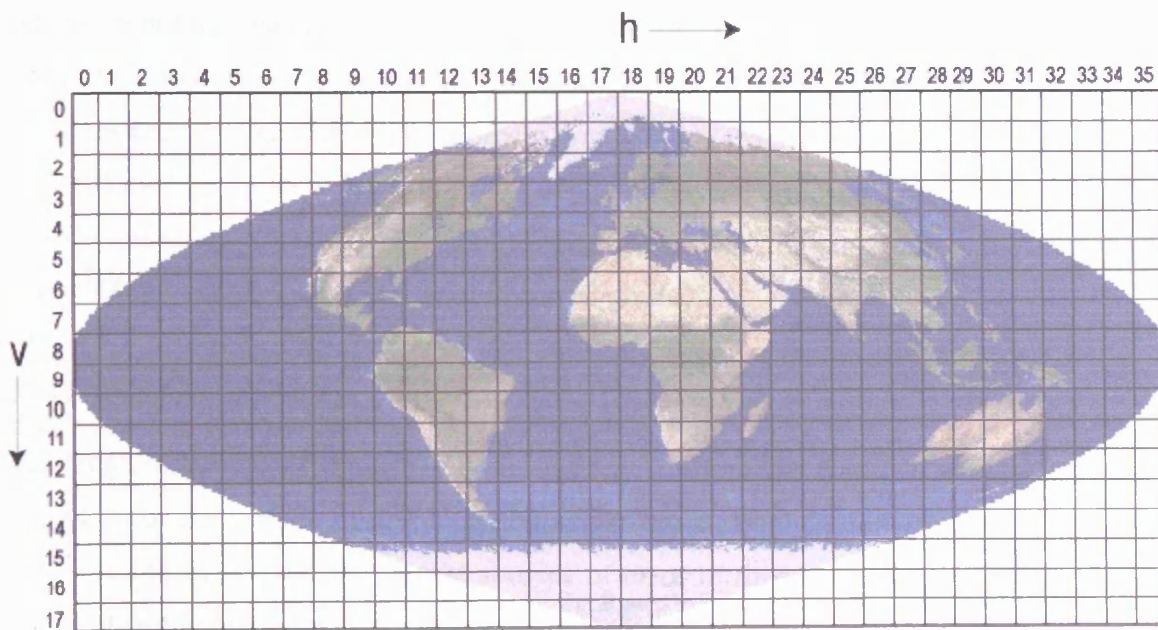


Figure 5.1: MODIS Sinusoidal grid (*Source:* <http://nsidc.org/data/modis/landgrid.html>)

land tiles (“h19v10” and “h20v10”) have been selected and the spatial extent of these is detailed in Figure 3.10. Three of the MODIS Land Products are used as inputs to the change detection model introduced in the previous chapter. A description of each of these is provided below.

5.2.3 Surface Reflectance

The MODIS surface reflectance product consists of the first seven MODIS wavebands (see Table 5.2) computed from the Level 1b radiances. An estimate of the surface spectral reflectance for each pixel for each band is documented as it would have been measured at ground level assuming no atmospheric scattering or absorption (Justice *et al.* 1998). The reflectances are corrected for the effects of atmospheric gases, aerosols and thin cirrus clouds. This is achieved by atmospherically correcting the calibrated radiances for each of the land bands (bands 1-7). The MODIS atmospheric products (MOD04: aerosols, MOD05: water vapour, MOD07: ozone, MOD35: cloud mask) as well as ancillary data (a Digital Elevation Model and information on atmospheric pressure) are used as inputs to the atmospheric correction process (Vermote and Vermeulen 1999b). The 6s radiative code (Vermote *et al.* 1997) is used to model the atmosphere, and the atmospheric point spread function (PSF) as well as atmosphere/BRDF coupling effects are accounted for. The surface reflectance product is used as input to several of the higher order land products including vegetation indices, land cover, thermal anomalies, and biophysical variables. Four Surface Reflectance products are available from MODIS at different spatial and temporal resolutions and with various levels of processing, ranging from atmospherically corrected Level 1B data (Level 2), to an 8-day composite of the calibrated atmospherically corrected gridded data. The reflectance data used as input to the change detection algorithm is the daily Level 3 gridded 500m bands 1-7 land surface reflectance product.

Atmospheric Correction

A challenge in the use of optical EO data for any study of the land surface is separating the contribution of the surface from the combined surface-atmosphere reflectance as measured by the sensor, and as a result the largest sources of error in time series data of the land surface are a result of the inaccurate calculation of this quantity (Vermote and Vermeulen 1999b). The explicit correction of atmospheric effects has frequently been avoided through the use of NDVI-type vegetation indices, or through compositing time series data sets as discussed in Chapter 2. The selection of the maximum value of a temporal composite of NDVI data reduces the impact of atmospheric effects, in particular the presence of subpixel clouds (Kaufman and Tanre 1992). The problems associated with the use of this compositing procedure are discussed in Section 2.2.

Explicit correction of atmospheric effects has typically been achieved through the use of radiative transfer codes. However for accurate calculations these need to be applied in conjunction with measurements of aerosol optical depth recorded by ground-based sunphotometers (Vermote and Vermeulen 1999b). As it is not feasible to provide these measurements globally, an alternative methodology is required. The approach used by MODIS is to make these measurements at the satellite itself. This is achieved by the incorporation of 7 bands between $0.41\mu m$ and $2.1\mu m$, in comparison to 2 bands of the AVHRR instrument, thus enabling the explicit derivation of aerosol optical depth and thereby allowing atmospheric correction for aerosol scattering and absorption at a global scale (Vermote and Vermeulen 1999b). In addition (i) smaller MODIS bandwidths minimize the need to correct for water vapour absorption, (ii) an increased spatial resolution of bands 1-2 (250m) compared to, for example the AVHRR (1.1km) leads to better detection of cloudy pixels and subpixel clouds, and (iii) the incorporation of a waveband at $1.38\mu m$ allows for the detection of thin cirrus clouds and stratospheric aerosols, all of which contribute to improved atmospheric correction and increased accuracy in measurements of surface reflectance (*ibid*). The atmospheric correction algorithm is applied to all daytime Level 1B data which has been acquired at a solar zenith angle of less than 85° to generate the Surface Reflectance products. A flow chart of the steps involved is displayed in Figure 5.2. The process requires inputs that describe the variable constituents that influence the signal measured at the top of the atmosphere, correct modelling of the atmospheric scattering and absorption, and correction for the atmospheric point spread function and coupling of the surface BRDF and atmosphere effects (Vermote and Vermeulen 1999a).

Geolocation Accuracy

Subpixel geolocation accuracy is necessary in order to perform studies of change detection and to accurately retrieve biophysical parameters of the land surface (Townshend *et al.* 1992). The MODIS land team therefore state an operational geolocation goal of an accuracy of 0.1 pixels at two standard deviations for the 1km bands (Justice *et al.* 1998). Geolocation is performed on-board using eight pieces of information: geodetic latitude and longitude (defined in the WGS84 system), height above the earth, satellite zenith and azimuth angles, range to the satellite, and solar zenith and azimuth angles (*ibid*). Earth ellipsoid, spacecraft ephemeris and attitude data are

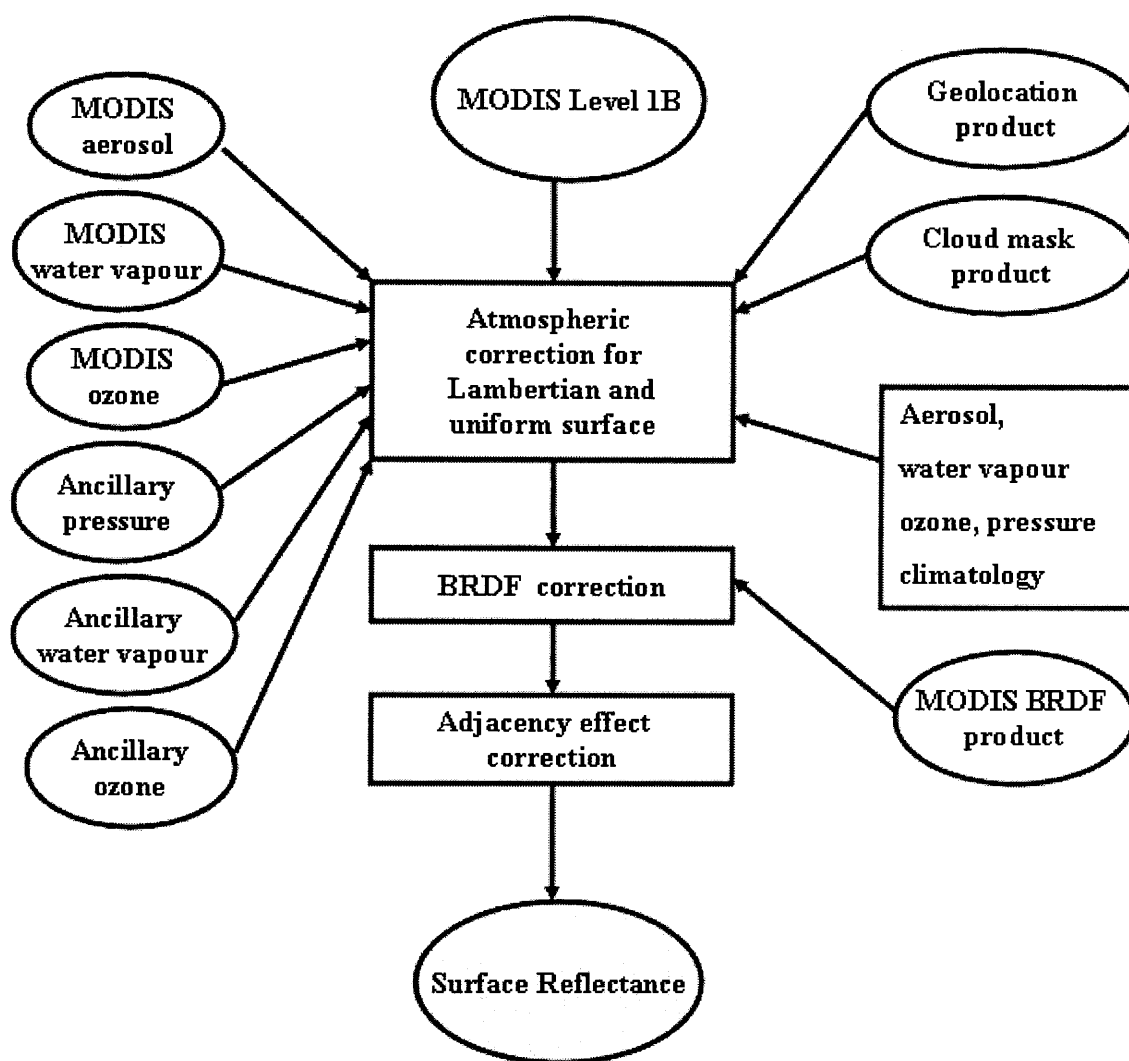


Figure 5.2: MODIS atmospheric correction (*Source: Adapted from Vermote and Vermeulen (1999a)*)

used in conjunction with knowledge of the sensor and satellite geometry and a 1km global digital elevation model in order to compute this information for each 1km spatial element (Nishihama *et al.* 1997). The 250m and 500m observations are then geolocated using a fixed offset relative to the 1km observations (Wolfe *et al.* 1998).

5.2.4 Surface State

The MODIS Surface State products provide information on the quality of the daily surface reflectance observations. The aim of the product is to identify and flag suspect or poor quality observations before they are released to the public (Justice *et al.* 1998). Errors in the data have a range of potential sources including; (i) inadequacies in the algorithms used to create the data, (ii) errors in the operational production, archiving and dissemination of the data, and (iii) errors caused by the satellite platform, the sensor, or in the transmission of the data. The Level 2 gridded Land Surface Reflectance State Quality Assurance product is created from the Level 1B data by placing the quality assurance data for the corresponding observation into each relevant 1km grid cell. The information is stored as a 16-bit integer with a range of 0-57335. The information contained in each bit is displayed in Table 5.4. For the purpose of the current research the quality assurance of each pixel is examined prior to input into the change detection model and only pixels with the values displayed in Table 5.5 are accepted (a value of 1 indicates which bits have been set). Thus only land pixels which are free of cloud and cloud shadow are considered suitable.

5.2.5 Geolocation Angles

The MODIS geolocation Level 2 gridded dataset contains information on the solar illumination geometry and the geometry of the sensor at the time of image acquisition. This information is required in order to model the geometric relationship and the distance between the sensor, the area of the earth's surface imaged by the sensor, and the sun (Nishihama *et al.* 1997). These data are then used to calibrate, atmospherically correct and geolocate the 1km MODIS observations. The geolocation datasets are thus used as input into various higher order products including the Surface Reflectance products described above. In order to model the directional component of surface reflectance using any of the models described in Section 4.2 information is required about

Data Bit	Description
0: Internal snow algorithm	1 - yes
	0 - no
1-2: BRDF correction performed	00 - none
	01 - Montana methodology
	10 - Boston methodology
3: Snow ice flag	1 - yes
	0 - no
4: Internal fire algorithm flag	1 - fire
	0 - no fire
5: Internal cloud algorithm flag	1 - cloud
	0 - no cloud
6-7: Cirrus detected	00 - none
	01 - small
	10 - average
	11 - high
8-9: Aerosol quality	00 - climatology
	01 - low
	10 - average
	11 - high
10-12: Land/water flag	000 - shallow ocean
	001 - land
	010 - coastlines and shorelines
	011 - shallow inland water
	100 - ephemeral water
	101 - deep inland water
	110 - continental/moderate ocean
	111 - deep ocean
13: Cloud shadow	0 - no
	1 - yes
	1 - yes
14-15: Cloud state	00 - clear
	01 - cloudy
	10 - mixed
	11 - not set, assumed clear

Table 5.4: MODIS Surface State product: Quality Assurance (QA) bits

Bit Number	Description	Pixel Value							
		8	72	136	200	2056	2120	2184	2248
0	Internal snow algorithm	0	0	0	0	0	0	0	0
1	BRDF correction performed	0	0	0	0	0	0	0	0
2		0	0	0	0	0	0	0	0
3	Snow ice flag	0	0	0	0	0	0	0	0
4	Internal fire algorithm flag	0	0	0	0	1	1	1	1
5	Internal cloud algorithm flag	0	0	0	0	0	0	0	0
6	Cirrus detected	0	0	0	0	0	0	0	0
7		0	0	0	0	0	0	0	0
8	Aerosol quality	0	0	1	1	0	0	1	1
9		0	1	0	1	0	1	0	1
10	Land/water flag	0	0	0	0	0	0	0	0
11		0	0	0	0	0	0	0	0
12		1	1	1	1	1	1	1	1
13	Cloud shadow	0	0	0	0	0	0	0	0
14	Cloud state	0	0	0	0	0	0	0	0
15		0	0	0	0	0	0	0	0

Table 5.5: MODIS Surface State product: Quality Assurance (QA) bits

the illumination and sensor geometry for each observation of reflectance. This information is documented in the MODIS Geolocation Angles product in the following fields; (i) solar azimuth (ii) solar zenith (iii) sensor azimuth and (iv) sensor zenith. All of these data fields are input into the change detection model.

5.3 Data preprocessing

All data products derived from EOS missions are stored in the Hierarchical Data Format (HDF). Developed by the National Center for Supercomputing Applications (NSCA) HDF-EOS (an extension of HDF-4) is a file format, an Application Programming Interface (API) and library which includes several important conventions for EOS data, including the placement of meta-data within the HDF file and the definition of compound data objects to represent satellite swaths as well as standard grid projections and point data structures (NASA Accessed: July 2005). The HDF has been found to be an extremely appropriate format for use with Earth observation data as it is self describing and portable across many computing systems, and has been designed explicitly for scientific use with predefined structures common to scientific data (*ibid*).

As discussed the examination of high temporal resolution surface changes such as those induced by fire requires daily images of surface reflectance. In order to account for the angular variations present in the surface reflectance data, information relating to the viewing and illumination geometry of each data acquisition is also required. Finally, in order to locate the presence of cloud and cloud shadow and to determine the quality of the surface reflectance data information relating to the quality of each observation is also needed. These three fields of MODIS data are archived as individual products as described in Sections 5.2.3, 5.2.5 and 5.2.4 above, with each daily product stored as a separate HDF file. A study of changes which have taken place at a single location over a period of a year thus requires the storage and manipulation of 1095 HDF files. While this in itself is not an excessively large number of files, the extraction of the information and its reformation into the required order does pose a problem.

In the original HDF format the data are stored band sequentially (BSQ) for each day as an array of 2400 by 2400 pixels for the 500m data, or an array of 1200 by 1200 pixels for the 1km products. In order to detect changes and to model the angular effects in the data using the change detection model described in the previous chapter the surface reflectance, surface state and geolocation information for each individual pixel is required as a temporal sequence. To extract this information for each pixel for a year it would be necessary to open all 1095 images at the same time. Under the Unix Solaris operating system however it is only possible to read a maximum of 256 files into memory at a single time, which would only allow for the extraction of data for a period of 85 days. The approach used is therefore to open each of the three files for

each day in the time series, loop over each pixel within a single row extracting the seven fields of reflectance information (seven wavebands), the four fields of angular information (view zenith, view azimuth, solar zenith, solar azimuth) and the single field of surface state information, and to save this as a single Band Interleaved by Pixel (BIP) file. This re-ordered dataset is subsequently used as input to the change detection model.

All of the preprocessing as well as the change detection operations have been performed on each of the two MODIS tiles (“h19v10” and “h20v10”) separately, with the final outputs mosaicked together to form a single result for the entire area. The processing has been performed on a cluster of 96 workstations running the Sun Grid Engine. For each of the processing and preprocessing steps the 2400 row 2400 column images are divided into 48 sections of 50 rows and 2400 columns. Each of these are submitted to a different node on the cluster. The preprocessing and processing operation to produce the outputs for a single month for each 50 row by 2400 column array of each MODIS tile takes approximately 6 hours.

5.4 Identifying fire induced surface change

The temporal BRDF algorithm described in Sections 4.5.1 and 4.7 is a generic approach to change detection which locates sudden changes within a temporal sequence of reflectance by minimising the global error (i.e. across all wavebands) in the model fit. The day of the step change is thus located as the point within the sequence which provides the lowest global rmse, irrespective of the type of change which has occurred. While this may be a suitable method to follow if the interest lies solely in identifying the greatest change which has occurred during the time series, there are various reasons why it may be more appropriate to follow an alternative approach. In particular locating parameter c (the day of the step) by minimising the global RMSE (i) incorporates no measure of the uncertainty in the prediction of a step on day c , (ii) provides no indication of the magnitude of the step and (iii) is not directly dependent on the spectral nature of the change. While the size, direction and spectral nature of the change may only be important if the aim is to identify specific types of surface change, the first point is important irrespective of the specificity of the model. However as the aim of the research documented here is the application of the model to the detection of fire induced surface change all three of these

points are of importance. The first two are addressed by the definition of a measure related to the uncertainty in the prediction of a step as well as the magnitude (i.e. size *and* direction) of a step at a particular point in the time series of observations. A spectral filter is subsequently defined which may be applied to this measure in order to specifically identify burn-type changes in the surface reflectance. Both of these are described in the following sections.

5.4.1 Determining the day of the change

The global error in model fit does not provide a direct indication of the uncertainty associated with the prediction of a step at a particular point in the time series. As the confidence of predicting a step will decrease at the ends of the temporal sequence and as a function of the angular sampling associated with a particular set of observations, it is necessary to take this into account in order to robustly identify changes in the surface state. A measure is therefore proposed which provides an indication of the confidence of the prediction of a step at each point in the temporal sequence. The weight of determination (Lucht and Lewis 2000) is directly related to the error associated with the model parameters (see Equation 4.33) and provides an indication of the uncertainty in the predictions as a result of the angular and temporal sampling of a particular set of observations. The weight of determination for a single pixel is shown in Figure 5.3 for a period of 120 days. Although it is relatively stable over the central portion of the time series it increases sharply at the edges of the sequence indicating a higher degree of uncertainty in the predictions at the tails of the data. In order to incorporate this uncertainty into the determination of parameter c (the day of the step change) it is proposed that the magnitude of the step (model parameter $s(\lambda)$) at each cloud free observation is weighted by the uncertainty in the prediction of a step as well as the noise in the data as an alternative approach to finding the best value of c . This measure is defined mathematically as:

$$M(\lambda) = \frac{s(\lambda)}{\left(\frac{1}{w} \times e(\lambda)\right)} \quad (5.1)$$

where $s(\lambda)$ is the magnitude of the step, $\frac{1}{w}$ is the weight of determination, and $e(\lambda)$ is the error in model fit (assumed to be an estimate of the noise in the data). The derivation of $e(\lambda)$ is

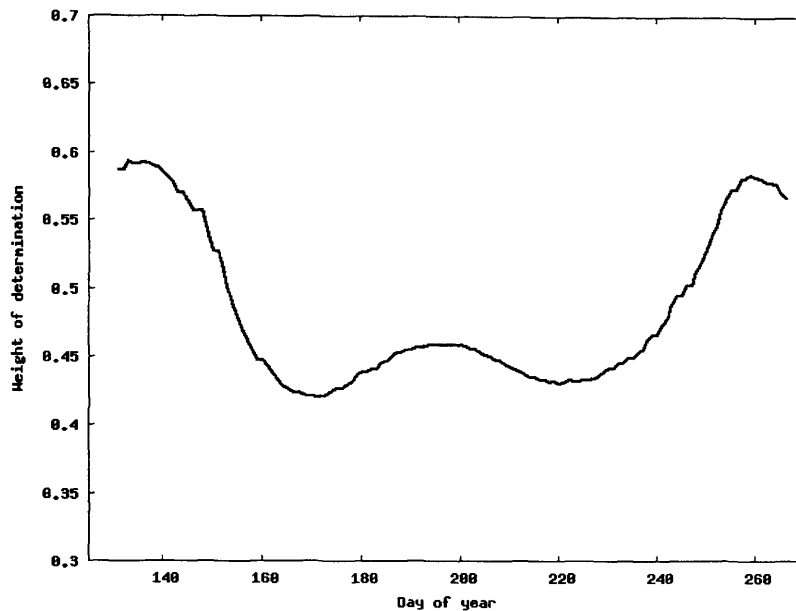
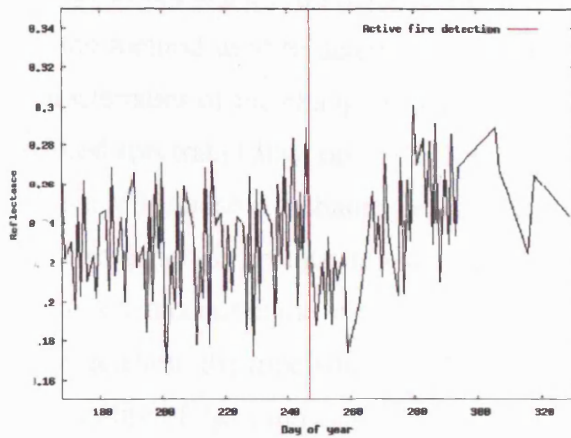


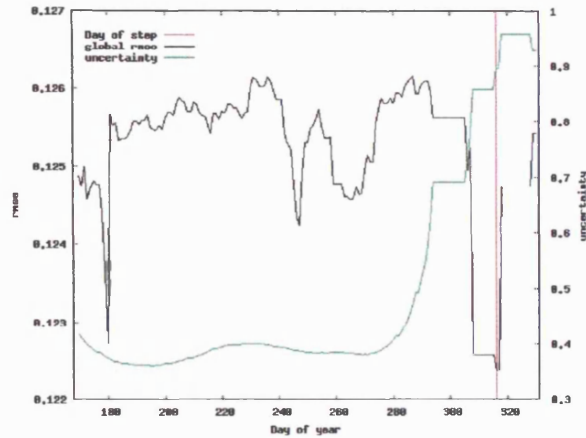
Figure 5.3: Uncertainty in predictions of reflectance

described in Equation 4.32. The benefit of using a measure which incorporates information relating to the noise in the data as well as the uncertainty associated with the prediction of the model parameters is evident from the example displayed in Figures 5.4. Figure 5.4a contains a sequence of MODIS band 2 reflectances for a pixel which was flagged as containing an active fire in the MODIS Thermal Anomalies product on day 247 (the 4th September) 2003. The pixel is located within central Angola as documented as Site 5A in Table A.1 and Figure A.1 in Appendix A. A clear step change occurs in the band 2 reflectances at this point. However when the model is inverted over this sequence and parameter c is determined by minimising the global error, the best fit value for c is day 316 where the minimum of the global error occurs. The global error in the model fit as well as the weight of determination for this temporal sequence are contained in Figure 5.4b. As in the example of Figure 5.3 the uncertainty increases towards the end of the time period resulting in a much larger uncertainty in the prediction of a step change on day 316 than at earlier points in the sequence. This is likely to be due to its location in the temporal sequence, in conjunction with an increase in cloud cover towards the end of the burn season which has resulted in a higher number of missing observations towards the end of the dataset. Figure 5.4c contains the values of model parameter $s(\lambda)$ - the magnitude of the step change - at each cloud free observation within the temporal sequence over which the model is inverted. In

comparison the measure ($M(\lambda)$) described in Equation 5.1 is displayed in Figure 5.4d. Weighting parameter $s(\lambda)$ by the uncertainty in prediction and the noise in the data reduces the impact of any predictions which have a high uncertainty. The global (i.e. across all wavebands) minimum of this measure now occurs on day 247 in agreement with the active fire detection.



(a) MODIS band 2 reflectances



(b) Uncertainty and error in prediction

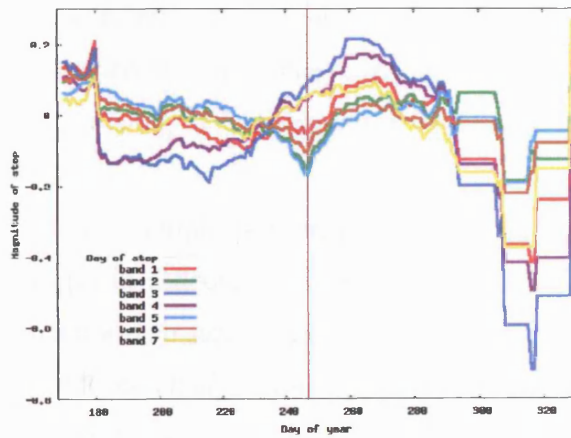
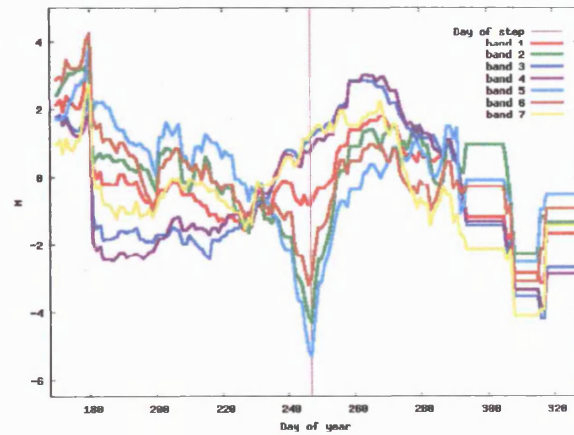
(c) Magnitude of step $s(\lambda)$ (d) Measure $M(\lambda)$

Figure 5.4: Locating the day of greatest change: Site 5A, central Angola

5.4.2 A spectral filter

The incorporation of the measure of uncertainty described in the previous section into the change detection algorithm provides a robust approach to the detection of sudden changes within a temporal sequence of reflectance data. If however the aim is to identify specific types of surface change as is the case in the current research, this may be achieved more effectively by weighting the method used to determine the location of the change by an expectation of the spectral characteristics of the change. As discussed in Section 3.5 the greatest and most consistent fire induced spectral change occurs in MODIS bands 2, 5 and 6, with changes in the other four land surface reflectance wavebands being considerably smaller and/or more variable. The occurrence of a fire generally results in a sudden decrease in MODIS bands 2, 5 and 6 reflectances, with changes that occur in the other four bands dependent on factors such as the condition and type of the vegetation, the time since the fire, atmospheric properties at the time of the acquisition and the stability of the atmospheric correction (Roy *et al.* 2002). Figure 5.5 displays the magnitude of the step change weighted by the uncertainty in the prediction of a step and the noise in the data (Equation 5.1) for the pixel used as an example in the previous section (Section 5.4) which was detected as containing an active fire on day 247. From these results a large negative step (a decrease in reflectance) can clearly be identified in bands 2, 5 and 6 on the day of the active fire detection, with comparatively minimal changes occurring in the other four wavebands at this point.

This example is representative of the spectral response of the vegetation to fire induced changes in reflectance over the area of interest, and suggests that not all seven MODIS land surface wavebands are necessary to detect changes in the surface due to fire. The separation of fire induced change from changes due to other causes may be achieved more successfully based on some measure relating to the nature of the change observed in bands 2, 5 and 6 as opposed to a global measure across all seven wavebands. As changes which are not due to fire may cause changes in reflectance at a greater magnitude than the changes caused by burning, the incorporation of wavebands which are insensitive to burning but which may be affected by other types of change may confuse the signal, resulting in a decrease in accuracy in the detection of fire induced change. In addition the fewer the number of wavebands used in the algorithm, the more computationally efficient it will be. As the changes which occur to bands 1, 3, 4 and 7 tend to be

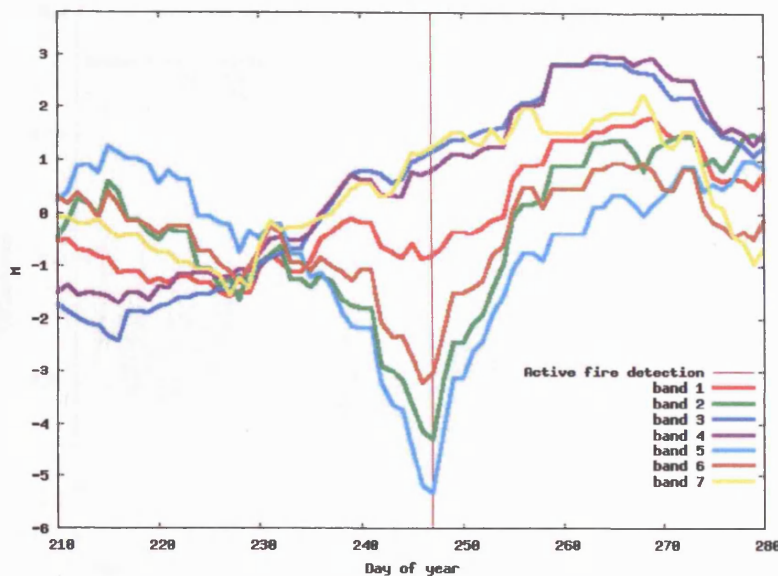


Figure 5.5: The prediction of a step change, Site 5A, central Angola

minimal and/or variable as a result of fire, it may not be necessary to incorporate them into the algorithm. However as types of surface change other than that caused by fire may result in similar changes to MODIS bands 2, 5 and 6 reflectances, it may be necessary to include additional wavebands as a check in order to eliminate changes of a similar spectral nature which are not a result of burning.

In particular problems have been identified in the data due to an increase in cloud cover which occurs over the area of interest towards the end of the burn season, resulting in a larger number of missing samples within the temporal sequence. The presence of noisy data and missing samples in conjunction with an increasing magnitude in the underlying phenological change due to the onset of the rainy season may result in the occurrence of a step change in the time series of MODIS band 2, 5 and 6 reflectances with a similar magnitude to that caused by fire, even though a fire has not actually occurred. This is demonstrated through the example of a single pixel location which burned on day 246 (the 3rd September) 2003. The pixel is located in southern Angola (Site 5B, Table A.1 and Figure A.1 in Appendix A). Band 2 reflectances for this pixel are shown in Figure 5.6 for a period of 120 days.

The reflectance state is relatively stable over the period before the burn and during the fifty days or so after the fire. However towards the end of the time series the data becomes increasingly

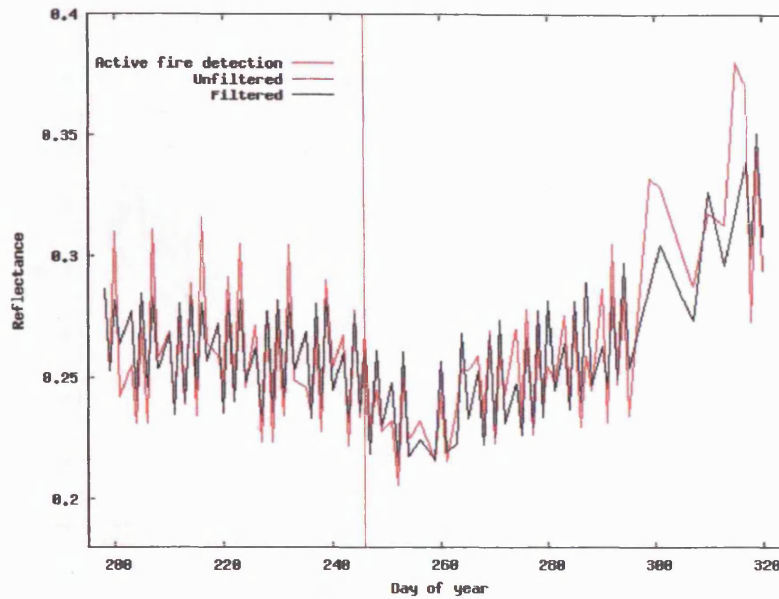


Figure 5.6: MODIS band 2 reflectances: Site 5B, southern Angola

variable with a larger number of ‘noisy’ observations. Although the method described in Section 4.6 is successful in identifying and removing most of these as is evident from the filtered data in Figure 5.6, if the outliers are not isolated events they will not be removed. Figure 5.7 contains the values of $M(\lambda)$ for this pixel calculated over the 120 day period. The effect which the combination of bad data, missing samples and the increasing magnitude of underlying surface change has on the model predictions can clearly be seen in these results. Although the largest negative step in band 2 and band 5 occurs on day 246 (in agreement with the active fire detection), the day of the greatest step change (based on the global minimum of the measure $M(\lambda)$) is identified as day 307. An examination of the values of $M(\lambda)$ contained in Figure 5.7 suggest that the surface change identified on this day is not only characterised by a decrease in bands 2, 5 and 6 reflectances, but at this point all seven MODIS land surface wavebands exhibit a decrease in reflectance with a larger and more pronounced negative step occurring in bands 1, 3, 4 and 7 in comparison to bands 2 and 5. In this case it is clearly not sufficient to use only bands 2, 5 and 6 to locate burn type changes in the surface. A spectral filter has therefore been defined in order to separate changes which occur due to fire from those that occur as a result of other causes. This involves the three conditions defined below:

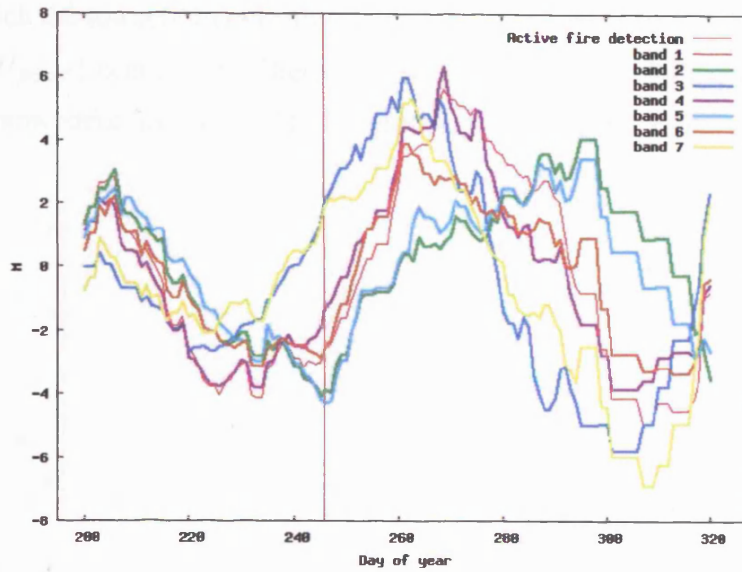


Figure 5.7: Step changes in reflectance ($M(\lambda)$) Site 5B, southern Angola

1. $M(\text{band2}) < 0$ and $M(\text{band5}) < 0$
2. $M(\text{band1}) > M(\text{band2})$ and $M(\text{band1}) > M(\text{band5})$
3. $M(\text{band7}) > M(\text{band2})$ and $M(\text{band7}) > M(\text{band5})$

In order for a pixel to be identified as a potential burn, it must have a negative value of $M(\text{band2})$ and $M(\text{band5})$ thus exhibiting a sudden decrease in reflectance in these two wavebands. MODIS bands 2 and 5 have been selected in preference to band 6 as the data presented in Chapter 3 as well as previous research has indicated that the changes which occur at band 6 wavelengths as a result of fire tend to be more dependent on the vegetation type and the time which has elapsed since the occurrence of the fire than those which occur at shorter infrared (bands 2 and 5) wavelengths (Trigg and Flasse 2000, Sa *et al.* 2003, Li *et al.* 2004, Roy *et al.* 2005b). In addition to the requirement for a negative change at bands 2 and 5 wavelengths, according to the criteria defined above the value of M must be smaller in both bands 1 and 7 than the value of both $M(\text{band2})$ and $M(\text{band5})$. If these conditions are met then the temporal location of the burn is assigned to the day corresponding to the largest negative value of $M(\text{band2})$ or $M(\text{band5})$. This filter is applied to the temporal sequence contained in Figures 5.6 and 5.7, with the value of $M(\lambda)$ set to zero if any of the three conditions are not met. The day of the change is then located as the point within

the series at which the lowest filtered value (i.e. meeting the three conditions defined above) of $M(\text{band}2)$ and $M(\text{band}5)$ occurs. The filtered results are contained in Figure 5.8 with the point of greatest change now identified as day 246 in agreement with the day of the active fire detection.

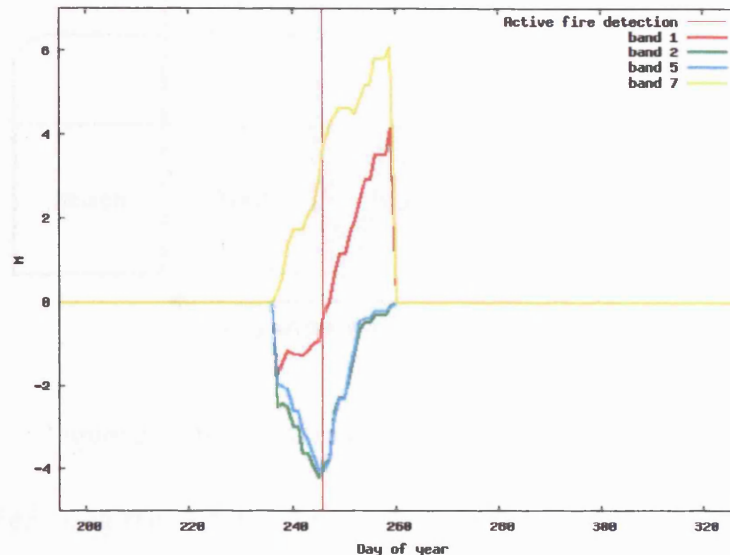


Figure 5.8: Prediction of burn-type change (Site 5B, southern Angola)

5.5 The creation of monthly burned area datasets

The change detection model introduced in Section 4.5 has been applied to daily MODIS surface reflectance data for the eight months of the annual southern Africa fire season (April–November) over a five year period (2000–2004), with the aim of providing daily burned area information for this period. The burn information has been produced by inverting the model over a single month of daily observations of reflectance with a thirty day buffer at either end, as illustrated in Figure 5.9. Thus for April 2000 for example 90 days of observations of reflectance (*window A*) for the time period beginning on the 2nd of March and ending on the 30th of May have formed the model input, with the model output consisting of a single inversion performed over this entire period for each pixel. However the observations contained within the 30 day buffer do not contribute to the identification of a step change, and thus the location of the greatest step change has only been identified within the month of interest (*window B*). The location of the greatest step change

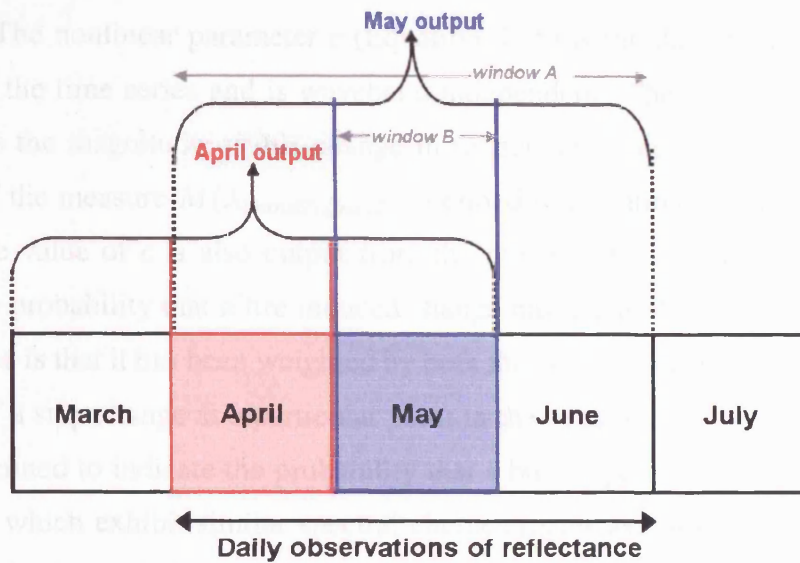


Figure 5.9: Temporal range of model inputs and outputs

has been identified using the statistical spectral measure described in Section 5.4, and is thus only based on the information contained in MODIS bands 1, 2, 5 and 7. The model output for each month is a band sequential image consisting of 34 layers including one for each of the seven model parameters plus the rmse of the model fit for each waveband, the day of the greatest change and the probability that a fire induced change has occurred on this day. The latter two data fields are waveband independent.

5.5.1 The selection of burn candidates

In order to produce the final maps detailing the location of fire affected areas, it is necessary to examine the change candidates and decide upon a threshold which will separate pixels according to the magnitude and type of change which has occurred. Although a spectral filter (M) has been used to determine the probability of the occurrence of a burn-type change at each temporal location within the time series (Section 5.4.1), not all pixels which exhibit a negative step change at the day selected as the point of greatest change according to M will have burned. A post-processing step is therefore necessary in order to threshold the change information and locate areas of high probability burning.

Three of the model outputs contain information relating directly to the occurrence of change

at the surface. The nonlinear parameter c (Equation 4.35) is the day at which the change has occurred within the time series and is waveband independent. The coefficient $s(\lambda)$ defined in Equation 4.34 is the magnitude of this change in reflectance at each waveband on day c , and the minimum of the measure $M(\lambda_{(band2),(band5)})$ defined in Equation 5.1 and used to locate the most appropriate value of c is also output from the model. Of these $s(\lambda)$ and M provide an indication of the probability that a fire induced change has taken place on day c . An advantage of the measure M is that it has been weighted by both the noise in the data and the uncertainty in the prediction of a step change at a particular point in the time series of observations. However as it has been defined to indicate the probability that a burn-type change has occurred at day c , surface changes which exhibit similar spectral characteristics as burned areas but at a smaller magnitude will also be included in the data and these will need to be identified and removed. The step change parameter $s(\lambda)$ is related to the characteristics of the observed reflectance and the magnitude of the change which has occurred on day c .

As the magnitude of the change (parameter $s(\lambda)$) provides multispectral information relating to the change which has occurred at the surface, it can be used to eliminate changes which exhibit a decrease in burn sensitive wavebands (MODIS bands 2 and 5) but which are not due to fire. In the case of the multiplicative model due to the non-linear formulation parameter $s(\lambda)$ is not a direct measure of the magnitude of the change in the surface reflectance. The modelled reflectance for the multiplicative temporal change detection model takes the form of Equation 5.2;

$$\begin{aligned} \ln \rho(\lambda, \Omega, \Omega') = & \ln \rho_0(\lambda) + \ln \rho_0(\lambda)t + \ln \rho_0(\lambda)t^2 + \ln \rho_0(\lambda)t^3 + f_1 \ln K_1 + f_2 \ln K_2 \\ & + f_1 \ln K_1 + f_2 \ln K_2 + f_3 \ln K_3 + s(\lambda) \end{aligned} \quad (5.2)$$

In order to determine the magnitude of the change which has occurred to the surface reflectance it is therefore necessary to calculate the inverse of $\ln \rho(\lambda)$ for the day of the change and the day after the change. The actual magnitude of the step change can then be calculated as the difference between the forward modelled reflectance on the day of the change (c) and the day after the change ($c + 1$). Under nadir illumination and viewing conditions ($\Omega = 0, \Omega' = 0$) this is

defined as:

$$\rho_{diff}(\lambda, \Omega, \Omega') = (\rho_{(c+1)} - \rho_{(c)}) \quad (5.3)$$

where ρ is the model predicted reflectance for waveband λ on the day after the step change $(c + 1)$ and the day of the step change (c) . For the multiplicative temporal model the forward modelled reflectance on day t where $t \leq c$ takes the form of Equation 5.4 for nadir viewing and illumination conditions:

$$\rho_0(\lambda, \Omega, \Omega') = e^{(f_{iso} + f_t t + f_{t_2} t^2 + f_{t_3} t^3)} \quad (5.4)$$

where f_{iso} is the isotropic parameter and f_{t_N} are the cubic temporal coefficients. For $t > c$ the multiplicative temporal model the forward modelled reflectance under nadir viewing and illumination conditions takes the form of Equation 5.5 where $s(\lambda)$ is the magnitude of the step change.

$$\rho_0(\lambda, \Omega, \Omega') = e^{(f_{iso} + f_t t + f_{t_2} t^2 + f_{t_3} t^3 + s)} \quad (5.5)$$

For the additive temporal model the reflectance level $\rho(\lambda, \Omega, \Omega')$ at day t under $\Omega = 0, \Omega' = 0$ for $t \leq c$ is defined as:

$$\rho(\lambda, \Omega, \Omega') = f_{iso} + f_t t + f_{t_2} t^2 + f_{t_3} t^3 \quad (5.6)$$

And for $t > c$;

$$\rho(\lambda, \Omega, \Omega') = f_{iso} + f_t t + f_{t_2} t^2 + f_{t_3} t^3 + s \quad (5.7)$$

Using the outputs from Equations 5.4 and 5.6 the magnitude of the change in surface reflectance under $\Omega = 0, \Omega' = 0$ is calculated following Equation 5.3.

As described in Section 3.6.1 the magnitude of fire induced changes in the surface reflectance are expected to vary both spatially and temporally as a function of the characteristics of the pre fire vegetation and the nature of the fire. The separation of areas which have been affected by fire

from those which have not according to the magnitude of the change which has occurred may therefore require a spatially and temporally varying threshold level. In addition to the difficulty in the definition of such a threshold due to the inherent heterogeneity of the surface, its requirement would result in the loss of generality of the algorithm and thereby reduce its applicability to different ecosystems. In contrast a proportional measure such as that defined in Equation 3.3 (Section 3.6.1) will allow for variations in the pre fire and post fire reflectance levels and provides an indication of the change which has occurred to the surface reflectance as a function of the reflectance level before the change. Following on from Equation 5.3 above, the proportional change in the modelled reflectances is calculated by weighting the magnitude of the change in the reflectance (ρ_{diff} in Equation 5.3) by the pre change reflectance level. This is defined as:

$$\delta\rho(\lambda, \Omega, \Omega') = \left(\frac{\rho_{diff}}{\rho_{(c-1)}} \right) \quad (5.8)$$

where $\rho_{(c-1)}$ is the reflectance on the day before the change as described in Equations 5.4 and 5.6. A further processing step is thus added to the burned area detection process which involves;

1. forward modelling the reflectance for each model on the day before the change (Equations 5.4 and 5.6) and the day after the change (Equations 5.5 and 5.7)
2. the calculation of the magnitude of the change in reflectance which has occurred between these two days (Equation 5.3)
3. the calculation of the proportional change in reflectance following Equation 5.8

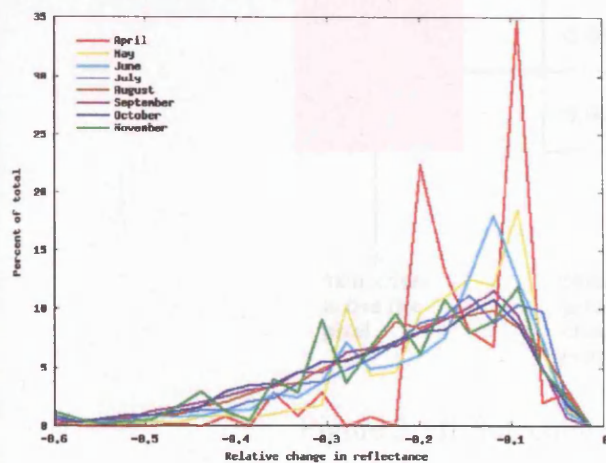
While the proportional change in reflectance may be a more robust measure if calculated under the mean solar zenith angle for each month and the viewing zenith angle of the observation, as a post-processing step this would require a significant amount of computationally expensive data manipulation as these information fields are not contained in the model output. The proportional change in reflectance is therefore calculated under nadir viewing and illumination conditions for each pixel.

5.5.2 The proportional change in reflectance

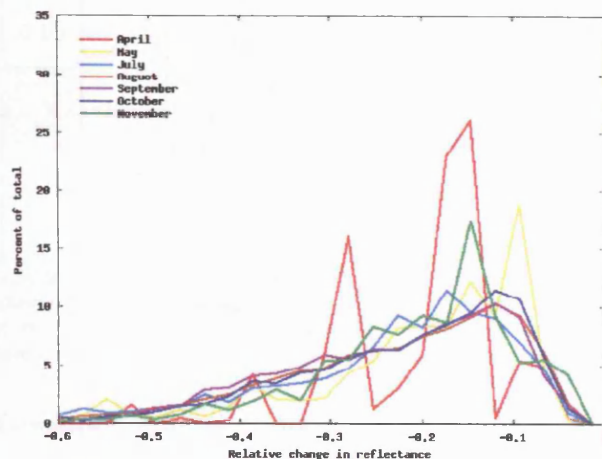
The MODIS Thermal Anomalies product documents the locations of high confidence active fire detections (see Section 3.4.1). Although errors of omission will be present in the data as the occurrence of fires may not coincide with the timing of the satellite overpass or may be precluded by the presence of smoke or cloud, this product has demonstrated minimal errors of commission for the southern Africa study area (Giglio *et al.* 2003a). While the original “version 3” product contained frequent false detections over deserts and sparsely vegetated land surfaces, the algorithm employed in the replacement “version 4” product addresses these problems and under a small scale validation has been shown to have very low errors of commission (*ibid*). The locations of active fires as documented in the MODIS Thermal Anomalies version 4 product will be used to verify the change detection algorithms, and to assist in the determination of a suitable threshold level for the identification of fire-affected areas from the model results.

The distribution of the values of $\delta\rho(\text{band5})$ calculated using the additive temporal model parameters for each month of the annual burn season for each of the five years and across the entire study area are displayed in Figure 5.10. These data correspond to pixel locations which have been identified as containing an active fire during the particular month of interest, as documented in the MODIS Thermal Anomalies product. However as the spatial resolution of the active fire data is 1km by 1km only the single 500m by 500m model output pixel which exhibits the greatest absolute change of the four corresponding pixels is selected. This procedure is followed in order to reduce potential errors of commission as a flaming fire needs only to be approximately $100m^2$ in order to have a 50 percent or greater chance of detection by the MODIS active fire algorithm (Giglio *et al.* 2003a). Therefore in the case of subpixel resolution fires not all four of the MODIS surface reflectance pixels which correspond to a single 1km active fire location will have burned. This selection process is described in Figure 5.11. The histogram values for the multiplicative model results are displayed in Figure 5.10 as a percentage of the total number of 1km active fire pixels detected each month which exhibit a negative step change for at least one of the four corresponding 500m resolution pixel locations. For the 2003 and 2004 annual fire seasons hotspot locations derived from MODIS Aqua data are used in addition to those detected by MODIS Terra.

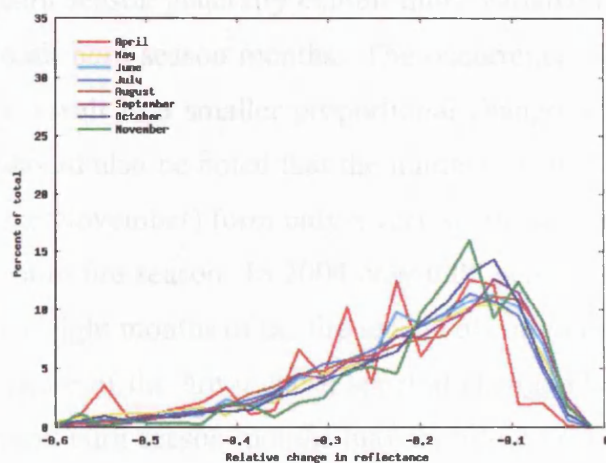
A visual examination of the distribution of $\delta\rho(\text{band5})$ values at active fire locations (Figure



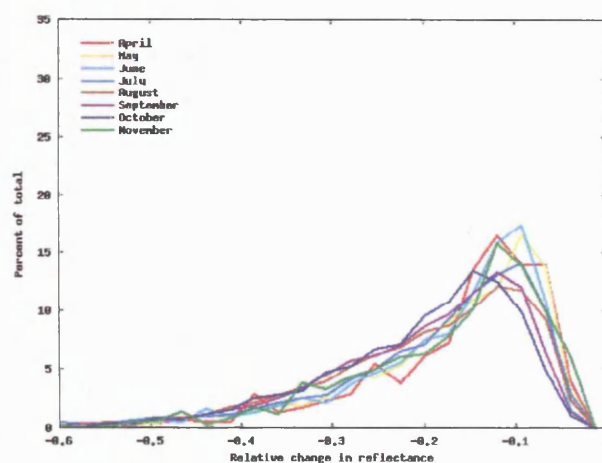
(a) 2000



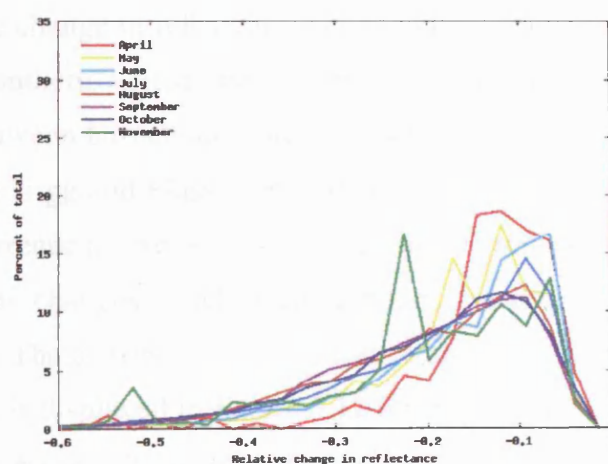
(b) 2001



(c) 2002



(d) 2003



(e) 2004

Figure 5.10: The proportional change ($\delta\rho$) in band 5 reflectances at active fire locations

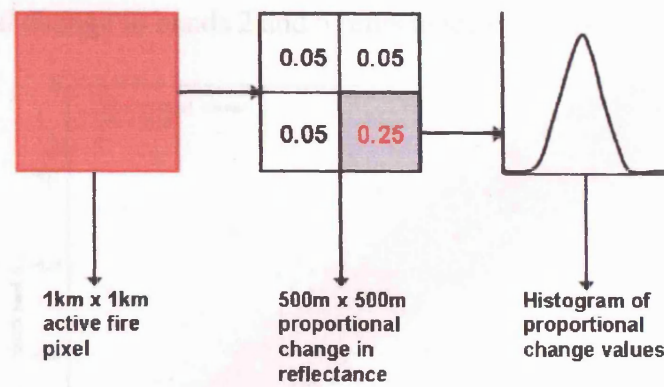


Figure 5.11: Selection of change candidate values

5.10) suggests that for all years other than 2003 fires which occur during the tail months of the burn season generally exhibit more variable changes than those which are detected during the peak burn season months. The occurrence of fires at the start of the burn season (April) tend to result in a smaller proportional change in the surface reflectance than later in the year. It should also be noted that the number of fires which occur at the tails of the burn season (April and November) form only a very small percentage of the total number of fires detected over the entire fire season. In 2004 only 0.05 percent of the total number of active fires detected during the eight months of the fire season occurred in April, and 1.7 percent in November. The variable nature of the fire induced spectral change identified during these months in comparison to the peak burn season months may therefore be a function of the smaller sample size of the data in addition to the characteristics of the fire regime at this time.

The short-wave infrared waveband (MODIS band 5) has been chosen to illustrate the distributions of the relative change in reflectance at active fire locations in Figure 5.10 as research has indicated that in southern African ecosystems this waveband (along with band 2) offers higher separabilities between burned and unburned vegetation than other MODIS land surface reflectance wavebands (Trigg and Flasse 2001, Roy *et al.* 2002, Li *et al.* 2004). As described in Section 3.5 the occurrence of fire results in a decrease in reflectance at MODIS bands 2 and 5 wavelengths, while the changes which occur at bands 1 and 7 tend to be more variable and of a smaller magnitude. The distribution of the relative change in the surface brightness ($\delta\rho(\lambda)$) across bi-spectral space is displayed in Figure 5.12 for pixels which have been detected as containing an active fire in August 2004 and subjected to the procedure described in Figure 5.11.

While the proportional change in bands 2 and 5 reflectance is typically very similar (Figure 5.12)

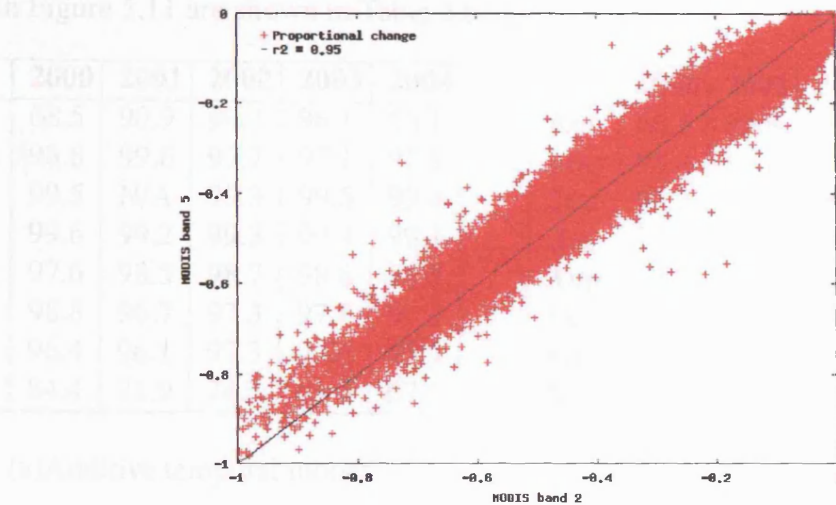


Figure 5.12: $\delta\rho(\text{band}2)$ and $\delta\rho(\text{band}5)$ at active fire locations

it tends to be slightly greater at band 5 than at band 2 wavelengths. However this is not always the case and changes in reflectance of a greater magnitude occasionally occur in the near infrared waveband at active fire locations. This difference in the proportional change in reflectance which occurs at MODIS bands 2 and 5 as a result of a fire is likely to be due to the characteristics and the condition of the vegetation at the time of burning. As demonstrated in Figure 3.11b (Section 3.5) the magnitude of the change which occurs at MODIS bands 2 and 5 will be affected by the level of senescence and thus the water content of the vegetation. At band 2 wavelengths a greater difference is evident between the measured spectra of a post-burn black ash surface and pre-burn green vegetation than at band 5 wavelengths, while in the case of dry vegetation the opposite is observed with a greater change in reflectance occurring at band 5 rather than at band 2 wavelengths. Therefore in order to exploit all of the spectral information available as well as to exclude confusing spectral changes (see Section 5.5.3 below) the proportional change in reflectance at both bands 2 and 5 will be examined in order to locate pixels which have been affected by fire. In addition to the increase in potential change information provided by the incorporation of band 2, the use of this waveband in conjunction to band 5 offers the further advantage of reducing the impact of a bad MODIS band 5 500m detector which results in missing scan lines every 10km (Roy *et al.* 2002).

The percentage of active fire detections each month which correspond to a decrease in re-

flectance (a negative value of $\delta\rho$) at band 2 *and* band 5 wavelengths following the method described in Figure 5.11 are shown in Table 5.6.

	2000	2001	2002	2003	2004
Apr	68.5	90.9	99.2	96.1	56.1
May	98.8	99.6	97.7	97.1	97.9
Jun	99.5	N/A	99.3	99.5	99.4
Jul	99.6	99.2	99.3	99.4	99.1
Aug	97.6	98.5	98.7	98.8	98.7
Sep	98.8	96.7	97.3	97.8	97.2
Oct	96.4	96.1	97.3	96.6	93.4
Nov	84.4	71.9	74.3	69.0	67.8

	2000	2001	2002	2003	2004
Apr	66.5	89.9	99.3	95.0	55.5
May	98.4	99.6	97.7	96.9	97.9
Jun	99.3	N/A	99.2	99.4	99.3
Jul	99.5	99.2	99.3	99.3	98.9
Aug	97.7	98.4	98.5	98.8	98.4
Sep	80.1	96.8	97.3	97.7	97.2
Oct	96.2	96.1	97.4	96.5	93.8
Nov	84.4	70.2	74.1	69.5	67.9

(a) Additive temporal model

(b) Multiplicative temporal model

Table 5.6: Percentage of MODIS active fire detections which exhibit a proportional decrease in MODIS band 2 *and* band 5 reflectances

Two features of interest are immediately apparent in this data; (i) the results from the two models are extremely similar and (ii) a much lower percentage of active fire locations exhibit a decrease in band 2 and band 5 reflectance during the tail months of the fire season. Thus while over 95% of active fire locations exhibit a corresponding decrease in band 2 and 5 reflectances between May and October each year, this figure is much lower for November for each of the five years and for April 2000, 2001 and 2004. This feature is discussed further in the following paragraph. The agreement between the detection of an active fire and a proportional change in band 2 *and* band 5 reflectances below a particular threshold level for each month are displayed in Table 5.7 as a percentage of the total number of pixels for the particular month which exhibit a decrease in reflectance at these wavelengths. As above (Table 5.6) the change information used in the analysis is the value of $\delta\rho(\text{band}2)$ and $\delta\rho(\text{band}5)$ for each pixel location across the entire study area, with the data subjected to the procedure described in Figure 5.11.

As discussed above the data contained in Table 5.6 and Table 5.7 indicate that the proportional changes in reflectance which occur at the corresponding 500m locations of active fire detections are generally of a much smaller magnitude at the tails of the southern Africa fire season, and tend to be more uniform during the months encompassing the peak of the fire season. This is likely to be due to the state of the vegetation and thus the characteristics of the fires which occur at the start and at the end of the annual fire season. The southern Africa fire season typically

	2000	2001	2002	2003	2004
Apr	51.1	71.1	86.7	65.3	48.3
May	73.6	74.9	77.7	65.0	68.3
Jun	76.7	N/A	74.0	66.9	67.9
Jul	80.9	79.6	76.1	69.6	67.9
Aug	76.1	74.0	71.8	67.9	68.2
Sep	75.1	73.8	71.0	66.9	69.0
Oct	76.1	75.9	69.9	69.5	66.6
Nov	72.9	71.7	71.6	59.5	68.2

Threshold: -0.1

(a) Additive temporal model

	2000	2001	2002	2003	2004
Apr	57.9	73.0	91.7	69.2	51.9
May	77.5	78.6	79.9	67.4	68.4
Jun	80.8	N/A	77.8	71.4	71.1
Jul	84.7	82.7	79.4	73.5	70.7
Aug	80.2	78.3	75.4	71.0	70.5
Sep	58.4	78.0	75.7	70.4	72.3
Oct	80.7	82.5	81.3	74.9	74.7
Nov	81.3	77.9	82.6	73.2	80.6

Threshold: -0.1

(b) Multiplicative temporal model

	2000	2001	2002	2003	2004
Apr	37.2	47.8	69.6	47.3	27.7
May	55.5	57.8	61.9	46.9	49.6
Jun	60.7	N/A	57.8	47.4	50.5
Jul	64.7	64.7	60.0	51.7	50.9
Aug	59.7	59.0	56.6	50.8	50.6
Sep	57.8	60.1	55.6	49.9	53.2
Oct	61.0	61.2	51.7	49.7	50.4
Nov	55.4	48.8	51.5	40.8	50.3

Threshold: -0.15

(c) Additive temporal model

	2000	2001	2002	2003	2004
Apr	39.1	50.6	76.9	50.1	26.5
May	59.0	59.8	64.5	48.5	48.6
Jun	64.5	N/A	61.5	51.2	53.5
Jul	69.3	68.1	63.8	55.2	53.9
Aug	64.5	63.0	59.2	53.7	53.1
Sep	42.3	62.8	59.2	52.3	56.0
Oct	65.6	66.8	60.7	53.7	57.0
Nov	65.4	58.8	62.4	52.8	61.8

Threshold: -0.15

(d) Multiplicative temporal model

	2000	2001	2002	2003	2004
Apr	23.4	33.3	55.0	35.2	16.6
May	40.0	43.6	45.7	32.5	35.3
Jun	46.0	N/A	42.5	32.8	36.6
Jul	49.3	50.9	45.4	37.2	37.1
Aug	43.7	45.7	43.6	36.1	36.7
Sep	42.8	47.6	42.0	36.0	40.1
Oct	46.6	47.0	38.8	35.8	38.0
Nov	40.0	31.9	34.2	29.6	35.5

Threshold: -0.2

(e) Additive temporal model

	2000	2001	2002	2003	2004
Apr	27.1	44.9	61.1	35.8	15.3
May	42.3	44.3	48.7	33.3	33.5
Jun	49.2	N/A	46.5	35.5	38.8
Jul	54.1	53.4	49.6	39.8	38.9
Aug	48.3	49.2	46.0	38.9	38.9
Sep	29.9	49.5	45.2	37.7	42.7
Oct	50.8	52.1	44.4	38.5	43.5
Nov	48.3	41.2	44.0	36.3	45.1

Threshold: -0.2

(f) Multiplicative temporal model

Table 5.7: Percentage of MODIS active fire detections which exhibit a proportional decrease in MODIS band 2 *and* band 5 reflectances below a particular threshold value

begins in April and follows the seasonal pattern of vegetation senescence starting at the end of the annual rainy season (Frost 1999). At the start of the fire season the vegetation is at the peak of its phenological cycle and is greener than at any other point during the fire season, as evident from the MODIS EVI data in Figure 3.8 (Section 3.4.2). Due to the higher water content of the vegetation at this point fires which do start are likely to be of a lower severity and the larger burns which are observed later in the year at the peak of the fire season are thus less likely to occur. Fires which are detected during April are therefore likely to be smaller and more fragmented than later in the year when the vegetation is drier and burns more easily. Consequently an explanation for the larger relative change in surface reflectance which occurs in April 2002 is that this may have been a dry year with the fire season starting earlier than in the other years. This is discussed further in Section 7.5. In 2002, 1.9 percent of the fires detected by MODIS Terra during the eight months of the annual fire season occurred in April, in comparison to 0.09, 0.05, 0.4 and 0.05 percent in 2000, 2001, 2003 and 2004 respectively. The lower relative changes observed at active fire locations during November over the five year period are likely to have a similar cause. As precipitation increases and wet conditions typically return to most of the interior African regions south of the equator during October (Cahoon *et al.* 1992), the lower magnitude of the burn signal in November each year may be a result of the increased moisture content of the vegetation, and the decrease in the occurrence of larger fires commonly observed in the previous months. An additional factor which may explain the lower agreement between the active fire detections and the proportional changes in reflectance at the tails of the fire season is greater cloud cover over the study area during this time resulting in fewer clear high quality observations of the surface than during the height of the dry season. The disagreement between the potential burn candidates and the locations of active fire detections at the tails of the fire season are thus likely to be due to the different spatial resolutions of the two data sources, the state of the vegetation and the characteristics of the fires, as well as the greater cloud cover during these months.

An examination of the results contained in Table 5.7 indicates that higher proportional changes in reflectance are identified at active fire locations from the multiplicative in comparison to those produced using the additive model (Table 5.7b, 5.7d and 5.7e). Using a threshold of -0.1 (a 10% decrease in reflectance) allows for an agreement of over 75% between the multiplicative modelled results and active fire locations for most months, and an agreement of at least 65% between the additive modelled results and active fire locations for almost all months over the five year

period. However thresholding either set of results at a level higher than -0.15 results in the incorporation of a large number of pixels which are unlikely to have burned but exhibit changes of a similar magnitude due to other causes. Thus in April 2003 68.8% of the land surface within the study area exhibits a proportional decrease (using the multiplicative modelled results) in MODIS band 2 and 5 reflectances of at least -0.1, while for August 2003 this figure is 17.3%.

Although the lack of a comprehensive burned area dataset for the area of interest makes it impossible to determine whether a pixel is not a burn and therefore all pixels which exhibit a negative step change in conjunction with the spectral characteristics exhibited by fire affected areas may potentially have burned, using a threshold of -0.1 clearly results in high errors of commission in particular at the tails of the fire season. While reducing the threshold to a value of -0.15 (an equivalent decrease in reflectance of 15%) reduces the errors of commission, a decrease in the agreement between the active fire detections (Table 5.7c and 5.7d) also occurs. An examination of the locations of active fire pixels which exhibit a proportional change in band 2 and band 5 reflectances above this threshold (i.e. are *not* potential burn candidates) suggests that this disagreement may largely be a function of the different spatial resolutions of the two data sources and the occurrence of subpixel (<1km) resolution fires.

Figure 5.14 contains two areas of 100km by 100km extracted from the additive modelled results for July 2003 which exhibit different patterns of burning. The location of these within the area of interest is displayed in Figure 5.13, and detailed in Table A.1 in Appendix A.

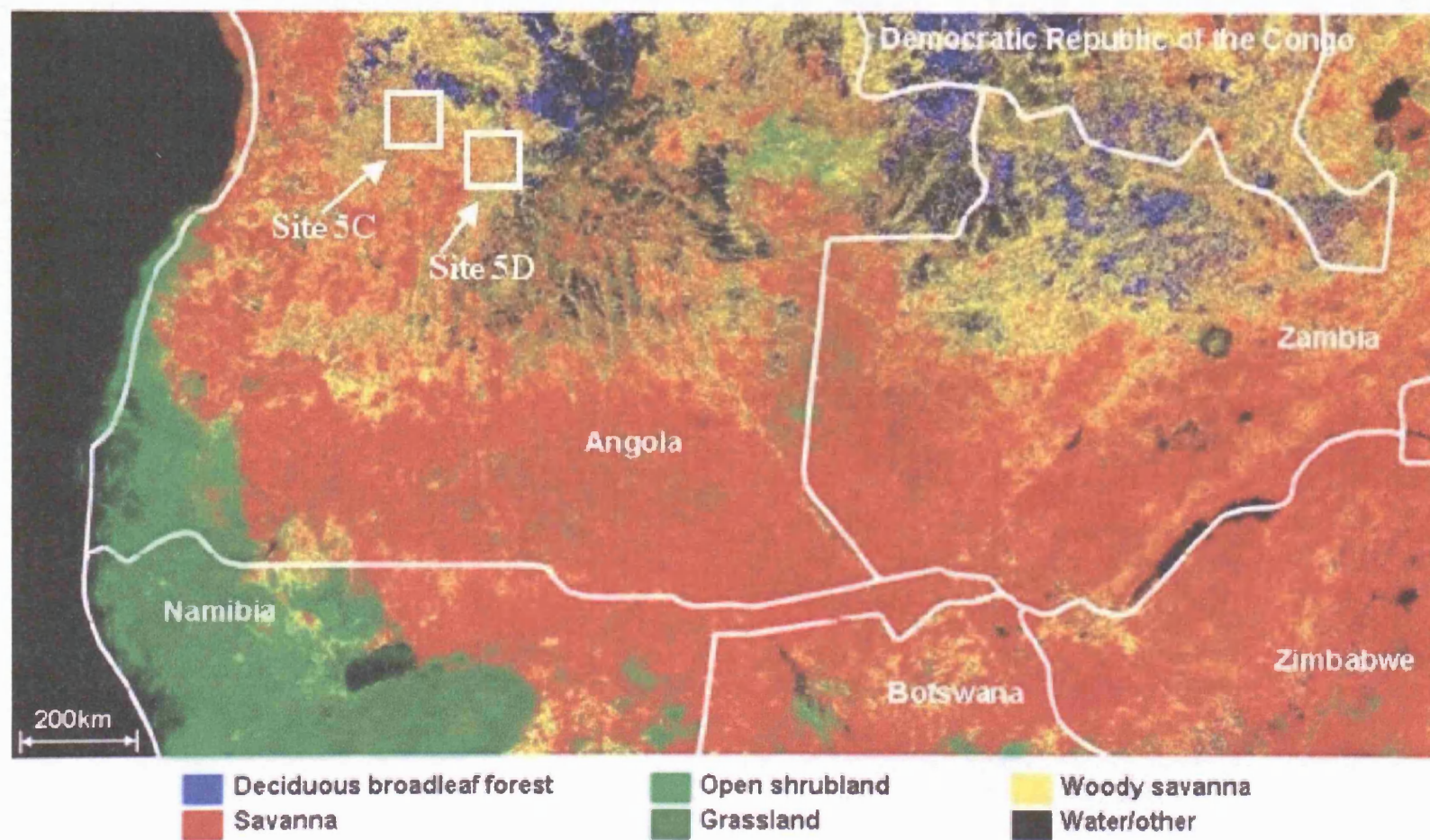
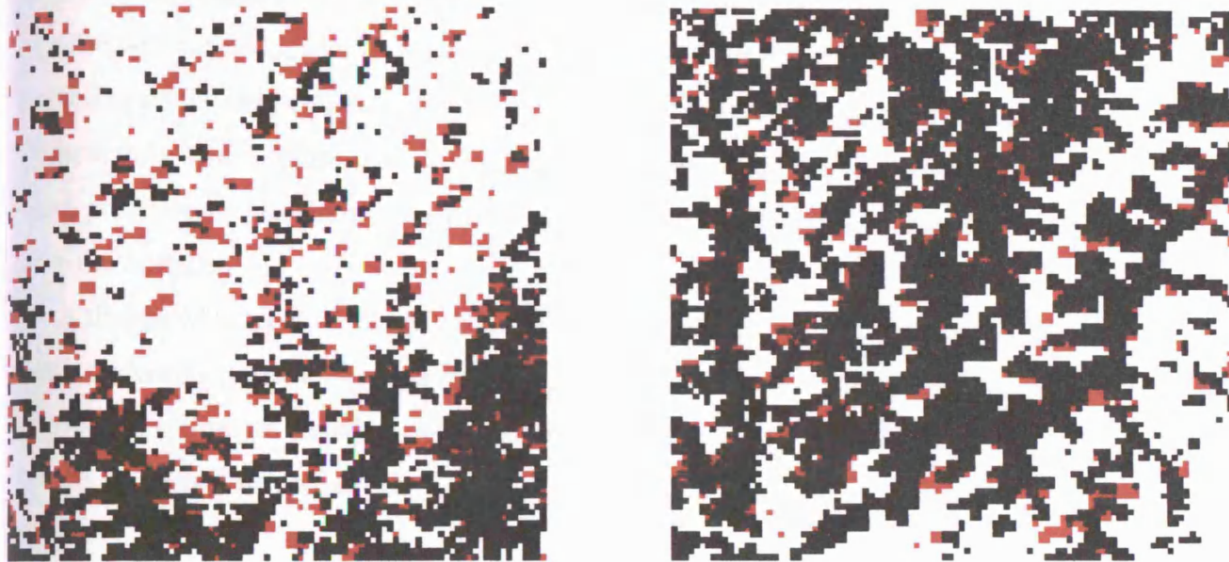


Figure 5.13: Sites 5C, 5D and MODIS Landcover Product

The red pixels correspond to those where an active fire has been detected but $\delta\rho(\text{band2}) > -0.15$ and/or $\delta\rho(\text{band5}) > -0.15$ at each of the corresponding 4 500m locations, and the black areas indicate pixels where $\delta\rho(\text{band2}) \leq -0.15$ and $\delta\rho(\text{band5}) \leq -0.15$ irrespective of whether an active fire has also been detected or not. A large proportion of active fire locations which are



(a) Site 5C (Angola) July 2003

(b) Site 5D (Angola) July 2003

Figure 5.14: Disagreement between 1km active fire locations and 500m potential burn candidates: red pixels indicate active fire detections which are not identified as burns; black areas indicate burn candidates

not identified as potential burns (i.e. exhibit proportional changes in reflectance smaller than the threshold) and are represented as the red pixels in both Figures 5.14a and 5.14b are located either between two burns, or along the perimeter of a burn. A higher agreement between the locations of active fire detections and potential burn candidates is apparent in Figure 5.14b where the burns tend to be larger than those in Figure 5.14a, where the burned areas are smaller and more fragmented. As a flaming fire only needs to be approximately $100m^2$ in order to have a 50 percent or greater chance of detection by the MODIS active fire algorithm (Giglio *et al.* 2003a) and the spatial resolution of this product is 1km, in the presence of small burns such as those displayed in Figure 5.14b it is likely that the size of the fires is overrepresented in the MODIS Thermal Anomalies product. The change which occurs in the MODIS band 2 and 5 reflectances due to burning will be dependent on the fraction of the 500m pixel which has burned. In the case

of small fires the fraction of a 500m pixel which has burned may not be sufficient to produce a proportional change in reflectance of at least 15% ($\delta\rho(\lambda)=-0.15$).

Under the assumption that a hotspot detected is actually a fire, the lower relative change in reflectance observed at many active fire locations may have several causes. In addition to the size of the fire discussed above, the quality of the observations on the days surrounding the occurrence of a fire will have an affect on the detection of a step change in the temporal sequence at this point as well as on the magnitude of the change identified. If there are missing observations on the days immediately after the fire due to the presence of smoke or cloud, the change in the reflectance from pre-burn to post-burn conditions may be of a smaller magnitude due to recovery of the post-fire surface.

A threshold level of -0.15 which corresponds to a 15 percent change in reflectance is therefore used to identify potential burn candidates, and several spectral constraints have been introduced in order to eliminate changes of a similar magnitude which are not due to fire. These are discussed in the following Section.

5.5.3 Excluding confusing spectral change

Vegetation

Various peturbing factors (see Section 3.5.3) may exhibit similar spectral changes to those induced by fire, resulting in confusion between areas which have been affected by fire and those which have not (Trigg and Flasse 2001, Roy *et al.* 2005b). Previous research has indicated that burning results in a decrease in near to middle infrared reflectances with MODIS bands 2 and 5 providing the highest separabilities and band 1 and 7 affording low or variable discrimination between burned and unburned surfaces (Roy *et al.* 2002, Sa *et al.* 2003, Li *et al.* 2004). Although as demonstrated by Figure 5.12 the response of MODIS bands 2 and 5 to burning are extremely similar, the results for both bands are used in the determination of fire affected areas in an attempt to exclude reflectance changes which are due to variations in the vegetation moisture content. Increases in plant water content which may occur, for example, due to leaf flushing caused by a sudden rainfall event (Roy *et al.* 2005b) will reduce the reflectance at band 5 and 7 wavelengths but will have less of an impact at shorter infrared wavelengths (Zarco-Tejada *et al.* 2003). This is demonstrated by Figure 5.15 which contains reflectances modelled at a canopy level using

the Kuusk canopy reflectance model (Kuusk 1996) for different values of leaf equivalent water thickness (C_w) under nadir illumination and viewing conditions. Figure 5.15a refers to a sparse vegetation canopy and has been modelled using an LAI value of 2, while Figure 5.15b refers to a dense canopy modelled with an LAI value of 8. The spectral locations of MODIS bands 2, 5 and 7 are indicated by the vertical lines. The effect of increasing the leaf water content is a decrease

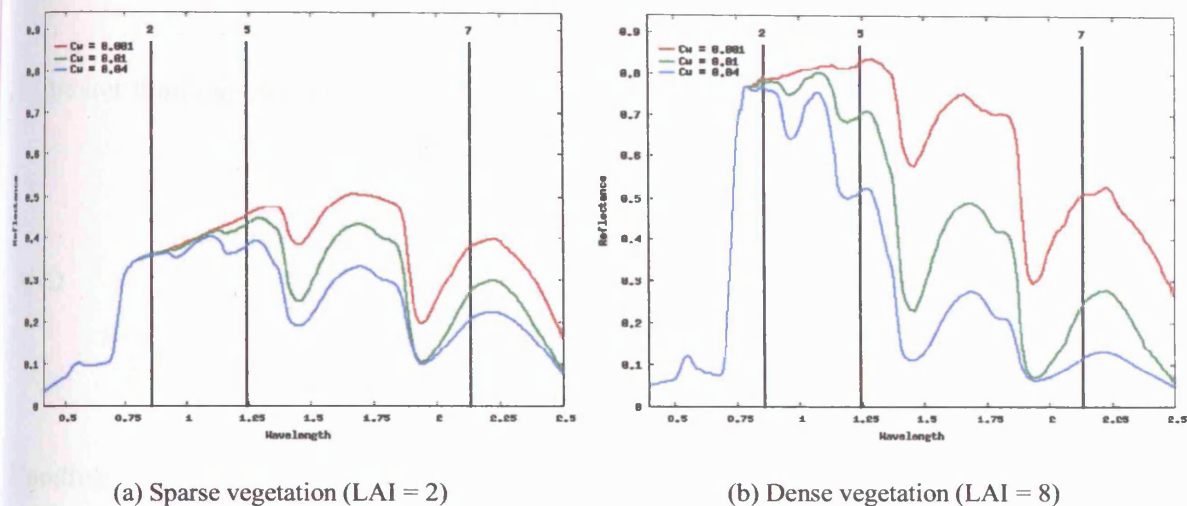


Figure 5.15: Canopy level reflectance modelled with different leaf equivalent water thickness using the Kuusk model (Kuusk 1996)

in MODIS bands 2, 5 and 7 reflectance for dense vegetation canopies, while for sparse canopies varying the moisture content has a minimal effect at band 2 wavelengths but results in a decrease in reflectance in MODIS bands 5 and 7. The larger impact of variations in the leaf water content on the reflectance from both canopies at MODIS band 7 and 5 wavelengths in comparison to the changes which occur at band 2 is clearly evident in Figure 5.15. The proportional changes in MODIS bands 2, 5 and 7 reflectances ($\delta\rho$) calculated for the data displayed in Figure 5.15 are contained in Table 5.8. These data suggest that using a band 5 proportional change threshold of -0.15 to identify potential burn candidates would result in the inclusion of the moisture induced changes described in Figure 5.15. Thus in order to reduce the possibility of identifying such changes as burns both MODIS band 2 and band 5 results are used, with potential burn candidates identified as those which exhibit a proportional change of -0.15 lower in band 2 *and* band 5. In addition the proportional decrease in reflectance at band 2 and band 5 wavelengths is required to

MODIS waveband	Sparse (LAI=2)	Dense (LAI=8)
2	-0.01	-0.03
5	-0.16	-0.38
7	-0.46	-0.77

Table 5.8: Proportional change ($\delta\rho$) in canopy level reflectance due to varying leaf equivalent water thickness

be greater than the change at band 7 wavelengths. This criteria is defined as;

$$\delta\rho_{(band2)} < \delta\rho_{(band7)} \quad (5.9)$$

AND

$$\delta\rho_{(band5)} < \delta\rho_{(band7)} \quad (5.10)$$

Flooding

Confusion between burned areas and water bodies has been reported by several authors (Pereira and Setzer 1993, Razafimpanilo *et al.* 1995, Eva and Lambin 1998a). In the GBA2000 burned area product (see Section 2.4.2) for example, when the algorithms were applied outside the main period of fire activity flooding was found to be the most common cause of false detections (Tansey *et al.* 2004a). The occurrence of flooding was thus one of the two main causes of comission errors (the other being hot bare surfaces) for the sub-Saharan region. This spectral confusion occurs as both water bodies and burned surfaces are characterised by low reflectances at near to middle infrared wavelengths. Although confusion does not arise between burned areas and areas of permanent water in the current research as the latter are identified in the MODIS QA product (Section 5.2.4) and flagged prior to input into the change detection model, flood events will still be present and may cause burned area detection errors.

The effect of flooding is a sudden large decrease in MODIS band 2, 5 and 7 reflectance, with a more variable response at band 1 wavelengths. These drops in reflectance are identified as a negative step change ($M(\lambda)$ and $s(\lambda)$) and a large proportional decrease ($\delta\rho(\lambda)$) in the band 2, 5 and 7 modelled results, and thus constitute a perturbing factor in the spectral separation of burned

and unburned areas. Figure 5.17 illustrates values of $\delta\rho(band2)$ for an area of 150km x 100km extracted from the south of the study area and located to the north east of the Okavango Delta. The location of the site within the area of interest is displayed in Figure 5.16, and is documented in Table A.1 in Appendix A as Site 5E.

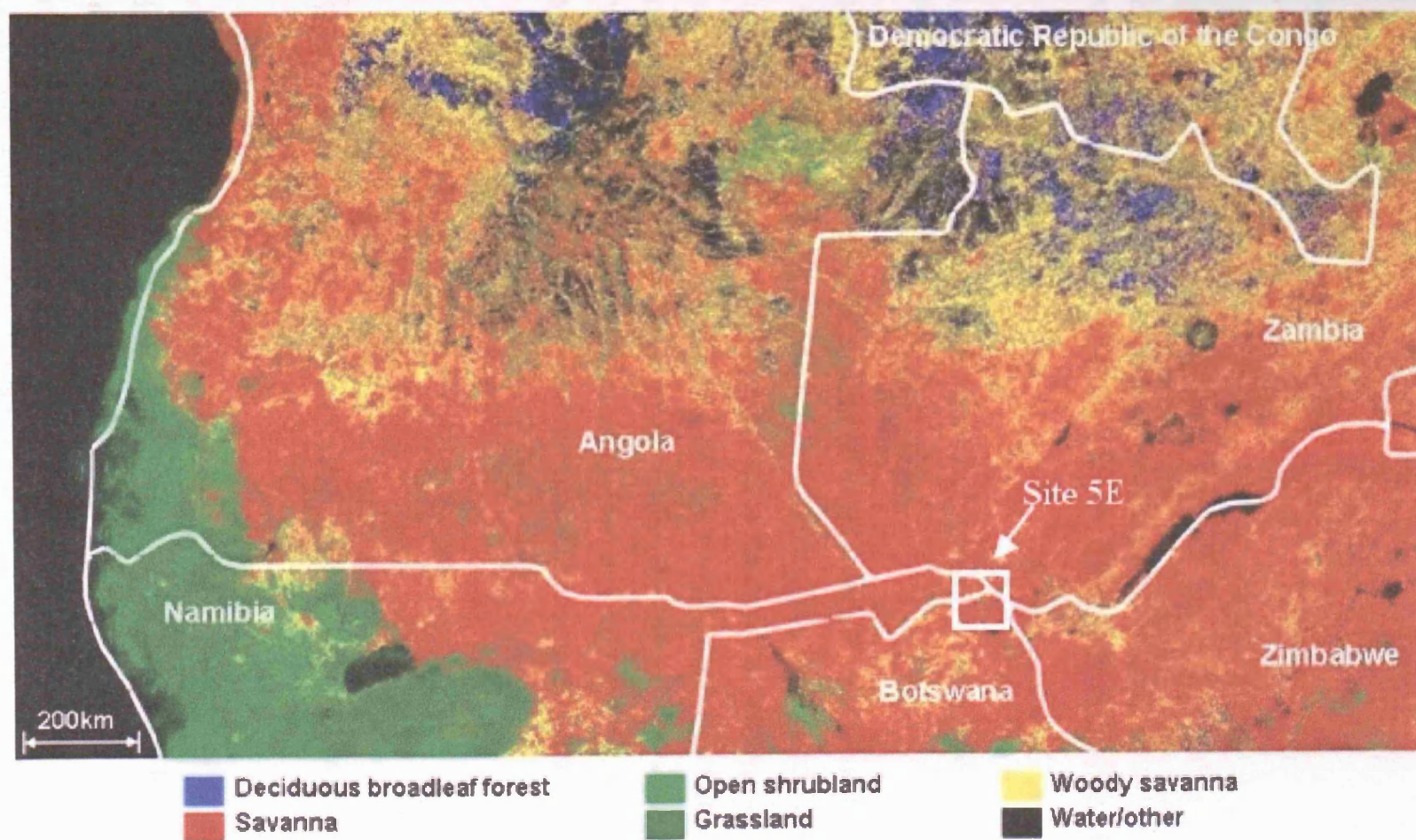


Figure 5.16: Site 5E and MODIS Landcover Product

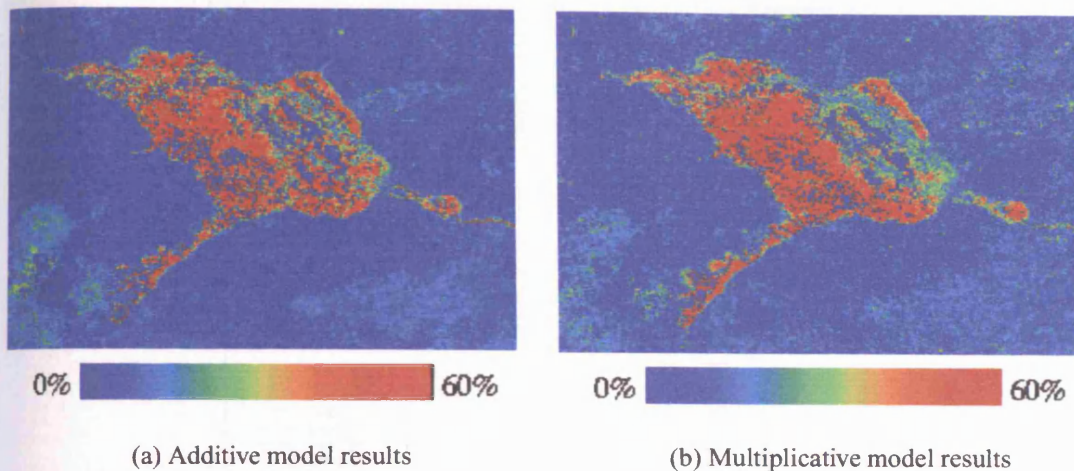


Figure 5.17: Proportional change in reflectance ($\delta\rho(\text{band2})$): Changes due to flooding, April 2003: Site 5E, Botswana

The locations which exhibit a high proportional decrease in reflectance (the red pixels) correspond to a non-permanent water body which floods in April during each of the five years of observation. The magnitude of the change ($M(\lambda)$) on the days surrounding the identified day of greatest change (day 99 - the 9th of April 2003) for a single pixel is displayed in Figure 5.18. The location corresponds to a red pixel extracted from the center of the water feature in Figure 5.17a. The proportional changes in reflectance ($\delta\rho\lambda$) at this pixel location are displayed in Table 5.9. Although band 7 reflectances typically exhibit either a small proportional decrease or an

	MODIS waveband			
	1	2	5	7
Additive	-0.69	-0.97	-0.88	-0.74
Multiplicative	-0.83	-0.90	-0.88	-0.93

Table 5.9: Proportional change in reflectance at a single pixel location due to flooding: 9th April 2003

increase of varying magnitude as a result of burning (see Section 3.6.1) this is not always the case and a large decrease in reflectance is sometimes observed at MODIS band 7 wavelengths as a result of burning.

Although pixels which exhibit comparably large decreases in band 7 reflectance tend to be located within the centre of a burn, fire induced decreases in MODIS band 7 reflectances are

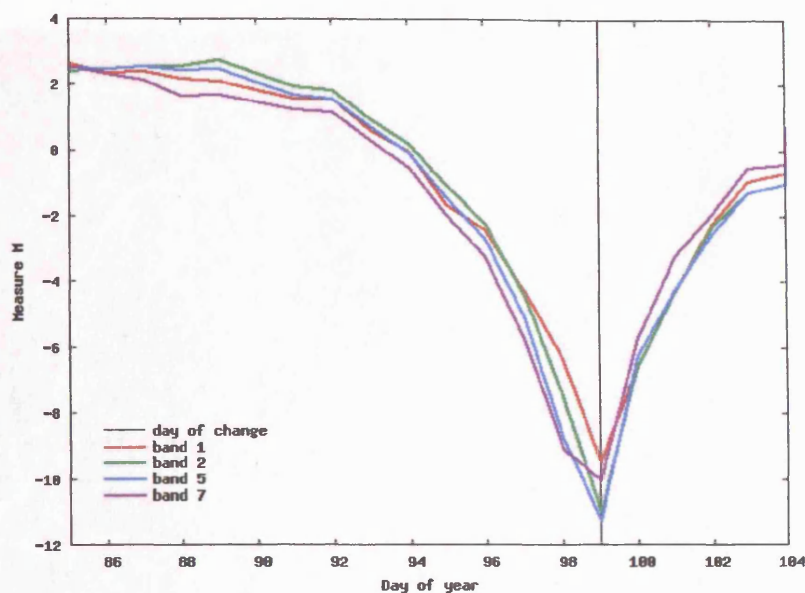


Figure 5.18: Magnitude of the change ($M(\text{band}2)$): Additive model results, site 5E, Botswana

occasionally identified over large homogenous areas of burning. An example of such a location is provided in Figure 5.20. This corresponds to an area of 25km by 50km in southern Angola which burned in July 2000, and is documented in Table A.1 and Figure A.1 in Appendix A as Site 5F. The geographical location of Site 5F is displayed in Figure 5.19.

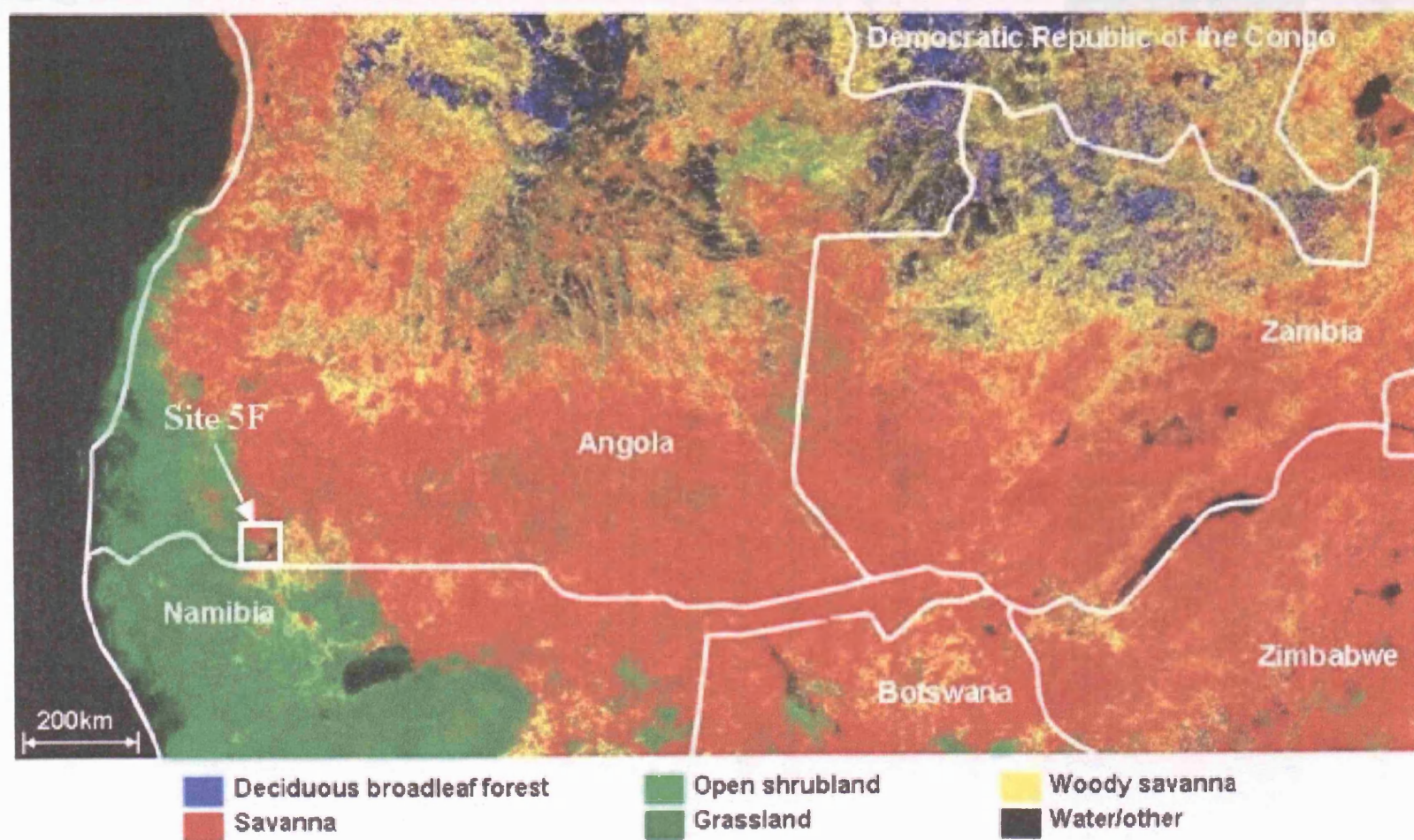


Figure 5.19: Site 5F and MODIS Landcover Product

Figure 5.20 displays the proportional change in MODIS band 2 and 7 reflectances across the area. Figure 5.21 displays the magnitude of the change ($M(\lambda)$) at a single pixel location extracted

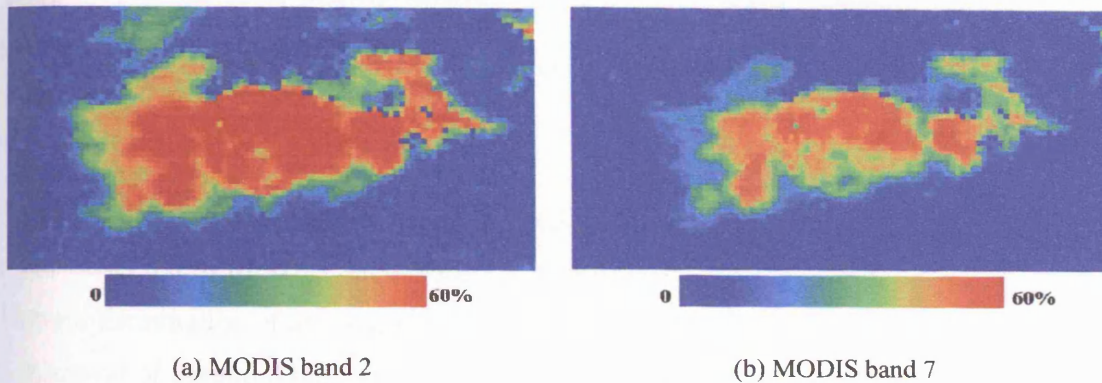


Figure 5.20: Proportional change in reflectance ($\delta\rho(\lambda)$) due to burning, July 2000: Multiplicative model results: Site 5F, southern Angola

from the centre of the burned in Figure 5.20. An active fire has been detected at this location on the day on which the burn has been identified - day 197 (the 15th July 2000). The proportional changes in reflectances ($\delta\rho(\lambda)$) which correspond to this pixel are contained in Table 5.10.

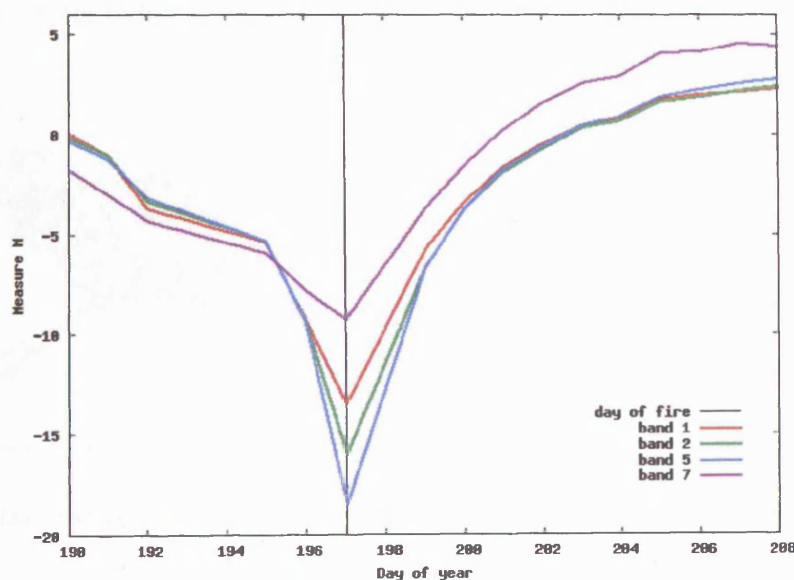


Figure 5.21: Magnitude of the change ($M(\text{band}2)$): Additive model results, Site 6F (southern Angola)

	MODIS waveband			
	1	2	5	7
Additive	-0.69	-0.66	-0.58	-0.37
Multiplicative	-0.69	-0.67	-0.64	-0.43

Table 5.10: Proportional change in reflectance at a single pixel location due to burning: 15th July 2000

It is evident from Figure 5.20 that a decrease in band 7 reflectance of a comparable magnitude to that observed in MODIS band 2 has occurred over a large number of pixels within this burn location. Elimination of areas of flooding based on the response of band 7 may thus also result in the removal of potential burn candidates. In order to reduce the possibility of excluding burned areas due to their spectral similarity with flood events, a flood mask is created from the daily data for each month of the annual fire season. Areas of flood candidates are identified using a threshold of $\delta\rho(\lambda) = -0.3$. Any pixels which exhibit a proportional decrease in reflectance equivalent to 30% or greater ($\delta\rho \leq -0.3$) at band 2 *and* band 5 *and* band 7 wavelengths are flagged as potential flood pixels. The black areas in Figure 5.22 (which correspond to the location displayed in Figure 5.17) are pixels which meet this criteria and are therefore flagged as areas of high probability water induced surface change.

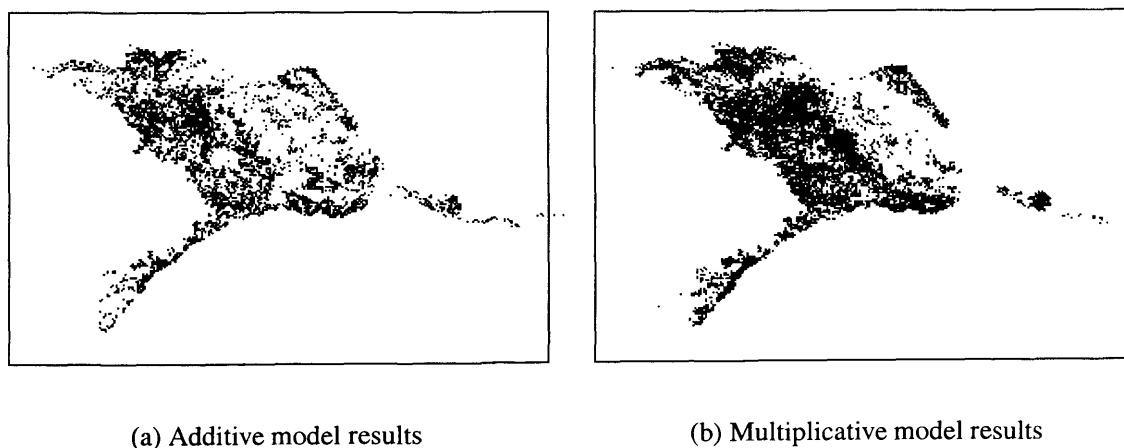


Figure 5.22: Changes due to flooding (black pixels), Site 5E (northern Botswana) April 2003

Water boundary pixels

In addition to flood induced surface change confusion occasionally arises between pixels situated along the boundaries of water bodies. These are located and removed through the application of a conservative water test according to the method of Roy *et al.* (2005b). Following this approach any pixels with a MODIS band 7 reflectance of less than 0.04 *and* an NDVI value of less than 0.1 are removed. The NDVI test is used in conjunction to the band 7 reflectance as dense green vegetation may also exhibit a low band 7 reflectance (see Figure 3.11 Section 3.5.2) but in contrast to water will have a high NDVI value. Under the current modelling framework these criteria are implemented as;

$$\rho_{(band7)}(\Omega, \Omega') < 0.04 \quad (5.11)$$

AND

$$\left(\frac{\rho_{(band2)}(\Omega, \Omega') - \rho_{(band1)}(\Omega, \Omega')}{\rho_{(band2)}(\Omega, \Omega') + \rho_{(band1)}(\Omega, \Omega')} \right) < 0.1 \quad (5.12)$$

where $\rho(\lambda, \Omega, \Omega')$ is calculated according to Equation 5.4 for the multiplicative model and Equation 5.6 for the additive model for $t = (c - 1)$ i.e. the day before the identified day of change. In addition in order to exploit all of the data available the criteria defined in Equation 5.12 is also applied using band 5. The behaviour of band 2 and band 5 is extremely similar for water, and thus the use of both bands increases the chances of identifying and removing water related change in the presence of bad or missing data or unmodelled noise in either band. Figure 5.23 contains an example of a water boundary pixels which would be identified as a burn candidate in April 2003 but is removed according to the criteria defined above. The pixel corresponds to Site 5G (Table A.1 and Figure A.1 in Appendix A) and is located on the land/water interface of a non-permanent water feature. The proportional changes in reflectance which correspond to the temporal sequence contained in Figure 5.23 for the day of the change (day 116 - the 26th April 2003) are -0.14, -0.46, -0.68 and 0.02 in bands 1, 2, 5 and 7 respectively. If not removed this pixel would therefore have been identified as a burn candidate in April 2003.

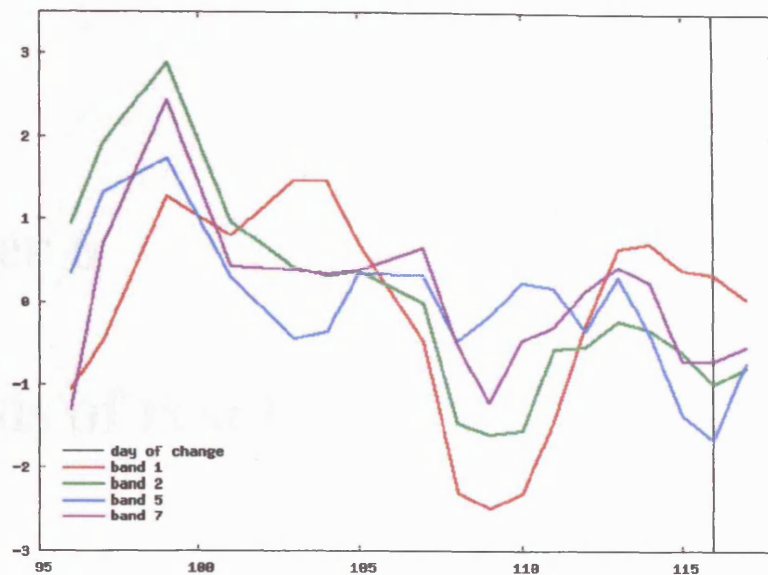


Figure 5.23: Magnitude of the change ($M(band2)$): Site 5G, central Angola

5.6 Summary

This chapter has described the data sources which have been used as inputs to the two temporal change detection models developed in the previous chapter. The production of monthly datasets documenting daily changes at a spatial resolution of 500m for the five year period and over the 2400 by 1200km area of interest requires an extremely large quantity of input data. The methods which have been used to manipulate, preprocess and process this data have been described.

The two models introduced in the previous chapter represent a generic approach to the detection of sudden changes within a temporal sequence of reflectance data. The second half of this chapter has therefore been concerned with the adaptation of these to the specific problem of identifying pixels which been affected by fire. In addition as spectral changes of a similar nature to those exhibited by burned surfaces occur due to other causes other than burning the separation of these from the changes of interest has been discussed. The various post-processing steps implemented to deal with these confusing spectral changes have been described.

The monthly burned area datasets produced following the methods described in this and the previous chapter are presented in the following two chapters.

Chapter 6

Analysis of results

The implementation of the change detection models and their application to the detection of fire affected areas has been described in the previous chapter. The lack of ground based burned area information over the area of interest at the time of writing has meant that validation of the burned areas has been limited to a comparison with two other independently produced burned area datasets as well as with the active fire information documented in the MODIS Thermal Anomalies product. The similarities and differences between these products are presented in this chapter.

6.1 MODIS 500m fire affected areas

Daily burned area information for the eight months of five annual fire seasons have been processed according to the steps described in Chapter 5. The outputs of the post processing steps are two fields of information for each 500m pixel location. The first is the proportional change in reflectance $\delta\rho(band2)$, and the second is the day of change. For illustrative purposes burned area results for August 2004 are displayed in Figure 6.2 for an area of approximately 225 by 125km located near the Angola/Namibia border (see Figure 6.1). This area is documented as Site 6A in Table A.1 and Figure A.1 in Appendix A. Figure 6.2a displays the $\delta\rho(band2)$ values at burn locations and Figure 6.2b displays the day of the change with day 214 corresponding to the 1st of August and day 244 the 31st of August 2004. The progression of burning on a day to day basis is evident in Figure 6.2b.

A higher resolution image is displayed in Figure 6.3 along with the 500m burned area results for visual purposes. In contrast to the data displayed in Figure 6.2, Figure 6.3 displays an area of approximately 26km by 30km located along the Zambia/Namibia border (Site 6B, Figure 6.1) which had burned by the 28th August 2001. A high resolution (30m) real colour composite (bands 3, 2, 1) Landsat ETM+ image of the area which was acquired on the 28th of August 2001 is displayed in Figure 6.3a, while Figure 6.3b contains the MODIS 500m burned area results for the same location. A large area of burning which stretches from southern Zambia into northern Namibia is evident in both images.

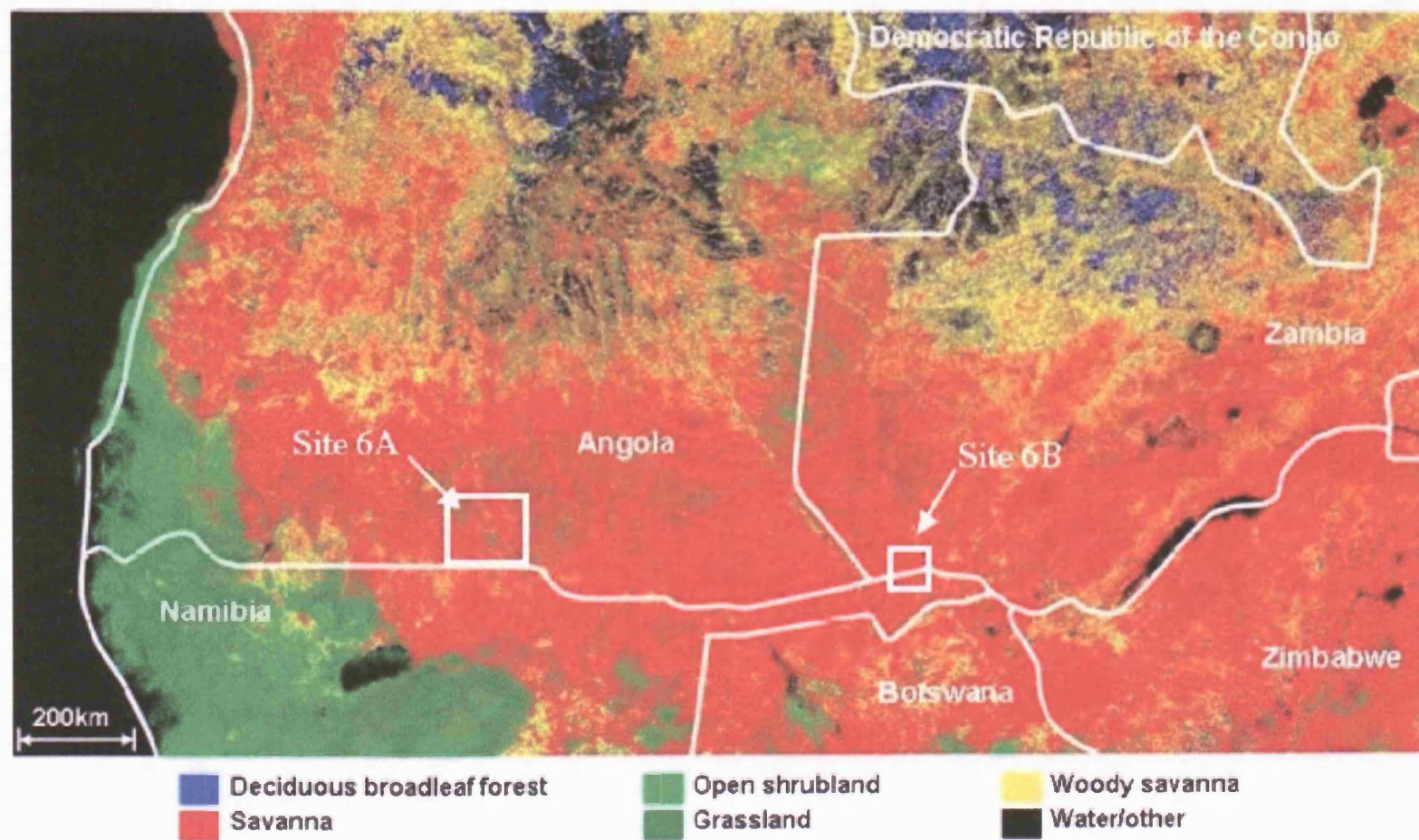


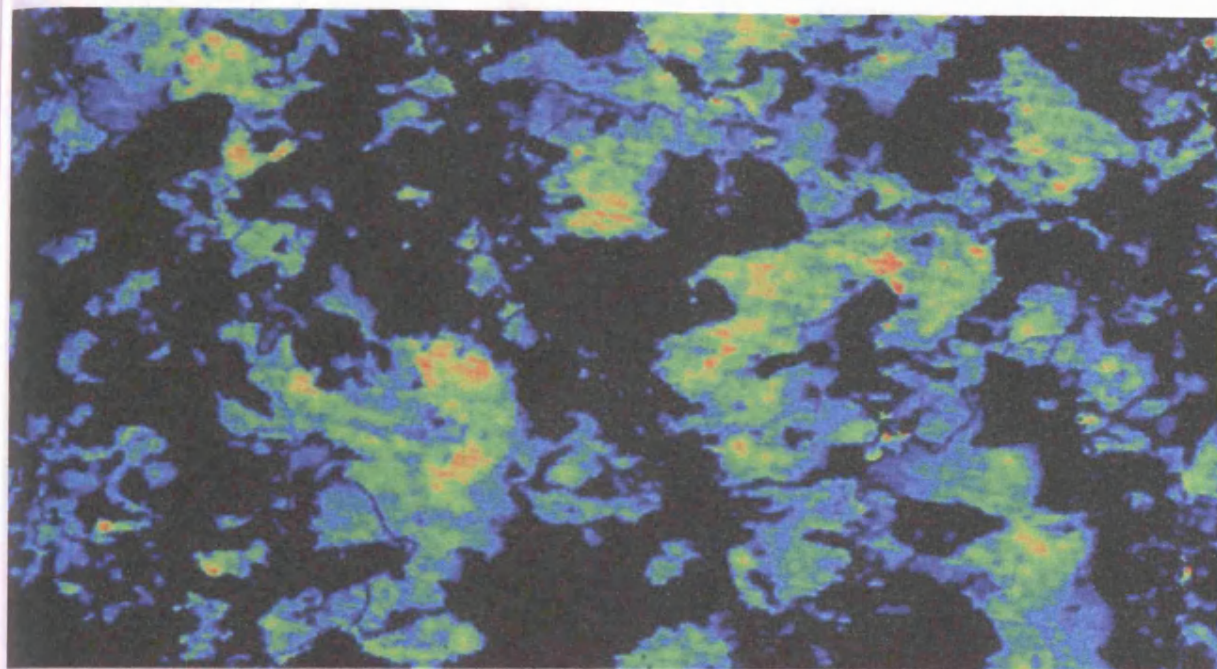
Figure 6.1: Sites 6A, 6B and MODIS Landcover Product

An analysis of the spatial and temporal distribution of burning over the five year period of observation as well as an interpretation of the fire regimes over this period are provided in Chapter 7. The aim of the following sections is to compare the results to other sources of burned area and active fire information available for the area of interest and over the time period of the current study. Three sources of fire related information which document the occurrence of active fires and burned areas across different temporal and spatial scales will be used for this purpose;

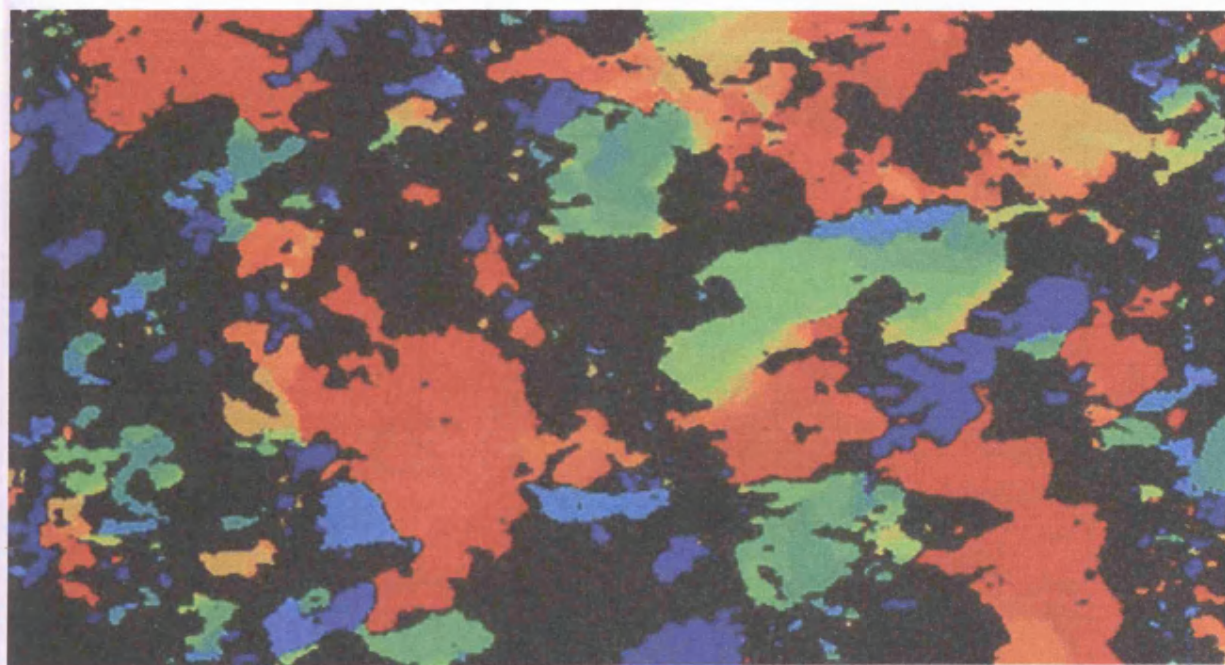
1. Daily MODIS Thermal Anomalies, April 2000 to November 2004 (Giglio *et al.* 2003a)
2. Monthly SAFARI 2000 MODIS 500m burned areas, July 2000 (Roy 2005)
3. Monthly GBA2000 1km burned areas, April - November 2000 (Gregoire *et al.* 2003)

6.2 MODIS 1km Thermal Anomalies

A description of the MODIS Thermal Anomalies product is provided in Section 2.4.1. This section investigates the spatial and temporal agreement between MODIS active fire detections and the burned area results. The data used in the analysis are the daily 1km day and night active fire detections from MODIS Terra and Aqua (for the 2003 and 2004 fire seasons). The percentage of the active fire detections which are identified as burned each month over the five year period are shown in Table 6.1. These have been calculated following the procedure described in Figure 5.11. In addition a seven day overlap is used at the beginning and end of each month in order to allow for differences in the detections of active fires and burning due to missing data or cloud. Possible reasons for the low agreement between the locations of active fire detections and burned pixels have been discussed in Section 5.5.2. In particular the discrepancies are likely to be a function of the different spatial resolutions of the data. In addition the increase in cloud cover towards the end of the fire season each year results in a lower number of observations of the surface during these months. These will result in a greater likelihood of underdetection of burned areas due to an insufficient number of cloud free observations. It should also be noted that the number of fires detected at the tail months of the fire season constitute an extremely small proportion of the total fires detected over the entire season. In April 2004, for example, only 1932 1km fire pixels were detected over the area of interest by both MODIS Terra and Aqua. These correspond to

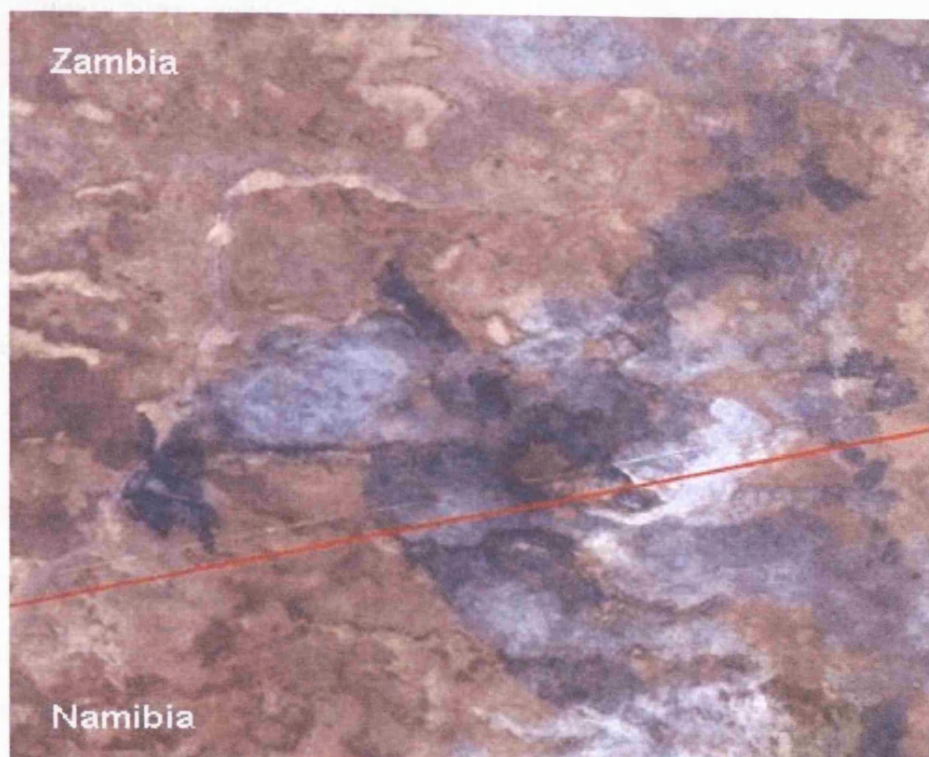


(a) Proportional change in band 5 reflectance: Site 6A, Angola/Namibia

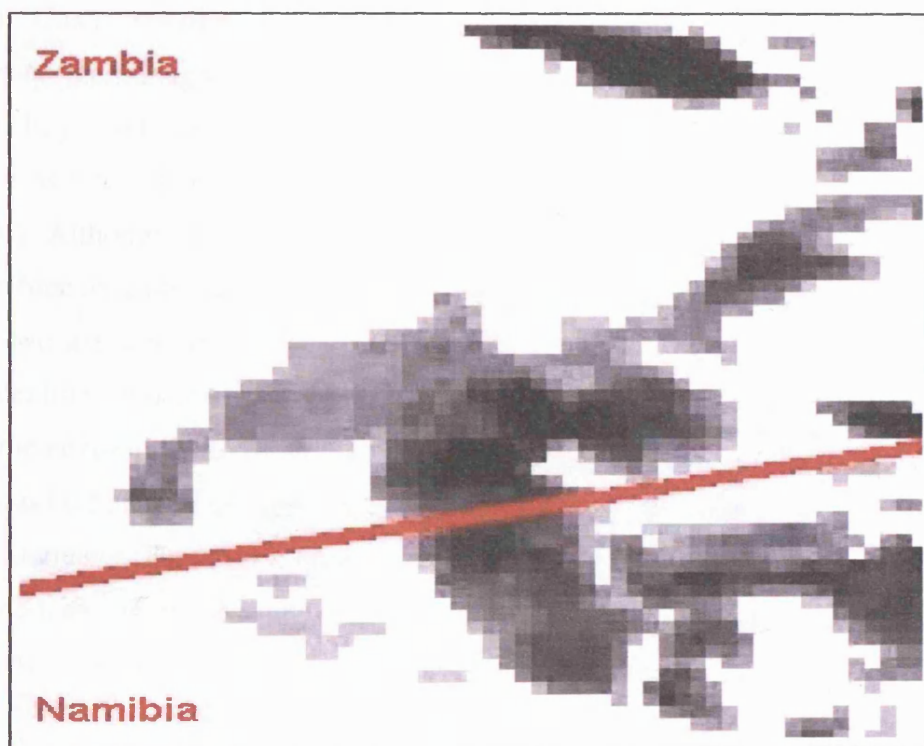


(b) Day of change: Site 6A, Angola/Namibia

Figure 6.2: Burned area information, August 2004: Multiplicative model results



(a) Landsat ETM+ real colour composite image (bands 3, 2, 1) 28th August 2001, Site 6B, Zambia/Namibia



(b) MODIS burned area results, August 2001, Site 6B, Zambia/Namibia

Figure 6.3: An area of burning, August 2001

	2000	2001	2002	2003	2004
Apr	35.5	51.5	64.8	44.5	14.3
May	55.6	42.5	61.8	47.9	50.8
Jun	60.7	N/A	58.8	48.9	52.6
Jul	64.0	62.2	60.6	51.9	51.8
Aug	58.0	58.8	56.4	51.7	51.6
Sep	59.2	59.4	55.2	50.7	52.8
Oct	58.0	57.9	50.5	48.0	46.8
Nov	39.4	27.8	35.7	25.8	31.2

(a) Additive temporal model

	2000	2001	2002	2003	2004
Apr	30.6	36.0	66.2	43.2	12.8
May	54.5	48.6	62.0	46.6	48.4
Jun	60.7	N/A	59.6	50.2	53.4
Jul	65.4	61.9	62.3	52.7	52.1
Aug	59.0	58.5	56.7	52.9	53.4
Sep	59.1	59.6	56.5	51.0	54.4
Oct	58.4	58.0	54.3	49.6	49.0
Nov	35.6	25.0	19.5	26.7	32.3

(b) Multiplicative temporal model

Table 6.1: Percentage of MODIS (Aqua and Terra) 1km active fire locations identified as burned

less than 1% of the total number of active fire pixels detected over the 8 months. The size of individual burn events is also much smaller during the tail months of the fire season, resulting in a greater disparity between the 1km active fire detections and the 500m burn pixels during this time. The smaller fire size in conjunction with the differing spatial resolutions of the datasets and the minimum requirements for the detection of an active fire are likely to contribute to the larger number of active fire locations which are not identified as burns during the start and end of the fire season. This is demonstrated through two small burn events displayed in Figure 6.5 which occurred in northern Angola in April 2003, and a third larger burn which occurred in northern Namibia in July 2003. The locations of these are documented in Table A.1 and Figure A.1 in Appendix A as Sites 6C-E. Their geographical position within the area of interest is displayed in Figure 6.4. Although both the active fire and the occurrence of burning has been identified at each of the three locations, there is clearly some spatial disagreement between the two datasets. At the first two sites (Figures 6.5a and 6.5b) where a smaller area has burned a large number of pixels are identified as active fires but not as burned areas (the red pixels). In both cases these are located on the edges of areas which have been identified as burns. At the third location a much larger area has burned, and the agreement between the locations of the active fire detections and burn pixels is greater. However a number of active fire pixels have not been identified as burns (the red pixels), and again these are generally contiguous to burn pixels. The disagreement at all three locations is likely to be a factor of the different spatial resolutions of the data as well as the

minimum requirements for the detection of an active fire. A flaming fire needs only be 100m² in size in order to have a 50% or greater chance of detection by the MODIS Thermal Anomalies algorithm. This is equivalent to approximately one 50th of the surface area of a 500m pixel. Following the procedure described in Section 5.5.1 a pixel is only identified as a burn candidate if a decrease in reflectance of at least 15% occurs at band 2 and band 5 wavelengths. The change in reflectance due to burning at MODIS band 5 wavelengths has been shown to be a function of both the combustion completeness of the fire and the fraction of a pixel which burns (Roy and Landmann 2005). As the heterogeneity of the fire effects will be greater at the perimeter of the fire both of these factors will contribute to a smaller proportion of the 500m surface area of an individual pixel. The change signal identified at such locations may therefore be insufficient for the pixel to be labelled as a burn.

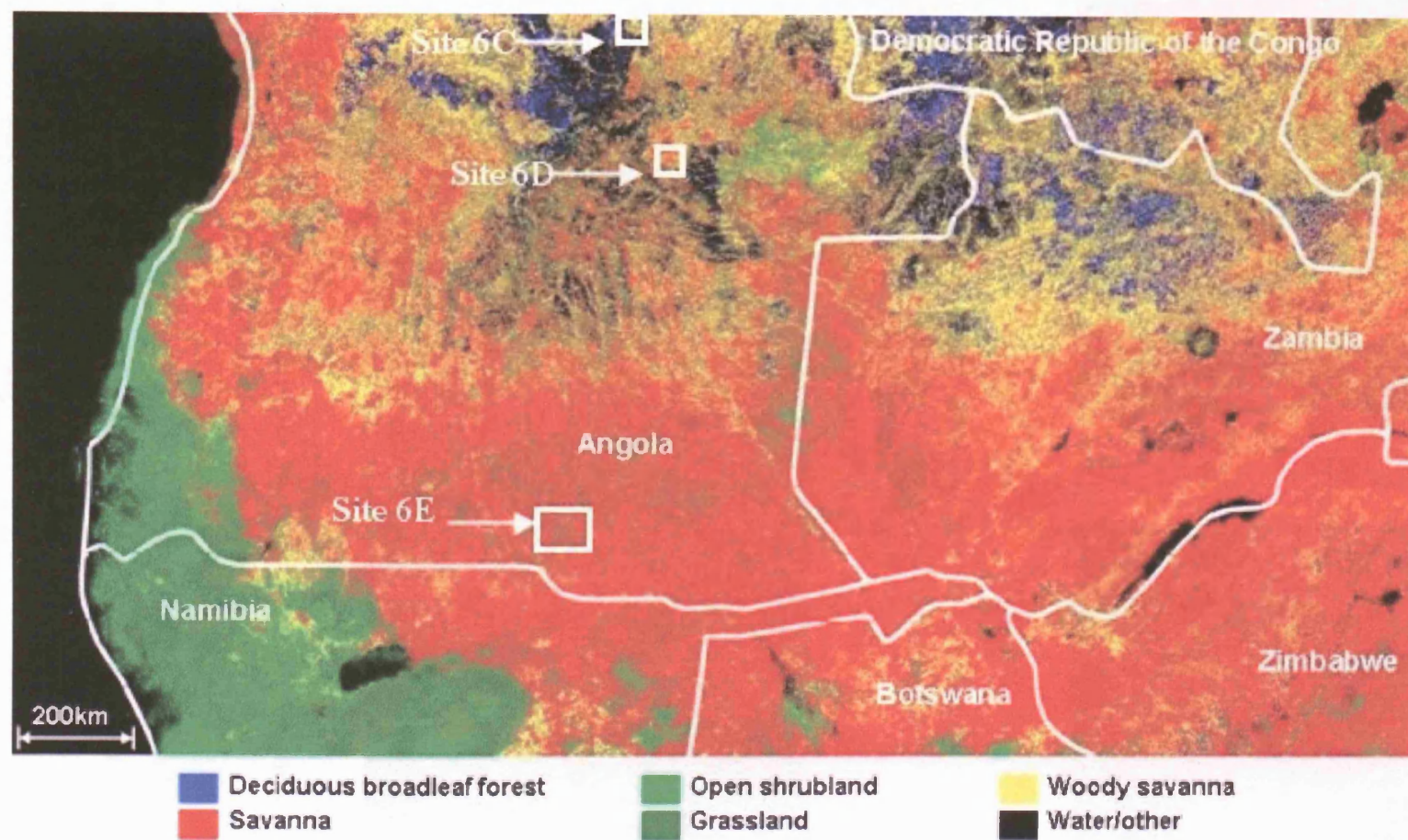


Figure 6.4: Sites 6C, 6D, 6E and MODIS Landcover Product

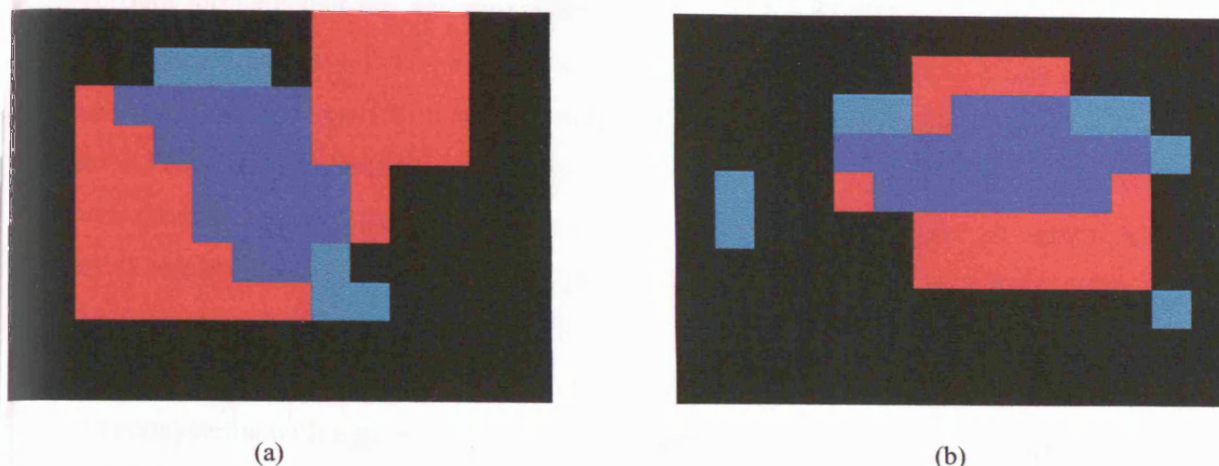


Figure 6.5: Discrepancies between 1km active fire detections and 500m burned areas (additive model results), April 2003: black pixels = no burn or fire, red pixels = fire only, green = burn only, dark blue = fire and burn (Sites 6C and 6D, Angola)

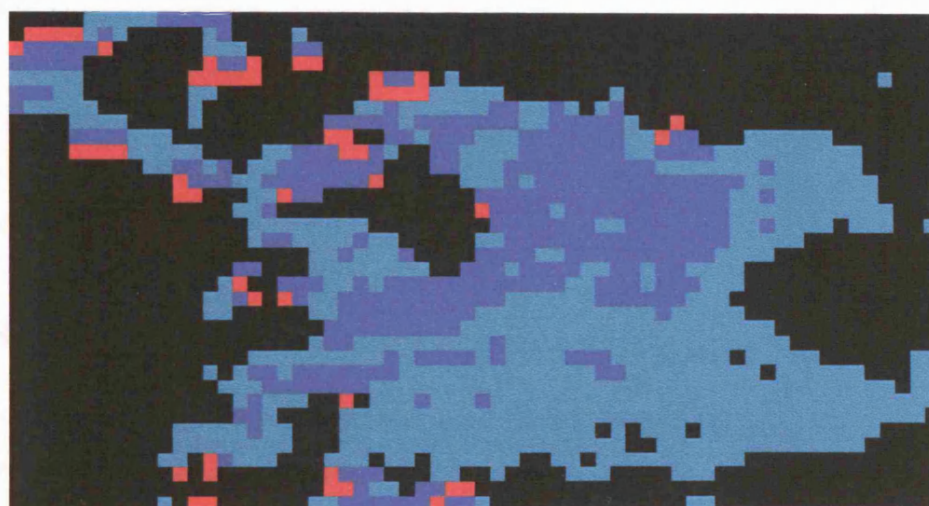


Figure 6.6: Discrepancies between 1km active fire detections and 500m burned areas (additive model results), July 2003: black pixels = no burn or fire, red pixels = fire only, green = burn only, dark blue = fire and burn (Site 6E, Angola)

The agreement between the location of active fires and burned areas has been investigated within each cover type in order to determine whether there is a consistent discrepancy between the two within a particular ecosystem. The percentage agreement has been calculated over the eight months of each annual fire season. The data are displayed in Table 6.2 as annual totals.

These data indicate that the agreement between the active fire detections and burned areas is lowest in deciduous broadleaf forests, and highest in grasslands. This is likely to be due to the characteristics of the vegetation and the nature of the fires which occur within these vegetation types. As described in Section 3.2 the majority of fires within southern African ecosystems are surface fires which burn through the herbaceous layer with little effect on established woody plants (Frost and Robertson 1985). The probability of detection of such fires will be lower in forested areas as the burned surface will be obscured by unburned canopy components. The spatial extent of individual fires may also be smaller and the burned surface more heterogenous within ecosystems with a greater woody plant density due to the greater heterogeneity of the fuel load. While the fuel load in grasslands is relatively homogenous, in woodlands the woody and grass fuel components coexist with more restricted grass production in the more closed canopy woodlands (Scholes *et al.* 2002). Research by Van der Werf *et al.* (2003) has identified a decrease in MODIS 500m burned areas per TRMM active fire count with increasing percent tree cover over the African continent, which the authors suggest may be due to differences in the rate of fire spread or differing detection capabilities within the different vegetation types. As illustrated in Figure 6.5 smaller burn events may result in greater overestimation of the active fire product (or underestimation of the area burned) and consequently a lower agreement between the active fire and burned area information.

6.2.1 Scaling between active fire counts and the area burned

A review of active fire detection methodologies, products and limitations is provided in Section 2.3. Although these data provide a useful information source detailing the location and occurrence of fires, they do not provide spatially explicit information relating to the occurrence of burning. Active fire counts are not a good indicator of the area burned as the fires may not coincide with the timing of the satellite overpass, or their detection may be precluded due to the presence of cloud. These data are therefore not the appropriate product with which to make quantitative statements relating to biomass burning emissions (Hoelzemann *et al.* 2004). Despite the errors of omission which will inevitably be present in active fire counts, these have nevertheless been used as a surrogate for the area burned. Scaling factors have typically been calculated through a comparison with the limited burned area information available and applied to regional or global

Additive model results					
	2000	2001	2002	2003	2004
Deciduous broadleaf forest	48.3	47.9	44.7	39.2	38.8
Open shrubland	56.7	58.9	56.1	49.8	50.6
Woody savanna	59.1	56.4	56.4	50.5	50.6
Savanna	60.5	60.1	60.1	53.4	54.7
Grassland	62.4	61.9	65.1	57.6	59.6

Multiplicative model results					
	2000	2001	2002	2003	2004
Deciduous broadleaf forest	49.8	49.0	47.2	41.6	41.7
Open shrubland	54.5	54.8	56.5	49.4	50.6
Woody savanna	59.6	56.7	57.4	51.4	51.8
Savanna	60.9	60.1	60.9	54.0	55.5
Grassland	60.4	56.5	65.7	57.6	59.5

Table 6.2: Percentage of MODIS (Terra and/or Aqua) 1km active fire locations identified as burned in each cover type

active fire counts in order to produce estimates of the total area burned. The relationship between TRMM active fire counts and burned areas has been derived using estimates of burned areas from MODIS data and ground based information for areas of Africa, Australia and Canada in order to quantify carbon emissions (Van der Werf *et al.* 2003). The relationship between the area burned and the fire counts was assumed to be a linear function of tree cover but was only found to hold in regions with a tree cover of less than 40%. Possible reasons for this have been discussed in the previous section, and include the characteristics of the fires which occur in forested areas as well as detection capabilities of both the fire counts and the area burned within these ecosystems. ATSR active fire counts have been used to estimate the relative pattern of biomass burning within the boreal forest of north America and Russia using burned area estimates produced from SPOT-VGT data and ground based regional fire statistics (Kasischke *et al.* 2003). However no significant correlation was found between the active fire counts and the area burned in the north American study area, although a linear relationship was found to exist over the Russian and Canadian study areas. Variations in the overpass time of the ATSR satellite are suggested as a possible explanation for this discrepancy, leading the authors to conclude that scaling between fire counts and burned areas is not a simple linear transformation as the

ATSR fire counts to do not represent an unbiased sample of fire activity. Biases which may be introduced if active fire counts are extrapolated to the area burned without detailed knowledge of the interannual as well as intraannual variabilities in the relationship between the two are described in Section 3.4.2.

The relationship between MODIS 1km active fire counts and 500m burned areas

No data exist quantifying the relationship between MODIS (Terra and/or Aqua) active fire detections and the area burned within different ecosystems or at different times of year. The representivity of the active fire counts as an indicator of the total area or the seasonal variations in the spatial extent of burning with southern Africa is unknown. The aim of the following paragraphs is to investigate the relationship between the daily MODIS 1km day and night active fire detections and the daily 500m burned areas for the eight months of each annual fire season over the five year period.

The percentage of the total area burned which has been detected as an active fire each month is displayed in Table 6.3 for the multiplicative model results. As the results are extremely similar, those produced by the additive model are documented in Appendix B. For the years which MODIS Aqua fire detections are available in addition to MODIS Terra for the entire annual fire season (2003 and 2004) the agreement between the burned area totals and the active fire counts for each satellite are shown, as well as for the total detections. As no MODIS data is available between the 14th of June and the 3rd of July 2001 burned areas have not been processed for the month of June this year. It is immediately apparent from these data that the relationship between the number of active fires detected (by MODIS Terra and/or Aqua) and the area burned varies from year to year, and is not linear across the annual fire season. The percentage of the total area burned detected as an active fire by MODIS Terra is lowest at the start and end (April and November) of the fire season during each of the five years of observations. A greater proportion of the total area burned is detected during the peak of the fire season, but this varies annually between the months of July and September. During these months the greatest percentage of burned areas detected as active fires by MODIS Terra is typically between 13-14%. The incorporation of MODIS Aqua data has a large impact on the relationship between the active fire counts and area burned, but again this is not uniform across the annual fire season with a much lower burned

area per fire count observed at the beginning and end of each fire season. In addition differences between the number of fires detected by MODIS Aqua during the afternoon overpass and the number of fires detected by MODIS Terra during the morning overpass is greater at the peak of the fire season than at the tails. This further complicates the relationship between the active fire counts and the area burned. The possible reasons for and implications of this observation have been discussed in Section 3.4.2 and include variations in meteorological conditions which will influence the fire rate of spread and the likelihood of ignition, the sources of ignition and the condition of the vegetation over the course of the fire season. All of these factors will contribute to the observed seasonal variability in the diurnal nature of the fire activity within the area of interest.

	2000 Terra	2001 Terra	2002 Terra	2003 Terra	Aqua	both	2004 Terra	Aqua	both
Apr	0.3	0.15	2.8	3.9	8.5	10.7	0.1	0.4	0.5
May	7.4	6.0	10.8	7.9	24.6	29.7	5.4	21.9	25.0
Jun	9.7	N/A	10.1	8.8	29.9	35.2	9.7	36.6	42.1
Jul	7.8	11.2	12.0	10.6	36.6	43.0	10.2	37.6	43.6
Aug	8.9	13.6	13.5	13.5	32.6	41.4	9.9	26.8	33.5
Sep	13.6	14.0	11.1	13.1	22.8	31.4	8.9	13.1	19.7
Oct	10.0	10.2	7.6	8.6	13.0	19.0	8.9	11.1	18.1
Nov	2.6	0.4	1.4	0.7	0.6	1.2	1.5	1.5	2.8
Total	9.3	11.1	10.5	10.6	26.6	33.4	8.9	23.7	29.6

Table 6.3: Percentage of 500m burned areas detected as active fires: Multiplicative model results

The relationship between the active fire counts and burned areas for each annual fire season has also been investigated as a function of vegetation type. These data are displayed as annual totals in Table 6.4 for the multiplicative model results. The monthly totals calculated for each vegetation type for both of the model results (additive and multiplicative) are contained in Table C.2, Appendix C. The data displayed in Table 6.4 indicate that the variations between the total area burned and the number of active fires detected within each cover type exhibit similar annual variations as the data displayed in Table 6.3. As discussed above the relationship between the two data sources is not uniform and varies annually as well as seasonally during each annual fire season. The inclusion of MODIS Aqua fire counts has a large impact on the percentage

	2000 Terra	2001 Terra	2002 Terra	2003 Terra	Aqua	Both	2004 Terra	Aqua	Both
Deciduous broadleaf	7.5	9.7	8.7	8.0	29.7	34.4	7.3	27.2	31.6
Open shrubland	8.5	9.2	8.9	8.7	21.3	27.1	8.2	19.3	25.1
Woody savanna	9.2	11.1	10.1	10.3	28.3	34.6	8.9	26.3	31.9
Savannas	9.9	11.9	11.2	11.6	26.0	33.6	9.4	22.2	28.7
Grasslands	9.0	10.1	11.1	10.3	22.4	29.4	9.0	20.4	26.9

Table 6.4: Percentage of 500m burned areas detected annually as active fires in each vegetation type: Multiplicative model results

of the total area burned identified as an active fire across all vegetation types. The agreement between the area burned and the active fire counts from MODIS Terra and Aqua within deciduous broadleaf forests is an interesting feature of these data. For each year the percentage of the total area burned detected as an active fire by MODIS Terra is lowest for areas of deciduous forests. However the opposite is true for the Aqua detections, with this cover type exhibiting the highest agreement between the area burned and the number of fire counts in comparison to all other vegetation types in both 2003 and 2004. The implications of this observation are that a higher proportion of fires within deciduous broadleaf forests occur during the afternoon in comparison to the other vegetation types. This results in a greater probability of detection by the afternoon (MODIS Aqua) satellite overpass.

In addition the higher agreement between the area burned and the total active fire counts (both Aqua and Terra) in deciduous broadleaf forest in comparison to grasslands, for example, suggests that the fires which occur within the former are of a smaller size than those which occur in the latter. The smaller the area which burns between each satellite overpass the higher the number of fire counts per area burned. As described above the burned area per fire count has been found to decrease with increasing tree cover over Africa by Van der Werf *et al.* (2003). It is suggested that this may be due to differences in the fire rate of spread with grassland fires spreading quickly and burning for a shorter period which results in a lower detection probability of the active fire and thus a higher burned area per fire count. In addition burning within deciduous forests may be obscured by the canopy, resulting in a lower burned area detection probability and an underestimation of the total area burned, which will contribute to a higher active fire count per area burned.

Although previous studies have identified significant correlations between fire counts and the area burned (Pereira and Setzer 1996, Scholes *et al.* 1996a) the authors have noted that these relationships may be limited by the characteristics of the particular fire events examined. The data presented in the previous paragraphs emphasises the variable nature of the relationship between the total area burned and the MODIS active fire counts. The relationship between these two quantities varies both spatially and temporally. The accurate scaling between active fires and burned areas and the extrapolation from active fire detections to the area burned therefore requires sensor, vegetation and season specific calibration factors.

6.3 SAFARI 2000 MODIS 500m burned areas

The aim of this section is to compare the burned area results with those produced under the SAFARI 2000 Dry Season campaign. The SAFARI 2000 project constitutes the first regional test for the prototype southern Africa 500m MODIS burned area product. These data have been created following the approach of Roy *et al.* (2002) which locates the 500m location and approximate day of burning using a change detection algorithm based on a bi-directional reflectance model-based expectation method, applied to MODIS band 5. This change detection algorithm is described in Section 4.3. The validation of the SAFARI 2000 burned area datasets is currently underway, although details are not yet available. The validation protocol involves the derivation of maps of the location and approximate day of burning through interpretations by members of the Southern Africa Fire Network (SAFNet) of multitemporal Landsat Enhanced Thematic Mapper data. A detailed description of the validation methods used can be found in Roy *et al.* (2005a).

The SAFARI 2000 burned area data is available in the Lambert Azimuthal Equal Area projection at a pixel size of 500m for the months of July and September 2000. Following the characteristics of the input data the monthly burned area information produced according to the methods described in the previous chapters is stored in a sinusoidal projection with a pixel size of 463.31m. In order to compare the results the burned area datasets have been reprojected from the MODIS Sinusoidal projection to the Lambert Azimuthal Equal Area projection with an output pixel size of 500m, for the area of overlap. To avoid confusion the Safari 2000 burned areas

will be referred to as the “SK2”, and the current results as the “Southern Africa Burned Area” (SABA) dataset. Due to the unavailability of MODIS data between the 5th and the 19th of August 2000 a buffer size of only 13 days has been used in the creation of the September 2000 SABA data (see Section 5.5). Due to this smaller sample size the burned area data for this month may be unreliable and are unrepresentative of the dataset as a whole. The subsequent comparison will therefore only be performed on the July 2000 burned areas.

6.3.1 Errors of omission

The SK2 dataset documents pixels which have burned between the 26th June and the 4th of August 2000. In order to allow for discrepancies between the two datasets due to the identified day of burning a four day buffer is applied at the beginning and end of the time series. SABA pixels which have been identified as burning between the 26th of June and the 4th of August are compared to SK2 pixels which have burned between the 30th of June and the 1st of August 2000. The number of 500m pixels identified as burned in both the SK2 and the SABA dataset and the percentage of the total SK2 burned area which this is equivalent to is documented in Table 6.5. These data indicate that approximately 70% of the SK2 burned areas are also documented as burned in the SABA dataset, while approximately 30% of the SK2 burned areas have not been identified as burned in the SABA dataset. Table 6.6 defines the criteria which have not been met

Additive model results		Multiplicative model results	
Pixel count	Percentage	Pixel count	Percentage
387446	67.7	406083	70.8

Table 6.5: Number of pixels and percentage of SK2 burned areas also identified as burned by SABA

during the production of the SABA dataset at pixel locations documented as burned in the SK2 but not is the SABA dataset. The first criteria (Table 6.6) indicates that approximately 5% of the pixels identified as burned by SK2 but have *not* been identified as burned in the SABA dataset have not been processed due to an insufficient number of good quality cloud free samples during the 91 days used in the production of the SABA data. Criteria two indicates the percentage of the errors or omission in the SABA dataset which are due to an insufficient burn signal identified in

band 2. According to the change detection approach defined in Section 5.5.2, a pixel is identified as a potential burn candidate if a proportional decrease in reflectance ($\delta\rho$) of at least 15% ($\delta\rho \leq -0.15$) occurs at band 2 *and* band 5 wavelengths. Criteria 3 indicates the percentage of the errors of omission in the SABA dataset which are due to a proportional decrease in band 2 of an insufficient magnitude (i.e. less than 15%) for the pixel to be labelled as a burn. Finally criteria 4 indicates the percentage of the errors of omission which are due to an insufficient burn signal identified in band 2 *and* band 5.

Criteria ($\delta\rho(\lambda)$)		Additive model	Multiplicative model
1	not processed	7.7	7.2
2	b2 ≤ -0.15 <i>and</i> b5 > -0.15	13.7	16.7
3	b2 > -0.15 <i>and</i> b5 ≤ -0.15	5.0	4.5
3	b2 > -0.15 <i>and</i> b5 > -0.15	72.3	63.9

Table 6.6: Rejection criteria of pixels identified as burns in the SK2 but not the SABA dataset

It is evident from the data contained in Table 6.6 that a large proportion of the errors of omission in the SABA dataset are due to the identification of an insufficient change signal. Following the procedure described in Section 5.5.2 above for the separation of areas which have been affected by fire from those which have not, pixels are only labelled as potential burn candidates in the SABA dataset if $\delta\rho(\text{band}2)$ *and* $\delta\rho(\text{band}5)$ are less than the threshold value which has been set to -0.15. The reasons for using both bands 2 and 5 are discussed in Section 5.5.2. In particular this criteria has been followed in an attempt to reduce potential confusion between changes in the surface reflectance at these wavelengths which are due to the effects of fire, from those which are due to changes in the conditions and characteristics of the vegetation (see Section 5.5.3). In contrast the SK2 dataset has been created following the method of Roy *et al.* (2002) described in Section 4.3. Under this approach burn candidates are identified as pixels which exhibit a decrease in MODIS band 5, and band 5 minus band 7 decreases due to burning. The response at MODIS band 2 wavelengths is therefore not considered. A subsequent refinement of this algorithm for global application however incorporates MODIS band 2 for similar reasons to those discussed in Section 5.5.3, with potential burn pixels identified as those where the difference between band 5 and band 7 *and* the difference between band 2 and band 7 decreases (Roy 2005). Two reasons for the high error of omission of the SABA dataset when compared against the SK2 burned areas

(Table 6.5) are therefore the exclusion of MODIS band 2 in the identification of the SK2 burned areas, and variations in the definition of the magnitude of the change in reflectance required for a pixel to be identified as a burn candidate. The latter point is discussed in the following paragraph.

A visual examination of the burned area data indicates a high spatial agreement between the location of fire affected areas in the two datasets. Discrepancies are apparent around the borders of individual burns, contributing to the low total agreement between the burn locations documented in Table 6.5. This is demonstrated by the two examples displayed in Figure 6.7. Each corresponds to an area of 45km by 60km (see Figure 6.8). Their geographical locations are

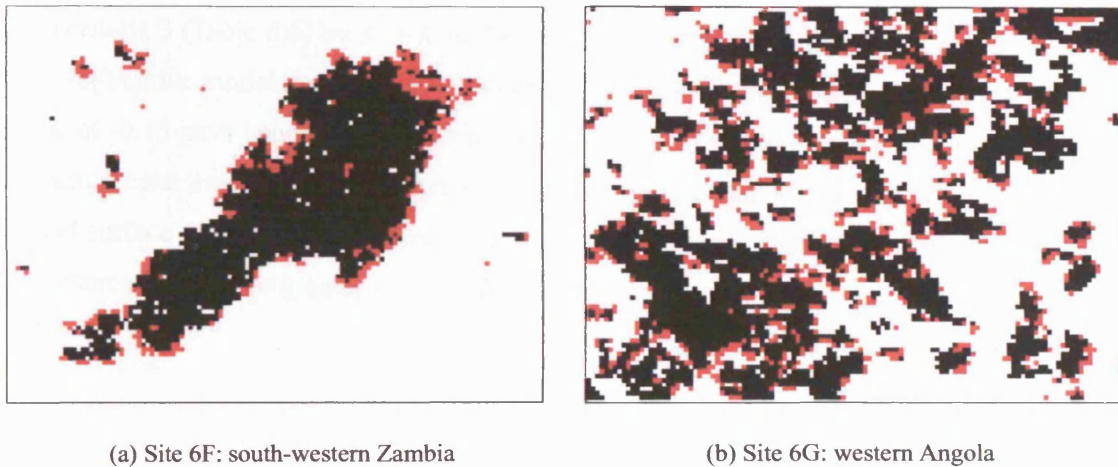


Figure 6.7: Discrepancies between SK2 500m burned areas and SABA (multiplicative model results): black pixels = burn in both, red pixels = burn in SK2 only, white pixels = no burn in SK2

displayed in Figure 6.8 and are detailed in Table A.1 in Appendix A as Site 6F and 6G. A large homogenous area has burned at Site 6F (south-western Zambia) while in contrast several more patchy burns have occurred at Site 6G (western Angola) during July 2000. The pixel locations which have been identified as burned in the SK2 but *not* in the SABA dataset correspond to the red pixels in Figures 6.7. The locations of the areas of disagreement (the red pixels) suggest that the discrepancies are due to the definition of what constitutes a burned area in terms of the magnitude of the change in reflectance which has occurred due to burning. Research has shown that the decrease in MODIS band 5 reflectance which occurs due to burning is a linear function of both the combustion completeness of the fire and the fraction of the observation area burned

(Roy and Landmann 2005). Pixels around the perimeters of fire affected areas are expected to exhibit lower decreases in reflectance due to both of these factors. The burned surface will exhibit greater heterogeneity around the perimeter and a lower proportion of the area within a 500m pixel may therefore have been affected by the fire at locations around the edge of a burn. In addition the intensity of the fire and thus combustion completeness will be lower at the perimeter of the burned area than at the centre. Following the approach described in Section 5.5.2 a 500m pixel is only identified as a potential burn candidate if it exhibits a proportional decrease in reflectance *greater* than 15% at both MODIS band 2 *and* band 5 wavelengths. Increasing the threshold of $\delta\rho(\lambda)$ to -0.1 (i.e. a proportional decrease in reflectance of 10%) reduces the error of omission due to criteria 3 (Table 6.6) by 37.8% in the case of the additive model results, and by 39.6% for the multiplicative model results. The effect of increasing this threshold and the reasons for using a value of -0.15 have been discussed in Section 5.5.2. In particular the use of a higher threshold results in greater errors of commission at the tails of the fire season with, for example, 68.8% of the land surface within the study area exhibiting a proportional decrease in MODIS band 2 and 5 reflectances of 10% or greater in April 2003.

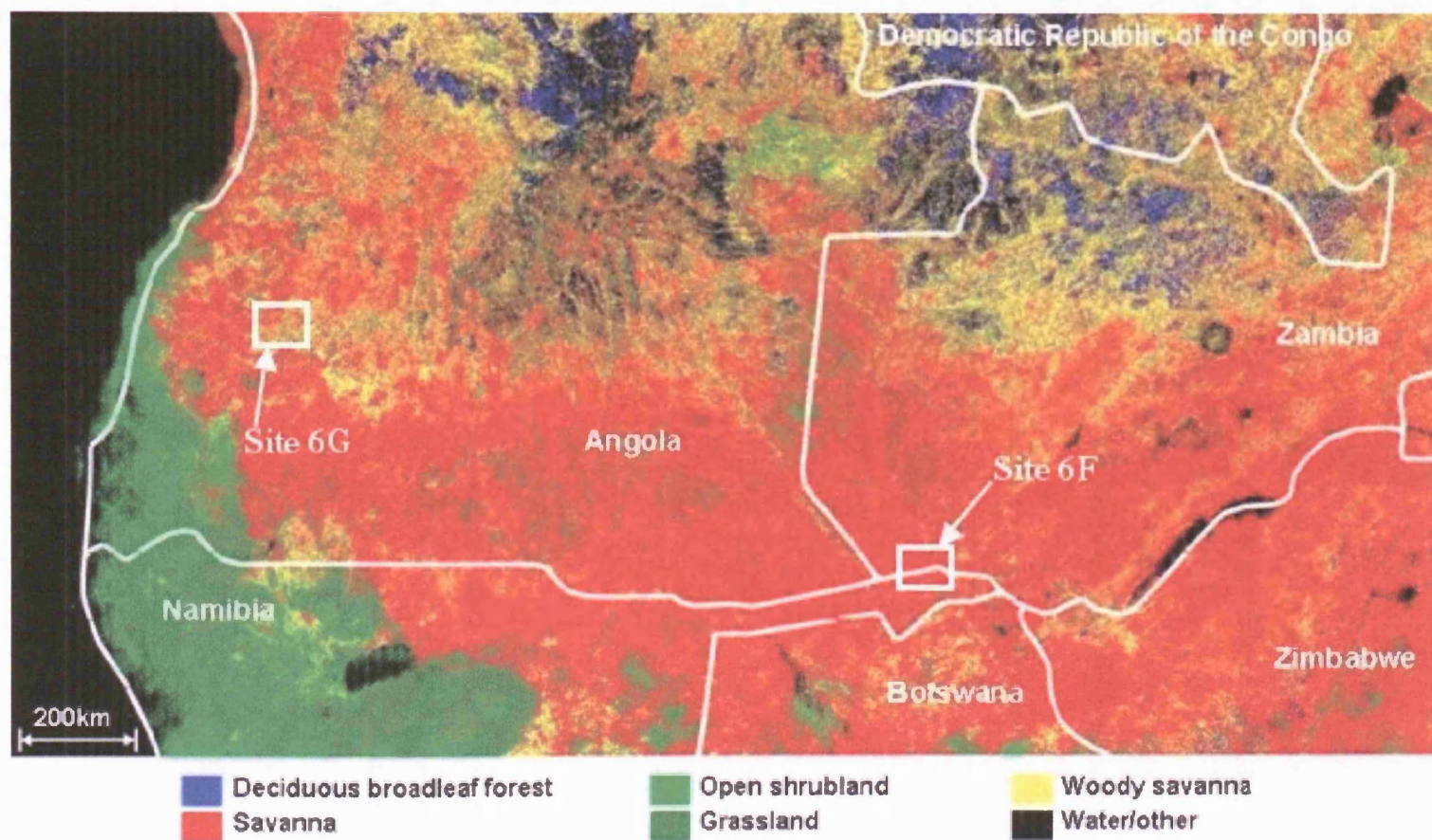


Figure 6.8: Sites 6F, 6G and MODIS Landcover Product

The distribution of the SABA errors of omission within each of the main vegetation types across the area of interest are displayed in Table 6.7. These data are calculated as the percentage of the total burns within each cover type identified by the SK2 algorithm which have *not* been mapped by the SABA approach. The errors of omission are distributed evenly across most cover types except for grasslands which exhibit a higher agreement between burned areas in the two datasets. The higher agreement in grasslands is unknown, but may be due to the greater probability of detection of burning within these ecosystems due to a clearer change signal in comparison to areas with greater tree cover. This has been discussed in Section 6.2 in reference to the detection of active fires.

Land cover	Percentage
Deciduous broadleaf forest	31.0
Open shrubland	31.2
Woody savanna	27.2
Savanna	31.7
Grassland	23.7

Table 6.7: Percentage of SABA burned areas *not* identified as burned in SK2 as a function of vegetation type

6.3.2 Errors of commission

Although errors of omission are present within the SABA data a large number of pixels which have been identified as burned in this dataset are not present in the SK2 data. The number of pixels and the percentage of the total area burned in the SABA data which this corresponds to is displayed in Table 6.8. Only SK2 pixels with a value of 0 (i.e. no burning has been detected) have

Additive model results		Multiplicative model results	
Pixel count	Percentage	Pixel count	Percentage
205775	23.8	275885	29.6

Table 6.8: Number of pixels and percentage of SABA burned areas *not* identified as burned in SK2

been considered in the comparison. In order to exclude discrepancies between the two dataset

due to the day of burning at the beginning and end of the temporal sequence, a four day buffer is applied at the start and end of July. SK2 areas which have been identified as burning between the 26th of June and the 4th of August 2000 are thus compared to pixels which are documented as burning between the 30th of June and the 1st August in the SABA dataset. A total area of 68971km^2 (275885 500m pixels) which is identified as burned in the SABA multiplicative dataset is not present in the SK2 data. This is the equivalent of just under 30% of the total fire affected area documented in the SABA dataset. Two areas of 45km by 60km have been extracted from the burned area data and are displayed in Figure 6.10 for illustrative purposes. Their locations within the study area are displayed in Figure 6.9 and are also detailed in Table A.1 in Appendix A as Sites 6H and 6I. The black pixels correspond to burned areas documented in the SABA dataset, and the red pixels to those identified as burned in SABA but *not* in SK2. At the first site (6H) burning has taken place over smaller and less spatially contiguous areas, while at the second site (6I) burning has occurred over larger areas. At both locations a large proportion of the burned areas which have not been identified in the SK2 data (the red pixels) are located around the perimeters of or adjacent to burn pixels. As discussed above reasons for these discrepancies may include factors such as the combustion completeness of the fire and the proportion of a pixel burned, as these will determine the magnitude of the change identified in the remote sensing signal. The threshold level used to separate areas of significant burn induced surface change from those where the effect of burning is considered minimal at an individual 500m pixel scale will also contribute to discrepancies in the location of the burn/noburn perimeter around an area of burning. Under the SABA approach a proportional change in reflectance of 15% or greater is required at MODIS band 2 and 5 for a 500m pixel to be labelled as burned. As discussed in Section 4.5 in contrast to the method of Roy *et al.* (2002) used in the production of the SK2 burned areas, the temporal change detection models used to create the SABA dataset account for phenological variations in the surface thereby allowing for the improved detection of more subtle changes. An examination of the locations which are identified as burns in the SABA dataset but *not* the SK2 product exhibit large changes at band 5 wavelengths. This is demonstrated through two pixels which have been selected at random from the errors of commission. The locations of these are documented in Table A.1 and Figure A.1 in Appendix A as Sites 6J and 6K. Site 6J is located in central Zambia, and Site 6K in southern Zambia. Both pixels have been identified as burned in the SABA but *not* in the SK2 dataset. The MODIS band 5 reflectances and the model

predicted values for July 2000 are displayed in Figures 6.11a and Figures 6.11c. Following the approach of Roy *et al.* (2002) the reflectances have been modelled using a 16 day moving window additive model (see Section 4.3). Burned areas in the SK2 dataset have been located by thresholding a Zscore time series, as described in Section 4.3. The corresponding Zscores for the two pixel locations are displayed in Figures 6.11b and 6.11d. For the first example a large negative Z-score is evident on the day of burning documented in the SABA dataset. The reasons why locations such as these have not been identified as burns in the SK2 product are unknown as they exhibit a clear change signal at MODIS band 5 wavelengths under a 16 day moving window BRDF inversion scheme.

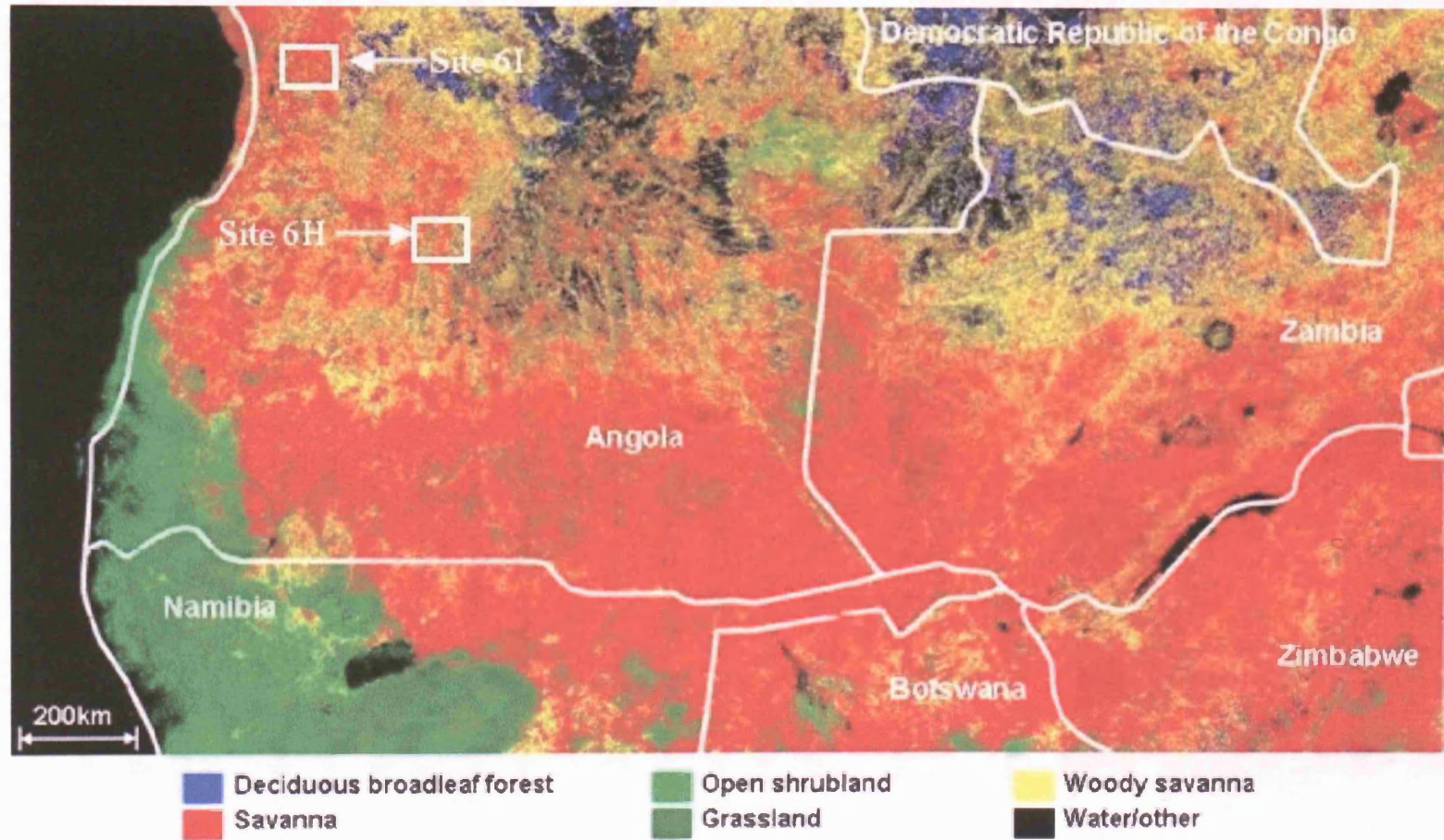


Figure 6.9: Sites 6H, 6I and MODIS Landcover Product

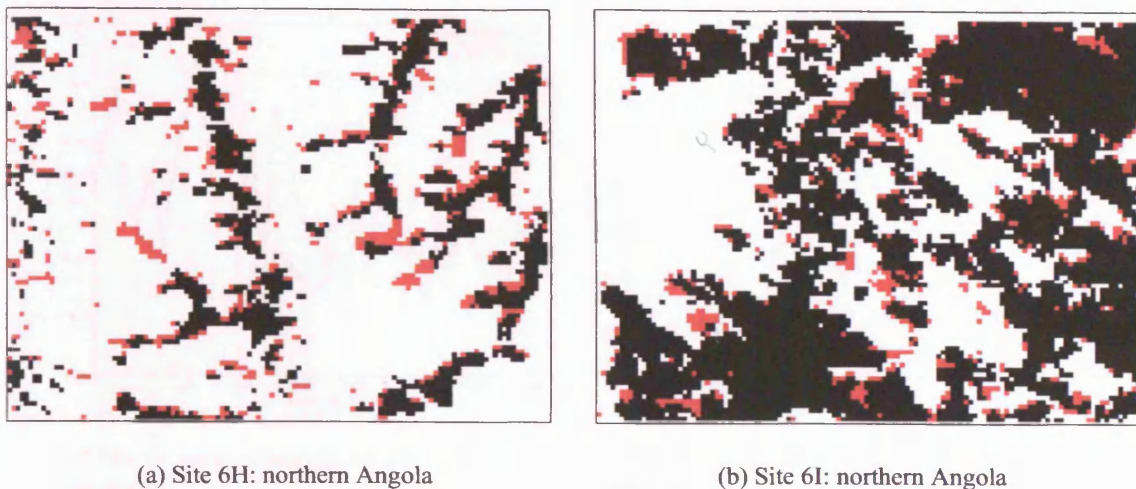
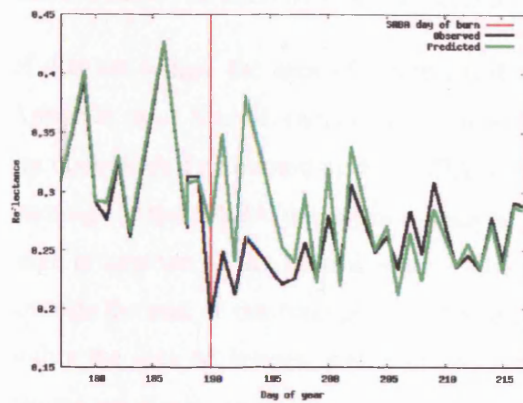


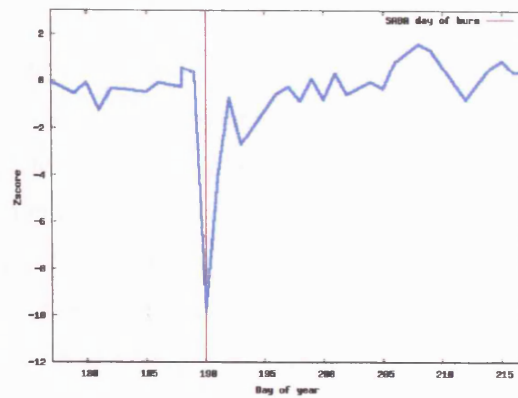
Figure 6.10: Discrepancies between SK2 500m burned areas and SABA (multiplicative model results): black pixels = burn in both, red pixels = burn in SABA only, white = no burn in SABA

At the second location (Site 6K) a large negative Zscore occurs on day 194, 9 days before the day of burning identified in the SABA dataset. This corresponds to an isolated decrease in the reflectance sequence (Figure 6.11c). This has been identified as an outlier in the temporal change detection approach (Section 4.5) used to create the SABA dataset and following this method has been removed from the sequence. In the change detection approach used to create the SK2 data although such outliers are not identified as burns due to the use of a temporal consistency threshold which excludes temporary changes they are not removed prior to model inversion and the authors note that the BRDF model inversion is insensitive to the inclusion of a single contaminated reflectance value (Roy *et al.* 2002). In scenarios such as that displayed in Figure 6.11c where the presence of a noisy observation is exacerbated by missing samples on the surrounding days, its inclusion clearly has an effect on the model predictions and therefore on the change signal (Figure 6.11d). When this is removed a large negative Zscore occurs on the day of burning documented in the SABA data (Figure 6.11d).

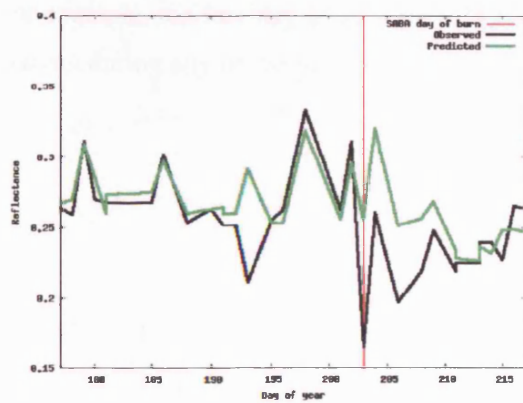
In addition to the errors of commission described above which are typically located on the perimeter of burned areas, several large and spatially homogenous fire affected areas identified in the SABA dataset are not documented in the SK2 product. This is demonstrated with an area of 100km by 160km extracted from the two datasets and displayed in Figure 6.13. The location



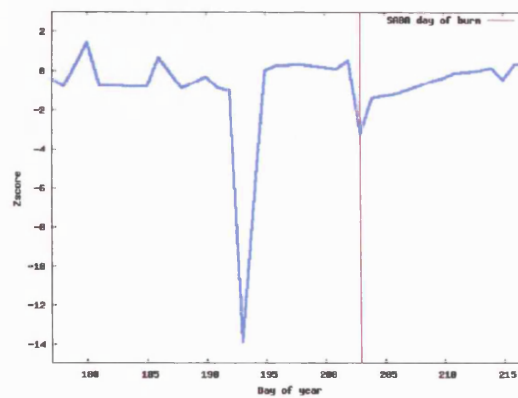
(a) Site 6J, central Zambia: MODIS band 5 reflectance



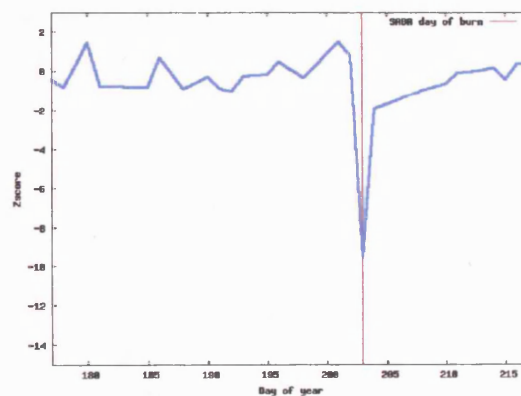
(b) Site 6J, central Zambia: 16 day moving window Zscore



(c) Site 6K, southern Zambia: MODIS band 5 reflectance



(d) Site 6K, southern Zambia: 16 day moving window Zscore



(e) Site 6K, southern Zambia: 16 day moving window Zscore - Cloud filtered

Figure 6.11: SABA errors of commission: 500m burn pixels not identified by the SK2 product

of this site within the area of interest is displayed in Figure 6.12 and detailed in Table A.1 in Appendix A as Site 6L (northern Angola). The red pixels in Figure 6.13a indicate pixels which are documented as burned in the SABA dataset, but not the SK2 product. The identified day of burning for the SABA dataset is displayed in Figure 6.13b. From these data it appears that a large proportion of the burned areas which are not identified in the SK2 dataset have occurred towards the end of the time period. The distribution of the day of burning for all of the pixels within the area of interest which are documented as burned in the SABA but *not* in the SK2 dataset are displayed in Figure 6.14. Approximately 27% of the SK2 unidentified burned areas have burned within the last four days of July (day 210-213). Due to the use of a four day buffer in the comparison of the two datasets locations identified as burned within the SABA dataset on, for example, the last day of July (day 213) have not been identified as burned within the SK2 dataset during any of the previous 34 or the subsequent four days.

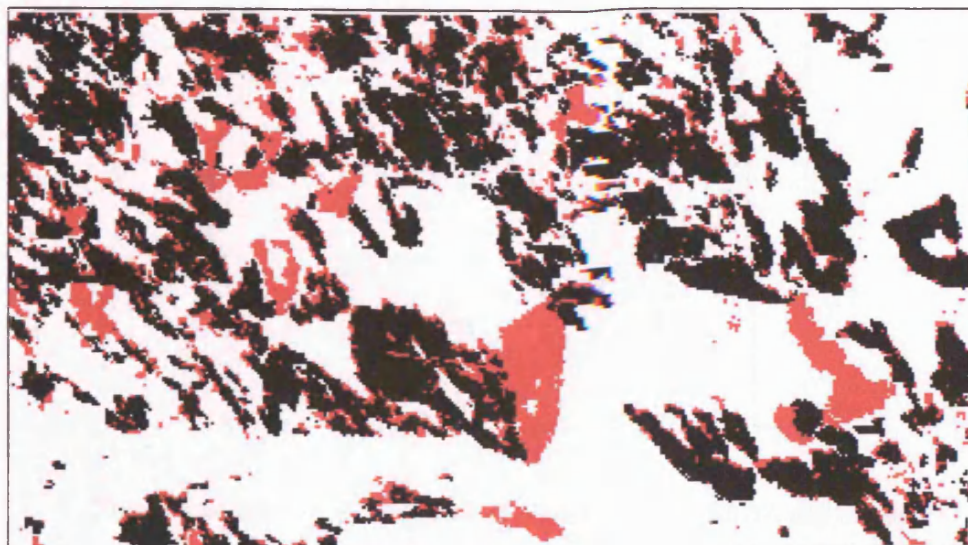
A large proportion of the burned areas documented in the SABA dataset for the temporal sequence starting on the 30th June and ending on the 1st August which are *not* identified as burning in the SK2 dataset between the 26th June and the 4th of August have burned between the 29th of July and the 1st of August. This is confirmed by an examination of a false colour composite of MODIS surface reflectance bands 2, 1 and 4 for the 2nd of August 2000, displayed in Figure 6.15b for the same location as that displayed in Figure 6.13. The red pixels correspond to areas of dense vegetation and the dark/black pixels to the recently burned surfaces. In particular it is evident from Figure 6.15b that the large burn in the centre of the site which has not been identified as a burn in the SK2 dataset (the red pixels in Figure 6.15a) but is labelled as burning on or around the 1st August in the SABA dataset (Figure 6.13) has been burned by the 2nd of August. The greater underestimation of burning towards the end of the temporal sequence by the SK2 data suggests that this may be due to a systematic problem in the identification of the day of burning at the ends of the time series.

The spatial distribution of the errors of commission have also been investigated as a function of land cover type. The number of unidentified SK2 burns within each vegetation type is displayed in Table 6.9 as a percentage of the total number of burn pixel identified by the SABA (multiplicative model) dataset within the particular cover type. The highest proportion of burned

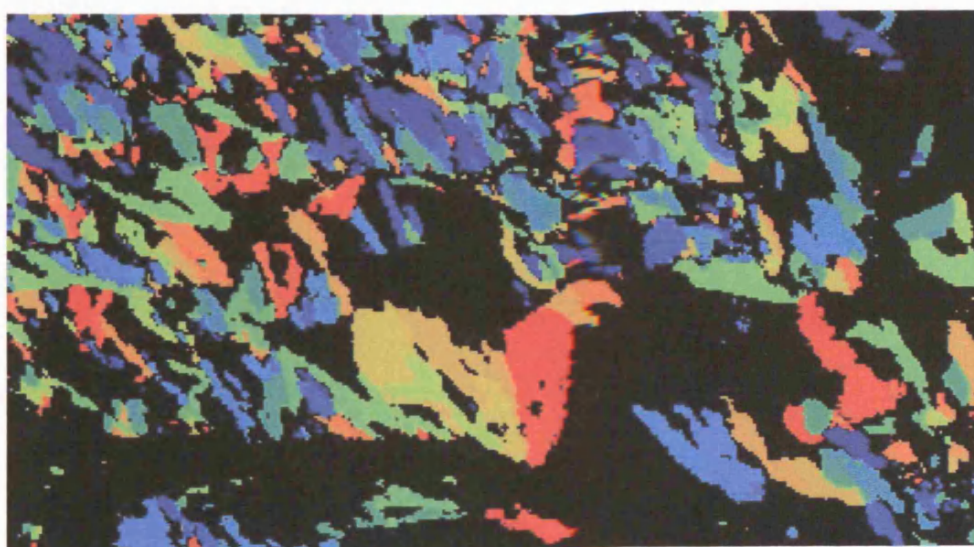
Land cover	Percentage
Deciduous broadleaf forest	31.3
Open shrubland	26.8
Woody savanna	25.3
Savanna	26.0
Grassland	23.2

Table 6.9: Percentage of SABA burned areas *not* identified as burned in SK2 as a function of vegetation type

areas which have *not* been identified by the SK2 methodology occur within deciduous broadleaf forests, and the lowest within grasslands. Preliminary validation of MODIS burned areas for 2001 and 2002 have indicated that the SK2 approach is underestimating the regional area burned (Roy *et al.* 2005a). A similar pattern is exhibited in the errors of omission, with the highest disagreement occurring within deciduous broadleaf forests and the lowest within grassland



(a) Site 6L, northern Angola: black pixels = burn in both, red pixels = burn in SABA only, white = no burn in SABA



182 213

(b) Site 6L, northern Angola: Day of burn

Figure 6.13: Discrepancies between SABA (multiplicative model results) and SK2 500m burned areas

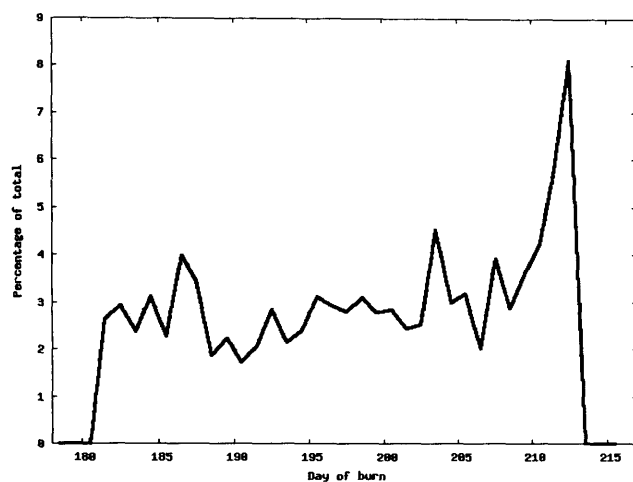
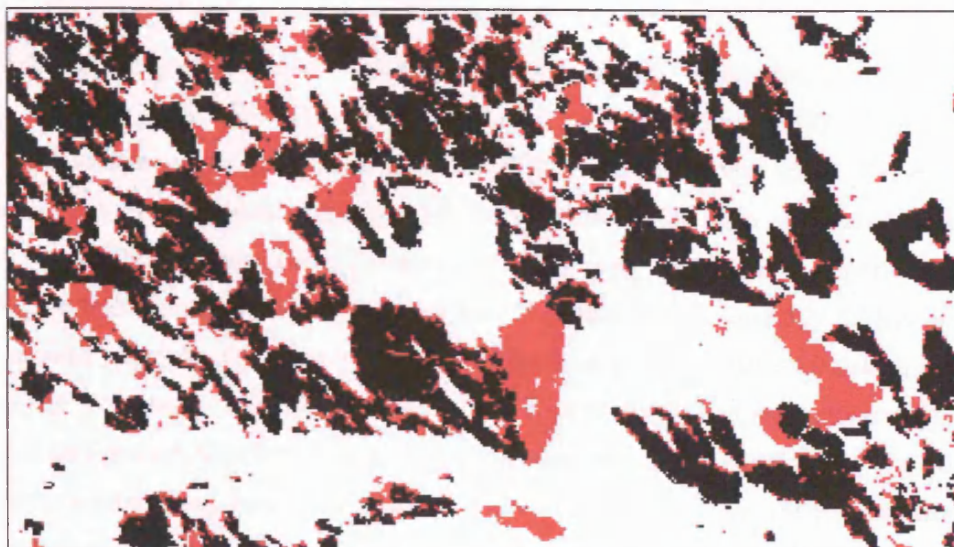
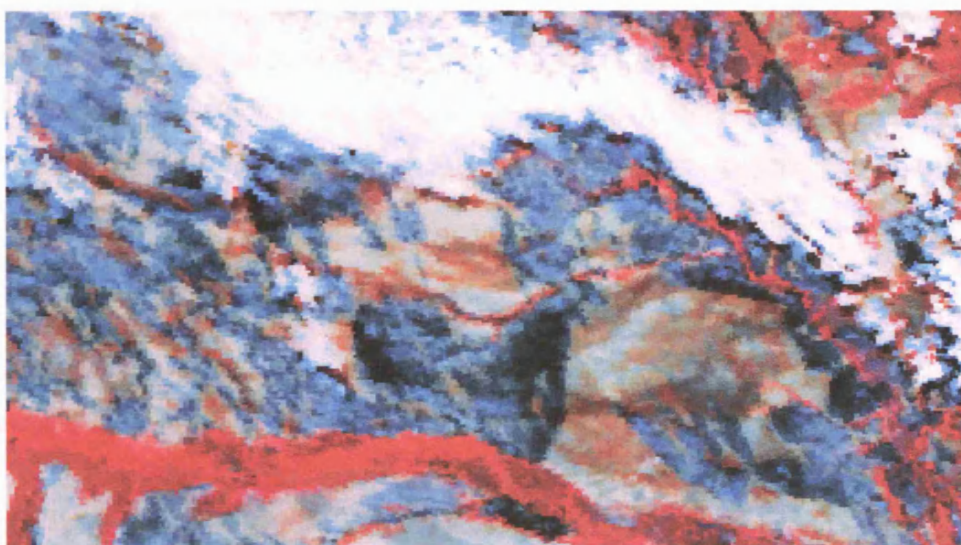


Figure 6.14: Errors of commission: distribution of SABA day of burn

ecosystems. The causes of these disagreements are unknown, and possible reasons are discussed in Section 6.2.



(a) Site 6L: black pixels = burn in both, red pixels = burn in SABA only, white = no burn in SABA



(b) Site 6L: False colour composite: MODIS bands 2 1 4, 2nd August 2000

Figure 6.15: Discrepancies between SABA (multiplicative model results) and SK2 500m burned areas, Site 6L (northern Angola)

6.4 GBA2000 1km burned areas

The GBA2000 dataset is a global inventory of biomass burning for the year 2000 (Gregoire *et al.* 2003, Tansey *et al.* 2004b). This product has been created from the SPOT VEGETATION S1 1km product using algorithms developed and calibrated at a regional scale. The methodology applied to the Africa region is described in Section 2.4.2. The data are available as monthly binary (burn/noburn) composites. The aim of the following paragraphs is to perform a comparison between the monthly burned areas of the GBA2000 and the monthly SABA data for the eight months (April to November) of the 2000 fire season. The GBA2000 data are stored in a geographic projection. The projection parameters have been adjusted manually and the data converted to the Lambert Azimuthal Equal Area projection with an output pixel size of 1km. In order to perform a comparison between the 1km GBA2000 burned areas and the 500m SABA data the latter have been aggregated to a resolution of 1km with an output pixel detailing the number of corresponding 500m burn pixels. The SABA pixel values at a spatial resolution of 1km thus vary between 0 where no burn has been identified in any of the corresponding four 500m pixels, and 4 where each of the SABA 500m pixels and thus 100% of the 1km pixel has been identified as a burn pixel. This approach reduces positional errors and provides a more accurate burned area assessment for subsequent analysis (Korontzi *et al.* 2004). Although a validation protocol is in place for this product (Boschetti *et al.* 2004) the burned areas have yet to be systematically validated.

6.4.1 Errors of omission

The number of pixels identified as burned in both the GBA2000 and SABA datasets, and the percentage of the total GBA2000 burned area which this corresponds to is documented in Table 6.10. The SABA datasets used in the analysis have included areas identified as burning on the last four days of the previous and the first four days of the subsequent month in order to account for variations in the day of burning due to missing and/or cloudy data.

A visual examination of the spatial distribution of pixels identified as burned in the GBA2000 dataset but *not* in the SABA dataset over the eight months of the 2000 fire season indicate that a large proportion of the errors of omission at the beginning of the annual fire season may be

Month	Additive model results		Multiplicative model results	
	Pixel count	Percentage	Pixel count	Percentage
April	4032	67.2	5155	86.3
May	2774	35.2	3060	38.8
June	6670	14.9	6732	15.0
July	8944	9.3	8698	9.1
August	10113	13.6	8999	12.1
September	20103	25.7	21303	27.2
October	3380	14.2	3586	15.1
November	2004	45.4	2218	50.2

Table 6.10: Number of 1km pixels and percentage of GBA2000 burned areas *not* identified as burned in the SABA dataset

due to flood events which have been misclassified as areas of burning in the GBA2000 product. The causes of the spectral confusion which occurs between water and burned areas has been discussed in Section 5.5.3. During the first two as well as the last month of the southern Africa fire season a large number of the pixels identified as burns in the GBA2000 dataset have been flagged as areas of flooding in the SABA dataset. The same 150km by 100km location which flooded in April 2003 and has been used as an illustrative example in Figure 5.17 Section 5.5.3 is displayed in Figure 6.17 for April 2000. The location of this area corresponds to Site 6M in Figure 6.16. The geographical location of the site is detailed in Table A.1 in Appendix A. The black pixels in Figure 6.17a correspond to areas which are identified as burns in April 2000 in the GBA2000 product, while the black pixels in Figure 6.17b have been flagged as potential flood events in the SABA April 2000 data. An examination of MODIS 500m band 2 reflectances for this location confirms that this is a semi-permanent water feature and *not* an area of burning. Figure 6.18 displays a 190 by 216km portion of a MODIS band 2 image acquired over this area on the 29th of April 2000. The site is located to the northeast of the Okavango Delta, and streams flowing into and out of the water feature are apparent in the northwest, southeast and southwest corners. The contribution of areas of flooding to the total errors of omission contained in Table 6.10 above are displayed in Table 6.11 as a percentage of the total number of 1km pixels identified as burned in the GBA2000 but not in the SABA dataset.

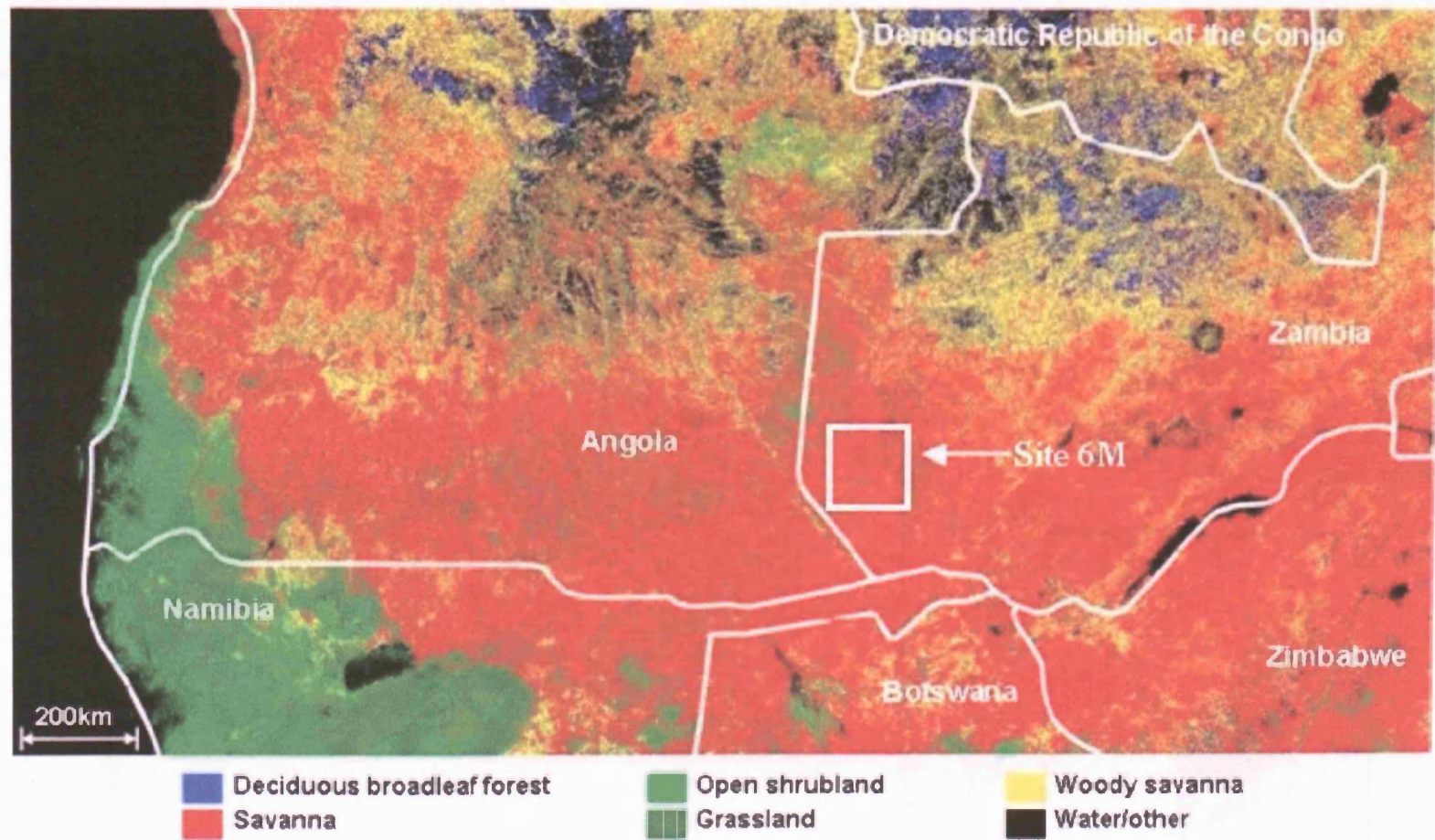
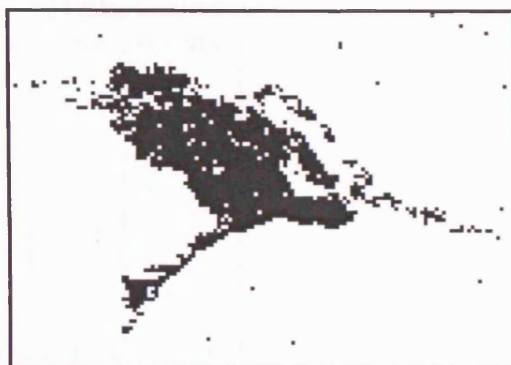


Figure 6.16: Site 6M and MODIS Landcover Product



(a) Black pixels are identified as burned areas in the GBA2000



(b) Black pixels are flagged as flooding in the SABA multiplicative model results

Figure 6.17: A semi-permanent water body identified as a burn in the GBA2000 product, Site 6M, Zambia, April 2000

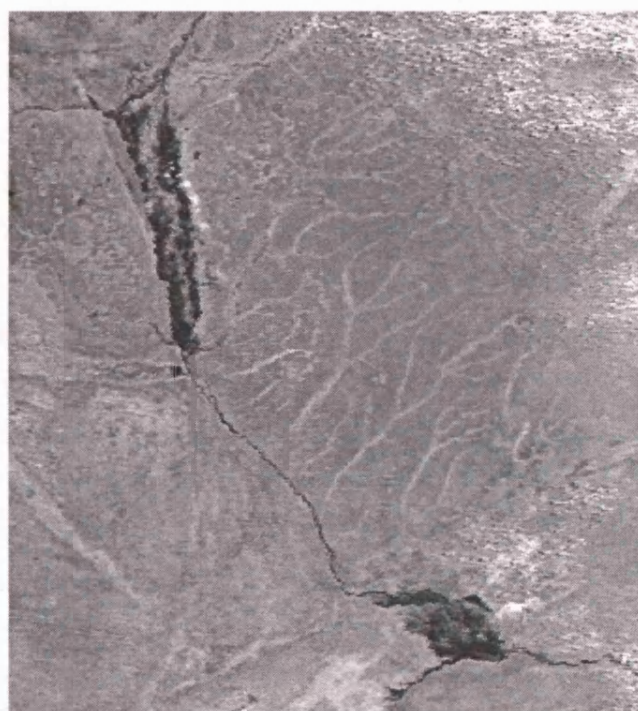


Figure 6.18: Semi-permanent water features, 29th April 2000, Site 6M (Zambia)

Higher errors of omission are expected to be present in the SABA dataset for the months

	Additive model results	Multiplicative model results
April	29.3	33.9
May	5.4	8.9
June	0.4	2.2
July	1.7	7.5
August	1.0	5.7
September	0.3	0.7
October	1.4	4.9
November	3.1	2.9

Table 6.11: Percentage of 1km GBA2000 burned areas identified water induced surface change

of August and September due to missing data, as MODIS was not operational between the 5th and the 19th of August 2000. Areas which burned between these dates will therefore not be documented in the SABA August 2000 dataset. As the day of burning is not calculated for the GBA2000 product it is not possible to exclude burns which have occurred during these days from the analysis. In addition as a 30 day time buffer is applied in the detection of burned areas in the SABA dataset (see Section 5.5) the results for September may be less reliable than for the other months due to the necessity of using a 13 day time buffer due to the missing data in August 2000. It should also be noted that MODIS data sensed prior to November 2000 are noisier than later acquisitions due to a poorly performing MODIS detector (Guenther *et al.* 2002), which may result in higher errors of omissions in the SABA 2000 data in comparison to subsequent years.

A large proportion of the errors of omission which are not due to flooding have a distinct spatial distribution. These tend to be isolated pixels located in a band along the coast of Angola and Namibia which are identified as burns in the SK2 but not in the SABA dataset. This is demonstrated with an area of 22km by 16km for May 2000 which is located near the coast of Angola and displayed in Figure 6.20. The geographical location of this area is detailed in Table A.1 Appendix A as Site 6N. The location of the site within the area of interest is displayed in Figure 6.19. The red pixels have been identified as burns in May 2000 by the GBA2000 product, but *not* in the SABA dataset. An examination of the proportional changes in reflectance which has occurred at these 500m pixel locations in May 2000 indicates that the changes which have taken place are small. The distributions of the $\delta\rho(\lambda)$ values for the red pixels in Figure 6.20

are displayed in Figure 6.21a. These locations have not been identified as burns in the SABA dataset as they exhibit proportional decreases in MODIS band 2 *and* band 5 reflectances of less than 15%. The MODIS band 2 and band 5 reflectances for the pixel (Site 6P, Table A.1 and Figure A.1 in Appendix A) indicated by the X in Figure 6.20 are displayed in Figure 6.21b for May 2000. The day of change identified for this sequence is day 135 (the 14th of May), and the proportional change values are 0.013 -0.010 -0.009 and 0.003 for MODIS bands 1, 2, 5 and 7 respectively. A proportional decrease in reflectance of 1% or less has been identified at MODIS band 2 and 5 wavelengths at this location, and the pixel has therefore not been labelled as a burn in the SABA dataset.

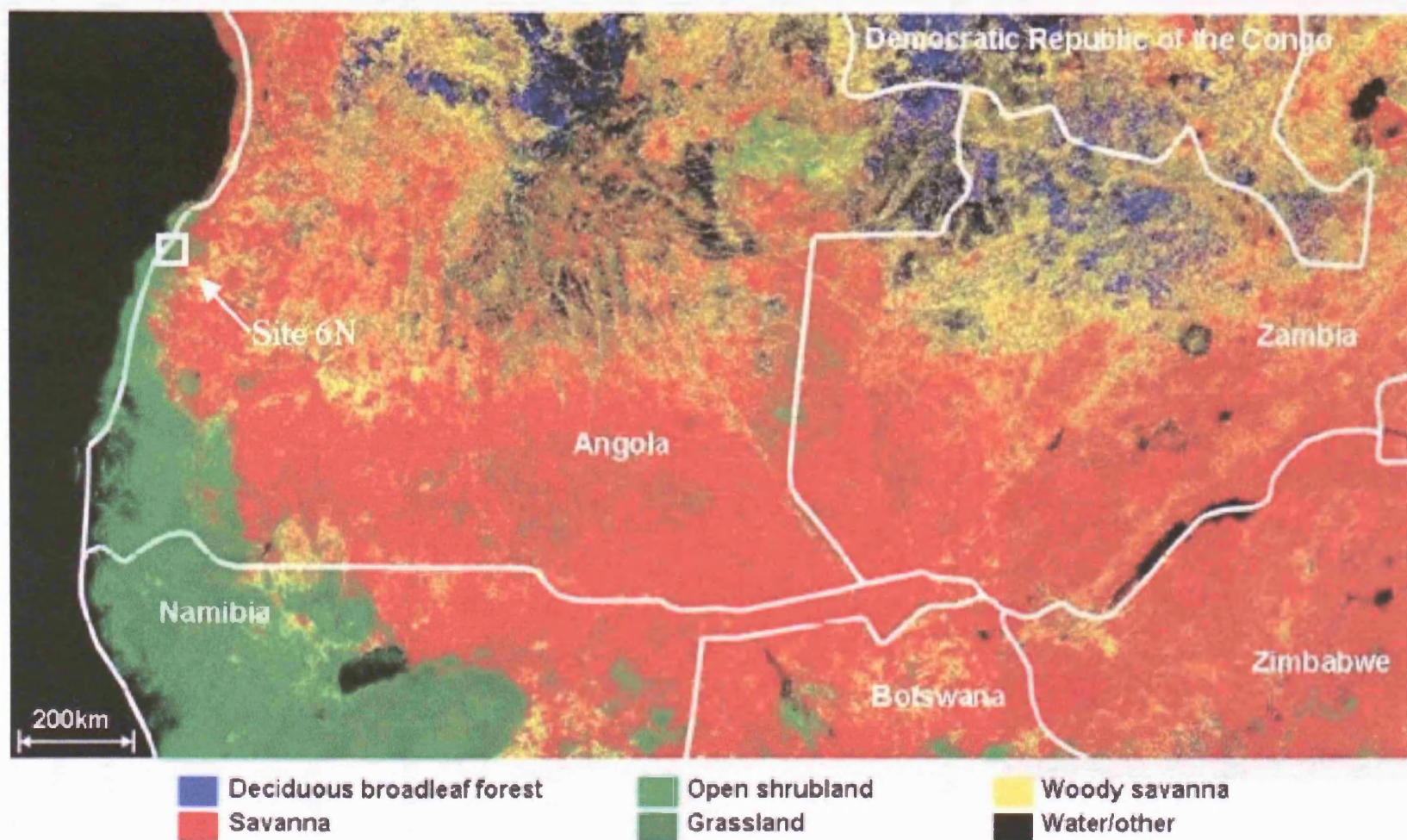


Figure 6.19: Site 6N and MODIS Landcover Product

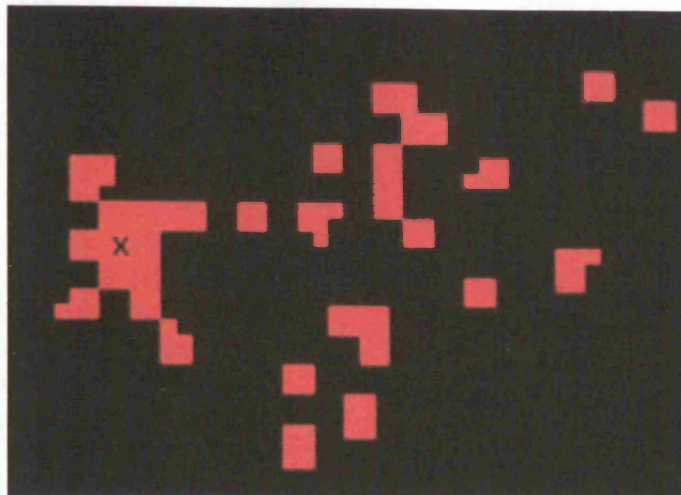
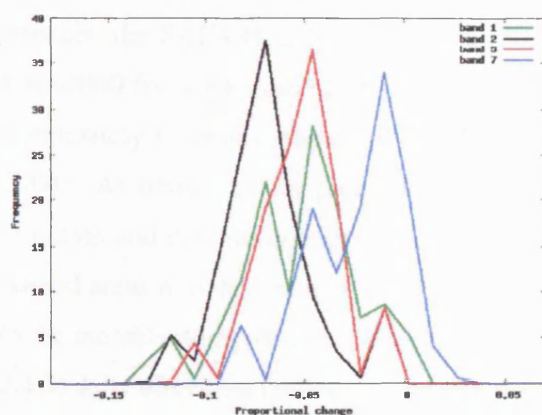
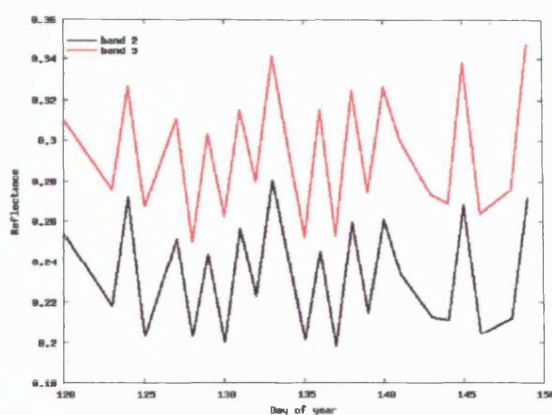


Figure 6.20: SABA errors of omission: GBA2000 burned areas, Site 6N, western Angola, May 2000



(a) Proportional change values: Multiplicative model results



(b) MODIS band 2 and 5 reflectances

Figure 6.21: SABA errors of omission: Site 6P, western Angola, May 2000

6.4.2 Errors of commission

Table 6.12 contains statistics describing the SABA errors of commission in relation to the GBA2000 product. The number of 1km pixels and the percentage of the total burned area documented in the SABA dataset but *not* identified as burned in the GBA2000 data are detailed for the eight

Month	Additive model results		Multiplicative model results	
	Pixel count	Percentage	Pixel count	Percentage
April	70284	97.3	45816	98.3
May	64186	92.6	55946	92.1
June	131582	77.5	133067	77.7
July	194373	69.1	201089	69.7
August	291851	82.0	302744	82.3
September	250411	81.1	261173	82.1
October	253890	92.6	258864	92.8
November	132586	98.2	119000	98.2

Table 6.12: Number of pixels and the percentage of SABA burned areas *not* identified as burned by GBA2000

months of the 2000 fire season. Although the percentage of SABA burned areas which are not identified in the GBA2000 product are large, similar results were found during a comparison between the SAFARI 2000 MODIS 500m (SK2) burned areas and those documented by the GBA2000 for September 2000, with the MODIS product mapping a total burned area of approximately 1.5 times greater across southern Africa than the GBA2000 product (Korontzi *et al.* 2004). As neither of the products have been systematically validated the respective errors of omission and commission are unknown. The differences in the algorithms used to produce the burned areas may however provide a theoretical explanation for the disagreements. In contrast to the monthly compositing approach used in the creation of the GBA2000 product (see Section 2.4.2) daily directional reflectances have been used to create the SK2 and SABA datasets. While the GBA2000 approach attempts to minimise the angular effects present in the daily reflectances through a minimum near-infrared compositing technique (Gregoire *et al.* 2003), the method used in the creation of the SABA and SK2 datasets accounts for these effects allowing for the identification of subtle changes which are of a similar magnitude as the directional effects, and would otherwise be masked by these.

The percentage of a 1km pixel (i.e. the number of corresponding 500m resolution pixels) documented as burned in the SABA dataset at the 1km GBA2000 locations which have *not* been identified as burned (i.e. those documented in Table 6.12) are displayed in Table 6.13 as a percentage of the total error of commission for each month. These data indicate that at the tail months of the fire season a large percentage of the errors of commission occur at locations

	Additive model results				Multiplicative model results			
	25%	50%	75%	100%	25%	50%	75%	100%
April	80.6	14.5	2.6	0.9	84.8	11.8	1.7	0.8
May	55.4	21.0	9.0	8.4	57.4	19.8	8.2	8.1
June	36.4	20.1	10.2	12.2	37.9	19.6	9.7	12.2
July	30.1	19.3	10.1	11.4	30.2	19.0	10.1	12.5
August	34.9	21.1	11.7	15.2	34.5	20.9	11.8	16.3
September	37.2	20.3	10.8	14.8	38.7	20.4	10.5	14.6
October	47.8	22.0	10.5	13.8	48.1	22.2	10.4	13.9
November	73.7	18.3	4.5	2.2	73.7	18.5	4.4	2.3

Table 6.13: Percentage of each 1km pixel identified as burned in SABA but *not* in GBA2000

which contain subpixel ($<1\text{km}$) burns. There are two possible explanations for this; (i) the overestimation of burning by the SABA algorithm, and/or (ii) the occurrence of smaller and less severe fires and the underestimation of burning by the GBA2000 during these months. Temporal variations in the severity of burning within the area of interest is discussed in the following chapter. An analysis of this variable indicates that fires which occur at the beginning and the end of the annual fire season are generally less severe than those which occur during the peak months. In addition due to the higher moisture content of the vegetation at this time as well as less favourable meteorological conditions fires will not spread as quickly resulting in smaller and less homogenous burned areas than those observed at the peak of the fire season. Generally higher spatial resolution sensors will detect burned areas more reliably than lower spatial resolution sensors, as increasing the fraction of a pixel which burns increases the fire induced reflectance change and consequently the likelihood of detection (Roy and Landmann 2005). The occurrence of smaller (in terms of their spatial extent) and less severe burns at the tails of the fire season may therefore be detected more reliably in the higher spatial resolution data. At the peak of the burn season (June-September) the errors of commission are less dependent on the percentage of a 1km pixel which has burned, with over 60% of 1km pixels not mapped as burned in the GBA2000 product during these months identified as containing two or more SABA 500m burn pixels.

A visual examination of the errors of commission suggest that these are not predominantly caused by overestimation of burned areas in the SABA dataset. This is illustrated by an area of 200 by 230km extracted from the northeast corner of the study area. This site is displayed in

Figure 6.22 as Site 6Q and is also documented in Table A.1 in Appendix A. Figure 6.23 displays the SABA 1km errors of commission. The corresponding 500m day of burning and proportional change in band 2 reflectances is displayed in Figure 6.24.

The errors of commission detailed in Table 6.12 have also been investigated as a function of vegetation type. The number of 1km pixels which are identified as burned in the SABA dataset but *not* in the GBA2000 product across each of the main vegetation types within the study area are displayed in Figure 6.25 as a percentage of the total number of SABA 1km burns within each cover type during the eight months of the annual fire season. These data indicate that a higher proportion of 1km SABA burn pixels which have not been mapped by the GBA2000 product are located within deciduous broadleaf forests. Conversely the lowest errors of commission are present over grasslands. The comparison of the SK2 burned areas for September 2000 against the GBA2000 product identified a similar trend, with the main difference between the two datasets associated with areas of higher percent tree cover (Korontzi *et al.* 2004). Possible reasons for the greater underestimation of the GBA2000 product in woodlands and forests include the characteristics of the fires which occur in these ecosystems, the spatial resolution of the two products and different detection capabilities of the algorithms employed. In particular the use of higher spatial resolution data allows for more accurate detection of understorey burned surfaces which may be partially obscured by unburned canopy components, as is often the case in the surface fire regimes of southern Africa.

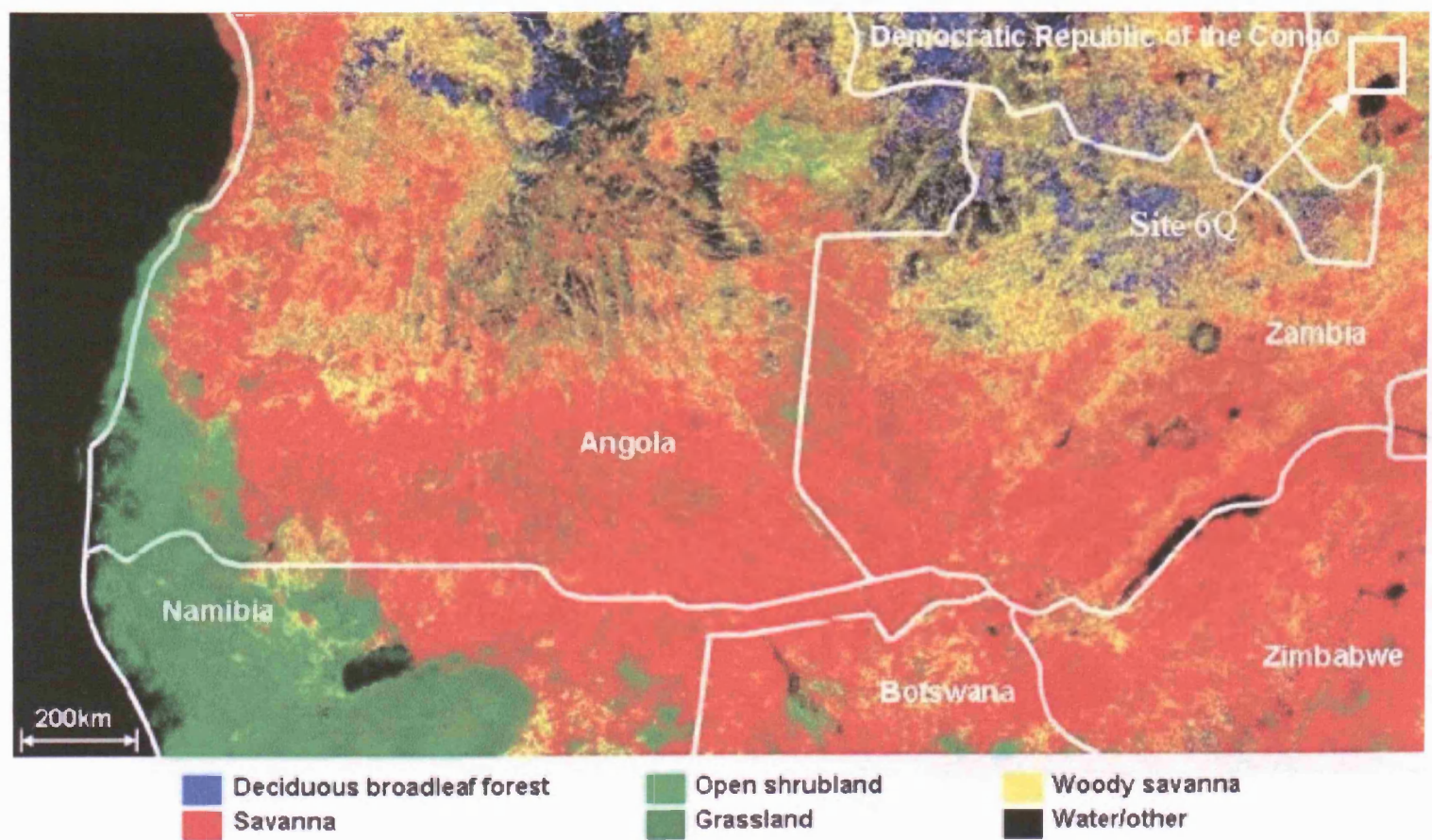


Figure 6.22: Site 6Q and MODIS Landcover Product

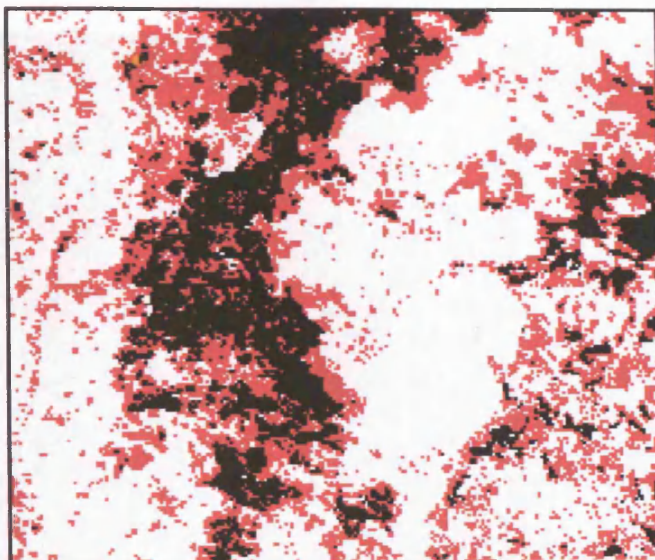
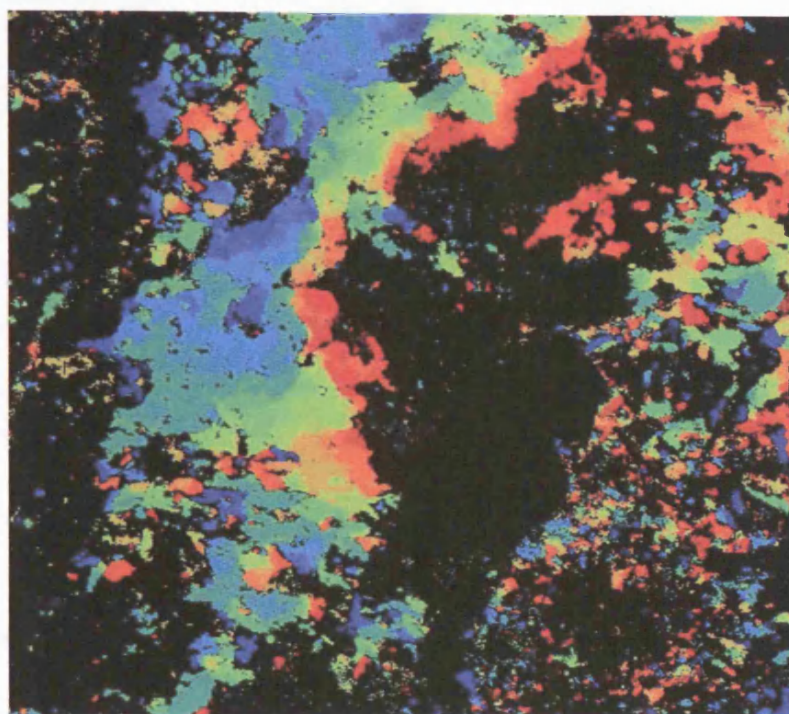
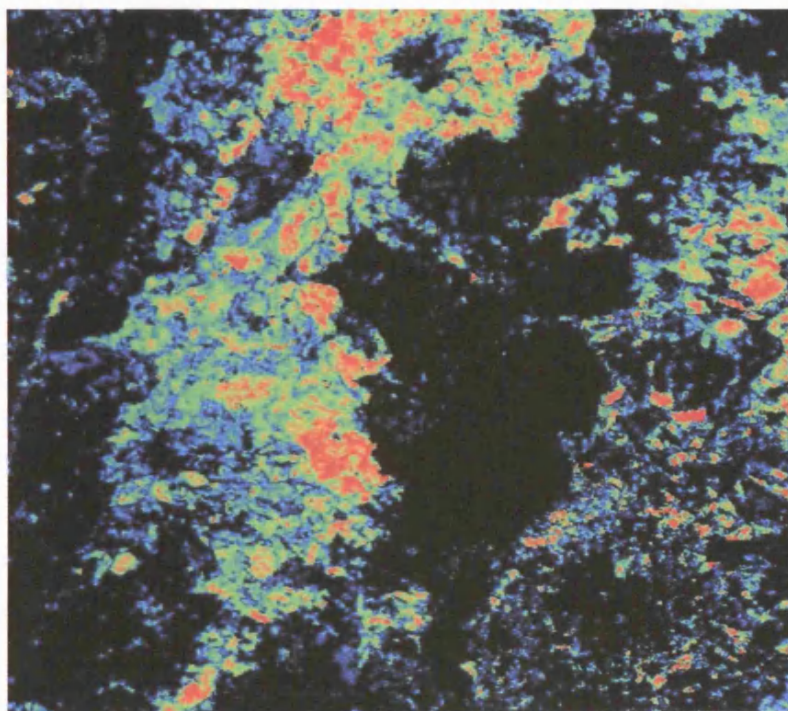


Figure 6.23: Errors of commission: black pixels = burn in both SABA and GBA2000, red pixels = burn in SABA only (Site 6Q)



245  274

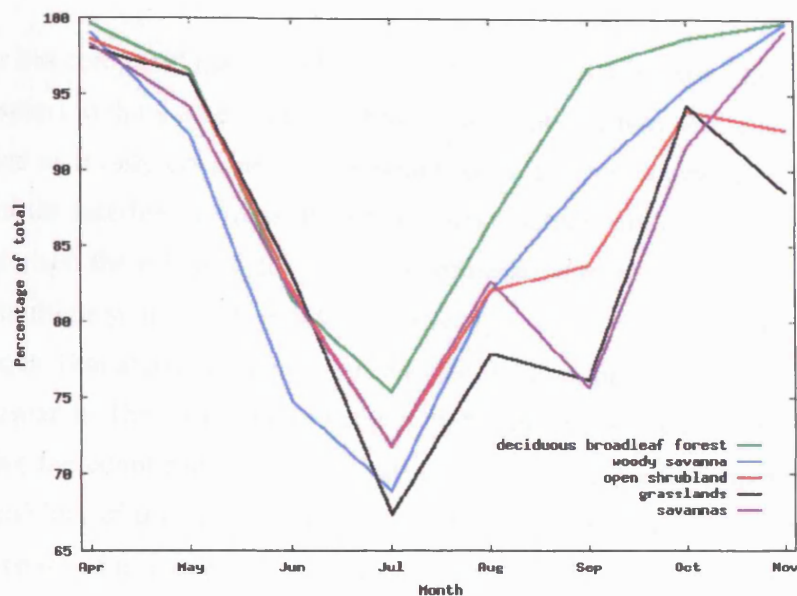
(a) Day of burning, September 2000



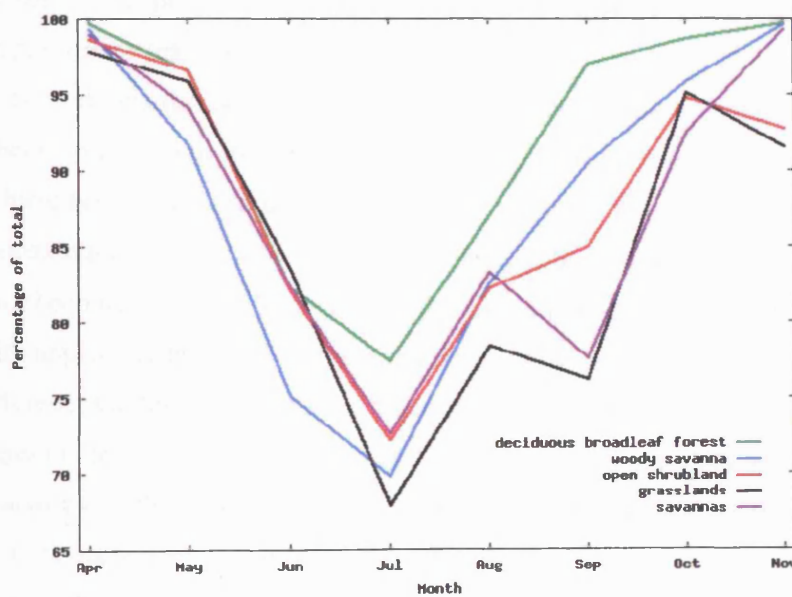
15%  60%

(b) Proportional change in band 2 reflectances, September 2000

Figure 6.24: SABA burned areas, Site 6Q, northern Zambia



(a) Additive model results



(b) Multiplicative model results

Figure 6.25: Distribution of SABA/GBA2000 errors of commission within each land cover class

6.5 Summary

This chapter has compared the burned area results produced using the methods described in the previous chapters to three other sources of fire-related information. Although the active fire data will be biased as it only documents fires which are active and unobscured by cloud or smoke at the time of the satellite overpass, it still provides a valuable information source. Few studies have characterised these biases due to a lack information quantifying burned areas over large regions and multiple years. Section 6.2.1 has investigated the relationship between daily MODIS Terra and Aqua 1km active fire detections and the 500m burned area dataset developed during the current research. The result of this analysis highlight the nonlinear nature of this relationship, with the active fire count per area burned varying both spatially and temporally. In addition the temporal variability of this relationship has a diurnal as well as a seasonal dependence. These diurnal, seasonal and interannual variations in the active fire count per area burned have implications for studies that use spatially or temporally limited scaling factors to extrapolate between active fire detections and the area burned. In particular the extrapolation from active fire counts to the area burned for the purpose of emissions calculations will introduce significant biases into the results if appropriate scaling factors are not applied.

The daily burned area dataset produced according to the methods described in the previous chapters has been compared to two additional sources of information. The SAFARI 2000 500m burned areas have been produced using the method of Roy *et al.* (2002) described in Section 4.3. While approximately 30% of the areas documented as burned within the SAFARI 2000 June dataset have *not* been identified as burned using the method developed in this thesis, the converse is also true with approximately 30% of these *not* mapped by the method of Roy *et al.* (2002). In addition to differences in the algorithms and wavebands used in the creation of these two datasets these disagreements may in part be due to differences in the input data as well as positional errors. Comparisons of the results produced using different change detection techniques may be performed more accurately by applying the different methodologies to the same data source, thereby excluding omission or commission errors which may arise due to the data as opposed to the results.

The second source of burned area information used in the analysis presented in this chapter is the monthly GBA2000 1km product. In contrast to the SAFARI 2000 burned areas this product

has been produced using a different source of moderate spatial resolution satellite data (SPOT-VGT as opposed to MODIS) and a very different change detection approach. Comparison of the two datasets indicates lower errors of omission than for the SAFARI 2000 burned areas, with a large proportion of these at the tail ends of the fire season occurring due to the misclassification of flood events as burns in the GBA2000 data. In contrast higher errors of commission are exhibited with over 60% of areas identified as burned according to the temporal BRDF model-based approach developed in this thesis *not* identified as burned in the GBA2000 product. This may be partially due to positional errors as well as differences in the spatial resolution of the two datasets. Although the contribution of commissional or omissional errors to the differences in these datasets are unknown as none of them have been systematically validated, the temporal change detection model developed in the previous chapters should theoretically provide a clearer definition of the remote sensing change signal. This is due to the incorporation of both the temporal and the angular model into the change detection approach. Both of these allow for the identification of subtle changes as well as better identification of these in the presence of missing or noisy data.

The burned area datasets developed in the previous chapters are analysed further in Chapter 7. The daily burned area information for the five annual fire seasons is used to investigate the spatial and temporal variability in the area burned within the area of interest during this time.

Chapter 7

Characterisation of the fire regime

7.1 The fire regime

Fire is an essential ecological factor in southern African ecosystems. It can also be one of the major causes of ecosystem degradation (Ruiz-Gallardo *et al.* 2004). An understanding of the disturbance history of an area is thus of importance in the sustainable management of resources. The characterisation of a fire regime is indispensable to land management as it portrays important features of wildland fire, such as severity, intensity and pattern across a landscape, which serve as important reference for future treatment activities (Keane *et al.* 2003). In particular as the occurrence of fire is one of the only determinants of savanna ecosystems which can be easily manipulated, it is an important variable in the management of these areas (Frost and Robertson 1985). Detailed information relating to the spatial and temporal characteristics (as well as the intensity and type) of fires within an ecosystem form important inputs to the fire management policy of a region. Fire suppression in ecosystems which are dependent on fire such as African savannas may result in previously adapted plants no longer adapted to the new regime (Thonicke *et al.* 2001). In addition while fire suppression policies have been shown to reduce the number of medium to large-scale fires the subsequent changes in the vegetation patterns have resulted in feedbacks to fire regimes with an increase in the occurrence of large-scale stand replacing fires due to higher fuel loads and changes in fuel arrangement (Stocks 1991, Brown *et al.* 1999). Fire suppression in ecosystems which are adapted to fire has also been shown to result in a decrease in biological diversity with a loss of up to 50% of plant species, with even greater species loss occurring when fire suppression leads to a complete biome switch such as from savanna to forest (Peterson and Reich 2001, Uys 2004). In contrast therefore prescribed burning is frequently used in southern Africa as a land management and fire prevention tool. Changes in the components of a fire regime such as the frequency of fires or their spatial patterning may however result in vegetation phases that comprise unstable landscape patterns which may not have enough time to equilibrate to these shifts (Brown *et al.* 1999). Although prescribed burning is a viable treatment alternative to reduce the potential for severe fires (Keane *et al.* 2001), its successful implementation clearly requires a thorough understanding of the fire regime of an ecosystem.

An understanding of the fire regime is not only of importance for the successful management of a region, as discussed in Section 1.1.1 detailed characterisation of the spatial and temporal dis-

tribution of fire is a prerequisite for understanding and monitoring carbon dynamics at a regional to global scale. Due to the impact of fires on the structure and functioning of an ecosystem the fire regime of an area will determine the quantities of emissions released as a result of burning, as well as the sequestration of carbon by the post-fire vegetation. The plant species composition within an ecosystem will be determined by both the timing of burning and the interval between recurrent fires. In semi-arid and arid grasslands for example the timing of burning will determine the assemblage of C_3 and C_4 grasses while the time which elapses between successive fires will determine the invasion of woody plants (Bragg 1995). In addition within ecosystems with poor nutrient stores such as African savanna, changes which occur to a fire regime may result in an overall loss of nutrients within the ecosystem (Thonicke *et al.* 2001). Thus while under a stable fire regime (i.e. with steady fire frequency conditions) the majority of carbon released due to burning will return to the land via vegetation regrowth, a changing fire regime may have large impacts on the overall ecosystem dynamics and the ability of the vegetation to sequester carbon (Amiro 2001, Candell *et al.* 2004). A temporal trend of increasing combustion will generate a net source of carbon, while a decreasing combustion trend will cause a sink (Chen *et al.* 2000). The characterisation of present and past fire regimes is thus of importance in understanding the current interactions of the carbon-climate-human system as well as for future predictions under various global change scenarios.

The term *fire regime* is typically used to characterise the pattern of fires within an area as a function of time and space. Initially defined by Gill (1975) numerous definitions have subsequently been put forward as to what constitutes a fire regime (Sousa 1984, Frost and Robertson 1985, Christensen 1993). The original definition of Gill (1975) used four main components to describe a fire regime; fire intensity, spatial extent, frequency and seasonality. Christensen (1993) also includes predictability as a component of a fire regime, while the definition of Frost and Robertson (1985) incorporates the type of fire and Bond and Keeley (2005) include fuel consumption and patterns of fire spread. The factors which contribute to the fire regime of an area and the complex interactions between the elements of a fire regime are displayed in Figure 7.1. The aim of the following sections is to characterise the fire regime of the southern African study area as a function of both time and space using the outputs from the change detection models presented in the previous chapter, and to investigate the interactions between the elements of the fire regime highlighted (in red) in Figure 7.1 and the vegetated surface.

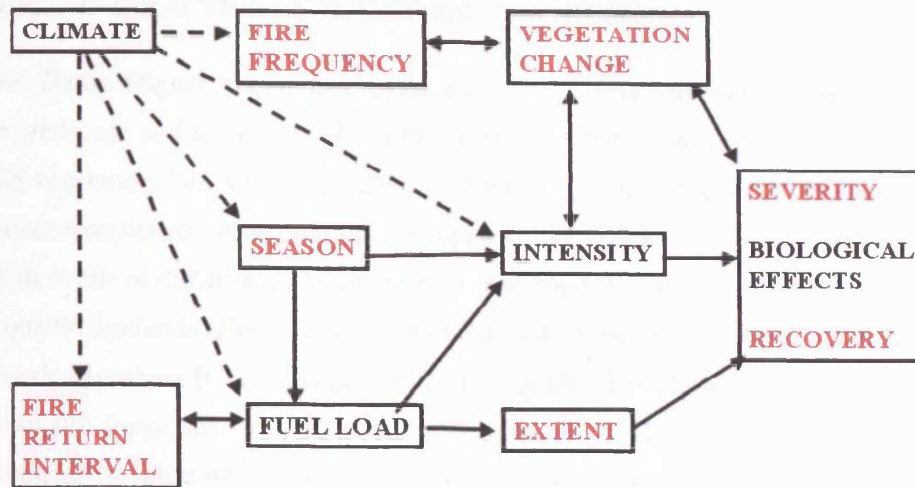


Figure 7.1: The determinants and components of a fire regime. Adapted from Diaz-Delgado *et al.* (2004)

7.2 The fire frequency

The fire frequency describes how often an area burns and is defined as the number of events per unit time. It will have an affect not only on the characteristics of an ecosystem but will also determine the quantities of gaseous and particulate emissions released due to burning. Diaz-Delgado *et al.* (2004) describe fire frequency as one of the most important patterns characterising fire regimes irrespective of the ecosystem type, as it enables the identification of recurrent burning thereby assisting the formulation of appropriate management plans. Fire recurrence will determine both the species diversity and composition within an ecosystem as it affects plant survival probability and thus determines the time available for plants to reach maturity (Diaz-Delgado *et al.* 2004). Single fires will generally have less of an effect on an ecosystem than a succession of fires (Frost 1999), and under a changing fire regime with an increasing fire frequency plants will have less time to recover between subsequent fire events. In addition ecosystems which are affected by recurrent burning will be characterised by soils with a low nutrient status (Eva and Lambin 2000). The impact of fire frequency on soil carbon pools has been investigated at a savanna site in southern Africa, with areas of low frequency burning (every five years) exhibiting an increase in soil carbon accumulation of approximately 10% while areas of high frequency (annual) burning exhibiting a decrease in carbon accumulation of approximately 10%

(Bird *et al.* 2000). Higher frequency fires have also been shown to result in greater heterogeneity of the landscape and a wider range in fire intensities due to the faster regrowth of the more flammable vegetation (Slocum *et al.* 2002). The effect of fire frequency on species diversity varies across ecosystems. Although theory suggests that species richness should be greatest at intermediate levels of disturbance, plant diversity has been shown to increase with fire frequency in the Scottish Highlands (Hobbs *et al.* 1984) but to decrease with increasing fire frequency in North American prairies (Collins *et al.* 1995). Few studies have however attempted to quantify the effect of fire frequency on species richness in southern African ecosystems, with variable results produced by those which have (Schwilk *et al.* 1997, Uys 2004).

As the frequency of fire occurrence is highly sensitive to meteorological conditions it is likely that it will change quickly under a changing climate (Hoffmann *et al.* 2002). Simulations of a Global Circulation Model (GCM) conducted by Hoffmann *et al.* (2002) identify a positive feedback loop with the clearance of tropical savannas resulting in a warmer and drier climate with accelerated fire frequencies and further loss of tree cover, with a complete clearance of savanna increasing fire frequency by up to 42%. Even under regimes where the majority of fires are started anthropogenically climate will still largely determine the fire frequency as meteorological conditions and the nature of the fuel load will influence the fire rate of spread and the total area burned (Barbosa *et al.* 1999, Hoffmann *et al.* 2002). An understanding of the fire frequency of an ecosystem is therefore not only of importance in the management of that ecosystem, but in predicting future climates and vegetation properties (Hoffmann *et al.* 2002). While fire regime models are typically used to evaluate the influence of a fire regime on ecosystem dynamics, such models require a definition of the fire frequency (as well as size distribution) as inputs (Li *et al.* 1999). The robust application of fire regime models and their use in gaining an understanding of landscape dynamics is therefore dependent on the accurate characterisation of the spatial and temporal occurrence of burning within an ecosystem.

Measurements of fire frequency have typically followed one of two approaches; the analysis of point frequencies or area frequencies. The reconstruction of fire histories prior to the satellite era and the availability of spatially explicit data have involved the use of point frequency information. Point frequencies assess fire occurrence at single locations using data such as tree ring scars (Swetnam *et al.* 1990, Buechling and Baker 2004). In contrast area frequencies assess fire occurrence at a landscape scale through the use of spatially continuous data. Studies based on

area frequencies have been performed using satellite data of burned areas (Diaz-Delgado *et al.* 2004) or compilations (“fire atlases”) of mapped observations of past fires (Rollins *et al.* 2001).

Characterisations of the frequency of fire occurrence have been performed at a variety of spatial and temporal scales and across different ecosystem types. Measurements of historical fire frequencies (for the past 800 years) have been reconstructed from fire scarred trees and inferred from forest stand ages in a pine forest in central Colorado (Brown *et al.* 1999), and using charcoal, pollen and peat macrofossil records for the last 1200 years for southern Patagonia (Huber and Markgraf 2003). Fire regimes and fire frequencies during the past decade have been determined using prescribed burning in the Everglades National Park in Florida (Slocum *et al.* 2002), at an individual country level using various satellite data (AVHRR, Landsat and SPOT) over a four year (1989-92) period as well as globally from a years worth (April 1992 - March 1993) of single source satellite data (Dwyer *et al.* 1999). An alternative approach has involved the inference of past fire events using fire frequency models. Diaz-Delgado *et al.* (2004) have applied three different fire frequency models using burned area maps of a region of north eastern Spain produced from remote sensing data as an ancillary data source for the period 1975-1993. The characterisation of the fire frequencies of the current study area is performed using the spatially explicit data described in the preceding chapters, with each 500m pixel considered as an individual burn/no-burn event.

7.2.1 Fire frequencies in southern Africa, 2000-2004

As daily burned area information is available the frequency of fire occurrence is investigated not only at the temporal resolution of a single fire season, but additionally within each of the five annual fire seasons. Table 7.1 contains the proportion of each cover type which burns at least once during each annual fire season. Pixels which have burned more than once correspond to areas where burning was identified on more than one date with a time interval of at least 7 days in between the observations. This temporal constraint was implemented in order to exclude pixels which were labelled as burns in consecutive months due to the timing of burning. Thus in the case of a burn event beginning at a pixel location at the end of one month and continuing at the same location during the beginning of the next month and therefore documented in each of the monthly burned area maps, it will only be counted as a single event.

	2000	2001	2002	2003	2004
1	84.1	86.6	85.8	86.5	87.4
2	13.8	12.2	12.4	12.0	11.2
3	1.8	1.1	1.6	1.3	1.2

(a)Additive temporal model

	2000	2001	2002	2003	2004
1	84.7	87.2	86.7	86.8	87.1
2	13.8	11.9	11.9	12.2	12.0
3	1.4	0.8	1.1	0.9	0.9

(b)Multiplicative temporal model

Table 7.1: Percentage of total area burned which burn between one and three times during a single fire season

It is immediately apparent from the data displayed in Table 7.1 that a relatively large percentage of areas which burn each year do so more than once during each annual fire season, with between approximately 12 and 15% of burn locations burning at least twice in a single annual fire season. The number of 500m pixels which this equates to is documented in Appendix D. The lowest number of multiple events has occurred in 2004, with a higher percentage of locations burning only once during the eight months of the 2004 burn season. The spatial distribution of burning and the relationship between the area burned and land cover type is investigated in Section 7.3. However as the purpose of this section is to characterise the frequency of burning, the percentage of each land cover type which burns more than once during any of the five annual burn seasons is documented in Table 7.2. Although croplands only account for 0.9% of the study area (see Section 3.3) they are included in Table 7.2 for interest as a substantially larger proportion of this cover type exhibits multiple burn events during a single fire season, in comparison to the five main cover types of the region. This is likely to be due to agricultural practices with land burned initially to prepare it for cultivation and subsequently to remove crop residues. Of the remaining five cover types which together constitute over 90% of the study area, the highest occurrence of multiple burning during a single fire season is exhibited by areas of woody savanna.

The fire frequency is defined here as the number of fire events which have occurred at each pixel location over the 5 year period, and is documented in Table 7.3 for the entire study area, and in Table 7.4 as a function of land cover type. As the results of the two models are typically very similar only the multiplicative model results are displayed. The results from the additive model can be found in Appendix E. Figure 7.2 shows the frequency of burning within each of the five main cover types over the five year period of observation. The results contained in Table 7.3 indicate that while approximately 21% of the land surface within the study area has burned only

Additive results	2000	2001	2002	2003	2004
Deciduous broadleaf	4.8	3.7	3.4	3.8	3.3
Open shrubland	2.3	2.0	2.0	1.8	1.9
Woody savanna	7.2	5.5	5.7	5.9	5.5
Savanna	4.3	3.3	3.9	3.3	3.1
Grassland	3.3	2.4	3.1	2.9	2.7
Cropland	8.5	6.3	9.6	6.2	6.3
Multiplicative results	2000	2001	2002	2003	2004
Deciduous broadleaf	4.8	3.6	3.3	4.0	4.2
Open shrubland	2.1	1.7	1.6	1.7	1.7
Woody savanna	7.3	5.3	5.4	6.0	5.8
Savanna	4.4	3.3	3.7	3.5	3.5
Grassland	2.7	1.9	2.6	2.7	2.5
Cropland	6.5	4.6	6.7	4.7	5.2

Table 7.2: Percentage of each land cover type which burns more than once in a single fire season

once between the beginning of April 2000 and the end of November 2004, approximately 40% has burned more than once during this five year period. In addition over 6% of the land surface (6.2% equates to an area of 131420 km²) has burned every year during the five year period of observation. These data (Table 7.4 and Figure 7.2) show that the distribution of fire frequencies

Frequency	Additive	Multiplicative
1	21.5	21.4
2	14.5	14.9
3	10.8	11.3
4	8.3	8.7
5	6.1	5.8

Table 7.3: Fire frequency across the study area: Percentage of land surface which burns between one and five times during the five year period

is not uniform across the different vegetation types. It is evident that a lower proportion of grasslands and open shrublands are subjected to burning over the five year period in comparison to the remaining three cover types. In addition a higher proportion of these two ecosystems burn only once during the five year period in comparison to the other three vegetation types which exhibit a

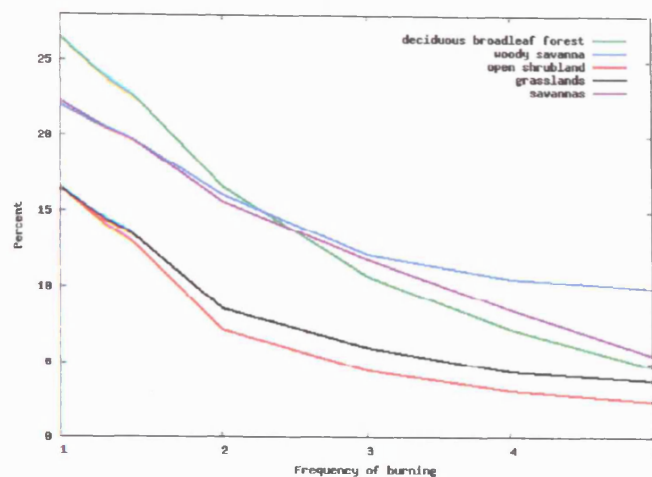


Figure 7.2: Fire frequency: Proportion of each cover type which burns more than once between 2000-2004

higher frequency of burning. This is discussed in more detail in Section 7.4 as a spatial aspect of the fire regime. In terms of the fire frequency, woody savannas exhibit the highest occurrence of recurrent burning with approximately 10% of this cover class (and approximately 13% of all burn locations) burning each year during the five year period. In contrast open shrublands exhibit the lowest fire frequencies with less than 3% burning five times during the five years. The reason for the higher fire frequencies in woody savannas is likely to be due to the vegetation composition within and the effect of fire on this ecosystem. Frequent low intensity fires can transform areas of woodland into open grassy savannas with only isolated fire-tolerant canopy trees and scattered understorey trees and shrubs, encouraging the regrowth of flammable vegetation and suppressing the regrowth of woody plants and preventing their recruitment into the canopy (Frost 1999). The higher fire frequency observed in woody savanna ecosystems may thus be a function of (i) the nature of the fire with frequent low intensity fires destroying only the herbaceous understorey layer, and (ii) the fast recovery of the post-fire surface. Both of these will result in higher fuel loads available for burning each year. In contrast in grassland ecosystems, for example, even low intensity fires may be more destructive to the vegetation than in ecosystems with a higher woody plant density. The latter two points are supported by the data presented in Table 3.8 Section 3.6.2 describing the persistence of the MODIS burn signal. It is evident from these data that areas of woody savanna exhibit a burn signal of a considerably lower duration than areas of grassland,

open shrubland or savanna. In addition within 7 days woody savanna ecosystems exhibit a faster recovery with reflectance levels closer to pre burn levels than the other cover classes, suggesting rapid regeneration of the vegetation and recovery of the post-fire surface. In contrast while a similar proportional change is observed in the MODIS (band 2) signal for grassland and woody savanna ecosystems immediately after the fire, in contrast to woody savannas a significant signal is still evident for grasslands 14 days after the fire, suggesting a higher level of destruction and a slower recovery of this ecosystem.

Land cover	Frequency	Proportion of total	Proportion of burns
Deciduous broadleaf forest	1	26.5	37.7
	2	16.9	26.0
	3	11.0	17.6
	4	7.4	11.8
	5	4.7	6.9
Open Shrubland	1	16.1	48.3
	2	7.2	21.6
	3	4.6	13.9
	4	3.3	9.8
	5	2.4	6.4
Woody Savanna	1	22.1	30.0
	2	16.3	23.4
	3	12.5	18.3
	4	10.8	15.5
	5	9.6	12.8
Savanna	1	22.4	34.02
	2	15.8	24.6
	3	12.1	19.2
	4	8.8	14.2
	5	5.3	8.0
Grassland	1	16.3	40.8
	2	8.6	21.4
	3	6.2	16.5
	4	4.6	12.4
	5	3.7	9.0

Table 7.4: Fire frequency across the study area: Percentage of each land cover type which burns between one and five times during the five year period: Multiplicative model results

The spatial distribution of fire frequencies across the study area (calculated from the multiplicative model results) is displayed in Figure 7.3. It is clear from Figure 7.3 that the areas which burn every year have a distinct spatial distribution, with a larger proportion of high fire frequency pixels in northern Angola and in central and north eastern Zambia. In contrast lower fire frequencies are evident in the Namibian, Botswanan and Zimbabwean portions of the area of interest. Two areas of 250km by 500km have been extracted from western and eastern Angola in order to demonstrate the level of detail and the spatial patterns of the fire frequency information. The locations of these are documented in Table A.1 and Figure A.1 in Appendix A as Site 7A and Site 7B. The red pixels thus represent areas which have a fire frequency of 5 and have burned during each of the five consecutive fire seasons. The spatial contiguity of the fire frequencies is emphasized and it is noted that no spatial operations have been performed in the creation of these results. Figure 7.5 displays the land cover classes for Sites 7A and 7B respectively, while Figure 7.6 displays a digital elevation model (DEM) for the two locations. The elevation data has been collected by a Spaceborne Imaging Radar (SIR-C) and dual X-band Synthetic Aperture Radar (X-SAR) as part of the Shuttle Radar Topography Mission (USGS 2006). The spatial resolution of the data is approximately 90m, with a vertical resolution of 1m.

The areas of high frequency burning within the site displayed in Figure 7.4a form an interesting spatial pattern which is likely to be a function of the vegetation type and composition as well as the topography. The vegetation type within the area is predominantly open shrublands, woody savanna and broadleaf forest, with the areas which have not burned (black) or have only burned once during the five year period (dark blue) corresponding to forested areas. The vertical lines and the tendrils of high frequency burning evident in Figure 7.4a thus correspond to areas of less dense vegetation located between areas of higher density vegetation. A visual examination of the topography of this region suggests that the areas of higher frequency burning (and less dense vegetation) correspond to the areas of lower altitude. The second site (Figure 7.4b) exhibits an area of high frequency burning to the west and an area of low frequency burning to the east. The western portion of the site is predominantly woody savannas, savannas and grasslands, while the eastern section is dominated by broadleaf forests. The areas of low frequency burning located within the areas of high frequency burning in the western half of the area correspond to patches of broadleaf forest which are surrounded by grasslands and savannas. A visual examination of the topography of the areas with less dense vegetation and a higher frequency of burning within

the western section of the region indicates that this area is both lower and flatter than the eastern half of the region.

The relationship between the fire frequency and vegetation type within the area of interest is investigated further through the characterisation of the fire return interval, which forms an additional component of the fire regime. This is discussed in the following section.

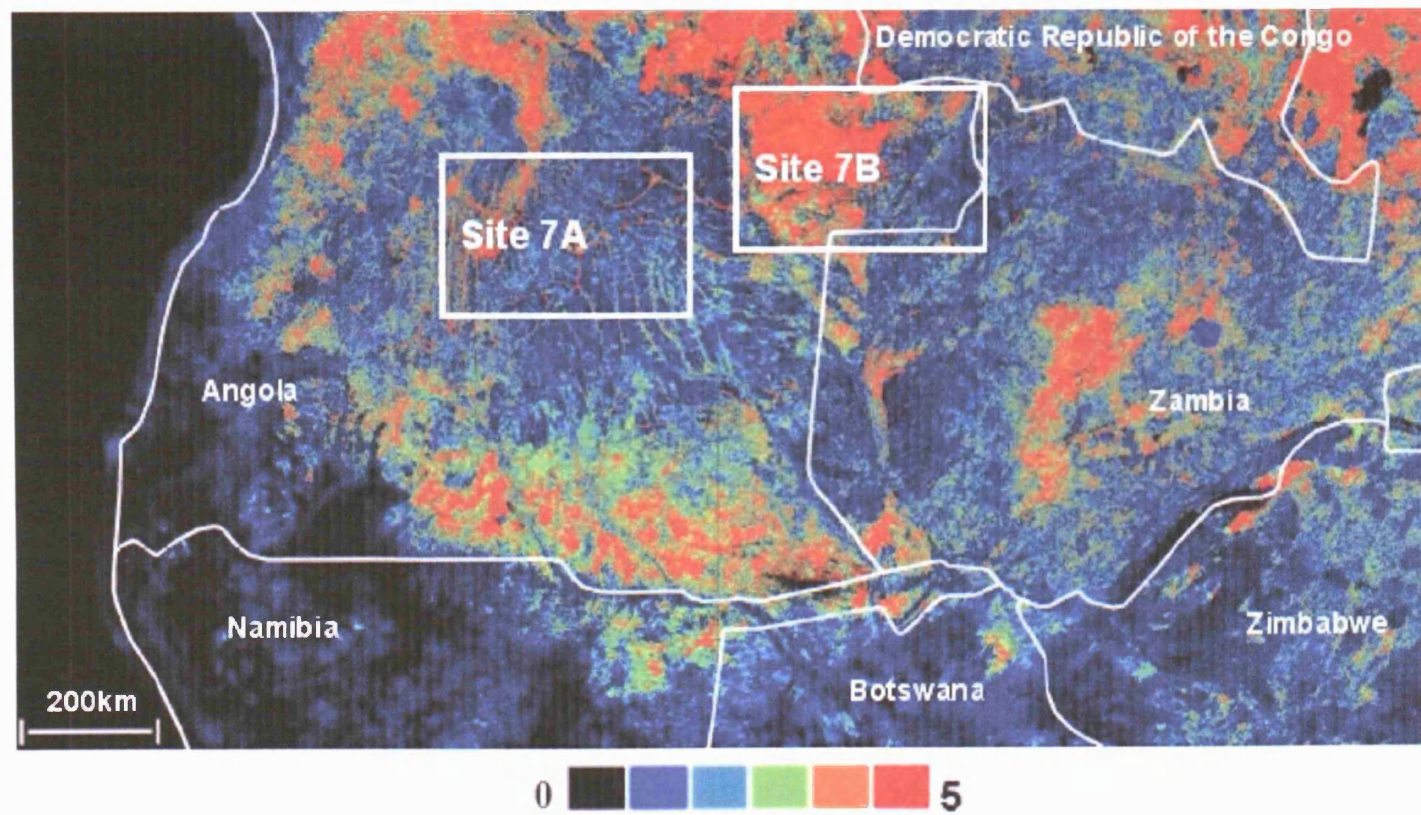
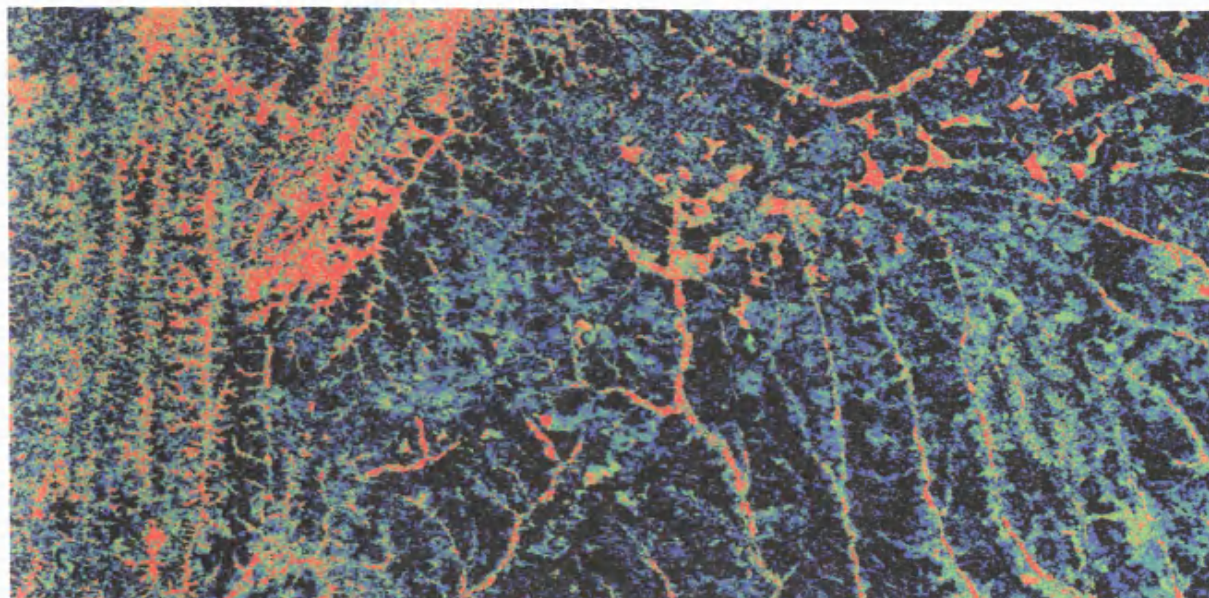


Figure 7.3: Fire frequency (2000-2004): Multiplicative model results



(a) Site 7A (Angola)

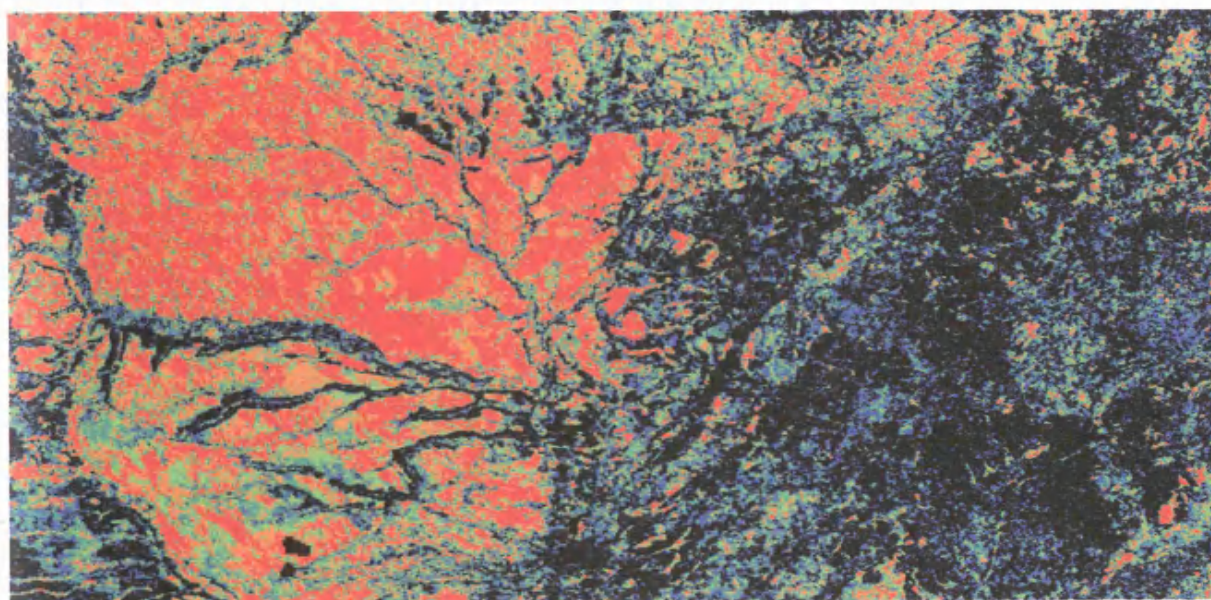
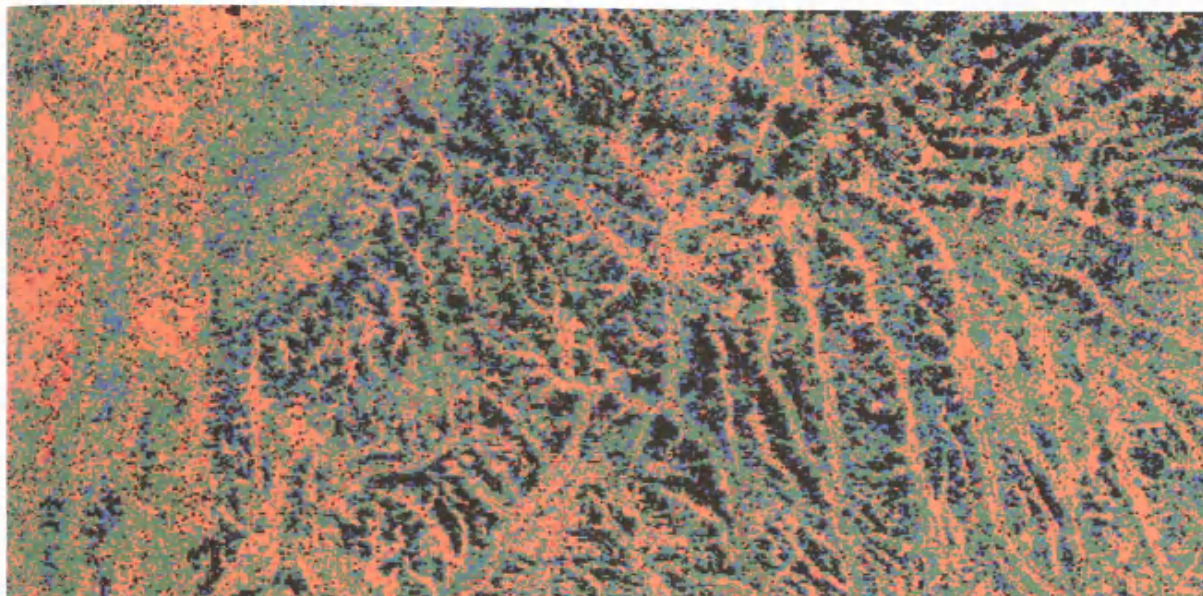


Figure 7.4: (b) Site 7B (Angola): Fire frequency (2000-2004): Multiplicative model results



(a) Site 7A (Angola)

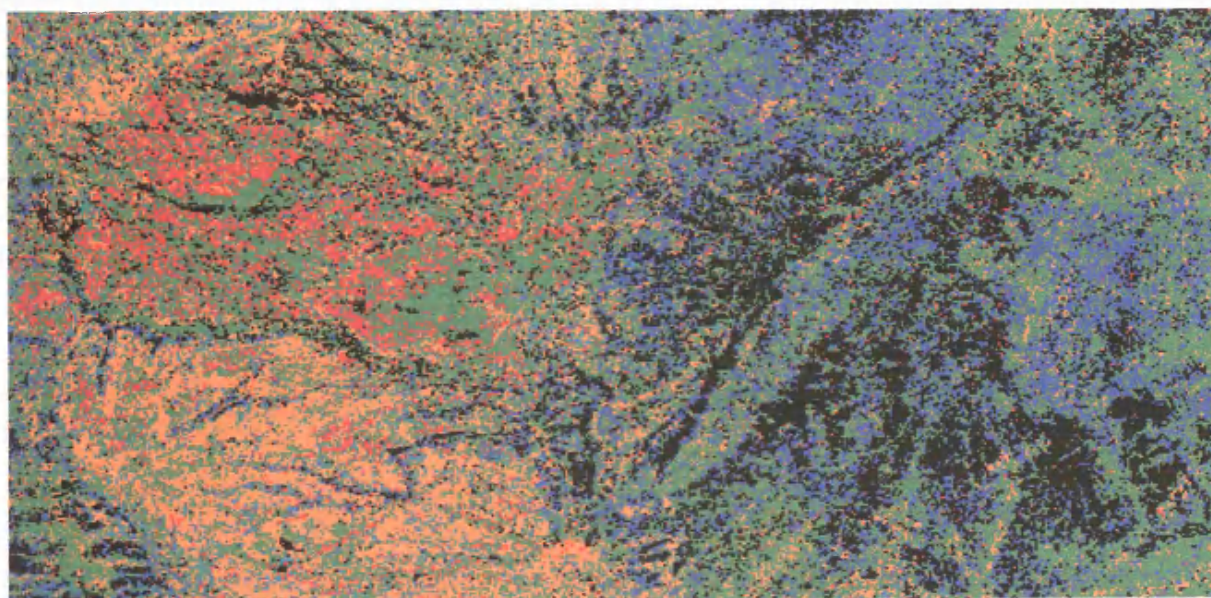
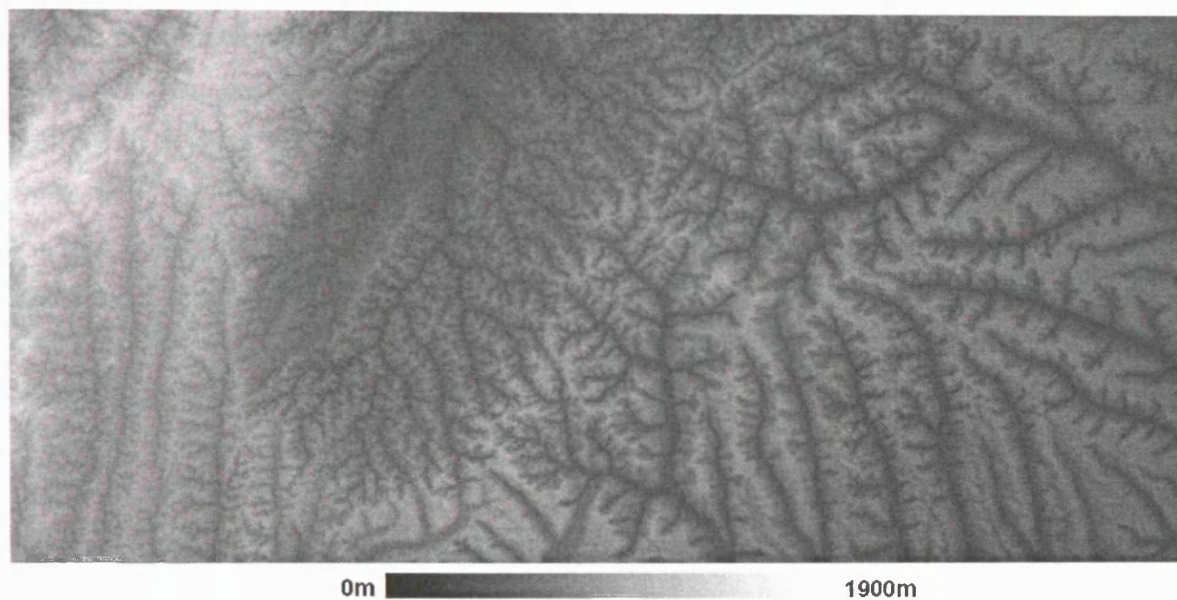
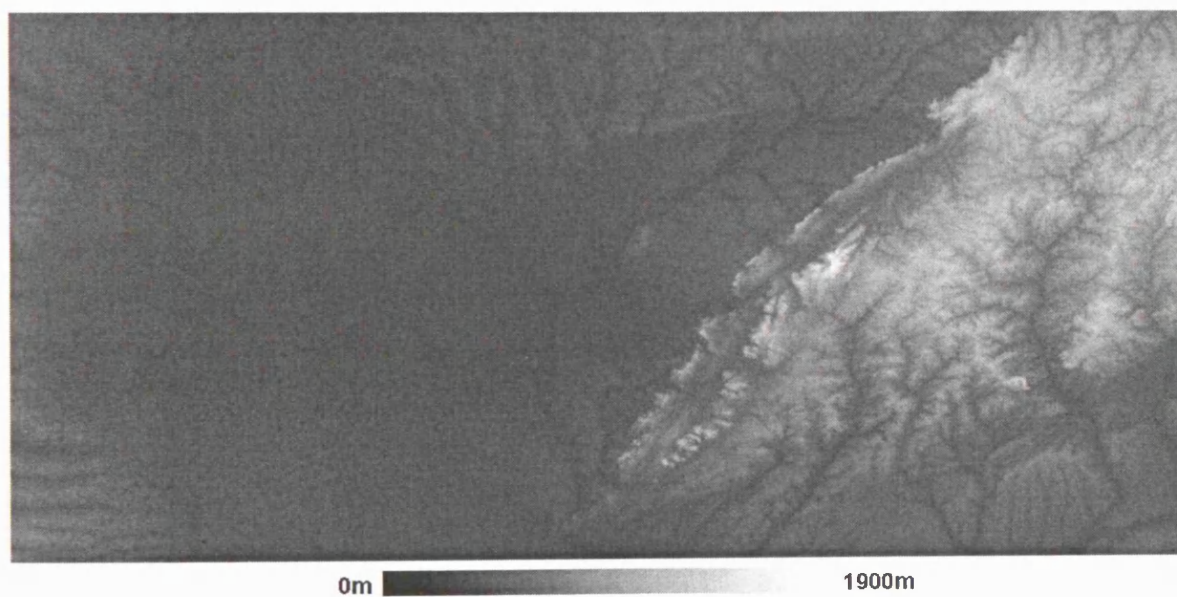


Figure 7.5: (b) Site 7B (Angola): Land cover



(a) Site 7A (Angola): Topography



(b) Site 7B (Angola): Topography

Figure 7.6: Digital Elevation Model, (Source: USGS 2006)

7.2.2 Fire return intervals

The fire return interval is related to the fire frequency and provides an indication of how often an area could burn, or the time expected before it will burn again. The impact of the frequency of burning on the structure, composition and dynamics of an ecosystem as well as on gaseous emissions due to burning is discussed in the previous section. In particular under a warming climate, changes in the fire return interval of a region can have a large effect on carbon sequestration, vegetation health and ecosystem sustainability (Kasischke *et al.* 1995). Minimal research exists characterising the recent fire frequency or fire return interval within southern African ecosystems. Although Barbosa *et al.* (1999) have mapped burned areas for the whole of Africa over three years during the period 1981-1991 this has been performed at a spatial resolution of 5km and over non-consecutive fire seasons. In contrast the GBA2000 product (Gregoire *et al.* 2003) documents areas burned at a spatial resolution of 1km, but only for the year 2000. Investigations into the fire return intervals within southern African ecosystems have typically been performed across a limited spatial area using fire records (Van der Werf *et al.* 2004), or simulated at a regional scale using a fire model (Thonicke *et al.* 2001). Frost (1999) describes the return interval of southern African savanna fires as 2-3 years, but notes that there are almost no data to support this. The following section thus characterises the fire return intervals within the study area over the past five years, at a spatial resolution of approximately 500m.

The fire return interval (FRI) is defined here as the mean number of months between successive fire events during the five year (2000-2004) period. The mean FRI calculated across the entire land area within the region of interest as a proportion of the total number of burn pixels is displayed in Figure 7.7 with the vertical black lines corresponding to yearly intervals. Only locations with a mean FRI of less than 56 months (i.e. which have burned more than once during the five years) are shown. The fire frequency information presented in the previous section (Table 7.3) indicated that approximately 40% of the land surface within the study area burned more than once during the past 5 years. The mean FRI across the study area (Figure 7.7) has four distinct peaks with fires recurring after 12, 24, 36 and 48 months, and two less distinct peaks at 16 and 18 months. The distributions of the FRI becomes wider as the time which has elapsed between successive fires increases. The data suggest that the mean time interval between successive fires is extremely consistent across the study area, with areas which burned during each year of observa-

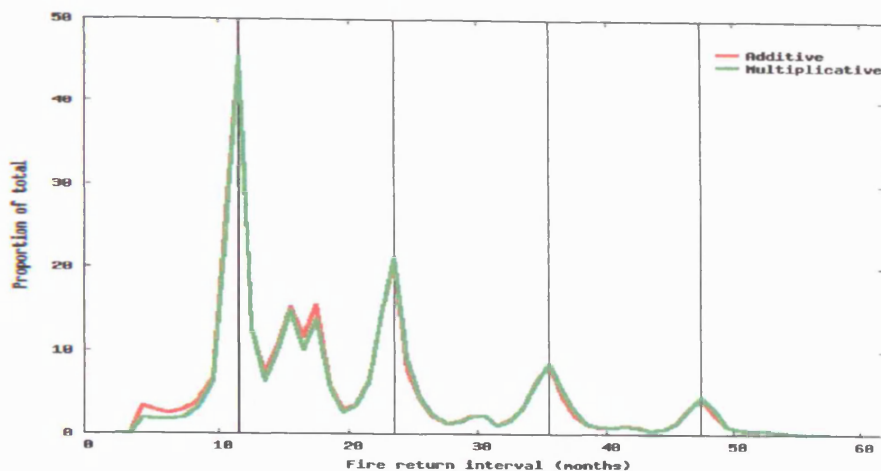


Figure 7.7: Mean fire return intervals (2000-2004)

tion (a fire frequency of 5) exhibiting a mean return interval of exactly one year. The implication of this information is that the fire regime of the area has been stable over the past five years and has a high degree of spatial consistency, with most of the areas which burned every year doing so at the same time each year. Under the assumption that the fire regime within the area is largely anthropogenically driven, then it may be that fires are started at a similar time each year for the same purpose, be it agricultural or for improving forage quality. As the fire frequency is highly sensitive to meteorological conditions which will determine the fuel loads available as well as their ignition potential, any interannual variations in climate would be expected to have an impact on the fire frequency and thus the FRI. The variability in FRIs within the Kruger National Park in South Africa between 1957 and 2002 have, for example, been shown to be strongly influenced by variations in the annual rainfall rather than by management approaches (Van der Werf *et al.* 2004). The mean FRI results displayed in Figure 7.7 in particular for the locations which have a fire frequency of 5 indicate that in general over the five year period the locations which burn every year do so at the same time every year. This suggests that although small scale variations may have occurred during this time in general the fire conditions (i.e. climatic potential and condition and availability of fuel) have been similar each year.

The distribution of the FRIs as a function of land cover class is displayed in Figure 7.8 as a percentage of the total number of pixels within each cover type which have burned during the five years. Open shrublands have the most even distribution of FRIs. In contrast woody sa-

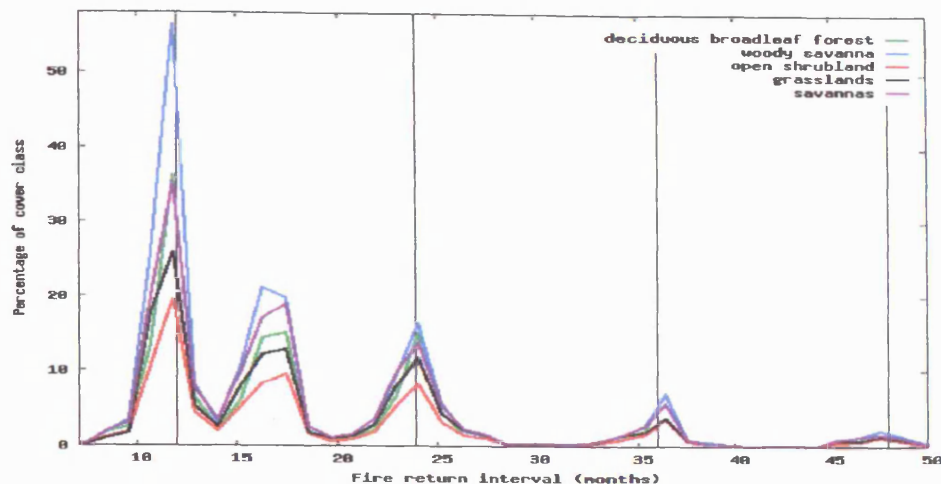


Figure 7.8: Mean fire return interval (2000-2004) as a function of land cover

vannas exhibit the most uneven distribution with a larger proportion of recurrent fires occurring at 12 month intervals than the other cover types. The reasons for this will be similar to those provided above for the higher fire frequencies observed within woody savannas. In particular in surface-fire regimes such as the savanna and grassland ecosystems of southern Africa, the fire will consume plants located in the grass layer but not trees taller than 2-4m (Bond and Keeley 2005). The affected vegetation recovers quickly through sprouting and thus while frequent fires may reduce the height of the dominant plants they do not necessarily reduce canopy photosynthesis (*ibid*). Fires are thus less destructive to ecosystems such as woody savannas than for example, grasslands, and the rate of recovery may therefore be faster. Alternately the higher FRIs observed in woody savannas may be due to land cover practices and the burning of the vegetation for cultivation. However in the absence of information relating to land cover practices in the area and over the time period of interest it is only possible to speculate as to the possible causes of the observed patterns in the frequency and time intervals between recurrent fires. As discussed the frequency of fire occurrence and the length of time which elapses between recurrent fires will be dependent on a variety of factors. In particular observed fire return intervals will be a result of interannual climatic variability, human influence and changes in vegetation dynamics over different time scales as well as the interactions of these (Thonicke *et al.* 2001).

7.3 The seasonality of burning

The season of burning is an important component of a fire regime as it will determine the effect of fires on the ecosystem as well as the ability of the ecosystem to recover. The effect of burning may be minimal to some plants while damaging the above ground components or completely destroying others. The level of destruction will depend not only on the intrinsic attributes of the plant species but also on their physiological state and the intensity and timing of the fires (Frost 1999). The intensity of burning will vary as a function of fuel type, fuel load, moisture content and the atmospheric conditions at the time of the fire (Frost and Robertson 1985). The timing as well as the frequency of burning will thus influence the intensity and patchiness of fires, and consequently the structure and composition of the vegetation (Slocum *et al.* 2002). The interactions between the characteristics of the vegetation and the components of the fire regime are displayed in Figure 7.1. As described above, within semi-arid and arid environments such as much of southern Africa the season of burning (assuming sufficient precipitation) will determine the final assemblages of C₃ and C₄ grasses, while the length of the fire return interval will determine the invasion of woody plants with frequent fires suppressing regrowth and recruitment to the canopy (Bragg 1995). The timing of burning (as well as the fire return interval) will thus determine the plant species composition through selection (Thonicke *et al.* 2001). In general dry season fires in southern Africa will have a greater effect on woody plants than grasses as the majority of these are dormant at this point, with late dry season fires always more destructive than those which occur earlier in the dry season (Frost 1999). This is because the late dry season is a period of nutrient cycling and rapid growth for woody plants. Frequent late dry season fires will transform areas of woodland into open savanna with only isolated patches of fire tolerant canopy trees and scattered understorey trees and shrubs while early dry season burning or complete suppression of fires will encourage the recruitment and growth of woody plants (Frost 1999).

The characteristics and the behaviour of the fire will also vary depending on the timing of ignition. Fuel consumption as well as the percentage of total fuels consumed, fire intensity and heat per unit area, and the fire rate of spread have all been shown to be greater in dormant as opposed to growing season fires (Sparks *et al.* 2002). An understanding of the duration and timing of burning is thus not only of importance in ecosystem management, but is an important parameter in the determination of the amount of trace gases and aerosol particles emitted from

vegetation fires (Dwyer *et al.* 2000). Fires which occur earlier in the dry season when the moisture content of the vegetation is greater will have a lower combustion completeness with a lower combustion efficiency in comparison to fires which occur later in the dry season (Hoffa *et al.* 1999). The characterisation of the temporal distribution of fire activity at a global scale as well as across southern Africa has typically been one of the more researched components of the fire regime from satellite data. At a global scale however this has only been performed across a single fire season (Cahoon *et al.* 1992, Dwyer *et al.* 2000, Gregoire *et al.* 2003), at the African continental scale across three (non-consecutive) fire seasons (Barbosa *et al.* 1999), and in southern Africa for a single fire season (Roy *et al.* 2002). The following paragraphs provide a temporal characterisation of burning (aggregated from daily data) within southern Africa over the past five years.

7.3.1 The temporal distribution of burning within the study area

The total area burned each month as a percentage of the total area burned over the eight months of the annual fire season are displayed in Figure 7.9 for each of the five years of observation. It should be noted that these data do not provide an indication of the *total* area burned annually which may vary considerably from year to year and is discussed in Section 7.4. The data displayed in Figure 7.9 are instead intended to provide a characterisation of the distribution of burning across each annual fire season as a proportion of the total area burned over the entire season. The timing of burning is similar from year to year with the greatest proportion of burn events identified in August every year except 2002. During this year the peak of burning occurred a month earlier. A higher proportion of burns also occur in April 2002 in comparison to the other four years, while conversely a lower proportion occur in November. These data therefore suggest that the burn season occurred earlier in 2002 in comparison to the other four years. The distribution of burn events over each annual burn season has also been investigated as a function of land cover type. These results are contained in Table 7.5. The general pattern of burning is similar across all of the vegetation types with a relatively uniform temporal distribution from year to year, with the highest proportion of each cover type burning between July and August during each of the five years. It should be noted that the distributions for the 2001 fire season may be affected by the lack of data for June during this year. The earlier occurrence of fires in 2002 in

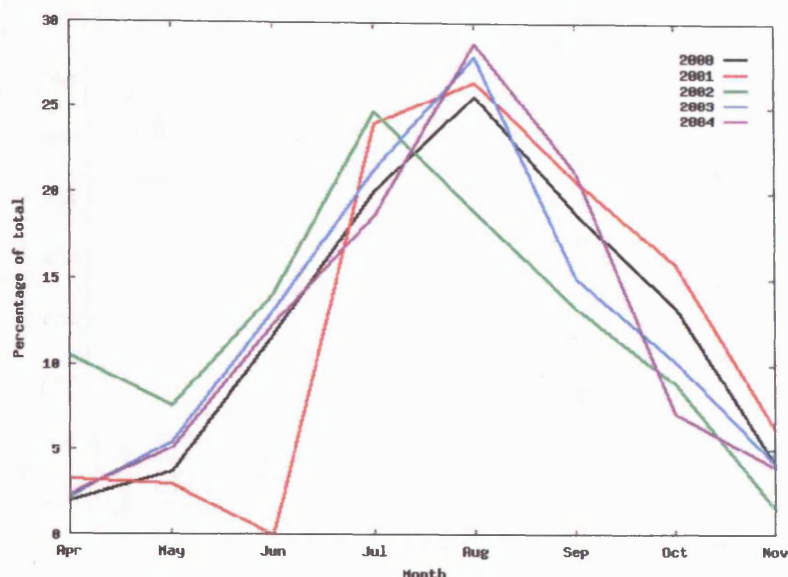


Figure 7.9: Monthly area burned as a proportion of the annual total: multiplicative model results

contrast to the other four years described above is also evident across all vegetation types.

Variations in the timing of burning such as those observed during 2002 are likely to be due to a combination of factors including the meteorological conditions and in particular the timing of the previous wet season and thus the onset of the dry season. In addition as the fire regime of southern Africa is largely driven by anthropogenic ignition sources (see Section 3.2), the temporal distribution of burning each year will be largely influenced by human activity. An examination of the spatial distribution of burning in April 2002 indicates that a greater number of fires have occurred in the eastern section of the area of interest and in particular around and to the west of the Okavango Delta in comparison to the other four years.

The reasons for the greater extent of burning observed within this region in April 2002 are unknown, and are likely to be due to a combination of the factors described above. An examination of the mean EVI data for the eastern portion of the study area for April 2000 to 2004 indicates that while the interannual variability in mean EVI values is relatively consistent between each vegetation type over the five year period, grasslands and open shrublands are much drier in April 2002 in comparison to the other years. Woody savannas and savannas also exhibit lower mean EVI values in April 2002 than in April during the other four years. An investigation into the impact of short-term rainfall fluctuations in sub-Saharan Africa on land cover change

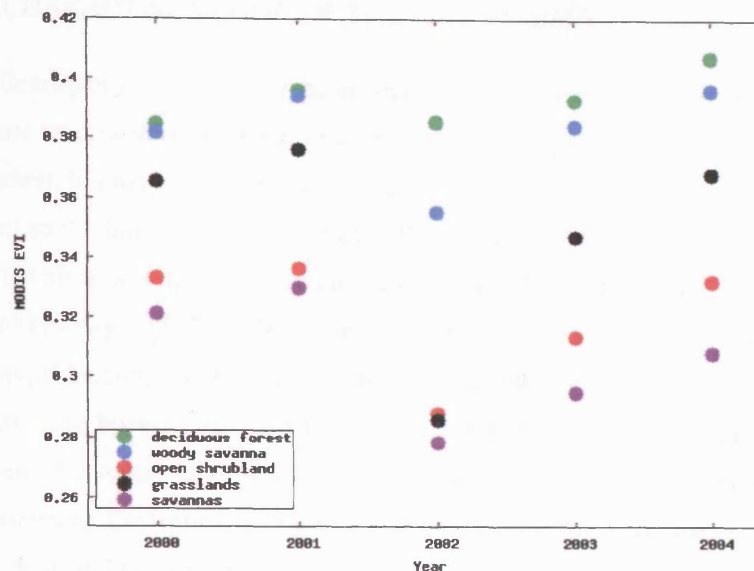


Figure 7.10: Eastern half of study area (MODIS tile “h20v10”): Mean MODIS EVI, 6th April 2000-2004

for the two year period October 2000 to 2002 has indicated that although the magnitude of land cover change during this time was significantly related to rainfall variability, the response of the vegetation to variations in precipitation was dependent on the phenology, morphology and physiology of the prevailing species (Vanacker *et al.* 2005). Grasslands and shrublands were found to be particularly sensitive to short-term rainfall fluctuations, with over a quarter of the variation in the magnitude of land cover change within these ecosystems explained by indices of rainfall variability, while in contrast the small changes observed in forest and woodland vegetation types were not found to be strongly associated with short-term rainfall variability. Reasons for these observations include the morphology and phenology of the plant species within each ecosystem. Species within grasslands and shrublands generally extract moisture from the upper soil layer through dense but shallow root systems. and their growth cycle is closely linked to instantaneous soil moisture availability (Vanacker *et al.* 2005). In contrast tree growth is less sensitive to the frequency or duration of precipitation events due to their well-developed root systems which penetrate deeper and enable trees to hold a large amount of moisture which can be released gradually over time (Scanlon *et al.* 2002). The observed interannual variations in the temporal distribution of burning within the area of interest is therefore likely to be a complex interaction of factors including the frequency and duration of precipitation events during the previous wet season, the

conditions and flammability of the vegetation, and the prevalence of ignition sources.

Regional scale studies have shown a north to south and as well as an eastward progression of fires across southern hemisphere Africa during the fire season (Cahoon *et al.* 1992). A similar pattern is evident in the burned area results over the region of interest. Figure 7.11 displays the day of burning for all pixels identified as burn candidates during 2004. Values thus range from day 92 (1st April) to day 335 (30th November) 2004. A general north to south progression is evident in the day of burning, with locations in the north tending to burn earlier in the year than those in the south. The burning also advances eastward as the year progresses, with the eastern extent of the area of interest tending to burn later in the year than the western portion. The factors which determine the timing of burning and their interactions are displayed in Figure 7.1. In particular the seasonality of burning within southern Africa has been shown to be dependent on the levels of precipitation over the preceding two years (Van der Werf *et al.* 2004) and thus the grass fuel loads available (Trollope and Trollope 2004). The following paragraph discusses the relationship between the seasonality of burning and the time which elapses between recurrent fires.

		2000	2001	2002	2003	2004
Deciduous broadleaf forest	Apr	1.7	3.5	5.6	1.5	4.2
	May	1.8	1.4	2.7	2.5	6.7
	Jun	9.7	N/A	9.8	9.9	9.2
	Jul	25.9	27.5	32.2	28.2	23.3
	Aug	33.0	39.0	29.2	30.1	33.7
	Sep	15.0	14.1	10.7	13.4	15.5
	Oct	10.3	10.2	8.3	12.2	5.8
	Nov	2.5	4.4	1.5	2.2	1.5
Open shrubland	Apr	3.0	5.7	13.9	3.4	3.7
	May	2.8	3.8	6.4	4.5	3.8
	Jun	8.7	N/A	11.7	10.9	10.7
	Jul	16.6	19.4	22.0	18.8	17.9
	Aug	23.3	22.1	16.7	24.6	25.2
	Sep	20.2	22.5	13.6	14.4	22.2
	Oct	20.3	17.8	14.2	13.7	8.3
	Nov	5.1	8.7	1.5	9.7	8.3
Woody savanna	Apr	2.0	3.4	7.5	2.0	2.8
	May	4.6	3.3	6.9	5.6	6.7
	Jun	14.4	N/A	16.9	15.5	16.0
	Jul	23.5	29.1	26.6	24.7	21.7
	Aug	24.5	26.4	19.5	24.7	25.8
	Sep	17.2	20.4	12.6	15.5	18.5
	Oct	10.8	12.9	8.6	9.1	6.0
	Nov	2.9	4.5	1.3	2.9	2.5
Savanna	Apr	2.1	2.6	13.0	2.3	1.7
	May	3.4	2.8	8.8	5.8	3.5
	Jun	10.5	N/A	12.7	11.8	10.3
	Jul	17.4	20.3	23.1	18.8	16.7
	Aug	25.5	26.4	17.6	30.5	30.8
	Sep	20.7	22.5	14.4	15.5	24.1
	Oct	15.1	18.0	8.6	10.4	8.2
	Nov	5.2	7.4	1.9	4.9	4.7
Grassland	Apr	2.2	4.2	8.8	2.8	2.1
	May	2.7	3.4	6.6	4.8	2.9
	Jun	9.6	N/A	16.9	16.9	14.5
	Jul	18.6	24.5	27.0	19.6	17.2
	Aug	25.8	16.9	17.7	27.9	26.6
	Sep	19.6	20.5	12.7	12.2	22.4
	Oct	15.9	23.2	9.2	9.3	5.9
	Nov	5.5	7.3	1.2	6.5	8.2

Table 7.5: Percentage of total annual area burned within each cover type: Multiplicative model results

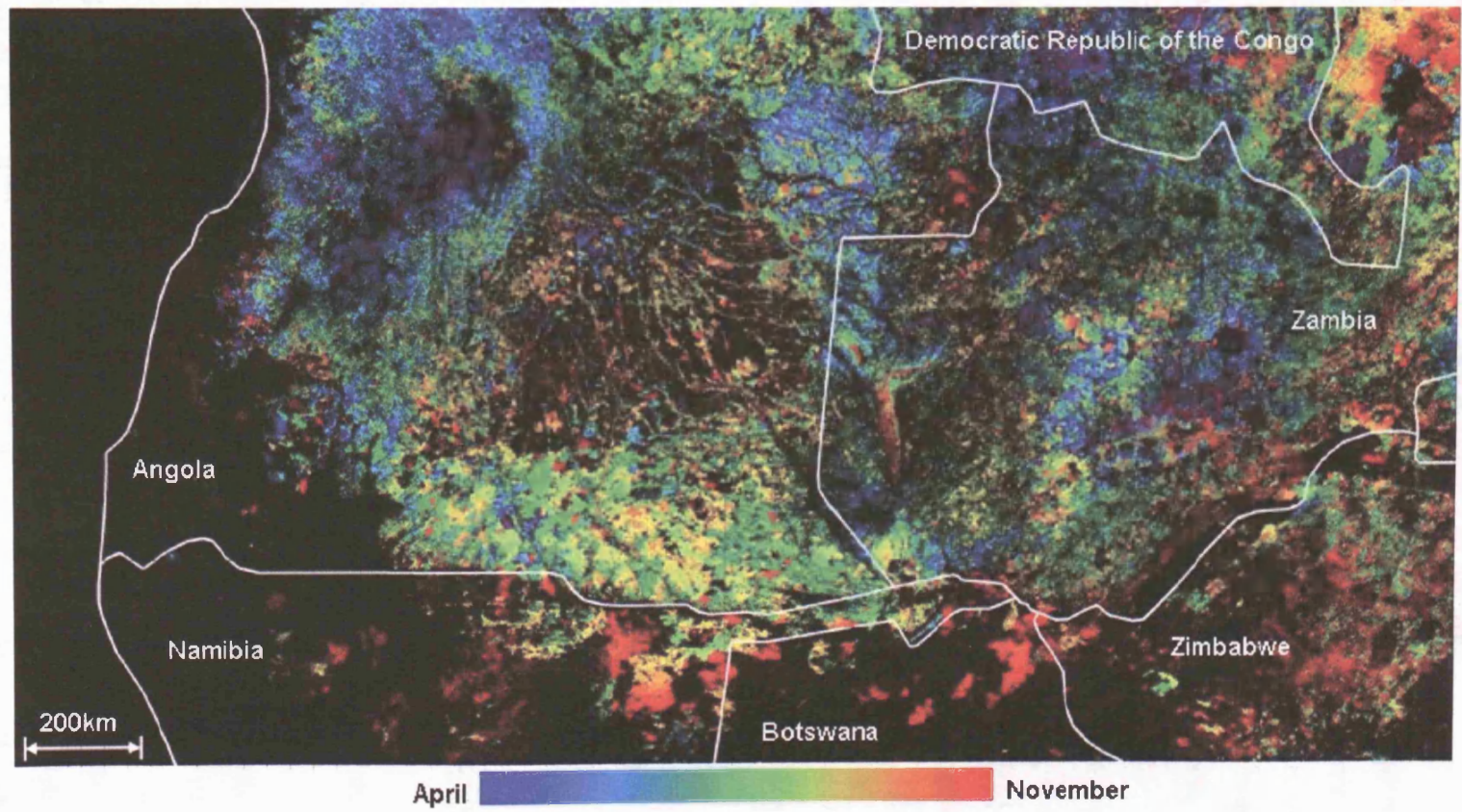


Figure 7.11: Seasonality of burning 2004: Multiplicative model results

The relationship between the timing and frequency of burning

As discussed above the effect of burning on an ecosystem will be dependent (amongst other factors, see Figure 7.1) on the timing of the fire as this will not only determine the quantity and characteristics of the available fuel loads, but also the ability of the plants to regenerate after burning. The timing of burning is thus expected to have an effect on the frequency of burning and the time which elapses between recurrent fires. This is investigated through the calculation of the mean fire return interval (see Section 7.2.2) as a function of the initial month of burning during the five year period. Figure 7.12 contains these results for all grassland pixels within the area of interest. The results are displayed as the proportion of the total number of grassland pixels identified as burning more than once during the five year period of observation. As the results are very similar for each cover type only the data for grasslands are shown. The overall

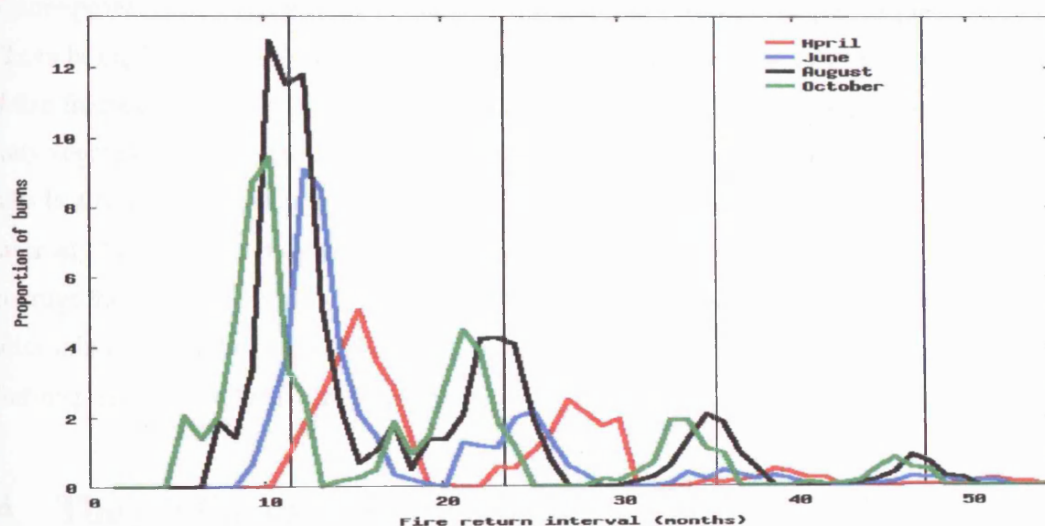


Figure 7.12: Mean fire return intervals of savanna fires as a function of the timing of initial burning

trend in the results displayed in Figure 7.12 is a decreasing mean fire return interval as the month of initial burning increases. Pixels which burn in April for the first time during the five year period of observation (2000-2004) across the entire study area exhibit mean return interval peaks at approximately 14 and 27 months. In contrast those which burn initially in June exhibit peaks at approximately 12 and 25 months, while those which burn initially during August peak at approximately 10 and 22 months. Fire return intervals are lowest at locations which burn

initially in November, with peaks at approximately 9 and 19 months. The implication of these results is that locations which burn later in the dry season have a shorter time interval between recurrent fires than those which burn earlier in the dry season. As discussed above the plant species composition within an ecosystem will be determined by both the timing of burning and the interval between recurrent fires. In grasslands the assemblage of C_3 and C_4 grasses will be determined by the timing of burning while the time which elapses between successive fires will determine the invasion of woody plants (Bragg 1995). Short fire return intervals will suppress the regrowth of woody plants, with frequent late dry season fires transforming areas of woodland into open grassy savannas with only isolated fire tolerant canopy trees and scattered understorey trees and shrubs (Frost 1999). In contrast early dry season burning favours the recruitment and the growth of woody plants (Trapnell (1959) in Frost (1999)). As grassland and savanna vegetation are more prone to widespread and frequent burning (Frost 1999) the results displayed in Figure 7.12 can be explained by the positive relationship between the occurrence of late dry season fires and fire frequency. Fires which occur later in the dry season thus have a greater effect on the woody vegetation while encouraging the regrowth of more flammable vegetation, which in turn results in a landscape more prone to frequent fires thereby exhibiting shorter fire return intervals. Conversely fires which occur earlier in the dry season are less destructive to the vegetation and encourage the growth of woody plants resulting in longer intervals between recurrent fires. The relationship between the timing of burning and the destruction to the vegetation (i.e. the severity of burning) is discussed further in Section 7.6.1.

7.4 The spatial extent of burning

The need for spatial and temporal information relating to the area burned has been discussed in Section 1.1.1. In particular quantifying the contribution of biomass burning to the global distribution of emissions of carbon into the atmosphere requires information relating to the area burned (Simon *et al.* 2004). The total area affected by fire is currently one of the parameters which provides the greatest uncertainty in the calculation of the quantity of biomass burned and the gases emitted at regional or global scales (Scholes *et al.* 1996a, Conard *et al.* 2002). In certain African countries (for example Angola and Namibia) annual estimates of the area burned at the

country level are unknown (Tansey *et al.* 2004b). Frost (1999) thus notes the lack of adequate data on the trends in the area burned annually in southern Africa. While various studies have since quantified the area burned at a continental or global scale, these have been performed at the scale of a single annual fire season (Gregoire *et al.* 2003, Simon *et al.* 2004) or across three (non-consecutive) fire seasons (Barbosa *et al.* 1999). The aim of the following paragraphs is therefore to quantify the total area burned within the area of interest over five annual fire seasons (2000-2004), as well as within each of the main vegetation types present within the study area.

7.5 Annual burned area totals

The total area burned each month across the entire area of interest is displayed in Table 7.6 for each year calculated from the multiplicative model results. The proportion of the land surface within the study area (i.e. excluding pixels identified as either water or permanent wetlands in the MODIS land cover product) which this equates to is documented in Table 7.7. The additive model results are contained in Appendix F. An examination of the results contained in Tables 7.6

	2000	2001	2002	2003	2004
Apr	1.46	1.99	6.74	1.52	1.66
May	2.55	1.85	4.85	3.60	3.44
Jun	8.09	N/A	9.00	8.61	8.27
Jul	13.89	14.61	15.81	14.05	12.50
Aug	17.72	16.07	12.11	18.39	19.21
Sep	13.05	12.60	8.54	9.91	14.19
Oct	9.25	9.66	5.71	6.73	4.79
Nov	2.92	3.80	1.05	2.77	2.65
Total	68.93	60.58	63.81	65.58	66.71

Table 7.6: Total area burned (million hectares): Multiplicative model results

and 7.7 indicates that over the five year period of observation the largest area burned in 2000, and the smallest in 2001. The total area burned during each of these two years differs by 8.35 million hectares. This is likely to be due to the missing data for the month of June 2001. No burned area information has been processed for this period as MODIS data are unavailable between the 14th of June and the 3rd of July. Excluding the 2001 fire season, at least 29% of the land surface

2002. The peak of burning occurs in July 2002 and comparatively lower burned area totals are evident for the remainder of the 2002 burn season. In comparison peak burning occurs in August in each of the other four years. The reasons for these variations are unknown but may include the climatic conditions and in particular the levels of precipitation during the 2001/2002 wet season. The relationship between rainfall and the magnitude of land cover change has been discussed in Section 7.3.1. In particular variations in the magnitude of land cover changes in sub-Saharan Africa have been shown to be significantly related to short-term rainfall fluctuations (Vanacker *et al.* 2005). The strength of this relationship is dependent on the vegetation type, with grassland and shrublands more sensitive to the timing, intensity and duration of rainfall events than forests or woodlands. The reasons for this are linked to the morphology of the prevailing plant species as discussed in Section 7.3.1. The temporal distribution of burning is thus likely to be related indirectly to variations in precipitation, which will determine the characteristics of the vegetation. Figure 7.14 displays interannual variations in mean MODIS EVI values for savanna pixels between the the end of each annual fire season and the start of the next. Day 275 (or 274 for

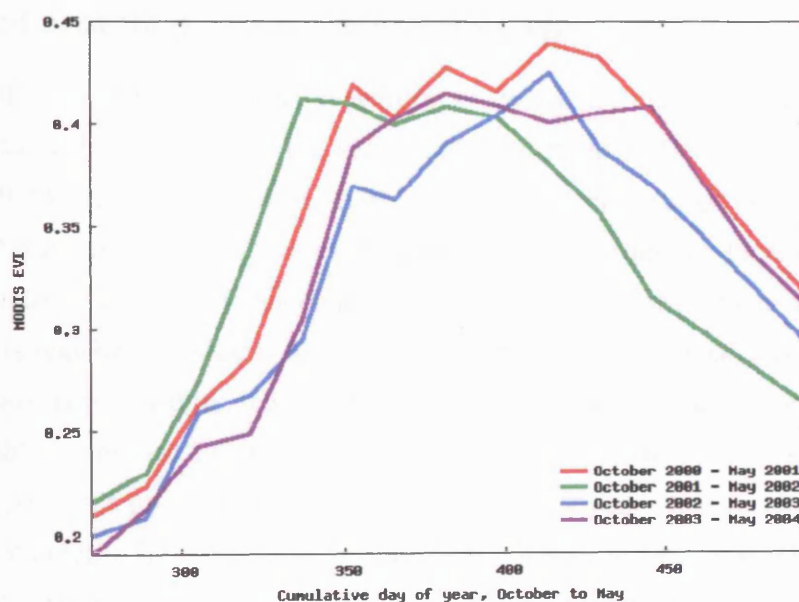


Figure 7.14: Vegetation phenology (savannas), October to May: MODIS EVI

the non-leap years) corresponds to the 1st October, and day 488 (or 487) to the 1st of May. The period between October 2001 and May 2002 clearly exhibits a different trend, with the growth cycle of the vegetation appearing to occur earlier than during the other years. Vegetation growth

peaks earlier (approximately day 335 - the 1st December 2001) and senescence begins earlier, with a decreasing trend in the mean EVI values occurring by day 400 (the 4th of February 2002). In comparison at the beginning of February in 2001, 2003 and 2004 the vegetation is not yet or is only just at the peak of its growth cycle. At the onset of the 2002 fire season (day 458) the vegetation is drier than at this point during any of the other years. The variations in the area burned and the temporal distribution of the burning in 2001 and 2002 in comparison to the other years of observation is thus likely to be due to the conditions of the vegetation at this point. The end of the annual fire season occurs due to the decrease in the fuel loads available and the onset of the rainy season. Conversely the beginning of the subsequent fire season follows the end of the rainy season and the associated increase in temperature and decrease in vegetation moisture. The longer duration of the 2001 fire season with considerably greater areas burned than, for example, November 2004, and the earlier start of the 2002 fire season is likely to be a result of interannual variations in precipitation, which determine the fuel loads available.

7.5.1 Burned area totals in each vegetation type

The total area of each of the five main vegetation types present within the study area which has burned during each of the annual fire seasons are contained in Table 7.8. The figures are displayed as 100,000 hectares. Thus in April 2000 435,700 hectares of deciduous broadleaf forest burned. The monthly totals as well as the additive model results are documented in Tables F to F.6 in Appendix F. The data displayed in Table 7.8 indicate that the total area burned within each cover type is relatively similar from year to year, with similar annual variations observed across all vegetation types. Although the total area of woody savannas and savannas burned each year is considerably larger than the other cover classes, this may be due to the larger quantities of this vegetation type within the study area. Table 7.9 contains the same data but as a percentage of each cover type in order to investigate the proportion of each vegetation class which burns each year. Figure 7.15 displays these data graphically at monthly intervals across the entire five year period in order to demonstrate the inter as well as intra annual variations.

The data contained in Tables 7.8 and 7.9 indicate that in comparison to the other vegetation types considerably lower proportions of grasslands and open shrublands burn every year. Thus while over 29% of deciduous broadleaf forests, woody savannas and savannas burn during each

	2000	2001	2002	2003	2004
Deciduous broadleaf forest	4.36	3.75	3.69	4.10	3.96
Open shrubland	2.22	2.03	19.63	20.4	2.03
Woody savanna	22.81	19.73	20.23	21.58	21.07
Savanna	32.52	29.51	31.60	31.48	32.99
Grassland	2.91	2.45	2.78	2.83	3.03

Table 7.8: Total area burned (million hectares): Multiplicative model results

	2000	2001	2002	2003	2004
Deciduous broadleaf forest	34.34	29.54	29.03	32.29	31.20
Open shrubland	14.72	13.50	13.04	13.56	13.51
Woody savanna	40.68	35.18	36.07	38.48	37.58
Savanna	32.04	29.08	31.14	31.02	32.51
Grassland	18.24	15.37	17.43	17.74	18.94

Table 7.9: Percentage of vegetation class which burns: Multiplicative model results

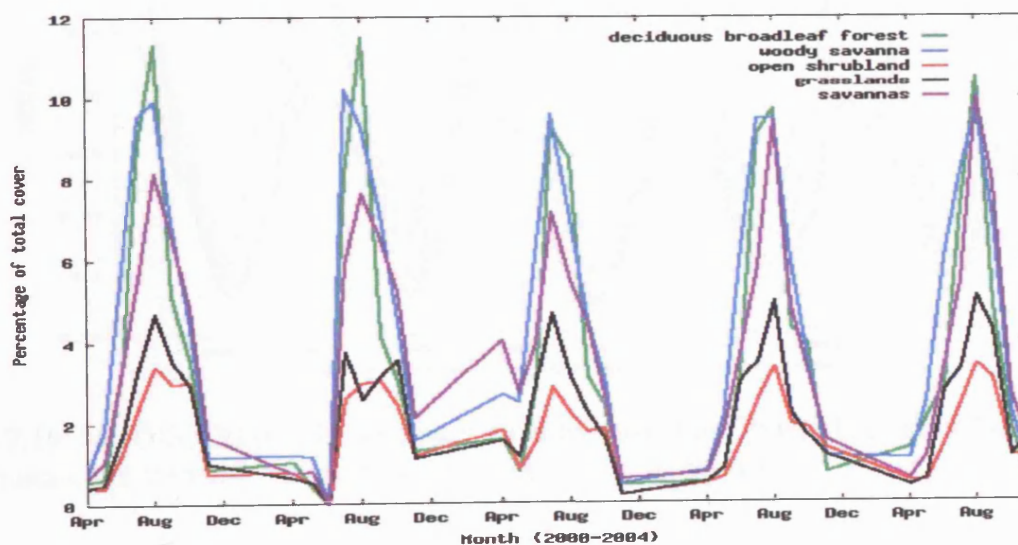


Figure 7.15: Proportion of each vegetation type burned per month between April 2000 and November 2004: Multiplicative model results

annual fire season, only 13-14% of open shrublands and 17-18% of grasslands typically do so. The reasons for this are unknown, but may be due to the characteristics of the vegetation as well as anthropogenic land cover practices within and around these cover types. As grasses are generally not sensitive to increasing levels of fire intensity and exhibit no significant differences in recovery with increasing levels of intensity (Trollope and Trollope 2002), the intensity and the severity of the fire (this is discussed further in Section 7.6.1) is unlikely to be a factor in the lower proportional burning within grassland ecosystems. A possible explanation is the lower quantities of available fuel loads within grassland and open shrubland ecosystems in comparison to those with a greater herbaceous and understorey canopy layer. Arid areas of southern hemisphere Africa may burn infrequently due to insufficient fuel loads available to carry a fire with several years of fuel accumulation (or an exceptionally wet growing season) required to generate sufficient fuel loads (Goldammer and Mutch 2001). Figure 7.16 displays MODIS EVI data for the five year period of interest. These data are the mean EVI values for each vegetation type calculated across the entire study area. The EVI data indicate that grasslands and open shrublands

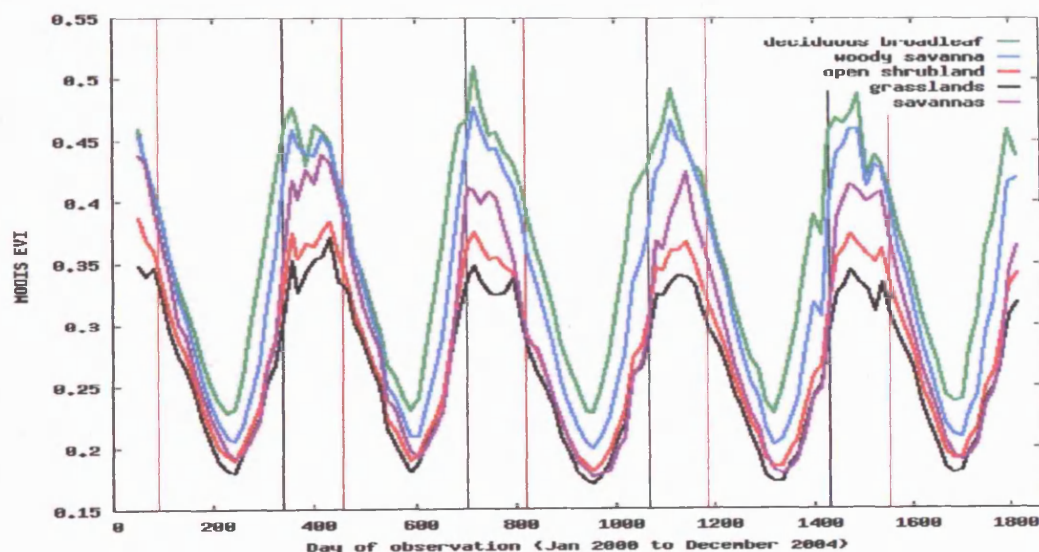


Figure 7.16: MODIS EVI profiles (January 2000 to November 2004). The vertical red and black lines indicate the start and end of the annual fire season respectively.

have the lowest values and thus lower biomass than deciduous broadleaf forests, woody savannas and savannas during each annual wet and dry season. While the EVI values for each vegetation type are low at the peak of the dry season, deciduous broadleaf forests and woody savannas in

particular, and savannas to a lesser extent exhibit large increases in biomass over the course of the wet season, (i.e. the period between the end of the annual fire season and the start of the next). The lower EVI values may provide an explanation for the lower proportions of grasslands and open shrublands burned during each annual fire season, as there may be insufficient fuel present to carry a fire. The lower fuel loads available in southern African grasslands may also be exacerbated by herbivory, reducing what little plant matter there is during the dry season even further. In contrast to forested and woodland areas grassland and open shrubland ecosystems may thus require multiple growing seasons after the occurrence of a fire before sufficient biomass has accumulated to fuel a subsequent fire event.

7.6 The severity of burning

The magnitude of an ecological disturbance consists of two components; (i) the intensity, which provides a measure of the strength of the disturbing force, and (ii) the severity, which provides a measure of the damage caused by the disturbing force (Sousa 1984). Although the two are often used interchangeably they are separate quantities. Fire severity is generally described broadly as the degree of ecosystem change as a result of burning and provides information on the spatial variation in the effects of fire on the landscape, while the intensity of a fire is typically defined as the rate of heat release over time, with the energy per length of fire front (the “fireline intensity”) increasingly used as a standard measure of fire intensity (Bond and Keeley 2005). The fireline intensity will be a function of the fuel heat content, the quantity of fuel consumed and the fire rate of spread (Diaz-Delgado *et al.* 2004). Although the intensity of a fire will often dictate its severity, depending on the measure used as an indicator of severity the two are not always well correlated (Neary *et al.* 1999). A consistent set of criteria for classifying levels of fire severity have yet to be defined and as a result a range of different measures have been used as indicators of fire severity (Ryan 2002). These include the depth of burn and the penetration of heat into the soil layers (Groot and Wein 2004), ash pH and soil microarthropod community (Henig-Sever *et al.* 2001), temperature residence time at the surface (Perez and Moreno 1998), and the degree of tree or aboveground mortality (Elliott *et al.* 1999, Miller and Yool 2002). Ryan (2002) notes however that the use of ground-based processes as indicators of fire severity may not be suitable as in addition to excluding the aboveground dimensions of severity, soil heating is typically shallow even if surface fires are intense. Focussing on the above ground impacts of fire, the amount of biomass combusted can be used as an indicator of severity (Oertel *et al.* 2004).

The effects of fire on plants and soil will vary according to the intensity of the fire, which will in turn be determined by a variety of factors (Perez and Moreno 1998, Diaz-Delgado *et al.* 2004). The quantity of fuel available is one of the most important factors influencing fire behaviour as it will determine the total amount of heat energy available for release during a fire (Trollope and Trollope 2002). The moisture content of the fuel is also of importance as it will affect the ease of ignition as well as the rate of combustion and the quantity of fuel consumed. Fuel moisture has a negative relationship with fire intensity due to the smothering effect of water vapour released during burning and the reduction in the quantity of oxygen in the proximity of burning, thereby

decreasing the rate of combustion (Trollope and Trollope 2002). Fires which occur in the middle of the southern African wet season are thus cooler and more patchy than those which occur during the dry season (Frost and Robertson 1985). Fire severity will also vary with vegetation structure. Crown height and bark thickness will determine levels of burn severity as will the intrinsic attributes and physiological state of the plants (Frost and Robertson 1985, Ryan 2002). Meteorological conditions and in particular the air temperature and relative humidity at the time of burning are also of importance. The intensity and severity of a fire will thus be linked to both the seasonality and frequency of burning, as these will affect all of the factors described above (Frost and Robertson 1985). In theory, fire severity will be inversely correlated to the time between successive fires (the fire return interval), with high intensity stand destroying crown fires exhibiting longer intervals between successive fire events than lower intensity surface fires (Sousa 1984, Brown *et al.* 1999). This is due to the higher fuel loads which accumulate under longer fire return intervals and subsequently result in more intense fires.

The characterisation of levels of fire severity is a requirement in sustainable ecosystem management. Severity is an important determinant of post-fire ecosystem development, with information relating to the severity of burning across a landscape as well as the heterogeneity of burn severity patterns within the perimeter of a fire of importance to land managers (Wagtendonk *et al.* 2004). While fires of low to medium severity may be beneficial for ecosystem stability and productivity high severity fires tend to have devastating ecological consequences (Oertel *et al.* 2004). Information relating to the severity of vegetation fires within a region is not only of importance in understanding the spatial impact of fires on the landscape, but also in quantifying the relationship between climate and fire intensity and severity. Changes in fire severity (as well as in the fire return interval) can have a large impact on carbon sequestration and ecosystem health and sustainability (Kasischke *et al.* 1995). The factors which determine the intensity and severity of a fire are highly sensitive to meteorological conditions and are thus likely to respond quickly to any climate change (Hoffmann *et al.* 2002). The severity of a fire will influence the quantity and type of emissions released as a result of burning, and variations in fire severity are thus of importance in estimating emissions (Kasischke *et al.* 2005). Higher intensity (flaming) fires are more efficient and have a higher degree of combustion completeness and release more CO₂ in comparison to less efficient (smoldering) fires which burn with a lower combustion completeness and release more CO (Ward *et al.* 1996). Research has shown that within sub-Saharan Africa

areas of grasslands and/or open woodlands exhibit the highest CO₂ emissions due to burning, while areas with a higher percent tree cover release more CO (Korontzi *et al.* 2004).

The recognition of the importance of fire intensity and the effects on different ecosystems has resulted in significant improvement in the use of fire as a management practice in African savannas and grasslands (Trollope and Trollope 2002). Few studies have however investigated levels of fire severity using remote sensing data, and those which have have done so over a limited temporal scale. Chafer *et al.* (2004) have used a single pre-fire and a single post-fire SPOT VEGETATION image to map fire severity in Australia based on NDVI differencing (see Section 2.1.1). Cocke *et al.* (2005) have used a similar approach, classifying a single fire event in Arizona into four severity levels based on a Difference Normalized Burn Ratio, while Diaz-Delgado *et al.* (2003) have used a longer time series consisting of eight Landsat TM images ranging from 13 days to 1165 days after a single large fire in Spain. The approach involved the comparison of pre-fire and post-fire NDVI images to determine levels of severity. The evaluation of pre and post-fire Landsat Normalized Burn Ratio (NBR) images are used by land managers in the USA to assess landscape level fire severity. Calculated as the difference between the near and middle infrared wavebands (MODIS equivalent bands 2 and 7) divided by their sum, this approach forms a component of the Fire Effects Monitoring and Inventory System (FIREMON) (Lutes *et al.* 2004). The severity information is subsequently used to (i) identify areas which require rehabilitation or post-fire treatment (ii) to validate and improve fire spread models, (iii) to update fuel models and vegetation layers for fire growth models, and (iv) to examine vegetation change effects for wildlife concerns (*ibid*). The drawbacks associated with the use of NDVI images and NDVI differencing is discussed in Section 2.1.1. In addition it is noted that within the area of interest a consistent burn signal is not observed at MODIS band 1 or band 7 wavelengths. As discussed in Section 5.5.3 changes in the spectral signal due to burning vary in both magnitude and direction at MODIS band 1 and 7 wavelengths. Thus while a decrease in reflectance is consistently observed at MODIS bands 2 and 5 over burned areas, burning results in either (i) an increase, (ii) a decrease, or (iii) minimal change in MODIS band 1 and 7 reflectances. Indices which assume a consistent change signal in either of these wavebands may therefore not be suitable as indicators of burn severity within the southern Africa study area. In addition Roy and Landmann (2005) note that values of a ratio spectral index computed using MODIS bands 5 and 7 decrease in a nonlinear manner with respect to either the combustion completeness of the

fire or the fractional area burned. This observation implies that ratio-type spectral indices may be sensitive in a nonlinear manner to the size and combustion completeness of the fire, and therefore may exhibit variable capabilities as indicators of fire properties (Roy and Landmann 2005).

Recently “process-based” functions relating to the fire behaviour have been used as indicators of fire severity. Kaufman *et al.* (1998) and Wooster *et al.* (2003) have investigated the use of the Fire Radiative Power (FRP, calculated as the total integrated instantaneous radiative energy) as a measure of fire intensity and a proxy for the total fuel combusted when integrated over time, while Smith *et al.* (2005) have used the duration of the fire, the maximum temperature attained and the integration of the fire temperature with time to determine fire severity. Despite these efforts coherent information relating to the spatial and temporal variations in fire characteristics such as intensity and severity remains limited, and the remote sensing of these variables is therefore a noted goal in wildfire research (Smith *et al.* 2005). The severity of burning is defined here as the degree of surface change which has occurred due to fire. The following subsections provide a characterisation of the relative severity of burning across the study area over the five year period using the proportional change in surface reflectance to determine the degree of surface change which has taken place as a proxy for burn severity.

7.6.1 An indicator of burn severity

Fire induced changes in the remote sensing signal at near to mid-infrared wavelengths (MODIS bands 2 and 5) occur as a result of the combustion of the vegetated surface layer. The nature of these changes is described in Section 3.5. The proportional change in reflectance ($\delta\rho(\lambda)$ in Equation 3.3) at MODIS band 2 and 5 wavelengths provides a measure of the relative change which has taken place at each 500m pixel location due to burning. The magnitude of the change in reflectance due to burning at near infrared wavelengths has been shown to be dependent on (i) the proportion of a MODIS 500m pixel which has burned, and (ii) the combustion completeness of the fire (and hence the degree of damage to the vegetation) (Roy and Landmann 2005). Increasing either (a) the fraction of a pixel which burns, or (b) the combustion completeness of the fire will result in a greater change in reflectance due to burning *ibid.* The proportional change in reflectance can therefore be used as an indicator of the degree of damage and thus a surrogate for burn severity. Higher severity burns are expected to exhibit a greater proportional decrease in

MODIS band 2 and 5 reflectances than lower severity burns, due to the greater destruction of the vegetation. This is supported by the spatial nature of the proportional change values observed across fire affected areas. Figures 7.18a and 7.18c illustrate the spatial distribution of $\delta\rho(\text{band}5)$ values for two sites, each covering an area of approximately 100km by 100km. For comparative purposes the Normalised Burn Ratio (calculated as the difference between MODIS bands 2 and 7 divided by their sum) is displayed in Figures 7.18b and 7.18d for the two regions. The NBR data been calculated from the band 2 and 7 forward modelled nadir reflectances (Equation 5.4). The two locations correspond to sites 7C and 7D (Figure 7.17). Their location is detailed in Table A.1 in Appendix A. A different pattern of burning is evident at each of the two locations with the first site containing fire affected areas of a smaller individual spatial extent but which exhibit a greater proportional decrease in reflectance than the second site where the spatial extent of burning is greater but the proportional decrease (and thus the degree of damage) is comparatively lower.

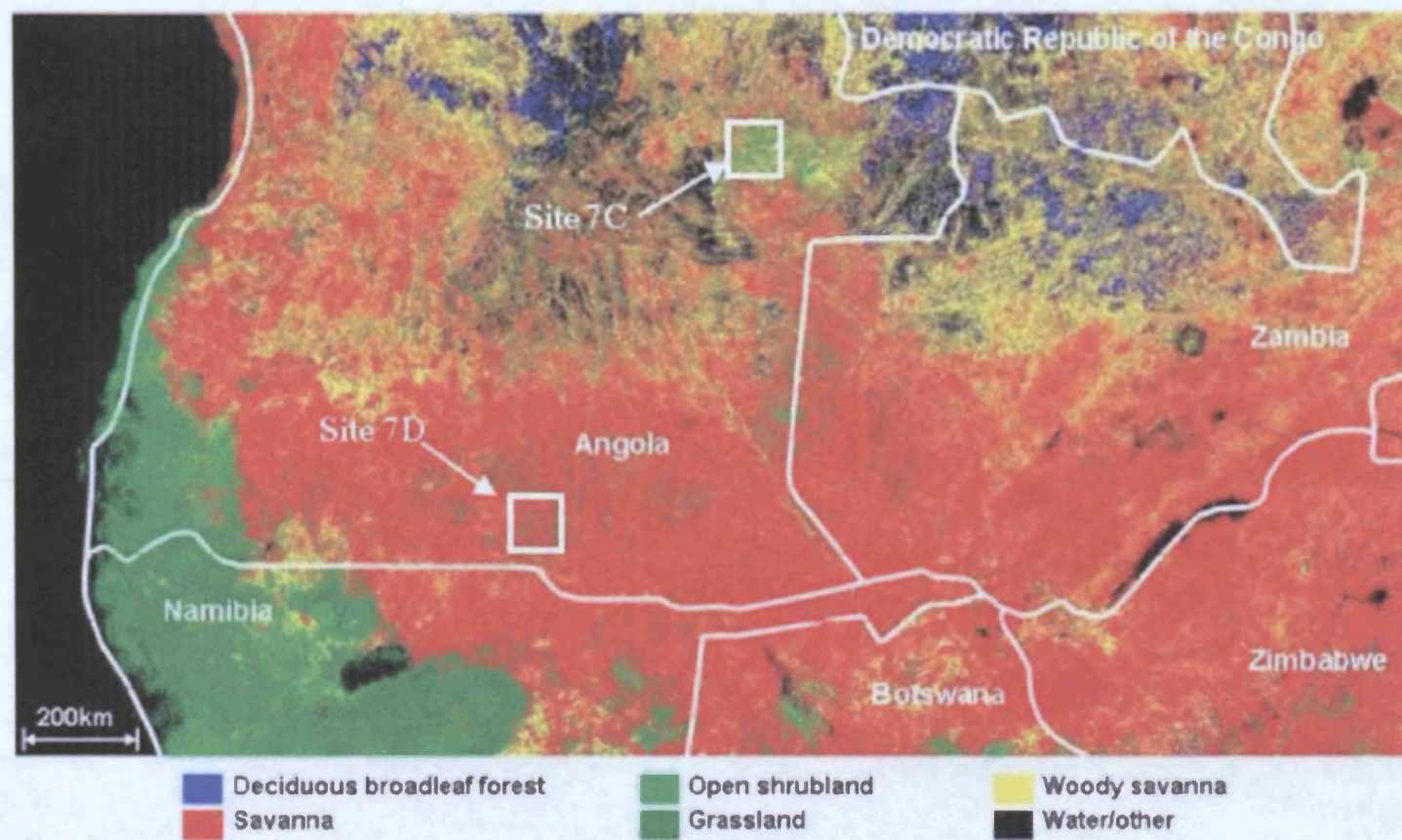
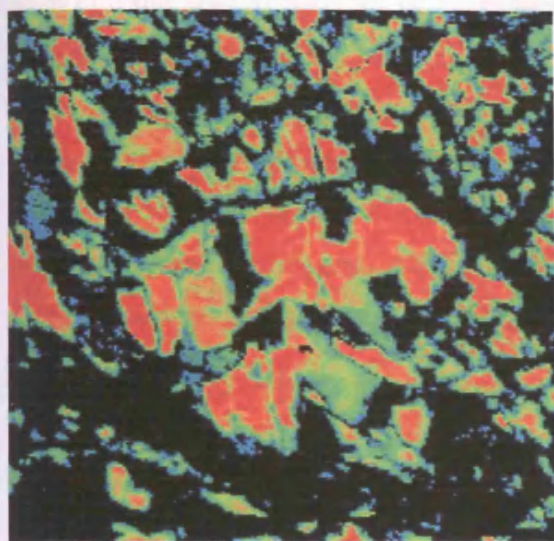
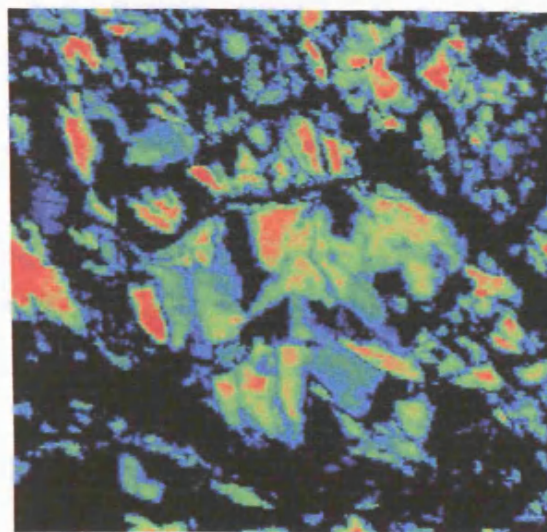


Figure 7.17: Sites 7C, 7D and MODIS Landcover Product



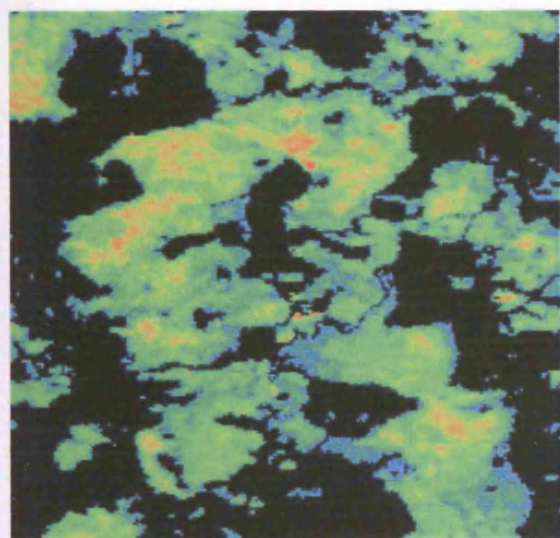
0 60%

(a) Site 7C (northern Angola) July 2004: proportional decrease in MODIS band 2



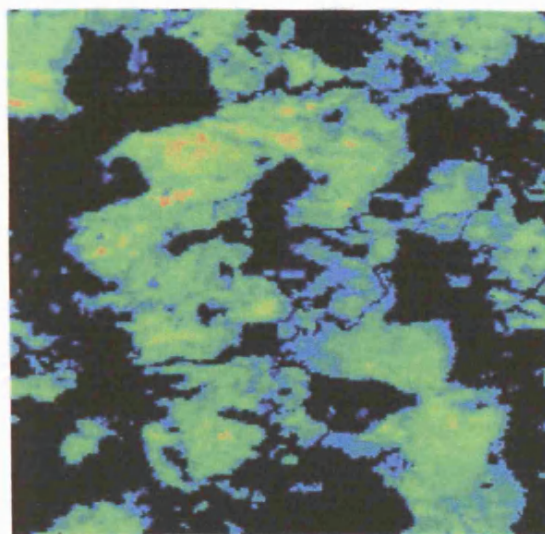
0 0.5

(b) Site 7C (northern Angola) July 2004: Normalised burn ratio



0 60%

(c) Site 7D (southern Angola) August 2004: proportional decrease in MODIS band 2



0 0.5

(d) Site 7D (southern Angola) August 2004: Normalised burn ratio

Figure 7.18: Spatial patterns of burn severity at two locations: Multiplicative model results

While the spatial patterns of high severity burning are generally comparable for the proportional decrease and the NBR data displayed in Figure 7.18, fewer areas of higher relative severity are identified in the NBR data for Site 7C (Figure 7.18b) in comparison to the proportional change results (Figure 7.18a). These areas correspond to pixels which exhibit a decrease in MODIS band 7 reflectance as a result of burning. The distribution of band 7 values for the two sites are displayed in Figure 7.19. These data indicate that a greater proportion of the burn pixels are characterised by a decrease in MODIS band 7 reflectances at Site 7C. As the NBR works on

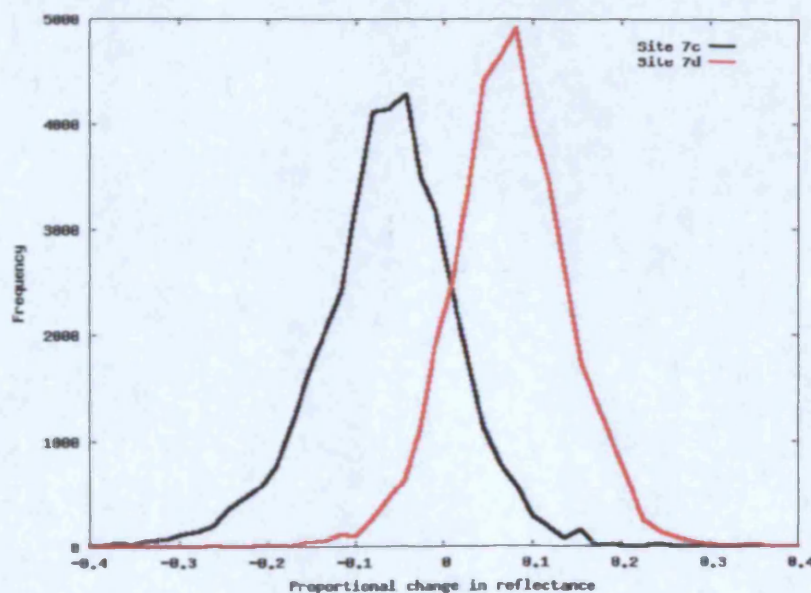


Figure 7.19: Distribution of MODIS band 7 proportional changes in reflectance: Sites 7C and 7D (northern and southern Angola)

the principal that the difference between band 2 and 7 reflectances decrease as a result of fire, the greater proportion of pixels which exhibit a decrease in band 7 reflectance at Site 7C explains the lower agreement between the two indicators of burn severity at this site. In situations where the band 7 reflectance decreases as well as the band 2 reflectance, this measure will not be a good indicator of burn severity. In particular as pixels which exhibit a decrease in band 7 reflectances as a result of burning also tend to exhibit a greater proportional decrease in MODIS bands 2 and 5 than those with a smaller or a positive change in band 7 reflectance, it is possible that these locations correspond to areas of high severity burning. If this is the case then the saturation of the NBR under such circumstances makes it an unsuitable indicator of burn severity.

The areas of high proportional change (the red pixels) at both sites (Figures 7.18a and 7.18c) are located within the boundaries of the fire affected areas and surrounded by areas of lower proportional change. This pattern of severity is expected as areas within the perimeter (and thus behind the firefront) of a fire will experience greater fire intensities and thus a higher severity of burning than locations on the perimeter of the fire. The proportional change values have been classified into three classes of burn severity (Table 7.10) in order to facilitate the following analysis. The classification of the two locations contained in Figure 7.18 into these three severity classes is displayed in Figure 7.20.




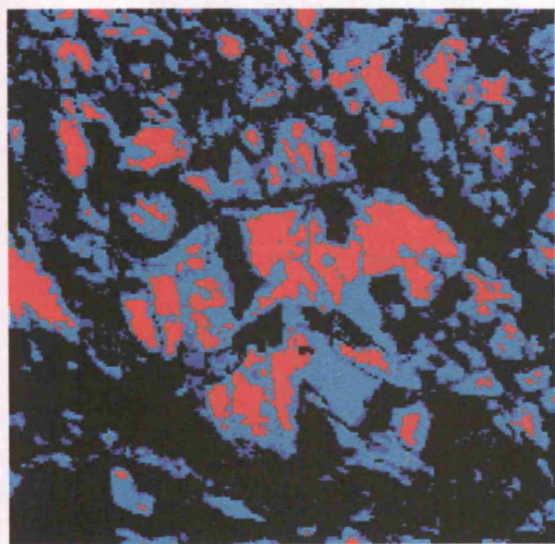
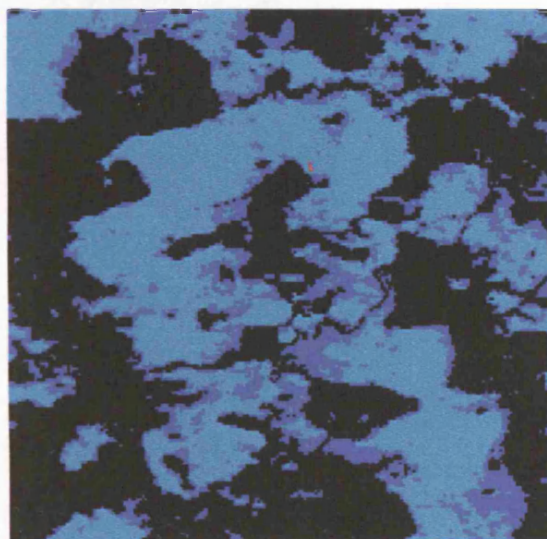
Severity class	Proportional change	Image key
Low severity	< 25%	
Moderate severity	25% to 50%	
High severity	≥ 50%	

Table 7.10: Classification of burn severity based on the proportional change in MODIS band 5 reflectances

The spatial distribution of (unclassified) burn severity ($\delta\rho(\text{band5})$) across the entire area of interest is displayed in Figure 7.21 for 2004, calculated from the multiplicative model results. Several areas of higher severity burning are evident during the 2004 fire season. In particular burning which has occurred in the northern section of Angola is of a higher severity than that which has occurred across the majority of the study area. Localised areas of higher severity burning are also evident in central Zambia, near the Botswana/Zambia border, and in southern Angola near the Angola/Namibia border. The relationship between the burn severity and (i) the land cover type, (ii) the time of year, and (iii) the fire frequency is discussed in the following subsections.



(a) Site 7C (northern Angola) July 2004



(b) Site 7D (southern Angola) August 2004

Figure 7.20: Spatial patterns of burn severity at two locations

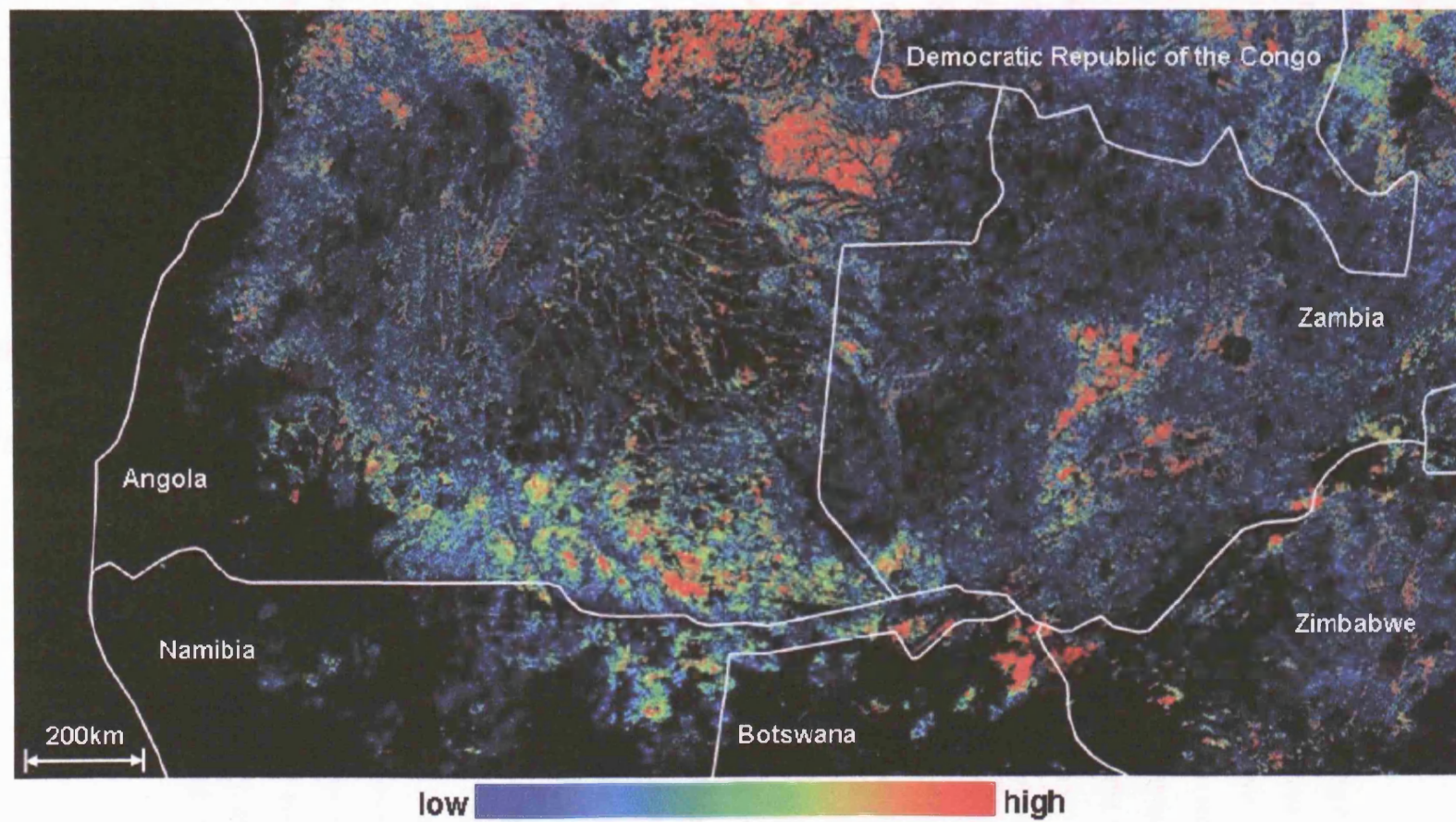
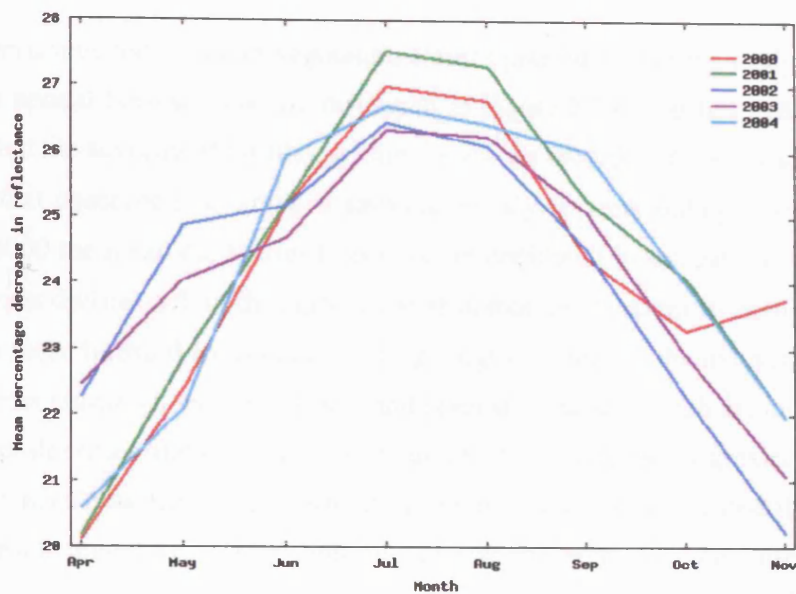


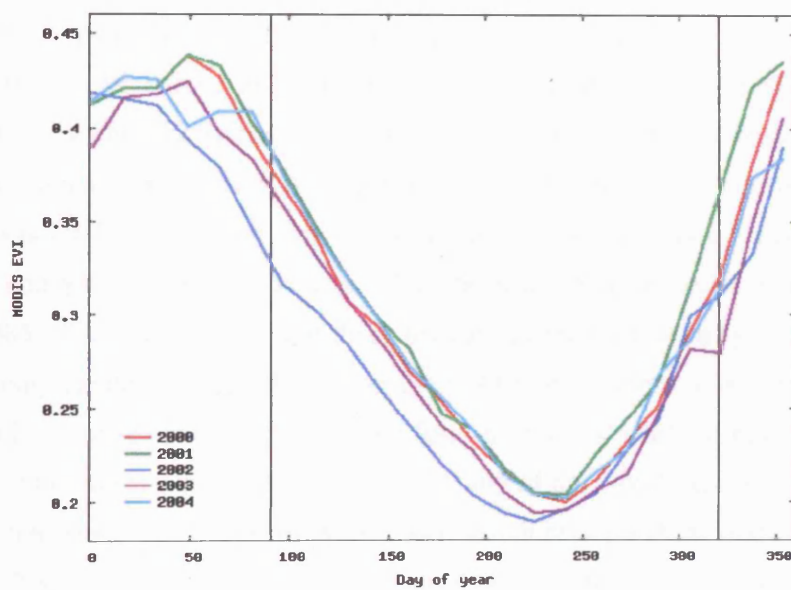
Figure 7.21: Burn severity 2004

The temporal distribution of burn severity

The factors which will determine the intensity of fires and the severity of burning have been discussed above, and the relationship between the severity of burning and the various components of the fire regime as well as external factors is represented graphically in Figure 7.1. As all of these will vary over the course of a single fire season as well as from year to year temporal variations in the severity of burning will occur. Figure 7.22a displays the mean proportional decrease ($\delta\rho(\lambda)$) in band 5 reflectances as a percentage change (a $\delta\rho$ value of -0.15 is the equivalent of a 15% decrease in reflectance) calculated for each month across the entire area of interest from the multiplicative model results. A temporal pattern in the mean severity of burning is apparent in these data, with a uniform trend exhibited over each of the five years. The mean burn severity is lowest at the start of the fire season and increases over the subsequent months with highest severities observed in either July or October each year. After this point the severity of burning decreases with lower mean values observed towards the end of the fire season which are of a similar magnitude to those observed at the beginning of the annual fire season. As discussed in Section 3.4.2 the temporal distribution of fire activity follows the vegetation growth cycle, with the peak of the fire season corresponding to the height of the dry season. The data in Figure 7.22a indicate that the most severe burns also occur during the peak months of the annual fire season. Figure 7.22b contains mean MODIS EVI profiles (see Section 3.4.2) calculated across the entire study area. The annual fire season is delimited by the vertical lines. The vegetation is at the lowest point in its growth cycle (and thus drier and more flammable) during the months which exhibit the highest burn severity, with vegetation senescence at its peak during July and August in each of the five years. In addition the vegetation is at its greenest and healthiest at the start and end of the fire season (April and November), when the observed burn severity is lowest. The severity of burning is expected to exhibit an inverse relationship with the moisture content of the vegetation as the ease of ignition as well as the rate of combustion and the quantity of fuel consumed will be dependent on the plant water content. This will not only vary temporally (as is evident in Figure 7.22) but also spatially with vegetation type and is investigated further in the following paragraph.



(a) Mean burn severity



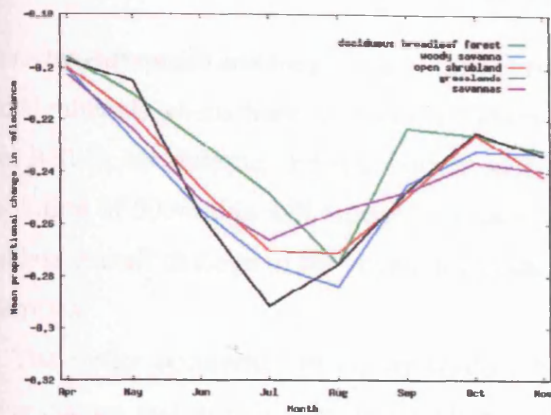
(b) Mean MODIS EVI

Figure 7.22: Temporal distribution of mean burn severity and MODIS EVI, 2000-2004

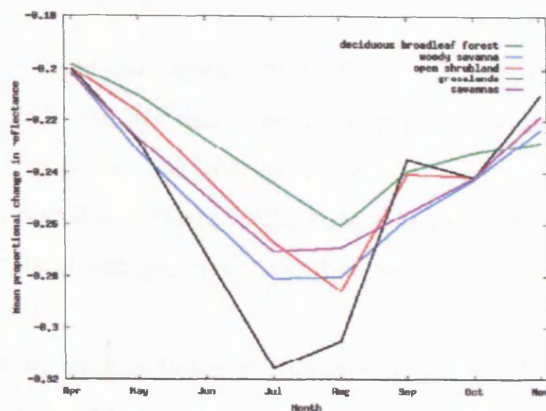
Burn severity and land cover type

The mean burn severities for the main vegetation classes present within the study area for each month of the five annual burn seasons are displayed in Figure 7.23. It is immediately apparent from these data that the severity of burning within deciduous broadleaf forests and grasslands is very different to that observed over areas of savanna, woody savanna and open shrublands. For all years except 2000 the mean burn severity is lower in deciduous broadleaf forests than any of the other cover types during each of the eight fire season months. In addition the highest severity of burning within these forested areas occurs during August in each of the five years. In contrast the three cover types (savanna, woody savanna and open shrublands) which are characterised by lower woody plant densities and canopy cover than deciduous forests but greater tree densities and canopy cover than grasslands (see Table 3.3) exhibit a more uniform distribution of burn severities across each annual fire season, with higher severity burns typically observed between July and August each year. In contrast higher severity burns within grassland ecosystems occur earlier in the year, with the highest mean severities evident during June and July for all years except 2001. In addition the severity of burning observed over areas of grassland is considerably higher than the peak burn severities observed over the other cover classes.

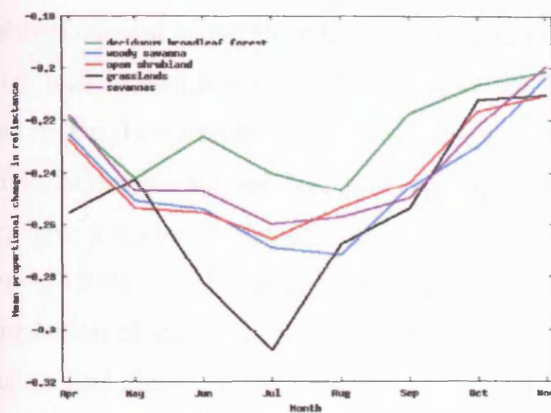
Explanations for the variations in burn severity described above include the type of fires which typically occur within the study area as well as the characteristics of the different vegetation types. In particular variations in the mean severity of burning observed for the different land cover classes is likely to be a function of the fire type. The majority of vegetation fires in southern African ecosystems are surface fires which burn through the herbaceous layer (Frost and Robertson 1985). The flame heights of these fires are generally low and plant matter above 3-4m is not normally ignited (*ibid*). Within southern African savanna ecosystems the majority of the fuel load comprises surface fuels in the form of grasses, while in grasslands the fuel load is entirely grass (Trollope and Trollope 2002). Many of the woody species within biomes subjected to high frequency fires have insulating bark which protects them from fire (Frost and Robertson 1985). The higher severity of burning observed within grassland ecosystems is thus likely to be a result of the higher quantities of surface fuels available, and the lower heterogeneity of flammable vegetation in contrast to ecosystems with higher woody plant densities. Vegetation types such as grasslands and open savannas which are spatially more homogenous are more



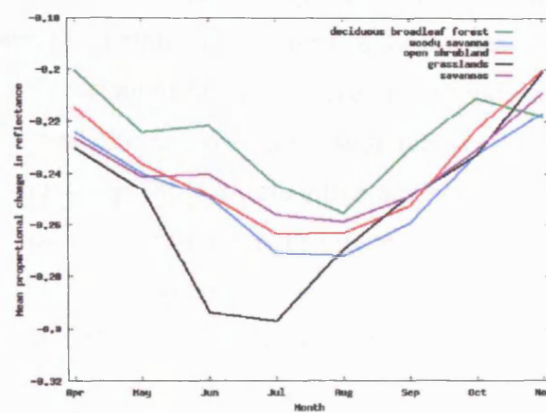
(a) 2000



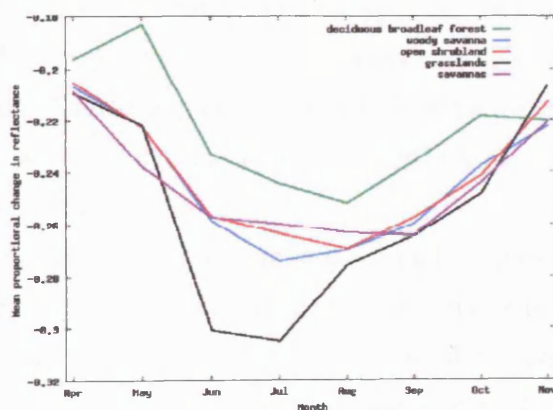
(b) 2001



(c) 2002



(d) 2003



(e) 2004

Figure 7.23: Mean severity of burning for each of the main vegetation types present in the study area

prone to widespread and frequent burning than other vegetation types (Frost 1999). In woodlands and shrublands where there is generally a lower grass biome and more uneven distribution of fuel fires will be less intense and will burn more patchily (Frost and Robertson 1985). At a spatial resolution of 500m this will equate to a lower proportional change in the nature of the surface and less overall damage to the vegetation at the scale of a single pixel, and therefore lower burn severities.

The earlier occurrence of higher severity burning in grasslands in comparison to the other cover classes and in particular to deciduous broadleaf forests may be due to (i) the source of ignition, and/or (ii) the vegetation characteristics. In southern African grassland ecosystems the herbaceous vegetation is either dead (annual grasslands) or dormant during the dry season. The moisture content is therefore low and the plant material is flammable for most of the dry season. In contrast in deciduous broadleaf forests the moisture content of the herbaceous understorey plant material may be higher as it is protected by the tree cover, and it may take longer for sufficiently flammable surface fuel loads to aggregate. Grasses growing within a tree neighbourhood may have a higher moisture content and retain moisture levels for longer into the dry season (Vetaas 1992). The build up of surface fuel loads in these ecosystems is also dependent on the contribution of leaf litter from deciduous trees (Frost 1999) and the presence of sufficient material to fuel higher intensity surface fires will therefore be dependent on the phenology of the vegetation. The difference in the timing of the higher severity fires may also be a function of the sources of ignition. As discussed in Section 3.2 the majority of vegetation fires in southern Africa are of anthropogenic origin. Different vegetation types may be burned at different times of year following specific land cover practices. Areas with higher tree densities for example may be burned later in the dry season (August-September) in order to clear the land for cultivation ready for the onset of the rains. However no data are available describing the reasons for anthropogenic burning at the different times of year.

The burn severity data for the five annual fire seasons and across each vegetation type has been classified into three severity classes according to the criteria described in Table 7.10. The proportion of each severity class is displayed in Table 7.11 for the multiplicative model results. The additive model results are contained in Table G.1, Appendix G. For all cover types except grasslands in 2002 and 2004 low severity burns account for over 50% of the total, while high severity burns account for less than 5% of all burns except for grasslands in both model results,

	Low	Moderate	High
2000	60.1	37.3	2.7
2001	61.0	36.8	2.2
2002	67.9	30.5	1.6
2003	65.1	33.0	1.9
2004	65.0	33.4	1.7

(a) Deciduous broadleaf forest

	Low	Moderate	High
2000	57.1	39.7	3.2
2001	59.4	37.4	3.2
2002	61.1	36.1	2.8
2003	60.9	36.5	2.6
2004	54.3	43.2	2.5

(b) Open shrublands

	Low	Moderate	High
2000	53.0	42.8	4.2
2001	52.6	42.9	4.5
2002	56.0	40.2	3.9
2003	54.2	41.8	4.1
2004	53.3	42.6	4.1

(c) Woody savannas

	Low	Moderate	High
2000	57.4	40.0	2.6
2001	54.6	43.0	2.4
2002	57.9	40.2	1.9
2003	57.7	40.3	2.0
2004	51.3	46.5	2.3

(d) Savannas

	Low	Moderate	High
2000	53.5	43.1	3.5
2001	54.6	39.3	6.1
2002	47.6	45.8	6.6
2003	50.6	43.5	5.9
2004	45.6	49.1	5.3

(e) Grasslands

Table 7.11: Proportion of low, moderate and high severity burns in each cover class between 2000-2004: Multiplicative model results

and woody savannas in the additive model results. Areas of deciduous broadleaf forest typically exhibit the lowest proportion of high severity burns and the highest proportion of low severity burns each year, with a general decrease in the proportion of high severity burns evident in the five year period. In contrast grasslands exhibit the highest proportions of high severity burning each year, with the proportion of higher severity burning in this cover type increasing to a peak in 2002 and subsequently decreasing. The reasons for these temporal variations within and between each cover type are likely to be complex and varied. In particular as the majority of fires in this region are fuelled by grass the intensity (and thus typically the severity) of burning will vary considerably between seasons, landscape units and vegetation types. In particular in grassland ecosystems the fuel layer is relatively homogenous, while in ecosystems with higher woody plant density and tree cover such as woodlands the woody and grass fuel components coexist, with lower grass production in the more closed canopy woodlands (Scholes *et al.* 2002). As the majority of southern African fires are surface fires which are fueled by the grass biomass (Frost and Robertson 1985), higher severity of burning may be expected to be observed within ecosystems with a greater and more homogenous fuel layer. Additional factors which will contribute to the observed patterns in burn severity include the prevailing climatic conditions, the moisture content of the fuel, the rate of fuel accumulation over the previous wet season, and the time which has elapsed since the previous fire. This latter point is investigated in the following subsections.

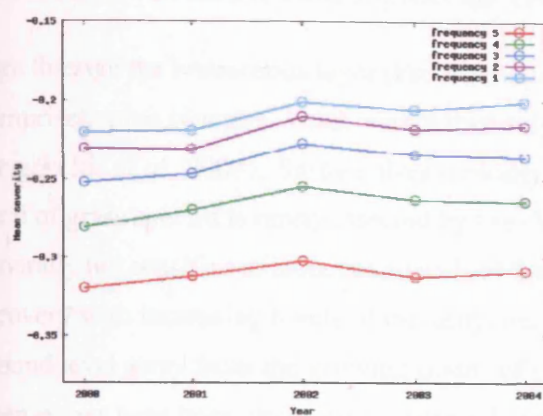
Burn severity and fire frequency

Under ecological theories of natural disturbance an inverse relationship exists between the severity of the disturbance and the disturbance frequency (Pickett and White 1985). In general the severity and intensity of fires are thought to be inversely related to fire frequency (Swetnam 1993, Brown and Smith 2000), although considerable variability exists within this generalisation (Goldammer and Mutch 2001). This relationship has been shown to hold in Californian forests with fire severity tending to decrease as fire frequency increased (Miller and Urban 2003), while in the Giant Sequoia forests of north America high severity stand replacing fires were found to occur under low frequency fire regimes, while mixed severity fires occurred in forests with high frequency fire regimes (Swetnam 1993). Conversely in the closed canopy tropical forests

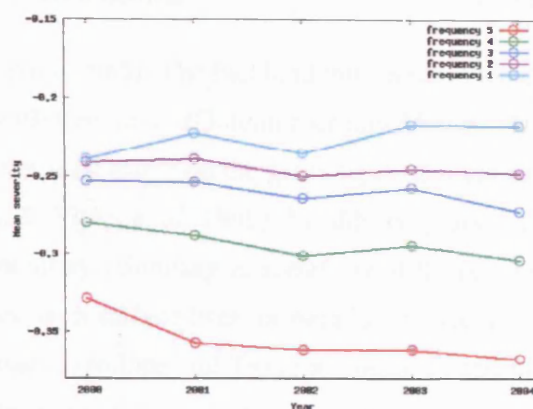
of South America fire severity is believed to increase with frequency, with previously burned forests more likely to burn than unburned forests, and second fires moving faster and burning more intensely than the initial fires (Cochrane *et al.* 1999). This pattern occurs as the first fire moves slowly along the ground consuming little besides the dry leaf litter and smaller trees and stems while the larger and thicker barked trees survive. Following the fire combustible fuels fall from the dead trees forming a flammable layer on the forest floor. Recurrent fires increasingly open the canopy causing fuel loads to rise substantially as highly combustible grasses and vines invade and the open canopy allows for greater solar heating and air movement to dry out the forest fuels, resulting in previously burned forests more susceptible to intense fires under dry season weather conditions (Cochrane *et al.* 1999). Little research exists documenting the relationship between the frequency of fires and the severity of burning in southern African ecosystems. While several studies have investigated the intensity of experimental fires over a limited spatial scale (Trollope and Trollope 2002, Smith *et al.* 2005), no data are available describing the spatial or temporal variations in the observed severity of burning at a regional scale, or the impact of the frequency of fires on the severity of burning. The aim of the following paragraphs is therefore to characterise this relationship within the different vegetation types present in the southern Africa study area.

The mean severity of burning in each of the five vegetation types within the area of interest is displayed in Figure 7.24 as a function of the frequency of burning. Pixels with a frequency value of 5 have burned during each annual fire season in the five year period of observation, while those with a frequency value of 1 have only burned once during this time. The frequency of burning within the study area and the time between recurrent fires has been discussed in detail in Sections 7.2.1 and 7.2.2. A very clear pattern is evident in the data contained in Figure 7.24. For all vegetation types and for each year of observation locations with a higher frequency of burning exhibit a higher mean burn severity. A positive relationship thus exists between the fire frequency and burn severity across all vegetation types within the study area. The reasons for this are likely to be due to factors which include the type of fire and the effect on the vegetation, the characteristics of the fuel loads and the regenerative power of the dominant plant species as well as the meteorological conditions between subsequent fires. These factors and their interactions are shown in Figure 7.1.

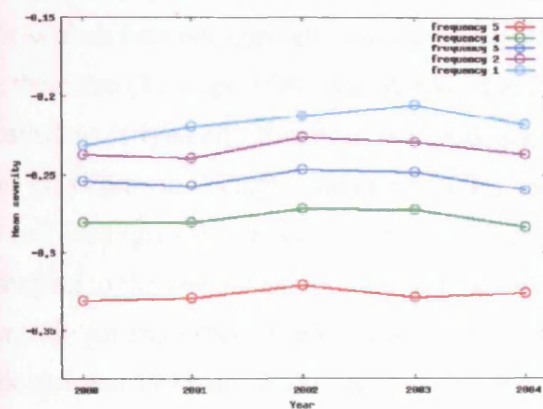
As discussed above the majority of vegetation fires in southern Africa are surface fires which



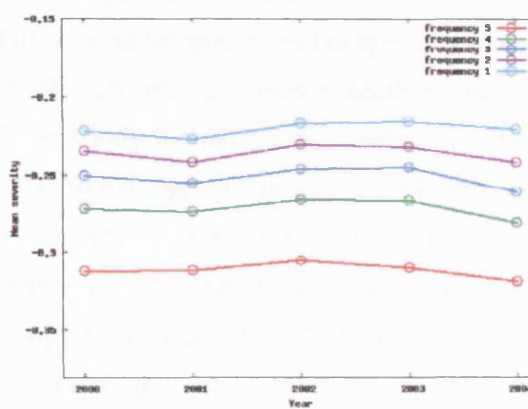
(a) Deciduous broadleaf forest



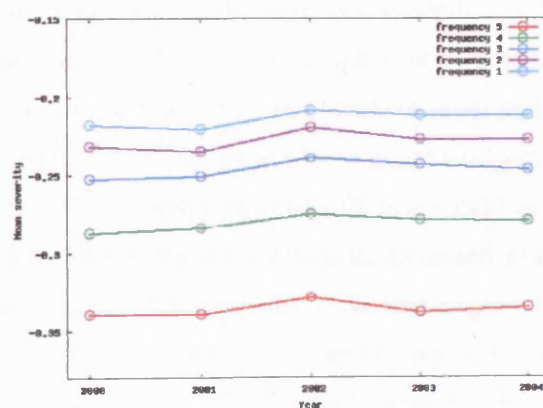
(b) Grasslands



(c) Open shrublands



(d) Savannas



(e) Woody savannas

Figure 7.24: The relationship between the mean burn severity and fire frequency in each vegetation type: Multiplicative model results

burn through the herbaceous layer (Frost and Robertson 1985). The fuel load thus predominantly comprises grass biomass which varies inversely with tree cover (Goldammer and Mutch 2001, Langevelde *et al.* 2003). Surface fires typically have least effect on the grass layer, and the survival of grass species is rarely affected by fire (Van de Vijver *et al.* 1999). In addition grasses are generally not sensitive to increasing levels of fire intensity exhibiting no significant differences in recovery with increasing levels of intensity, because with surface fires the heat is released above ground level away from the growing points of grasses (Trollope and Trollope 2002). In contrast intense fires have been observed to cause a direct decline in the cover of woody biomass by either killing trees or reducing them to smaller size classes (Langevelde *et al.* 2003). The probability of tree mortality as a result of fire is a function of both the stem height and the fire intensity, with surface fires not normally intense enough to kill African savanna trees but typically affecting their size (Trollope 1982, Van der Werf *et al.* 2004). The effect of fires in southern African ecosystems is typically therefore the reduction of the woody biomass which indirectly stimulates grass growth (Langevelde *et al.* 2003). It would follow that this results in an increase in the fuel load (grass biomass) and the occurrence of fires which are more intense (and thus more damaging to the vegetation i.e. are more severe), which leads to an increased decline in woody biomass. An analysis of fire occurrence in the subtropical savannas of the Everglades National Park between 1995 and 2000 suggests that frequent fires result in an increase in patchiness and a wider range of intensities, with higher intensities appearing to result from the regrowth of more flammable vegetation (Slocum *et al.* 2002).

Vegetation changes in savanna ecosystems have been modelled by Langevelde *et al.* (2003) using a model of tree-grass dynamics. Under the assumption of no negative effects of fire on grass growth, the relationship between fire frequency and levels of grass and woody biomass are displayed in Figure 7.25. Increasing the fire frequency has a negative effect on woody biomass, with woody biomass highest under fire frequency regimes of 5 years and lowest under annual burning conditions. Conversely higher fire frequencies result in increased grass biomass with highest levels occurring with annual burning. The existence of alternate (grass and woody biomass) stable states will thus depend critically on the relationship between the fuel load (grass biomass) and the fire intensity (Langevelde *et al.* 2003). Unstable equilibria may arise when events such as drought reduce the grass biomass below a break point value (the dashed line) where there is insufficient fuel to carry a fire, allowing bush encroachment to occur (*ibid*). These data (Figure

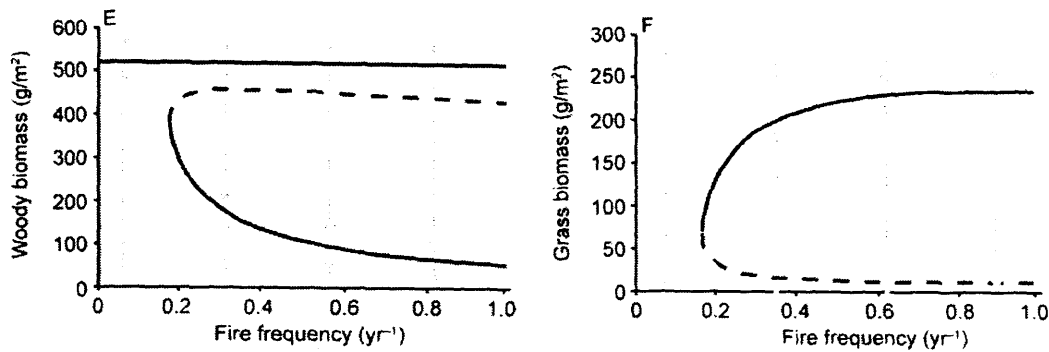


Figure 7.25: Changes in woody and grass biomass with levels of fire frequency. Solid lines indicate stable equilibria, dashed lines unstable equilibria, and arrows the direction of development. Source: Langevelde *et al.* (2003)

7.25) support the theory that grass biomass is maintained by frequent fires while fire regimes with a short fire return interval will result in an increase in the grass biomass.

The increase in burn severity with increasing fire frequency observed across all vegetation types (Figure 7.24) is thus likely to be due to the effects of burning on the grass and woody biomass discussed above. Burning results in an increase in grass biomass and a reduction in woody biomass below a certain height (less than 2-4m (Bond and Keeley 2005)), which in turn contributes to more intense fires due to the higher fuel load (grass biomass) available, which are subsequently more damaging to the woody biomass. A positive feedback thus exists between the frequency of fire and the fuel load. High frequency fires maintain the grass biomass preventing tree and bush encroachment, which result in higher fuel loads available for the next fire event. Increasing grass production is shown to negatively influence tree density by making it more difficult for seedlings to establish, and by effectively increasing the fire intensity and therefore reducing the opportunities for woody vegetation to develop into fire-resistant size classes (Higgins *et al.* 2000). Conversely under a regime of infrequent fires woody biomass increases and grass biomass decreases reducing the quantity of flammable vegetation and thus the intensity of fires and the resultant damage to the vegetation. This would explain the lower mean severity of burning observed under lower frequency fire events. It should be noted however that this relationship will only hold if the fires are surface fires with fuel loads comprising grass biomass. Crown fires are only thought to occur in southern Africa under extreme atmospheric conditions characterised by high temperatures, low humidities and strong winds (Trollope 2000). Should a

crown fire occur fuel loads in the form of the woody biomass will be high, resulting in greater fire intensities and greater damage (and thus a higher burn severity) to the vegetation. Although high intensity stand destroying crown fires are generally expected to exhibit longer intervals between successive fire events than lower intensity surface fires (Sousa 1984, Brown *et al.* 1999), this may not be the case in southern African ecosystems as the replacement of the woody biomass with herbaceous vegetation may actually result in an increase in fire frequency.

Under the assumption of steady climatic conditions over the five years of observations, the implications of the results displayed in Figure 7.24 are that the fuel load of southern African fires is (i) maintained, and (ii) increased under a regime of frequent burning. A positive feedback thus exists between the frequency of burning and the accumulation of combustible material, and subsequently the severity of burning.

7.7 Summary

Little quantitative information exists describing the fire regimes of southern African ecosystems at a regional or multi-annual scale. While the spatial and temporal distribution of burning across this region has been mapped at a spatial resolution of 1km for a single year (Gregoire *et al.* 2003) and over three non-consecutive fire seasons at a spatial resolution of 5km (Barbosa *et al.* 1999) no data exist describing the interannual variability in fire frequencies or characteristics across multiple fire seasons. This chapter has investigated the occurrence of biomass burning within the area of interest over over five consecutive annual fire seasons and at a spatial resolution of 500m. The fire regimes within the area of interest have been characterised in terms of four main variables. The main findings are summarized below.

1. Frequency The frequency of fire occurrence within the area of interest has been documented for the past five annual fire seasons (April 2000 to November 2004). During this time approximately 40% of the land surface has burned, with 6% (an area of approximately 131,420km²) burning during each of the five annual fire seasons. Higher fire frequencies are identified in savanna and grassland ecosystems, with shrublands and deciduous broadleaf forests burning less frequently. Fire return intervals indicate that locations which burn every year do so at the same time each year. These areas also have a distinct spatial pattern and are predominantly located in

the northern section of Angola, southern Zaire and northern Zambia, as well as in a belt along the Namibia/Angola/Botswana borders.

2. Seasonality The majority of burning occurs between April and November each year. The general pattern of burning is similar across all vegetation types with the greatest proportion of burn events identified in either July or August in each of the five years. A general north to south progression is evident in the timing of burning every year with areas in the north of the region burning earlier in the year than those in the south. In addition the fires spread eastward over the course of each annual fire season. The timing of burning has an effect on the time which elapses between recurrent fires, with areas which burn initially at the beginning of the fire season during the five years exhibiting longer time intervals between subsequent burn events than those which burn later in the year.

3. Spatial extent Between 27% and 32% of the study area has burned during each of the five years of observation. This equates to an area of approximately 610,000 to 690,000km². The distribution of burning within each of the main vegetation types is similar from year to year, with a much larger proportion of deciduous broadleaf forests, woody savannas and savannas burning each year in comparison to shrublands and grasslands. Thus in 2004 for example while 38, 33 and 32% of woody savannas, savannas and deciduous broadleaf forests burned over the course of the annual fire season only 19 and 14% of grasslands and shrublands did so.

3. Severity The severity of burning exhibits a distinct temporal pattern, with a higher mean severity of burning identified across all vegetation types during the peak months (June to September) of each annual fire season. The mean burn severity is lowest at the start of the fire season and increases over the subsequent months. Areas which burn at the end of the annual fire season do so with a severity of a similar magnitude to the start. Fires which occur in deciduous broadleaf forests burn tend to result in lower severity burns. The fires which cause greatest damage to these ecosystems occur in August each year. In contrast grassland fires are much more severe with the most damaging fires occurring earlier each year (June to July). A positive relationship is identified between the fire frequency and the severity of burning irrespective of vegetation type, with areas which burn every year doing so with a higher severity than those which burn less

frequently.

The characteristics of the fire regimes within the area of interest are determined by a complex interaction between human activity, changes in vegetation dynamics and interannual variability in climate. The temporal distribution as well as the severity of burning follows the vegetation growth cycle with the largest area and most severe burning occurring when the fuel layer has senesced. Distinct patterns of recurrent fire activity are evident within the area of interest, with the same locations burning each year. The vegetation recovers quickly after the passage of fire, with the frequency of burning exhibiting a positive relationship with burn severity. The more frequent the fires, the greater the severity of burning. These data support the theory that the grass biomass is maintained by recurrent fires, and these fire-prone ecosystems of southern Africa are dependent on the frequent occurrence of burning.

Chapter 8

Conclusions

The focus of this study has been the development of a new, generic approach to change detection applicable to high temporal and moderate spatial resolution satellite data. This has been applied to the problem of locating and delineating daily burned areas at a regional scale over a five year period. Conclusions specific to each section of the study have been presented in the summaries at the end of each chapter. The aim of this chapter is to draw the main conclusions from the work presented in the previous chapters in terms of the objectives of the research stated in Chapter 1.

8.1 Summary of work

Chapter 2 has provided a review of the methods traditionally applied to the detection of land cover change from remote sensing data. The limitations of these are discussed and the requirements for a change detection model are defined in terms of the major shortcomings of these approaches. Three key issues are identified. These are stated as the need to (i) account for angular variations in the remote sensing signal, (ii) account for phenological variations in the surface, and (iii) identify and remove noisy observations from the temporal sequence. Chapter 3 provides a discussion of the causes and ecological impacts of fire within southern African ecosystems. The diurnal, seasonal and interannual distribution of burning are characterised through an analysis of daily MODIS active fire detections over a five year period, and the spectral features of burned surfaces and their temporal persistence in the remote sensing signal are investigated. These findings enable the definition of a further set of requirements for the application of a change detection model to the identification of fire affected areas. Chapter 4 reviews the approaches typically used to correct remote sensing data for directional effects. Following on from this a new, generic approach to the detection of land surface change from high temporal and moderate spatial resolution data is introduced.

The second half of the study is concerned with the application of the change detection model to the identification of burned surfaces, and the analysis of the results. Chapter 5 introduces the data sources used and the pre-processing steps applied to these. The adaptation of the model to the explicit detection of sudden changes in the surface is described, and a set of post-processing steps developed in order to separate burned areas from those which exhibit similar spectral

changes. Following the methods introduced in Chapters 4 and 5 daily burned area datasets for five annual fire seasons (2000-2004) are produced. These are compared to three other sources of active fire and burned area information in Chapter 6. Finally a characterisation of the fire regime within the area of interest over the five year period is provided in Chapter 7 based on an analysis of the burned area results.

8.2 Aims of the study

The principal objectives of the research were stated in Chapter 1 as;

1. **The development of an algorithm suitable for the detection of sudden surface change from daily moderate spatial resolution optical remote sensing data**
2. **The application of this methodology to the identification and delineation of burned areas in southern Africa on a daily basis for a five year period (2000-2004)**
3. **The characterisation and analysis of the fire regimes of southern African ecosystems from the data produced via Objectives 1 and 2 over the five annual fire seasons**

The following sections assess the accomplishment of these objectives in this Thesis. A discussion of the key issues associated with each is provided, and conclusions are drawn.

8.2.1 Objective 1: A change detection model

A review of the literature (Chapter 2) has highlighted three main limitations associated with the methods traditionally applied to the detection of land cover change from optical remote sensing data sources. The first involves the presence of directional effects in the remote sensing signal. These are of particular importance in data acquired by wide field of view sensors such as the AVHRR, MODIS and SPOT-VGT, and may introduce variations in reflectance of a similar magnitude to that caused by the changes which are to be identified. If these angular effects are not accounted for they have the potential to mask the changes of interest, reducing the accuracy with which these may be detected. Change detection studies have typically either ignored, or attempted to minimise these effects through the use of temporal compositing techniques designed

to select near-nadir observations with reduced cloud and atmospheric contamination. This approach is not ideal as the reduction of the dataset to include only near-nadir observations results in a considerably smaller sample size. This decrease in samples has implications for the detection of changes which exhibit low temporal persistence in the remote sensing signal. In addition some compositing criteria have been shown to preferentially select off nadir observations due to directional effects rather than reduced atmospheric or cloud contamination.

The second limitation is concerned with the temporal dynamics of the surface during the time period of the investigation. Change detection studies generally assume the overall phenological conditions to be comparable over the temporal extent of the study. While anniversary date images are typically used to minimise these effects, the identification of sudden and short lived changes in the surface requires high temporal resolution data over long time periods. Low frequency variations in the surface which occur during this time will complicate the identification of the changes of interest. If they are not accounted for these variations will decrease the accuracy with which land cover changes may be identified.

Temporal variations in the characteristics of the surface may also have implications for the first issue stated above. Models which account for the angular component of the remote sensing signal reviewed in Chapter 4 are typically inverted over a short temporal window. Directional observations acquired over a 16 day period with a requirement for a minimum of 7 cloud free samples during this time are generally used to provide a prediction of reflectance under a subsequent angular scenario, with the assumption that the surface remains static over this temporal period (Strahler *et al.* 1999a, Roy *et al.* 2002). The presence of missing samples in a time series of remote sensing data due to cloud or atmospheric effects may necessitate the inversion of the BRDF model over a longer time period. This will invalidate the model assumption of static surface properties which control the BRDF over this time.

The third issue associated with the detection of land cover changes identified in Chapter 2 is the presence of atmospheric and cloud effects in the remote sensing data. All change detection techniques will be sensitive to noise in the data resulting from cloud or cloud shadows and atmospheric contamination. The presence of these will significantly reduce the capability of the change detection algorithm to accurately identify the changes of interest, and as with the issues highlighted above may result in the inaccurate identification of change events.

Objective 1 has been met through the development of a change detection model which ad-

addresses the three key issues identified above. The model accounts for the directional effects present within moderate spatial and high temporal resolution optical remote sensing data, through the inversion of a BRDF model. The second issue is addressed through the incorporation of an empirical temporal model along with the angular model. This accounts for low frequency variations in the surface, allowing for the application of the temporal BRDF model to much longer time periods than the traditional “static” 16 day moving window approach. Sudden changes in the surface are identified explicitly using a “step function kernel”. This statistical framework allows for the calculation of uncertainty in the model parameters under different angular sampling scenarios, as well as the estimation of noise within the observations. Noisy data are identified through the definition of a Zscore which is related to the probability of a prediction of reflectance belonging to the same set as that used in the model inversion. These are removed from the time series and therefore do not contribute to subsequent predictions. The use of the BRDF model accounts for angular variations in the remote sensing signal, while the temporal model accounts for phenological changes and facilitates the inversion of the angular model over longer time periods. In conjunction with the statistical identification and removal of outliers this results in a clearer change signal and thus the improved detection of surface change.

8.2.2 Objective 2: Mapping fire affected areas

The successful implementation of a change detection model requires a detailed understanding of the nature of the change to be identified. This is achieved in Chapter 3 through an analysis of (i) the spatial and temporal distribution of fire activity, and (ii) the spectral characteristics of burned surfaces within the southern Africa study region. Following on from this a set of criteria for the identification of fire affected areas from remote sensing data sources are defined, and the change detection model developed under Objective 1 is adapted to the problem of locating and delineating burned areas.

The spatial and temporal distribution of fire activity has been determined through the analysis of daily active fire detections from the MODIS sensor over the five year period from January 2000 to December 2004. Fires are identified within each of the main vegetation types across the study area during this time, with over 99% of the annual fire activity each year occurring between the months of April and November. The pattern of burning follows the phenology of

the vegetation with the peak of the annual fire season corresponding to the point at which the vegetation is driest. The locations of active fires have been used to characterise the spectral nature of the burned surfaces as well as their post-fire evolution. Although only near-nadir ($\pm 10^\circ$) observations (which reduces the number of observations by approximately 40%) have been used in the analysis, the pre-burn and post-burn surfaces are statistically similar and their separability is very low. MODIS bands 2, 5 and 6 provide the highest separabilities between burned and un-burned surfaces while the changes observed at the remaining 4 wavelengths tend to be small and variable. The burned surfaces exhibit a fast recovery with a burn signal detectable in certain ecosystems (deciduous broadleaf forests and woody savannas) for only seven days after the fire. These findings reinforced the need to address the issues identified under Objective 1 in order to increase the detectability of potentially low magnitude changes in the remote sensing signal. The persistence of these changes is also of significance and indicates that recovery of the burned surfaces may occur rapidly after the fire. In order to ensure the maximum probability of detection of these burned areas it is clearly necessary to acquire images as near to the day of burning and with as high a revisit period as possible. Near-daily satellite acquisitions from high temporal resolution sensors provide the only feasible means of identifying these changes.

With a consideration of these characteristics, Objective 2 is met through the application of the temporal change detection models developed under Objective 1 to daily, moderate (500m) spatial resolution satellite data for a five year period. The southern Africa fire season is defined as the eight months from the beginning of April until the end of November each year, as this encompasses over 99% of the fires detected annually. The fast recovery of the post-fire surface in addition to the possibility of missing observations due to cloud or smoke necessitates the use of daily data for the accurate detection of fire-induced surface change. The literature reviewed and the analysis performed in Chapter 3 indicate that MODIS band 2 and 5 reflectances provide the highest separabilities between pre-burn and post-burn surfaces. The temporal change detection models were therefore applied to temporal sequences of these two wavebands. In addition as changes due to causes other than burning may result in similar spectral changes bands 1 and 7 were used in order to exclude confusing spectral change. From an analysis of the results it was clear that changes other than burning were identified through the minimum band 2/band 5 criteria described in Chapter 5. Several post-processing steps were therefore introduced in order to meet Objective 2. These involved (i) the calculation of a proportional change measure, (ii)

thresholding this to identify significant change, and (iii) the identification and removal of water induced surface change. The results of these steps are monthly datasets documenting the daily occurrence of burning at a spatial resolution of 500m for five annual fire seasons.

8.2.3 Objective 3: Analysis of the fire regime of southern Africa

The datasets produced under Objective 2 contain a wealth of information describing the occurrence of burning within southern Africa at a variety of scales. The third objective of the research was therefore to analyse this data and to perform a characterisation of the fire regime within the study area and over the time period of interest. This has been achieved indirectly through a comparison with other sources of fire-related information in Chapter 6, and directly through the analysis and interpretation of the burned areas in Chapter 7.

Due to the lack of ground based validation data the burned areas have been compared to three independent sources of fire-related information. These are; (i) daily 1km day and night active fire detections from MODIS Terra and Aqua, (ii) SAFARI 2000 500m burned areas for July 2000 (Roy 2005), and (iii) GBA2000 1km monthly burned areas, April to November 2000 (Gregoire *et al.* 2003). Similarities and differences are apparent in all three of these sources and are likely to be due to differences in the spatial resolutions and characteristics of the input data in addition to the algorithms used in their creation. While the reasons for the disagreements have been investigated in Chapter 6 the relative errors of omission and commission are unknown as none of the burned area datasets have been systematically validated and the active fire counts only provide a snapshot of the fire activity.

Chapter 7 is more directly concerned with fulfilling Objective 3. This chapter has involved the characterisation of fire regimes within southern African ecosystems from the data produced via Objectives 1 and 2. Four key aspects relating to the occurrence of fires within the study area have been analysed; (i) frequency, (ii) seasonality, (iii) spatial extent, (iv) severity. The characterisation of these provide a detailed description of the fire regimes within southern African ecosystems over the past five years. The patterns identified within each of these aspects of the fire regime have been interpreted by drawing on information contained within the literature as well as through an examination of additional data sources.

8.3 Principal contributions

This study has made a number of contributions to both the field of remote sensing change detection and the fire ecology of southern Africa. These can be separated into two themes. The first constitutes the bulk of the experimental work and involves the development of the change detection model. The second is concerned with the analysis of the fire affected areas and the characterisation and interpretation of the southern African fire regime.

The temporal BRDF model developed in this study allows for the normalisation of the angular effects within remote sensing data over long time periods. BRDF models are typically inverted over time periods of two weeks to a month under the assumption that the properties which control the surface BRDF remain static over this period. In the presence of missing samples or noisy data due to cloud or atmospheric effects, there may be an insufficient number of samples over which to perform a reliable inversion. The incorporation of the temporal component allows for the inversion of the BRDF model over much greater time periods than the “static” version. The application of the BRDF models to longer time periods enables better estimation of noise within the data due to the greater number of samples. This subsequently allows for the improved identification of noisy observations within the time series and the removal of these results in better estimation of model parameters and improved predictions of reflectance. Temporal sequences of reflectance which have been corrected for angular effects and noisy observations are required by the scientific community for the retrieval of vegetation structural attributes such as the leaf area index, to calculate biophysical variables such as vegetation indices, and in climatology studies to derive the land surface albedo (Strahler *et al.* 1999a). The temporal BRDF model developed in this study therefore has potential uses beyond the detection of land cover change.

The model developed in this study constitutes a generic approach to the detection of land cover change. Sudden changes in the characteristics of the surface are modelled through the incorporation of a “step function kernel” along with the temporal BRDF model. The detection of the day on which the change occurs (parameter c) has been adapted to identify burn-type changes in reflectance through the definition of a spectral filter. The criteria used to locate the most appropriate value of c may be defined according to the changes of interest. Identifying c based on the global error in the model fit, for example, will locate the greatest change which has occurred across all wavebands. The model may therefore be applied to the detection of

surface changes caused by factors other than fire. The results presented in Section 5.5.3 (Chapter 5) indicate that the change detection model may be applied to the problem of identifying flood events based on the sudden decrease in near to middle infrared reflectances which occur.

The burned area datasets created in the first half of the study and the analysis of these performed in the second half has produced a wealth of information relating to fire regimes of southern Africa over the past five years. Spatially explicit burned area information for southern Africa is currently only available at a spatial resolution of 500m for July and September 2000 (Roy 2005), at a resolution of 1km for the year 2000 (Gregoire *et al.* 2003), and at a resolution of 5km for three fire seasons between 1989 and 1991 (Barbosa *et al.* 1999). This study has developed daily burned area information at a spatial resolution of 500m for the eight months of five consecutive fire seasons. The effective management of vegetation fires as well as the sustainability of fire dependent ecosystems requires a sound understanding of the spatial and temporal distribution of burning. Appropriate land management schemes cannot be conceived without a consideration of the fire ecology of an ecosystem. Due to the lack of spatially explicit and multi-annual burned area information, little is known about the characteristics and variations of fire regimes across southern Africa. The effects of climate change on the fire regimes of these ecosystems and the determination of the feedbacks involved cannot be determined without a detailed knowledge of the fire ecology of these. The analysis and characterisation of the fire regime within the area of interest at an interannual as well as intraannual scale provides valuable information relating to the fire ecology of these ecosystems. Variations in the spatial and temporal distribution of burning within different ecosystems has been quantified, areas subjected to annual burning identified, and the severity of burning investigated. A novel indicator for burn severity has been introduced and used to characterise the temporal and spatial variability of this, as well as the relationship between the severity and the frequency of burning.

The fire regime of a region will determine both the quantity and type of gases emitted by biomass burning. Detailed burned area information is therefore of importance in the accurate modelling of biomass burning emissions and in the creation of emissions inventories. The area and type of vegetation which burns annually currently provide the greatest uncertainty in the calculation of gaseous and aerosol emissions due to burning (Tansey *et al.* 2004b). The spatial and temporal variability of biomass burning has therefore typically been excluded from models of emission inventories due to the lack of systematic and consistent burned area information

(Schaaf *et al.* 2002). The burned area datasets produced in this study constitute an important characterisation of the distribution and temporal variability of burning within southern African ecosystems, while the change detection model provides a rigorous modelling framework for the identification of burning on a daily basis at regional to global scales.

8.4 Further Research

The work documented in this thesis has developed a new, generic approach to change detection which in this case has been applied to the problem of locating and delineating fire affected areas, and the creation of a five year dataset documenting the daily occurrence of burning within the study area. Although the data has been compared to three other independently produced active fire and burned area datasets, it requires further validation. The validation of spatially and temporally large datasets will always be problematic, and is especially so due to the nature of the changes of interest. Consequently there is little heritage for fire-product validation, and none of the burned area datasets currently available to the scientific community have been systematically or consistently validated (Roy *et al.* 2005a). Protocols are however in place for the validation of the SAFARI 2000 and GBA2000 burned area products used in the analysis in Chapter 6 (Boschetti *et al.* 2004, Roy *et al.* 2005a). In particular the protocol developed for the validation of the SAFARI 2000 burned areas has involved the interpretation of (11) high spatial resolution Landsat images to derive maps of the location and approximate date of burning, which have subsequently been verified with ground based information. Should this dataset be made available to the scientific community it will greatly facilitate and be extremely valuable in the validation of other fire-related products.

The change detection approach developed in this study is based on the inversion of a temporal BRDF model, under the assumption that fire induced changes in the overall “brightness” of the surface are not too great. While the validity of this assumption is dependent on the characteristics of the pre-fire surface and the extent to which the structure of the vegetation has been altered by the fire, the algorithm has been shown to model the burned surfaces within the area of interest with sufficient accuracy to enable the identification of step changes in reflectance. The application of the model to different ecosystems however requires further investigation. The suitability

of the methods developed to the identification of burning within different vegetation types and under different fire regimes (for example crown as opposed to surface fires) will be dependent on the nature of the pre-fire and post-fire surfaces, and the changes which occur in the shape of the surface BRDF as a result of burning. In addition the applicability of the model to different types of surface change is a path for future investigation. Although the model developed constitutes a generic approach to change detection which may be adapted to the nature of the changes which are to be identified, its applicability to surface changes other than those induced by burning has yet to be investigated.

The analysis of the burned area results has enabled the characterisation of the fire regimes of southern African ecosystem over the last five years. While this has provided information which was previously lacking, the interpretation of the trends identified would inevitably benefit from further analysis and in particular the integration with additional data sources. An understanding of the mechanisms which determine the positive relationship between the severity and frequency of burning identified in Chapter 7 would, for example, be improved through an analysis of data describing the productivity of these ecosystems after the occurrence of fire. Parameters related to ecosystem processes such as the Net Primary Productivity (NPP) available globally every 8 days as a 1km MODIS product may provide useful information in the interpretation of this relationship. In addition an understanding of the determinants of the temporal variability of burning identified in Chapter 7 would greatly benefit from the analysis of climate data, in particular precipitation rates over the five year period. Short term rainfall variability has been shown to account for a large proportion of the interannual variability in land cover changes within southern African ecosystems (Vanacker *et al.* 2005).

Finally, the aspects of the fire regime characterised in Chapter 7 constitute useful inputs to large scale ecological models. As fires play an essential role in determining the global distribution of vegetation they are being increasingly represented in models of global vegetation dynamics. Although numerous fire models have been developed for various applications at a variety of spatial and temporal scales, they require a definition of the frequency of fire occurrence and the time which elapses between subsequent fires. The quantification of the frequency of burning and the fire return interval within southern African ecosystems is thus a useful input to such models.

In conclusion, this study has developed a new, generic approach to the detection of changes from high temporal and moderate spatial resolution satellite data. The model accounts for angu-

lar effects present in the remote sensing signal and incorporates a temporal model of the surface. As such it may be applied to longer time series than traditional approaches and provides a “clean” time series of reflectance for use in a further analysis. While the potential applications of this model are wide, in the context of this study it has been applied specifically to the problem of locating and delineating fire affected areas. The burned area datasets constitute a source of information previously unavailable which have potential application to a wide range of environmental monitoring problems.

References

- ABUELGASIM, A., GOPAL, S., IRONS, J., and STRAHLER, A., 1996, Classification of ASAS multiangle and multispectral data using artificial neural networks. *Remote Sensing of Environment*, **57**, 79–87.
- ADAMS, J., SABOL, D., KAPOV, V., FILHO, R., ROBERTS, D., SMITH, M., and GILLESPIE, A., 1995, Classification of multispectral images based on fractions of endmembers: Application to land cover change in the Brazilian Amazon. *Remote Sensing of Environment*, **52**, 137–154.
- AL-RAWI, K., CASANOVA, J., and CALLE, A., 2001, Burned area mapping system and fire detection system, based on neural networks and NOAA-AVHRR imagery. *International Journal of Remote Sensing*, **22**, 2015–2032.
- AMIRO, B., 2001, Paired-tower measurements of carbon and energy fluxes following disturbance in the boreal forest. *Global Change Biology*, **7**, 253–268.
- ANDREAE, M., 1991, *Global Biomass Burning: Atmospheric, Climatic and Biospheric Implications* (MIT Press, Cambridge MA), pp. 3–21.
- ANDREAE, M., 1998, The IGAC Biomass Burning Experiment (BIBEX): Rationale and Evolution, <http://www.igac.noaa.gov/newsletter/15/bibex.php>, Accessed: August 2005.
- ANDREWS, P., and QUEEN, L., 2001, Fire modelling and information system technology. *International Journal of Wildland Fire*, **10**, 343–352.
- ARINO, O., and MELINOTTE, J., 1997, Fire index atlas. *Earth Observations Quarterly*, **50**, 11–16.

- ARINO, O., and PLUMMER, S., 2000, Along Track Scanning Radiometer World Fire Atlas: Validation of the 1997-98 Active Fire Product.
- ARINO, O., ROSAZ, J., and GOLOUB, P., 1999, The ATSR World Fire Atlas: A synergy with "POLDER" aerosol products. *Earth Observations Quarterly*, **64**, 1–6.
- ASNER, G., 2000, Contributions of multi-view angle remote sensing to land-surface and biogeochemical research. *Remote Sensing Reviews*, **18**, 137–162.
- BARBOSA, P., GREGOIRE, J., and PEREIRA, J., 1999, An algorithm for extracting burned areas from time series of AVHRR GAC data applied at a continental scale. *Remote Sensing of Environment*, **69**, 253–263.
- BARBOSA, P., PEREIRA, J., and GREGOIRE, J., 1998, Compositing criteria for burned area assessment using multitemporal low resolution satellite data. *Remote Sensing of Environment*, **65**, 38–49.
- BARNESLEY, M., ALLISON, D., and LEWIS, P., 1997, On the information content of multiple view-angle (MVA) images. *International Journal of Remote Sensing*, **18**, 1937–1960.
- BARTHOLOME, E., and BELWARD, A., 2005, GLC2000: A new approach to global land cover mapping from Earth Observation data. *International Journal of Remote Sensing*, **In Press**.
- BATESON, A., and CURTISS, B., 1996, A method for manual endmember selection and spectral unmixing. *Remote Sensing of Environment*, **55**, 229–243.
- BELWARD, A., ESTES, J., and KLINE, K., 1999, The IGBP-DIS Global 1-km Land-Cover Data Set DISCover: A Project Overview. *Photogrammetric Engineering and Remote Sensing*, **65**, 1013–1020.
- BELWARD, A., KENNEDY, P., and GREGOIRE, J., 1994, The limitation and potential of AVHRR GAC data for continental scale fire studies. *International Journal of Remote Sensing*, **15**, 2215–2234.
- BIRD, M., VEENENDAAL, E., MOYO, C., LLOYD, J., and FROST, P., 2000, Effect of fire and soil texture on soil carbon in a sub-humid savanna. *Geoderma*, **9**, 71–90.

- BOND, W., and KEELEY, J. E., 2005, Fire as a global 'herbivore': The ecology and evolution of flammable ecosystems. *Trends in Ecology and Evolution*, **20**, 387–394.
- BOND, W., WOODWARD, F. I., and MIDGLEY, G., 2004, The global distribution of ecosystems in a world without fire. *New Phytologist*, 525–538.
- BOREL, C., GERSTL, S. A., and POWERS, B., 1991, The radiosity method in optical remote sensing of structured 3-D surfaces. *Remote Sensing of Environment*, **36**, 13–44.
- BOSCHETTI, L., EVA, H., BRIVIO, P., and GALLEG0, J., 2004, The validation protocol of GBA2000 global burned area maps. *Proceedings, Igarss*, 1–4.
- BOUSQUET, P., PEYLIN, P., CIAIS, P., LE QUERE, C., FRIEDLINGSTEIN, P., and TANS, P., 2000, Regional changes in carbon dioxide fluxes of land and oceans since 1980. *Science*, **290**, 1342–1346.
- BRAGG, T., 1995, *The changing prairie, North American grasslands* (Oxford University Press, New York), pp. 49–81.
- BRIVIO, P., MAGGI, M., BINAGHI, E., and GALLO, I., 2003, Mapping burned surfaces in Sub-Saharan Africa based on multi-temporal neural network classification. *International Journal of Remote Sensing*, **24**, 4003–4018.
- BROWN, J., and SMITH, J., 2000, Wildland fire in ecosystems: Effects of fire on flora, Technical report, Department of Agriculture, Forest Service, Rocky Mountain Research Station.
- BROWN, P., KAUFMANN, M., and SHEPPERD, W. D., 1999, Long-term landscape patterns of past fire events in a montane ponderosa pine forest of central Colorado. *Landscape Ecology*, **14**, 513–532.
- BRUSTET, J., VICKOS, J., FONTAN, J., MANISSADJAN, K., PODAIRE, A., and LAVENU, F., 1991, *Global Biomass Burning: Atmospheric, Climatic and Biospheric Implications* (MIT Press, Cambridge MA), pp. 47–52.
- BUECHLING, A., and BAKER, W., 2004, A fire history from tree rings in a high-elevation forest of Rocky Mountain National Park. *Canadian Journal for Forest Research*, **34**, 1259–1273.

- CAHOON, D., LEVINE, J., MINNIS, P., TENNILLE, G., YIP, T., HECK, P., and STOCKS, B., 1991, *Global Biomass Burning: Atmospheric, Climatic and Biospheric Implications* (MIT Press, Cambridge MA), pp. 61–66.
- CAHOON, D., STOCKS, B., LEVINE, J.S. AND COFER, W., and O'NEILL, K., 1992, Seasonal distribution of African savanna fires. *Nature*, **359**, 812–815.
- CANDELL, J., CIAIS, P., and COX, P. AND HEIMANN, M., 2004, Quantifying, understanding and managing the carbon cycle in the next decades. *Climatic Change*, **67**, 147–160.
- CHAFER, C., NOONAN, M., and MACNAUGHT, E., 2004, The post-fire measurement of fire severity and intensity in the Christmas 2001 Sydney wildfires. *International Journal of Wildland Fire*, **13**, 227–240.
- CHEN, J., CHEN, W., and LIU, J., 2000, Annual carbon balance of Canada's forests during 1895–1996. *Global Biogeochemical Cycles*, **14**, 839–849.
- CHEN, J., and CIHLAR, J., 1997, A hotspot in a simple bidirectional reflectance model for satellite applications. *Journal of Geophysical Research*, **102**, 25907–25913.
- CHEN, J., and LEBLANC, S., 2000, A four-scale bidirectional reflectance model based on canopy architecture. *IEEE Transactions on Geoscience and Remote Sensing*, **35**, 1316–1337.
- CHRISTENSEN, N., 1993, *Fire in the environment: The ecological, atmospheric and climatic importance of vegetation fires* (Wiley, New York), pp. 233–245.
- CHUVIECO, E., and MARTIN, M., 1994, A simple method for fire growth monitoring using AVHRR channel 3 data. *International Journal of Remote Sensing*, **15**, 3141–3146.
- CHUVIECO, E., MARTIN, M., and PALACIOS, A., 2002, Assessment of different spectral indices in the red-near-infrared spectral domain for burned land discrimination. *International Journal of Remote Sensing*, **23**, 5103–5110.
- CIHLAR, J., 1994, Detection and removal of cloud contamination from AVHRR images. *IEEE Transactions on Geoscience and Remote Sensing*, **32**, 583–589.

- CIHLAR, J., MANAK, D., and VOISIN, N., 1994, AVHRR bidirectional reflectance effects and compositing. *Remote Sensing of Environment*, **48**, 77–88.
- COCHRANE, M., ALENCAR, A., SCHULZE, M., SOUZA, C., NEPSTAD, D., LEFEBVRE, P., and DAVIDSON, E., 1999, Positive feedbacks in the fire dynamic of closed canopy tropical forests. *Science*, **284**, 1832–1835.
- COCKE, A., FULE, P., and CROUSE, J., 2005, Comparison of burn severity assessments using Differenced Normalized Burn Ratio and ground data. —*International Journal of Wildland Fire*, **14**, 189–198.
- COHEN, W., and FIORELLA, M., 1998, *Remote sensing change detection: Environmental monitoring methods and applications* (Sleeping Bear Press), pp. 89–102.
- COLLINS, J., and WOODCOCK, C., 1994, Change detection using the Gramm-Schmidt transformation applied to mapping forest mortality. *Remote Sensing of Environment*, **50**, 267–279.
- COLLINS, J., and WOODCOCK, C., 1995, An assessment of several linear change detection techniques for mapping forest mortality using multitemporal Landsat TM data. *Remote Sensing of Environment*, **56**, 66–77.
- COLLINS, S., GLENN, S., and GIBSON, D., 1995, Experimental analysis of intermediate disturbance and initial floristic composition: Decoupling cause and effect. *Ecology*, **76**, 486–492.
- CONARD, S., SUKHININ, A., STOCKS, B., CAHOON, D., DAVIDENKO, E., and IVANOVA, G., 2002, Determining effects of area burned and fire severity on carbon cycling and emissions in Siberia. *Climatic Change*, **55**, 197–211.
- COPPIN, P., JONCKHEERE, I., NACKAERTS, K., MUYS, B., and LAMBIN, E., 2004, Digital change detection methods in ecosystem monitoring: A review. *International Journal of Remote Sensing*, **25**, 1565–1596.

- COPPIN, P., NACKAERTS, K., QUEEN, L., and BREWER, K., 2001, Operational monitoring of green biomass change for forest management. *IEEE Transactions on Geoscience and Remote Sensing*, **67**, 603–611.
- COPPIN, R., and BAUER, M., 1994, Processing of multi-temporal Landsat imagery to optimize extraction of forest cover change features. *IEEE Transactions on Geoscience and Remote Sensing*, **32**, 918–927.
- CRUTZEN, P., and ANDREAE, M., 1990, Biomass burning in the tropics: Impacts on atmospheric chemistry and biogeochemical cycles. *Science*, **250**, 1669–1677.
- DAI, X., and KHORRAM, S., 1998, The effects of image misregistration on the accuracy of remotely sensed change detection. *IEEE Transactions on Geoscience and Remote Sensing*, **36**, 1566–1577.
- DESANKER, P., FROST, P., JUSTICE, C., and SCHOLES, R., 1995, The Miombo Network: Framework for a terrestrial transect study of land-use and land-cover change in the Miombo ecosystems of Central Africa, Technical report, The International Geosphere-Biosphere Programme.
- DIAZ-DELGADO, R., LLORET, F., and PONS, X., 2003, Influence of fire severity on plant regeneration by means of remote sensing imagery. *International Journal of Remote Sensing*, **24**, 1751–1763.
- DIAZ-DELGADO, R., LLORET, F., and PONS, X., 2004, Statistical analysis of fire frequency models for Catalonia (NE Spain, 1975–1998) based on fire scar maps from Landsat MSS data. *International Journal of Wildland Fire*, **13**, 89–99.
- DINER, D., J., B., REILLY, T., BRUEGGE, J., CONEL, J., KAHN, A., MARTCHONIK, J., ACKERMAN, T., DAVIES, R., GERSTL, S., GORDON, H., MULLER, J.-P., MYNENI, R., SELLERS, P., PINTY, B., and VERSTRAETE, M., 1998, Multi-angle Imaging SpectroRadiometer instrument description and experiment overview. *IEEE Transactions on Geoscience and Remote*, **36**, 1072–1087.

- DISNEY, M., LEWIS, P., and NORTH, P., 2000, Monte Carlo methods in optical canopy reflectance modelling. *Remote Sensing Reviews*, **18**, 163–196.
- DOZIER, J., 1981, A method for satellite identification of surface temperature fields of subpixel resolution. *Remote Sensing of Environment*, **11**, 221–229.
- DWYER, E., GREGOIRE, J., and MALINGREAU, J., 1998, A global analysis of vegetation fire using satellite images: Spatial and temporal dynamics. *Ambio*, **27**, 175–181.
- DWYER, E., PEREIRA, J., GREGOIRE, J., and DACAMARA, C., 1999, Characterisation of the spatio-temporal patterns of global fire activity using satellite imagery for the period April 1992 to March 1993. *Journal of Biogeography*, **27**, 57–69.
- DWYER, E., PINNOCK, S., GREGOIRE, J., and PEREIRA, J., 2000, Global spatial and temporal distribution of vegetation fire as determined from satellite observations. *International Journal of Remote Sensing*, **21**, 1289–1302.
- EASTWOOD, J., PLUMMER, S., and WYATT, B., 1998, The potential of SPOT-Vegetation data for fire scar detection in boreal forests. *International Journal of Remote Sensing*, **19**, 3681–3687.
- ELLIOTT, K., HENDRICK, A., MAJOR, J., VOSE, J., and SWANK, W., 1999, Vegetation dynamics after a prescribed fire in the southern Appalachians. *Forest Ecology and Management*, **114**, 199–213.
- ESRI, 1999, *ESRI data and maps*, Redlands, CA.
- EVA, H., and LAMBIN, E., 1998a, Burnt area mapping in Central Africa using ATSR data. *International Journal of Remote Sensing*, **18**, 3473–3497.
- EVA, H., and LAMBIN, E., 1998b, Remote sensing of biomass burning in tropical regions: Sampling issues and multisensor approach. *Remote Sensing of Environment*, **64**, 292–315.
- EVA, H., and LAMBIN, E., 2000, Fires and land-cover change in the tropics: A remote sensing analysis at the landscape scale. *Journal of Biogeography*, **27**, 765–776.

- EVA, H. MALINGREAU, J., GREGOIRE, J., BELWARD, A., and MUTLOW, C., 1998, The advance of burnt areas in Central Africa as detected by ERS-1 ATSR-1. *International Journal of Remote Sensing*, **19**, 1635–1637.
- FERNANDEZ, A., ILLERA, P., and CASANOVA, J., 1996, Automatic mapping of surfaces affected by forest fires in Spain using AVHRR NDVI composite image data. *Remote Sensing of Environment*, **60**, 153–162.
- FIERENS, F., 2002, GLOBSCAR final report, Technical report, VITO, Belgium.
- FISHMAN, J., FAKHRUZZAMAN, K., CROS, B., and NGANGA, D., 1991, Identification of widespread pollution in the southern hemisphere deduced from satellite analyses. *Science*, **252**, 1693–1696.
- FLASSE, S., and CECCATO, P., 1996, A contextual algorithm for AVHRR fire detection. *International Journal of Remote Sensing*, **17**, 419–424.
- FRASER, R., FERNANDES, R., and LATIFOVIC, R., 2002, Multi-temporal burned area mapping using logistic regression analysis and change metrics. *Proceedings, Igarss*, **3**, 1486–1488.
- FRASER, R., and LI, Z., 2002, Estimating fire-related parameters in boreal forest using SPOT VEGETATION. *Remote Sensing of Environment*, **82**, 95–110.
- FRASER, R., LI, Z., and CIHLAR, J., 2000a, Hotspot and NDVI Differencing Synergy (HANDS): A new technique for burned area mapping over boreal forest. *Remote Sensing of Environment*, **74**, 362–376.
- FRASER, R., LI, Z., and LANDRY, R., 2000b, SPOT VEGETATION for characterizing boreal forest fires. *International Journal of Remote Sensing*, **21**, 3525–3532.
- FROST, P., 1999, Fire in southern African woodlands: Origins, impacts, effects and control, In *Proceedings of an FAO meeting on Public Policies Affecting Forest Fires*, volume 138 of *FAO Forestry Paper*, pp. 181–205.
- FROST, P., and ROBERTSON, F., 1985, *Determinants of Tropical Savannas* (IRL Press, Oxford), pp. 93–140.

- FULLER, D., and FULK, M., 2001, Burned areas in Kalimantan Indonesia mapped with NOAA AVHRR and Landsat TM imagery. *International Journal of Remote Sensing*, **22**, 691–697.
- FUNG, T., 1990, An assessment of TM imagery for land cover change detection. *IEEE Transactions on Geoscience and Remote Sensing*, **28**, 681–684.
- FUNG, T., and LEDREW, E., 1987, Application of principal components analysis to change detection. *Photogrammetric Engineering and Remote Sensing*, **53**, 1649–1658.
- FUNG, T., and LEDREW, E., 1988, The determination of optimal threshold levels for change detection using various accuracy indices. *Photogrammetric Engineering and Remote Sensing*, **54**, 1449–1454.
- GAO, F., SCHAAF, C., JIN, Y., LUCHT, W., and STRAHLER, A., 2003, Deriving albedo from coupled MERIS and MODIS surface products, In *Proceedings, MERIS Workshop, Frascati, Italy*, pp. 1–11.
- GARCIA-HARO, F., GILABERT, M., and MELIA, J., 2001, Monitoring fire-affected areas using Thematic Mapper data. *International Journal of Remote Sensing*, **22**, 533–549.
- GER, 2000, GER 3700 Specifications, <http://www.ger.com/3700.html>, Accessed: June 2005.
- GIGLIO, L., DESCLOITRES, J., JUSTICE, C., and KAUFMAN, Y., 2003a, An enhanced contextual fire detection algorithm for MODIS. *Remote Sensing of Environment*, **87**, 273–282.
- GIGLIO, L., KENDALL, J., and JUSTICE, C., 1999, Evaluation of global fire detection algorithms using simulated AVHRR infrared data. *International Journal of Remote Sensing*, **20**, 1947–1985.
- GIGLIO, L., KENDALL, J., and MACK, R., 2003b, A multi-year active fire dataset for the tropics derived from the TRMM VIRS. *International Journal of Remote Sensing*, **24**, 4505–4525.
- GIGLIO, L., and PINZON, G., 2003, Comment on "Seasonal, intraseasonal, and interannual variability of global land fires and their effects on atmospheric aerosol distribution" by Y.Ji and E.Stocker. *Journal of Geophysical Research*, **108**, 4754–4758.

- GILL, A., 1975, Fire and the Australian flora: A review. *Australian Forestry*, **38**, 2–25.
- GITAS, I., MITRI, G., and VENTURA, G., 2004, Object-based image classification for burned area mapping of Creus Cape, Spain, using NOAA-AVHRR imagery. *Remote Sensing of Environment*, **92**, 409–413.
- GOEL, N., 1989, *Theory and applications of optical remote sensing* (Wiley, New York), pp. 205–241.
- GOEL, N., and THOMPSON, R., 2000, A snapshot of canopy reflectance models, and a universal model for the radiation regime. *Remote Sensing Reviews*, **18**, 197–225.
- GOFC, 2005, GOFC-GOLD-FIRE: Overview, <http://gofc-fire.umd.edu/>, Accessed: August 2005.
- GOFC-GOLD, 2003, GOFC-GOLD: Overview, <http://www.fao.org/gtos/gofc-gold/overview.html>, Accessed: August 2005.
- GOLDAMMER, J., and MUTCH, R., 2001, Global forest fire assessment 1990-2000, Technical report, FAO.
- GOPAL, S., and WOODCOCK, C., 1996, Remote sensing of forest change using artificial neural networks. *IEEE Transactions on Geoscience and Remote Sensing*, **34**, 398–404.
- GOVAERTS, Y., PEREIRA, J., PINTY, B., and MOTA, B., 2002, Impact of fires on surface albedo dynamics over the African continent. *Journal of Geophysical Research*, **107**, 1–12.
- GREGOIRE, J., TANSEY, K., and SILVA, J., 2003, The GBA2000 initiative: Developing a global burnt area database from SPOT-VEGETATION imagery. *International Journal of Remote Sensing*, **24**, 1369–1376.
- GROOT, W., and WEIN, W., 2004, Effects of fire severity and season of burn on *Betula glandulosa* growth dynamics. *International Journal of Wildland Fire*, **13**, 287–295.
- GUENTHER, B., XIONG, X., SALOMONSON, V., BARNES, W., and YOUNG, J., 2002, On orbit performance of the earth observing system Moderate Resolution Imaging Spectroradiometer; first year of data. *Remote Sensing of Environment*, **83**, 16–30.

- HALL, F., BOTKIN, D., STREBEL, D., WOODS, K., and GOETZ, S., 1991, Large scale patterns of forest succession as determined by remote sensing. *Ecology*, **21**, 1331–1364.
- HANSEN, M., DEFRIES, R., TOWNSEND, J., and SOHLBERG, R., 2000, Global land cover classification at the 1km spatial resolution using a classification tree approach. *International Journal of Remote Sensing*, **21**, 1331–1364.
- HAO, W., and LIU, M., 1994, Spatial and temporal distribution of tropical biomass burning. *Global Biogeochemical Cycles*, **8**, 495–503.
- HAO, W., LIU, M., and CRUTZEN, P., 1990, *Fire in the tropical biota* (Springer-Verlag, NY), pp. 440–462.
- HENIG-SEVER, N., POLIAKOV, D., and BROZA, M., 2001, A novel method for estimation of wild fire intensity based on ash pH and soil microarthropod community. *Pedobiologia*, **45**, 98–106.
- HENYEY, L. G., and GREENSTEIN, T. L., 1941, Diffuse radiation in the galaxy. *Astrophysics*, **93**, 70–83.
- HICKE, J. A., ASNER, G. P., KASISCHKE, E., H.F., N., RANDERSON, J. T., COLLATZ, G., STOCKS, B., TUCKER, C., SIETSE, L., and FIELD, C., 2003, Postfire response of North American boreal forest net primary productivity analysed with satellite observations. *Global Change Biology*, **9**, 1145–1157.
- HIGGINS, S. I., BOND, W. J., and TROLLOPE, W., 2000, Fire, resprouting and variability: A recipe for grass-tree coexistence in savanna. *Journal of Ecology*, **88**, 213–229.
- HOBBS, R. J., MALLIK, A. U., and GIMINGHAM, C., 1984, Studies on fire in Scottish heathland communities: Vital attributes of the species. *Journal of Ecology*, **72**, 963–976.
- HOELZEMANN, J., SCHULTZ, M., BRASSEUR, G., and GRANIER, C., 2004, Global Wildland Fire Emission Model (GWEM): Evaluating the use of global burnt area satellite data. *Journal of Geophysical Research*, **109**, 3666–3684.

- HOFFA, E., WARD, D., HAO, W., SUSOTT, R., and WAKIMOTO, R., 1999, Seasonality of carbon emissions from biomass burning in a Zambian savanna. *Journal of Geophysical Research*, **104**, 13841–13854.
- HOFFMANN, A., SCHROEDER, W., and JACKSON, R., 2002, Positive feedbacks of fire, climate, and vegetation and the conversion of tropical savanna. *Geophysical Research Letters*, **29**, 2052–2056.
- HOLBEN, B. N., 1986, Characteristics of maximum-value composite images from temporal AVHRR data. *International Journal of Remote Sensing*, **7**, 1417–1434.
- HU, B., LUCHT, W., LI, X., and STRAHLER, A. H., 1997, Validation of kernel-driven semi-empirical models for the surface bidirectional reflectance distribution function of land surfaces. *Remote Sensing of Environment*, **62**, 201–214.
- HUBER, U., and MARKGRAF, V., 2003, European impact on fire regimes and vegetation dynamics at the steppe-forest ecotone of southern Patagonia. *The Holocene*, **13**, 567–579.
- HUDAK, A. T., and BROCKETT, B. H., 2004, Mapping fire scars in a southern African savannah using Landsat imagery. *International Journal of Remote Sensing*, **25**, 3231–3243.
- HUETE, A., JUSTICE, C., and LEEUWEN, W., 1999, *MODIS Vegetation Index: Algorithm Theoretical Basis Document*.
- HUETE, A. R., and JACKSON, R. D., 1988, Soil and atmosphere influences on the spectra of partial canopies. *Remote Sensing of Environment*, **25**, 89–105.
- IGBP, 1988, *The International Geosphere Biosphere Program: A study of global change* (Stockholm).
- IPCC, 2001, Radiative forcing of climate change, http://www.grida.no/climate/ipcc_tar/wg1/216.htm, Accessed: July 2005.
- JACQUEMOUD, S., and BARET, F., 1990, PROSPECT: A model of leaf optical properties spectra. *Remote Sensing of Environment*, **34**, 75–91.

- JAKUBAUSKAS, M. E., LULLA, K. P., and MAUSEL, P., 1990, Assessment of vegetation change in a fire-related forest landscape. *IEEE Transactions on Geoscience and Remote Sensing*, **56**, 371–377.
- JENSEN, J., 1996, *Introductory digital image processing: A remote sensing perspective* (Englewood Cliffs; NJ: Prentice-Hall).
- JHA, C., and UNNI, N., 1994, Digital change detection of forest conversion of a dry tropical forest region. *International Journal of Remote Sensing*, **15**, 2543–2552.
- JI, Y., and STOCKER, E., 2002, Seasonal, intraseasonal and interannual variability of global land fires and their effects on atmospheric aerosol distribution. *Journal of Geophysical Research*, **107**, 4697–4710.
- JOHNSON, R., and KASISCHKE, E., 1998, Change vector analysis: A technique for the multi-spectral monitoring of land cover and condition. *International Journal of Remote Sensing*, **19**, 411–426.
- JUSTICE, C., KENDALL, J., DOWTY, P., and SCHOLES, R., 1996, Satellite remote sensing of fires during the SAFARI campaign using NOAA AVHRR data. *Journal of Geophysical Research*, **101**, 23851–23863.
- JUSTICE, C., VERMOTE, E., TOWNSHEND, J. R. G., DEFRIES, R., ROY, D. P., HALL, D. K., SALOMONSON, V. V., PRIVETTE, J., RIGGS, G., STRAHLER, A., LUCHT, W., MYNENI, R., KNJAZIHHIN, Y., RUNNING, S., NEMANI, R., WAN, Z., HUETE, A., VAN LEEUWEN, W., WOLFE, R., GIGLIO, L., MULLER, J.-P., LEWIS, P., and BARNSLEY, M., 1998, The Moderate Resolution Imaging Spectroradiometer (MODIS): Land remote sensing for global change research. *IEEE Transactions on Geoscience and Remote Sensing*, **36**, 1228–1249.
- JUSTICE, C. O., GIGLIO, L., KORONTZI, S., OWENS, J., MORISETTE, J. T., ROY, D., DESCLOITRES, J., ALLEAUME, S., PETITCOLIN, F., and KAUFMAN, Y., 2002, The MODIS fire products. *Remote Sensing of Environment*, **83**, 244–262.

- KALLURI, S., ZHANG, Z., JAJA, J., LIANG, S., and TOWNSHEND, J., 2001, Characterizing the land surface anisotropy from AVHRR data at a global scale using high performance computing. *International Journal of Remote Sensing*, **22**, 2171–2191.
- KALLURI, S., ZHANG, Z., LIANG, S., JAJA, J., and TOWNSHEND, J., 1997, Retrieval of bidirectional reflectance distribution function (BRDF) at continental scales from AVHRR data using high performance computing, In *Proceedings of the International Geoscience and Remote Sensing Symposium, Singapore*, pp. 174–176.
- KASISCHKE, E., CHRISTENSEN, N., and STOCK, B., 1995, Fire, global warming and the carbon balance of boreal forests. *Ecological applications*, **5**, 437–451.
- KASISCHKE, E., and FRENCH, N., 1995, Locating and estimating the areal extent of wildfires in Alaskan boreal forests using multiple-season AVHRR NDVI composite data. *Remote Sensing of Environment*, **51**, 263–275.
- KASISCHKE, E., FRENCH, N., HARRELL, P., CHRISTENSEN, N., USTIN, S., and BARRY, D., 1993, Monitoring of wildfires in boreal forests using Large Area AVHRR NDVI composite image data. *Remote Sensing of Environment*, **45**, 61–71.
- KASISCHKE, E., HEWSON, J., STOCKS, S., and VAN DER WERF, G., 2003, The use of ATSR active fire counts for estimating relative patterns of biomass burning - a study from the boreal forest region. *Geophysical Research Letters*, **30**, 1969–1972.
- KASISCHKE, E., HYER, E., NOVELLI, P., BRUHWILER, L., FRENCH, N., SUKHININ, A., HEWSON, J., and STOCKS, B., 2005, Influences of boreal fire emissions on Northern Hemisphere atmospheric carbon and carbon monoxide. *Global Biogeochemical Cycles*, **19**, 1–16.
- KAUFMAN, Y., C.O., J., FLYNN, L., KENDALL, J., PRINS, E., GIGLIO, L. AND WARD, D., MENZEL, W., and SETZER, A., 1998, Potential global fire monitoring from EOS-MODIS. *Journal of geophysical research*, **103**, 32215–32238.
- KAUFMAN, Y., ICHOKU, C., GIGLIO, L., KORONTZI, S., CHU, D., HAO, W., LI, R., and JUSTICE, C., 2003, Fire and smoke observed from the Earth Observing System MODIS

- instrument - products, validation and operational use. *International Journal of Remote Sensing*, **24**, 1765–1781.
- KAUFMAN, Y., and JUSTICE, C., 1998, *MODIS Fire Products: Algorithm Theoretical Basis Document*.
- KAUFMAN, Y., and TANRE, D., 1992, Atmospherically Resistant Vegetation Index (ARVI) for EOS-MODIS. *IEEE Transactions on Geoscience and Remote Sensing*, **30**, 261–270.
- KAUFMAN, Y., TUCKER, C., and FUNG, I., 1990, Remote sensing of biomass burning in the tropics. *Journal of Geophysical Research*, **95**, 9926–9939.
- KAUTH, R., and THOMAS, G., 1976, The tasseled cap - A graphic description of the spectral-temporal development of agricultural crops as seen by Landsat, In *LARS: Proceedings of the Symposium on Machine Processing of Remotely Sensed Data*, pp. 41–51.
- KEANE, R., BURGAN, R., and WAGTENDONK, J., 2001, Mapping wildland fuels for fire management across multiple scales: Integrating remote sensing, GIS and biophysical modeling. *International Journal of Wildland Fire*, **10**, 301–319.
- KEANE, R., CARY, G., and PARSONS, R., 2003, Using simulations to map fire regimes: An evaluation of approaches, strategies and limitations. *International Journal of Wildland Fire*, **12**, 309–322.
- KENNEDY, P., BELWARD, A., and GREGOIRE, J., 1994, An improved approach to fire monitoring in West Africa using AVHRR data. *International Journal of Remote Sensing*, **15**, 2235–2255.
- KORONTZI, S., ROY, D., JUSTICE, C., and WARD, D., 2004, Modeling and sensitivity analysis of fire emissions in southern Africa during SAFARI 2000. *Remote Sensing of Environment*, **92**, 376–396.
- KOUTSIAS, N., 2003, An autologistic regression model for increasing the accuracy of burned surface mapping using Landsat Thematic Mapper data. *International Journal of Remote Sensing*, **24**, 2199–2204.

- KOUTSIAS, N., and KARTERIS, M., 1998, Logistic regression modelling of multitemporal Thematic Mapper data for burned area mapping. *International Journal of Remote Sensing*, **19**, 3499–3514.
- KOUTSIAS, N., and KARTERIS, M., 2000, Burned area mapping using logistic regression modelling of a single post-fire Landsat-5 Thematic Mapper image. *International Journal of Remote Sensing*, **21**, 673–687.
- KUSHARDONO, D. K., FUKUE, H., SHIMODA, T., and SAKATA, T., 1995, Comparison of multi-temporal image classification methods. *Proceedings, IGARSS*, 1282–1284.
- KUUSK, A., 1995, A fast, invertible canopy reflectance model. *Remote Sensing of Environment*, **1951**, 342–350.
- KUUSK, A., 1996, A computer-efficient plant canopy reflectance model. *Computers and Geoscience*, **22**, 149–163.
- LAMBIN, E., 1996, Change detection at multi-temporal scales: Seasonal and annual variation in landscape variables. *Photogrammetric Engineering and Remote Sensing*, **62**, 931–938.
- LAMBIN, E., and EHRLICH, D., 1996, The surface temperature-vegetation index space for land cover and land-cover change analysis. *International Journal of Remote Sensing*, **17**, 463–487.
- LAMBIN, E., and EHRLICH, D., 1997, Land-cover changes in sub-Saharan Africa (1982-1991): Application of a change index based on remotely sensed surface temperature and vegetation indices at a continental scale. *Remote Sensing of Environment*, **61**, 181–200.
- LAMBIN, E., and STRAHLER, A., 1994a, Change vector analysis in multi-spectral space: A tool to detect and categorize land cover change processes using high temporal resolution satellite data. *Remote Sensing of Environment*, **48**, 321–344.
- LAMBIN, E., and STRAHLER, A., 1994b, Indicators of land cover change for change vector analysis in multitemporal space at coarse spatial scales. *International Journal of Remote Sensing*, **15**, 2099–2119.

- LANGAAS, S., 1993, A parameterised bispectral model for savanna fire detection using AVHRR night images. *International Journal of Remote Sensing*, **14**, 2245–2262.
- LANGENFELDS, R., FRANCEY, R., PAK, B., STEELE, L., LLOYD, J., TRUDINGER, C., and ALLISON, C., 2002, Interannual growth rate variations of atmospheric CO₂ and $\delta^{13}\text{C}$, H₂, CH₄ and CO between 1992 and 1999 linked to biomass burning. *Global Biogeochemical Cycles*, **16**, 1048–1072.
- LANGEVELDE, F., VIJVER, C., KUMAR, L., KOPPE, J., RIDDER, N., ANDEL, J., SKIDMORE, A., HEARNER, J., STROOSNIJDER, L., BOND, W., PRINS, H., and RIETKERK, M., 2003, Effects of fire and herbivory on the stability of savanna ecosystems. *Ecology*, **84**, 337–350.
- LATIFOVIC, R., CIHLAR, J., and CHEN, J., 2003, A comparison of BRDF models for the normalization of satellite optical data to a standard sun-target-sensor geometry. *IEEE Transactions on Geoscience and Remote Sensing*, **41**, 1889–1898.
- LEROY, M., and HAUTECOEUR, O., 1999, Anisotropy-corrected vegetation indexes derived from POLDER/ADEOS. *IEEE Transactions on Geoscience and Remote Sensing*, **37**, 1698–1708.
- LEVINE, J., 1991, *Global Biomass Burning* (MIT Press, Cambridge MA), pp. 197–202.
- LEWIS, P., and MULLER, J.-P., 1992, The advanced radiometric ray-tracer: ARARAT for plant canopy reflectance simulations. *International Archives of Photogrammetry and Remote Sensing*, **24**, 281–293.
- LI, C., CORNS, I., and YANG, R., 1999, Fire frequency and size distribution under natural conditions: A new hypothesis. *Landscape Ecology*, **14**, 533–542.
- LI, R., KAUFMAN, Y., HAO, W., SALMON, J., and GAO, B., 2004, A technique for detecting burn scars using MODIS data. *IEEE Transactions on Geoscience and Remote Sensing*, **42**, 1300–1308.

- LI, X., GAO, F., WANG, J., and STRAHLER, A., 2001, *A priori* knowledge accumulation and its application to linear BRDF model inversion. *Journal of Geophysical Research*, **106**, 11925–11935.
- LI, X., and STRAHLER, A. H., 1985, Geometric-optical modeling of a conifer forest canopy. *IEEE Transactions on Geoscience and Remote Sensing*, **23**, 705–721.
- LI, X., and STRAHLER, A. H., 1992, Geometric-optical bidirectional reflectance modeling of the discrete crown vegetation canopy: Effect of crown shape and mutual shadowing. *IEEE Transactions on Geoscience and Remote Sensing*, **30**, 276–292.
- LI, Z., CIHLAR, J., MOREAU, L., HUANG, F., and LEE, B., 1997, Monitoring active fires in the boreal ecosystem. *Journal of Geophysical Research*, **102**, 29611–29624.
- LI, Z., NADON, S., and CIHLAR, J., 2000a, Satellite based detection of Canadian boreal forest fires: Development and application of the algorithm. *International Journal of Remote Sensing*, **21**, 3057–3069.
- LI, Z., NADON, S., CIHLAR, J., and STOCKS, B., 2000b, Satellite based mapping of Canadian boreal forest fires: Evaluation and comparison of algorithms. *International Journal of Remote Sensing*, **21**, 3071–3082.
- LIANG, S., STRAHLER, A. H., BARNESLEY, M., BOREL, C., GERSTL, S., DINER, D., PRATA, A., and WALTHALL, C., 2000, Multiangle remote sensing: Past, present and future. *Remote Sensing Reviews*, **18**, 83–102.
- LINDESAY, J., ANDREAE, M., GOLDAMMER, J., HARRIS, G., ANNEGARN, H., GARSTANG, M., SCHOLLES, R., and VAN WILGEN, B., 1996, International Geosphere-Biosphere Programme/International Global Atmospheric Chemistry SAFARI-92 experiment: Background and overview. *Journal of Geophysical Research*, **101**, 23521–23530.
- LOBERT, J., KEENE, W., LOGAN, J., and YEVICH, R., 1999, Global chlorine emissions from biomass burning: Reactive chlorine emissions inventory. *Journal of Geophysical Research*, **104**, 8373–8389.

- LOPEZ, M., and CASELLES, V., 1991, Mapping burns and natural reforestation using Thematic Mapper data. *Geocarto International*, **1**, 31–37.
- LU, D., MAUSEL, P., BRONDIZIO, E., and MORAN, E., 2004, Change detection techniques. *International Journal of Remote Sensing*, **25**, 2365–2407.
- LUCHT, W., 1998, Expected retrieval accuracies of bidirectional reflectance and albedo from EOS-MODIS and MISR angular sampling. *Journal of Geophysical Resources*, **103**, 8763–8778.
- LUCHT, W., and LEWIS, P., 2000, Theoretical noise sensitivity of BRDF and albedo retrieval from the EOS-MODIS and MISR sensors with respect to angular sampling. *International Journal of Remote Sensing*, **21**, 81–98.
- LUCHT, W., and ROUJEAN, J., 2000a, Considerations in the parametric modeling of BRDF and Albedo from multiangular satellite sensor observations. *Remote Sensing Reviews*, **18**, 343–379.
- LUCHT, W., and ROUJEAN, J., 2000b, Considerations in the parametric modelling of BRDF and albedo from multiangular satellite sensor observations. *Remote Sensing Reviews*, **18**, 343–379.
- LUCHT, W., SCHAAF, C., and STRAHLER, A., 2000, An algorithm for the retrieval of Albedo from space using semiempirical BRDF models. *IEEE Transactions on Geoscience and Remote Sensing*, **38**, 977–998.
- LUTES, D., KEANE, R., CARATTI, J., KEY, C., BENSON, N., and GANGI, L., 2004, FIRE-MON: Fire Effects Monitoring and Inventory System, Technical report, US Department of Agriculture, Rocky Mountain Research Station.
- LYON, 1998, A change detection experiment using vegetation indices. *Photogrammetric Engineering and Remote Sensing*, **64**.
- MACLEOD, R., and CONGALTON, R., 1998, A quantitative comparison of change detection algorithms for monitoring Eelgrass from remotely sensed data. *Photogrammetric Engineering and Remote Sensing*, **64**, 207 – 216.

- MALINGREAU, J., STEPHENS, G., and FELLOWS, L., 1985, Remote sensing of forest fires: Kalimantan and North Borneo in 1982-83. *Ambio*, **14**, 314 – 321.
- MARCHONIK, J., DINER, D., PINTY, B., VERSTRAETE, M., MYNENI, R., KNYAZIKHIN, T., and H., G., 1998, Determination of land and ocean reflective, radiative and biophysical properties using multiangle imaging. *IEEE Transactions on Geoscience and Remote Sensing*, **36**, 1266–1281.
- MAS, J.-F., 1999, Monitoring land-cover changes: A comparison of change detection techniques. *International Journal of Remote Sensing*, **20**, 139 – 152.
- MATSON, M., and DOZIER, J., 1981, Identification of subresolution high temperature sources using a thermal infra-red sensor. *Photogrammetric Engineering and Remote Sensing*, **47**, 1311–1318.
- MENAUT, J., ABBADIE, L., and VITOUSEK, P., 1993, *Fire in the environment: The ecological, atmospheric and climatic importance of vegetation fires* (Wiley, New York), pp. 215–231.
- MILLER, C., and URBAN, D., 2003, A model of surface fire, climate and forest pattern in the Sierra Nevada, California. *Ecological Modelling*, **114**, 113–135.
- MILLER, J., and YOOL, S., 2002, Mapping forest post-fire canopy consumption in several over-story types using multi-temporal Landsat TM and ETM data. *Remote Sensing of Environment*, **82**, 481–496.
- MINNAERT, M., 1941, The reciprocity principle in Lunar photometry. *Journal of Astrophysics*, **93**, 403–410.
- MIURA, T., HUETE, A., VAN LEEUWEN, W., and DIDAN, K., 1998, Vegetation through smoke filled AVIRIS images: An assessment using MODIS band passes. *Journal of Geophysical Research*, **47**, 1311–1318.
- MUCHONEY, D. M., and HAACK, B., 1994, Change detection for monitoring forest defoliation. *Photogrammetric Engineering and Remote Sensing*, **60**, 1243–1251.

- MYNENI, R., NEMANI, R., and RUNNING, S., 1997, Estimation of global leaf area index and absorbed PAR using a radiative transfer model. *IEEE Transactions on Geoscience and Remote Sensing*, **35**, 1380–1393.
- NASA, 2001, MODIS data versioning and maturity, <http://geography.bu.edu/landcover/userguide/c>, Accessed: January 2005.
- NASA, Accessed: July 2005, HDF-EOS tools and information center, <http://hdfeos.gsfc.nasa.gov/hdfeos/index.cfm>.
- NEARY, D., KLOPATEK, C., DEBANO, L., and FFOLLIOTT, P., 1999, Fire effects on below ground sustainability: A review and synthesis. *Forest Ecology and Management*, **122**, 51–71.
- NELSON, R., 1983, Detecting forest canopy change due to insect activity using Landsat MSS. *Photogrammetric Engineering and Remote Sensing*, **9**, 1303–1314.
- NI, W., LI, X., WOODCOCK, C., CAETANO, M., and STRAHLER, A., 1999, An analytical hybrid GORT model for bidirectional reflectance over discontinuous plant canopies. *IEEE Transactions on Geoscience and Remote Sensing*, **37**, 987–999.
- NICODEMUS, F., RICHMOND, J., HSIA, J., GINSBERG, W., and LIMPERIS, T., 1977, Geometrical considerations and nomenclature for reflectance. *Applied Optics*, **9**, 1474–1475.
- NILSON, T., and KUUSK, A., 1989, A reflectance model for the homogenous plant canopy and its inversion. *Remote Sensing of Environment*, **27**, 157–167.
- NISHIHAMA, M., WOLFE, R., and SOLOMON, D., 1997, *MODIS Level 1A Earth Location: Algorithm Theoretical Basis Document*.
- OERTEL, D., ZHUKOV, B., BARBOSA, P., CSISZAR, I., GEORGE, C., HELD, A., HAYASAKA, H., SIEGERT, F., and WOOSTER, M., 2004, BIRD-CHRIS joint experiments for fire mapping, In *Proceedings, 2nd CHRIS/Proba Workshop, Frascati, Italy*.
- OKIN, G., ROBERTS, D., MURRAY, B., and OKIN, W., 2001, Practical limits on hyperspectral vegetation discrimination in arid and semiarid environments. *Remote Sensing of Environment*, **77**, 212–225.

- OLSON, J., 1994, Global ecosystem framework: Definitions, Technical report, USGS EROS Data Centre, Sioux Falls, SD.
- PATTERSON, M., and YOOL, S., 1998, Mapping fire-induced vegetation mortality using Landsat Thematic Mapper data: A comparison of linear transformation techniques. *Remote Sensing of Environment*, **65**, 132–142.
- PEREIRA, J., 1999, A comparative evaluation of NOAA/AVHRR vegetation indices for burned surface detection and mapping. *IEEE Transactions on Geoscience and Remote Sensing*, **37**, 217–226.
- PEREIRA, J., CHUVIECO, E., BEUDAIN, A., and DESBOIS, N., 1997, Remote sensing of burned areas: A review, Technical report, Universidad de Alcalá, Alcalá de Henares.
- PEREIRA, J., SA, A., SOUSA, A., SILVA, J., SANTOS, M., and CARREIRAS, J., 1999, *Spectral characterisation and discrimination of burnt areas* (Springer-Verlag, Berlin), pp. 123–138.
- PEREIRA, J., and SETZER, A., 1993, Spectral characteristics of fire scars in Landsat-5 TM images of Amazonia. *International Journal of Remote Sensing*, **14**, 2061–2078.
- PEREIRA, J., and SETZER, A., 1996, Comparison of fire detection in savannas using AVHRR's Channel 3 and TM images. *International Journal of Remote Sensing*, **17**, 1925–1937.
- PEREZ, B., and MORENO, J., 1998, Methods for quantifying fire severity in shrubland-fires. *Plant Ecology*, **139**, 91–101.
- PETERSON, D., and REICH, P., 2001, Prescribed fire in oak savanna: Fire frequency effects on stand structure and dynamics. *Ecological Applications*, **11**, 914–927.
- PETICOLIN, F., and VERMOTE, E., 2002, Land surface reflectance, emissivity and temperature from MODIS middle and thermal infrared data. *Remote Sensing of Environment*, **83**, 112–134.
- PICCOLINI, I., and ARINO, O., 2000, Towards a global burned surface world atlas. *Earth Observations Quarterly*, **65**, 14–18.

- PICKETT, S., and WHITE, E., 1985, *The ecology of natural disturbance and patch dynamics* (Academic Press, New York).
- PILON, P., HOWARTH, P., BULLOCK, R., and ADENIYI, P., 1988, An enhanced classification approach to change detection in semi-arid environments. *Photogrammetric Engineering and Remote Sensing*, **54**, 1709–1716.
- PINTY, B., and VERSTRAETE, M., 1992, GEMI: A nonlinear index to monitor global vegetation from satellites. *Vegetation*, **101**, 15–20.
- PRAKASH, A., and GUPTA, R. P., 1998, Land-use mapping and change detection in a coal mining area - a case study in the Jharia coalfield, India. *International Journal of Remote Sensing*, **19**, 391–410.
- PRIVETTE, J. L., ECK, T. F., and DEERING, D. W., 1997, Estimating spectral albedo and nadir reflectance through inversion of simple BRDF models with AVHRR/MODIS-like data. *Journal of Geophysical Research*, **102**, 29529–29542.
- QIN, W., and LIANG, S., 2000, Plane-parallel canopy radiative transfer modelling: Recent advances and future directions. *Remote Sensing Reviews*, **18**, 281–305.
- RADELOFF, V., MLADENOFF, D., and BOYCE, M., 1999, Detecting Jack Pine budworm defoliation using spectral mixture analysis: Separating effects from determinants. *Remote Sensing of Environment*, **69**, 156–169.
- RAHMAN, H., PINTY, B., and VERSTRAETE, M., 1993a, Coupled surface-atmosphere reflectance (CSAR) model. 2. Semi-empirical surface model usable with NOAA Advanced Very High Resolution Radiometer data. *Journal of Geophysical Research*, **98**, 20791–20801.
- RAHMAN, H., VERSTRAETE, M., and PINTY, B., 1993b, Coupled surface-atmosphere reflectance (CSAR) model. 1. Model description and inversion on synthetic data. *Journal of Geophysical Research*, **98**, 20779–20789.

- RANDRIAMBELO, T., BALDY, S., BESSAFI, M., PETIT, M., and DESPINOV, M., 1998, An improved detection and characterization of active fires and smoke plumes in South-Eastern Africa and Madagascar. *International Journal of Remote Sensing*, **19**, 2623–2638.
- RAZAFIMPANILO, H., FROUIN, R., and IACOBELLIS, S., 1995, Methodology for estimating burned area from AVHRR reflectance data. *Remote Sensing of Environment*, **54**, 273–289.
- RICHARDS, J., 1984, Thematic mapping from multitemporal image data using the principal components transformation. *Remote Sensing of Environment*, **16**, 35–46.
- RIDD, M., and LIU, J., 1998, A comparison of four algorithms for change detection in an urban environment. *Remote Sensing of Environment*, **63**, 95–100.
- ROAN-CUESTA, R, M., RETANA, J., GRACIA, M., and RODRIGUEZ, R., 2003, A quantitative comparison of methods for classifying burned areas with LISS-III imagery. *International Journal of Remote Sensing*, **26**, 1979–2003.
- ROGAN, J., FRANKLIN, J., and ROBERTS, D. A., 2002, A comparison of methods for monitoring multitemporal vegetation change using thematic mapper imagery. *Remote Sensing of Environment*, **80**, 142–157.
- ROGAN, J., and YOOL, S., 2001, Mapping fire-induced vegetation depletion in the Peloncillo mountains, Arizona and New Mexico. *International Journal of Remote Sensing*, **22**, 3101–3121.
- ROLLINS, M., SWETNAM, T., and MORGAN, P., 2001, Evaluating a century of fire patterns in two Rocky Mountain wilderness areas using digital fire atlases. *Canadian Journal of Forest Research*, **31**, 2107–2123.
- ROSS, J., 1981, *The radiation regime and architecture of plant stands* (W.Junk, Netherlands).
- ROUJEAN, J., LEROY, M., and DESCHAMPS, P., 1992, A bi-directional reflectance model of the Earth's surface for the correction of remote sensing data. *Journal of Geophysical Research*, **97**, 20455–20468.

- ROY, D., 1997, Investigation of the maximum NDVI and the maximum surface temperature (Ts) AVHRR compositing procedures for the extraction of NDVI and Ts over forest. *International Journal of Remote Sensing*, **18**, 2383–2401.
- ROY, D., 2000, The impact of misregistration upon composited wide field of view satellite data and implications for change detection. *IEEE Transactions on Geoscience and Remote Sensing*, **38**, 2017–2031.
- ROY, D., 2005, SAFARI 2000 MODIS 500-m Burned Area Products, Southern Africa, Dry Season 2000, <http://daac.ornl.gov>.
- ROY, D., FROST, P., JUSTICE, C., LANDMANN, T., LE ROUX, J., GUMBO, K., MAKUNGA, S., DUNHAM, K., DU TOIT, R., MHWANDAGARA, K., ZACARIAS, A., TACHEBA, B., DUBE, O., PEREIRA, J., MUSHOVE, P., MORISETTE, J., VANNAN, S., and DAVIES, D., 2005a, The Southern Africa Fire Network (SAFNet) regional burned-area product-validation protocol. *International Journal of Remote Sensing*, **In press**.
- ROY, D., GIGLIO, L., KENDALL, D., and JUSTICE, C., 1999, Multi-temporal active-fire based burn scar detection algorithm. *International Journal of Remote Sensing*, **20**, 1031–1038.
- ROY, D., JIN, Y., LEWIS, P., and JUSTICE, C., 2005b, Prototyping a global algorithm for systematic fire-affected area mapping using MODIS time series data. *Remote Sensing of Environment*, **97**, 137–162.
- ROY, D., and LANDMANN, T., 2005, Characterizing the surface heterogeneity of fire effects using multi-temporal reflective wavelength data. *International Journal of Remote Sensing*, **In press**.
- ROY, D., and LEWIS, P., 2000, Burned area mapping from multitemporal surface bi-directional reflectance, American Geophysical Union Spring 2000 Meeting, Session B04: Remote Sensing of the Biosphere, Washington DC, May 30 - June 3.
- ROY, D., LEWIS, P., and JUSTICE, C., 2002, Burned are mapping using multi-temporal moderate spatial resolution data - a bi-directional reflectance model-based expectation approach. *Remote Sensing of Environment*, **83**, 263–286.

- RUIZ-GALLARDO, J., CASTANO, S., and CALERA, A., 2004, Application of remote sensing and GIS to locate priority intervention areas after wildland fires in Mediterranean systems: A case study from south-eastern Spain. *International Journal of Wildland Fire*, **13**, 241–252.
- RUNNING, S., JUSTICE, C. O., SALOMONSON, V., HALL, D., BARKER, J., KAUFMAN, Y., STRAHLER, A. H., HUETE, A., MULLER, J.-P., VANDERBILT, V., WAN, Z.-M., TEILLET, P., and CARNEGIE, D., 1994a, Terrestrial remote sensing science and algorithms planned for EOS-MODIS. *International Journal of Remote Sensing*, **15**, 3587–3620.
- RUNNING, S., LOVELAND, T., and PIERCE, L., 1994b, A vegetation classification logic based on remote sensing for use in global scale biogeochemical models. *Ambio*, **23**, 77–81.
- RYAN, K., 2002, Dynamic interactions between forest structure and fire behaviour in boreal ecosystems. *Silva Fennica*, **36**, 13–39.
- SA, A., PEREIRA, J., VASCONCELOS, M., SILVA, J., RIVEIRO, N., and AWASSE, A., 2003, Assessing the feasibility of sub-pixel burned area mapping in miombo woodlands of northern Mozambique using MODIS imagery. *International Journal of Remote Sensing*, **24**, 1783–1796.
- SAARNAK, C., 2001, A shift from natural to human driven fire regimes: Implications for trace-gas emissions. *The Holocene*, **11**, 373–375.
- SALVADOR, R., VALERIANO, J., PONS, X., and DIAZ-DELGADO, R., 2000, A semi-automatic methodology to detect fire scars in shrubs and evergreen forests with Landsat MSS time series. *International Journal of Remote Sensing*, **21**, 655–671.
- SAVAGE, M., and VERMEULEN, K., 1983, Microclimate modification of tall moist grasslands of Natal by spring burning. *Journal of Range Management*, **36**, 172–175.
- SCANLON, T., ALBERTSON, J., CAYLOR, K., and WILLIAMS, C., 2002, Determining land surface fractional cover from NDVI and rainfall time series for a savannah ecosystem. *Remote Sensing of Environment*, **3682**, 376–388.

- SCHAAF, C., GAO, G., STRAHLER, A., LUCHT, W., LI, X., TSANG, T., STRUGNELL, N. C., ZHANG, X., JIN, Y., MULLER, J., LEWIS, P., BARNSELY, M., HOBSON, P., DISNEY, M., ROBERTS, G., DUNDERDALE, M., DOLL, C., D'ENTREMONT, R., HU, B., LIANG, S., PRIVETTE, J., and ROY, D., 2002, First operational BRDF, Albedo and Nadir reflectance products from MODIS. *Remote Sensing of Environment*, **83**, 135–148.
- SCHOLES, R., DOWTY, P., CAYLOR, K., PARSONS, D., FROST, P., and SHUGART, H., 2002, Trends in savanna structure and composition along an aridity gradient in the Kalahari. *Journal of Vegetation Science*, **13**, 419–428.
- SCHOLES, R., KENDALL, J., and JUSTICE, C., 1996a, The quantity of biomass burned in southern Africa. *Journal of Geophysical Research-Atmospheres*, **101**, 23667–23676.
- SCHOLES, R., WARD, D., and JUSTICE, C., 1996b, Emissions of trace gases and aerosol particles due to vegetation burning in southern hemisphere Africa. *Journal of Geophysical Research*, **101**, 23677–23682.
- SCHWILK, D., KEELEY, J., and BOND, W., 1997, The intermediate disturbance hypothesis does not explain fire and diversity pattern in fynbos. *Plant Ecology*, **132**, 77–84.
- SEILER, W., and CRUTZEN, P., 1980, Estimates of gross and net fluxes of carbon between the biosphere and the atmosphere from biomass burning. *Climatic Change*, **2**, 207–247.
- SELLERS, P., LOS, S., TUCKER, C., JUSTICE, C., DAZLICH, D., COLLATZ, G., and RANDALL, D., 1994, A global 1x1 degree NDVI data set for climate studies. Part 2: The generation of global fields of terrestrial biophysical parameters from the NDVI. *International Journal of Remote Sensing*, **24**, 3311–3340.
- SERRA, P., PONS, X., and SAURI, D., 2003, Post-classification change detection with data from different sensors: Some accuracy considerations. *International Journal of Remote Sensing*, **24**, 3311–3340.
- SETO, K., WOODCOCK, C., SONG, C., HUANG, X., LU, J., and KAUFMAN, R., 2002, Monitoring land-use change in the Pearl River Delta using Landsat TM. *International Journal of Remote Sensing*, **23**, 1985–2004.

- SETZER, A., and PEREIRA, M., 1992, Operational detection of fires in Brazil with NOAA-AVHRR, In *Proceedings 24th International Symposium of Remote Sensing of Environment*, pp. 469–482.
- SILJESTROM, P., and MORENO, A., 1995, Monitoring burnt areas by principal components analysis of multitemporal TM data. *International Journal of Remote Sensing*, **16**, 1577–1587.
- SILVA, J., CADIMA, J., PEREIRA, J., and GREGOIRE, J.-M., 2004, Assessing the feasibility of a global model for multi-temporal burned area mapping using SPOT-VEGETATION data. *International Journal of Remote Sensing*, **25**, 4889–4913.
- SIMON, M., PLUMMER, S., FIERENS, F., HOELZEMANN, J., and ARINO, O., 2004, Burnt area detection at global scale using ATSR-2: The GLOBSCAR products and their qualification. *Journal of Geophysical Research*, **109**, 1–18.
- SINGH, A., 1989, Digital change detection techniques using remotely-sensed data. *International Journal of Remote Sensing*, **10**, 989–1003.
- SLOCUM, M., PLATT, W. J., and COOLEY, H., 2002, Effects of differences in prescribed fire regimes on patchiness and intensity of fires in subtropical savannas of Everglades National Park, Florida. *Restoration Ecology*, **11**, 91–102.
- SMITH, A., 2004, *Determining nitrogen volatilised within African savanna fires via ground-based remote sensing*, Ph.D. thesis, King's College London.
- SMITH, A., WOOSTER, M., DRAKE, N., DIPSO, F., FALLOWSKI, M., and HUDAK, A., 2005, Testing the potential of multi-spectral remote sensing for retrospectively estimating fire severity in African savannas. *Remote Sensing of Environment*, **97**, 92–115.
- SOHL, T., 1999, Change analysis in the United Arab Emirates: An investigation of techniques. *Photogrammetric Engineering and Remote Sensing*, **65**, 475–484.
- SOSA, W., 1984, The role of disturbance in natural communities. *Annual Reviews of Ecological Systems*, **15**, 353–391.

- SPARKS, J., MASTERS, R., ENGLE, D., and BUKENHOFER, G., 2002, Season of burn influences fire behaviour and fuel consumption in restored shortleaf pine-grassland communities. *Restoration Ecology*, **10**, 714–722.
- STOCKS, B., 1991, *The extent and impact of forest fires in northern circumpolar countries* (MIT Press, Cambridge MA), pp. 197–202.
- STRAHLER, A., LUCHT, W., SCHAAF, C., TSANG, T., GAO, F., LI, X., MULLER, J., LEWIS, P., and BARNESLEY, M., 1999a, *MODIS BRDF/Albedo Product: Algorithm Theoretical Basis Document*.
- STRAHLER, A., MUCHONEY, D., BORAK, J., FRIEDL, M. AND GOPAL, S., LAMBIN, E., and MOODY, A., 1999b, *MODIS Land cover product: Algorithm Theoretical Basis Document*.
- STROMGAARD, P., 1992, Immediate and long-term effects of fire and ash fertilization on a Zambian Miombo woodland soil. *Agriculture, Ecosystems and Environment*, **41**, 19–37.
- STRONACH, N., and MCNAUGHTON, S., 1989, Grassland fire dynamics in the Serengeti ecosystem, and a potential method of retrospectively estimating fire energy. *Journal of Applied Ecology*, **26**, 1025–1033.
- STROPPIANA, D., GREGOIRE, J., and PEREIRA, J., 2003, The use of SPOT VEGETATION data in a classification tree approach for burnt area mapping in Australian savanna. *International Journal of Remote Sensing*, **24**, 2131–2151.
- STROPPIANA, D., PINNOCK, D., and GREGOIRE, J., 2000, The Global Fire Product: Daily fire occurrence from April 1992 to December 1993 derived from NOAA AVHRR data. *International Journal of Remote Sensing*, **21**, 1279–1288.
- STROPPIANA, D., PINNOCK, D.S. PEREIRA, J., and GREGOIRE, J., 2002, Radiometric analysis of SPOT-VEGETATION images for burnt area detection in Northern Australia. *Remote Sensing of Environment*, **82**, 21–37.

- STRUGNELL, N., and LUCHT, W., 2001, Continental-scale albedo inferred from AVHRR data, land cover class and field observations of typical BRDFs. *Journal of Climate*, **14**, 1360–1376.
- STRUGNELL, N., LUCHT, W., and SCHAAF, C., 2001, A global albedo dataset derived from AVHRR data for use in climate simulations. *Geophysical Research Letters*, **28**, 191–194.
- SUSAKI, J., HARA, K., KAJIWARA, K., and HONDA, Y., 2004, Robust estimation of BRDF model parameters. *Remote Sensing of Environment*, **89**, 63–71.
- SWAP, B., 2000, SAFARI-2000: A Southern African Regional Science Initiative, <http://www.igac.noaa.gov/newsletter/15/safari-2000.php>, Accessed: August 2005.
- SWETNAM, T., 1993, Fire history and climate change in giant Sequoia groves. *Science*, **262**, 885–889.
- SWETNAM, T., TOUCHAN, R., BAISAN, C., CAPRIO, A., and BROWN, P., 1990, Giant Sequoia fire history in Mariposa Grove, Yosemite National Park, In *Natural Areas and Yosemite: Prospects for the future*, pp. 1–16.
- TANSEY, K., GREGOIRE, J., BINAGHI, E., BOSCHETTI, L., BRIVIO, P., ERSHOV, D., FLASSE, S., FRASER, R., GRAETZ, D., MAGGI, M., PEDUZZI, P., PEREIRA, J., SILVA, J., SOUSA, A., and STROPPIANA, D., 2004a, A global inventory of burned areas at 1km resolution for the year 2000 derived from Spot Vegetation data. *Climatic Change*, **67**, 345–377.
- TANSEY, K., GREGOIRE, J., STROPPIANA, D., SOUSA, A., SILVA, J., PEREIRA, J., BOSCHETTI, L., MAGGI, M., BRIVIO, P., FRASER, R., FLASSE, S., ERSHOV, D., BINAGHI, E., GRAETZ, D., and PEDUZZI, P., 2004b, Vegetation burning in the year 2000: Global burned area estimates from SPOT VEGETATION data. *Journal of Geophysical Research*, **109**, 661–677.
- THONICKE, K., VENEVSKY, S., SITCH, S., and CRAMER, W., 2001, The role of fire disturbance for global vegetation dynamics: Coupling fire into a Dynamic Global Vegetation Model. *Global Ecology and Biogeography*, **10**, 661–677.

- TOMPKINS, S., MUSTARD, J., PIETERS, C., and FORSYTH, D., 1997, Optimization of end-members for spectral mixture analysis. *Remote Sensing of Environment*, **59**, 472–489.
- TOWNSHEND, J., JUSTICE, C., GURNEY, C., and MCMANUS, J., 1992, The impact of mis-registration on change detection. *IEEE Transactions on Geoscience and Remote Sensing*, **30**, 1054–1060.
- TOWNSHEND, J., JUSTICE, C., LI, C., GURNEY, C., and MCMANUS, J., 1991, Global land cover classification by remote sensing: Present capabilities and future possibilities. *Remote Sensing of Environment*, **35**, 243–255.
- TOWNSHEND, J., JUSTICE, C., SKOLE, D., MALINGREAU, J., CIHLAR, J., TEILLET, P., SADWOSKI, F., and RUTTENBERG, S., 1994, The 1km resolution global data set - needs of the International Geosphere Biosphere program. *International Journal of Remote Sensing*, **15**, 3417–3441.
- TRAPNELL, C., 1959, Ecological results of woodland burning experiments in Northern Rhodesia. *Journal of Ecology*, **47**, 129–168.
- TRIGG, S., and FLASSE, S., 2000, Characterizing the spectral-temporal response of burned savannah using *in situ* spectroradiometry and infrared thermometry. *International Journal of Remote Sensing*, **21**, 3161–3168.
- TRIGG, S., and FLASSE, S., 2001, An evaluation of different bi-spectral spaces for discriminating burned shrub savannah. *International Journal of Remote Sensing*, **22**, 2641–2647.
- TRIGG, S., ROY, D., and FLASSE, S., 2005, An *in situ* study of the effects of surface anisotropy on the remote sensing of burned savannah. *International Journal of Remote Sensing*, **26**, 1–9.
- TROLLOPE, W., 1982, *Ecological effects of fire in South African Ecosystems* (Springer Verlag, New York).
- TROLLOPE, W., 2000, Effects and use of fire in southern African savannas, In *Proceedings, Natural forests and savanna woodlands symposium II*, volume 1, pp. 149–163.

- TROLLOPE, W., and TROLLOPE, L., 2002, *Forest fire research and wildland fire safety* (Millpress, Rotterdam), pp. 1–17.
- TROLLOPE, W., and TROLLOPE, L., 2004, Prescribed burning in African grasslands and savannas for wildlife management. *Aridlands*, **55**, 1–8.
- TUCKER, C., 1979, Red and photographic infrared linear combinations for monitoring vegetation. *Remote Sensing of Environment*, **8**, 127–150.
- USGS, 2006, Seamless Shuttle Radar Topography Mission, <http://seamless.usgs.gov/website/seamless/products/srtm3arc.asp>.
- UYS, R., 2004, The effects of different fire regimes on plant diversity in southern African grasslands. *Biological Conservations*, **118**, 489–499.
- VANACKER, V., LINDERMAN, M., LUPO, F., FLASSE, S., and LAMBIN, E., 2005, Impact of short-term rainfall fluctuation on interannual land cover change in sub-Saharan Africa. *Global Ecology and Biogeography*, **14**, 123–135.
- VAQUEZ, A., CUEVAS, J., and GONZALEZ-ALONSO, F., 2001, Comparison of the use of WiFS and LISS images to estimate the area burned in a large forest fire. *International Journal of Remote Sensing*, **22**, 901–907.
- VERMOTE, E., TANRE, D., DEUZE, J., HERMAN, M., and MORCETTE, J., 1997, Second simulation of the satellite signal in the solar spectrum: An overview. *IEEE Transactions on Geoscience and Remote Sensing*, **35**, 675–686.
- VERMOTE, E., and VERMEULEN, A., 1999a, *Atmospheric correction algorithm, spectral reflectances: Algorithm Theoretical Basis Document*.
- VERMOTE, E., and VERMEULEN, A., 1999b, *Atmospheric Correction Algorithm: Spectral Reflectances (MOD09)*, University of Maryland, Department of Geography.
- VETAAS, O., 1992, Micro-site effects of trees and shrubs in dry savannas. *Journal of Vegetation Science*, **3**, 337–344.

- VAN DE VIJVER, C., FOLEY, C., and OLFF, H., 1999, Changes in the woody component of an East African savanna during 25 years. *Journal of Tropical Ecology*, **15**, 545–564.
- VOGELMANN, J., 1988, Detection of forest change in the Green Mountains of Vermont using multi-spectral scanner data. *International Journal of Remote Sensing*, **9**, 1187–1200.
- WAGTENDONK, J., ROOT, R., and KEY, C., 2004, Comparison of AVIRIS and Landsat ETM+ detection capabilities for burn severity. *Remote Sensing of Environment*, **92**, 397–408.
- WALTHALL, C., NORMAN, J., WELLES, J., CAMPBELL, G., and BLAD, B., 1985, Simple equation to approximate the bidirectional reflectance from vegetative canopies and bare soil surfaces. *Applied Optics*, **24**, 383–387.
- WANG, G., and KEVIN, K., 2005, Effects of fire severity on early development of understorey vegetation. *Canadian Journal of Forest Research*, **2**, 254–262.
- WANNER, W., LI, X., and STRAHLER, A., 1995, On the derivation of kernels for kernel driven models of bi-directional reflectance. *Journal of Geophysical Research*, **100**, 21077–21090.
- WANNER, W., STRAHLER, A., HU, B., LEWIS, P., MULLER, J.-P., LI, X., SCHAAF, C., and BARNSELY, M., 1997, Global retrieval of bi-directional reflectance and albedo over land from EOS MODIS and MISR Data: Theory and algorithms. *Journal of Geophysical Research*, **102**, 17143–17162.
- WARD, D., HAO, W., SUSOTT, R., BABBITT, R., SHEA, R., KAUFFMAN, J., and JUSTICE, C., 1996, Effect of fuel composition on combustion efficiency and emission factors for African savanna ecosystems. *Journal of Geophysical Research*, **101**, 23569–23576.
- VAN DER WERF, G., RANDERSON, J., COLLATZ, G., and GIGLIO, L., 2003, Carbon emissions from fires in tropical and subtropical ecosystems. *Global Change Biology*, **9**, 547–562.
- VAN DER WERF, G., RANDERSON, J., COLLATZ, G., GIGLIO, L., KASIBHATLA, P., ARELLANO, A., OLSEN, S., and KASISCHKE, E., 2004, Continental-scale partitioning of fire emissions during the 1997 to 2001 El Nino/La Nina period. *Science*, **303**, 73–76.

- WIELICKI, B., BARKSTROM, B., BAUM, B., CHARLOCK, T., GREEN, R., KRATZ, D., LEE, R., MINNIS, P., SMITH, G., TAKMENG, W., YOUNG, D., CESS, R., COAKLEY, J., CROMMELYNCK, D., DONNER, L., KANDEL, R. AND KING, M., MILLER, A., RAMANATHAN, V., RANDALL, D., STOWE, L., and WELCH, R., 1998, Clouds and the Earth's Radiant Energy System (CERES): Algorithm overview. *IEEE Transactions on Geoscience and Remote Sensing*, **36**, 1127–1141.
- WOLFE, R., ROY, D., and VERMOTE, E., 1998, MODIS land data storage, gridding, and compositing methodology: Level 2 grid. *IEEE Transactions on Geoscience and Remote Sensing*, **36**, 1324–1338.
- WOOSTER, M., CECCATO, P., and FLASSE, S., 1998, Indonesia fires observed using AVHRR. *International Journal of Remote Sensing*, **19**, 383–386.
- WOOSTER, M., ZHUKOV, B., and OERTEL, D., 2003, Fire radiative energy release for quantitative study of biomass burning: Derivation from the BIRD experimental satellite and comparison to MODIS fire products. *Remote Sensing of Environment*, **86**, 83–107.
- YAMAGUSHI, Y., KAHLE, A., TSU, H., KAWAKAMI, K., and PNIEL, M., 1998, Overview of Advanced Spaceborne Thermal Emission and Reflection Radiometer (ASTER). *IEEE Transactions on Geoscience and Remote Sensing*, **36**, 1062–1071.
- YUAN, D., ELVIDGE, C., and LUNETTA, R., 1999, *Remote sensing change detection: Environmental monitoring methods and applications* (Sleeping Bear Press), pp. 21–39.
- YUANBO, L., NISHIYAMA, S., and YANO, T., 2004, Analysis of four change detection algorithms in bi-temporal space with a case study. *International Journal of Remote Sensing*, **25**, 2121–2139.
- ZARCO-TEJADA, P., RUEDA, C., and USTIN, S., 2003, Water content estimation in vegetation with MODIS reflectance data and model inversion methods. *Remote Sensing of Environment*, **85**, 109–124.
- ZAVALA, M., and HOLDO, R., 2005, Delayed effects of fire on habitat use by large herbivores in Acacia Drepanolobium savanna. *African Journal of Ecology*, **43**, 155–157.

- ZHAN, Y.-H., WOOSTER, M., TUTUBALINA, O., and PERRY, G., 2003, Monthly burned area and forest fire carbon emission estimates for the Russian Federation from SPOT VGT. *Remote Sensing of Environment*, **87**, 1–15.
- ZHANG, Z., KALLURI, S., JAJA, J., LIANG, S., and TOWNSHEND, J., 1998, Models and high performance computing algorithms for global BRDF retrieval. *IEEE Transactions on Geoscience and Remote Sensing Computer Science and Engineering*, **4**, 16–29.

Appendices

Appendix A

Sitemap

Site	Row	Column	Number of rows	Number of columns	Latitude (degrees, minutes, seconds)	Longitude (degrees, minutes, seconds)
2A	1499	4704	1	1	30° 49' 36.83" E	16° 14' 30" S
4A	869	2918	1	1	22° 47' 59.86" E	13° 36' 60" S
4B	772	4447	1	1	29° 18' 35.91" E	13° 12' 45" S
4C	781	3409	1	1	24° 52' 0.92" E	13° 14' 60" S
4D	397	2695	1	1	21° 40' 35.38" E	11° 38' 60" S
4E	1533	1576	1	1	17° 16' 7.03" E	16° 22' 60" S
4F	1000	2346	1	1	20° 23' 43.15" E	14° 9' 30" S
4G	235	3045	1	1	23° 6' 39.50" E	10° 58' 30" S
4H	232	3145	1	1	23° 32' 3.86" E	10° 57' 45" S
5A	1238	1712	1	1	17° 45' 5.05" E	15° 9' 15" S
5B	1678	1570	1	1	17° 17' 19.74" E	16° 59' 30" S
5C	450	1500	200	200	16° 36' 36.63"	11° 10' 15"
5D	640	1520	200	200	16° 44' 28.65"	22° 39' 45"
5E	1760	3110	340	200	24° 3' 2.87" E	17° 19' 45" S
5F	1695	815	100	50	14° 0' 47.15" E	17° 3' 30" S
5G	1361	1198	1	1	15° 33' 44.16" E	15° 39' 60" S
6A	1525	1530	250	450	17° 3' 57.33" E	16° 20' 60" S
6B	1821	2993	60	52	23° 36' 3.08" E	17° 33' 45" S
6C	38	2550	1	1	20° 55' 41.93" E	10° 8' 60" S
6D	668	2350	1	1	20° 17' 56.76" E	12° 46' 30" S
6E	1588	2126	1	1	19° 40' 50.07" E	16° 36' 45" S
6F	1747	3028	90	120	23° 41' 9.27" E	17° 16' 30" S
6G	995	957	90	120	14° 25' 31.62" E	14° 8' 30" S
6H	730	1450	90	120	16° 28' 0.91" E	13° 2' 15" S
6I	110	990	90	120	14° 21' 51.20" E	10° 27' 15" S
6J	713	4733	1	1	30° 29' 57.56" E	12° 57' 60" S
6K	1836	3405	1	1	25° 22' 41.51" E	17° 38' 45" S
6L	360	2400	200	350	20° 24' 36.81" E	11° 29' 45" S
6M	815	1545	110	150	16° 53' 51.85" E	13° 23' 30" S
6N	774	615	33	45	12° 54' 20.76" E	13° 13' 45" S
6P	790	622	1	1	12° 56' 19.79" E	13° 17' 15" S
6Q	15	2000	200	230	18° 37' 13.08" E	10° 3' 30" S
7A	570	1370	500	1000	16° 4' 57.09" E	12° 22' 15" S
7B	275	2450	500	1000	16° 4' 57.09" E	11° 8' 30" S
7C	400	2680	100	100	21° 36' 49.15" E	11° 39' 45" S
7D	1570	1750	100	100	18° 2' 19.10" E	16° 32' 15" S

Table A.1: Pixel locations referred to in the text: Sites which are of a greater spatial extent than a single pixel are indexed by the upper left row and column, while the latitude and longitude refer to the centre of the pixel. Each site is indexed by the chapter number in which it appears.

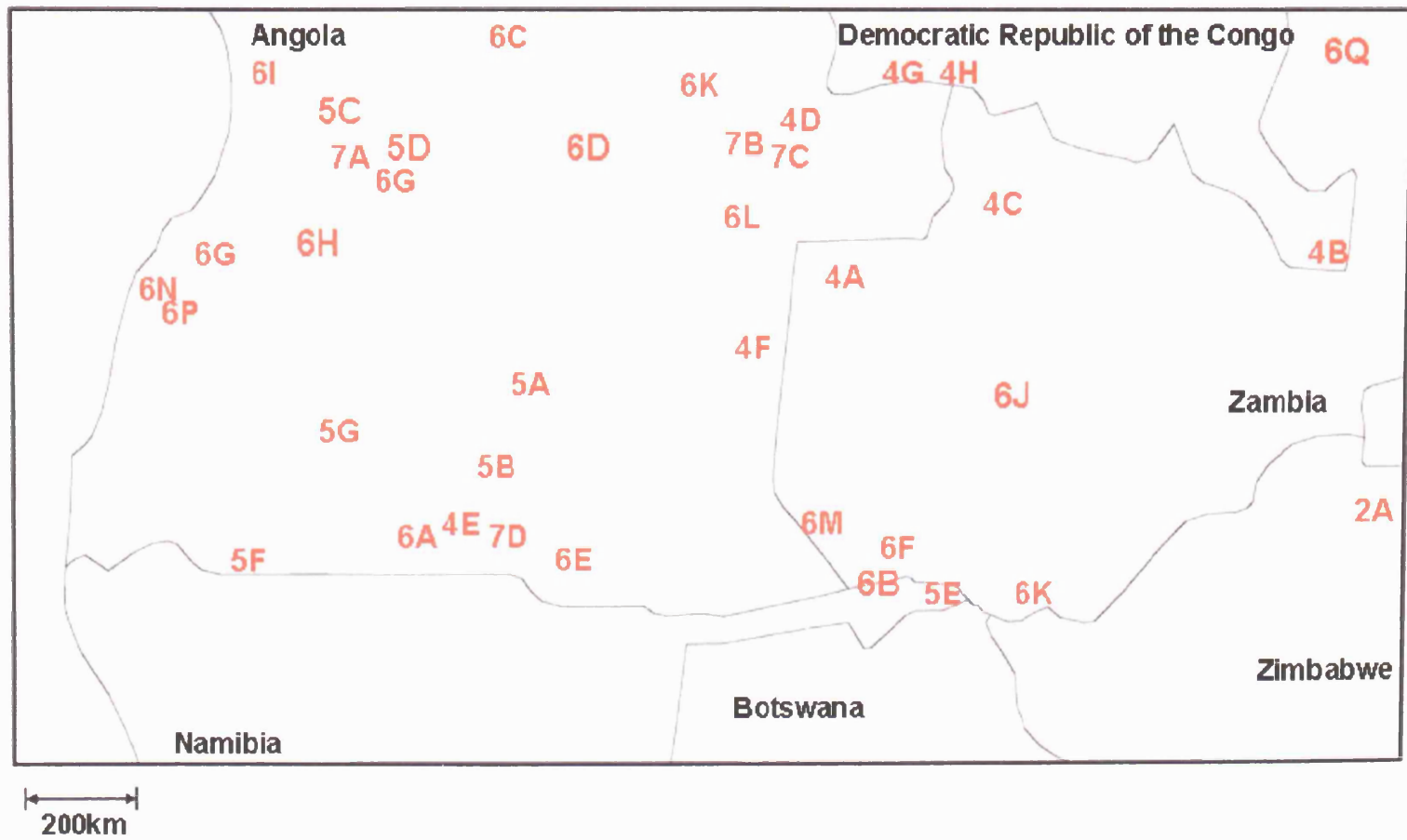


Figure A 1: The locations of pixel examples used in the text

Appendix B

Active fires and burned areas

Additive model results									
	2000 Terra	2001 Terra	2002 Terra	2003 Terra	Aqua	both	2004 Terra	Aqua	both
Apr	0.3	0.1	1.7	2.4	5.5	6.7	0.1	0.4	0.4
May	6.9	5.1	10.5	7.7	24.3	29.2	5.0	20.6	23.5
Jun	9.8	N/A	10.0	8.8	29.8	35.1	9.5	35.6	41.0
Jul	7.8	11.1	11.9	10.5	36.3	42.7	10.1	36.8	42.7
Aug	8.9	13.0	13.3	13.3	31.8	40.4	9.6	25.5	32.0
Sep	13.8	14.0	11.6	12.9	22.4	31.0	8.9	13.1	19.7
Oct	10.1	10.3	8.2	8.9	13.2	19.4	9.9	12.2	19.9
Nov	2.8	0.41	2.2	0.09	0.8	1.7	2.1	2.1	3.9
Total	9.2	10.6	9.9	10.5	26.3	33.1	8.9	23.6	29.5

Table B.1: Percentage of 500m burned areas detected as active fires: Additive model results

Appendix C

Monthly burned area totals

	2000 Terra	2001 Terra	2002 Terra	2003 Terra	Aqua	both	2004 Terra	Aqua	both
Deciduous broadleaf forest									
Apr	0.0	0.1	0.8	1.0	2.9	3.4	0.0	0.1	0.1
May	7.1	4.5	8.0	6.1	23.2	27.0	3.5	15.8	17.9
Jun	9.1	N/A	8.5	7.5	32.5	36.7	8.3	38.0	42.5
Jul	7.3	10.6	10.6	8.9	40.8	45.8	9.1	41.0	45.9
Aug	8.0	12.3	12.1	10.3	37.4	43.3	9.6	34.0	39.8
Sep	10.2	10.7	6.8	9.8	22.9	29.3	6.0	9.9	14.5
Oct	3.4	4.6	2.2	2.7	6.6	8.4	3.7	5.8	8.8
Nov	0.9	0.2	0.4	0.5	0.6	1.0	1.2	1.7	2.8
Open shrublands									
Apr	0.0	0.1	2.5	2.4	3.8	4.9	0.0	0.1	0.2
May	5.2	2.2	9.3	7.0	18.7	22.9	3.4	12.2	14.5
Jun	10.4	N/A	9.1	7.3	26.4	31.2	8.5	29.8	35.5
Jul	7.0	10.3	10.9	9.4	30.5	36.8	9.0	31.6	37.5
Aug	8.1	11.6	11.2	11.9	28.1	36.2	8.0	21.3	27.1
Sep	12.0	11.7	8.6	10.6	19.23	26.3	8.8	13.1	19.8
Oct	8.	8.6	6.0	6.7	10.3	15.3	8.6	9.1	16.2
Nov	8.7	0.5	2.2	1.1	0.9	1.7	2.0	1.2	2.9
Woody savannas									
Apr	0.34	0.1	1.7	1.5	5.2	6.0	0.1	0.4	0.5
May	9.0	6.1	9.3	7.5	24.4	29.1	5.1	22.7	25.4
Jun	10.6	N/A	9.7	9.1	32.0	37.4	9.9	37.9	43.1
Jul	7.9	11.6	10.9	10.1	37.5	43.5	10.2	38.1	43.9
Aug	8.1	12.6	12.9	11.9	32.9	40.4	9.3	27.5	33.6
Sep	14.4	14.5	11.2	13.9	24.5	33.2	9.5	14.2	20.9
Oct	8.5	8.5	8.0	8.2	12.4	17.8	8.7	10.4	17.3
Nov	0.9	0.3	1.0	0.6	0.6	1.1	1.8	1.9	3.4
Savannas									
Apr	0.2	0.1	1.3	2.7	6.3	7.7	0.2	0.4	0.5
May	5.9	5.2	11.5	8.2	25.5	30.9	6.1	22.4	25.9
Jun	9.1	N/A	10.7	8.9	28.1	33.5	9.6	34.3	40.0
Jul	7.9	11.0	13.0	11.6	36.0	43.2	10.5	36.2	42.5
Aug	9.7	13.9	14.3	14.9	31.2	41.0	9.9	23.5	30.5
Sep	14.7	14.7	13.1	13.4	22.1	31.1	9.1	13.0	19.8
Oct	12.6	12.5	10.4	11.1	15.8	23.5	11.3	14.4	23.1
Nov	2.3	0.5	3.3	0.9	0.8	1.7	2.2	2.4	4.3
Grasslands									
Apr	0.1	0.1	6.4	4.1	4.3	6.8	0.1	0.4	0.5
May	3.6	3.2	10.5	7.3	19.0	24.0	2.9	12.8	14.5
Jun	9.1	N/A	8.5	8.2	28.4	33.9	7.6	31.9	36.6
Jul	7.4	10.3	13.1	10.1	28.1	34.8	9.5	30.5	36.9
Aug	9.0	11.1	11.8	14.0	26.1	35.5	9.9	21.2	28.1
Sep	9.5	11.2	11.4	9.7	16.7	23.6	9.2	12.5	19.5
Oct	10.2	12.2	5.5	9.1	14.1	20.7	12.8	12.2	22.7
Nov	12.4	0.7	2.9	0.6	0.5	1.07	1.8	1.6	3.2

Table C.1: Percentage of 500m burned areas detected as active fires: Additive model results

		2000 Terra	2001 Terra	2002 Terra	2003 Terra	Aqua	Both	2004 Terra	Aqua	Both
Deciduous Broadleaf Forest	Apr	0.0	0.1	1.3	1.5	4.5	5.3	0.0	0.1	0.1
	May	6.8	4.9	8.3	6.0	22.3	26.1	2.3	11.6	13.0
	Jun	8.8	N/A	8.2	7.2	32.0	36.2	8.4	38.7	43.1
	Jul	7.4	10.4	10.2	8.7	40.4	45.2	8.9	41.1	46.0
	Aug	8.0	12.5	12.2	10.3	37.7	43.6	9.6	34.6	40.4
	Sep	10.0	10.3	6.4	9.6	22.4	28.7	5.5	9.4	13.6
	Oct	3.5	5.0	2.5	2.9	7.2	9.1	3.4	5.6	8.3
	Nov	1.0	0.2	0.3	0.5	0.5	0.9	0.9	0.9	1.7
Open shrublands	Apr	0.0	0.1	3.7	4.7	7.1	9.4	0	0.2	0.2
	May	6.7	3.5	10.7	8.0	20.7	25.7	4.5	15.5	18.6
	Jun	9.9	N/A	9.8	7.7	28.3	33.2	9.1	31.6	37.8
	Jul	7.2	10.7	11.4	9.6	31.3	37.8	9.3	33.1	39.3
	Aug	8.3	12.2	11.6	12.1	28.9	37.1	8.4	22.7	28.7
	Sep	11.8	11.3	8.1	10.9	19.7	26.8	9.0	13.3	20.2
	Oct	7.6	8.4	5.5	5.7	9.0	13.2	8.3	9.0	15.8
	Nov	7.4	0.5	2.3	0.6	0.4	0.1	2.3	1.2	3.3
Woody savannas	Apr	0.5	0.1	2.8	2.5	7.8	9.3	0.1	0.4	0.5
	May	9.2	6.9	9.4	7.7	24.9	29.6	5.5	24.3	27.3
	Jun	10.5	N/A	9.7	9.1	32.0	37.3	10.1	38.7	44.0
	Jul	8.1	11.7	10.8	10.0	37.6	43.6	10.3	38.9	44.6
	Aug	8.1	13.2	13.1	12.1	33.6	41.1	9.6	28.6	34.9
	Sep	14.2	14.3	10.8	13.9	24.7	33.5	9.1	13.7	20.2
	Oct	8.4	8.3	7.7	8.2	12.4	17.9	7.8	9.2	15.4
	Nov	1.0	0.3	0.7	0.5	0.5	0.9	1.3	1.4	2.6
Savannas	Apr	0.3	0.1	2.4	4.3	9.5	11.8	0.2	0.6	0.7
	May	6.2	5.4	11.7	8.2	25.2	30.6	6.9	25.2	29.3
	Jun	9.1	N/A	10.8	8.8	30.0	33.4	9.7	35.0	40.7
	Jul	7.8	11.2	13.2	11.7	36.3	43.5	10.6	36.9	43.2
	Aug	9.5	14.5	14.4	15.3	31.9	42.0	10.3	24.8	32.0
	Sep	14.5	14.8	12.4	13.6	22.6	31.8	9.3	13.3	20.3
	Oct	12.4	12.1	9.3	10.7	15.2	22.8	10.2	13.0	21.0
	Nov	2.4	0.4	1.8	0.7	0.6	1.2	1.5	1.6	2.9
Grasslands	Apr	0.2	0.1	9.6	8.4	8.6	13.5	0.1	0.8	0.9
	May	5.4	5.9	11.9	8.4	20.0	25.7	4.1	17.6	19.9
	Jun	9.5	N/A	9.0	8.5	29.2	34.8	8.2	34.0	39.1
	Jul	7.4	10.6	13.7	10.6	29.6	36.5	10.0	31.8	38.4
	Aug	9.0	12.1	12.4	14.8	27.4	37.3	10.5	22.7	30.0
	Sep	10.1	11.2	11.3	10.1	17.2	24.3	9.8	12.9	20.4
	Oct	10.4	11.8	5.3	8.2	12.5	18.4	11.6	11.3	20.8
	Nov	10.6	0.6	1.7	0.4	0.3	0.6	1.2	1.4	2.5

Table C.2: Percentage of 500m burned areas detected as active fires: Multiplicative model results

Appendix D

Number of burn pixels

Frequency	2000	2001	2002	2003	2004
1	2633239	2460266	2565300	2543889	2585172
2	431723	390623	371253	352369	331861
3	57049	36319	46974	38980	35789

(a) Additive temporal model

	2000	2001	2002	2003	2004
1	2719132	2462568	2581935	2652820	2707261
2	443177	336553	355108	371424	372260
3	45678	22650	32494	28529	26859

(b) Multiplicative temporal model

Table D.1: Number of pixels identified as burning between one and three times during a single fire season

Appendix E

Fire frequencies

Land cover	Frequency	Proportion of total of total	Proportion of burns of burns
Deciduous broadleaf forest	1	26.4	39.9
	2	18.18	25.4
	3	12.3	16.6
	4	8.2	11.1
	5	4.8	7.0
Open Shrubland	1	116.2	48.0
	2	7.2	21.5
	3	4.6	13.6
	4	3.3	9.7
	5	2.1	7.2
Woody Savanna	1	22.0	31.0
	2	17.1	22.9
	3	13.3	17.5
	4	11.3	15.1
	5	9.3	13.5
Savanna	1	22.3	34.8
	2	16.1	24.5
	3	112.6	18.8
	4	9.3	13.7
	5	5.2	8.2
Grassland	1	15.7	41.4
	2	8.3	21.7
	3	6.3	15.7
	4	4.8	11.7
	5	3.5	9.5

Table E.1: Fire frequency across the study area: Percentage of each land cover type which burns between one and five times during the five year period: Additive model results

Appendix F

Burned area totals

	2000	2001	2002	2003	2004
Apr	2.32	3.47	11.60	2.61	2.34
May	2.93	2.38	4.96	4.04	4.01
Jun	7.94	N/A	8.07	7.87	7.65
Jul	12.82	14.16	14.21	13.47	12.56
Aug	16.62	15.51	11.36	17.29	18.82
Sep	12.57	11.84	8.28	9.72	12.08
Oct	8.867	9.48	4.31	6.28	4.32
Nov	3.13	3.83	1.38	1.83	1.72
Total	67.19	60.67	64.19	63.11	63.48

Table F.1: Total area burned (million hectares): Additive model results

	2000	2001	2002	2003	2004
Apr	1.06	1.59	5.30	1.19	1.07
May	1.34	1.09	2.27	1.85	1.83
Jun	3.62	N/A	3.69	3.59	3.49
Jul	5.85	6.46	6.49	6.15	5.73
Aug	7.59	7.08	5.19	7.90	8.59
Sep	5.74	5.40	3.78	4.44	5.51
Oct	4.05	4.33	1.99	2.87	1.97
Nov	1.47	1.75	0.6	0.83	0.78
Total	30.72	27.70	29.3	28.82	28.97

Table F.2: Percentage of the total land area which has burned: Additive model results

		2000	2001	2002	2003	2004
Deciduous broadleaf forest	Apr	0.96	1.90	3.61	1.08	1.73
	May	0.85	0.59	1.10	1.11	1.88
	Jun	3.79	0	2.95	3.33	3.13
	Jul	9.65	9.23	9.76	10.26	8.80
	Aug	13.85	13.33	9.70	11.21	12.13
	Sep	5.92	4.90	3.75	5.35	4.934
	Oct	5.16	4.04	2.71	4.94	1.97
	Nov	1.4	2.18	0.87	0.78	0.35
Total		41.58	36.17	34.45	38.06	34.92
Open shrubland	Apr	1.10	1.98	4.17	1.45	1.46
	May	0.88	1.32	1.38	1.16	1.14
	Jun	2.00	N/A	2.14	2.19	2.11
	Jul	3.48	3.85	4.02	3.74	3.70
	Aug	4.97	4.52	3.06	4.81	5.00
	Sep	4.39	4.60	2.66	2.88	4.27
	Oct	4.22	3.86	1.85	2.34	1.44
	Nov	1.43	1.64	0.77	1.08	1.21
Total		22.47	21.77	20.05	19.65	20.33
Woody savanna	Apr	7.09	12.01	25.84	7.62	7.97
	May	11.47	8.29	15.37	13.85	16.80
	Jun	32.06	0	30.69	30.43	30.83
	Jul	49.51	54.98	48.83	50.92	46.02
	Aug	53.57	49.42	36.98	49.53	51.14
	Sep	36.68	37.62	24.64	32.85	33.44
	Oct	23.93	24.24	13.98	18.63	11.00
	Nov	7.12	9.74	3.91	4.62	3.22
Total		221.43	196.3	200.24	208.45	200.42
Savanna	Apr	10.93	13.63	72.30	11.82	7.93
	May	12.22	9.48	26.73	19.62	14.51
	Jun	33.81	0	35.89	33.86	31.55
	Jul	52.66	59.29	65.89	57.24	55.46
	Aug	75.85	76.05	52.31	90.87	102.70
	Sep	66.33	61.94	44.26	47.87	67.03
	Oct	45.70	51.33	19.39	30.23	24.99
	Nov	17.41	20.60	6.53	9.74	9.97
Total		314.91	292.32	323.3	301.25	314.14
Grassland	Apr	1.37	2.18	3.73	1.70	1.62
	May	1.39	1.76	1.90	1.69	1.39
	Jun	2.67	N/A	4.34	4.41	4.22
	Jul	5.27	5.56	6.83	5.61	5.28
	Aug	7.05	4.45	4.80	7.59	7.89
	Sep	5.98	5.16	3.58	3.40	6.14
	Oct	4.23	6.00	1.61	2.46	1.68
	Nov	2.20	1.57	0.70	1.03	1.67
Total		35.12	31.07	32.03	32.46	34.83

Table F.3: Total area burned (100000 hectares): Additive model results

		2000	2001	2002	2003	2004
Deciduous broadleaf forest	Apr	0.73	1.31	2.05	0.63	1.67
	May	0.80	0.52	0.99	1.03	2.64
	Jun	4.24	N/A	3.63	4.04	3.64
	Jul	11.29	10.31	11.83	11.54	9.24
	Aug	14.40	14.60	10.76	12.33	13.32
	Sep	6.52	5.28	3.95	5.48	6.14
	Oct	4.49	3.81	3.07	4.99	2.31
	Nov	1.10	1.63	0.57	0.91	0.61
Total		43.57	37.46	36.85	40.95	39.57
Open shrubland	Apr	0.66	1.17	2.73	0.70	0.76
	May	0.63	0.77	1.26	0.91	0.77
	Jun	1.93	N/A	2.29	2.22	2.17
	Jul	3.68	3.93	4.32	3.84	3.63
	Aug	5.152	4.49	3.28	5.02	5.11
	Sep	4.48	4.59	2.68	2.93	4.52
	Oct	4.50	3.622	2.78	2.81	1.68
	Nov	1.12	1.76	0.29	1.97	1.69
Total		22.15	20.33	19.63	20.4	20.33
Woody savanna	Apr	4.58	6.71	15.14	4.37	5.94
	May	10.50	6.61	14.02	12.07	14.02
	Jun	32.95	N/A	34.27	33.46	33.69
	Jul	53.71	57.43	53.90	53.21	45.75
	Aug	55.78	52.10	39.41	53.34	54.39
	Sep	39.24	40.21	25.58	33.43	39.04
	Oct	24.63	25.39	17.32	19.61	12.67
	Nov	6.69	8.83063	2.63	6.29	5.19
Total		228.08	197.28	202.27	215.78	210.69
Savanna	Apr	6.81	7.77	41.00	7.389	5.56
	May	10.93	8.26	27.74	18.34	11.69
	Jun	34.04	N/A	40.22	37.14	34.09
	Jul	56.68	59.79	73.02	59.15	54.93
	Aug	82.95	77.80	55.56	95.87	101.61
	Sep	67.52	66.48	45.42	48.66	79.49
	Oct	49.22	53.23	27.13	32.79	26.93
	Nov	17.03	21.77	5.95	15.48	15.57
Total		325.18	295.1	316.04	314.82	329.87
Savanna	Apr	0.65	1.04	2.45	0.79	0.64
	May	0.80	0.85	1.83	1.36	0.89
	Jun	2.78	N/A	4.70	4.77	4.39
	Jul	5.41	6.01	7.50	5.556	5.19
	Aug	7.52	4.14	4.91	7.89	8.06
	Sep	5.72	5.02	3.54	3.47	6.78
	Oct	4.63	5.69	2.57	2.620	1.79
	Nov	1.60	1.79	0.32	1.85	2.49
Total		29.11	24.54	27.82	28.31	30.23

Table F.4: Total area burned (100000 hectares): Multiplicative model results

		2000	2001	2002	2003	2004
Deciduous broadleaf forest	Apr	0.76	1.49	2.85	0.86	1.36
	May	0.67	0.47	0.86	0.87	1.48
	Jun	2.99	N/A	2.33	2.63	2.47
	Jul	7.62	7.28	7.70	8.09	6.94
	Aug	10.93	10.51	7.6	8.84	9.56
	Sep	4.67	3.87	2.96	4.22	3.89
	Oct	4.07	3.19	2.13	3.90	1.56
	Nov	1.10	1.72	0.69	0.61	0.28
Total		32.81	28.53	27.12	30.02	27.54
Open shrubland	Apr	0.73	1.32	2.77	0.96	0.97
	May	0.59	0.88	0.92	0.77	0.76
	Jun	1.33	N/A	1.42	1.45	1.40
	Jul	2.31	2.56	2.67	2.48	2.46
	Aug	3.30	3.01	2.03	3.19	3.33
	Sep	2.92	3.06	1.77	1.91	2.84
	Oct	2.81	2.57	1.23	1.56	0.96
	Nov	0.95	1.09	0.51	0.71	0.80
Total		14.94	14.49	13.32	13.03	13.52
Woody savanna	Apr	1.26	2.14	4.61	1.36	1.42
	May	2.05	1.48	2.74	2.47	3.00
	Jun	5.72	0	5.47	5.43	5.50
	Jul	8.83	9.81	8.71	9.08	8.21
	Aug	9.55	8.81	6.59	8.83	9.12
	Sep	6.54	6.71	4.39	5.86	5.96
	Nov	4.27	4.32	2.49	3.32	1.96
	Oct	1.27	1.74	0.70	0.82	0.57
Total		39.49	35.01	35.71	37.17	35.74
Savanna	Apr	1.08	1.34	7.12	1.16	0.78
	May	1.20	0.93	2.63	1.93	1.43
	Jun	3.33	N/A	3.54	3.34	3.11
	Jul	5.19	5.84	6.49	5.64	5.47
	Aug	7.47	7.49	5.15	8.95	10.12
	Sep	6.54	6.10	4.36	4.72	6.61
	Oct	4.50	5.06	1.91	3.00	2.46
	Nov	1.72	2.03	0.64	1.00	0.98
Total		31.03	28.81	31.86	29.68	30.96
Grassland	Apr	0.86	1.37	2.34	1.06	1.02
	May	0.87	1.10	1.19	1.06	0.87
	Jun	1.67	N/A	2.72	2.76	2.65
	Jul	3.30	3.48	4.28	3.51	3.30
	Aug	4.41	2.79	3.01	4.76	4.94
	Sep	3.74	3.23	2.24	2.13	3.85
	Oct	2.65	3.75	1.01	1.54	1.05
	Nov	1.38	0.98	0.44	0.64	1.05
Total		18.88	16.7	17.23	17.46	18.73

Table F.5: Percentage of vegetation class which has burned: Multiplicative model results

		2000	2001	2002	2003	2004
Deciduous broadleaf forest	Apr	0.56	1.04	1.61	0.49	1.32
	May	0.63	0.41	0.78	0.81	2.08
	Jun	3.34	N/A	2.86	3.19	2.87
	Jul	8.90	8.13	9.33	9.10	7.28
	Aug	11.35	11.51	8.48	9.72	10.51
	Sep	5.15	4.17	3.11	4.32	4.84
	Oct	3.54	3.00	2.42	3.94	1.82
	Nov	0.87	1.28	0.44	0.72	0.48
Total		34.34	29.54	29.03	32.29	31.20
Open shrubland	Apr	0.44	0.78	1.82	0.47	0.51
	May	0.42	0.51	0.84	0.61	0.51
	Jun	1.28	N/A	1.52	1.48	1.44
	Jul	2.45	2.61	2.87	2.55	2.41
	Aug	3.42	2.98	2.18	3.34	3.40
	Sep	2.97	3.04	1.78	1.95	3.00
	Oct	2.99	2.42	1.85	1.86	1.12
	Nov	0.75	1.17	0.19	1.31	1.13
Total		14.72	13.50	13.04	13.56	13.51
Woody savanna	Apr	0.82	1.20	2.70	0.78	1.06
	May	1.87	1.18	2.50	2.15	2.50
	Jun	5.88	N/A	6.11	5.97	6.01
	Jul	9.58	10.24	9.61	9.49	8.16
	Aug	9.95	9.29	7.03	9.51	9.70
	Sep	7.00	7.17	4.56	5.96	6.96
	Oct	4.39	4.53	3.09	3.50	2.26
	Nov	1.19	1.57	0.47	1.12	0.93
Total		40.68	35.18	36.07	38.48	37.58
Savanna	Apr	0.67	0.77	4.04	0.73	0.55
	May	1.08	0.81	2.73	1.81	1.15
	Jun	3.35	N/A	3.96	3.66	3.36
	Jul	5.59	5.89	7.20	5.83	5.41
	Aug	8.17	7.67	5.48	9.45	10.01
	Sep	6.65	6.55	4.48	4.79	7.83
	Oct	4.85	5.25	2.67	3.23	2.65
	Nov	1.68	2.15	0.59	1.53	1.53
Total		32.04	29.08	31.14	31.02	32.51
Grassland	Apr	0.41	0.65	1.54	0.50	0.40
	May	0.50	0.53	1.14	0.85	0.56
	Jun	1.74	0	2.94	2.99	2.76
	Jul	3.39	3.77	4.70	3.48	3.25
	Aug	4.71	2.60	3.08	4.94	5.05
	Sep	3.58	3.14	2.22	2.17	4.24
	Oct	2.90	3.56	1.61	1.64	1.12
	Nov	1.00	1.12	0.20	1.16	1.56
Total		18.24	15.37	17.43	17.74	18.94

Table F.6: Percentage of vegetation class which has burned: Multiplicative model results

Appendix G

Burn severity classes

	Low	Moderate	High
2000	61.0	36.1	2.9
2001	61.0	36.0	3.1
2002	67.7	30.3	2.0
2003	64.4	33.2	2.4
2004	63.7	34.0	2.3

(a)Deciduous broadleaf forest

	Low	Moderate	High
2000	56.5	38.9	4.6
2001	58.6	36.8	4.6
2002	61.1	34.8	4.1
2003	58.6	37.2	4.1
2004	53.7	42.2	4.1

(b)Open shrublands

	Low	Moderate	High
2000	53.3	41.9	4.8
2001	53.2	41.4	5.4
2002	56.4	38.9	4.7
2003	53.9	41.1	5.0
2004	52.8	42.0	5.2

(c)Woody savannas

	Low	Moderate	High
2000	56.0	38.7	3.3
2001	55.7	41.1	3.2
2002	61.1	36.5	2.4
2003	59.0	38.2	2.7
2004	52.7	44.3	3.0

(d)Savannas

	Low	Moderate	High
2000	52.7	42.3	5.1
2001	54.2	38.2	7.6
2002	49.0	42.2	8.8
2003	50.6	40.9	8.5
2004	46.4	46.1	7.4

(e)Grasslands

Table G.1: Proportion of low, moderate and high severity burns in each cover class between 2000-2004: Additive model results

Appendix B

Active fires and burned areas

Additive model results									
	2000 Terra	2001 Terra	2002 Terra	2003 Terra	Aqua	both	2004 Terra	Aqua	both
Apr	0.3	0.1	1.7	2.4	5.5	6.7	0.1	0.4	0.4
May	6.9	5.1	10.5	7.7	24.3	29.2	5.0	20.6	23.5
Jun	9.8	N/A	10.0	8.8	29.8	35.1	9.5	35.6	41.0
Jul	7.8	11.1	11.9	10.5	36.3	42.7	10.1	36.8	42.7
Aug	8.9	13.0	13.3	13.3	31.8	40.4	9.6	25.5	32.0
Sep	13.8	14.0	11.6	12.9	22.4	31.0	8.9	13.1	19.7
Oct	10.1	10.3	8.2	8.9	13.2	19.4	9.9	12.2	19.9
Nov	2.8	0.41	2.2	0.09	0.8	1.7	2.1	2.1	3.9
Total	9.2	10.6	9.9	10.5	26.3	33.1	8.9	23.6	29.5

Table B.1: Percentage of 500m burned areas detected as active fires: Additive model results

Appendix C

Monthly burned area totals

	2000	2001	2002	2003			2004		
	Terra	Terra	Terra	Terra	Aqua	both	Terra	Aqua	both
Deciduous broadleaf forest									
Apr	0.0	0.1	0.8	1.0	2.9	3.4	0.0	0.1	0.1
May	7.1	4.5	8.0	6.1	23.2	27.0	3.5	15.8	17.9
Jun	9.1	N/A	8.5	7.5	32.5	36.7	8.3	38.0	42.5
Jul	7.3	10.6	10.6	8.9	40.8	45.8	9.1	41.0	45.9
Aug	8.0	12.3	12.1	10.3	37.4	43.3	9.6	34.0	39.8
Sep	10.2	10.7	6.8	9.8	22.9	29.3	6.0	9.9	14.5
Oct	3.4	4.6	2.2	2.7	6.6	8.4	3.7	5.8	8.8
Nov	0.9	0.2	0.4	0.5	0.6	1.0	1.2	1.7	2.8
Open shrublands									
Apr	0.0	0.1	2.5	2.4	3.8	4.9	0.0	0.1	0.2
May	5.2	2.2	9.3	7.0	18.7	22.9	3.4	12.2	14.5
Jun	10.4	N/A	9.1	7.3	26.4	31.2	8.5	29.8	35.5
Jul	7.0	10.3	10.9	9.4	30.5	36.8	9.0	31.6	37.5
Aug	8.1	11.6	11.2	11.9	28.1	36.2	8.0	21.3	27.1
Sep	12.0	11.7	8.6	10.6	19.23	26.3	8.8	13.1	19.8
Oct	8.	8.6	6.0	6.7	10.3	15.3	8.6	9.1	16.2
Nov	8.7	0.5	2.2	1.1	0.9	1.7	2.0	1.2	2.9
Woody savannas									
Apr	0.34	0.1	1.7	1.5	5.2	6.0	0.1	0.4	0.5
May	9.0	6.1	9.3	7.5	24.4	29.1	5.1	22.7	25.4
Jun	10.6	N/A	9.7	9.1	32.0	37.4	9.9	37.9	43.1
Jul	7.9	11.6	10.9	10.1	37.5	43.5	10.2	38.1	43.9
Aug	8.1	12.6	12.9	11.9	32.9	40.4	9.3	27.5	33.6
Sep	14.4	14.5	11.2	13.9	24.5	33.2	9.5	14.2	20.9
Oct	8.5	8.5	8.0	8.2	12.4	17.8	8.7	10.4	17.3
Nov	0.9	0.3	1.0	0.6	0.6	1.1	1.8	1.9	3.4
Savannas									
Apr	0.2	0.1	1.3	2.7	6.3	7.7	0.2	0.4	0.5
May	5.9	5.2	11.5	8.2	25.5	30.9	6.1	22.4	25.9
Jun	9.1	N/A	10.7	8.9	28.1	33.5	9.6	34.3	40.0
Jul	7.9	11.0	13.0	11.6	36.0	43.2	10.5	36.2	42.5
Aug	9.7	13.9	14.3	14.9	31.2	41.0	9.9	23.5	30.5
Sep	14.7	14.7	13.1	13.4	22.1	31.1	9.1	13.0	19.8
Oct	12.6	12.5	10.4	11.1	15.8	23.5	11.3	14.4	23.1
Nov	2.3	0.5	3.3	0.9	0.8	1.7	2.2	2.4	4.3
Grasslands									
Apr	0.1	0.1	6.4	4.1	4.3	6.8	0.1	0.4	0.5
May	3.6	3.2	10.5	7.3	19.0	24.0	2.9	12.8	14.5
Jun	9.1	N/A	8.5	8.2	28.4	33.9	7.6	31.9	36.6
Jul	7.4	10.3	13.1	10.1	28.1	34.8	9.5	30.5	36.9
Aug	9.0	11.1	11.8	14.0	26.1	35.5	9.9	21.2	28.1
Sep	9.5	11.2	11.4	9.7	16.7	23.6	9.2	12.5	19.5
Oct	10.2	12.2	5.5	9.1	14.1	20.7	12.8	12.2	22.7
Nov	12.4	0.7	2.9	0.6	0.5	1.07	1.8	1.6	3.2

Table C.1: Percentage of 500m burned areas detected as active fires: Additive model results

		2000 Terra	2001 Terra	2002 Terra	2003 Terra	Aqua	Both	2004 Terra	Aqua	Both
Deciduous Broadleaf Forest	Apr	0.0	0.1	1.3	1.5	4.5	5.3	0.0	0.1	0.1
	May	6.8	4.9	8.3	6.0	22.3	26.1	2.3	11.6	13.0
	Jun	8.8	N/A	8.2	7.2	32.0	36.2	8.4	38.7	43.1
	Jul	7.4	10.4	10.2	8.7	40.4	45.2	8.9	41.1	46.0
	Aug	8.0	12.5	12.2	10.3	37.7	43.6	9.6	34.6	40.4
	Sep	10.0	10.3	6.4	9.6	22.4	28.7	5.5	9.4	13.6
	Oct	3.5	5.0	2.5	2.9	7.2	9.1	3.4	5.6	8.3
	Nov	1.0	0.2	0.3	0.5	0.5	0.9	0.9	0.9	1.7
Open shrublands	Apr	0.0	0.1	3.7	4.7	7.1	9.4	0	0.2	0.2
	May	6.7	3.5	10.7	8.0	20.7	25.7	4.5	15.5	18.6
	Jun	9.9	N/A	9.8	7.7	28.3	33.2	9.1	31.6	37.8
	Jul	7.2	10.7	11.4	9.6	31.3	37.8	9.3	33.1	39.3
	Aug	8.3	12.2	11.6	12.1	28.9	37.1	8.4	22.7	28.7
	Sep	11.8	11.3	8.1	10.9	19.7	26.8	9.0	13.3	20.2
	Oct	7.6	8.4	5.5	5.7	9.0	13.2	8.3	9.0	15.8
	Nov	7.4	0.5	2.3	0.6	0.4	0.1	2.3	1.2	3.3
Woody savannas	Apr	0.5	0.1	2.8	2.5	7.8	9.3	0.1	0.4	0.5
	May	9.2	6.9	9.4	7.7	24.9	29.6	5.5	24.3	27.3
	Jun	10.5	N/A	9.7	9.1	32.0	37.3	10.1	38.7	44.0
	Jul	8.1	11.7	10.8	10.0	37.6	43.6	10.3	38.9	44.6
	Aug	8.1	13.2	13.1	12.1	33.6	41.1	9.6	28.6	34.9
	Sep	14.2	14.3	10.8	13.9	24.7	33.5	9.1	13.7	20.2
	Oct	8.4	8.3	7.7	8.2	12.4	17.9	7.8	9.2	15.4
	Nov	1.0	0.3	0.7	0.5	0.5	0.9	1.3	1.4	2.6
Savannas	Apr	0.3	0.1	2.4	4.3	9.5	11.8	0.2	0.6	0.7
	May	6.2	5.4	11.7	8.2	25.2	30.6	6.9	25.2	29.3
	Jun	9.1	N/A	10.8	8.8	30.0	33.4	9.7	35.0	40.7
	Jul	7.8	11.2	13.2	11.7	36.3	43.5	10.6	36.9	43.2
	Aug	9.5	14.5	14.4	15.3	31.9	42.0	10.3	24.8	32.0
	Sep	14.5	14.8	12.4	13.6	22.6	31.8	9.3	13.3	20.3
	Oct	12.4	12.1	9.3	10.7	15.2	22.8	10.2	13.0	21.0
	Nov	2.4	0.4	1.8	0.7	0.6	1.2	1.5	1.6	2.9
Grasslands	Apr	0.2	0.1	9.6	8.4	8.6	13.5	0.1	0.8	0.9
	May	5.4	5.9	11.9	8.4	20.0	25.7	4.1	17.6	19.9
	Jun	9.5	N/A	9.0	8.5	29.2	34.8	8.2	34.0	39.1
	Jul	7.4	10.6	13.7	10.6	29.6	36.5	10.0	31.8	38.4
	Aug	9.0	12.1	12.4	14.8	27.4	37.3	10.5	22.7	30.0
	Sep	10.1	11.2	11.3	10.1	17.2	24.3	9.8	12.9	20.4
	Oct	10.4	11.8	5.3	8.2	12.5	18.4	11.6	11.3	20.8
	Nov	10.6	0.6	1.7	0.4	0.3	0.6	1.2	1.4	2.5

Table C.2: Percentage of 500m burned areas detected as active fires: Multiplicative model results

Appendix D

Number of burn pixels

Frequency	2000	2001	2002	2003	2004
1	2633239	2460266	2565300	2543889	2585172
2	431723	390623	371253	352369	331861
3	57049	36319	46974	38980	35789

(a) Additive temporal model

	2000	2001	2002	2003	2004
1	2719132	2462568	2581935	2652820	2707261
2	443177	336553	355108	371424	372260
3	45678	22650	32494	28529	26859

(b) Multiplicative temporal model

Table D.1: Number of pixels identified as burning between one and three times during a single fire season

Appendix E

Fire frequencies

Land cover	Frequency	Proportion of total of total	Proportion of burns of burns
Deciduous broadleaf forest	1	26.4	39.9
	2	18.18	25.4
	3	12.3	16.6
	4	8.2	11.1
	5	4.8	7.0
Open Shrubland	1	116.2	48.0
	2	7.2	21.5
	3	4.6	13.6
	4	3.3	9.7
	5	2.1	7.2
Woody Savanna	1	22.0	31.0
	2	17.1	22.9
	3	13.3	17.5
	4	11.3	15.1
	5	9.3	13.5
Savanna	1	22.3	34.8
	2	16.1	24.5
	3	112.6	18.8
	4	9.3	13.7
	5	5.2	8.2
Grassland	1	15.7	41.4
	2	8.3	21.7
	3	6.3	15.7
	4	4.8	11.7
	5	3.5	9.5

Table E.1: Fire frequency across the study area: Percentage of each land cover type which burns between one and five times during the five year period: Additive model results

Appendix F

Burned area totals

	2000	2001	2002	2003	2004
Apr	2.32	3.47	11.60	2.61	2.34
May	2.93	2.38	4.96	4.04	4.01
Jun	7.94	N/A	8.07	7.87	7.65
Jul	12.82	14.16	14.21	13.47	12.56
Aug	16.62	15.51	11.36	17.29	18.82
Sep	12.57	11.84	8.28	9.72	12.08
Oct	8.867	9.48	4.31	6.28	4.32
Nov	3.13	3.83	1.38	1.83	1.72
Total	67.19	60.67	64.19	63.11	63.48

Table F.1: Total area burned (million hectares): Additive model results

	2000	2001	2002	2003	2004
Apr	1.06	1.59	5.30	1.19	1.07
May	1.34	1.09	2.27	1.85	1.83
Jun	3.62	N/A	3.69	3.59	3.49
Jul	5.85	6.46	6.49	6.15	5.73
Aug	7.59	7.08	5.19	7.90	8.59
Sep	5.74	5.40	3.78	4.44	5.51
Oct	4.05	4.33	1.99	2.87	1.97
Nov	1.47	1.75	0.6	0.83	0.78
Total	30.72	27.70	29.3	28.82	28.97

Table F.2: Percentage of the total land area which has burned: Additive model results

		2000	2001	2002	2003	2004
Deciduous broadleaf forest	Apr	0.96	1.90	3.61	1.08	1.73
	May	0.85	0.59	1.10	1.11	1.88
	Jun	3.79	0	2.95	3.33	3.13
	Jul	9.65	9.23	9.76	10.26	8.80
	Aug	13.85	13.33	9.70	11.21	12.13
	Sep	5.92	4.90	3.75	5.35	4.934
	Oct	5.16	4.04	2.71	4.94	1.97
	Nov	1.4	2.18	0.87	0.78	0.35
Total		41.58	36.17	34.45	38.06	34.92
Open shrubland	Apr	1.10	1.98	4.17	1.45	1.46
	May	0.88	1.32	1.38	1.16	1.14
	Jun	2.00	N/A	2.14	2.19	2.11
	Jul	3.48	3.85	4.02	3.74	3.70
	Aug	4.97	4.52	3.06	4.81	5.00
	Sep	4.39	4.60	2.66	2.88	4.27
	Oct	4.22	3.86	1.85	2.34	1.44
	Nov	1.43	1.64	0.77	1.08	1.21
Total		22.47	21.77	20.05	19.65	20.33
Woody savanna	Apr	7.09	12.01	25.84	7.62	7.97
	May	11.47	8.29	15.37	13.85	16.80
	Jun	32.06	0	30.69	30.43	30.83
	Jul	49.51	54.98	48.83	50.92	46.02
	Aug	53.57	49.42	36.98	49.53	51.14
	Sep	36.68	37.62	24.64	32.85	33.44
	Oct	23.93	24.24	13.98	18.63	11.00
	Nov	7.12	9.74	3.91	4.62	3.22
Total		221.43	196.3	200.24	208.45	200.42
Savanna	Apr	10.93	13.63	72.30	11.82	7.93
	May	12.22	9.48	26.73	19.62	14.51
	Jun	33.81	0	35.89	33.86	31.55
	Jul	52.66	59.29	65.89	57.24	55.46
	Aug	75.85	76.05	52.31	90.87	102.70
	Sep	66.33	61.94	44.26	47.87	67.03
	Oct	45.70	51.33	19.39	30.23	24.99
	Nov	17.41	20.60	6.53	9.74	9.97
Total		314.91	292.32	323.3	301.25	314.14
Grassland	Apr	1.37	2.18	3.73	1.70	1.62
	May	1.39	1.76	1.90	1.69	1.39
	Jun	2.67	N/A	4.34	4.41	4.22
	Jul	5.27	5.56	6.83	5.61	5.28
	Aug	7.05	4.45	4.80	7.59	7.89
	Sep	5.98	5.16	3.58	3.40	6.14
	Oct	4.23	6.00	1.61	2.46	1.68
	Nov	2.20	1.57	0.70	1.03	1.67
Total		35.12	31.07	32.03	32.46	34.83

Table F.3: Total area burned (100000 hectares): Additive model results

		2000	2001	2002	2003	2004
Deciduous broadleaf forest	Apr	0.73	1.31	2.05	0.63	1.67
	May	0.80	0.52	0.99	1.03	2.64
	Jun	4.24	N/A	3.63	4.04	3.64
	Jul	11.29	10.31	11.83	11.54	9.24
	Aug	14.40	14.60	10.76	12.33	13.32
	Sep	6.52	5.28	3.95	5.48	6.14
	Oct	4.49	3.81	3.07	4.99	2.31
	Nov	1.10	1.63	0.57	0.91	0.61
Total		43.57	37.46	36.85	40.95	39.57
Open shrubland	Apr	0.66	1.17	2.73	0.70	0.76
	May	0.63	0.77	1.26	0.91	0.77
	Jun	1.93	N/A	2.29	2.22	2.17
	Jul	3.68	3.93	4.32	3.84	3.63
	Aug	5.152	4.49	3.28	5.02	5.11
	Sep	4.48	4.59	2.68	2.93	4.52
	Oct	4.50	3.622	2.78	2.81	1.68
	Nov	1.12	1.76	0.29	1.97	1.69
Total		22.15	20.33	19.63	20.4	20.33
Woody savanna	Apr	4.58	6.71	15.14	4.37	5.94
	May	10.50	6.61	14.02	12.07	14.02
	Jun	32.95	N/A	34.27	33.46	33.69
	Jul	53.71	57.43	53.90	53.21	45.75
	Aug	55.78	52.10	39.41	53.34	54.39
	Sep	39.24	40.21	25.58	33.43	39.04
	Oct	24.63	25.39	17.32	19.61	12.67
	Nov	6.69	8.83063	2.63	6.29	5.19
Total		228.08	197.28	202.27	215.78	210.69
Savanna	Apr	6.81	7.77	41.00	7.389	5.56
	May	10.93	8.26	27.74	18.34	11.69
	Jun	34.04	N/A	40.22	37.14	34.09
	Jul	56.68	59.79	73.02	59.15	54.93
	Aug	82.95	77.80	55.56	95.87	101.61
	Sep	67.52	66.48	45.42	48.66	79.49
	Oct	49.22	53.23	27.13	32.79	26.93
	Nov	17.03	21.77	5.95	15.48	15.57
Total		325.18	295.1	316.04	314.82	329.87
Savanna	Apr	0.65	1.04	2.45	0.79	0.64
	May	0.80	0.85	1.83	1.36	0.89
	Jun	2.78	N/A	4.70	4.77	4.39
	Jul	5.41	6.01	7.50	5.556	5.19
	Aug	7.52	4.14	4.91	7.89	8.06
	Sep	5.72	5.02	3.54	3.47	6.78
	Oct	4.63	5.69	2.57	2.620	1.79
	Nov	1.60	1.79	0.32	1.85	2.49
Total		29.11	24.54	27.82	28.31	30.23

Table F.4: Total area burned (100000 hectares): Multiplicative model results

		2000	2001	2002	2003	2004
Deciduous broadleaf forest	Apr	0.76	1.49	2.85	0.86	1.36
	May	0.67	0.47	0.86	0.87	1.48
	Jun	2.99	N/A	2.33	2.63	2.47
	Jul	7.62	7.28	7.70	8.09	6.94
	Aug	10.93	10.51	7.6	8.84	9.56
	Sep	4.67	3.87	2.96	4.22	3.89
	Oct	4.07	3.19	2.13	3.90	1.56
	Nov	1.10	1.72	0.69	0.61	0.28
Total		32.81	28.53	27.12	30.02	27.54
Open shrubland	Apr	0.73	1.32	2.77	0.96	0.97
	May	0.59	0.88	0.92	0.77	0.76
	Jun	1.33	N/A	1.42	1.45	1.40
	Jul	2.31	2.56	2.67	2.48	2.46
	Aug	3.30	3.01	2.03	3.19	3.33
	Sep	2.92	3.06	1.77	1.91	2.84
	Oct	2.81	2.57	1.23	1.56	0.96
	Nov	0.95	1.09	0.51	0.71	0.80
Total		14.94	14.49	13.32	13.03	13.52
Woody savanna	Apr	1.26	2.14	4.61	1.36	1.42
	May	2.05	1.48	2.74	2.47	3.00
	Jun	5.72	0	5.47	5.43	5.50
	Jul	8.83	9.81	8.71	9.08	8.21
	Aug	9.55	8.81	6.59	8.83	9.12
	Sep	6.54	6.71	4.39	5.86	5.96
	Nov	4.27	4.32	2.49	3.32	1.96
	Oct	1.27	1.74	0.70	0.82	0.57
Total		39.49	35.01	35.71	37.17	35.74
Savanna	Apr	1.08	1.34	7.12	1.16	0.78
	May	1.20	0.93	2.63	1.93	1.43
	Jun	3.33	N/A	3.54	3.34	3.11
	Jul	5.19	5.84	6.49	5.64	5.47
	Aug	7.47	7.49	5.15	8.95	10.12
	Sep	6.54	6.10	4.36	4.72	6.61
	Oct	4.50	5.06	1.91	3.00	2.46
	Nov	1.72	2.03	0.64	1.00	0.98
Total		31.03	28.81	31.86	29.68	30.96
Grassland	Apr	0.86	1.37	2.34	1.06	1.02
	May	0.87	1.10	1.19	1.06	0.87
	Jun	1.67	N/A	2.72	2.76	2.65
	Jul	3.30	3.48	4.28	3.51	3.30
	Aug	4.41	2.79	3.01	4.76	4.94
	Sep	3.74	3.23	2.24	2.13	3.85
	Oct	2.65	3.75	1.01	1.54	1.05
	Nov	1.38	0.98	0.44	0.64	1.05
Total		18.88	16.7	17.23	17.46	18.73

Table F.5: Percentage of vegetation class which has burned: Multiplicative model results

		2000	2001	2002	2003	2004
Deciduous broadleaf forest	Apr	0.56	1.04	1.61	0.49	1.32
	May	0.63	0.41	0.78	0.81	2.08
	Jun	3.34	N/A	2.86	3.19	2.87
	Jul	8.90	8.13	9.33	9.10	7.28
	Aug	11.35	11.51	8.48	9.72	10.51
	Sep	5.15	4.17	3.11	4.32	4.84
	Oct	3.54	3.00	2.42	3.94	1.82
	Nov	0.87	1.28	0.44	0.72	0.48
Total		34.34	29.54	29.03	32.29	31.20
Open shrubland	Apr	0.44	0.78	1.82	0.47	0.51
	May	0.42	0.51	0.84	0.61	0.51
	Jun	1.28	N/A	1.52	1.48	1.44
	Jul	2.45	2.61	2.87	2.55	2.41
	Aug	3.42	2.98	2.18	3.34	3.40
	Sep	2.97	3.04	1.78	1.95	3.00
	Oct	2.99	2.42	1.85	1.86	1.12
	Nov	0.75	1.17	0.19	1.31	1.13
Total		14.72	13.50	13.04	13.56	13.51
Woody savanna	Apr	0.82	1.20	2.70	0.78	1.06
	May	1.87	1.18	2.50	2.15	2.50
	Jun	5.88	N/A	6.11	5.97	6.01
	Jul	9.58	10.24	9.61	9.49	8.16
	Aug	9.95	9.29	7.03	9.51	9.70
	Sep	7.00	7.17	4.56	5.96	6.96
	Oct	4.39	4.53	3.09	3.50	2.26
	Nov	1.19	1.57	0.47	1.12	0.93
Total		40.68	35.18	36.07	38.48	37.58
Savanna	Apr	0.67	0.77	4.04	0.73	0.55
	May	1.08	0.81	2.73	1.81	1.15
	Jun	3.35	N/A	3.96	3.66	3.36
	Jul	5.59	5.89	7.20	5.83	5.41
	Aug	8.17	7.67	5.48	9.45	10.01
	Sep	6.65	6.55	4.48	4.79	7.83
	Oct	4.85	5.25	2.67	3.23	2.65
	Nov	1.68	2.15	0.59	1.53	1.53
Total		32.04	29.08	31.14	31.02	32.51
Grassland	Apr	0.41	0.65	1.54	0.50	0.40
	May	0.50	0.53	1.14	0.85	0.56
	Jun	1.74	0	2.94	2.99	2.76
	Jul	3.39	3.77	4.70	3.48	3.25
	Aug	4.71	2.60	3.08	4.94	5.05
	Sep	3.58	3.14	2.22	2.17	4.24
	Oct	2.90	3.56	1.61	1.64	1.12
	Nov	1.00	1.12	0.20	1.16	1.56
Total		18.24	15.37	17.43	17.74	18.94

Table F.6: Percentage of vegetation class which has burned: Multiplicative model results

Appendix G

Burn severity classes

	Low	Moderate	High
2000	61.0	36.1	2.9
2001	61.0	36.0	3.1
2002	67.7	30.3	2.0
2003	64.4	33.2	2.4
2004	63.7	34.0	2.3

(a)Deciduous broadleaf forest

	Low	Moderate	High
2000	56.5	38.9	4.6
2001	58.6	36.8	4.6
2002	61.1	34.8	4.1
2003	58.6	37.2	4.1
2004	53.7	42.2	4.1

(b)Open shrublands

	Low	Moderate	High
2000	53.3	41.9	4.8
2001	53.2	41.4	5.4
2002	56.4	38.9	4.7
2003	53.9	41.1	5.0
2004	52.8	42.0	5.2

(c)Woody savannas

	Low	Moderate	High
2000	56.0	38.7	3.3
2001	55.7	41.1	3.2
2002	61.1	36.5	2.4
2003	59.0	38.2	2.7
2004	52.7	44.3	3.0

(d)Savannas

	Low	Moderate	High
2000	52.7	42.3	5.1
2001	54.2	38.2	7.6
2002	49.0	42.2	8.8
2003	50.6	40.9	8.5
2004	46.4	46.1	7.4

(e)Grasslands

Table G.1: Proportion of low, moderate and high severity burns in each cover class between 2000-2004: Additive model results